A METALLOGENIC STUDY

OF THE CENTRAL VIRGINIAN GOLD-PYRITE BELT

by

Norman Albert Duke

Department of Earth Sciences

Submitted in partial fulfilment

of the requirements for the degree of

Doctor of Philosophy

to:

The Faculty of Graduate Studies

University of Manitoba,
Winnipeg, Manitoba.

✓ c Norman Albert Duke 1983

A METALLOGENIC STUDY

OF THE CENTRAL VIRGINIAN GOLD-PYRITE BELT

by

Norman Duke

A thesis submitted to the Faculty of Graduate Studies of
the University of Manitoba in partial fulfillment of the requirements
of the degree of

DOCTOR OF PHILOSOPHY

© 1984

Permission has been granted to the LIBRARY OF THE UNIVERSITY OF MANITOBA to lend or sell copies of this thesis, to the NATIONAL LIBRARY OF CANADA to microfilm this thesis and to lend or sell copies of the film, and UNIVERSITY MICROFILMS to publish an abstract of this thesis.

The author reserves other publication rights, and neither the thesis nor extensive extracts from it may be printed or otherwise reproduced without the author's written permission.

ABSTRACT

A Metallogenic Study of the Central Virginian Gold-Pyrite Belt
by Norman A. Duke

The pyritic base metal massive sulphide and lode gold occurrences of the central Virginian Piedmont are hosted in the Chopawamsic metavolcanic (schist) belt. This terrane is characterized by strongly bimodal volcanic suites interlayered with considerable epiclastic and chemical sedimentary rocks, indicating that it originated as a volcanically active rift setting. The fault-bounded rift deposits are flanked on the west by the low greenschist facies metapelitic schists of the inner Piedmont and on the east by the amphibolite facies gneissic lithology of the outer Piedmont, which includes both Grenvillian basement exposures and late Paleozoic granitoid intrusions.

A three-stage evolutionary model is proposed for the setting. Laterally extensive fissure volcanism during latest Precambrian through Cambrian times produced a western metavolcanic suite dominated by felsic pyroclastic rocks, a central metavolcanic suite of interlayered epiclastic sediments and bimodal volcanic lithologies, and an eastern amphibolite gneiss facies. This initial stage culminated in a period of high level intrusion accompanied by regional deposition of lean iron formation, local pyroclastic eruptions, and epiclastic sedimentation into volcani-tectonic sinks. The area remained a non-volcanic shale successor basin during most of the Ordovician. After being greatly foreshortened during late Paleozoic metamorphism, it remained stable until the Mesozoic when the widespread intrusion of diabase dykes and the formation of deep molassic graben accompanied the opening of the Atlantic.

Both low-K mantle-derived and high-K crustal magmas formed the igneous suites. Where intruded, the low-K partial melt fractions from the mantle commonly underwent gravitational differentiation to ultramafic cumulates, layered gabbro, and fractionated tonalite-trondhjemite compositions. In contrast, the low-K metavolcanic suites are strongly bimodal; possibly these formed through liquid immiscibility and the splitting off of conjugate iron-rich basaltic and trondhjemitic liquids. The high-K lineage accounts for large diorite to granodiorite stocks, the western pyroclastic rocks, and the late ash flow tuff deposits. The uniform magnesian amphibolite horizons which occasionally accompany the latter facies have ultramafic-igneous compositions; these are tentatively identified as metakomatiite flows.

Heat flow within the rift peaked in the near-surface environment during the late high level intrusive and pyroclastic volcanic stage. Enhanced hydrothermal activity at this time resulted in pervasive alteration of the volcanic rocks and derivation of the lithologically diverse iron formation - aluminous quartzite association which caps the metavolcanic suites. The pyritic massive sulphide and lode gold mineralization found in the Chopawamsic can also be directly related to syndepositional hydrothermal processes. The marked increase in the spessartine contents of garnet with proximity to sulphide mineral concentrations documents the existence of primary manganese enrichment haloes, a characteristic feature of many exhalative sulphide settings. The garnet-grunerite iron formation - cummingtonite and tschermakitic hornblende-bearing ironstone - metakomatiite lithological association which hosts the gold is common to many gold districts in metamorphosed iron formation terranes. The metallogeny of the Chopawamsic setting reflects variations in the syndepositional hydrothermal regime. The initial high water/rock ratios existing prior to loss of formational brines resulted in the deposition of massive sulphide near discharge sites while the much lower water/rock ratios existing subsequent to dewatering enriched gold within multifacies iron formation.

ACKNOWLEDGMENTS

The preparation of this thesis has entailed many debts. The author wishes to thank Dr. H.D.B. Wilson for his interest and advice during preliminary phases of the project and also Dr. P. Laznicka for his invaluable assistance after Dr. Wilson's retirement. The manuscript was read in addition by Dr. L.D. Ayres and Dr. W.R. Brisbin, whose thoughtful appraisals proved very helpful. Special thanks are due as well to Callahan Mining Corp. for its sponsorship of extensive field research in the study area, to K. Ramlal for the analytical work carried out at the University of Manitoba, and to R.L. Barnett for the microprobe analyses done at the University of Western Ontario. The author is also greatly indebted to G. McGregor for her assiduous and discriminating labour in editing, drafting, and typing.

The work was partially supported by a University of Manitoba Fellowship during 1976-79.

TABLE OF CONTENTS

		Page
1.	INTRODUCTION	1-1
	1.1 Statement of Thesis	1-1
	1.2 Tectonic Setting of the Chopawamsic Metavolcanic Belt Within the Appalachian Orogen	1-3
	1.3 Methodology: Problems and Solutions	1-15
	1.3.1 Compensating for Lack of Outcrop	1-17
	1.3.2 Sample Collection and Classification	1-20
	1.4 Presentation of Data	1-21
2.	REGIONAL GEOLOGICAL FRAMEWORK	2-1
	2.1 Structural Features	2-1
	2.1.1 Minor Structures	2-2
	2.1.2 Major Structures	2-4
	2.1.3 A Regional Structural Schema	2-8
	2.2 Stratigraphic Framework	2-10
	2.2.1 A Regional Stratigraphic Schema	2-27
	2.3 Tectonic Analysis	2-29
	2.3.1 Tectonic Setting of the Chopawamsic Metavolcanic Schist Belt	2-33
3.	PETROGENY	3-1
	3.1 The Geochemical Effects of Metamorphic-Metasomatic Overprinting	3-2
	3.2 Petrogenesis of Intrusives	3-10
	3.2.1 Intermediate to Felsic Intrusives	3-13
	3.2.2 Ultramafic to Mafic Intrusives	3-17
	3.3 Petrogenesis of the Volcanic Suites	3-25
	3.4 Petrogenesis of the Hydrothermal Deposits	3-34
	3.5 Magma Genesis and Regional Hydrothermal Metasomatism	3-43
4.	METALLOGENY	4-1
	4.1 Regional Geological Setting of the Mineral Deposits	4-5
	4.1.1 The Mineral District	4-5
	4.1.1.1 Western Arminius Trend	4-6
	4.1.1.2 Central Cofer Trend	4-11
	4.1.1.3 Eastern Fisher Lode Trend	4-15
	4.1.2 The Columbia-Tellurium Gold Camp	4-17
	4.1.2.1 Western Tellurium Trend	4-18
	4.1.2.2 Central Moss Trend	4-19
	4.1.2.3 Eastern Grannison Tract	4-19
	4.1.3 New Canton Trend	4-21
	4.1.4 Mineral Deposits Along the Long Island Trend	4-23
	4.1.4.1 Louisa Iron Formation	4-24
	4.1.4.2 Gold Prospects Near Palmyra	4-26
	4.1.4.3 Penlan Massive Sulphide Mineralization	4-27
	4.1.4.4 The London & Virginia "Vein" System	4-28

4.1.5 The Andersonville District 4-29
4.1.5.1 The Morrow Mine 4-31
4.1.5.2 Zone 3 Sulphide Mineralization (Atkins Property) 4-33
4.1.5.3 Zone 9 Sulphide Mineralization (Nixon-Benedict Property) 4-35
4.1.5.4 Zone 24 Sulphide Mineralization (Morris Property) 4-36
4.1.5.5 Zone 18 Sulphide Mineralization 4-37
4.1.5.6 Geological Setting of the Andersonville District Massive Sulphides 4-38
4.1.6 Copper-Gold Mineralization Affiliated With Greenstone 4-39
4.2 Metallogenic Processes as Indicated by Mineral Chemistry 4-40
4.2.1 Mineral Chemical Data Reported in Other Studies 4-42
4.2.1.1 Sulphides 4-42
4.2.1.2 Carbonates 4-45
4.2.1.3 Oxides 4-45
4.2.1.4 Silicates 4-48
4.2.2 Regional Variation in Garnet Chemistry 4-50
4.2.3 Regional Variation in Amphibole Chemistry 4-57
4.3 Regional Metallogenic Synthesis 4-65
5. CONCLUSION
5.1 Historical Review 5-1
5.2 Petrogenetic and Metallogenic Summary 5-1
5.3 Depositional Environment 5-6
5.4 Assessment of the Effectiveness of the Methodology 5-10
6. REFERENCES 6-1
7. APPENDIX A: Nomenclature System Used For Classifying Schists
8. APPENDIX B: Systematic Description of Lithologies
9. APPENDIX C: Bulk Rock Major and Trace Element Data
10. APPENDIX D: Microprobe Analyses of Garnet and Amphiboles

LIST OF PHOTOS

		Page
1.	Lateritic soil developed on saprolitic quartz-sericite schist south of Mineral, Virginia	1-17a
2.	The Willis Mountain Kyanite Mine on the highest ridge crest in the map area	1-17a
3.	Hardware magnesian schist: Delicate microfolding defined by discontinuous magnetite laminae in talc schist	2-11a
4.	Hardware magnesian schist: Highly fissile chlorite schist with acicular tremolite and disseminated magnetite porphyroblasts	2-11a
5.	Cumulate-textured intrusives: Serpentinized peridotite with original cumulus olivine outlined by magnetite ± chromite	3-18a
6.	Cumulate-textured intrusives: Uralitized pyroxenite with remnant hypersthene partially rimmed by green hornblende	3-18a
7.	Magnesian amphibolites (metakomatiites): A typical matte textured magnesian amphibolite with Mg-chlorite and minor talc hosting randomly oriented acicular tremolitic - hornblende microlites	3-18b
8.	A peculiar textural variant of magnesian amphibolite comprising coalescing tremolitic hornblende sheaves with minor interstitial Mg-chlorite	3-18b
9.	Pillow structures in the Shores greenstone occurring on the western margin of the Chopawamsic metavolcanic belt	3-25a
10.	A slabbed specimen of banded amphibolite from the high grade gneiss terrane forming the eastern part of the Chopawamsic metavolcanic belt	3-25a
11.	Palmyra metavolcanics: Porphyritic andesite with plagioclase (An_{20}) phenocrysts in a moderately foliated groundmass of albitic plagioclase, actinolite, and minor quartz and biotite	3-25b
12.	Accretionary lapilli tuff with intergranular textured andesite rimmed by albitic plagioclase and quartz	3-25b
13.	Mineral metarhyolite: A quartz-feldspar porphyry with randomly oriented alkali feldspar occurring in a fine-grained groundmass of quartz and feldspar with minor sericite and calcite	3-25c
14.	Buffards quartz-mica schist (metarhyolite): A multiply foliated quartz-mica schist from the core of the Arvonia structure	3-25c
15.	Ironstones capping the Palmyra metavolcanics: Crosscutting magnetite stylolites terminating in discontinuous magnetite seams at the contact between underlying quartz-carbonate-rich and overlying chlorite-rich marl	3-35a
16.	Marked compositional banding defined by quartz-, chlorite-, and magnetite-rich layers	3-35a

17. Ironstones capping the Mineral metavolcanics: Marked compositional banding defined by hornblende-rich and quartz-albite-cummingtonite-rich layers in two-amphibole ironstone 3-35b
18. A polygonal textured quartz-albite-magnetite assemblage hosting randomly oriented cummingtonite splays 3-35b
19. Large staurolite and small gahnite porphyroblasts hosted in a decussate textured biotite-calcite-quartz assemblage 3-35c
20. Pyrite laminae in well foliated quartz-sericite schist 3-35c
21. Hydrothermal chloritite (Mineral District): Mg-chlorite phlogopite matte hosting staurolite crosses and irregularly shaped sulphides 3-35d
22. Hydrothermal chloritite (Andersonville District): Coarse coalescing garnet and staurolite porphyroblasts hosted in a matte of intimately intergrown phlogopite and Mg-chlorite 3-35d
23. Columnar kyanite and dimensionally elongate quartz and pyrite impart a marked foliation fabric to the kyanite quartzite horizons 3-35e
24. A mineralogically complex quartz-sillimanite-garnet-sericite-hematite-chlorite-tourmaline-zircon schist characteristic of the uppermost parts of the Buffards Formation 3-35e
25. Basal shale silicate iron formation: Oolitic chlorite occurring below the almandine isograd 3-35f
26. Characteristic radial inclusion pattern in garnet porphyroblasts growing in the oolitic chloritite above the almandine isograd 3-35f

LIST OF TABLES

		Page
1.	Age Dating of Basement Exposures in the Southern Appalachians	1-5b
2.	Ortho and Paragneiss Succession Overlying Grenville Basement	1-5c
3.	Stratigraphy and Lithofacies Variations Within the Late Precambrian Rift Facies Assemblage as Represented by the Lynchburg and Correlative Fauquier Formations	1-6c
4.	Stratigraphic Correlations of the Inner Piedmont Late Precambrian-Cambrian Volcanic-Sedimentary Schist Series	1-8a
5.	Stratigraphic Relationships of the Palmyra Metavolcanic Suite	2-12a,b
6.	Stratigraphic Relationships of the Mineral Metavolcanic Suite	2-15a
7.	Stratigraphic Relationships of the Diverse Upper Chopawamsic Group	2-17a
8.	Metamorphic Mineral Assemblages	3-3a
9.	Metal Ratios in the Various Massive Sulphide Lenses of the Cofer Deposit	4-12
10.	The Metal Content in the Long Island Iron Formation	4-25
11.	FeS Variation of Sphalerite in Differing Mineral Assemblages (Cox 1979)	4-44
12.	Compositional Variation in Gahnite (Sandhaus 1981)	4-46
13.	Variation in the Mg/Fe Ratio in Biotite and Chlorite Occurring at the Cofer Deposit (Feuer 1980)	4-55
14.	Core-to-Rim Elemental Zonation in Garnet	4-50b
15.	Preferential Partitioning of MnO Into Cummingtonite Over Ca-Amphibole	4-60
16.	Examples of Multi-Facies Iron Formation Hosting Gold and/or Sulphide Mineralization	4-65a

LIST OF FIGURES

		Page
1.	Tectonic Map of the Southern Appalachians	1-5a
2.	Location of Project Area Within the State of Virginia	1-19a
3.	Regional Geological Map of the Lake Anna to Appomattox River Segment of the Chopawamsic Metavolcanic Belt	2-1a
4.	Regional Structural Schema	2-9a
5.	Regional Stratigraphic Correlation Schema	2-28a
6.	Three-Stage Tectonic Evolutionary Model for the Chopawamsic Metavolcanic Belt	2-40a
7.	Metamorphic Petrogenetic Grid Showing Approximate P-T Gradient Across the Chopawamsic Metavolcanic Belt	3-3b
8.	Normative Mineral Plots for Felsic Intrusive Rocks	3-13a
9.	MgO-CaO-Al_2O_3 Ternary for Ultramafic to Mafic Intrusive Rocks	3-19a
10.	Normative Cation % OL-CPX-PL Ternary for Ultramafic to Mafic Intrusive Rocks	3-21a
11.	Al, Fe^2+Fe^3+Ti, Mg Cation Ternary for Ultramafic and Mafic Intrusive Rocks	3-21b
12.	Al_2O_3 vs $FeO^T/FeO^T/MgO$ Binary for Ultramafic to Mafic Intrusive Rocks	3-22a
13.	(a) Cr, (b) Ni, and (c) Ti vs MgO Binary Diagrams for Ultramafic to Mafic Intrusive Rocks	3-22b
14.	Alkali Variation Diagram for Chopawamsic Metavolcanic Suites	3-26a
15.	Total Alkalies vs Silica Binary of Chopawamsic Metavolcanic Suites	3-28a
16.	K_2O vs SiO_2 Binary for Chopawamsic Metavolcanic Suites	3-29a
17.	AFM Ternary for Chopawamsic Metavolcanic Suites	3-29b
18.	Al, Fe^2+Fe^3+Ti, Mg Cation for Chopawamsic Mafic Metavolcanics	3-31a
19.	Al_2O_3 vs Normative Plagioclase Binary for Chopawamsic Metavolcanic Suites	3-31b
20.	Normative Mineral An, Ab^1, Or Ternary for Chopawamsic Metavolcanic Suites	3-32a
21.	Differentiation Index vs Degree of Silica Saturation Binary for Chopawamsic Metavolcanic Suites	3-32b
22.	AFM Ternary for Hydrothermal Deposits in the Chopawamsic Meavolcanic Belt	3-36a
23.	Na_2O-CaO-K_2O Ternary for Hydrothermal Deposits in the Chopawamsic Metavolcanic Belt	3-37a
24.	SiO_2-FeO^T+MgO-Al_2O_3 Ternary for Hydrothermal Deposits in the Chopawamsic Metavolcanic Belt	1-38a

25. $MgO-CaO-Al_2O_3$ Ternary for Hydrothermal Deposits in the Chopawamsic Metavolcanic Belt 3-39a
26. $MgO-FeO^T-Al_2O_3$ Ternary for Hydrothermal Deposits in the Chopawamsic Metavolcanic Belt 3-39b
27. Location of Massive Sulphide and Gold Mineralization in the Mineral District 4-6a
28. Geological Longitudinal Section Arminius North to Sulphur North, Mineral District 4-6b
29. Geological Crossection of the Arminius Deposit, Mineral District 4-8a
30. Geological Crossection of the Cofer Deposit, Mineral District 4-11a
31. Geological Crossection of the New Canton Massive Sulphide Trend 4-21a
32. Geological Crossection of the Penlan Massive Sulphide Mineralization, Long Island Trend 4-27a
33. Geological Crossection of Zone 3 (the Atkins Property), Andersonville District 4-34a
34. Geological Crossection of Zone 9 (the Nixon-Benidict Property), Andersonville District 4-35a
35. Geological Crossection of Zone 24 (the Morris Property), Andersonville District 4-36a
36. Geological Crossection of Zone 18, Andersonville District 4-37a
37. Almandine-Spessartine-Grossular Content of Garnets in Relation to Massive Sulphide Mineralization 4-50a
38. Schematic Representation of Product (Garnet) - Reactant (Chlorite) Equilibria in T-X Space (Trzienski 1977) 4-53a
39. Schematic Representation of the Conceptual Model for the Distribution of Mn:Fe Rations in Sedimentary Rocks at Heath Steele Mines Massive Sulphide Deposit (Whitehead (1973) 4-56a
40. Classification of Iron-Magnesium-Manganese Amphiboles (Leake 1978) 4-58a
41. Classification of Calcic Amphiboles (Leake 1978) 4-58b
42. Miscibility Gaps Between Coexisting Amphiboles 4-58c
43. Phase Diagram for the Pseudobinary Join Cummingtonite-Actinolite (Cameron 1975) 4-61a
44. Tremolite-Hornblende Miscibility in Progressive Skagit Metamorphic Suite (Misch & Rice 1975) 4-63a
45. Al^{iv} vs Al^{vi} Diagram for Calcic Amphiboles 4-64a

1. INTRODUCTION

1.1 Statement of Thesis

This study examines the geological setting of the pyritic massive sulphide and lode gold mineralization occurring in the central Virginian segment of the southern Appalachian Chopawamsic metavolcanic belt. The author originally became interested in the metallogeny of mineral deposits hosted within such orogenic metavolcanic schist belt terranes as this in the course of several reconnaissance projects in the northern Brooks Range and the central Alaskan Range of Alaska and in the Virginian Piedmont. The latter was chosen to form the focus of this thesis primarily because of its easier accessibility. The exploration carried out by the author in the area between 1975 and 1981 for Callahan Mining Corp. afforded an ideal opportunity for investigating regional geology and elucidating the mineral deposit types characteristic of the Virginian Chopawamsic metavolcanics.

The term "schist belt" does not appear in the A.G.I. geological glossary, nor have the more established geological terms "greenstone belt," "slate belt" or "gneissic belt" yet been officially defined. The term "belted metamorphics," which according to common sense would seem to be broadly applicable to all of these various types of metamorphic terranes, is in fact, according to the glossary, a geomorphic designation for "mountainous areas of folded and faulted metamorphosed sedimentary and igneous rocks which have been

differentially eroded in distinct but irregular elongate subparallel ridges and valleys." Although this definition does comprehend the geomorphology of the schist belts familiar to the writer, it has no general application because the older metamorphic terranes, such as the greenstone and gneiss belts occurring in Precambrian shields, have been typically eroded to a peneplain. It would seem, therefore, that none of the various geological terms commonly used in reference to the characteristically belted lithological distribution demonstrated by various types of metamorphic terranes have any "official" status. In the present study the informal geological term "schist belt" is used to denote a distinct, irregularly elongate metamorphic terrane largely constituted of schists. So defined, schist belt terranes are intermediary in metamorphic rank between slate belts and gneiss belts. A metavolcanic schist belt, such as the one under investigation here, includes significant schist after primary felsic to mafic volcanic precursors. These particular belts may also include greenstone, but they are not dominated by mafic metavolcanics as are the greenstone belts so-called.

Metallogenic studies in schist belt terranes are invariably hampered by regional metamorphic overprinting. The effects of metamorphism not only mask original rock types but make reconstruction of regional structural-stratigraphic frameworks exceptionally problematic. In his investigation of the Virginian Chopawamsic metavolcanic belt, the author's aims encompassed two interdependent but essentially separate tasks. The initial thrust of the investigation was towards a clarification of regional geology. Subsequent to this primary phase, an attempt was then made to explicate the petrogenesis of the host volcanic schists and unravel the metallogeny of the pyritic massive sulphide and lode gold mineralization. This progression from the broad perspective of a paleotectonic setting to a more detailed examination of

specific rock types proved a particularly fruitful methodological strategy. Just as regional structural-stratigraphic relationships reflect historical development, the geological evolution so delineated offers a natural context for investigating how specific lithologies originated. More important, by making the attempt to place each given petrogenetic problem against a specific geological background, one ensures that genetic interpretations for individual rock types will be consistent with and add to an overall historical schema.

The present investigation, then, is basically an attempt to vindicate the thesis that the delineation of regional geological frameworks is an important key to understanding petrogenesis. Accepting as an axiom the view that local geological phenomena can best be understood within their regional contexts, the author would stress the need for geological synthesis. The regional approach, in other words, is considered to provide a necessary link between detailed observations made at the outcrop level and general tectonic interpretations. Isolated outcrop observations not placed in a general context remain collector's items of limited geological meaning. Conversely, tectonic models not continually tested against such specific observations remain imaginative fictions rather than enhancing our geological understanding.

1.2 Tectonic Setting of the Chopawamsic Metavolcanic Belt Within the Appalachian Orogen

On a broad scale the lithological distribution observed across the Appalachian orogen yields neatly to interpretation in terms of a geosynclinal tectonic framework. In the southern Appalachians the westerly migeocline, represented by the shelf sediments of the Valley and Ridge Province, is

separated from the easterly eugeocline by the topographically prominent Blue Ridge Grenvillian miogeanticline. The eugeocline comprises the weakly metamorphosed sediments flanking the Grenvillian basement core of the Blue Ridge Province and the more highly metamorphosed schists of the Piedmont Province. Along its eastern edge the Piedmont Province is onlapped by the unconsolidated sediments of the Atlantic Coastal Plain. Beyond these gross correlations, however, the rather simplistic spatial dynamic of this model proves inadequate to comprehend the complexities of this area. In attempting to come to terms with specific interrelationships among differing regional tectofacies the author thus found it necessary to utilize a more mobilistic plate tectonic framework.

The evolutionary schema which emerges from such a framework hinges critically on the hypothetical existence of an event known as the Iapetus cycle. This period of active oceanic spreading followed by foreshortening in late Precambrian-early Paleozoic times was first hypothesized by Wilson (1966) and Dewey and Bird (1971) to account for the remnants of ophiolitic oceanic crust discovered in the northern Appalachians. Since then, however, numerous researchers have utilized the concept as a means of rationalizing geological relationships within the southern Appalachians as well. As the consensus of opinion would have it (Hatcher 1972, Rankin 1975, Williams 1978, Cook et al 1980), late Precambrian rifting in this area as in the north broke up the Grenvillian craton, leaving trailing fragments of continental crust in the wake of separation and the eventual opening up of the ancient Iapetus ocean. The present study, while pointing up a number of inconsistencies in detail, has tended to substantiate at least the gross outlines of this scenario. Certainly on present evidence there would seem to be enough continuity throughout the orogen as a whole to permit tectonic schemata worked out with

respect to the north to be applied at least loosely to the southern terrane as well. In line with this presumption, the tectonic subdivisions shown on Figure 1 correspond fairly directly with those yielded by Williams' (1978) study of the Appalachians.

Approached in these terms, the regional tectonic setting of the Chopawamsic metavolcanic belt is brought into substantially clearer focus. To begin with the westernmost lithologies, the Grenvillian basement exposed regionally along the Blue Ridge and locally as windows (such as the Sauratown Mountains anticlinorium) in the inner Piedmont, together with an overlying ortho- and paragneiss succession, likely represents the margin of ancient North America; i.e., Williams' Humber zone. The reported age dates of this basement, summarized in Table 1, indicate that sediments as old as Helikian, along with interlayered igneous rocks, were transformed by the Grenvillian orogeny into a cratonic complex of ortho- and paragneiss intruded by Grenvillian age plutons. In addition to this, Conley (1978) has also noted a younger ortho- and paragneiss succession overlying the Grenville basement. These younger gneissic lithologies, summarized in Table 2, consist primarily of mica gneiss interbedded with quartzite and calc-silicate gneiss overlying and interfingering with garnet amphibolite units. Where gneissic domes intruded by Grenvillian granitic bodies have been documented in the outer Piedmont (Conley 1978, Glover et al 1978), the Grenvillian basement is again overlain by younger ortho- and paragneisses, specifically the Sabot amphibolite and Maidens quartzite and biotite gneiss. As will be discussed later, the latter basement association could correlate with the basement of Williams' Gander zone, a terrane purportedly constituted of cratonic fragments from the east side of the ancient ocean.

Williams' Dunnage zone, postulated to contain vestiges of relict oceanic

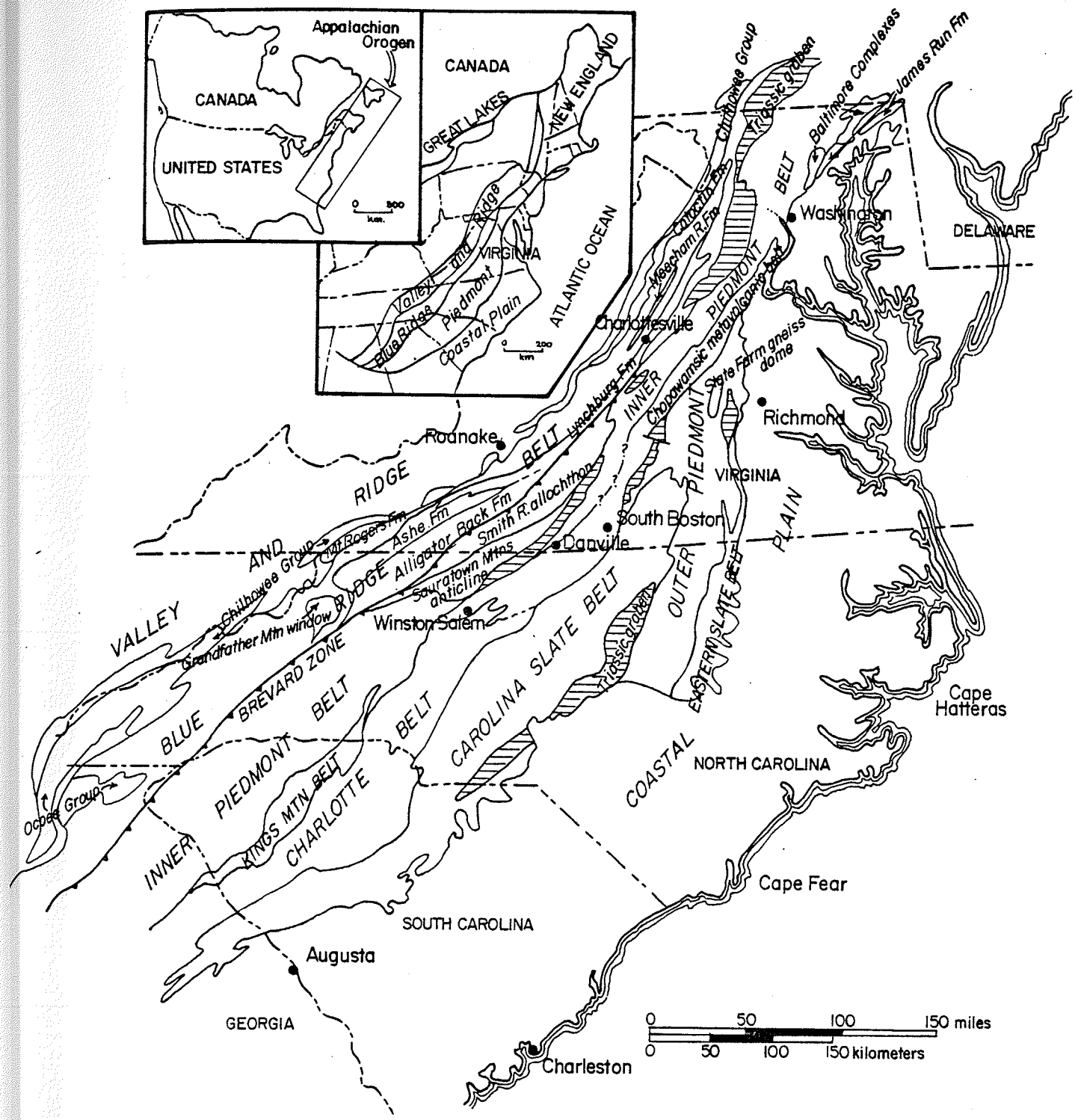

FIGURE 1: TECTONIC MAP OF THE SOUTHERN APPALACHIANS

(modified from: King 1959, Conley 1978, Pavlides 1981, Williams & Hatcher 1982)

Table 1: Age Dating Of Basement Exposures In The Southern Appalachians

Late Precambrian Plutonism Along Blue Ridge Core	alkali granite & syenite	U/Pb 730-750 m.y. (Allan 1963)
	granodiorite	Rb/Sr 820 m.y. (Davis 1974)
Gneiss West of Blue Ridge Core	unnamed paragneiss	Rb/Sr 1040-1370 m.y. (King 1959)
	charnokite	Zircon 1070-1150 m.y. (Davis et al 1958)
Gneiss East of Blue Ridge Core	unnamed paragneiss	Zircon 913 m.y. metamorphic 1870 m.y. sedimentary (Davis 1974)
Sauratown Mountains - Inner Piedmont	gneiss	Rb/Sr 1192 m.y. (Rankin et al 1971)
State Farm Gneiss - Outer Piedmont	granite gneiss	Rb/Sr 1000 m.y. (Glover et al 1978)

Table 2: Ortho- and Paragneiss Successions Overlying Grenville Basement (after Conley 1978)

Inner Piedmont		Outer Piedmont
Smith River Allochthon	Sauratown Mountains anticlinorium	State Farm gneiss dome
Fork Mountain Formation	garnet-mica schists	Evington schist series?
garnet-mica schist with staurolite-sillimanite porphyroblasts interbedded with mafic sills and flows	garnet-mica schist with staurolite-kyanite porphyroblasts interbedded with mafic sills and flows	
x -- x -- x -- x -- x -- x - metamorphic hiatus - x -- x -- x -- x -- x -- x		
Bassett Formation	mica gneisses	Maidens gneiss
amphibolite with pyroxene granofels	garnet amphibolite	biotite gneiss interbedded with mica schist and quartzite
biotite gneiss with boudins of quartzite and calc-silicate gneiss	muscovite-biotite gneiss interbedded with mica schist, quartzite, and calc-silicate gneiss	Sabot Formation
garnet amphibolite and talc gneiss	garnet amphibolite	massive amphibolite interbedded with biotite gneiss
= = = = = = = = = = = = = = Grenville basement = = = = = = = = = = = = = =		

crust, is more difficult to identify in the southern Appalachians as no complete ophiolite suites have as yet been documented in this area. Nevertheless, a major episode of the late Precambrian-Cambrian rifting is signified by the weakly metamorphosed clastic sedimentary and mafic igneous rocks flanking the Blue Ridge (see Table 3). The basal proximal turbidites of the Lynchburg Formation lie unconformably on the 820-730 m.y. intrusives of the Blue Ridge in the type area near the city of Lynchburg (Brown 1958, Conley 1978). Throughout its southern extension the Lynchburg flysch-type sediments interfinger with mafic and ultramafic igneous rocks. Just south of Lynchburg mafic igneous complexes replace much of the turbidite succession. Although this turbiditic sediment-mafic igneous lithological association cannot be identified with mature ophiolitic oceanic crust, one may hypothesize that it might represent an immature continental margin oceanic rift setting analogous to the present day Guymas Basin in the Gulf of California (Lonsdale & Lawver 1980). Such a comparison seems even more appropriate when the more northerly correlatives of the Lynchburg Formation are also taken into account. The co-extensive Fauquier Formation and lithologically similar Meechum River Formation, a narrow band of sediment in the Blue Ridge core, are both composed mainly of fluviatile arkose (Conley 1978). Significantly, similar Recent sediments occur in the present Great Valley of California where the oceanic rift impinges on the continental margin (Dickinson & Rich 1972).

Collectively the formations of late Precambrian terrigenous clastic sediments and the turbidite-mafic igneous association of the Lynchburg Formation signify rifting of the Grenvillian basement. The Meechum River Formation represents a narrow ensialic graben along the Blue Ridge core, and the Fauquier Formation a marginal sedimentary trough encroached upon by eastward prograding deltaic sands. The Fauquier near-shore half-graben

Table 3: Stratigraphy and Lithofacies Variations
Within the Late Precambrian Rift Facies Assemblage as Represented by
the Lynchburg and Correlative Fauquier Formations

SW Lynchburg Marginal Oceanic "Rift Basin"	NE Fauquier Intercratonic "Graben"
pelites with graphite	pelite with carbonate
quartz-mica pelites with local quartzite-carbonate lenses	fluviatile crossbedded arkose
distal turbidites (varved siltstones) with mafic sills and flows and mica schist	
proximal turbidites with lenses near base interlayered with gabbroic and ultramafic sills and mica schist	arkosic conglomerate and grits
amphibolite	

-- x -- x -- x -- x -- x -- unconformity -- x -- x -- x -- x -- x -- x --

Moneta biotite gneiss

Grenville basement

changes facies southward into the more offshore turbidite deposits comprising the Lynchburg. The mafic igneous rocks interfingering with the turbidites may indicate "oceanic" ridge segments but, perhaps due to the high sedimentation rates, spreading conditions apparently did not evolve to the extent of generating mature ophiolitic suites.

Contact relationships between this immature oceanic rift tectofacies and the inner Piedmont vary along strike. Over its southern extension the boundary is definitely structural, as this is the site of the Brevard fault zone, one of the major crustal sutures in the southern Appalachians (Hatcher 1978, Cook et al 1980). It is controversial how far north the Brevard zone can be traced, but Conley (1978) suggests that thrusting related to the Brevard zone pinches out upper Lynchburg sediments and overlying Catoctin basalt south of Charlottesville in central Virginia. From Charlottesville north, however, the contact between the rift assemblage and the inner Piedmont appears to be a depositional unconformity. Subaereal deposits demarking the zone include the restricted ash flow tuff deposits of the Swift Run Formation and the regionally extensive olivine basalt flows of the Catoctin Formation (Nelson 1962).

The extensive Catoctin plateau basalts have been attributed to a mantle plume (Davies et al 1978) which presumably caused the Blue Ridge Grenvillian basement, together with bordering rift deposits, to be tectonically uplifted and subaereally eroded prior to the active volcanic phase. The widespread outpouring of basalt during this event emanated from extensive volcanic fissures along both western and eastern borders of the uplifted block. To the west the plateau basalts of the Catoctin Formation transit through an interval of interbedded mafic flows and paralic sediments comprising the Louden Formation into basal infra-Cambrian and Cambrian Chilhowee sediments deposited

at the outer margin of the miogeocline. To the east a similar zone of transition occurs, though Louden-type sediments have only been identified locally; more regionally the Catoctin basalts appear to be conformably overlain by the extensive pelitic schists which characterize the inner Piedmont (Conley 1978). The fact that greenstone strata with ocean floor basalt geochemical affinity (Davis 1977, Bland 1978) occur as swarms within inner Piedmont pelitic schist suggests a type of immature oceanic setting.

Considerable confusion exists in the literature as to the naming and subdivision of the inner Piedmont pelitic schist terranes. Most commonly they are known as the Evington schists in Virginia and the Glenarm schists in Maryland (Pavlides et al 1974, Conley 1978). The broad subdivisions of these regional assemblages are listed in Table 4, where a tentative correlation is drawn with the infra-Cambrian to Cambrian Chilhowee Series that overlies the Catoctin Formation along the northwestern flank of the Blue Ridge. East of the Catoctin Formation in central Virginia the overlying Candler Formation (western part of the Evington schists) changes facies eastward from low greenschist micaceous pelites hosting thin, often lenticular, quartzite (Mt. Athos member; Ern 1968) and carbonate (Everona member; Mack 1965) units, through monotonous chlorite-quartz-sericite±calcite schists, to more quartzose and diversified mid-greenschist lithologies along its easterly extent. This across-strike variation has been interpreted by Conley (1978) to indicate the deepening of a marine basin to the east. Significantly, the greatest concentration of greenstone beds within Candler (Smith et al 1964, Ern 1968, Brown 1969) occurs along the eastern margin.

Along its eastern extremity the Candler metasedimentary schists border on the Chopawamsic metavolcanic belt which comprises the western part of the regional Evington schist assemblage. The boundary between Candler

Table 4: Stratigraphic Correlations of the
Inner Piedmont Late Precambrian-Cambrian Volcanic-Sedimentary Schist Series

NW of Blue Ridge	SW of Blue Ridge	
Chilhowee Series	Evington Series, Va.	Glenarm Series, Md.
Antiem quartzite	Chopawamsic volcanics	James Run volcanics
Harpers carbonate		
Weverton phyllite	Candler schists	Wissahickon schists
Louden schists / Catoctin	Catoctin / Louden schists	Catoctin
- x -- x -- x -- x -- x -- x -- x -- x -- x -		
	Lynchburg	
— x -- x -- x -- x -- x -- x -- x -- x -- x -- x -- x -- x -- x -- x -- x --		
	Grenville Basement	

metasediments and Chopawamsic metavolcanics falls along a regional magnetic ridge, connecting a series of elliptical metagabbro intrusive bodies identified by Pavlides et al (1974) as dismembered ophiolitic material (this interpretation is queried in the present study). Although Conley (1978) and Marr (1981) consider the Candler-Chopawamsic contact to be transitional in nature, both Pavlides (1976) and Brown (1976) have classified it, at least locally, as a zone of tectonic melange. The discovery of widespread, highly deformed magnesian schists along this boundary during the present investigation supports the more complex structural interpretation; this will be discussed in more detail in later sections.

Numerous workers during the last decade have suggested that the narrow (10-25 km) belt of felsic and lesser amphibolitic schist, which strikes from Montgomery County, Maryland across central Virginia at S 20°-30°W for a possible 300 kilometers to the vicinity of Danville near the North Carolina state line, delineates a major paleo-volcanic locus. Southwick et al (1971) named this metavolcanic belt the Chopawamsic Formation after its type section exposed along Chopawamsic creek in northern Virginia. This formational name is still commonly attributed only to the northern-to-central Virginian part, as neither the lithological relationships with bordering assemblages nor the along-strike correlations are at present well-defined. Pavlides et al (1974) have demonstrated, however, that the northern-to-central Virginian segment is delineated by an uninterrupted regional magnetic ridge. The correlative rocks further north in Maryland are generally known as the James Run Formation (Pavlides 1981, Gair and Slack 1980). The unnamed felsic and mafic metavolcanics occurring between Danville and South Boston in southern Virginia are also tentatively considered to be an extension of the Chopawamsic metavolcanic belt (Glover 1974, Henika 1977). It should be noted, though, that

no modern work has been done between the southern extent of the segment of the Chopawamsic metavolcanic belt covered by the present investigation and Henika's (1977) mapping to substantiate this southerly correlation.

The north to central Virginian segment of the Chopawamsic metavolcanic belt has also been called the Virginian gold-pyrite belt (Taber 1913, Cline et al 1921, Lonsdale 1927, Luttrel 1966) on account of the numerous lode gold and massive pyritic sulphide occurrences along its length. Interestingly, these early workers considered the belt to be dominantly of sedimentary origin, and named the most prominent part -- that which hosts the mineralization -- the Peter's Creek "quartzite." South of the James River the gold-pyrite belt was thought to merge with a more laterally extensive kyanite belt (Jonas 1932, Stose & Stose 1948, Espenshade & Potter 1960) which included both the greenschist facies gold-pyrite belt of rocks and the higher grade amphibolite gneisses outcropping along the east side of this belt. The easterly, higher grade gneiss terrane has more recently been recognized by Brown (1969), Conley (1978), Marr (1981), and Pavlides (1981) to be constituted of Chopawamsic lithologies at higher metamorphic rank. In the northern Virginian part Pavlides has identified an extensive mafic gneiss terrane (the Ta River Metamorphic Suite) as an easterly oceanic facies of the Chopawamsic. This mafic gneiss terrane is co-extensive with mafic gneisses occurring along the eastern side of the central Virginian segment as well; these latter comprise a significant part of the Hatcher complex defined by Brown (1969). As the Hatcher complex occurs in the east-central part of the segment of the Chopawamsic belt covered by the present investigation, this also will be discussed in more detail in subsequent sections.

Boundary relationships on the east side of the Chopawamsic metavolcanic belt have only relatively recently been defined. This is the site of the

Spotsylvania lineament (Neuschel 1970, Pavlides 1980b) which, with the Chopawamsic Ta River amphibolitic gneisses to the west and the Po River biotite gneisses to the east, separates terranes of vastly contrasting aeromagnetic, aeroradiometric, and lithological character. Little is yet known of the Po River rocks, but Pavlides (1981, personal communication) considers this to be an older basement paragneiss succession unrelated to the Chopawamsic metavolcanic belt. A tentative correlation might perhaps be drawn between these gneisses and the aforementioned Maidens biotite gneiss bordering on the Grenvillian State Farm gneiss dome that occurs about 15 km east of the Spotsylvania lineament.

The outer Piedmont terrane is one of the least well documented areas of the southern Appalachians since the amount of outcrop decreases appreciably as one approaches the onlapping unconsolidated coastal plain sediments. Although characterized by high grade gneisses, it differs from the inner Piedmont in having large tracts underlain by mid-Paleozoic granitic intrusions. The various granitoid plutons in the Fredricksburg area have been zircon-dated between 410 and 330 m.y. by Pavlides et al (1979). The Petersburg granite which forms large batholithic intrusions along the margin of the coastal plain onlap has also been zircon-dated at 330 m.y. (Wright et al 1975). Collectively these features would seem to substantiate what was suggested above, that the outer Piedmont is similar in many respects to the Gander terrane defined by Williams (1978). Counter to this is the fact that the northern extension of the Carolina Slate Belt, which has been identified by Williams and Hatcher (1982) as an Avalon tectonic terrane, appears to interfinger with the Gander-like elements in southeastern Virginia. On Figure 1 the Gander and Avalon elements in the outer Piedmont are represented as high grade gneissic and low grade slate belt rocks respectively.

The sparse age-dating of metavolcanics and local intrusives along the Chopawamsic belt indicates a late Precambrian-lower Paleozoic time span for the igneous activity. Interestingly, the oldest ages have been derived from the higher grade gneissic facies along the eastern margin of the belt. The whole rock Rb/Sr dates reported by Brown (1969) from the Hatcher complex gneisses are the oldest, indicating an origin in late-Precambrian times between 740 and 606 m.y. The Columbia granite intrusion at the northern end of the Hatcher complex gave an Rb/Sr whole rock age of 590 m.y. (Fullagar 1971) and a zircon date of 574 m.y. (Bourland & Glover 1979). Collectively the zircon ages obtained by Tilton et al (1970), Southwick et al (1971), and Higgins et al (1971) on the more westerly greenschist facies felsic metavolcanics indicate: (1) that this part of the Chopawamsic belt is of early Cambrian age (550 m.y.), and (2) that the Virginian Chopawamsic and Maryland James Run metavolcanics are indeed coeval. The zircon dating of felsic volcanics in southern Virginia by Glover (1974) yielded a similar age (580 m.y.). The mid- to upper Ordovician fauna documented in both the Arvonia Formation (Watson & Powell 1911, Tillman 1970) and the Quantico Formation (Pavlides et al 1980), both of which form major metashale synclinoria within the Chopawamsic belt, put an upper limit on the age of the volcanic activity. The K/Ar date of the Arvonia metashale (Harper et al 1973) establishes a late Paleozoic age (300 m.y.) for the latest regional metamorphic overprint.

Relationships between the Chopawamsic metavolcanic belt and the outer Piedmont Avalonian slate belt terranes have been the subject of some speculation but remain relatively obscure. The Virginian Chopawamsic Formation and the Maryland James Run Formation were included with the Carolina Slate Belt as part of the "Atlantic Seaboard Volcanic Province" by Higgins (1972). This particular categorization has, however, proven extremely

controversial. Zircon ages from Carolina Slate Belt felsic metavolcanics indicate a time interval between 740 and 575 m.y. (Glover et al 1971); the youngest ages thus overlap those of the Chopawamsic metavolcanics. Counter to this, the work of Higgins et al (1977) suggests that zircon ages may be of limited reliability as a tool for dating metavolcanic and metaplutonic rocks in the Piedmont since the zircons here may have been contaminated by older Precambrian seed crystals and/or may have lost lead and uranium during subsequent Paleozoic regional metamorphism. In consequence of such problems, Pavlides (1976) argues that the sparse paleontological data yielded by these two terranes should be given considerable weight. The documentation of late Precambrian fossils by St. Jean (1973) in the Carolina Slate Belt permits the broad correlation of this area with the Avalon Peninsula of Newfoundland. In contrast, the only known fossils in the Chopawamsic metavolcanic belt are of mid- to late Ordovician age, and comparable to fauna of similar age in rocks of the Appalachian miogeocline (Williams and Hatcher 1982). The differing faunal associations thus indicate that the Chopawamsic and Carolina belts do not in fact belong to the same volcanic province as Higgins suggests.

Many investigators including Wright et al (1975), Pavlides (1976), and Conley (1978) consider that the Virginian Chopawamsic metavolcanic belt may be a northward extension of the Charlotte belt in North Carolina. Charlotte belt gneisses have been dated at 740 m.y. and granodiorite bodies intruding these gneisses at 575 m.y. by Rb/Sr whole rock techniques (Glover et al 1971). It is possible, therefore, that south of the North Carolina border the Chopawamsic metavolcanic belt may transit into the mafic-felsic plutonic gneiss complex constituting the Charlotte belt. In this regard it is interesting that recent seismic data (Cook et al 1980) demonstrates a Moho decrease from 40-45 km below the Blue Ridge and inner Piedmont to 30-33 km below the Charlotte belt:

this differential could signify a transition from Grenvillian craton to former Iapetus oceanic crust.

Considering all these various correlations, the setting of the Chopawamsic metavolcanic belt, for all its differences from the more northerly segments of the orogen, would seem at least generally amenable to the plate tectonic interpretation. This is not to imply that the approach does not entail some significant problems as well. For one thing, as noted above, without the corroborating evidence of ophiolites it is questionable whether the Iapetus event -- as conventionally modelled -- may be assumed for this area at all. Beyond this, too, there are questions of spatial correlation. Even if one simply accepts the base scenario as given, in other words, it is difficult to determine how, specifically, the proto-environment thus invoked would relate to extant geological features. The evidence itself is not merely inconclusive but in some ways conflicting. According to Williams' regional reconstruction -- which is supported by geochemical studies by Davis (1977) and Bland (1978) showing that greenstones in the Candler Formation exhibit ocean floor basalt geochemical affinity -- the Chopawamsic belt would most likely comprise part of an island arc assemblage generated along the eastern margin of the postulated ancient ocean. According to Pavlides (1981), however, exactly the opposite was the case. Observing that the Ta River gneisses to the east <u>also</u> demonstrate an ocean floor-type geochemical signature, this latter researcher hypothesizes that the terrane in question was developed as a paleo-island arc along the <u>western</u> margin of that same hypothetical body. These divergent possibilities will be discussed in greater detail in the following chapters. In the meantime it might be noted that Williams and Hatcher (1982) included the Chopawamsic among the "suspect terranes" of the Appalachian eugeocline, a designation which both reflects and

underlines the many enigmas concerning its origin.

1.3 Methodology: Problems and Solutions

As the previous discussion indicates, the tectonic setting represented by the Chopawamsic metavolcanic belt has not as yet been satisfactorily defined. This poses a very real problem to ongoing investigations in that, as recent work demonstrates (Pereira & Dixon 1971, Mitchell & Garson 1976, Sawkins 1976), one of the most fruitful approaches to metallogenetic problems entails the recognition that differing ore deposit types are specific to particular tectonic settings. The mere fact of being able to invoke analogues gives a researcher a considerable headstart in unravelling metallogenic processes and placing ore-forming events within their regional geological context. One of the major obstacles to formulating such analogues for the current study was the lack of adequate mapping for the relevant area. At the outset of the project only limited portions of the belt had previously been covered in any detail. The author was thus faced with the arduous and time-consuming chore of constructing a geologic map before he could even begin to elucidate regional structural-stratigraphic relationships. Other extant data was equally scanty. Although brief descriptions of most of the old workings within the belt can be found in the literature (Luttrell 1966), and although a few detailed analyses of specific deposits had recently been undertaken as thesis projects, no broad-based metallogenic study critically addressing the diverse origins of differing deposits -- indeed, no previous systematic petrological or geochemical survey of any kind -- had ever been carried out. Explicating the petrogenesis of the meta-igneous rocks and the metallogenesis of the various types of ore deposits thus became defined as the primary goal

of this investigation.

The task was hampered not only by the sparseness of previous work but by the physical characteristics of the area, and especially by the extreme scarcity of fresh outcrop. The central Virginian Piedmont, with an altitude varying from about 100 to 300 m above sea level, has warm summers, relatively mild winters, and an average of 41.8 inches of rainfall per year (Carter & Wills 1972). These temperate climatic conditions tend to produce luxuriant vegetation. More critical, the ample moisture fosters continued leaching, causing the regional formation of saprolite which, due to the minimal erosion on this wooded, slightly dissected terrain, is preserved in a thick zone up to 70 m in depth. The red-yellow podzolic soils developed on top of this saprolite (see Photo 1) are Pleistocene or earlier in age (Cady 1951, Carroll 1970). With few exceptions, fresh outcrop can only be found in the deeper stream valleys and road cuts. Under the circumstances, geological investigation is inevitably rather onerous. Indeed, in much of the area detailed surface work is futile if not infeasible. Prospecting for economic mineral deposits and property evaluation thus tend to be both risky and expensive. Until a geophysical or geochemical target is actually drilled it is usually impossible to define either the host rock or the mineralization type with any certainty. Often even subsequent to drilling it is hard to assess the full potential of ore zones because the local rock distribution is so poorly understood. It was in direct response to this problem that the regional mapping survey which forms the basis for the present study was initiated. Without a better understanding of the regional structural-stratigraphic framework investigators found themselves totally unable to determine the significance of the individual showings along the belt.

Beyond the practical impediments posed by the terrain, over the course of the mapping survey the author came up against a number of theoretical impediments as well. In particular it was difficult to know how to classify schists of similar mineralogy but, as indicated by remnant textures and bedding characteristics, stemming from different (i.e., primary volcanic, sedimentary, or mixed volcani-sedimentary) precursors. The nomenclature problem was critical, for unless the various schist lithologies could be differentiated precisely in the field it would have been impossible to delineate even major lithofacies changes within the belt, far less to contend with the more subtle petrographic features indicative of metallogenic processes in areas of mineralization. In combination with the purely physical obstacles, such complications as these made the task of devising a suitable methodology for this project both difficult and essential.

1.3.1 Compensating for the Lack of Outcrop

The effects of rock weathering can be recognized as two stages of a complete process: (1) oxidation and leaching of fresh rock into rotten rock or saprolite, and (2) continued alteration of saprolitized rock to soils by biological activity. Unless at an advanced stage of breakdown, saprolitized rock can generally be treated as outcrop. Although the primary mineralogy may be more or less completely altered to clays, original rock fabrics are commonly well preserved. Fortunately, considering the lack of fresh outcrop in the Piedmont, saprolitic exposures are widespread along most stream and roadcuts in the project area.

Soil patterns in the region are controlled to a considerable extent by drainage systems, but at least under some circumstances specific soil

1. Lateritic soil developed on saprolitic quartz-sericite schist south of Mineral, Virginia.

2. The Willis Mountain Kyanite Mine on the highest ridge crest in the map area. The dense woods in the foreground are characteristic of the central Virginian Piedmont.

associations (Carter & Wills 1972) may also yield hard evidence about bedrock type. Unfortunately the value of soil mapping in geological interpretation is limited somewhat by the response of differing lithologies to weathering. A compositionally uniform rock such as an intrusive body can be correlated with a given soil type easily enough, but areas of considerable internal compositional variation (such as a thinly banded siliceous/mafic schist terrane) can also be characterized by reasonably uniform soils. Although soil associations may allow differentiation between the intrusives and the schists, therefore, they do little to facilitate distinctions within the latter. Outside of those few cases of rock-types resistant to chemical breakdown (such as the major metashale horizons, which tend to include considerable saprolitic microfloat), soil mapping is thus useful primarily as a means to delineating more regional lithological breaks.

The drainage system which together with bedrock determines soil patterns is itself strongly controlled by differential weathering of rock types. This regional topographic feature proved to be a considerable aid in geological mapping. Most of the Chopawamsic belt demonstrates a well developed reticulate drainage with larger streams paralleling the regional northeast strike. Within this system the more incompetent schistose lithologies tend to form stream valleys while the comparatively resistant quartzites and amphibolites and the dense metashale units form the ridges. Smaller creeks draining the heights typically enter major streams at regular intervals at right angles. This regularity makes the contrast all the more striking when the characterizing pattern is interrupted by areas of more uniform bedrock, where dendritic drainage patterns are better developed. The contacts of larger intrusive bodies can often be inferred simply by observing where the dendritic and reticulate styles of drainage interfere.

Another resource utilized by the author to compensate for the lack of outcrop was a substantial body of private and public airborne geophysical data. An electromagnetic survey was flown by Geoterrex Ltd. for Callahan Mining Corp. during the periods November 8-11 and March 5-8, 1976. Flight lines were oriented approximately N50°W over the northern portion and N65°W over the southern portion of the mapped area and spaced one quarter mile apart. The aircraft used by Geoterrex was equipped with a Barringer Mark V INPUT system and a Geometrics G-803 nuclear procession magnetometer. Navigation was by visual means, utilizing photo-mosaics. A mean clearance of 400 feet was maintained throughout and the geophysical data was presented on a series of EM plan maps at a scale of 1 inch = .25 mile. For regional mapping purposes this data was reduced to a 1 inch = .4 mile scale and plotted on Virginia State 7.5' quadrangle maps. The detailed geophysical picture thus derived was invaluable insofar as it demonstrated the along-strike continuity of numerous magnetic and/or conductive intervals within the belt. Ground proofing confirmed that many of these particular strata could be used as reasonably persistent marker beds.

In addition to Callahan Mining's detailed airborne EM data, Virginia State magnetic and aeromagnetic maps at 1 inch = 1 mile were also obtained for the project area, being utilized primarily as a means of extending coverage through a small strip along the northeastern border of the belt lying outside the range of the Callahan survey. Replotted with the EM on the 7.5' quadrangle maps, the aeroradiometric data proved useful as well for picking up granitic intrusive bodies and delineating the regional metashale deposits.

The final preparatory stage of the project entailed an attempt to compile all extant geological data at the same 1 inch = .4 mile scale. Areas previously mapped along the belt are listed on Figure 2. As demonstrated, the

Figure 2: Location of the Project Area
within the State of Virginia

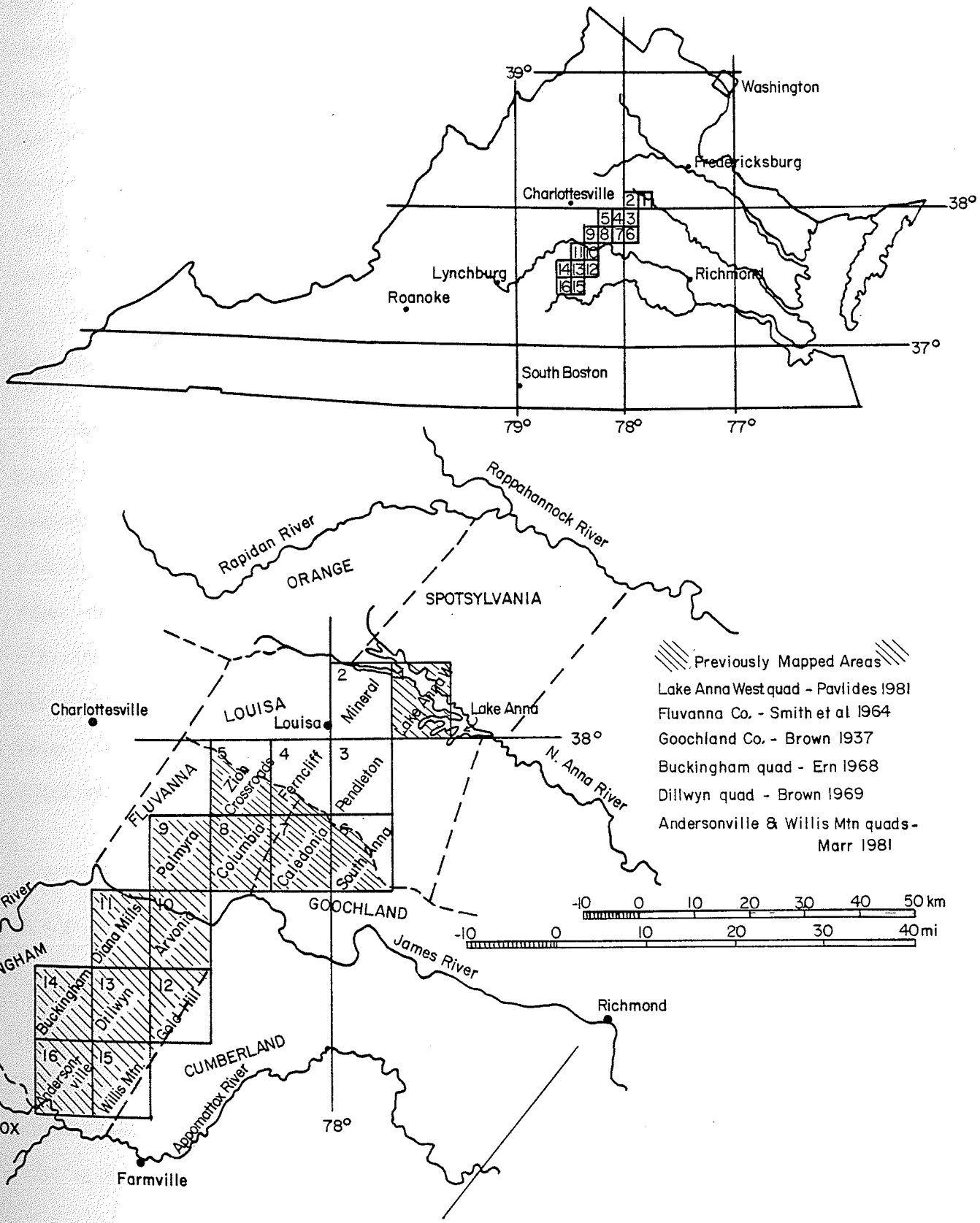

part of the belt lying south of the James River has attacted more attention than the more northerly sections. The only notable exception to this is the recent regional geological map published by Pavlides (1981) which at least overlaps the northern edge of the project area, providing a useful context for the present study by delineating regional lithological relationships in an immediately adjacent territory. Other mapping is of varying reliability. Nevertheless, all useful information, cross-referenced and at times reinterpreted in conjunction with the geophysical data, was synthesized on 7.5' topographic sheets to provide a set of "working" maps to serve as bases for the regional survey.

The survey itself was conducted by car and foot traversing. Excellent road access exists for the whole area, with a well developed network of primary and secondary roads as well as a myriad of small bush roads and trails. Foot travel is generally good along ridge crests, though the major creek valleys tend to be marshy and locally some of the bramble thickets are virtually impenetrable. Despite these problems the coverage achieved overall was reasonably systematic, although the economic thrust of the investigation meant that the mineralized trends along the core of the belt received considerably more attention than the outlying areas.

1.3.2 Sample Collection and Classification

Fresh outcrop being so scarce in the area, a concerted effort was made to glean maximum geological information from what was available. In addition to 110 core samples from 25 holes drilled by Callahan Mining Corp. across the mineralized zones, a total of 2665 handsamples were collected from 1120 out of 1280 different outcrop sites along the belt, all of which were slabbed and

classified. Because, as mentioned above, in many instances schists with the same mineralogy proved to have decidedly different geneses, a dual style of nomenclature was utilized with an interpretive genetic name following the metamorphic one. Genetic interpretations were not always possible, of course, but under the mid-greenschist conditions prevailing over much of the area, remnant textures and primary bedding characteristics are commonly preserved. Generally, indeed, the metamorphic overprint proved less of an obstacle to identification than the difficulty of consistently defining and differentiating species characterized by significant but exceedingly subtle petrographic variations. Particularly difficult to categorize were rocks of mixed volcanic-sedimentary parentage. It was necessary, therefore, to devise a rock classification system (see Appendix A) capable of encompassing not merely pure pyroclastic, epiclastic, and exhalative types but also mixed types falling somewhere between these categories. Following the classification process, a representative suite including both surface and drill core samples was selected for more detailed petrological study. Of this, 275 specimens were singled out for thin sectioning, 142 specimens for bulk rock geochemical analysis, and 52 specimens for microprobe mineralogical analysis.

1.4 Presentation of Data

In total, sixteen 7.5' quadrangles were included in the survey; these are shown on Figure 2. Collectively these cover the segment of the Chopawamsic metavolcanic belt occurring between Lake Anna to the north and the Appomatox River to the south -- approximately 125 km of strike length. The information on these original 1:24,000 scale (1 inch = .4 mile) maps was then reduced and redrafted onto a 1:126,000 (1 inch = 2 miles) base in order to produce a

regional composite of useable size. As much as possible of the geological detail from this composite is reproduced on Plate 1 in the pocket at the back of this volume. Plate 2, also in this pocket, comprises a more generalized version of the map, showing the dispositions of the major lithological suites, the intrusive bodies, and the mineral trends with respect to the main geographical features of the area.

In addition to the author's own work, the regional geological compilation, as mentioned above, incorporates all relevant earlier work done on the area. Much of this data has, however, been subjected to considerable reinterpretation. Contacts mapped by previous workers have been replotted in accordance with the more detailed geological and geophysical information yielded by the present investigation. The names of units have also been updated. Most earlier mapping tended to differentiate only metamorphic rock types and in many instances differing schist assemblages were given formational status. Counter to this, for the purposes of the present study it was felt that retaining as much of the lithological detail as possible would facilitate the delineation of regional lithofacies variation. On Plate 1, accordingly, the various rock types are labelled with their genetic classifications. In addition, because the lithologies comprising the Chopawamsic metavolcanic belt have been regionally metamorphosed and include a considerable meta-igneous component, the amendment to the stratigraphic code suggested by Sohl (1977) has been adopted for stratigraphic nomenclature. In line with this, major schist assemblages have been classified as metamorphic suites rather than formations wherever the former usage seems more appropriate.

The results of the petrological investigations carried out in conjunction with the mapping survey are discussed in the following chapters. The

petrographic data gleaned from outcrop, sawn handsamples, and thin section study have been synthesized and presented in the form of detailed petrographic descriptions of rock units in Appendix B. Along with the regional geological map, these lithological descriptions form the basis for the discussion of the regional geological framework comprising Chapter 2. The bulk rock geochemical data on selected rock types presented in Appendix C provide a backdrop to the discussion of petrogenesis in Chapter 3. Similarly, the mineral chemical data presented in Appendix D form a basis for the discussion of metallogeny in Chapter 4. The findings of the study as a whole are summarized in Chapter 5.

2. REGIONAL GEOLOGICAL FRAMEWORK

As demonstrated on Plate 2, the segment of the Chopawamsic metavolcanic belt between Lake Anna and the Appomattox River comprises several differing metavolcanic and metasedimentary schist assemblages as well as a variety of intrusive bodies. A simplified version of this map is presented as Figure 3 for easy reference in conjunction with the following geological summary. Since systematic descriptions of the lithological constitution of the various metamorphic suites and intrusive complexes are given in Appendix B, petrographic details are kept to a minimum in the present chapter, the author's primary aim at this point being to reconstruct the regional structural-stratigraphic framework as a whole.

2.1 Structural Features

Many questions concerning the history of deformation in the project area remain unresolved since the lack of bedrock exposure severely inhibits the mapping out of meso-scale structural features. Nevertheless, such structural features as are evident have not only attracted considerable attention but stimulated a number of controversies. Although no agreement has yet been reached about a specific structural interpretation, there is at least a general consensus that the terrane has undergone multiple or polyphase deformation.

FIGURE 3: REGIONAL GEOLOGICAL MAP OF THE LAKE ANNA TO APPOMATTOX RIVER SEGMENT OF THE CHOPAWAMSIC METAVOLCANIC BELT

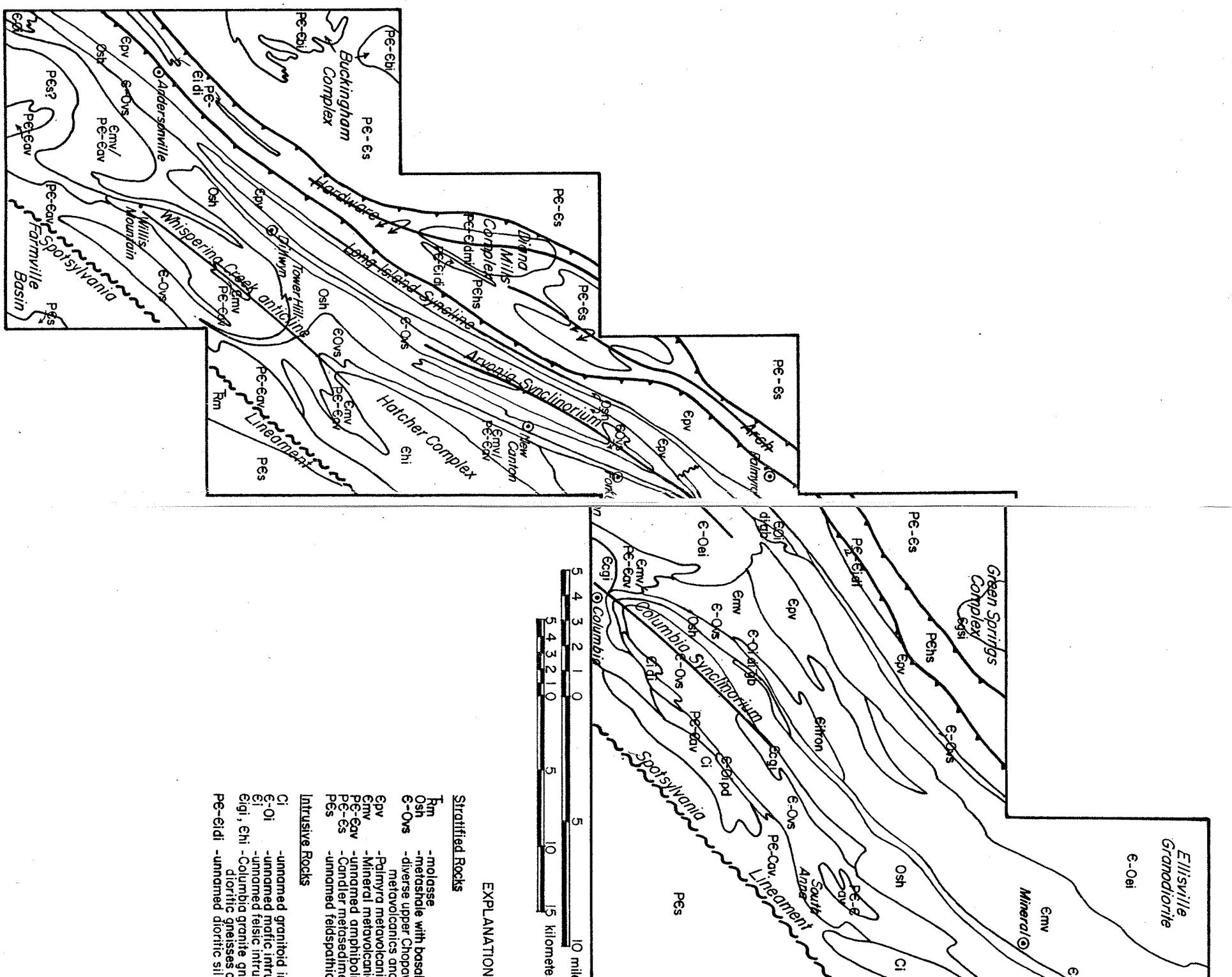

EXPLANATION

Stratified Rocks

Rm - molasse
Osh - metashale with basal silicate iron formation
Є-Ovs - diverse upper Chopawamsic group of metavolcanics and metasediments
Єpv - Palmyra metavolcanic suite
Єmv - Mineral metavolcanic suite
PЄ-Єav - unnamed amphibolitic metavolcanics
PЄ-Єs - Candler metasediments
PЄs - unnamed feldspathic paragneiss

Intrusive Rocks

Ci - unnamed granitoid intrusives
Є-Oi - unnamed mafic intrusive bodies
Єi - unnamed felsic intrusive bodies
Єigi, Єhi - Columbia granite gneiss and granitic to dioritic gneisses of the Hatcher Complex
PЄ-Єidi - unnamed dioritic sills

2.1.1 Minor Structures

The polyphase model is certainly supported by structural features evident at the outcrop, handsample, and thin section scales. As the descriptions presented in Appendix B indicate, all lithologies except those of Triassic age show the effects of regional metamorphic overprinting. A steep northeast trending schistosity is the predominant planar fabric. However, the type and intensity of s-surface development varies considerably with rock type. Quarzites commonly have a closely spaced rock cleavage rather than a schistosity; slaty cleavage characterizes the metashales and gneissic banding the eastern gneisses. Two generations of foliation have been recognized locally, while some rock species are typified by multiple foliations. Where two distinct foliation sets are in evidence the dominant steep (vertical to about 60° east-dipping) axial planar schistosity or slaty cleavage is commonly transected by a much shallower (15-35° east-dipping) crenulation cleavage. This crosscutting cleavage usually demonstrates nearly the same strike orientation as the dominant axial planar foliation. Intense multiple foliation sets defining a pervasive phacoidal structural overprint characterize the Hardware magnesian schists, the Buffards quartz mica schists in the core of the Arvonia synclinorium, and the New Canton chloritite occurring along the eastern side of the Arvonica synclinorium south of the James River.

Other structural features commonly observed at meso and micro scales include minor folds, lineations, and cross-fractures. Greatly drawn out drag folds are occasionally observed in schistose rocks; less commonly, apparently rootless intrafolial folds are found in the easterly gneisses. Very rarely (observed only near massive sulphide mineralization in the Mineral district)

the primary layering forms chaotic convolutions indicative of pre-tectonic slumping. Most minor folds of tectonic origin have axes plunging less than 20 from the horizontal. These typically lie in the plane of schistosity and regionally show reversals in plunge from northeast to southwest. Besides minor fold axes, other common lineations include bedding-foliation intersections, mullion structures in quartzites, stretched inclusions, and mineral alignment. In general the lineations so defined have the same orientation as minor fold axes in the same vicinity. Northwest trending, steeply dipping cross-fractures are the only structural features consistently demonstrating a strike orientation other than that of the dominant schistosity. Zones of intense cross-fracturing are locally accompanied by crenulation cleavages with axes plunging steeply in the same northwesterly direction. Most of the widespread Triassic diabase dykes in the area appear also have been intruded along northwest striking cross-fractures.

Although penetrative deformation fabrics are the rule, the intensity of overprint is not particularly uniform. Some lithologies and local areas demonstrate a far less intense metamorphic overprint than others. The metarhyolite flows of the Palmyra metavolcanic suite and the quartz-feldspar porphyry bodies in the Mineral district, for instance, may be surprisingly free of metamorphic overprinting. Also, the intrusive bodies often retain vestiges of their primary igneous textures and at times these are remarkably well preserved. The only cases where this is not true are the border zones of the mafic complexes along the Hardware Arch, the severely cataclasized granophyric and quartz diorite bodies in the Mineral metavolcanic suite, and the orthogneisses along the eastern margin of the belt. In general the westerly Palmyra metamorphic suite has a much less well developed schistosity than does the central Mineral metavolcanic suite; the latter in turn lacks the

coarse recrystallization manifested by the easterly gneisses. This evident variability in metamorphic overprinting suggests two further features that might be seen as characteristic of the regional deformation style: (1) the deformation increases in intensity with the general increase in metamorphic rank from west to east across the Chopawamsic metavolcanic belt, and (2) locally the development of deformation fabrics is controlled to a considerable extent by rock type.

Primary layering is readily discernible over most of the area, but tends to be obscured by the eastward increase in the intensity of metamorphism across the belt. The dominant schistosity generally lies subparallel to bedding; only locally (near fold hinges) do these crosscut at high angles. This relationship has generally been interpreted to indicate a tight to isoclinal fold regime with a strong axial planar schistosity. Where the metamorphic fabric is most highly developed, the primary bedding has been largely transposed into the plane of this schistosity. In such cases compositional layering is accentuated by mimetic crystallization. Primary layering is most difficult to distinguish from metamorphic differentiation in the strongly recrystallized gneisses along the eastern margin of the belt. It is likely, however, that most of the compositional layering characteristic of this lithology stems from original stratification.

2.1.2 Major Structures

Regionally a linear structural pattern typifying the western part of the Chopawamsic metavolcanic belt contrasts markedly with broad domal structures along the eastern side of the belt. The contrasting deformation styles merge across the major Arvonia and Columbia metashale synclinoria, broadly

coinciding with the change from westerly greenschist to easterly amphibolite facies metamorphic conditions. In the context of a general structural schema, this change in deformation across the belt reflects interference between a westerly near-vertical, tight to isoclinal fold generation (F_1) and an easterly broad fold generation with a generally similar axial strike but showing a moderately east-dipping axial planar orientation (F_2).

On the western side of the belt there is little evidence for F_2 interference outside of the minor warping of F_1 foliations and the local development of a shallow-dipping crenulation cleavage. The Palmyra metavolcanic suite is characterized by a single foliation paralleling primary compositional banding. The Long Island syncline coring the Palmyra metavolcanics has been identified by Smith et al (1964) and Brown (1969) as a simple isoclinal infold of metashale. Although this interpretation is supported in its broadest sense by the author, the fact that tight minor folds (ranging in amplitude from microscopic to several meters) occurring along the core of the Long Island syncline are commonly disrupted by a spaced axial planar cleavage indicates that intense axial planar shear displacement accompanied the isoclinal folding event.

The thesis that the central Arvonia and Columbia folds are anticline-cored synclinoria exhibiting F_1-F_2 interference is supported by recent interpretations of these structures by Conley (1978) and Conley and Marr (1979). In the case of the Columbia structure such an interpretation hinges on (1) identifying the lithology coring the structure as older than the metashale and basal shale silicate facies iron formation occurring along the limbs, and (2) noting a change from steep 60-70° east-dipping attitudes along the western limb to moderately shallow 20-40° east-dipping attitudes in the core and along the eastern limb. The marked asymetry is thought to be due to

the change from F_1 to F_2 dominated structural domains. The case of the Arvonia is somewhat more controversial since the favoured interpretation is decidedly at odds with Brown's (1969) view that this feature comprises a simple fold with older metashale limbs and younger clastic sediment and felsic pyroclastic deposits exposed along the core. Conley and Marr (1979) essentially turned Brown's stratigraphy upside down by identifying Chopawamsic metavolcanics between the two metashale limbs, an interpretation clearly conducing to the conclusion that the limbs of the Arvonia structure are individual synclinal folds. Within the anticlinal core of this structure a near-vertical foliation paralleling bedding along the west limb gives way to shallower bedding attitudes and a multiple foliation overprint along the eastern limb. The asymetry and increasing complexity in internal fabric is again attributed to F_1-F_2 interference.

Broad asymetric anticlinal to domal F_2 structures with moderately east-dipping axial planes control structural patterns along the eastern side of the Chopawamsic metavolcanic belt. These structures are best developed in the southeastern part of the map area in the Andersonville district, but are also well defined by the so-called Whispering Creek "anticline" (identified by Espenshade and Potter 1960) occurring on the east flank of the Arvonia synclinorium. The presence of a domal feature perhaps also accounts for the abrupt thickening of Columbia metashale where the South Anna River transects the anticline-cored Columbia synclinorium. The axis of the Whispering Creek anticline may well lie on strike with the axis of the Columbia synclinorium (Marr 1981, personal communication). Indeed, the Whispering Creek anticline shows many of the same features as the Columbia synclinorium, with older Mineral metavolcanics in the core rimmed sequentially by deposits of the diverse upper Chopawamsic group and by the basal metashale silicate facies

iron formation. The attitudes of the peripheral younger rocks define a similar asymetry with steeper northwest and shallower southeast fold limbs. It seems evident, therefore, that the Whispering Creek "anticline" forms the core of a broad asymetric domal structure with a synclinal rim, differing from the Columbia and Arvonia synclinoria only in that it has a more extensive exposed core zone. The morphological differences between the generally rounded major fold structures along the eastern side of the belt and the central elongate synclinal structures are due largely to shallower axial planes and more frequent reversals of axial plunge in the former. The structural saddles developed between areas of opposing axial plunge commonly show the most intense development of northwest cross-fracturing.

Delineation of major faults in the area is hampered not only by the sparsity of outcrop but also by the difficulty of distinguishing shear zones in schistose rocks. The most intense zone of shearing recognized over the course of the present survey occurs along the Hardware structure on the western border of the Chopawamsic metavolcanic belt. The Hardware magnesian schists coring this feature typically show multiple foliations, and included quartz stringers have been folded, boudinaged, and granulated. These characterizing extreme deformation fabrics indicate that the structure is considerably more complex than the simple anticline postulated by Smith et al (1964).

The multiple foliations overprinting the Buffards quartz mica schists coring the Arvonia synclinorium and the New Canton chloritite occurring on the eastern limb of the Arvonia structure signify that these particular lithologies have also been subjected to extreme deformation. The phacoidal structural overprint of the Buffards quartz mica schists indicates that the anticlinal core of the Arvonia synclinorium underwent intense shearing. The

similar intense shear deformation of the New Canton chloritite possibly relates to a zone of weakness along the outside of the eastern limb of the Arvonia structure which may separate the domal structures in the Andersonville district from the Whispering Creek anticline.

A major high angle fault zone is represented by the Spotsylvania lineament bounding the east side of the Chopawamsic belt. This lineament is considered by Pavlides (1981) to be a major crustal suture separating the Chopawamsic metavolcanic belt from the outer Piedmont, as these two terranes have vastly differing regional geophysical expression. As summarized by Johnson (1981), northwest of the lineament northwest-trending magnetic ridges and low value radiometric anomalies lie parallel to the strike of the Chopawamsic belt. Southeast of the lineament magnetic values are much lower and radiometric values considerably higher; together these features define more northerly trends. In Pavlides' view, the geophysical expression along the lineament would seem to suggest a broad (2-3 km wide) zone of discontinuous en echelon shears rather than a single fault. Significantly, the youngest major structure in the map area, the Triassic Farmville basin occurring in the southeast corner of the map area, is bordered on the west by a strand of the Spotsylvania lineament called the Lakeside fault zone by Glover (1974). The coarse fanglomerate along the west side of the basin reveals that this border fault formed an appreciable fault scarp in Triassic times. Glover noted that Triassic dykes crossing the fault are offset, testifying to post-Triassic movement.

2.1.3 A Regional Structural Schema

Collectively these structural features indicate that the Chopawamsic

metavolcanic belt is bound on both the east and the west by major fault loci. The belt itself constitutes a terrane characterized by somewhat incoherent folding. The western part, typified by steep F_1 isoclines accompanied by variable intensities of axial planar shearing, transits eastward into a gneissic terrane where broad asymetric F_2 folds dominate the structural pattern. The major Columbia and Arvonia synclinoria occur at the transition from F_1-dominated to F_2-dominated structural domains, and as a result these show the effects of F_1-F_2 interference. A graphic representation of these regional structural features is presented on Figure 4.

The specific age relationships between F_1 and F_2 fold generations are not yet well defined. The fact that the F_2 folds have moderate east-dipping axial planes and that crenulation cleavages of the same attitude transect the dominating steep F_1 axial planar schistosity clearly reveals that F_2 overprinted F_1 in the area where both generations occur. Although warping of F_1 structures by broad F_2 overprints is apparent on a regional scale, however, refolded folds are not evident in outcrops. This may indicate that the F_1 and F_2 fold generations were in fact coaxial, with the early F_1 folds being further warped during a protracted deformational regime culminating in F_2 doming. This late doming phase requires considerably more elucidation before definitive conclusions may be drawn, but the marked asymetry and moderate east-dipping axial planes shown by F_2 folds implies that a strong east-to-west directed compression accompanied the event. The effects of such subhorizontal compression are amply demonstrated by both the Columbia and the Whispering Creek structures, both of which show evidence of vestigial nappe-fold development. Notwithstanding such indicators, it seems clear from extant lithological patterns that both these folds are constituted by anticlinal cores and synclinal limbs rather than by the stacked recumbent F_1 isoclines

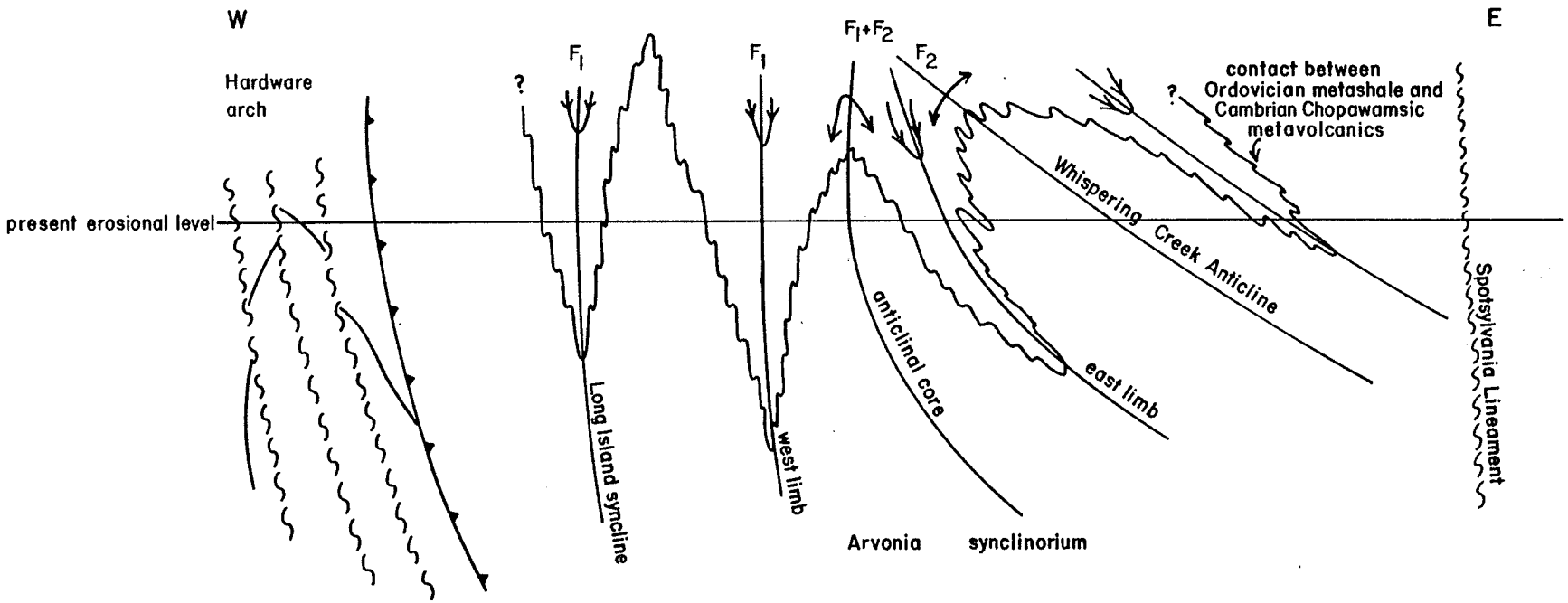

Figure 4: Regional Structural Schema

characteristic of more advanced stages of nappe folding.

Evidence for post F_1-F_2 fold deformation is restricted to zones of northwest trending cross-fracturing which are sometimes accompanied by steeply plunging crenulations of the same azimuth. Although these cross-fractures transect the northeast trending fold fabrics, the fact that they (a) concentrate in the saddles between the F_2 domal folds and (b) coincide with the en echelon displacement of the major Arvonia and Columbia F_1-F_2 synclinoria strongly suggests that they came into play only at the culmination of folding. This northwesterly tectonic grain did, however, play a critical role in controlling the attitude of emplacement of the Triassic dykes.

2.2 Stratigraphic Framework

Stratigraphic explication of the area of this investigation is hindered by many factors including the lack of outcrop, the polyphase style of deformation, the occurrence of schist assemblages consisting of thin and discontinuous lithological units, the absence or metamorphic eradication of facing directions, and the scarcity of reliable marker beds. Nevertheless, when specific lithological relationships are viewed collectively in conjunction with the regional distribution pattern, a stratigraphic framework applying at least on a broad scale is decipherable.

As illustrated on Figure 3, the Chopawamsic metavolcanic belt is bordered on the west by the regionally extensive Candler Formation. Along its eastern margin this latter comprises a basinal metasedimentary succession dominated by pelitic paper schists with interlayered impure quartzite and metagreywacke units. Unfortunately, the boundary between the metasediments and the

Chopawamsic metavolcanics occurs along a broad, little dissected upland typified by deep saprolitization and extensive soil cover. As a result, the outcrop situation is poor even by the standards of the region, making lithological relationships here particularly difficult to define. Magnesian schists are widespread along the contact but may not form such a persistent band as that depicted on the present map; it is quite possible that more Candler-type metasedimentary material may occur within the 1-4 km wide tract than the author has shown. The contacts as drawn do, however, bound the area over which magnesian schists were observed by the writer; they also broadly coincide with the magnetic ridge observed by Pavlides et al (1974) to connect the regional linear of mafic intrusive complexes and with the Hardware arch, the structure after which these schists have informally been named. Within the map area the Hardware schist lithology comprises, wholly or partially, the country rock to the Buckingham, Diana Mills, and Green Springs intrusive complexes. The ubiquitous minor magnetite occurring in the Hardware magnesian schists can well account for the regional magnetic high.

The extreme deformation textures demonstrated by these schists (photos 3 & 4), as well as the regional lithological change from westerly Candler metasediments to easterly Chopawamsic metavolcanics, pose a serious challenge to the interpretation put forward by Smith et al (1964) that the Hardware structure is a simple anticline. This zone is undoubtedly much more complexly deformed than these workers recognize. Nevertheless, the lithological overlap demonstrated by the interlayering of greenstone beds within the west bordering Candler metasediments, the Hardware magnesian schists, and the east bordering Chopawamsic metavolcanics does suggest a tectonized facies boundary rather than the tectonic juxtaposition of unrelated metamorphic and lithologic suites. The contact between the Candler metasediments and the Chopawamsic

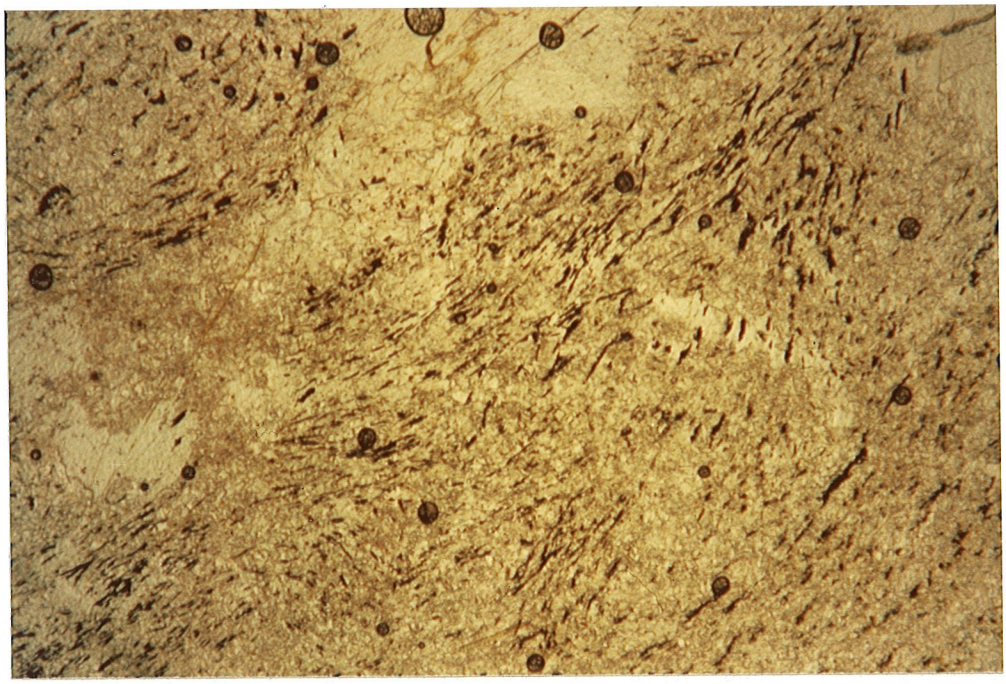

3. Hardware magnesian schist: Delicate microfolding defined by discontinuous magnetite laminae in talc schist (sample Fe-17, ppl, X250).

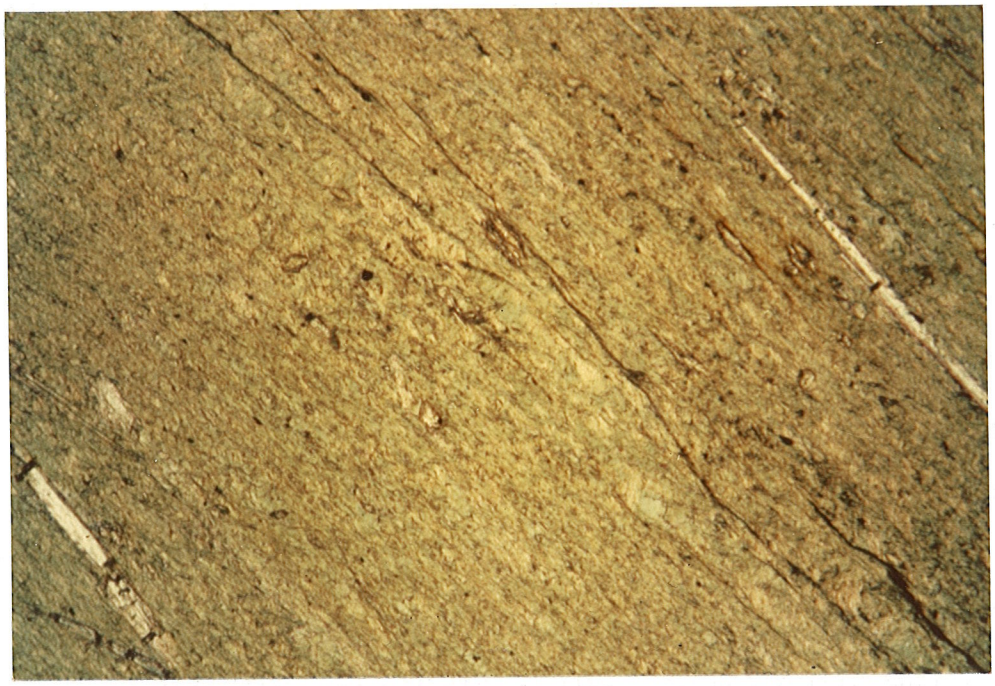

4. Hardware magnesian schist: Highly fissile chlorite schist with acicular tremolite and disseminated magnetite porphyroblasts (sample Fe-2, ppl, X200).

metavolcanics is consequently here interpreted to be a highly deformed facies boundary with the older substratum, represented by the Hardware magnesian schists and intrusive complexes, exposed along a severely tectonized structural arch.

The stratigraphic relationship between the mafic intrusives along this border and either the Candler metasediments or the Hardware schists is not at present well understood. It is considered significant, however, that the strongly differentiated sill complexes, represented by the southerly Buckingham and central Diana Mills bodies, show much the same lithological interlayering as the greenstone units. The fact that the greenstones form an integral basal member of the Palmyra metavolcanic suite suggests that the injection of the mafic sills was probably roughly coeval with basal Chopawamsic volcanism. The occurrence of the late quartz-diorite differentiate peripheral to the Buckingham and Diana Mills complexes and the predominance of diorite-granodiorite compositions in the northerly, more plug-like Green Springs complex, however, both imply long-lived magmatism which likely continued well into Candler and Chopawamsic times.

The Palmyra metavolcanic suite located on the west side of the Chopawamsic belt (see reconstructed stratigraphic column in Table 5) exhibits a sharp western contact against the multiply deformed Hardware magnesian schists. The suite consists of a low to mid-greenschist facies felsic pyroclastic succession characteristically overprinted by a single, near vertical foliation parallel to primary banding in the felsic tuffs. Because of the evident contrast in deformation across it, the western boundary of the belt is interpreted to be a high angle fault. Where greenstone beds occur along the contact, they show the same near vertical attitudes as do the felsic tuffs; these lithologies are evidently conformable. Indeed, particular

Table 5: Stratigraphic Relationships of the Palmyra Metavolcanic Suite

Long Island Metashale

---conformable contact---

Diverse Upper Chopawamsic Group

---conformable contact---

Palmyra Metavolcanic Suite

West of Long Island Syncline

Approximately 3000 meters of thin-banded (mm-cm scale), fine-grained metarhyolite tuff occur interlayered with occasional 10-100 meter-thick felsite sills. Very localized metarhyolite flows are found in the top third of the tuff succession. The felsic metavolcanics conformably overlie the 600 meter-thick Shores greenstone unit west of Palmyra, and discontinuous intervals of spilite-keratophyre are interlayered with the felsic tuffs along the westerly fault contact with the Hardware magnesian schists.

East of Long Island Syncline

Approximately 1200 meters of medium-banded (cm-m scale), medium-grained metadacitic and lesser rhyodacitic crystal tuff occur southwest of the Ellisville intrusion. Thin (100-200 m) meta-andesite tuff and flow units comprise a minor part of this intermediate metavolcanic succession.

Northeast of the Ellisville intrusion there are approximately 3000 meters of poorly differentiated, thick-banded (m scale), medium-grained intermediate tuffs including meta-andesite accretionary lapilli units. This particular tuff succession interfingers with the Mineral metavolcanic suite and is intruded by the Ellisville granodiorite sill at its base.

greenstones such as the major Shores unit striking through central Palmyra quadrangle and a few lithologically similar but thinner units interbedded with the felsic tuffs appear to form an intrinsic basal facies to the Palmyra suite.

To the north the Palmyra metavolcanics are truncated by the Ellisville porphyritic granodiorite intrusion. Where the northerly stock-like part of this Ellisville body necks down to a sill-form, the Palmyra rocks may be observed along both flanks. To the south the suite continues past the area mapped. Throughout, its core is demarked by the thin but regionally persistent Long Island syncline. The metashale preserved in this synclinal infold and the ferruginous lithologies which border it together cap the Palmyra suite. The facies change from felsic pyroclastics to rocks enriched in iron-bearing minerals is a very gradual one, with considerable interbedding of felsic tuffs and ferruginous metapelite and/or quartzite. These iron-enriched species are herein identified as the most westerly occurrence of the lithologically diverse upper Chopawamsic group. The overlying metashale is slightly coarser grained but otherwise lithologically correlative to the Arvonia and Columbia metashale preserved in the larger synclinoria further east.

The internal facies variations within the Palmyra metavolcanics are not well understood as the poor outcrop conditions tend to frustrate this level of geological investigation. A few distinctive lithological distributional features do, however, become evident on the regional scale. Thin-banded rhyolitic dust tuff dominates the western part of the assemblage, transiting through coarser crystal tuff to areally restricted cherty rhyolite flows bordering on the Long Island metashale. This would seem to suggest small localized rhyolite flow centers peripherally bordered by proximal crystal tuff

and more distal dust tuff. The stratigraphic relationship between the rhyolitic facies and the typically coarse grained dacitic to andesitic pyroclastics and lesser flows that dominate the eastern part of the Palmyra suite, occurring between the Long Island and Arvonia metashale units and on the eastern flank of the Ellisville granodiorite sill, remains, in contrast, largely unknown. From the standpoint that the Palmyra suite possibly comprises a mafic to felsic volcanic succession, it is tempting to consider that the intermediate facies might (at least in gross terms) underlie the rhyolitic lithologies, but such an inference cannot be substantiated by the present level of mapping. Rather, what seems evident is that the rhyolitic and more intermediate subfacies are in general separated by younger rock types such as the Long Island metashale to the south and the Ellisville granodiorite to the north.

Stratigraphic relationships between the westerly Palmyra metavolcanic suite and the mid to upper greenschist facies Mineral metavolcanic suite (informally named after the town of Mineral) which underlies the central part of the Chopawamsic metavolcanic belt are also obscured by younger rocks occurring along their border. Generally speaking the two metavolcanic suites are separated by the Arvonia metashales in the south and by the Ellisville stock in the north. Apparent interfingering of the Palmyra intermediate tuffs and Mineral volcaniclastics may be observed on the eastern flank of the Ellisville sill, however, indicating that their deposition overlapped, at least locally. Unfortunately, there is not enough outcrop in this area to allow detailed mapping of contacts, so the general structural-stratigraphic schema can only be inferred from regional lithological changes. This is discussed below in conjunction with facies changes within the Mineral metavolcanic suite.

The Mineral suite (see reconstructed stratigraphic column in Table 6) continues both north and south of the map area. Its western boundary is demarked by another granodiorite intrusion in the Appomattox River drainage at the south end of the Andersonville district. Internally, its major lithofacies variations are best demonstrated in the Mineral district itself. Here in the north the general across-strike lithological changes include an increase in the amount of epiclastic sediment to the west and a slight increase in the ratio of silicic to mafic metavolcanics accompanying the general increase in primary metavolcanics to the east. Towards the eastern margin the primary volcanic units become interbanded with and eventually give way to various facies of lean iron formation or ironstone. These ironstones in turn transit into the diverse upper Chopawamsic group which forms the base of the Columbia metashale, separating the Mineral suite from the higher grade gneiss and intrusive terrane further east.

The contact between Mineral and upper Chopawamsic rocks is a rather arbitrary one, having simply been placed where the ironstones interlayered with the mafic and silicic metavolcanics transit into a regionally extensive two-amphibole ironstone near or at the boundary of the metashale. This to-amphibole ironstone, which caps the Mineral metavolcanic suite, also forms the most persistent lithology of the diverse upper Chopawamsic group; it is described with the latter in Appendix B.

The Mineral suite demonstrates a considerable along-strike lithological variation as well. South of the Mineral district these metavolcanics underlie a broad tract along the west limb of the Columbia synclinorium. The westerly epiclastic-rich part of the suite is pinched out through interfingering with the felsic pyroclastics of the Palmyra assemblage on the east flank of the sill-shaped part of the Ellisville intrusion. Meta-andesitic tuff

Table 6: Stratigraphic Relationships of the Mineral Metavolcanic Suite

Arvonia Metashale

---conformable contact---

Diverse Upper Chopawamsic Group

---conformable contact---

Mineral Metavolcanic Suite

southern Andersonville District	central New Canton Trend	northern Mineral District
An indeterminate thickness of thin- to medium-banded (cm-m scale) amphibolite (after metabasaltic tuff and flows) intercalated with feldspathic and biotitic gneiss (after epiclastic sedimentary material). This lithological assemblage is complexly interfolded with and rimmed by members of the diverse upper Chopawamsic group. The banded amphibolite zone coring the Andersonville district is also likely correlative with the amphibolites of the eastern gneiss terrane.	Approximately 2000 meters of thick-banded (m scale) amphibolite gneiss interlayered with lesser feldspathic gneiss (after mafic metavolcanics and epiclastic sedimentary material respectively) occur along the western border of the Hatcher complex. Less highly metamorphosed massive metabasalt flows up to 50 meters thick and lesser 10-50 m thick schistose metarhyolites occur in the zone of interbanding with overlying diverse upper Chopawamsic units along the contact with the metashale.	Approximately 6000 meters of intercalated, thin-bedded (cm scale), fine-grained, immature quartzo-micaceous metasediment and bimodal metavolcanics flank the eastern side of the Ellisville intrusive stock. The metavolcanics dominate discontinuous 200-1000 meter-thick intervals of the succession and include massive to thickly banded (m scale) amphibolitic metabasalt and lesser amounts of schistose metarhyolite. This mixed volcanic-sedimentary assemblage hosts small (up to 1200 m thick) trondhjemite bodies and includes appreciable thin-banded (mm-cm scale) ironstone where interbanded with the overlying diverse upper Chopawamsic group. The metabasalts increase appreciably to the south and dominate a 2000 meter interval along the western limb of the Columbia synclinorium. This mafic facies grades into the amphibolite gneisses bordering the Hatcher complex.

Columbia Metashale

intercalated with drab green chloritic metasiltstones occurs at the facies change from Palmyra metatuff to Mineral epiclastic quartz biotite schist, indicating overlapping andesitic pyroclastic activity and epiclastic sedimentation in the area immediately north of where the Ellisville granodiorite again thickens to underlie much of the area between the Arvonia and Columbia synformal structures. The Mineral mafic-silicic metavolcanic and ironstone assemblage, together with included minor dioritic intrusive material, appears to pinch out near the termination of metashale at the nose of the Columbia structure. The core of the Columbia synclinorium, though poorly exposed, comprises lithologies belonging to the diverse upper Chopwamasic group.

The Mineral assemblage is also observed as a thin (1 km) interval forming the New Canton trend along the eastern border of the Arvonia synclinorium. South along the New Canton trend the metavolcanic suite loses definition due to interference by the higher grade metamorphic conditions prevailing in the Hatcher complex as defined by Brown (1969). Southwest of this complex, however, minor amounts of Mineral-type metamorphic lithologies are observed to accompany the dominating upper Chopawamsic rocks in the core of the Whispering Creek anticline. In the Andersonville district near the southern end of the map area the Mineral suite comprises an atypically mafic-metavolcanic-rich core zone bordered immediately by ironstone-iron formation which is in turn rimmed by a poorly differentiated volcaniclastic, pyroclastic, and bimodal primary volcanic assemblage. The Andersonville core zone has no counterpart in other areas underlain by Mineral metavolcanics, so it may be that this particular terrane correlates more specifically with the amphibolitic gneisses of the eastern plutonic terrane.

By far the most complex stratigraphic relationships in the map area are

those observed between the upper Chopawamsic group (see reconstructed stratigraphic column in Table 7) and the regional metashale formations. A variety of facies of ironstone-iron formation conformably caps much of both the Palmyra and Mineral assemblages. In the case of the Palmyra suite, these wholly or partially chemically precipitated lithologies range from localized, laminated, ferruginous metapelite-metamarl successions to much more regionally extensive ferruginous quartzite-oxide iron formation deposits. In the Mineral assemblage more localized facies of hornblendic, pyritic, and carbonate-bearing ironstone transit into a regionally extensive two-amphibole hornblende-cummingtonite ironstone - ferruginous quartzite - oxide iron formation capping. Although an iron formation-ironstone association typifies the metavolcanic-metashale contact on a regional scale, this boundary is also a locus for areally restricted deposits along the entire length of the belt covered by this investigation. While not laterally persistent, these particular upper Chopawamsic deposits are nevertheless volumetrically significant in the areas where they occur.

The stratigraphic relationship sustained by the restricted Buffards quartz-mica schists (rhyolite flow tuffs) and the various feldspathic, kyanitic, and mineralogically complex quartzites with the regionally extensive ironstone-iron formation deposits on the one hand and the metashales on the other provides a key to the stratigraphic links between the metashale formations and the Chopawamsic metavolcanics. The lithological change from upper Chopawamsic ironstone - ferruginous quartzite - oxide iron formation to basal shale silicate facies iron formation defines this contact regionally. As these particular lithologies form the best regional markers, the detailed stratigraphic relationships among the regionally extensive upper Chopawamsic ironstone-iron formation, the more restricted Buffards quartz-mica schist, the

Table 7: Stratigraphic Relationships of the Diverse Upper Chopawamsic Group

Long Island Metashale (basal silicate iron formation on west limb)	Arvonia Metashale (basal silicate iron formation along eastern limb)	Columbia Metashale (basal silicate iron formation inside of west limb and in core)	Whispering Creek (basal shale silicate iron formation along periphery)
---conformable contact---		---conformable contact---	
A variably thick (up to 300 m) interval consisting primarily of well banded (cm-m scale) ferruginous quartzite occurring between the Palmyra metavolcanics and metashale. There are about 100 meters of interlayering of quartzite and felsic tuff at the base, and thin bands (cm scale) of hematite-magnetite iron formation increase in frequency towards the top. Thick (1-2 m) oxide iron formation bands interlayer with the basal shale silicate iron formation. Very locally, the Palmyra metarhyolites persist to the metashale contact and in these areas thin bands (cm-m scale) of chloritic metamarl, metacarbonate, metachert, and oxide-sulphide iron formation occurs as thin interlayers within felsic tuff underlying the metashale.	A variably thick (up to 100 m) basal shale oolitic chloritite (iron formation) occurs interbedded with the top of the variably thick Bremo feldspathic quartzite in the nose of the Arvonia structure. Up to about 1200 meters of very highly deformed Buffards quartz-mica schist (metarhyolite ash flow tuff) occupies the core. Approximately 500 meters of thin to medium-banded (cm-m scale) two-amphibole ironstone and ferruginous quartzite, lesser oxide iron formation, and rare metakomatiite occurs along the outside of the eastern limb. A broad zone of indeterminate thickness of poorly differentiated upper Chopawamsic rocks rims the mafic amphibolite core to the Andersonville district. Persistent, thin (1-300 m) ferruginous quartzite - oxide iron formation units locally host metakomatiite beds.	A variably thick (up to 1200 m) interval of thin to medium-banded (cm-m scale) ferruginous quartzite - two-amphibole ironstone, and oxide iron formation occurs along the west limb of the Columbia metashale. Up to 500 meters of Buffards metarhyolite, up to 500 meters of metakomatiite, and up to 200 meters of kyanite quartzite form discontinuous units near/at the metashale contact. Local 500-1000 meter-thick diorite-gabbro bodies occur in this assemblage near the nose, and an indeterminate thickness of poorly differentiated upper Chopawamsic rocks cores the Columbia structure. About 100 meters of basal shale garnet-grunerite iron formation and 200 meters of Buffards metarhyolite border on the inside of the metashale. Persistent 1-200 m units of silicate iron formation, kyanite quartzite, and feldspathic quartzite occur in the core and along the eastern limb.	The Whispering Creek anticline is cored by an indeterminate thickness of Buffards metarhyolite, ferruginous quartzite, and two-amphibole ironstone. Persistent 1-300 meter-thick units of basal shale silicate iron formation, oxide iron formation, and kyanite quartzite, and more localized metakomatiite are interlayered around the periphery.
---completely gradational contact---		--- completely gradational contact---	
Palmyra Metavolcanic Suite	Mineral Metavolcanic Suite	Eastern Amphibolite Gneiss	

various types of quartzite deposit, and the metashales are best demonstrated by their respective relationships with the basal shale silicate facies iron formation marker unit. The latter occurs as a rather recessive oolitic chloritite below the almandine garnet isograd but above the isograd appears as a coarsely porphyroblastic garnet-grunerite. Because this is both the most readily recognizable and the most resistant rock type in the higher grade part of the belt it provides by far the best stratigraphic marker. Occurring not only in all three (Long Island, Arvonia, and Columbia) metashale synforms but in the Whispering Creek anticline as well, its regional distribution has great enough extent to make this unit extremely useful in the task of determining regional stratigraphic interrelationships.

In the Long Island syncline the basal silicate iron formation shows its best development along the west limb at the locale where the thickest development of shale occurs immediately east of Palmyra. In this area the most basal parts of the iron formation are coarsely conglomeratic with intraclasts of magnetite-quartzite occurring in a matrix of oolitic chloritite. These intraclastic conglomerate strata sometimes show upward fining to a dense oolitic chloritite, and this subfacies transits into the overlying metashale through a zone of interbedding with chloritic meta-argillite and metasiltstone. Such features are interpreted to signify that tectonic disturbances at the time of change from chemical precipitation of ferruginous chert and oxide iron formation to oolitic iron chlorite deposition caused slumping of initially interbanded ferruginous chert and oolitic chloritite. Where these rocks are observed further north near the northern boundary of the map area, evidence of turbidite resedimentation is not present and the chloritite subfacies occurs interbedded with strongly developed oxide iron formation. The most northerly outcrop observed is found at the junction of

the sill and stock parts of the Ellisville granodiorite. In this exposure the chloritite bands are recrystallized to a coarsely porphyroblastic garnet-chlorite rock, suggesting that a narrow thermal metamorphic aureole associated with the northern part of the intrusive body overprinted the iron formation.

The metamorphic transition from oolitic chloritite to a coarsely porphyroblastic garnet-grunerite rock is best demonstrated where the almandine isograd transects the east limb of the Arvonia synclinorium. At this location remnant oolites are observed both in unrecrystallized patches of matrix and occasionally within garnet porphyroblasts themselves. Within the Arvonia synclinorium the silicate iron formation is developed on the west side of the eastern metashale syncline between the metashale and the crossbedded Bremo feldspathic quartzite. The marker forms a continuous stratum from the nose of the Arvonia structure south of the James River to a point where intertonguing of the quartzite and the metashale causes thinning of the former. Notably, this same locale also marks the across-strike northerly extent of the Buffards quartz-mica schist which cores the Arvonia synclinorium. The occurrence of thin bands of a coarsely porphyroblastic garnet-kyanite-iron oxide rock interbedded with this latter formation at its contact with the metashale on the eastern flanks of Buffards Mountain is considered a subfacies correlative to the silicate iron formation marker; this is the most southerly location at which this key unit has yet been observed in the Arvonia synclinorium.

The thickest known development of the garnet-grunerite marker occurs within the Whispering Creek anticline near Tower Hill about four kilometers southeast of Buffards Mountain where it is again interbanded and/or interfolded with Buffards quartz-mica schist. Three in particular of the lithological relationships shown by this marker in this area are regionally

significant: (1) the basal silicate facies iron formation is essentially the only facies of the metashale to occur at this location, suggesting that this easterly terrane actually formed the easterly limit of shale deposition; (2) the garnet-grunerite is locally interbedded with and, on a more regional scale, transits into ferruginous quartzite-oxide iron formation, indicating that these units were deposited coevally; and (3) the garnet-grunerite marker locally interbeds with the extensive kyanite quartzite units that rim the Whispering Creek anticline, implying that kyanite quartzite was also generated at the same time as the basal shale silicate iron formation. The close stratigraphic overlap demonstrated here might suggest that the coarsely porphyroblastic garnet-kyanite-iron oxide bands interbedded in Buffards quartz-mica schist in fact comprise a transitional subfacies between garnet-grunerite and kyanite quartzite end members, and further, that both these facies developed near or at the close of Buffards volcanism.

The garnet-grunerite marker is also well developed in the Columbia synclinorium south of the abrupt thickening of this structure in the South Anna River area, occurring on the eastern side of the westerly metashale limb and appearing to comprise the only subfacies of the metashale observed along the eastern limb. As with the Whispering Creek anticline, these marker rocks are once more, at least in the latter location, accompanied by extensive kyanite quartzite. This quartzite, which continues considerably further north along this limb than the silicate iron formation, is found both to the southwest and to the northeast along-strike from the laminated feldspathic quartzite deposit in the South Anna River area, indicating that the latter deposit was also laid down at about the same time. The basal marker was not observed to accompany the main Columbia metashale along the western limb north of Interstate 64; however, oolitic structures were observed in a sample of

unusually chlorite-rich basal metashale from the Mineral district, suggesting that even though the highly ferruginous chloritite precursor was apparently not deposited this far north, the environmental conditions leading to the formation of oolites were present here as well. Significantly, a thin bed of kyanite quartzite occurs on the western metashale contact in the southern part of the Mineral district. This particular kyanite quartzite interval shows conformable relationships with both the westerly hornblende-cummingtonite-ironstone-oxide iron formation assemblage regionally capping the Mineral assemblage and the easterly metashale.

It should be stressed that the broadly conformable conditions the author infers from stratigraphic relationships between the diverse upper Chopawamsic lithologies and the basal shale silicate facies iron formation are markedly inconsistent with interpretations of the stratigraphic relationships between metashale and Chopawamsic metavolcanics offered by numerous previous investigators. Conley (1978), Pavlides (1976, 1981), and Marr (1981) all consider the contact a structural non-conformity, citing (1) the occurrence of more complex deformation fabrics in the Chopawamsic metavolcanic lithologies with respect to those of the metashale, (2) the fact that the Ellisville granodiorite intrudes Chopawamsic lithologies but not the shale deposits, and (3) the occurrence of conglomeratic metasediments in the basal part of the shale as evidence for this view. The divergent hypothesis put forth by the present study stems, first, from the recognition of the stratigraphic significance of the basal shale silicate iron formation marker, and second, from a different genetic interpretation for the upper Chopawamsic quartz-mica schists and the variety of quartzite deposits.

Marr (1981), focusing on rarely preserved sedimentary structures such as crossbedding and channel fills with "jelly bean gravels," classifies the

quartz-mica schists and quartzites as unconformity-related sediments derived from weathering of Chopawamsic volcanics. Indeed, he actually treats these rocks as a lower conglomeratic micaceous schist unit of the Arvonia metashale and correlates banded quartzites at the base of the metashale with the kyanite quartzite at Willis Mountain. In contrast, the present writer would contend that these particular lithofacies stem from a late Chopawamsic volcanic episode related to the intrusion of voluminous granodiorite magma along the Chopawamsic belt. The varying products of this igneous event would include the Ellisville body and the unnamed intrusive in the Appomattox area at the south end of the map area. The pervasively saussuritized but weakly metamorphosed dioritic sills occurring both peripheral to the Ellisville granodiorite and along the flanks of the Columbia synclinorium may also have been intruded at this time. The ultramafic facies locally affiliated with these latter bodies, moreover, suggests peridotitic magma as a possible source for the peculiar magnesian amphibolite bodies that locally occur at the base of the metashales and regionally interband with upper Chopawamsic oxide iron formation along the entire length of the belt.

Lithological support for a direct link between the quartz-mica schist and the granodiorite intrusives is provided, first, by the transition from porphyritic granodiorite to quartz eye porphyry where the Ellisville granodiorite borders on the closure of the Arvonia synclinorium, and second, by the occurrence of a felsitic border zone between quartz-mica schist and granodiorite in the case of the Appomattox River body. Further evidence for a volcanic-related origin may be inferred from the nature of the lithologies themselves. Over the course of the present investigation, the sedimentary structures noted by Marr were observed only rarely, and the author is of the opinion that these can be adequately explained as the products of local

winnowing and redeposition of pyroclastic volcanics prior to lithification. The "jelly bean gravels" cited as evidence for conglomeratic sedimentation, similarly, can equally well be interpreted as uniform quartz eye tuffs locally winnowed into lag "quartz eye conglomerate" deposits. Above and beyond such interpretive differences as these, however, is the fact that the occurrence of porphyritic felsite beds interbanded with quartz-mica schist in the Tower Hill area militates quite definitively against any such wholly sedimentary genetic scheme as Marr advocates for this particular facies.

The varied quartzite deposits occurring at this same basal metashale stratigraphic position are admittedly far more elusive from the standpoint of genesis. It obviously must be conceded that such deposits as the crossbedded Bremo feldspathic quartzite with its common quartz pebbles and shale rip-up clasts signify a sedimentary environment such as a delta debouching into a shale basin. However, in the case of the laminated feldspathic quartzite deposit in the South Anna River area, rocks of roughly similar composition to the Bremo quartzite, evidence for current activity is completely lacking.

The origin of the stratigraphically correlative and spatially related kyanite quartzite units has been and remains a geological enigma. The genesis of the Willis Mountain kyanite quartzite was by far the most debated topic at the 1981 symposium held in Farmville, Virginia, where the results of Marr's (1981) mapping of Andersonville and Willis Mountain quadrangles were presented. The internal bedded nature and considerable strike length were cited in support of a sedimentary origin while its unusual composition was considered by many as indicative of a link to hydrothermal volcanic processes. If, indeed, the Willis Mountain kyanite quartzite did have its origin in the clastic sedimentary processes hypothesized by Marr, the large, regular, three to four meter beds evident in the east ridge pit of the active

kyanite mining operation suggest a subtidal depositional regime and not a fluviatile origin as he postulates (Good 1981, personal communication). It is, however, considered by this author easier to account for the strataform nature of the kyanite quartzite without invoking a strictly clastic sedimentary regime than it is to account for the peculiar compositional characteristics, particularly the presence of beds with abundant disseminated pyrite, within such a regime. This holds even more for the sometimes related, mineralogically complex gahnite-staurolite-bearing quartzites and tourmalinites. As a result of these ambiguities the specific petrogenesis of these rocks remains problematic. The issue will be considered again on geochemical grounds in the following chapter.

This interpretation of a volcanogenic origin for what have been considered unconformity-related sediments forces a reconsideration of the entire regional stratigraphic relationship between the upper Chopawamsic metavolcanics and the overlying metashales along the belt. Although the base of the Buffards quartz-mica schist is not exposed in the core of the Arvonia synclinorium, ironstone and quartz-mica schists are so intimately interbedded in the core of the Whispering Creek anticline and again in the core of the Columbia synclinorium that these lithologies cannot be wholly differentiated from each other on a regional scale. Certainly there is no indication of a structural discontinuity between them. It therefore seems probable that at their base the quartz-mica schists transit into the regionally extensive cummingtonite-hornblende - ironstone-oxide iron formation assemblage that caps the Mineral assemblage. Locally the quartz-mica schists change facies to fluviatile sandstones (represented by the Bremo feldspathic quartzite) and laminated aquagene tuffs (represented by the South Anna feldspathic quartzite), and collectively these latter deposits are either capped by or

transit laterally into the extensive kyanite quartzite units. This assemblage as a whole forms a complex which deposition of the basal shale silicate facies iron formation both overlapped and capped.

In the light of these features, the change from Chopawamsic volcanism to pelagic sedimentation appears not to have been marked by a period of non-deposition, as is implied by the unconformity hypothesis, nor is there evidence that the metashales were deposited on a previously metamorphosed substratum. Rather, it seems more plausible that the late intrusion of voluminous granodiorite along the Chopawamsic metavolcanic belt which initiated widespread pyroclastic activity was accompanied by tectonic instability and possibly by a regional metamorphic pulse as well. It is hence hypothesized that the diverse upper Chopawamsic group of lithologies actually signifies a synintrusive and/or synmetamorphic depositional regime. Such an intriguing geological environment could account for the seeming paradox suggested by the at least locally more complex deformation that has been cited by Conley (1978) and Pavlides (1981) in the Chopawamsic metavolcanics with respect to the metashale and also the regionally conformable stratigraphic relationships implied by the results of the present investigation. The hypothesis of a synmetamorphic depositional regime is considered further in the following sections on petrogenesis and metallogenesis.

Whether or not the regional metashale formations can be considered a "time line" is a further important consideration for stratigraphic interpretations along the belt. The occurrence of mid to upper Ordovician fauna in the Arvonia slate quarries (Tillman 1970) and again in the Quantico slates near Washington (Pavlides et al 1980) supports the likelihood that the onset of fine terrigenous to pelagic sedimentary conditions was indeed synchronous along the belt. Considering that the metashale synforms in the

area of this investigation are so spatially close and that the metashales are to a great extent lithologically similar in all cases, it seems probable that we are indeed looking at the remnants of a formerly continuous shale sheet.

Stratigraphic relationships east of the major Columbia and Arvonia metashale synclinoria have not yet been definitively resolved. It is clear that the lithologies comprising the Whispering Creek anticline on the southeast flank of the Arvonia synclinorium and the grossly similar lithologies on the east limb of the Columbia synclinorium must be considered as part of the Chopawamsic metavolcanics inasmuch as they can be directly correlated with lithologies along the core of the belt. The amphibolitic gneisses and granitic intrusive material comprising the Hatcher complex and the more or less continuous easterly plutonic gneiss terrane between the metshale synclinoria and the Spotsylvania lineament, however, bear a much more obscure stratigraphic relationship with the Chopawamsic suite.

The occurrence of amphibolitic gneisses in the core of the Andersonville district and the transition from amphibolitic gneisses into Mineral metavolcanics at the north end of the Hatcher complex along the western limb of the Columbia synclinorium are interpreted to indicate that the eastern amphibolite gneiss facies represents a mafic volcanic terrane generated contemporaneously with the Mineral metavolcanic suite. These amphibolite gneisses are therefore considered to be correlative with Pavlides' (1981) Ta River Metamorphic Suite of the northern Virginian Piedmont. Indeed, the amphibolitic gneisses forming a continuous tract along the eastern margin of the central Virginian segment of the Chopawamsic covered by this investigation appear to be co-extensive with the Ta River amphibolite gneisses. In this regard it is interesting that on the basis of his work in northern Virginia Pavlides also considers these gneisses to be an easterly facies of Chopawamsic

metavolcanics.

Other stratigraphic relationships are somewhat more problematic. It is possible that the paragneiss facies and perhaps also such orthogneiss lithologies as the Columbia granodiorite gneiss and the granitic to dioritic gneisses of the Hatcher complex are higher grade metamorphic equivalents to the siliceous components of the Mineral metavolcanic suite. More difficult to classify, however, is the large area of paragneiss interlayered with amphibolite gneiss in south central Andersonville quadrangle at the southern end of the project area. These particular rocks could be correlative with the undifferentiated paragneisses occurring east of the Spotsylvania lineament and the Farmville basin and exposed here in a domal structure, but on present evidence any such inference must be considered a highly speculative one. This latter group of gneisses is itself of uncertain age. Pavlides (1981) considers the correlative Po River gneisses near Fredericksburg to comprise older basement to the amphibolitic Ta River gneisses which he identifies as higher grade Chopawamsic equivalents. Inasmuch as a 1000 m.y.-old gneiss dome occurs about fifteen kilometers east of the present survey boundary in Goochland County (the State Farm gneiss dated by Glover, 1978), testifying to the presence of Grenvillian cratonic basement in this area, it seems likely that the Chopawamsic belt is bounded on the east by an older basement gneiss terrane comprising the outer Piedmont.

2.2.1 A Regional Stratigraphic Schema

Perhaps above all else the foregoing discussions have demonstrated that regional structural-stratigraphic interpretations have been and remain a controversial issue. Most of the problems which have plagued regional

geological interpretations stem from the fact that the Chopawamsic metavolcanic belt demonstrates the stratigraphic complexity typical of volcanic-sedimentary terranes in which lateral facies variations at the time of active volcanism played as important a role in producing lithological diversity as did temporal change. For this reason, "layer cake" stratigraphic models that portray only time-controlled aspects of stratigraphic distribution are not particularly informative; any adequate stratigraphic schema for an area such as this also has to take into account the space-related variation in any given "layer."

With these considerations in mind, the stratigraphic framework to be inferred from the results of the present investigation is reconstructed schematically in Figure 5. As illustrated, the basements to both the Candler metasediments and the Chopawamsic metavolcanics are currently unknown. Within the Chopawamsic belt, younger metashale synclinoria occur at the boundaries between the differing metavolcanic suites, making the stratigraphic relationships among the older suites difficult to ascertain. Broadly conformable stratigraphic relationships are, however, defined by overlapping deposition of various members of the diverse upper Chopawamsic group of rocks with the basal shale silicate facies iron formation. It therefore seems apparent that the Chopawamsic metavolcanic belt, with the possible exception of some of the high grade gneisses along the eastern border, comprises a stratigraphically coherent lithological enclave in which older volcanics transit into younger sediments.

It should be stressed that the ages attributed to the various lithological assemblages on Figure 5 are somewhat speculative. Only the mid-upper Ordovician age of the shale, the late Paleozoic age of the major orogenic event, and the Mesozoic age of the Farmville basin sediments and

Figure 5: Regional Stratigraphic Correlation Schema

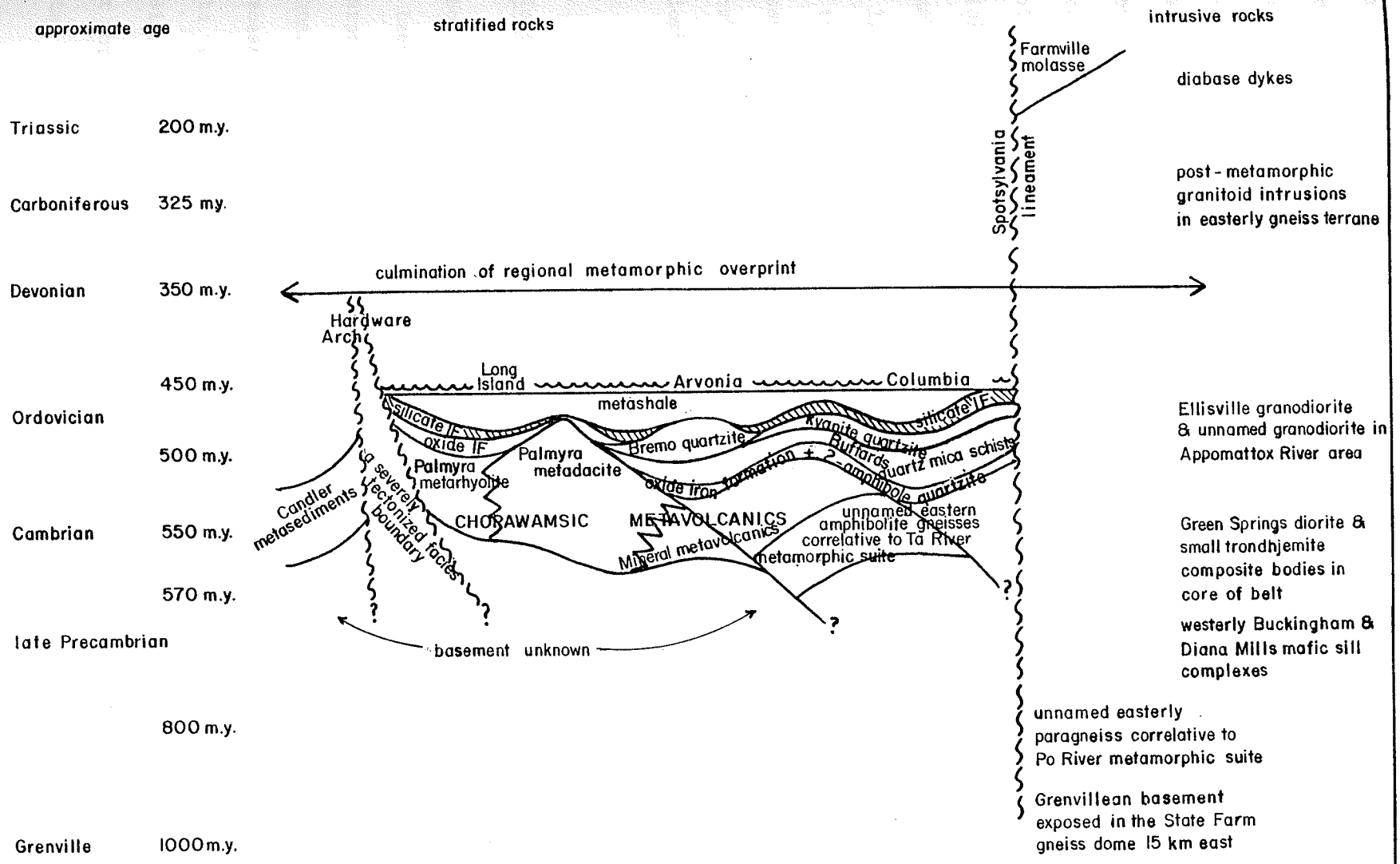

diabase dykes are known with any certainty. However, the fossils of Cambrian age recently discovered in Candler metasediments (Conley 1981, personal communication) would seem, on the structural-stratigraphic criteria cited above, also to suggest a Cambrian age for Chopawamsic volcanism. Complementing this, the sparse age dating (cited in the introduction) on comparative Chopawamsic metavolcanics outside the area of this investigation supports a general late Precambrian - Cambrian age for the various metavolcanic suites comprising the belt. The allocation of a middle to lower Ordovician age for the basal shale silicate facies iron formation, an age near the Cambrian-Ordovician boundary for the diverse upper Chopawamsic group, an older late Precambrian - Cambrian age for the Hardware magnesian schists and mafic intrusive complexes, and a post-Grenvillian age for the undifferentiated gneisses east of the Spotsylvania lineament is, however, supported only by the respective stratigraphic relationships between these lithologies and the lithologies for which ages are known.

2.3 Tectonic Analysis

Now that the structural features and broad stratigraphic relationships have been examined in isolation, our next task entails a synthesis and reinterpretation of the information collectively yielded by the preceding sections. Neither body of data can be adequately appreciated in isolation. The necessary interdependence and inter-reflectivity of these two critical aspects is, in fact, the single most important key to regional geological analysis. When structure is viewed in the light of stratigraphy, it is far easier for the researcher to differentiate between accidental and meaningful effects. Once the style of deformation is unravelled, conversely, it is

possible to reconstruct original lithological relationships with much more accuracy. It is, moreover, specifically in terms of this element of interplay between structure and stratigraphy that one may best define the unique tectonic framework of any area, thus laying the groundwork for a more complete historical/genetic recapitulation.

As we have seen, the most significant structural feature of the present study area is the presence of unusual folds in which younger rocks on fold limbs are flanked both on the outside and in fold cores by older lithologies. Conley (1978) and Conley and Marr (1979) suggest that the major Arvonia and Columbia fold structures comprise earlier synclinal folds wrapped around later antiforms, and that the fishhook-shaped outcrop pattern associated with the pinchout of the eastern synclinal metashale limbs in both of these structures results from early isoclinal fold closures. The author subscribes to the general thrust of this interpretation of synclinal limbs on antiformal cores, but the early, more northwesterly trending isoclinal folding event postulated by Conley and Marr is at odds with his opinion that, F_1 and F_2 being coaxial, there is no evidence to substantiate the existence of two temporally discrete overprints.

One important structural peculiarity of this area that any interpretation must come to terms with is the marked asymetry shown by steep westerly limbs and moderately shallow easterly limbs on both major synclinoria. This phenomenon, as noted above, is attributed by the present writer to interference of a steeply dipping F_1 isoclinal fold generation by broad, rather shallow F_2 fold structures such as the Whispering Creek anticline. Although widespread F_1-F_2 interference deformation patterns have not yet been demonstrated by any investigator, this may to a large extent be due to poor

outcropping conditions. Though one cannot ignore the fact that such patterns are not readily apparent even in the lithologies comprising the main F_2 structure, the discrepancy can perhaps be accounted for by the coaxial nature of F_1-F_2 events. Under such circumstances interference patterns would only be evident at fold closures. The repetition of marker beds like the garnet-grunerite iron formation and the kyanite quartzite units along the borders of the Whispering Creek anticline probably reflects the interference of broad F_2 warps on earlier F_1 isoclinal folds. Similarly, the shallowing of attitudes of earlier isoclinal folds by F_2 interference is considered to be responsible for the apparently disconnected nature of the basal shale silicate iron formation and kyanite quartzite strata along the eastern limb of the Columbia synclinorium. It is significant that the garnet-grunerite iron formation, as mentioned, is essentially the only subfacies of metashale found in the Whispering Creek structure. On the whole it seems reasonable to conclude that this anticline is a general structural and stratigraphic analogue to the Columbia synclinorium, with the difference in shape being largely attributable to regional variation in axial plunge. Such variation is also considered to account for the abrupt bulging of the Columbia structure in the South Anna River area.

The foregoing structural-stratigraphic hypotheses are graphically interpreted on the crossections included with Plate 1. It should be noted that many of the high angle axial planar shears or small scale thrust faults shown are inferred in places where parts of the stratigraphy seems to be missing. The most significant along-strike variations demonstrated by the major fold structures are illustrated by the three longitudinal sections. These latter are more speculative than the crossections as not enough lineation data is yet available to substantiate the shallow plunge reversals depicted.

When stratigraphy and structure are viewed in conjunction, numerous interesting regional geological features become evident. Foremost among these is the fact that the metashale infolds everywhere occur at major lithological breaks in the underlying Chopawamsic metavolcanic complex. This might mean that rather distal parts of the original volcanic terrane were structurally juxtaposed across shale infolds during foreshortening. Alternately, from a slightly different perspective, it could be taken to suggest that the original shale bed was thickest between volcanic ridges of varying character and these local basins became collapsed infolds during deformation. It is interesting, too, that the restricted upper Chopawamsic quartz-mica schist and diverse quartzite deposits are concentrated in the cores of major fold structures, a feature which also suggests that these major fold structures relate to original paleogeographic factors controlling deposition in late Chopawamsic times. Considering the foregoing lithological discussion, these may well have originally been rather isolated volcani-tectonic collapse structures attributable to crustal instability at the time of voluminous granodiorite magma intrusion. If this scenario is an accurate one, each particular volcani-tectonic sink must have had a slightly different depositional history in order to produce such broadly correlative but uniquely dissimilar lithologies as the Bremo crossbedded feldspathic sandstone in the Arvonia synclinorium and the South Anna laminated feldspathic aquagene tuff in the Columbia synclinorium.

Differing paleoenvironmental conditions affecting these depositional sites are considered to have been responsible for the production of such vastly different rock types as the basal shale silicate facies iron formation and the kyanite quartzite. It was probably environmentally significant, for

instance, that the former of these is always developed on only one side of any given metashale syncline. If the original oolitic chloritite documents above-wave base depositional environs, this presumably indicates that each individual shale syncline has a shallower and deeper water facies. Facies relationships among the various lithologies underlying the silicate facies iron formation are complex, but on the basis of regional distribution it seems apparent that the kyanite quartzite units cap the quartz-mica schist deposits and give way laterally to locally thick successions of feldspathic quartzite. A full explication of the original facies distributions in these early volcani-tectonic sink structures is beyond the scope of the present study, but it is the view of the author that lateral depositional facies variation may well account for much of the apparent structural complexity. As with the previously noted facies change from westerly shale to easterly basal shale silicate facies iron formation in both the Columbia synclinorium and again in the Whispering Creek anticline, that is, the identification of non-recognized lateral variations can provide simple, plausible alternatives to unwieldy and unduly complicated structural interpretations.

2.3.1 The Tectonic Setting of the Chopawamsic Metavolcanic Schist Belt

Having established our basic terms of reference, it is now time to reconsider the regional tectonic considerations outlined in the introduction in the light of the specific structural-stratigraphic framework inferred for the central Virginian segment of the Chopawamsic metavolcanic belt in order to determine whether the internal tectonic elements demonstrated by this terrane can in fact be adequately modelled by the favoured island arc interpretation.

To summarize, the Chopawamsic metavolcanic belt is separated from the Blue Ridge Grenvillian miogeanticline (which probably demarks the eastern edge of ancient North America) sequentially to the east by (1) the Lynchburg immature oceanic rift clastic sediment - mafic igneous rock associations, (2) the restricted Swift Run ash flow tuff and extensive Catoctin plateau basalts, and (3) the Candler basinal assemblage of mixed chemical sediment, distal terrigenous clastics, and greenstone of oceanic geochemical affinity. The boundary between Candler metasediments and Chopawamsic metavolcanics is a structural locus for uparched "basement" composed of localized mafic intrusive complexes in more regional severely cataclasized magnesian schists. The suggestion made by Pavlides et al (1974) and Drake and Morgan (1981) that the mafic complexes along this contact are dismembered slices of ophiolite, implying the existence of a mature oceanic basement, was found to have no supporting evidence. Rather, the mafic intrusive complexes are herein interpreted to stem from high level mafic diapirism which resulted in near-surface multiple sill injections and greenstone extrusion. There seems to be no support for the contention that the alignment of mafic diapirs was ever an active spreading ridge. It is possible, however, that individual diapirs may have related to a more or less continuous but "non-spreading" ridge, as this would acount for their present distribution along a regional lineament. On this basis one might conceivably postulate that the Hardware arch comprises a tectonic melange of a type of immature oceanic basement, but certainly not one generated by an actively spreading ridge such as those of present mature ocean basins.

The overlapping of greenstone units in Candler metasediments and Chopawamsic metavolcanics together with the increased volcanogenic components along the eastern margin of the Candler schists indicates that the contact

between these two assemblages was originally a facies break. Perhaps the non-spreading oceanic ridge signified by the lineament of mafic diapirs acted as the depositional facies barrier. The Palmyra assemblage felsic pyroclastics appear abruptly east of the ridge of mafic material. This might suggest a feature typically shown by modern island arcs; i.e., that in moving from oceanic to continental side the first volcanics form an abrupt igneous front, with the volume of eruption greatest at or immediately behind this front. The sharpness of the western Chopawamsic boundary and the differential deformation exhibited by the magnesian schists and Palmyra pyroclastics, however, may be taken as evidence that the contact is now a high angle thrust. On the other hand, it is obvious that not too much displacement occurred, as the presence of greenstones interbedded with Palmyra pyroclastics along the western edge would seem to suggest that we are still looking at original contact relationships.

Another feature that must be taken into account in deriving a tectonic model for this area is the fact that the voluminous Palmyra assemblage of felsic pyroclastics, rather than being deposited on a thick mafic volcanic substratum, was laid down on extensive but relatively thin greenstones. This high felsic to mafic volcanic ratio is in itself anomalous when compared to modern arcs. Although the dominating pyroclastic mode of extrusion shown by the Palmyra metavolcanic suite could be held to be analogous to the pyroclastic nature of volcanism in arcs, internal characteristics of these particular volcanics would seem to rule out such an interpretation in this case. Regionally the Palmyra assemblage comprises a laterally extensive belt composed primarily of a subaqueous accumulation of fine tuff, and there is no evidence to date to suggest that any large centralized stratavolcanoes with broad mafic bases and more restricted upper parts (as are typical of modern

island arc volcanism) ever existed here. More significantly, no lithology yet documented gives evidence of a major centralized vent area. To be sure, the metarhyolite flows in the vicinity of Little Mountain south of Palmyra do suggest nearness to an extrusive source area, but even here features are more consistent with a regional fissure system given to sporadic non-centralized extrusive activity along its length than with island arc-type volcanoes.

The evident lateral separation of the westerly rhyolitic and easterly intermediate volcanic facies of the Palmyra assemblage is also at variance with the characteristics of modern arcs, where this facies change is typically vertical due to earlier intermediate and later rhyolitic volcanic facies being extruded. The slightly coarser nature of the intermediate pyroclastics in the case of the Palmyra metavolcanic suite might suggest that the lateral differentiation could result in part from the coarser intermediate lithologies being more proximal to a single locus of fissuring represented today by the Ellisville granodiorite to the north and the intermediate pyroclastic and flow series between the Long Island and Arvonia metashale infolds. It is the opinion of this writer, however, that the gross differentiation into a westerly rhyolite facies with its attendant interlayered felsite sills and an easterly intermediate facies accompanied by crystal tuffs and flows argues more strongly for differing lateral vent systems tapping magma sources of differing composition. This is an aspect of modern arcs which is evident only on a mega-scale, signalled by such features as the regular increase of potassium content with the depth of the Benioffe zone across the arc complex (Dickenson 1975). The apparent close spatial proximity coupled with the fact that the rhyolitic and intermediate facies do in part overlap in the case of the Palmyra assemblage militates quite decidedly against any such mega-scale mechanism being an effective control on the apparent lateral variation shown

in this assemblage. On the whole it would seem that although some gross parallels can be drawn between the Palmyra assemblage and frontal arc volcanics, there are even more significant differences.

The Mineral assemblage, composed as it is of considerable epiclastic sediment interlayered with bimodal mafic-silicic volcanics and ironstone, is lithologically distinct from the Palmyra assemblage, evidently deriving from a different volcanic depositional setting. The greater amount of epiclastic sediments suggests a much more active sedimentational regime. In the northern area the mafic and to some extent the silicic units as well are quite persistent along strike and could conceivably stem from a focus for fissure effusion along a trend located slightly east of the center of the assemblage, since volcanic flow units intensify in this zone. The extensive development of ironstone-iron formation along the eastern side of the assemblage, moreover, suggests that hydrothermal activity within the setting was particularly long-lived. Collectively, then, the lithologies of the Mineral assemblage may plausibly be interpreted as having their source in a volcanically active rift in the central eastern part of the belt.

This postulated active volcanic rift east of the Palmyra "volcanic front" can be roughly compared to the back arc basins developed in modern island arc terranes. Just as the Palmyra feature differs significantly from the volcanic fronts of modern arcs, however, the Mineral assemblage also differs considerably from deposits in modern back arc basins. The latter are typically somewhat similar to modern ocean basins in being floored by mafic volcanics overlying oceanic crust with very little sedimentary cover (Karig 1971). The Mineral rift, in contrast, was a site for the deposition of considerable epiclastic sediment, for a significant silicic volcanic input,

and for a prolonged hydrothermal period (reflected in the presence of extensive ironstone-iron formation); none of these lithological features are particularly characteristic of the modern back arc basin. Also, it must be emphasized that there is no evidence known to date to suggest ophiolitic components. This in itself strongly argues against any direct comparison with the kind of active spreading regime commonly evident in modern back arc basins. It is true, as previously noted, that Pavlides (1981) imputes an ocean floor basalt affinity to the geochemical signatures of the Ta River mafic gneisses (correlative with the amphibolitic gneisses along the eastern side of the Chopawamsic belt), but it nevertheless remains debatable whether this easterly mafic volcanic facies was in fact generated at a mature ocean floor spreading ridge.

From all this it seems clear that the favoured interpretation of the Chopawamsic metavolcanic belt as a paleo-island arc site is far from unequivocal. The comparison is a useful one if only because it helps to elucidate the specific ways in which the present terrane diverges from the conventional setting, but once the similarities and differences are catalogued the question remains: what kind of tectonic model will comprehend all the peculiarities of this area. If nothing else, we can be fairly confident that these metavolcanics were indeed generated in late Precambrian-early Paleozoic times. We also know, notwithstanding all the foregoing qualifiers, that the original environment was at least in some ways similar to that of a modern island arc. Occurring along the east margin of the ancient Iapetus Ocean and at the west boundary of a Grenvillian cratonic fragment (undifferentiated gneisses east of the Spotsylvania lineament), this setting evidently comprised segments roughly analogous to a "volcanic front" (Palmyra suite) and a "back arc volcanic rift" (Mineral suite and easterly amphibolitic gneisses). Having

gone so far, however, we come up against the incontrovertible fact that little viable correlation can be made between the Chopawamsic metavolcanics and actual modern island arc volcanics on a lithological level. And here is where we have to part company with the island arc model. Recognizing that the lineament of mafic intrusive bodies along the western margin of the complex may quite plausibly be taken to reflect a non-spreading oceanic ridge and assuming, further, that the Palmyra assemblage could equally well be interpreted as representing separated westerly rhyolitic and easterly intermediate fissure systems and the Mineral assemblage a central, volcanically active rift setting subject to considerable sedimentary influx, one might suggest as a viable alternative the following scenario. Although the Grenvillian craton would seem to have undergone widespread extensional tectonism in late Precambrian-Cambrian times, the tensional conditions were never resolved by mature ocean spreading processes, giving rise instead to multiple lateral volcanically active fissure systems. The upwelling of voluminous buoyant granodiorite magma late in the history of rifting resulted in further unstable tectonic conditions that are now reflected in the distribution of the diverse upper Chopawamsic group of rocks. Following the late intrusive period, the terrane evolved as a sedimentary (successor) basin that served as a depository for extensive shale.

This three-stage tectonic evolutionary model for the central Virginian segment of the Chopawamsic metavolcanic belt is illustrated in Figure 6. The question of scale is left open on this diagram. Considering the marked facies changes that may be observed across the present shale infolds, the original volcanic terrane was most certainly considerably more laterally extensive than is now apparent, but how wide remains entirely speculative. In any case, as there is no evidence that any mature ophiolitic oceanic crust was obducted

during the later foreshortening events, there is no basis for postulating that the internal tectonic elements were brought into their present conjunction by modern plate-tectonic ocean-closing mechanisms.

The major regional metamorphic overprint postdated shale deposition. The 300 m.y. K/Ar age date on the Arvonia shales reported by Harper et al (1973) signifies the age at which metamorphic temperatures cooled enough to inhibit further argon loss. According to Fullagar (1971), a similar (342±70 m.y.) age for metamorphism is indicated by the K/Ar dating on biotite and potassium feldspar separates from the Columbia granodiorite gneiss. Many of the intrusive facies occurring in the eastern plutonic terrane, moreover, also derive from a late-Paleozoic time. A variety of intrusives examined by Pavlides et al (1979), for instance, are reported to fall in the 410-330 m.y. range. Finally, the 330±8 m.y. age reported by Wright et al (1975) for the Petersburg granite that forms masses of batholithic dimension in the outer Piedmont testifies to a metamorphic event culminating in late Paleozoic times which resulted in widespread intrusive activity in the Grenvillian fragment east of the Chopawamsic belt.

At present it is not known specifically how the deformation recognized throughout the belt is related to this late-Paleozoic regional metamorphism. However, the fact that F_1 and F_2 are coaxial implies that they probably resulted from a prolonged period of episodic northwest to southeast-oriented compressional tectonism. Also, one might speculate that since the late north-northwest cross structures lie approximately parallel to the direction of compression, this tectonic grain could have resulted from variation in deformation rates along the length of the deforming belt. The only remaining tectonic developments of any importance to have affected the area stemmed from

FIGURE 6: A THREE-STAGE TECTONIC EVOLUTIONARY MODEL FOR THE CHOPAWAMSIC METAVOLCANIC BELT

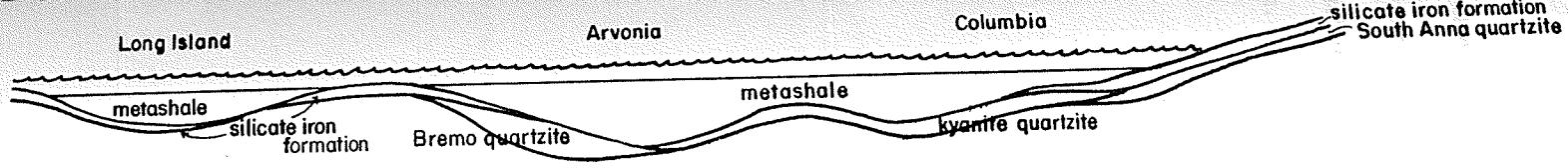

Stage III
Post Volcanic Successor Shale Basin

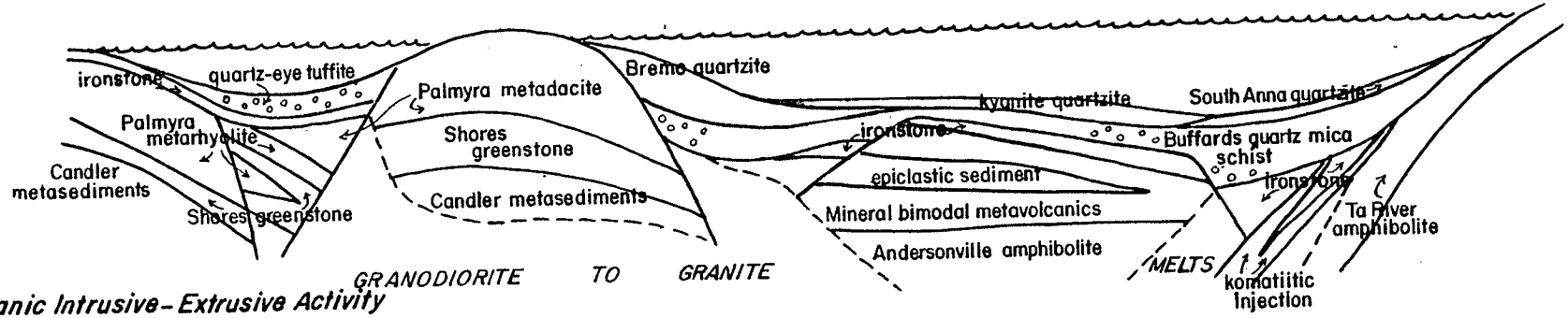

Stage II
Late Volcanic Intrusive-Extrusive Activity

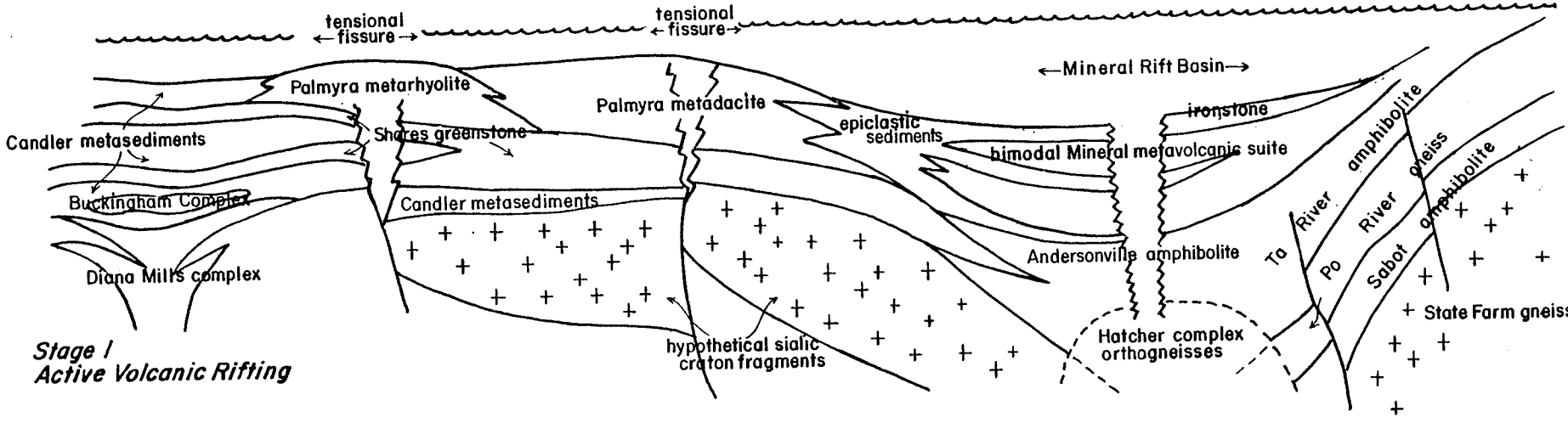

Stage I
Active Volcanic Rifting

the extensional conditions consequent upon the opening up of the Atlantic in Triassic times (Clifford 1968). This particular event resulted in the formation of the Farmville basin and the widespread emplacement of diabase dykes.

3. PETROGENY

Having now viewed the central Virginian segment of the Chopawamsic metavolcanic belt within its broader tectonic milieu and, on the basis of the regional geological framework, derived an evolutionary schema for the belt itself, attention may be turned to the more critical task comprising the ultimate objective of this investigation, i.e., elaboration of the key petrogenetic processes inherent within this particular setting. Numerous petrogenetic processes have, of course, been alluded to throughout the foregoing chapter as well as in Appendix B of physical rock descriptions, and it is expressly not the aim of the present chapter to reiterate what is already implicit in this data. Rather, this section addresses itself specifically to such broader petrogenetic aspects as magma types, volcanic lineages, hydrothermal processes, and so on, which have played primary roles in creating general petrogenetic conditions for the belt as a whole.

This part of the study is based essentially on geochemical criteria. The supporting data includes whole rock major and trace element analysis on a suite of 142 representative samples selected from drill core and surface handsamples free of weathering. Forty-eight 20-element analyses were completed at the University of Manitoba and 94 22-element analyses carried out by X-Ray Assay laboratories Ltd., Don Mills, Ontario. In both batches, combined XRF and A.A. analytical techniques were employed. As FeO, CO_2, and H_2O were not analysed by X-RAL, these particular elements were determined at the University of Manitoba for all specimens. This whole rock data is listed

in Appendix C, and in the text to follow the chemical features are illustrated on graphical plots selected to highlight diagnostic geochemical signatures.

Before elaborating on the regional petrogenetic processes as reflected in these geochemical signatures, we will briefly consider the chemical effects of metamorphic-metasomatic overprinting, as the possibility of post-depositional elemental mobility has an important bearing on the interpretation of the geochemical data. Inasmuch as evidence for the nature of metamorphic recrystallization and/or hydrothermal alteration processes must essentially reside in petrographic criteria, this discussion will draw heavily on the petrographic descriptions summarized in Appendix B. Following this, the bulk compositional signatures demonstrated by key lithologies will be examined in some detail with the aim of determining which specific petrogenetic processes have been most significant in the development of rock types within the belt. Throughout this inquiry, which will focus exclusively on igneous rocks and those thought to reflect hydrothermal processes, there will be a concerted attempt to explicate the petrogenesis of individual facies with specific reference to the regional geological framework previously established. The chapter concludes with a few comments on magma genesis and hydrothermalism within the belt.

3.1 The Geochemical Effects of Metamorphic-Metasomatic Overprinting

Classical treatments of the petrogenesis of regionally metamorphosed rocks have generally focused on the problem of determining the metamorphic conditions to which the rocks were subjected. Given a certain bulk composition and assuming isochemical metamorphic recrystallization, these

regional conditions are specified by coexisting mineral assemblages, which will change systematically with mineral reactions across any metamorphic gradient. The study of metamorphic mineral reactions (Winkler 1976, Thompson 1976 a & b, Mueller & Saxena 1977) has accordingly culminated in petrogenetic grids illustrating the pressure-temperature conditions over which particular coexisting mineral assemblages are stable. In the case of the study area, a regional metamorphic gradient ranging from westerly low grade (mid-greenschist facies) to easterly medium grade (amphibolite facies) conditions has been previously alluded to. The coexisting mineral assemblages that signal the existence of such a gradient are listed in Table 8. When the relevant reactions of this series are plotted on a petrogenetic grid (Figure 7), they collectively indicate a Barrovian style of regional metmorphism that ranges in an approximate manner from low grade (~500°C and 5 kb) conditions along the western side of the belt, through a low to medium grade transition (600°C and 6 kb) along the core of the belt, to higher medium grade conditions (700°C and 7 kb) in the easterly gneiss terrane. Notwithstanding the ostensible clarity of these gross results, however, more recent studies on mineral equilibria in naturally occurring metamorphic rocks reveal that a full understanding of phase equilibria requires chemical analysis of all the coexisting minerals in order to determine the effects of different metamorphic conditions and of bulk rock composition on mineral chemistry. For instance, because (as demonstrated by Laird, 1980) many of the minerals in mafic schists show complex solid solutions, rather than the coexisting mineral assemblages changing with metamorphic grade (as they do more readily in pelitic rocks), mineral compositions and modal proportions vary continuously. A precise unravelling of phase equilibria in many non-pelitic compositions is consequently impossible without full chemical analysis of both the bulk rock and all the coexisting minerals. This kind of detailed study is obviously beyond the

Table 3-1 Metamorphic Mineral Assemblages

WEST	LOW GRADE	LOW GRADE/MEDIUM GRADE TRANSITION	MEDIUM GRADE	EAST
	Long Island	Arvonia North	Arvonia South & Columbia	
Metashale				
qtz+ser+chl±bio		qtz+ser+chl+bio±chld	qtz+ser+bio+gnt±chl±chld±staur	
Silicate Iron Formation				
iron chl+qtz+ser		iron chl+qtz	gnt+qtz+grun±chl±bio	
Diverse Upper Chopawamsic Group				
ferruginous metapelite qtz+ser±chl±ep±bio±Mn gnt		kyanite quartzite qtz+ky±musc		
metamarl chl+ep+carb+qtz±bio±act		feldspathic quartzite qtz+ab+kspar±musc		
		quartz mica schist qtz+musc+kspar+silli+bio+gnt ±chld±ky		
		two-amphibole ironstones qtz+hb+cum+ab±gnt±chl±staur±ky		
		magnesian amphibole anth+trem±Mg chl±tc		
Palmyra Assemblage		Mineral Assemblage		Eastern Gneiss Terrane
metarhyolite alk feld+qtz+ser±ct±bio		epiclastics qtz+ser+bio+feld+gnt±ep±carb		granitic orthogneiss alk feld+qtz+bio+musc±hb±ep±gnt
metadacites ep+feld+qtz+chl+ser±bio		silicic volcanics alk feld+qtz+ser±bio±gnt±ep±carb		paragneiss plag+qtz+bio+micro+musc±hb±ep±gnt
metaandesites plag+hb+ep+qtz±chl±ser		pyritic ironstones qtz+ser+ab+Mg chl+bio+gnt		amphibolitic orthogneiss plag+hb+qtz+gnt±ep±bio±musc
		biotite carbonate ironstones carb+bio+qtz+gnt±chl±chld±musc± staur±ep±ky		
		mafic ironstones ab+hb+qtz+bio+gnt±cum±act±ep± chl±musc±staur±carb±ky		
		mafic volcanics plag+hb+qtz+act+bio+ep+gnt±carb		
		chloritites Mineral District Mg chl+gnt+staur+Mg bio+tc± musc±silli±ky		
		New Canton trend Mg chl+gnt+qtz+musc±silli±staur		
		Andersonville district gnt+Mg chl+Mg bio+qtz+staur± cum±anth		
Candler metapelite qtz+chl+ser±bio±carb				
Hardware Magnesian schists Mg chl+tc+musc+phlog+qtz±serp± ep±trem				

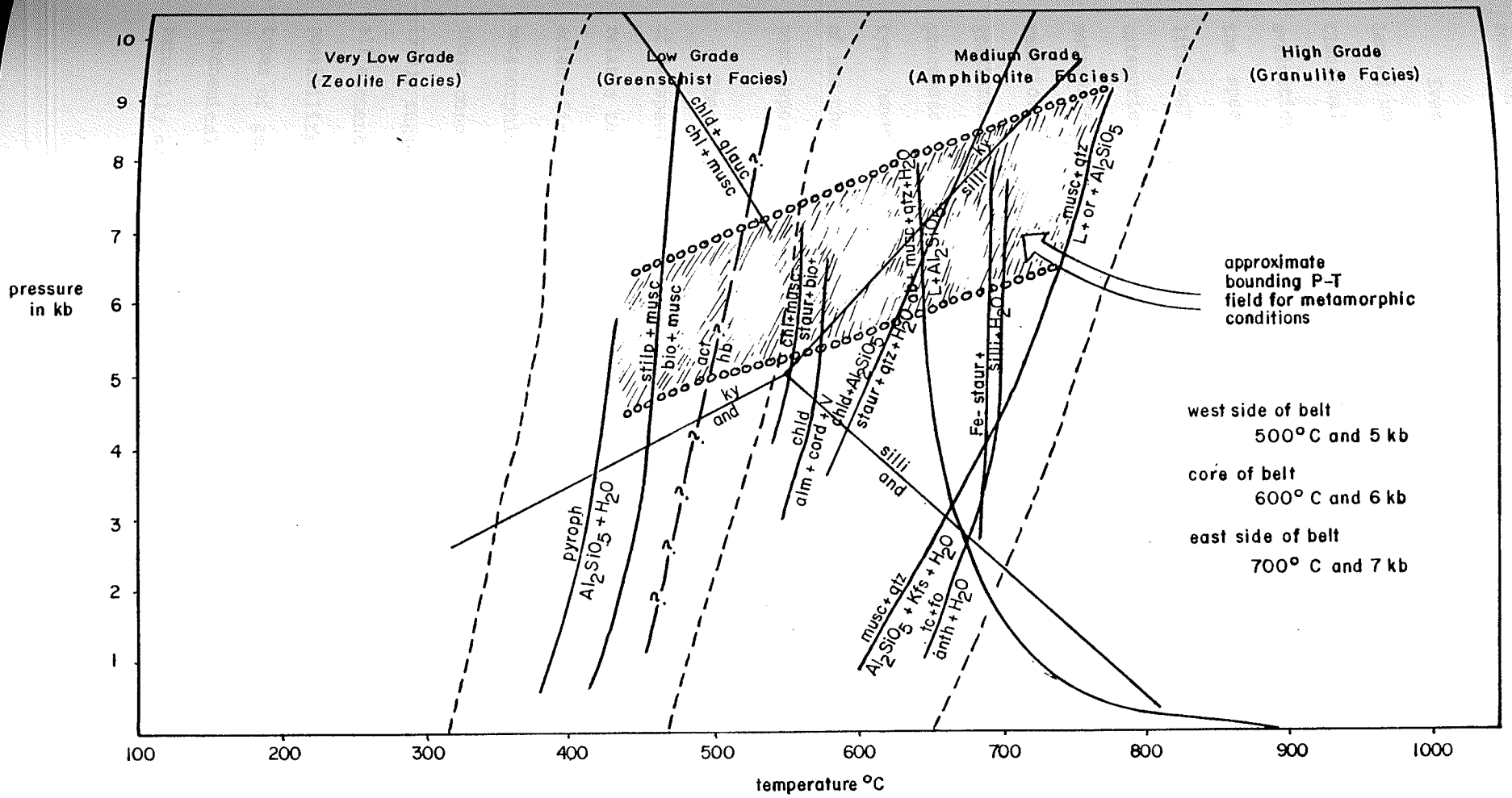

Figure 7: Metamorphic Petrogenetic Grid Showing Approximate P-T Gradient Across the Chopawamsic Metavolcanic Belt

stilp + musc out/bio + musc in
approximate stability limit of actinolite } Winkler 1976
chlt + Al_2SiO_5 → staur + qtz H_2O – Greve & Fawcett 1974
pyroph → Al_2SiO_5 + H_2O – Kerrick 1968
all other boundaries from Mueller & Saxena 1977

scope of the present investigation.

Even aside from methodological difficulties, the traditional approach leaves unanswered many of the questions this writer considers crucial. Classical studies have not in general striven for any sort of critical evaluation of premetamorphic petrogenetic phenomena nor, typically, addressed the specific problem of how the particular bulk composition of a given lithology was originally derived, focusing rather on general compositional categories, such as pelitic, mafic, and ultramafic rocks, and investigating metamorphic reactions with the object only of determining what isochemical reactions would occur within such generalized categories across a metamorphic gradient. When considering what specific premetamorphic petrogenetic processes might be reflected in the geochemical signature of a particular rock type, however, it is of paramount importance that one has a full understanding of how the bulk composition of that particular rock type was affected by post-depositional overprinting.

There is a good deal of work being carried out at present from a variety of perspectives to discover how the bulk composition of metamorphic rocks relates to their premetamorphic progenitors. Without criticizing either the scientific basis or the relevance of classical studies of isochemical metamorphic mineral reactions, numerous recent investigations, particularly those concerned with the modern sea floor (Spooner & Fyfe 1973, Wolery & Sleep 1976), suggest regionally extensive allochemical processes wherein most if not all elements are to some extent mobile under some PTX conditions. With the possibility of wholesale chemical exchange systems operative within certain types of geological environment, it begins to seem as though traditional isochemical studies have, in some cases at least, oversimplified a number of naturally occurring "hydrothermal metamorphic" phenomena. On the other hand,

the study of these phenomena being yet in its infancy, it is somewhat problematic whether or not such regimes should be classified as metamorphic environments at all, considering the possibility that wholesale chemical exchange may here be diagnostically more important than the actual intensity of the metamorphic overprint. For this reason this particular type of regime is for the purposes of the present study designated simply as a regional hydrothermal metasomatic one. The advantages to this approach are substantial. By differentiating hydrothermal metasomatic from metamorphic processes in such a way one may limit the category of metamorphic phenomena to solid state transformations which may then be considered along traditional lines; i.e., allowing for such chemical mobility as dewatering and desilication but typically not accommodating wholesale hydrothermal metasomatic adjustments. Alternately, environments wherein regional hydrothermal metasomatism has been operative can be considered as something quite apart from common regional metamorphic overprints.

Significantly, in presentday settings where regional hydrothermal metasomatic conditions are still active, such as the ocean floor, the hydrothermal metasomatic processes are operative contemporaneous with deposition. If one may take such environments as exemplary, it seems only reasonable to conclude that correlative settings where such conditions reigned in the past should be treated similarly, that is, as depositional sites characterized by intrinsic anomalously high hydrothermal-geothermal conditions at the time the lithological succession was laid down. More specifically, recent geothermal and hydrothermal studies of hot zones in the modern sea floor (Hayman & Kastner 1981, Corliss et al 1979) have indicated that temperatures of several hundreds of degrees C can exist at least locally very close to the rock-water interface. That such anomalous conditions can

accompany some depositional sites today seems to offer irrefutable proof that hydrothermal metasomatism is in fact not a later, secondarily imposed event, as has been the traditional view of metamorphism, but, rather, a syndepositional petrogenetic phenomenon. Regions subject to such intrinsic hydrothermal adjustment would subsequently be overprinted in the same manner as other depositional environments by quasi-isochemical metamorphic events, though in such secondary development only the fugitive elements would be to any degree mobile.

In establishing the utility (as opposed to the theoretical viability) of such an interpretation it is admittedly necessary to demonstrate how primary hydrothermal metasomatic overprints can be differentiated from later metamorphic ones. In the case of the present investigation, at least some aspects of these differing types of overprint are considered to be readily distinguishable on textural criteria, inasmuch as evidence may be derived for two distinct episodes of overprint. Where the overprinting of earlier syndepositional hydrothermal metasomatic effects by late metamorphic fabrics may be observed most clearly is in mafic metavolcanics, particularly the greenstone bodies that occur along the western contact of the Palmyra assemblage. From microscopic to megascopic scales these greenstones are heterogeneous, with late metamorphic fabrics and mineralogy clearly overprinting an earlier spilitization regime (the degree of elemental mobility during the metamorphic event is perhaps best reflected in the common nodular segregation of epidote in the metaspilities). The felsic metavolcanics are far less obviously affected by syndepositional hydrothermal alteration, and where evidence of such alteration is present it is localized essentially in flows, taking the form of crosscutting stringery vein systems. These veins, however, show the same effects of the late metamorphic overprint as does the

host rock (i.e., the hydrothermal vein paragenesis has typically recrystallized to metamorphic assemblages rich in a variety of porphyroblasts), thus implying the same basic history as the mafics, albeit more subtly. Against this, it is noticeable that the epiclastic sedimentary facies typically do not manifest any petrographic features indicative of early hydrothermal alteration at all, exhibiting only late metamorphic recrystallization features such as aligned mineral fabrics and the growth (commonly syntectonic) of porphyroblasts. This apparent absence of evidence for hydrothermalism may perhaps be accounted for by postulating that the epiclastics were not so much in disequilibrium with the ambient hydrothermal fluids as were the primary volcanic rocks.

The differentiation of late metamorphic from early hydrothermal metasomatic effects on such textural criteria does not, of course, specify the timing of the regional hydrothermal metasomatic processes with respect to the depositional period. The textural features indicate only that widespread hydrothermal alterations occurred at some time before the late metamorphic overprint, not necessarily that this was contemporaneous with deposition. However, throughout the area of investigation numerous intimate lithological relationships may be observed to occur between rocks which are obviously hydrothermally altered on the one hand and chemical sediments on the other. As pointed out by Ern (1968), for instance, many of the quartzite units in the Candler metasedimentary series occur in close proximity to the greenstone; on the basis of this lithological association one might postulate that greenstone extrusive events were accompanied by an increased silica supply in the immediate vicinity of the mafic flows, resulting in the enhanced precipitation of silica to form the quartzites. As the greenstone beds are themselves pervasively spilitized it is conceivable that a syndepositional hydrothermal

metasomatic regime was a major determinant in creating the chemical anomalies which produced the enhanced silica precipitation. Similarly, convergence of spilitized greenstone with marly metasediments and felsic metavolcanics with ferruginous metapelites, as is the case in the Palmyra assemblage, and of mafic metavolcanics with mafic ironstones and silicic metavolcanics with pyritic ironstones, as is the case in the Mineral assemblage, is considered to provide unmistakeable evidence for syndepositional hydrothermal regimes in which volcanics were pervasively hydrothermally altered and chemical sediments resulted from chemical anomalies related to the discharge of hydrothermal fluid onto the sea floor. Significantly, the irregular zones of hydrothermal alteration affecting the volcanics are not evident in the strikingly well-banded "hydrothermal sediments." The fact that both the former and the latter are conspicuously overprinted by metamorphic fabrics, showing such features as varied porphyroblastic populations specifically determined by local bulk rock compositional variations, indicates clearly, however, that both the earlier "syndepositional" hydrothermally altered rocks and the hydrothermal sediments are overprinted by the late quasi-isochemical metamorphic recrystallization.

The recognition of a widespread syndepositional metasomatic regime helps substantially in resolving such petrological problems as the origin of the enigmatic ironstones interlayered with metavolcanics, the peculiar hydrothermal chloritite found accompanying massive sulphide mineralization hosted in the Mineral assemblage, and the numerous facies (tourmalinite; varied species of iron formation; ironstone; pyritic, kyanitic, staurolitic, and gahnite-bearing quartzite) of the diverse upper Chopawamsic group. The effects of syndepositional hydrothermal conditions may also be reflected in the petrographic nature of the magnesian amphibolites exhibiting rather

massive fibrous to radiating textures which, not being obviously either remnant igneous or metamorphic in character, may conceivably signify subsolidus hydrothermal cooking in an anomalous geothermal-hydrothermal zone subsequent to the initial high level injection of ultramafic magma.

In the light of all these considerations it seems clear that textural criteria do indeed provide a useful and discrimating tool for differentiating between syndepositional hydrothermal metasomatism and late quasi-isochemical metamorphic overprinting events. In fact there is ample evidence to indicate that the scale of elemental mobility manifested texturally for these respective overprints differs remarkably. For the purposes of the ensuing discussion of geochemistry, the metamorphic elemental mobility which is evident at the thin section scale but does not affect rock volumes as large as a handsample is considered "quasi-isochemical." Conversely, elemental mobility which is evident not only at the handsample level but at outcrop and even larger scales is classified as hydrothermal metasomatic in origin. In this regard, it is important to remember that although the whole rock geochemical data discussed below does reflect premetamorphic bulk compositions, it necessarily entails as well the effects of syndepositional hydrothermal metasomatic readjustment. To be more specific, where hydrothermal alteration has occurred, although the premetamorphic composition can be determined easily enough through analysis, one must be cognizant that the composition prior to hydrothermal alteration is going to be irretrievable unless the altered zones can be traced into unaltered precursors. It should be noted, on the other hand, that even very subtle hydrothermal alterations are often accentuated by porphyroblastic growth zones produced during the metamorphic overprint, so it is generally possible to differentiate the hydrothermally altered and unaltered zones within the parental lithologies without much trouble.

The following discussion of the petrographic implications of whole rock geochemical data is grossly structured by an evolutionary schema based on the regional geological framework elaborated upon in Chapter 2. The petrochemical characteristics of intrusives, extrusives, and rocks of hydrothermal origin are discussed sequentially under separate headings. Within these subsections the compositions of similar rock types from the different lithological assemblages are compared for the purpose of illustrating varying petrologic conditions. In addition to this, different rock types from the same assemblages are compared and evident geochemical affinity considered from a petrogenetic standpoint.

3.2 Petrogenesis of Intrusives

Intrusive rocks along the segment of the Chopawamsic belt covered by the present investigation include: (1) the ultramafic, mafic, and intermediate facies constituting the intrusive complexes along the western side of the belt, (2) minor isolated but regionally widespread granophyric-quartz diorite bodies in the Mineral assemblage, (3) the Ellisville porphyritic sill and stock with peripherally associated late gabbro-diorite bodies which also locally have affiliated ultramafic facies, and (4) granitoid orthogneisses together with postmetamorphic intrusives in the easterly gneiss terrane. The ultramafic magnesian amphibolites, occurring in the diverse upper Chopawamsic group capping the Mineral assemblage are also provisonally assigned to this intrusive suite in order to facilitate a comparison of the composition of this facies with recognizable igneous ultramafics along the belt.

As previous petrographic descriptions of these rocks suggest, the western intrusive facies occurring in the low grade (mid-greenschist) metamorphic

terrane have evidently been to a large extent immune to overprinting by metamorphic fabrics and as a result commonly retain igneous textures. Only the border zones of the main intrusive complexes and the thin affiliated apophoses show common metamorphic schistosity. It is notable, however, that although much of this intrusive material manifests primary igneous textures, its pyrogenetic mineralogy is pseudomorphed by greenschist facies mineralogy; i.e., the mafic minerals are commonly uralitized and/or chloritized and the plagioclase saussuritized. Minerals most in disequilibrium conditions -- such as olivine, pyroxene, and calcic plagioclase -- typically show the highest degree of breakdown. Primary hornblende in these rocks has not in most cases been replaced but rather shows only the development of yellowish rims on the characteristically green primary grains. These particular types of mineral replacement or readjustment are not considered to be indicative of pervasive hydrothermal metasomatism wherein wholesale chemical exchange may have occurred, but are rather interpreted as a prograde effect under ambient greenschist facies metamorphic conditions. The common lack of the metamorphic fabric expected to accompany regional greenschist metamorphism is attributed to the generally greater competency of the intrusive bodies in comparison with bordering and interlayered Hardware schists and/or Candler schists. Also, because such local features as the occurrence of orbicular segregations in the Diana Mills body are identified as being late stage (deuteric) magmatic in origin, there is essentially no petrographic evidence to indicate even more localized or focused zones where pervasive hydrothermal metasomatic processes were active. On these grounds, the whole rock chemistry of the westerly intrusives is considered to be more or less intact, except for the hydration indicated by the breakdown of pyroxene to uralite-chlorite aggregates and the serpentinization of olivine.

With intensification of the metamorphic overprint to the east, however, the intrusive facies in contrast are typically structurally as well as mineralogically affected. Indeed, the presence of a pervasive metamorphic fabric overprint is evident as far west as the Ellisville sill, though the northern stock-like part of this body is only texturally overprinted near its margins. The effects of dynamic metamorphic overprinting are particularly evident in the case of the small quartz diorite to granophyric intrusive bodies widespread in the Mineral assemblage, as these have generally reacted to the deformation regime cataclastically. The more mafic intrusive material typically shows pervasive alteration to a uralite-saussurite paragenesis that pseudomorphs rather disrupted igneous textures. The ultramafic facies along the eastern side of the belt only rarely bears evidence of its igneous origin, and in some instances -- as with the magnesian amphibolites -- even the basic fact of igneous origin is suspect. At higher metamorphic grades in the easterly gneiss terrane the granitoid orthogneiss facies is characteristically well banded, and metamorphic differentiation has in all probability been instrumental in developing gneissic structure. Because of the more intense deformational effects of the metamorphic overprint at higher medium grade metamorphic conditions in this eastern part of the belt, the whole rock chemistry is thought to have been modified. It must be stressed, though, that in general the intrusive facies as a group do not manifest petrographic features indicative of pervasive hydrothermal metasomatic adjustments and for this reason, whatever the chemical changes, they are thought to have arisen during the late regional metamorphic event.

Because of their particular relevance to petrogenesis, those various types of intrusive believed to be at least in part contemporaneous with volcanism are emphasized in the following discussion. Due to the complexities

inherent in geochemical investigations of orthogneisses where metamorphic differentiation is suspected to have modified original intrusive compositions, an examination of the Columbia "granodiorite" facies of the eastern terrane was not undertaken. Also, because the late intrusives in this terrane are unrelated to the early formative stage of the belt, these also were not included in the study. The section is partitioned, for the sake of clarity of presentation, into subsections on intermediate to felsic intrusives and mafic intrusives, the latter being deemed to include the ultramafic amphibolites of problematic origin.

3.2.1 Intermediate to Felsic Intrusives

Normative mineral plots of various intermediate to felsic intrusive rocks representative of the granophyric bodies in the Mineral metavolcanic suite, of quartz diorite sills occurring west of the Palmyra assemblage peripheral to the Diana Mills complex, and of the Green Springs and Ellisville stocks are shown in Figure 8, a and b. As demonstrated on the AB-OR-AN diagram (Figure 8a), isolated intrusive bodies in the Mineral assemblage plot in a relatively tight cluster in the trondhjemite field. Significantly, a sample from a quartz diorite body (123) occurring along the western boundary of the Palmyra assemblage in Zion Crossroads quadrangle also plots in the trondhjemite field and, as previously noted, petrographically similar quartz diorite sills form apophoses to the mafic intrusive complexes along the western side of the belt. One sample of diorite from the Diana Mills body and three from the Green Springs intrusive indicate a wide compositional spread over the boundary between tonalite and granodiorite. Of note, also, is the fact that a sample from the Green Springs intrusive and the lone sample from the Ellisville stock

Figure 8: Normative Mineral Plots of Felsic Intrusive Rocks

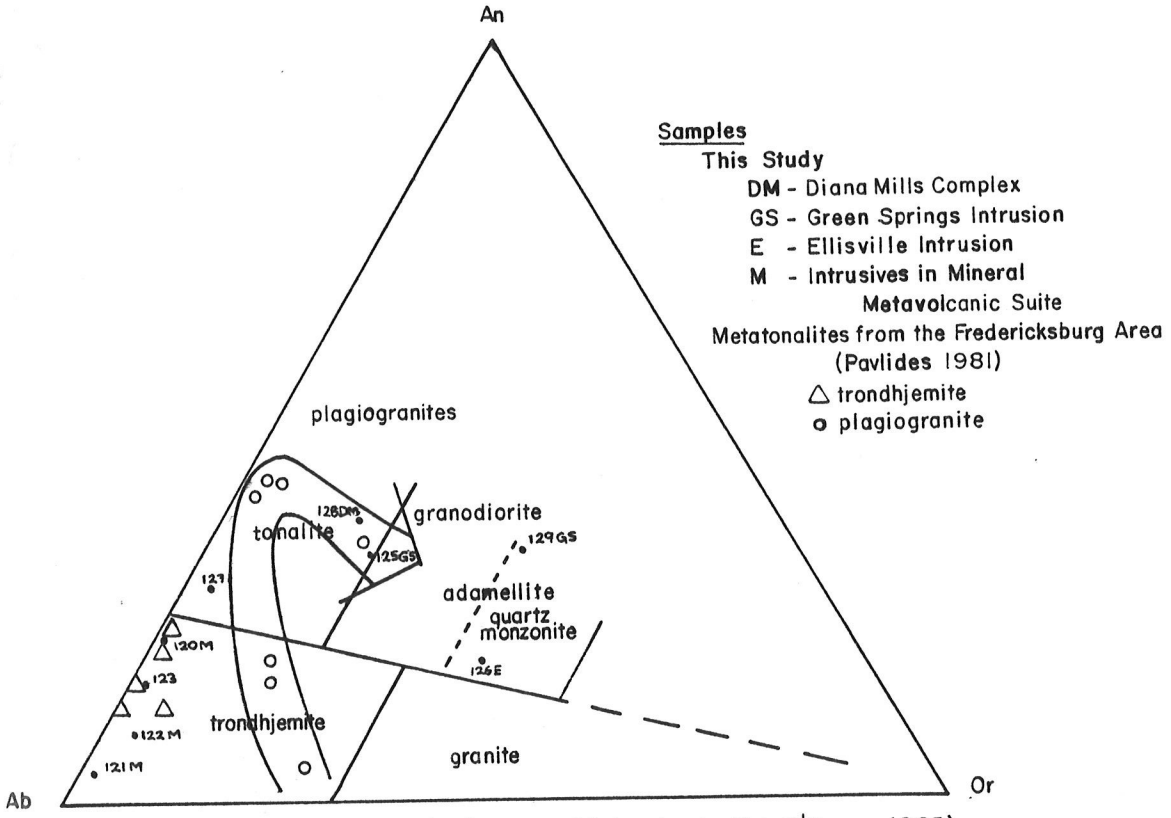

(a) Mesonormative Ab-Or-An Diagram (Fields of Intrusives after O'Connor 1965)

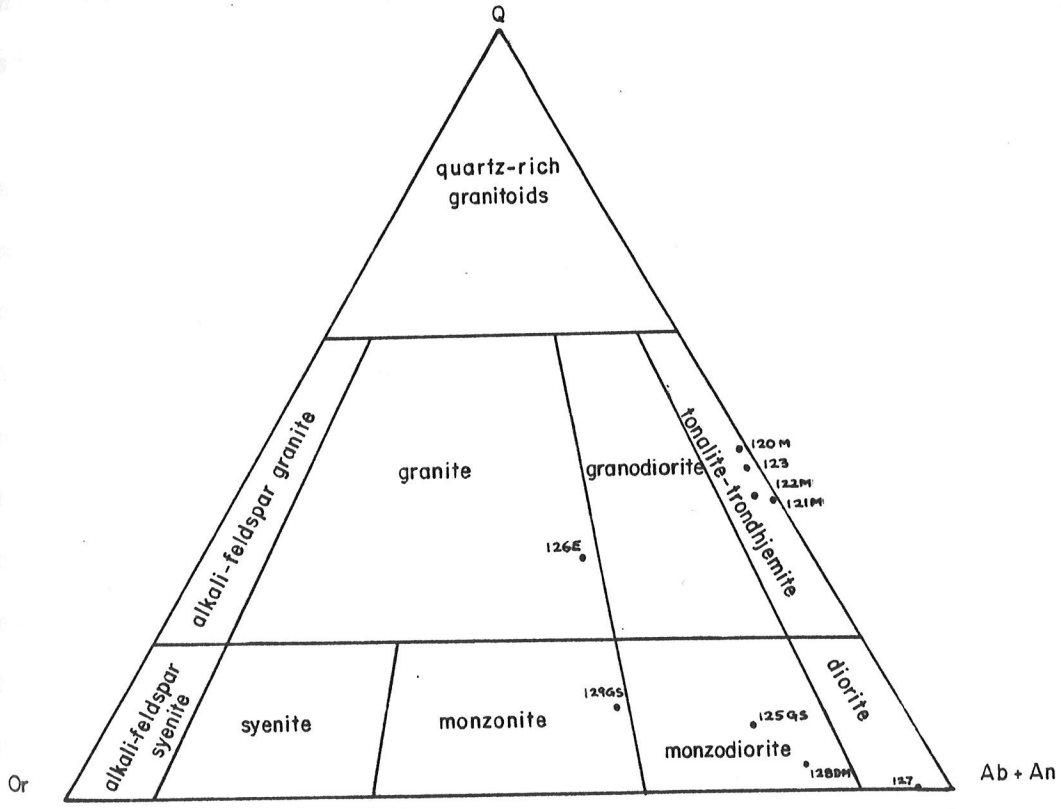

(b) Mesonormative Q, Or, Ab + An Diagram
(Fields of Intrusives after Coleman & Peterman 1975)

both plot as quartz monzonite in the adamellite field, although the latter sample plots much closer to the granite boundary. The lone sample of late Ellisville-age diorite (127) collected from near the Columbia metashale contact falls in the tonalite field, but not in any close proximity to other tonalitic or trondhjemitic types. On the Q-Or-Ab+An diagram (Figure 8b) the trondhjemitic intrusives of Figure 8a again form a tight cluster in the tonalite-trondhjemite field, while the Green Springs samples plot as monzodiorite and monzonite and the Ellisville sample as a granite near the granite-granodiorite boundary. The single Ellisville-age late diorite here plots very near the plagioclase corner, and would seem to be compositionally distinct.

The petrogenesis of trondhjemitic intrusives has been critically reviewed by Barker (1979). As numerous recent studies show, these types of intrusives have widespread occurrence in numerous tectonic settings. Plutons of trondhjemite-tonalite and quartz diorite are abundant in and around Archaean greenstone belts (Card 1982). Plagiogranites of batholithic dimension have been found intruding Proterozoic and Paleozoic geosynclinal successions (Barker 1979, Popilitov 1979), mature island arcs (Ishizoka & Yanagi 1977), and immature arcs of oceanic affinity (Gill& Stork 1979). Plagiogranites can also occur as small discrete bodies in the upper parts of ophiolitic suites (Coleman & Peterman 1975, Dixon & Rutherford 1979). Despite this variability, on the basis of recent experimental work it is possible to differentate the trondhjemites from differing tectonic settings on geochemical grounds. Knowing the compositions of the trondhjemitic bodies in a given area can thus help significantly in the attempt to elucidate the original tectonic setting for that area. The data available on the trondhjemites of the present study are somewhat limited, but it is perhaps possible to use this interpretive tool

indirectly, by invoking an analogue.

To this end, the compositions of a metatonalite suite recently identified by Pavlides (1981) as intrusive into Chopawamsic metavolcanics in the Fredericksburg area have been plotted on Figure 8 for purposes of comparison. The parallels pointed up by this exercise are instructive ones. Pavlides subdivides his assemblage into a younger, less metamorphosed trondhjemite and an older, more highly deformed plagiogranite; as illustrated, there is a striking overlap demonstrated between the former group and the trondhjemite samples from the current project area. This petrochemical correlation is supported, moreover, by the common granophyric textures observed in trondhjemites both by Pavlides and by this writer. The samples from the Green Springs and Ellisville intrusive bodies, in contrast, do not compare well either compositionally or texturally with the Fredericksburg suite -- despite the fact that the plagiogranite-metatonalites as a group are quite compositionally varied, at times encroaching upon granodioritic compositions. Considering these factors in combination it seems reasonable to assume a meaningful relation between the Fredericksburg trondhjemites and the trondhjemites of the present study. More significant for present purposes, it also seems reasonable to assume that Pavlides' petrogenetic analysis of the Fredericksburg rocks, based on trace-element geochemical signatures, provides important evidence not merely about the setting of his own investigation but also about what we may take as a broadly analogous terrane. The most salient points to emerge from this study may be summarized as follows:

(1) The trondhjemitic rocks include both corundum-normative and diopside-normative types regardless of SiO_2 content. This is in contrast with normal calc-alkaline magmas where, as demonstrated by Cawthorn et al (1976), there is a change from diopside to corundum-normative when the SiO_2 content reaches about 65 weight %. Significantly, the trondhjemites of the present study area include similar corundum-normative and diopside normative samples regardless of SiO_2. The Fredericksburg plagiogranites, on

the other hand, are all corundum-normative and hence demonstrate a normal calc-alkaline normative feature.

(2) All the trondhjemites plot in the low Al (less than 14.5% Al_2O_3) oceanic field of Arth's (1979) Al_2O_3 vs Y diagram for differentiating oceanic and continental trondhjemite varieties. The trondhjemites of the present study area have similar low Al_2O_3 contents in the 11-13 weight % range. Although the plagiogranites plot in the low Al oceanic field, they occasionally also plot in the high-Al continental field.

(3) Most trondhjemites have flat REE patterns with negative Eu anomalies, but some show spurious HREE and Ce-enrichment. Disregarding the spurious enrichments, these REE patterns compare best with patterns obtained from island arc trondhjemites. The plagiogranites, on the other hand, have REE patterns showing LREE enrichment and positive Eu anomalies. Such patterns are typical of normal calc-alkaline suites, and compare best with those obtained from siliceous (greater than 65% SiO_2) continental trondhjemites from Finland (Arth 1979).

On the basis of these particular geochemical features, Pavlides suggests that the Fredericksburg area metatonalite suite has an island arc affinity. That the trondhjemitic subfacies has characteristics common to low alumina oceanic trondhjemites further suggests an oceanic island arc. However, the fact that the plagiogranites show both the REE patterns typical of continental trondhjemites and the low Al_2O_3 contents of oceanic types indicates a crustal situation intermediate between these types. Collectively, then, the geochemical signatures demonstrated by the older plagiogranites and younger trondhjemites of the Fredericksburg metatonalite suite could be interpreted to signify early continental margin crustal conditions giving way in time to a more oceanic crustal setting. On the basis of their close petrographic and petrochemical kinship with the latter of these species, the trondhjemitic intrusives of the present study area are considered to reflect an oceanic crustal environment as well.

Not enough geochemical work has yet been carried out on either the Green Springs or the Ellisville stock to justify any definitive petrogenetic conclusions at present. The few samples that were analysed in this study

indicate clearly that the compositions of these broadly adamellitic bodies, as of the Ellisville-age diorites, differ significantly from those of the trondhjemitic intrusives. There is nevertheless some evident overlapping between lithologies comprising the Green Springs intrusive and the plagiogranites of the Fredericksburg area metatonalite suite on the one hand and between the Green Springs and Ellisville lithologies on the other. Three facts in particular could be taken as evidence for petrogenetic continuity among all the intrusive species present: (1) the Green Springs intrusive occupies the same structural position as the Buckingham and Diana Mills mafic intrusive complexes, (2) the dioritic facies common to all of these complexes compositionally overlap, and (3) all have affiliated trondhjemitic quartz diorite border facies. At this point in the discussion, the Green Springs body is tentatively identified as being broadly tonalitic-granodioritic in composition but including intermediary facies bridging the gap between an earlier peridotite-gabbro-tonalite-trondhjemite suite and a later Ellisville-age diorite-granodiorite-quartz-monzonite-granite suite. This hypothesis will be developed further in the following discussion of the mafic intrusive complexes and again in the section on magma genesis concluding this chapter.

3.2.2 Ultramafic to Mafic Intrusives

In contrast to the intermediate to felsic intrusives, those of ultramafic to mafic composition do not form large equidimensional stock-like bodies such as the Ellisville and Green Springs intrusives. Instead, the ultramafic to mafic material either forms sill injection zones like the Buckingham and Diana Mills complexes or small composite peridotite-gabbro-diorite bodies such as

those observed near and at the contact between Long Island metashales and the Ellisville sill and again on both limbs of the Columbia structure. Due to their higher stratigraphic position the ages of the latter composite mafic-ultramafic intrusive bodies are considered to be later -- perhaps early Ellisville? -- than those of the western sill complexes. Further ultramafic material occurs regionally as massive magnesian amphibolite strata interlayered with iron formation, ironstone, and, occasionally, coarse hornblendites of the diverse upper Chopawamsic group capping the Mineral assemblage. As this particular ultramafic facies is devoid of igneous textures, however, it is debatable whether or not it derives from an ultramafic igneous parentage. It is included here with ultramafic rocks of known igneous origin primarily for the purpose of testing the hypothesis that they are magmatic.

With the increasing west-to-east metamorphic gradient, the ultramafic intrusives and, to a lesser degree also the mafic facies show progressively more intense metamorphic overprinting. The Buckingham and Diana Mills sills retain much of their igneous fabric (photos 3 & 4), although commonly the pyrogenetic mineralogy of these bodies shows alteration to greenschist facies mineral assemblages. The ultramafic material observed along the Long Island trend is typically pervasively serpentinized, with igneous textures nearly or completely obliterated by metamorphic foliation fabrics. The mafic gabbro-diorite facies, on the other hand, generally manifests remnant igneous textures. In marked contrast to both of these, the uniform fibrous matte textures (photos 5 & 6) which typify the magnesian amphibolites along the Columbia metashale contact, in the Whispering Creek anticline, and in the Andersonville area show no evidence of an original igneous textured ultramafic parentage.

5. Cumulate textured intrusives: Serpentinized peridotite with original olivine outlined by magnetite ± chromite. Postcumulus minerals altered to talc and green hornblende (sample A-144, ppl, X75).

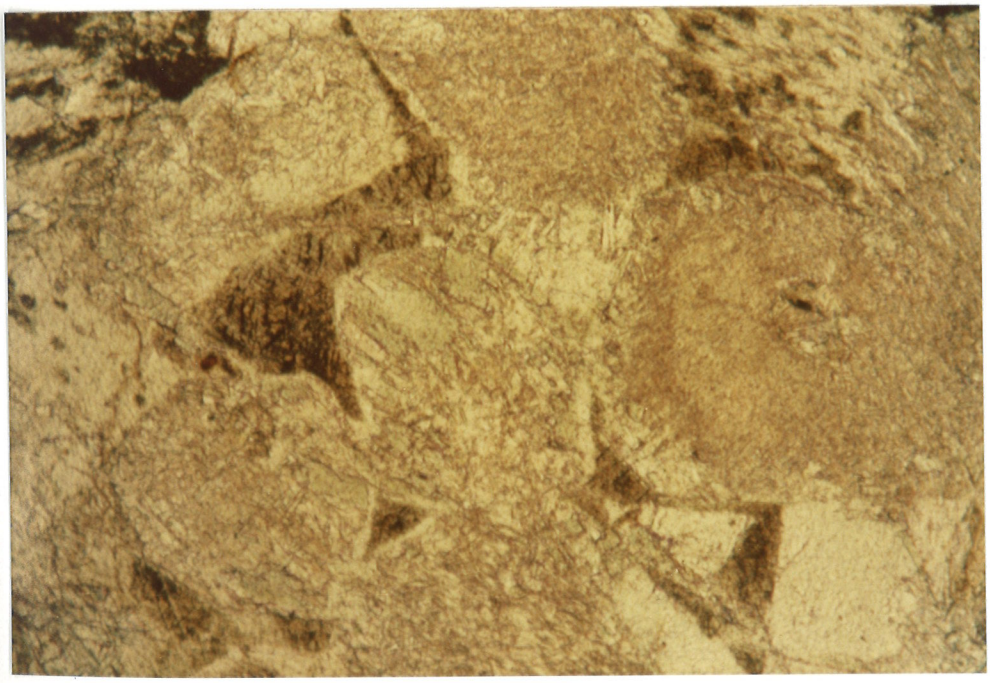

6. Cumulate textured intrusives: Uralitized pyroxenite with remnant cumulus hypersthene partially rimmed by green hornblende (sample Ca-1, ppl, X75).

7. Magnesian amphibolites (metakomatiites): A typical matte textured magnesian amphibolite with Mg-chlorite and minor talc hosting randomly oriented acicular tremolitic hornblende microlites (sample Law 6, ppl, X175).

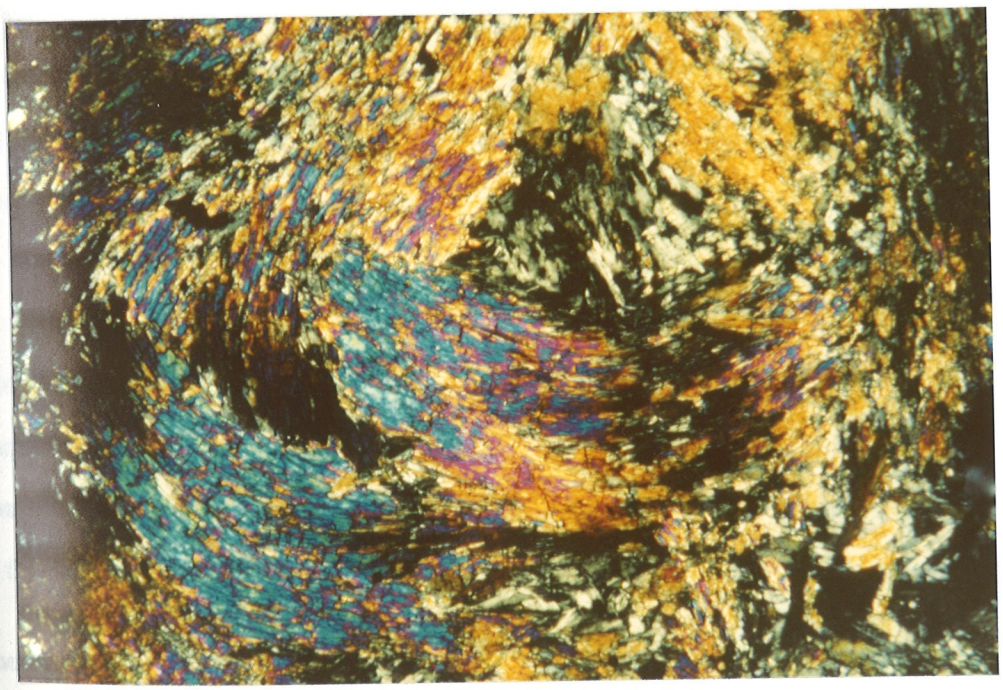

8. A peculiar textural variant of magnesian amphibolite comprising coalescing tremolitic hornblende sheaves with minor interstitial Mg-chlorite (sample A-190, xnicols, X175).

The main petrochemical variation characteristic of the ultramafic-mafic intrusives is well illustrated on the MgO-CaO-Al_2O_3 diagram (Figure 9). The most striking compositional feature demonstrated on this ternary derives from the fact that most compositions define a relatively narrow tract leading directly away from the MgO corner. This indicates that forsteritic olivine was the dominant residual mineral during partial melting and/or the major cumulate phase in magmatic differentiation. The greater breadth of the compositional tract in the low MgO range might be attributed to the increased role of Ca-plagioclase, augite, or hornblende. As there is a significant gap in the peridotite composition between the pyroxenite field and the serpentinized dunites, it is premature to suggest that the analysed samples define a continuous trend over the compositional range shown. However, as samples from the western sill complexes do show compositions over the whole range from tholeiitic basalt to peridotite (as defined by Arndt et al, 1977), such a continuous trend seems likely; more sampling should close the apparent gap. Significantly, the generally high CaO/Al_2O_3 ratio (≤ 1) demonstrated by such a compositional tract has been suggested by Nesbitt and Sun (1976, 1979) to be a characteristic of komatiitic magmas. It must be remembered, of course, that inasmuch as we are here dealing with fractionated intrusives with cumulate textured ultramafic to mafic facies the analysed samples do not necessarily represent original magma compositions. Under the circumstances, features which may appear to be diagnostic of komatiite could just as easily derive from tholeiite fractionation.

The general compositional overlap of the recognizable igneous rocks with the ultramafic amphibolites of dubious origin is interpreted to support an igneous parentage for these latter bodies. It is considered very significant that the ultramafic amphibolites generally lie in a fairly tight cluster in

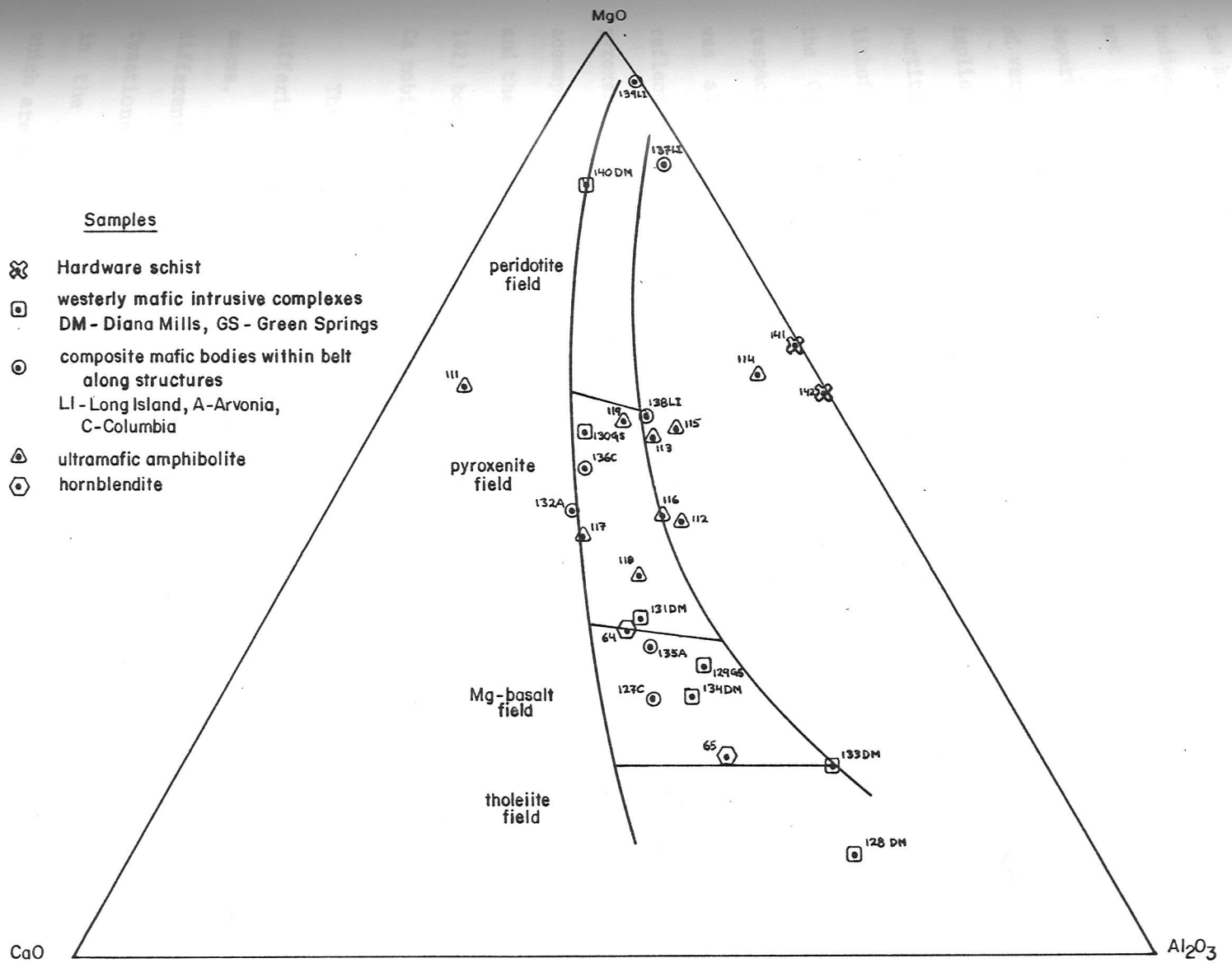

Figure 9: $MgO-CaO-Al_2O_3$ Ternary for Ultramafic to Mafic Rocks
(compositional fields of komatiitic to tholeiitic magmas after Arndt et al 1976)

the pyroxenite field, suggesting, first, that these particular rocks could stem from a magma of fairly uniform composition, and second, that unlike both the mafic intrusive complexes along the western border and the composite bodies along the limbs of the Long Island and Columbia structures, they did not undergo significant differentiation in place. The compositions that depart to any notable extent from the tight cluster (such as 111 and 114) are of very schistose rock respectively rich in tremolite and chlorite. This implies that hydration of the primary pyronxenite may have led to the partitioning of the Ca and Al components into mineralogically distinct lithofacies. Interestingly, both the Al-depleted tremolitic schist (111) and the Ca-depleted Mg-chlorite schist (114) are slightly enriched in MgO with respect to the pyroxenitic cluster, a fact which may indicate either that MgO was also beneficiated during hydration or that these species do in fact reflect the local presence of slightly more Mg-rich differentiate within pyroxenitic sills. There is also evidence, however, that Ca-depletion accompanied the serpentinization of the Long Island dunitic facies (137, 139) and the metamorphic overprinting of the Hardware magnesian schist facies (141, 142) bordering the western sill complexes; this would support the postulate of Ca mobility during hydration.

The broad compositional overlap of mafic-to-ultramafic intrusives of differing age suggests repeated high level injections of mafic to ultramafic magma. The earlier hypabyssal sill injection zones characteristically differentiated in place to dunitic and pyroxenitic cumulate and gabbro fractions. The degree of <u>in situ</u> differentiation decreased markedly, however, in the later, near-surface intrusive or extrusive magnesian amphibolites, which are constituted of homogeneous pyroxenitic magma. Indeed, the uniform compositions of these rocks in conjunction with their field relationships

(laterally extensive units interlayered with iron formation) suggest that here, at least, we are dealing with true metakomatiites. It is interesting that the gabbroic facies including the main stage crystallates of the westerly sill complexes and of the composite bodies, as well as the coarse hornblendites which sometimes accompany the magnesian amphibolite units, all plot in the komatiitic basalt field, indicating that these mafic fractions are also quite magnesian in composition.

Many of the compositional features demonstrated in Figure 9 are also evident on the normative OL-CPX-PL ternary (Figure 10), a projection from the quartz corner of the basalt tetrahedron of Yoder and Tilley (1962). This particular diagram further illustrates that although pyroxenite is a favoured composition, CPX is not a major normative mineral. In fact, many of the pyroxenitic magnesian amphibolites plot very near the OL-PL tie-line. This normative mineral feature possibly reflects a primary partition of Ca and Al into plagioclase and/or amphibole phases in magma which from the onset had characteristically high CaO/Al_2O_3 ratios. Such a compositional aspect may be further evidenced by the occurrence of very feldspar-rich diorites in the western differentiated intrusive sill complexes and, possibly, the association of coarse hornblendites with the magnesian amphibolites along the eastern side of the belt, if indeed these were cogenetic.

A plot commonly utilized in differentiating komatiitic compositions from other magmatic types such as the calc-alkaline and tholeiitic species is the Al, Fe^2+Fe^3+Ti, Mg cation ternary. On this graph, as shown in Figure 11, the trend of the westerly mafic intrusive complexes of the present project area can be seen to traverse all the respective fields as outlined by Jenson (1976). It is particularly interesting with respect to the question of precursors that each age of intrusive appears here as petrochemically distinct

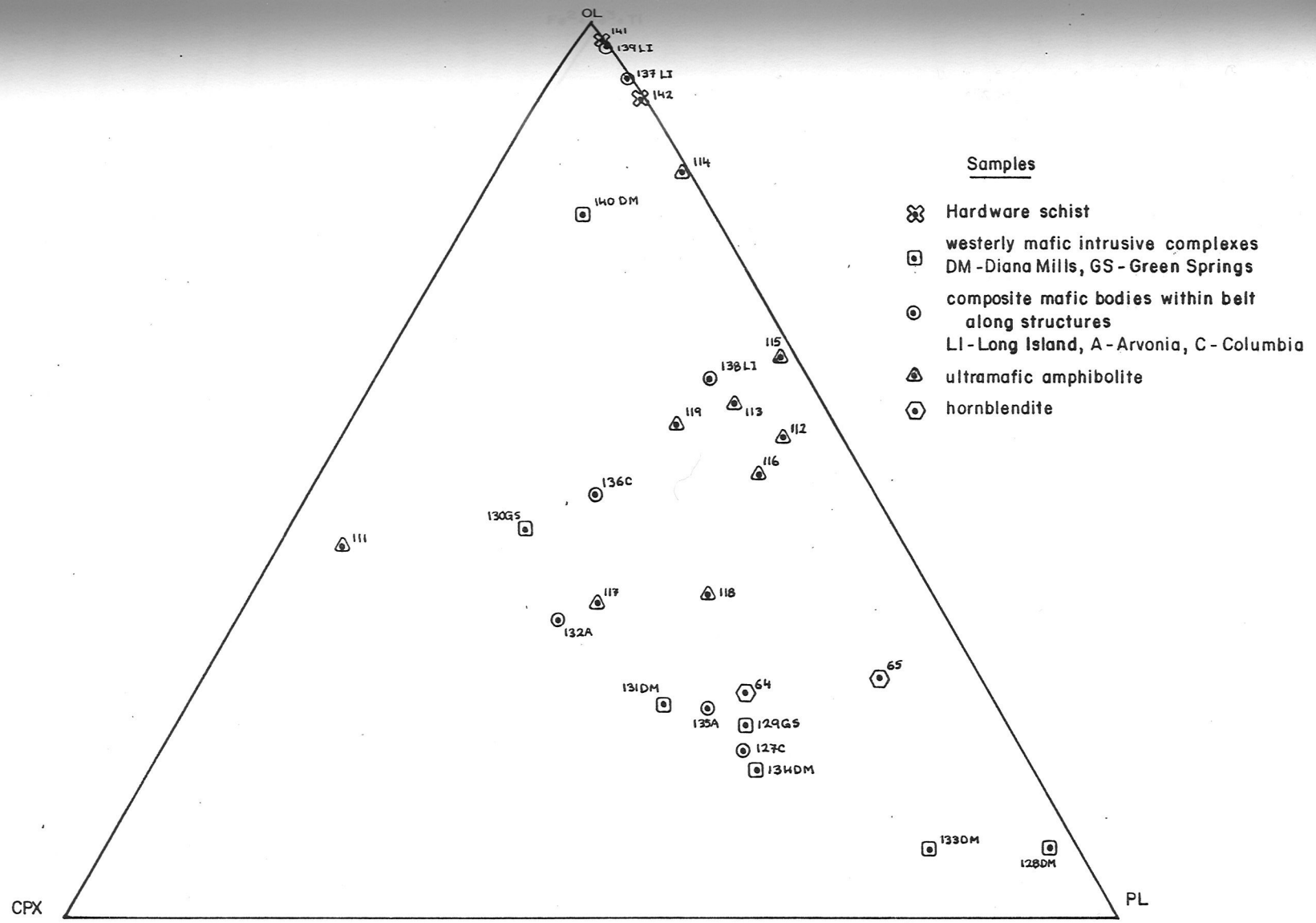

Figure 10: Normative Cation % OL-CPX-PL Ternary for Ultramafic to Mafic Intrusive Rocks
(the projection from the quartz corner the basalt tetrahedron of Yoder & Tilley 1962)

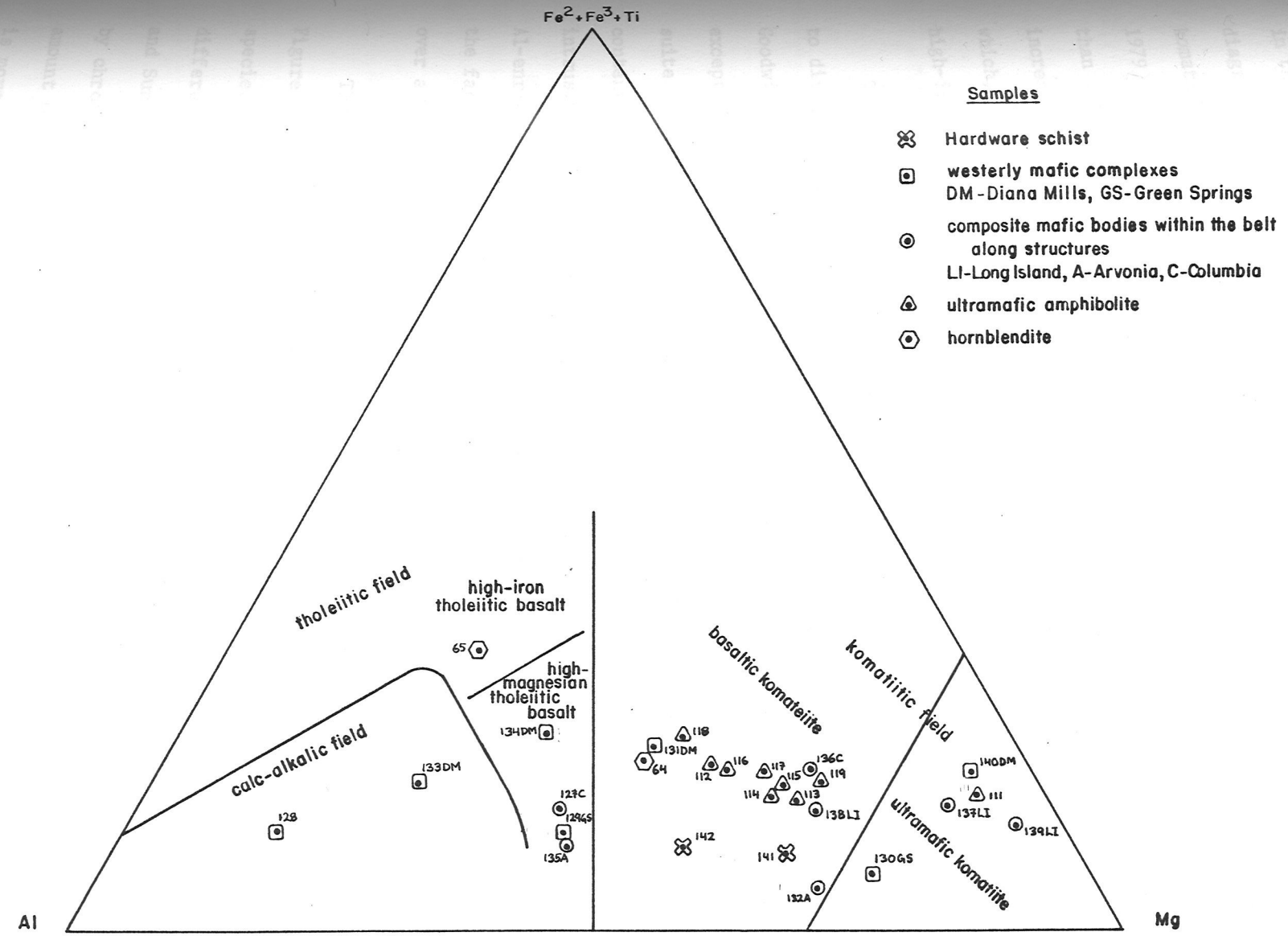

Figure 11: Al, Fe^2+Fe^3+Ti, Mg Cation Ternary for Ultramafic and Mafic Rocks
(compositional fields for komatiite, tholeiite and calc-alkaline magmas after Jensen 1976)

in the Fe^2+Fe^3+Ti component. Reinforcing the inference made above, on this diagram the magnesian amphibolites plot out as basaltic komatiites. Since komatiites have been found to be characteristically low in TiO_2 (Nesbitt & Sun 1979), moreover, the fact that the TiO_2 content in all these samples is less than .5% also contributes important evidence of their parentage. Marked increases in TiO_2 contents are demonstrated by the accompanying hornblendites, which, in contrast to the magnesian amphibolite group, locally plot in the high-iron tholeiitic basalt field.

The Al_2O_3 vs FeO^T/FeO^T+MgO graph (Figure 12) has also often been utilized to discriminate between komatiitic and tholeiitic magma types (Naldrett & Goodwin 1977, Arndt et al 1977, Peredery 1979). When plotted on this diagram, except for the serpentinites and tremolitic schists all samples in the present suite fall well within the komatiitic field due to comparatively low Al O contents. Significant compositional differences are shown among differing intrusive bodies, with those in the core of the belt demonstrating moderate Al-enrichment over the Diana Mills ultramafic-mafic suite. Most notable is the fact that the Hardware magnesian schists show exceptional Al-enrichment over all intrusive material.

The three additional plots of Cr, Ni, and Ti vs MgO (illustrated in Figure 13, a, b, and c) are included to demonstrate whether these particular species acted in accordance with a primary magmatic crystallization differentiation and/or a partial melt genetic scheme. As reviewed by Nesbitt and Sun (1976), the Cr content in komatiitic rocks is essentially controlled by chromite and clinopyroxene contents. At compositions less than 15% MgO the amount of Cr increases with increasing olivine. Above 15% MgO the Cr content is more or less constant, suggesting that at this point both clinopyroxene and chromite were exhausted in the residuum. These geochemical features are to a

Figure 12: Al_2O_3 vs $FeO^T/FeO^T + MgO$ Binary for Ultramafic to Mafic Intrusive Rocks (the boundary separating komatiitic from tholeiitic fields after Naldrett & Goodwin 1977; fields of metaperidotite-serpentinite, cortlandite and amphibolite after Papunen et al 1979)

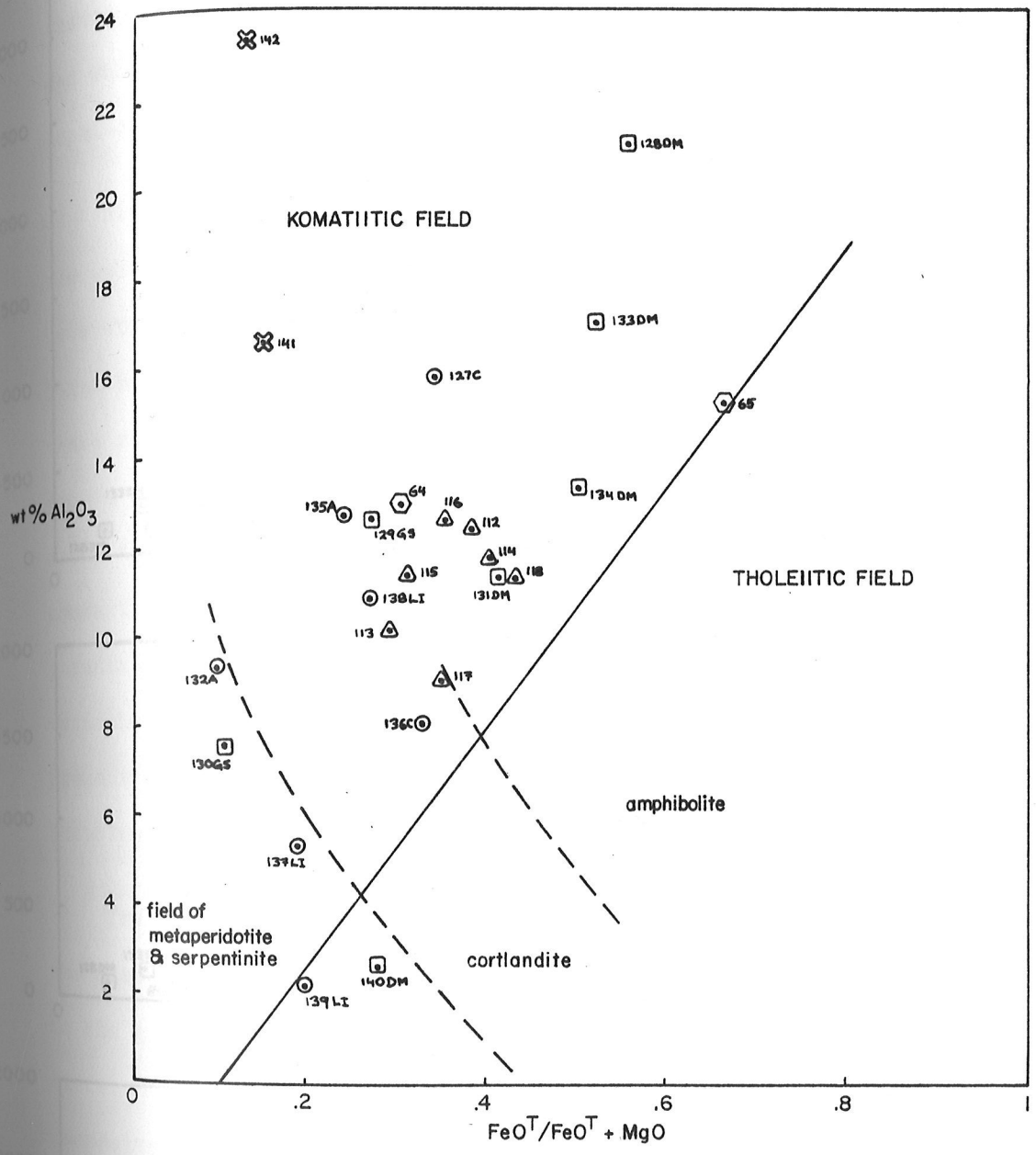

Samples

- Hardware schist
- westerly mafic intrusive complexes DM-Diana Mills, GS-Green Springs
- composite mafic bodies within belt along structures LI-LongIsland, A-Arvonia, C-Columbia
- ultramafic amphibolite
- hornblendite

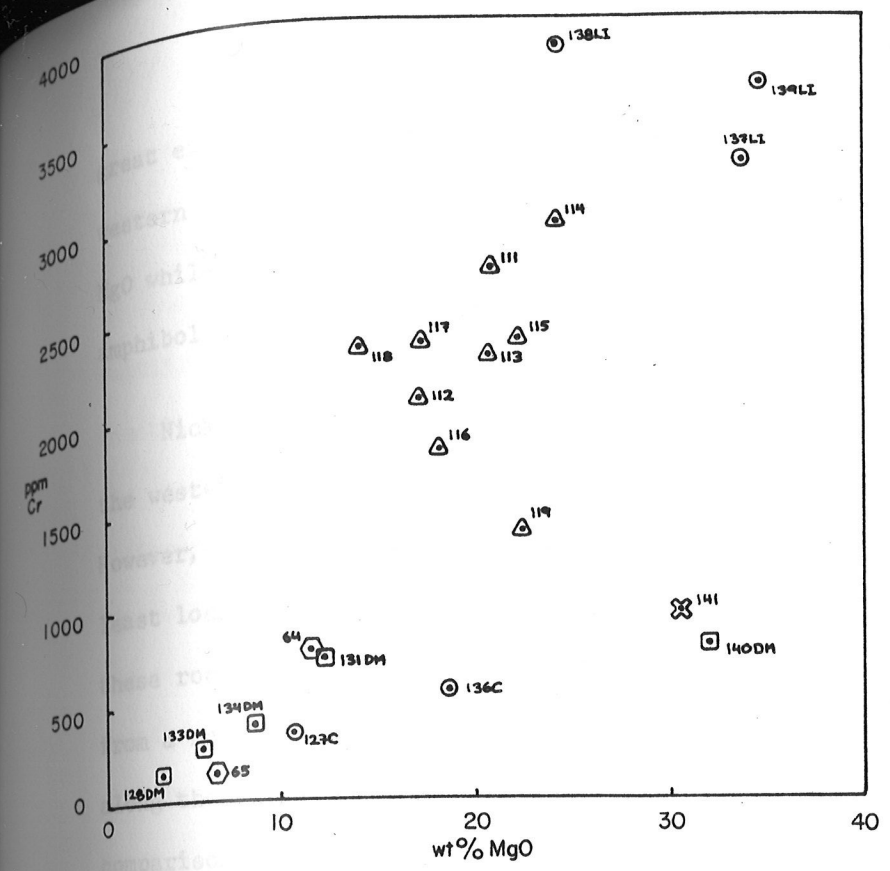

a) Cr vs MgO

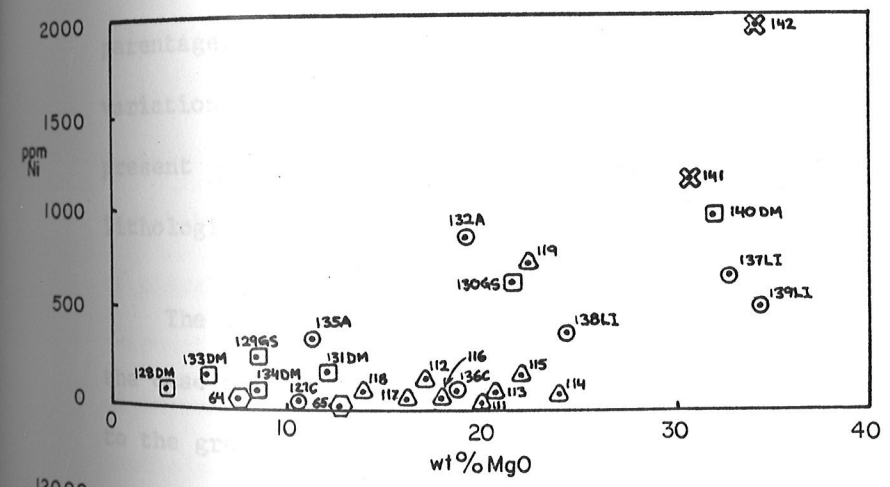

b) Ni vs MgO

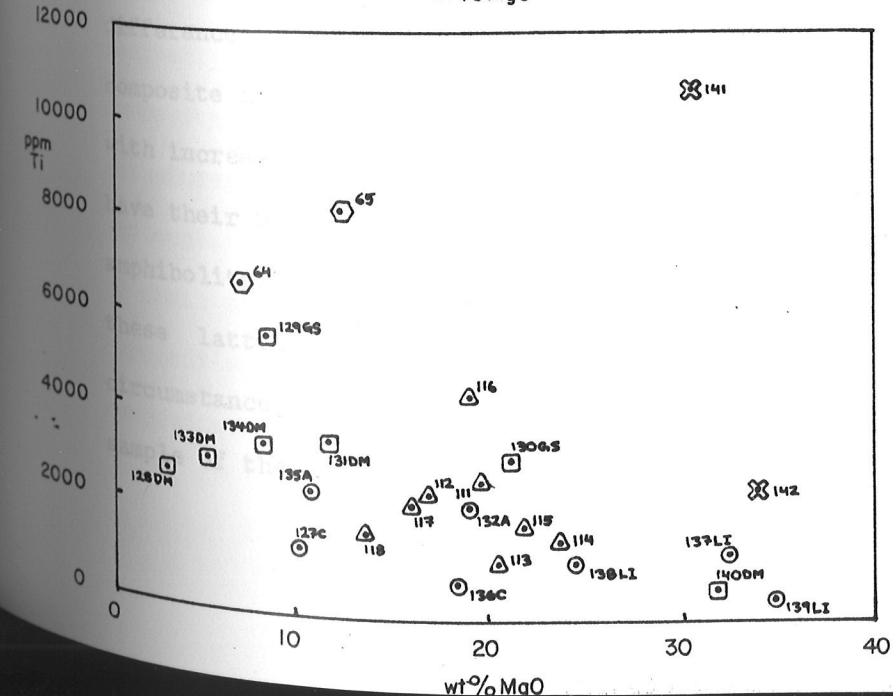

c) Ti vs MgO

Figure 13: Three Binaries for Utramafic to Mafic Rocks

Samples

- Hardware schist
- westerly mafic intrusive complexes
  DM - Diana Mills, GS-Green Springs
- composite mafic bodies within belt along stuctures
  LI - Long Island
  A - Arvonia
  C - Columbia
- ultramafic amphibolites
- hornblendite

great extent borne out by the present analytic results. The differentiated western intrusive sill complexes demonstrate positive Cr-MgO trends below 15% MgO while both the serpentinites along the Long Island trend and the magnesian amphibolites at MgO>15% show different but uniformly high Cr values.

Nickel shows a consistently positive relation with MgO contents in both the westerly sill complexes and the composite mafic bodies within the belt. However, the Hardware magnesian schists bordering these sill complexes are at least locally highly enriched in Ni over the intrusive facies, suggesting that these rocks may not simply comprise highly sheared intrusive material but stem from a more nickeliferous parent. In contrast, the magnesian amphibolites along the eastern side of the belt show uniformly low Ni contents in comparison with MgO contents, which would seem to imply a nickel-depleted parentage. As an alternative explanation one could, of course, attribute such variation simply to nickel mobility during hydration of ultramafic rocks. On present evidence, the interpretation of the role of nickel in these lithologies must remain speculative.

The Ti vs MgO plot shows considerable scatter but as one would expect in the case of a magmatic origin, a general negative correlation may be imputed to the group as a whole. Within this broad pattern, however, considerable differences are demonstrated to exist among the invidual members. While the composite mafic bodies near the shale contacts show a definite drop in TiO_2 with increasing MgO, for instance, the westerly differentiated sill complexes have their highest TiO_2 contents at about 10% MgO. As a subgroup the magnesian amphibolites form a cluster defining no trend. The hornblendites accompanying these latter rocks, however, are highly enriched in TiO_2 -- a predictable circumstance in light of their postulated tholeiitic parentage. Notably, one sample of the magnesian Hardware schist bordering the westerly sill complex is

also extremely enriched in this element, again testifying that this is not simply metamorphosed ultramafic sill material.

Considered collectively, these geochemical features would seem to offer fairly convincing substantiation for the postulate that episodic tholeiitic to komatiitic magmatism was a source for these mafic and ultramafic rocks. In the westerly sill complexes tholeiitic to komatiitic magma apparently differentiated in place to a dunitic cumulate at the base, gabbros in the main zones, and minor late stage feldspathic diorites at the top. The fact that these bodies are accompanied by peripheral late tonalitic diorite and trondhjemitic quartz diorite could be taken to indicate that late differentiates of tonalite-trondhjemite compositions stemmed from the main stage of crystallization of the ultramafic-mafic parent magma. Such an interpretation does not, however, take into account the compositionally similar but volumetrically larger stock-like intrusives (like the Green Springs body) which are also found in this area. Inasmuch as it is highly improbable that such a quantity of tonalite could have evolved from the amount of ultramafic-mafic material evident in the sill complexes, it seems more reasonable to suppose that we are looking at the results of an extended period of magmatism in the course of which early mafic to ultramafic magma from a mantle source eventually gave way to more voluminous tonalitic magma derived partially through differentiation and partially through crustal anatexis. The composite mafic-ultramafic bodies along the Long Island, Arvonia, and Columbia structures generally overlap in composition with the westerly intrusives although, as demonstrated particularly by the consistently higher Cr contents of their serpentinized dunite fractions, there are still some important compositional differences. Similarly, the main gabbro-diorite facies of these composite bodies seem to be roughly analogous to the gabbroic facies of the

western sills, though varying in some elements such as Fe^2+Fe^3+Ti.

In general, the geochemistry of the magnesian amphibolites broadly identifies these rocks as stemming from pyroxenitic komatiite of uniform composition. The local fluctuation in composition reflects variation in their now-hydrous mineralogy. The high chlorite facies is depleted in Ca while the tremolitic facies is depleted in Al; both are slightly enriched in Mg. Beyond this little can be said. Much more petrochemical work is needed on this ultramafic lithology before it will be possible to elucidate its origin with any certainty. Considering its peculiar textures, it is possible that hydration occurred during early pervasive hydrothermal metasomatism. It is also significant, however, that the ultramafic amphibolite beds are interlayered with iron formation and accompanied by coarse hornblendic units which are compositionally transitional between basaltic komatiite and high-iron tholeiite. This particular association will be examined again in the discussions of the petrogenesis of the volcanic extrusives and hydrothermal deposits to follow.

3.3 Petrogenesis of the Volcanic Suites

Extrusive rocks along the segment of the Chopawamsic metavolcanic belt covered by the present investigation include: (1) the greenstone suite along the western border, (2) the Palmyra and Mineral metavolcanic suites, (3) the restricted Buffards quartz mica schist deposits of the diverse upper Chopawamsic group, and (4) the amphibolitic orthogneisses in the easterly gneiss terrane. As the petrographic descriptions of these rocks indicate, all of the various extrusive types, and the mafic facies in particular, have been readily susceptible to early syndepositional hydrothermal metasomatic readjustments and therefore their petrochemical features reflect not only

9. Pillow structures in the Shores greenstone occurring on the western margin of the Chopawamsic metavolcanic belt. Note patchy chlorite-epidote distribution. Hammer is 14" in length.

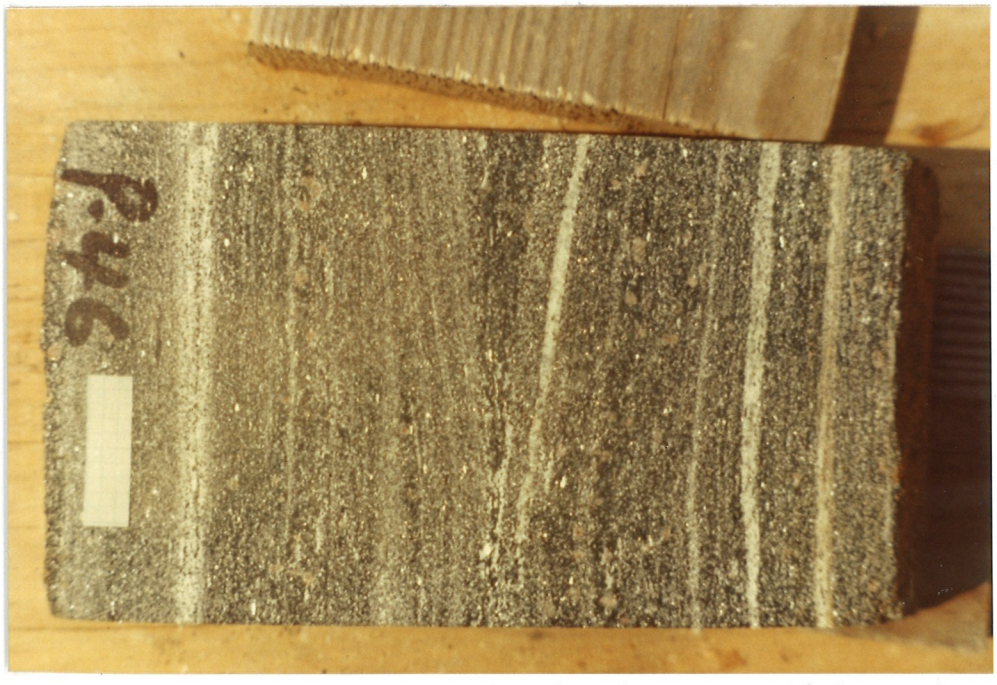

10. A slabbed specimen of banded amphibolite from the high grade gneiss terrane forming the eastern part of the Chopawamsic metavolcanic belt (sample P-46, note 1" scale).

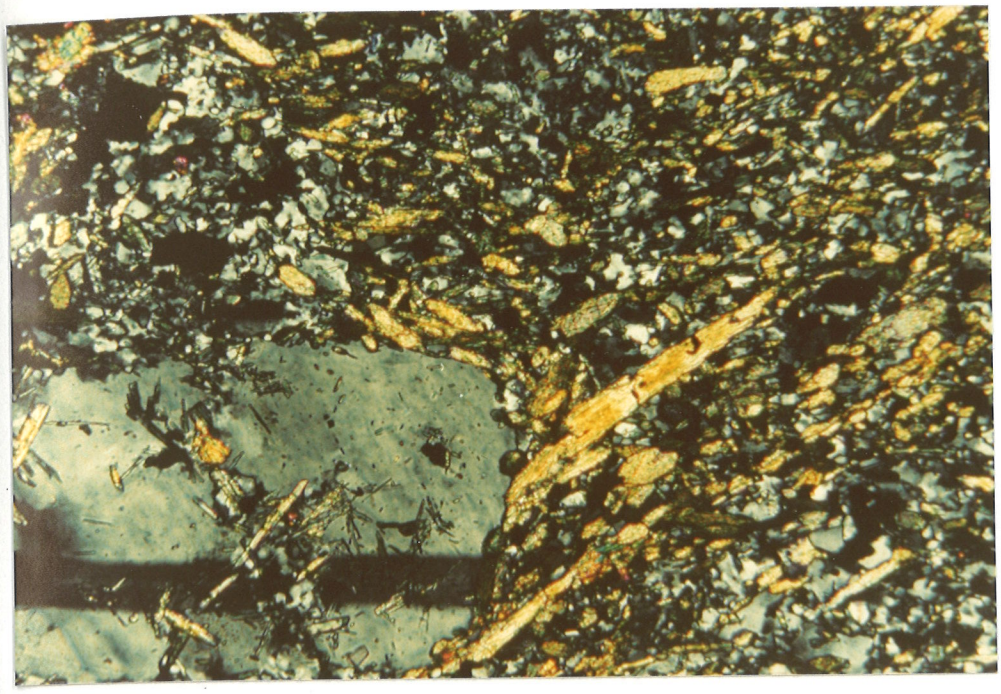

11. Palmyra metavolcanics: Porphyritic andesite with plagioclase (An20) phenocrysts in a moderately foliated groundmass of albitic plagioclase, actinolite, and minor quartz and biotite (sample Co-27, xnicols, X100).

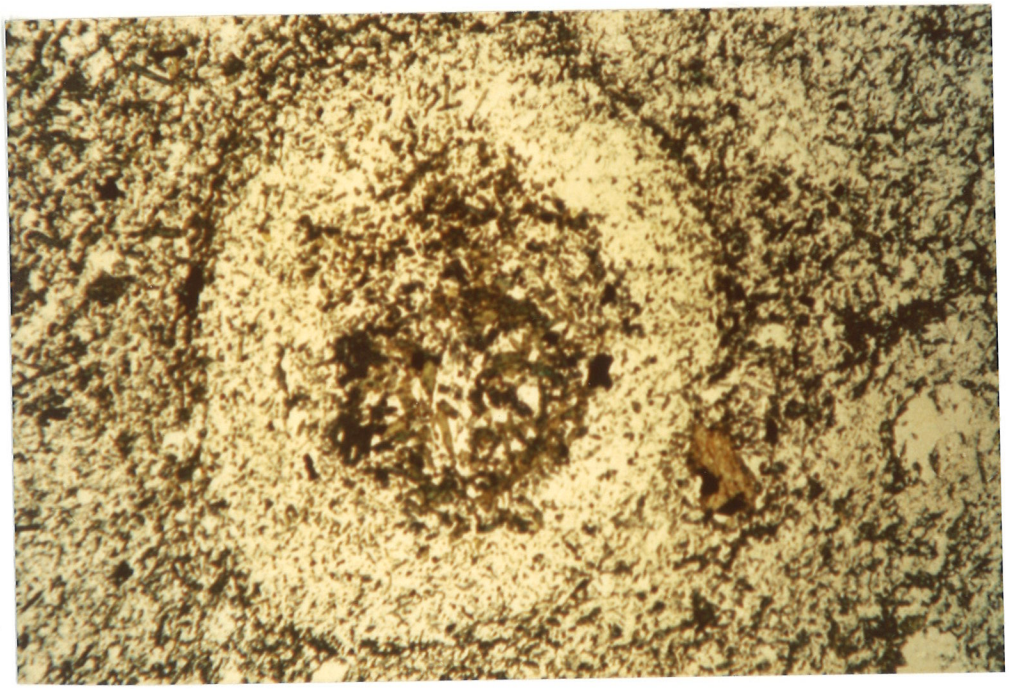

12. Accretionary lapilli tuff with intergranular textured andesite rimmed by albitic plagioclase and quartz (sample C-48, ppl, X150).

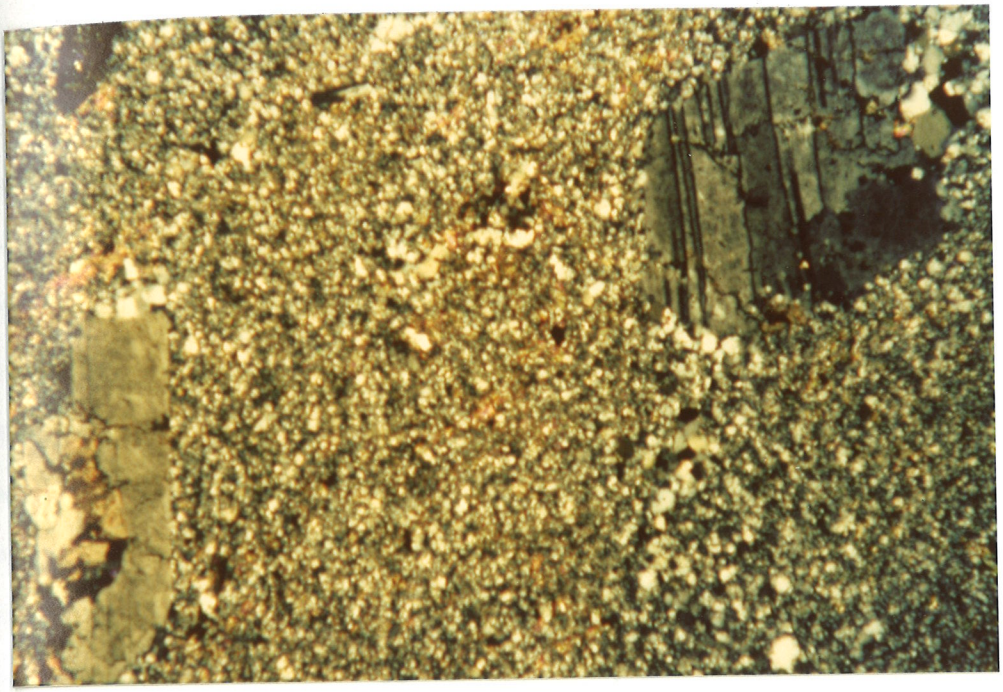

13. Mineral metarhyolite: A quartz-feldspar porphyry with randomly oriented alkali feldspar occurring in a fine-grained groundmass of quartz and feldspar with minor sericite and calcite (sample Cu-85-1900', ppl, X100).

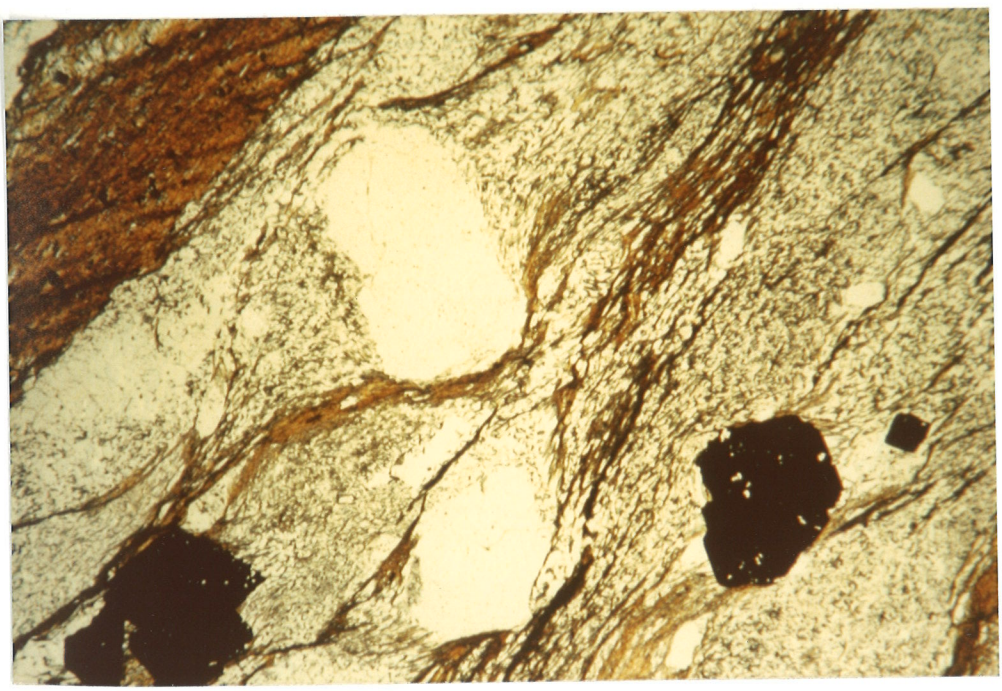

14. Buffards quartz-mica schist (metarhyolite): A multiple foliated quartz-mica schist from the core of the Arvonia structure. Note the quartz eye and rounded alkali feldspar porphyroclasts (phenocrysts), iron oxide porphyroblasts, and marked crenulation in the biotite-rich laminae (sample Buff, ppl, X100).

primary source magma compositions but the extent to which a given sample has been hydrothermally overprinted.

The effects of early hydrothermal metasomatism do not intensify with the west-to-east increase in metamorphic rank across the belt. Indeed, the most pervasive hydrothermal overprint is manifested by the greenstones along the western side of the belt. However, the fact that irregular saussuritic zones are present in the amphibolitic mafics in the more easterly parts of the belt indicates that these were susceptible to early spilitization as well. As has been previously noted, pervasive hydrothermal overprinting is not nearly as petrographically evident in the felsic volcanics except where focused in areas of rhyolite flows. This suggests that hydrothermal processes affecting felsics intensified near original vent areas. Whether or not these rocks were subject to unfocused regional hydrothermal metasomatism similar to pervasive spilitization of the mafics will be examined on geochemical grounds below.

In order to facilitate comparisons, the following discussion is not partitioned into separate headings for mafic, intermediate, and silicic extrusive facies. Rather, the broad geochemical features of all the various extrusive types are demonstrated together on graphical plots typically used to differentiate among volcanic suites from differing tectonic settings.

As shown on the total alkalies vs wt % K_2O/K_2O+Na_2O diagram (Figure 14), all the differing metavolcanic suites have broad alkali variation. As pointed out by Hughes (1973), this particular petrochemical feature is a common one for spilite-keratophyre-quartz keratophyre suites. Although broad compositional ranges in alkali contents are demonstrated, the fact that the samples from each given suite do occupy differing parts of the alkali field suggests that the parental magmas to the various suites had differing alkali

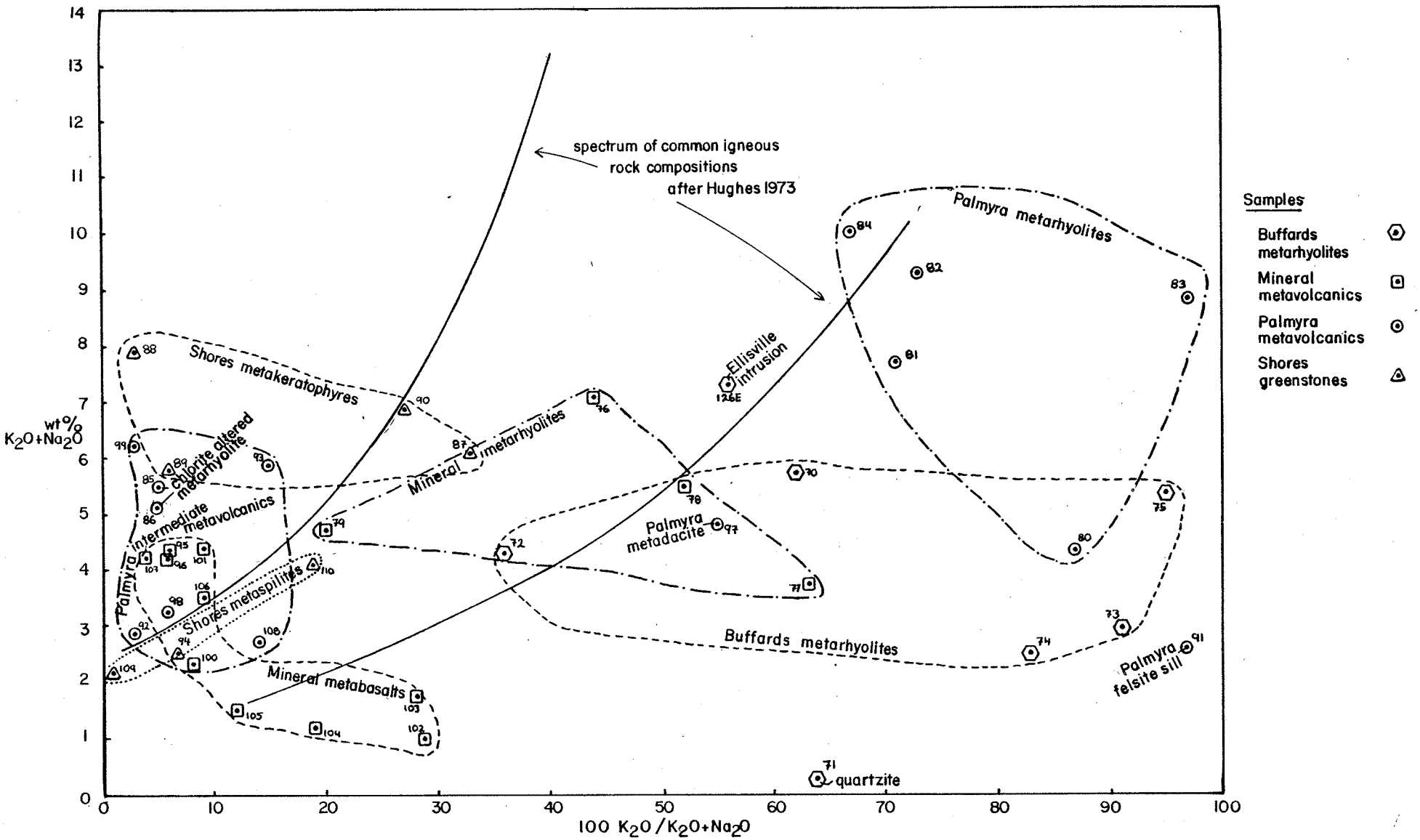

Figure 14: Alkali Variation Binary for the Chopawamsic Metavolcanic Suites

contents. The divergence is not so apparent at the mafic end of the spectrum as most mafics cluster in the low-K field and generally show elevated Na values over what is typical for igneous rocks. This is not always the case, however, as several samples of the Mineral metabasalts are apparently depleted in total alkalies with a greater loss in Na, which results in higher K_2O/Na_2O ratios. The felsic volcanics from the different suites, on the other hand, show considerable variation in their occurrence on the alkali field. The quartz keratophyres from the Shores greenstone suite, like the spilites, are restricted to the low-K end of the diagram. Although the metadacite facies of the Palmyra suite are also restricted to the low-K end, the Palmyra metarhyolites define a broad field at the high-K end of the diagram; these particular samples have the highest total alkali content of any volcanic type. Notably, there is evidence of marked bimodality in K_2O contents in the Palmyra suite, with only one intermediate volcanic (97) occurring in the gap between 15-65 wt % K_2O/K_2O+Na_2O.

The Mineral metavolcanics prove to be generally poorer in total alkalies and richer in Na in comparison to the Palmyra metavolcanics. Also, although there is again a marked bimodality evident in the fields of the mafic and silicic end members, the wt % K_2O/K_2O+Na_2O ratios in this case overlap and the different fields are determined primarily by a variation in total alkali content. The Buffards ash flow tuffs define a very broad field typified by a wide range in wt % K_2O/K_2O+Na_2O; this is interpreted to be indicative of extreme alkali mobility in this suite. Even at high K_2O relative to Na_2O values these particular rocks show only moderate total alkali values, suggesting a net alkali loss. As illustrated by sample 71, the quartzites interbedded with Buffards quartz mica schist deposits demonstrate extremely low alkali contents.

Most of the research on the effects of hydrothermal metasomatic overprints on volcanic rocks has dealt with basaltic compositions, and for this reason spilitization is a well-documented phenomenon. How felsic rocks respond to similar hydrothermal overprints is much less well known. Because the chemical readjustments in rocks composed essentially of quartz and feldspar are far less evident petrographically than are the effects of spilitization of mafics, chemical exchange during hydrothermal metasomatic overprinting of felsics has typically gone unrecognized. However, the fact that keratophyres and quartz keratophyres do show a wide range of Na_2O and K_2O values indicates that there has been considerable mobility of these components. A recent investigation of this phenomenon by Munha et al (1980) reveals that alkali exchange during hydrothermal overprinting of rhyolite at temperatures up to about 145°C results in the substitution of K for Na in albite to form adularia. Such alkali exchange may thus plausibly be invoked to account for the general alkali scatter demonstrated by the felsic volcanics of this study.

Due to the general mobility of alkalies in these rocks, they do not lend themselves to discrimination on the basis of their alkali content. As demonstrated on Figure 15, the samples plot in all the various fields delineated by the boundaries suggested by Kuno (1966). With respect to the Irvine and Baragar (1971) boundary, the overwhelming majority fall in the subalkaline field. Only two samples of metabasalt from the Mineral suite and two samples from the Palmyra suite (97, an andesite, and 83, a rhyolite dust tuff) fall in the alkaline field, and except for the dust tuff these fall near enough to the boundary line to be considered transitional. With respect to Kuno's fields, most of the mafic compositions would seem to be transitional in nature, ranging from mildly alkaline to subalkaline.

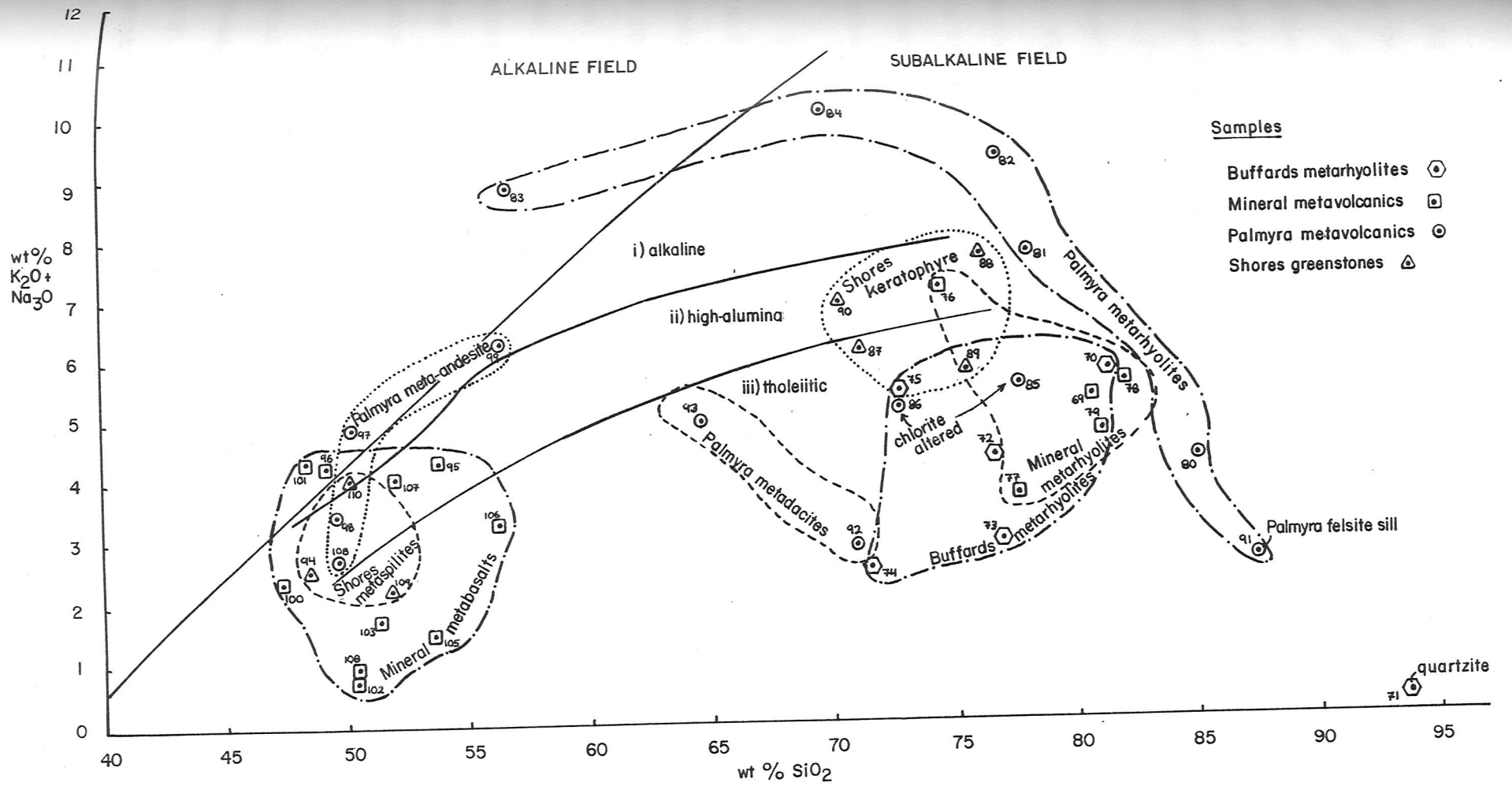

Figure 15: Total Alkalies vs Silica Binary for the Chopawamsic Metavolcanic Suites
(boundary defining alkaline and subalkaline fields after Irvine and Baragar 1971;
boundaries defining i alkaline, ii high-alumina, iii tholeiitic fields after Kuno 1966)

Although the alkali vs SiO_2 diagram is not particularly useful for differentiating the volcanic assemblages with respect to volcanic lineage, it does reveal further geochemical characteristics of the various groups. Striking bimodality is again demonstrated by the Mineral metavolcanics, revealing as they do a marked silica gap between 57 and 74%. The Shores greenstones also show strong bimodality, with a similar hiatus between 52-70% SiO . In contrast, the Palmyra suite exhibits intermediate compositions, as reflected in the andesitic lapilli tuff (99) and in the metadacites (92 and 93). The compositional spread of the Buffards quartz mica schist is tightened considerably and confined within the 71-82% SiO_2 range. It is significant that the total alkali content of all the higher silica rocks and of the Buffards samples in particular falls well below the Irvine and Baragar discriminate in the sub-alkaline field.

The K_2O vs SiO_2 plot may also be used to distinguish between low-K and high-K volcanic suites. As illustrated on Figure 16, the siliceous lithologies demonstrate too broad a K_2O scatter for such a diagnostic tool to be useful at this end of the compositional spectrum. However, it is notable that the mafic rocks are collectively characterized by very low (generally less than .5%) K_2O content. It is also considered significant that the majority of the Shores quartz keratophyres and Mineral silicic metavolcanics plot with low-K values while the Buffards ash flows and, even more so, the Palmyra metarhyolites plot as groups as high-K lithological types.

Much of the scatter apparent on the AFM diagram (Figure 17) also reflects alkali mobility. The scatter of the Buffards ash flow tuff samples is so broad, however, that further mechanisms of interference must also come into play. Although rhyolitic in general composition, this group tends to be erratically enriched in iron; this is interpreted to reflect their submarine

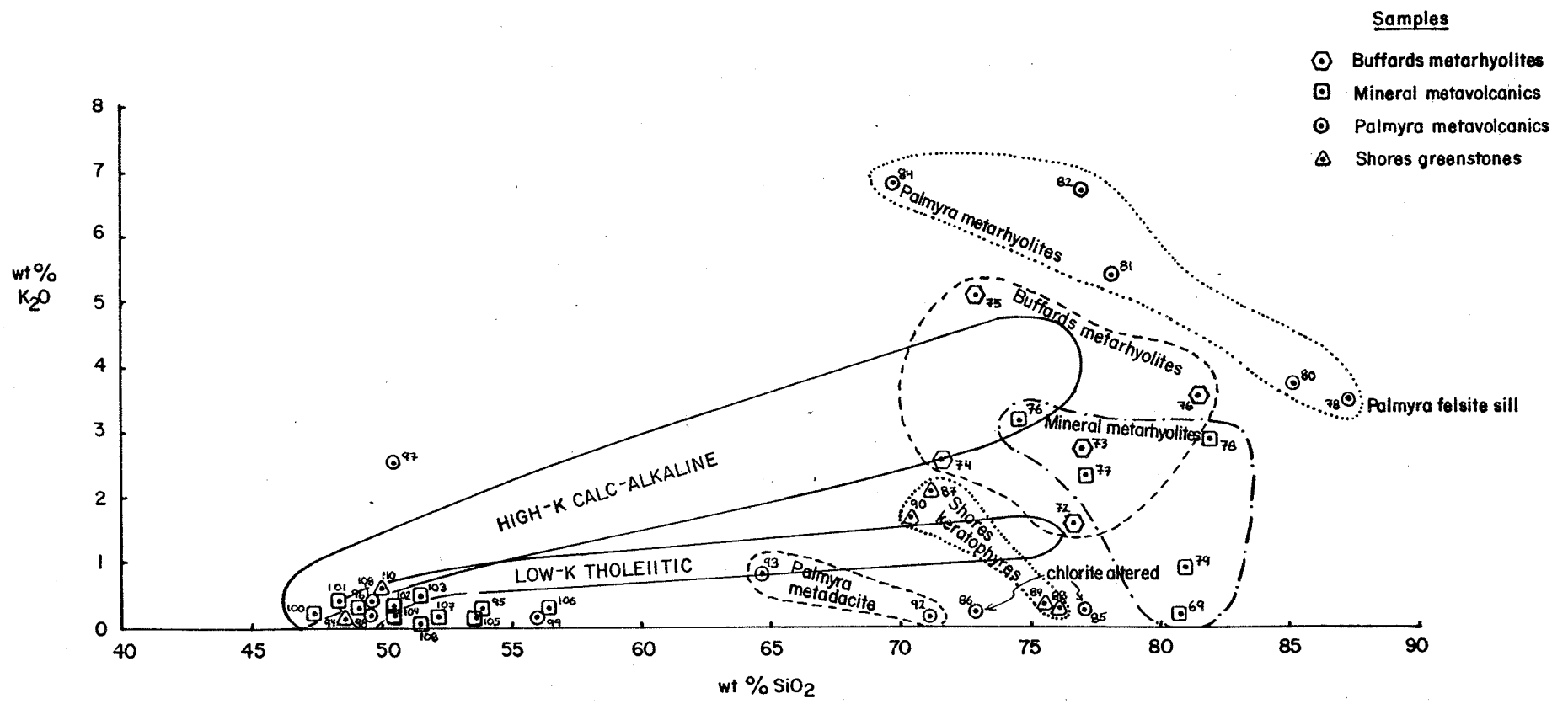

Figure 16: K_2O vs SiO_2 Binary for the Chopawamsic Metavolcanic Suites
(high and low-K fields defined by Johnson et al 1978)

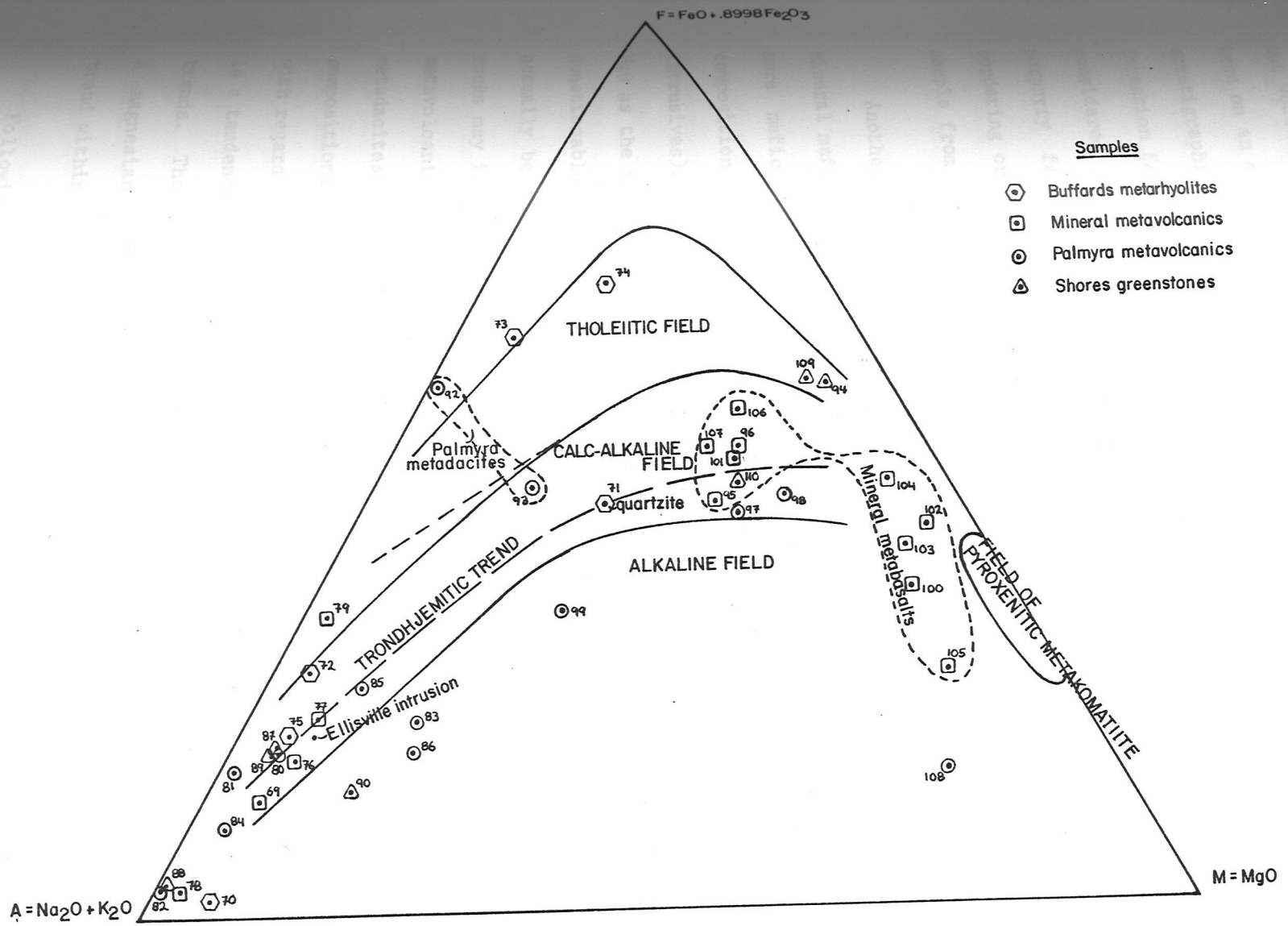

Figure 17: AFM Ternary for the Chopawamsic Metavolcanic Suites
(solid-line boundaries for tholeiitic, calc-alkaline and alkaline fields after Kuno 1968;
short, dashed boundary proposed by Irvine & Baragar 1971;
trondhjemitic trend within the alkaline field after Barker & Arth 1976)

depositional medium. These aquagene tuffs were not only leached of alkalies but would seem to have been deposited in a medium which was precipitating out iron on an ongoing basis. Such a regime is also suggested by their regional stratigraphic affiliation with the ferruginous quartzite - ironstone - iron formation facies along the belt. With respect to the Buffards, it is also considered significant that on this diagram sample 75 from the quartz eye porphyry facies along the eastern margin of the Arvonia metashale and bordering on the Ellisville granodiorite porphyry plots very close to the sample from Ellisville (126E) included for comparison.

Another interesting feature shown by the AFM diagram is the fact that the Mineral mafic metavolcanics again appear to comprise two rough groupings, the more mafic one containing signficantly higher MgO and trending towards the composition of pyroxenitic metakomatiite (see preceding discussion on the intrusives). The two samples 105 and 108, which have approximately the same MgO as the metakomatiites, turn out to contain appreciably more alkali. It is questionable, on the other hand, whether compositions of this type can actually be taken as diagnostic of any particular source magma, since these rocks may in fact have undergone pervasive metasomatism. Although the Palmyra metavolcanics do show a broad compositional range, it is notable that the metadacites are depleted in alkalies, plotting with the basaltic compositions. Again the characterizing feature -- particularly conspicuous with regard to the felsics but noted in the more mafic compositions as well -- is a tendency for the general scatter to overlap with various compositional trends. The pattern most consistently observed reveals the mafics lying along a magnesian tholeiite trend and the felsics falling near the trondhjemitic trend within the calc-alkaline field.

Following up the indication on the AFM plot that some of the Mineral

metabasalts encroach on komatiite compositions, the mafics from the various suites were also plotted on the Jensen (1976) cation plot (Figure 18), a diagram commonly found useful for discriminating among komatiitic, tholeiitic, and calc-alkalic volcanic suites. Here the majority of the samples are observed to cluster in the high-iron tholeiitic basalt field. However, three samples from the Mineral assemblage and one from the Shores greenstone comprise a subgroup that bridges the high magnesian tholeiite and basaltic komatiite fields. Considering the field of the pyroxenitic metakomatiite illustrated on the diagram for comparative purposes, it would seem evident that the more magnesian metabasalts are indeed characterized by intermediary mafic-ultramfic compositions. Also of note on the Jenson plot is the fact that the two samples (105 and 108) showing magnesian contents comparable to the komatiites have appreciably higher Al_2O_3. This would indicate that if these rocks are, as interpreted on petrographic criteria, in fact extrusive in origin, they have quite peculiar compositions, at least with respect to commonly recognized igneous rocks.

Two further diagrams often used to help discriminate among volcanic suites are shown in Figures 19 and 20. As demonstrated on the Al_2O_3 vs norm wt % plagioclase, all the mafic compositions lie within the tholeiite field but as a general rule the volcanics encroach on the calc-alkaline field with decreasing wt % An content. The only exceptions to this are the Buffards and Mineral metarhyolites, which plot as restricted groups well below this field. It should be noted that here again the Mineral metabasalts show considerable compositional variation with the more magnesian tholeiites having substantially higher wt % An. The normative An-Ab^{I}-Or diagram was utilized by Irvine and Baragar (1971) for distinguishing K-poor, common, and K-rich variants of subalkaline rocks, and differentiating the sodic and potassic

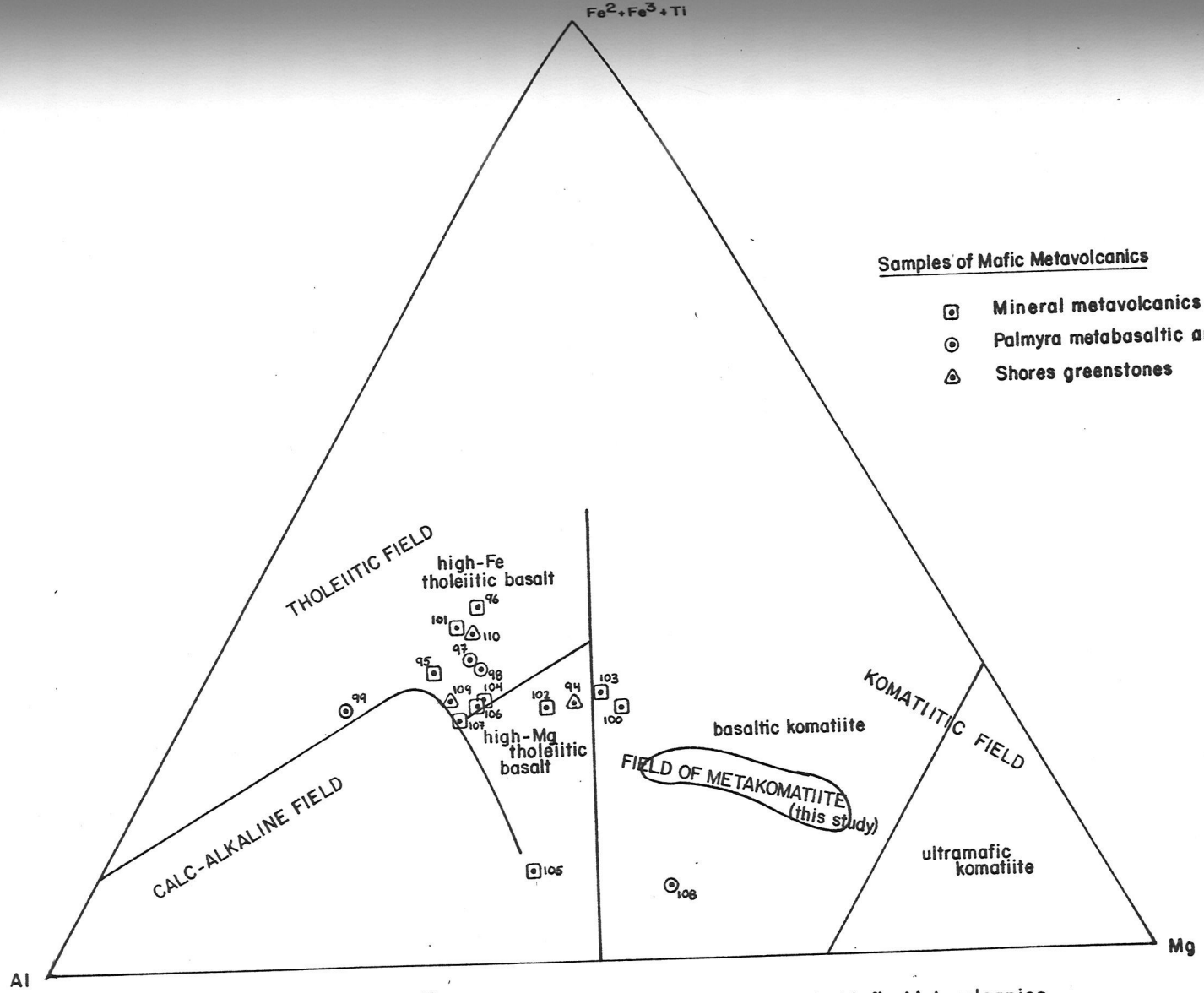

Figure 18: Al, Fe^2 + Fe^3 + Ti Cation Ternary for Chopawamsic Mafic Metavolcanics (field boundaries after Jenson 1976)

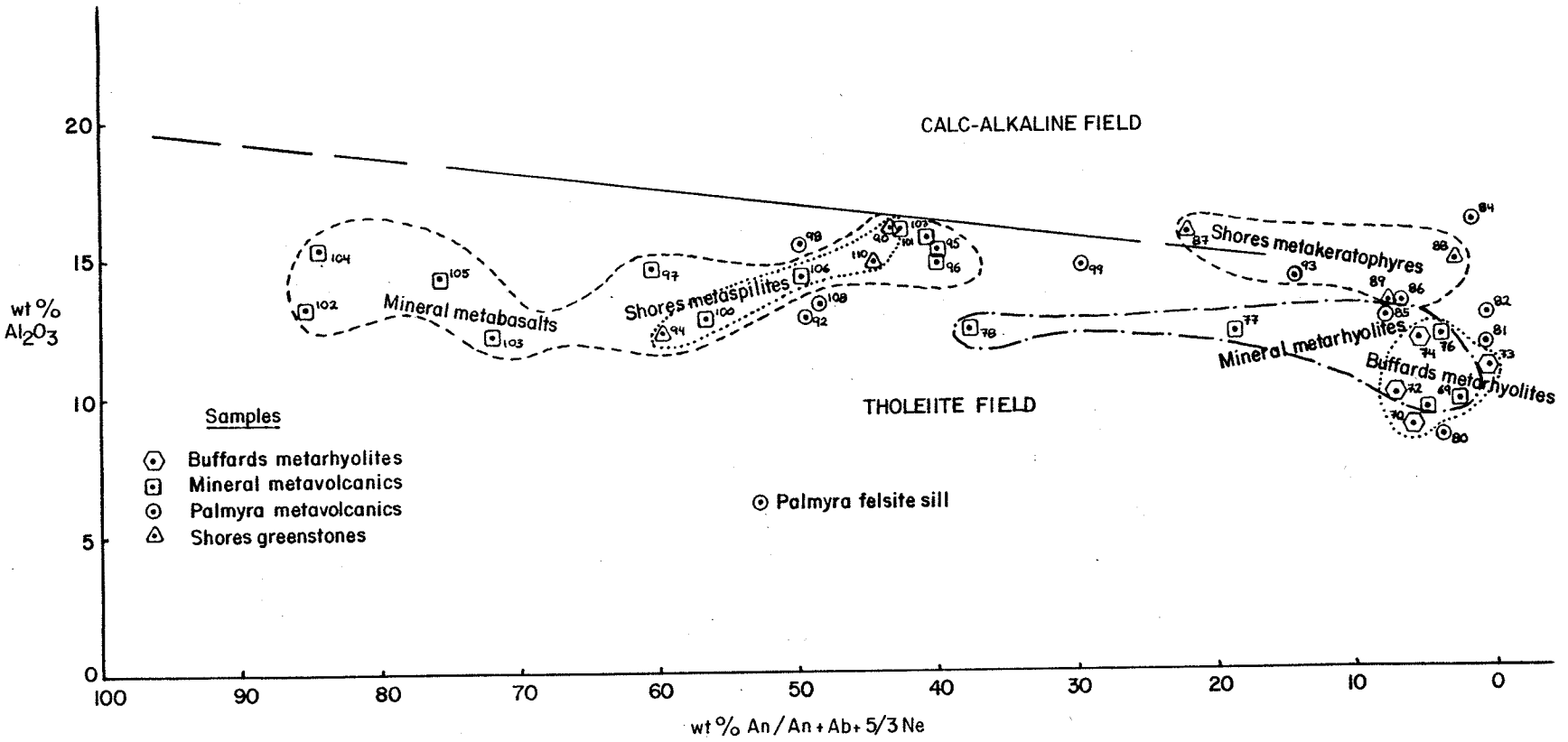

Figure 19: Al_2O_3 vs Normative Plagioclase Binary for the Chopawamsic Metavolcanic Suites
(discriminate between calc-alkaline and tholeiitic fields after Irvine & Baragar 1971)

series of the alkaline volcanics. On this particular plot (Figure 20), all the mafics cluster as K-poor types over a broad range along the An-Ab tie-line. Once more the scatter in the more alkali-rich siliceous rocks defies allocation to a specific volcanic type. Most of the Mineral silicic metavolcanics and the quartz keratophyre facies of the westerly Shores greenstone plot in the Ab corner, however, while the Palmyra metarhyolites and Buffards ash flow tuffs are primarily more K-rich types plotting near the Ab^{1}-Or tie-line.

In general the geochemical features of the volcanic lithologies suggest that the mafics broadly stem from a primitive low-K tholeiitic parentage. Many of these rocks, particularly from the Mineral suite, are quite magnesian, and a transition from basaltic komatiite through magnesian tholeiite to high iron tholeiite is in evidence. The more siliceous facies are characterized by considerable mobility of alkalies, so much so that these generally overlap the discriminates normally used to differentiate among various volcanic lineages, hence proving more difficult to classify. The different groupings of metarhyolitic rocks do demonstrate significant spread, however; this is interpreted basically to reflect compositional differences in source magmas. Both the Mineral silicic metavolcanics and the quartz kertatophyres from the Shores greenstone are low-K, sodic (trondhjemitic) types. In contrast, the Palmyra metarhyolites and the Buffards ash flow tuffs are broadly high-K calc-alkaline types.

It is considered significant that there are marked gaps in the collective composition demonstrated by the volcanics. This is interpreted to imply that these rocks are not all derived by fractional differentiation of a common source magma. The compositional discontinuities are particularly well shown by the DI vs degree of silicic saturation diagram of Figure 21. As notated

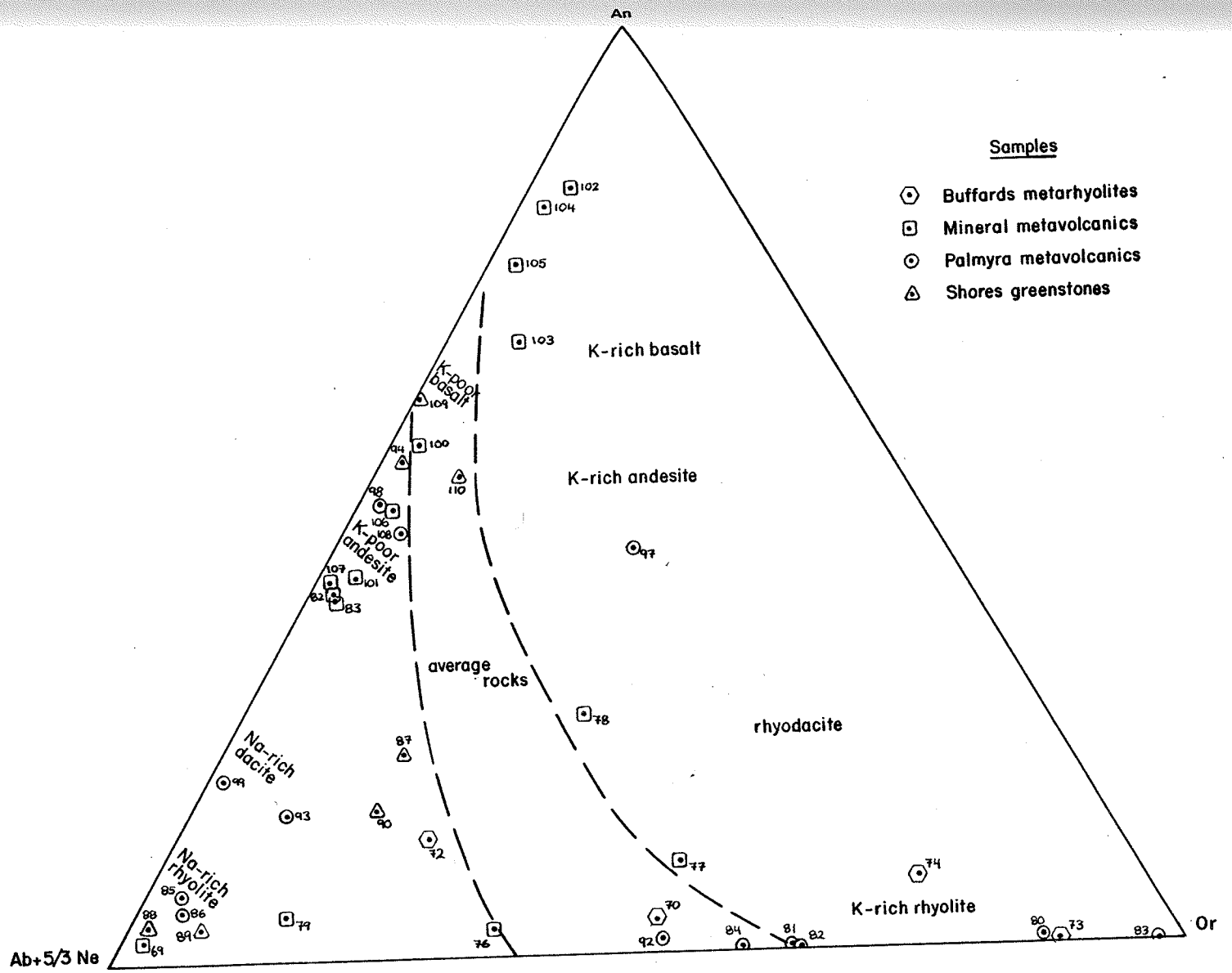

Figure 20: Normative Mineral An, Ab', Or Ternary for the Chopawamsic Metavolcanic Suites (field boundaries after Irvine & Baragar 1971)

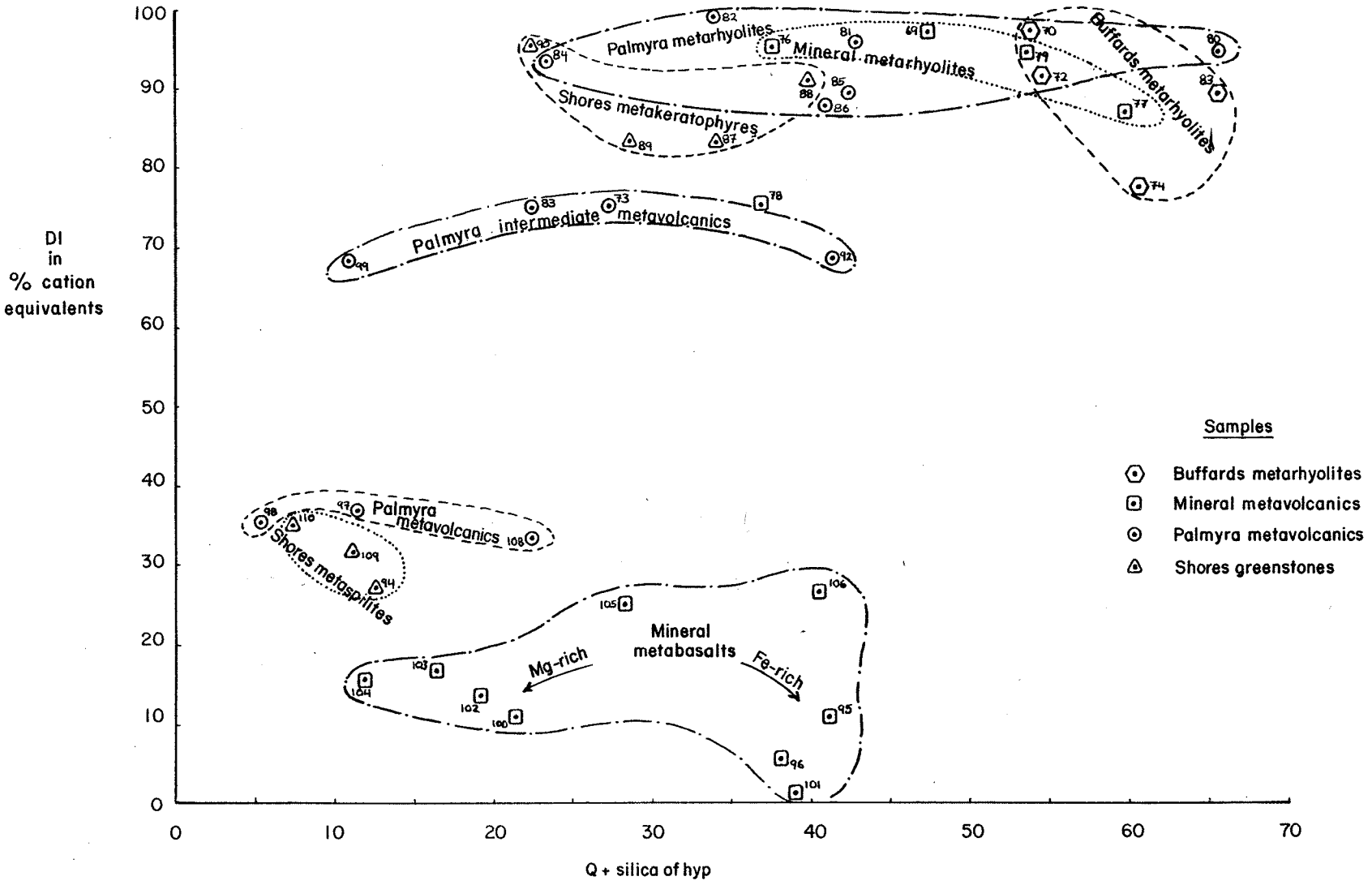

Figure 21: Differentiation Index vs Degree of Silica Saturation Binary for the Chopawamsic Metavolcanic Suites

here, the felsic volcanics from the Shores greenstone, the Mineral metavolcanics, and the Buffards quartz mica schists generally form very tight groups. With respect to the associated mafic silicic volcanic couplets evident in both the Shores and Mineral suites, one is struck particularly by their extreme bimodality. In contrast to this distinctive pattern, the Palmyra metavolcanic suite is characterized by rather broad compositional ranges in all of the various facies; this aspect is considered indicative of a more differentiated calc-alkaline volcanic series.

In a recent geochemical investigation of the Chopawamsic metavolcanics in the Fredericksburg area, Pavlides (1981) utilized a combination of immobile minor elements in conjunction with REE patterns to help identify magma types. His findings reveal that striking elemental distribution differences in the high valence cations, particularly Nb and REE, may be correlated with specific geographically defined suites. The main results of that study may be summarized as follows:

> (1) Rocks in suite A, mainly from the northern part of the Chopawamsic belt and comprising metabasaltic-keratophyric types, are characteristically highly sodic, have relatively low Nb contents (2.7-7.1 ppm) and generally flat REE patterns;
>
> (2) Rocks in suites B and C from the area south of Fredericksburg comprising primarily silicic metavolcanics petrographically similar to those in suite A have high valent cation contents which are distinctive both with respect to each other and with respect to suite A. The Nb content in suite B ranges from 27-34 ppm and in suite C from 11-17 ppm, while both suites B and C have LREE patterns;
>
> (3) The Ta River amphibolites are metabasaltic ($\leq$53% SiO_2) and although not particularly sodic are otherwise similar in high valent cation content to suite A. Although the REE patterns here are generally flat, Pavlides notes that these patterns change slightly among the various amphibolite facies and on occasion LREE trends are in evidence.

Based on these particular geochemical features, Pavlides determines that these metavolcanics originated in an island arc setting. Suite A and the Ta River

amphibolites are recognized as being tholeiitic, while suites B and C are identified as more alkalic parts of this hypothetical arc. The eastern Ta River amphibolites, alternately, are classified as a temporally equivalent oceanward facies. Although deposited more or less contemporaneously, all these different volcanic suites are considered to have been derived from compositionally distinct source magmas.

At the present stage of investigation the petrogenesis of the Chopawamsic metavolcanics appears amazingly complex. The results of Pavlides' study suggests major along-strike geochemical variations, while the present author's work identifies major across-strike variation between the differing volcanic assemblages. In both cases, the likelihood of multiple source magmas, at least for the felsic types, seems high. In general the findings of the present study indicate that the mafic volcanics comprise primitive low-K tholeiites that likely originated in the same source area as the komatiitic magmas found to comprise sill complexes and possibly flows as well. The low-K (sodic) felsics probably stem from a tholeiitic parentage, although the strong bimodality revealed by the tholeiite-sodic rhyolite suites is difficult to account for by fractional differentiation. The high-K felsics are identified as more normal calc-alkaline volcanic types, derived, at least in part, through crustal anatexis. The petrogenesis of the volcanics will be considered briefly again in the summary section on magma genesis and hydrothermal processes within the Chopawamsic belt.

3.4 Petrogenesis of the Hydrothermal Deposits

As has previously been noted, the hydrothermal deposits are considered to derive from syndepositional hydrothermal metasomatic processes. These

deposits comprise a highly varied suite of enigmatic origin. In light of such features as the petrographic-lithological convergence between hydrothermal and volcanic facies documented in Appendix B, it is virtually impossible to determine whether and to what extent they were formed through either chemical precipitation or complete breakdown of primary volcanics. One of the more important petrographic differences demonstrated by these rock types lies in the fact that while the generally more massive volcanics characteristically show the irregular overprinting effects of hydrothermal metasomatism, the hydrothermal deposits are instead typified by regular banding (a structural feature they share with banded iron formation) and are not themselves metasomatically overprinted. Both types, on the other hand, are metamorphically overprinted, as shown by metamorphic fabrics and varied porphyroblast populations. As the effects of the late metamorphic event are considered to have been isochemical, however, the whole rock geochemistry of the hydrothermal deposits is also thought to reflect original compositions.

The various facies of hydrothermal deposits selected for analytical work include oxide and silicate facies iron formation; kyanite quartzites; metacherts; cummingtonitic, hornblendic, biotitic carbonate-bearing, and sericitic pyrite-bearing ironstones; chloritites; and metamarl. The magnesian amphibolites, identified as pyroxenitic komatiites in the previous discussion on intrusives, are again considered with this group for comparative purposes since in the absence of igneous textures the hypothesized igneous origin cannot be assumed. Most of the specimens selected for analysis were collected from the Mineral metavolcanic suite and the overlying upper Chopawamsic group, but analogous facies capping the Palmyra metavolcanics were included to provide an external point of reference. The latter are differentiated on the diagrams chosen to illustrate the general geochemical nature of the group.

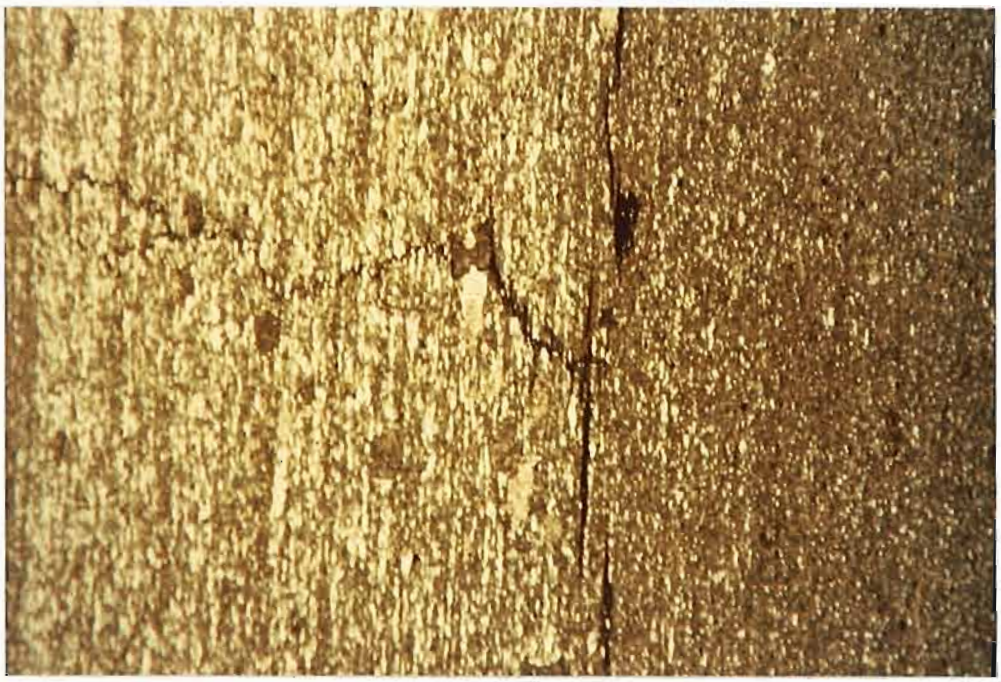

15. Ironstones capping the Palmyra metavolcanics: Crosscutting magnetite stylolites terminating in discontinuous magnetite seams at contact between underlying quartz carbonate-rich and overlying chlorite-rich marl (sample Cu-56-175, ppl, X100).

16. Marked compositional banding defined by quartz-, chlorite-, and magnetite-rich layers (sample Co-24, ppl, X100).

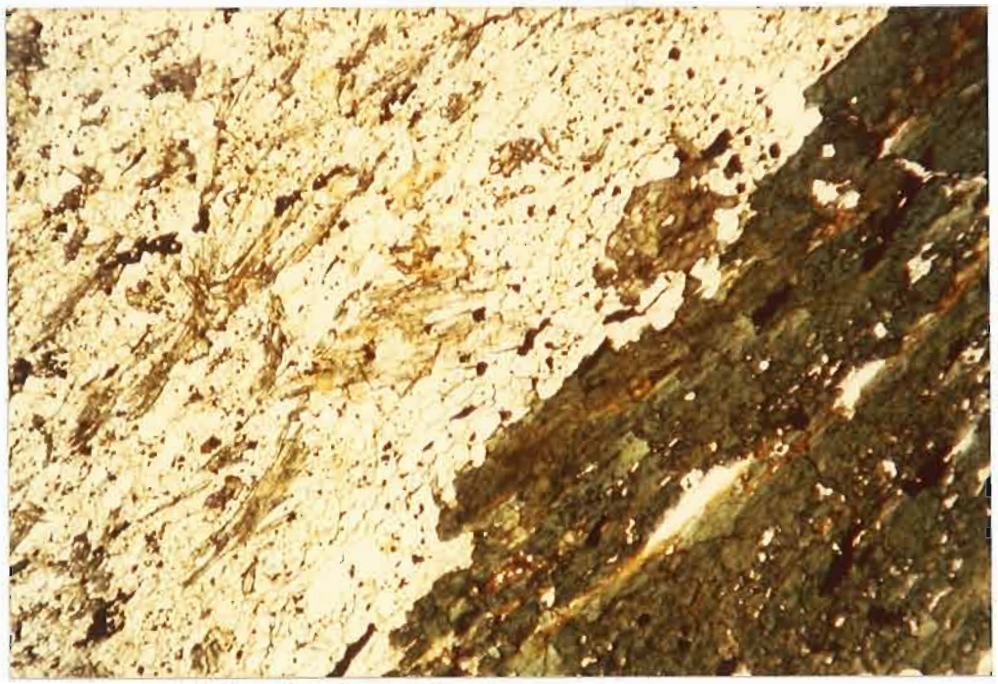

17. Ironstones capping the Mineral metavolcanics: Marked compositional banding defined by hornblende-rich and quartz-albite-cummingtonite-rich layers in two-amphibole ironstone.

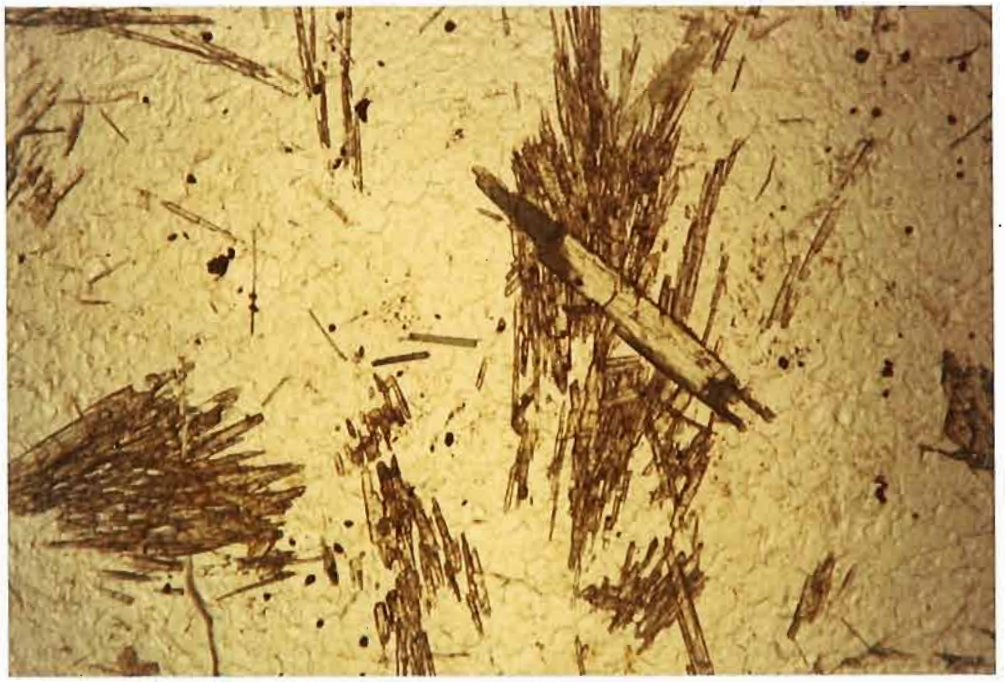

18. Ironstones capping the Mineral metavolcanics: A polygonal textured quartz-albite-magnetite assemblage hosting randomly oriented cummingtonite splays. Note the hornblende terminations on the large cummingtonite idioblast crsosscutting one of the cummingtonite bundles (sample Ca-2, ppl, X150).

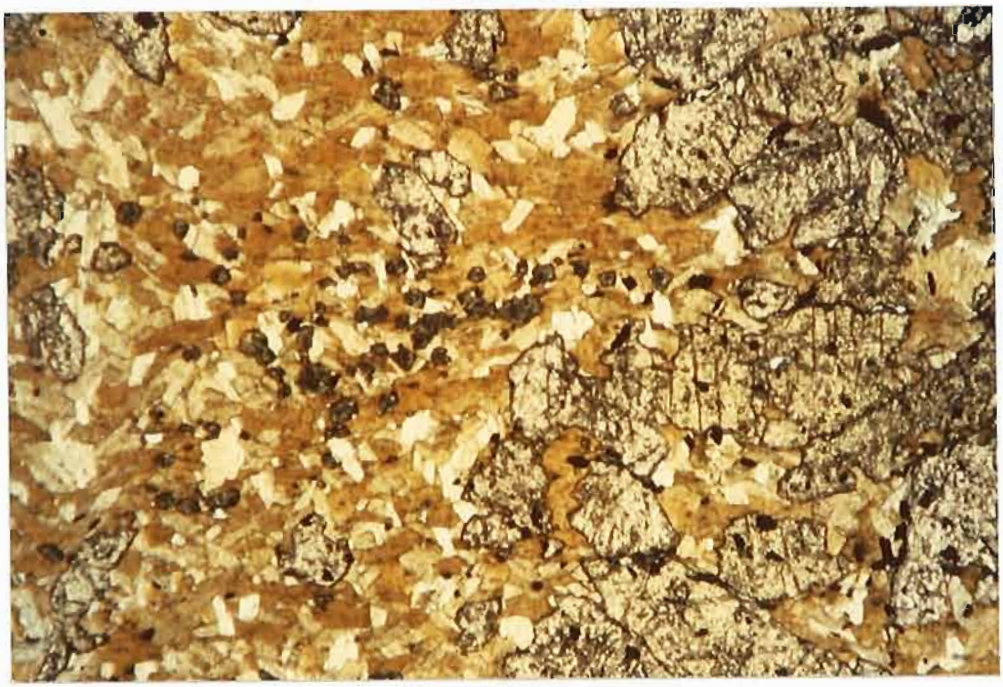

19. Large staurolite and small gahnite porphyroblasts hosted in a decussate textured biotite-calcite-quartz assemblage (a biotite-carbonate ironstone) (sample Cu-87-781', ppl, X100).

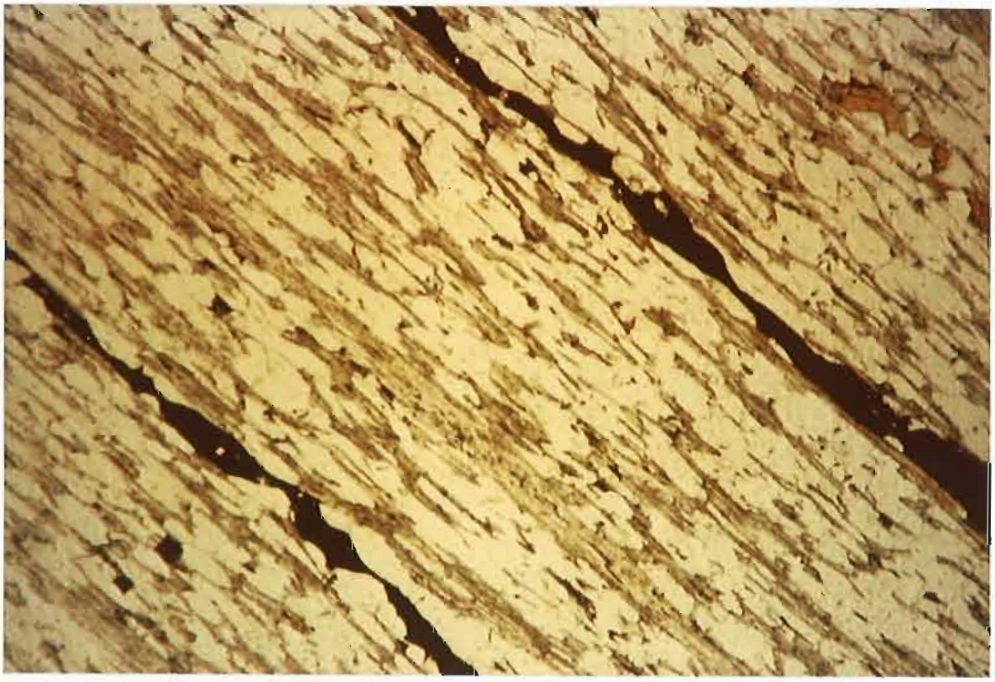

20. Pyrite laminae in well foliated quartz-sericite schist (pyritic ironstone) (sample Ar-8, ppl, X175).

21. Hydrothermal chloritite (Mineral district): Mg-chlorite-phlogopite matte hosting staurolite crosses and irregularly shaped sulphides. The patchy quartz appears to be related to the crystallization of staurolite (sample ST, ppl, X100).

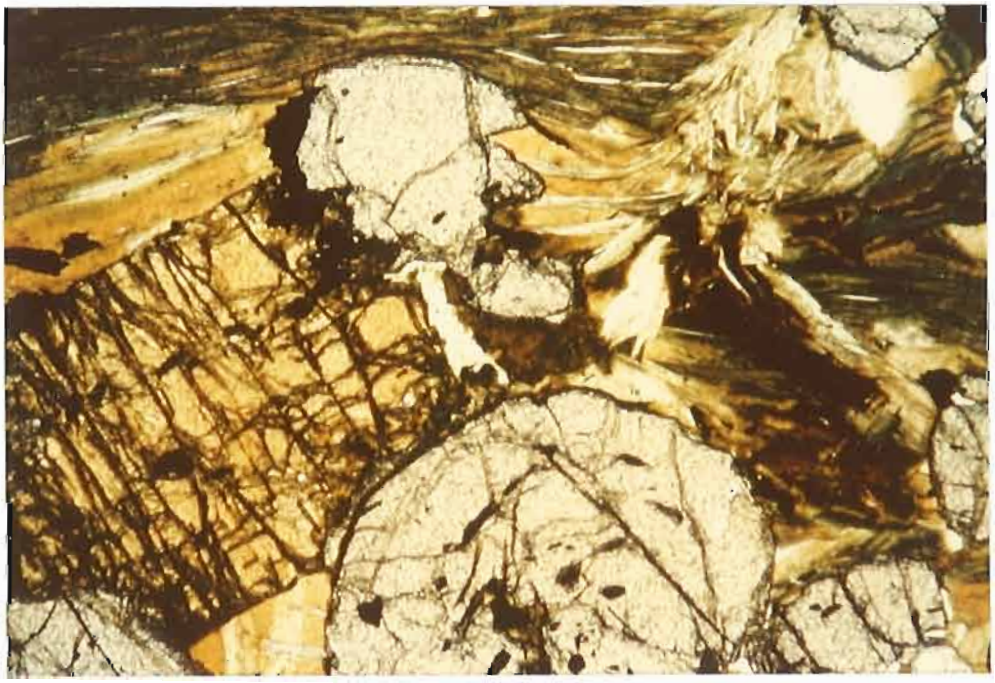

22. Hydrothermal chloritite (Andersonville district): Coarse coalescing garnet and staurolite porphyroblasts hosted in a matte of intimately intergrown phlogopite and Mg-chlorite (sample NB-2-416', ppl, X75).

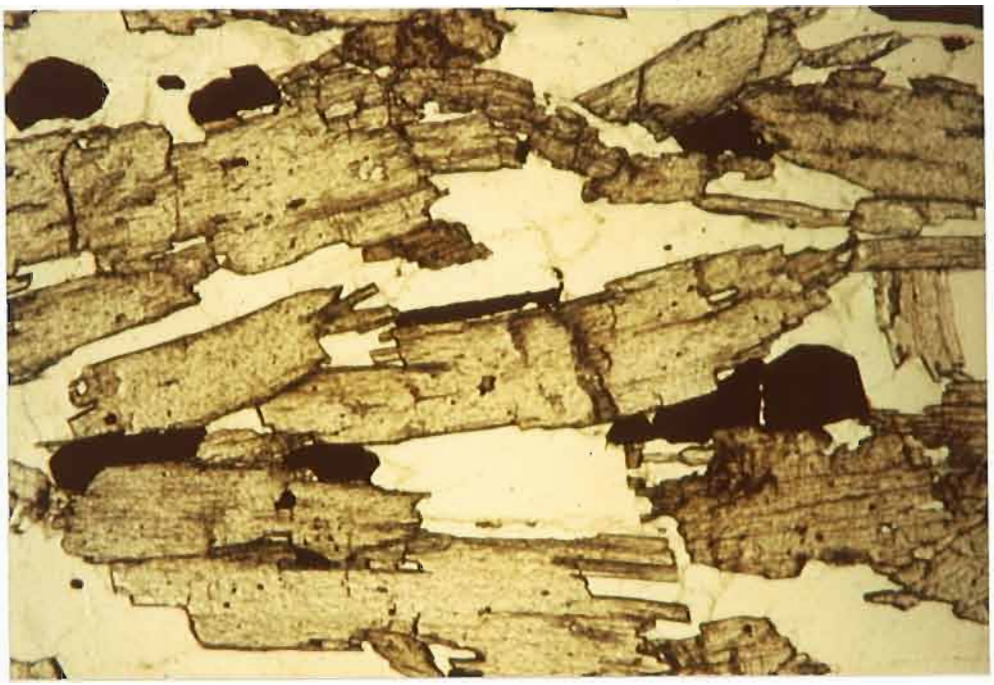

23. Columnar kyanite and dimensionally elongate quartz and pyrite impart a marked foliation fabric to the kyanite quartzite horizons (sample D-13, ppl, X75).

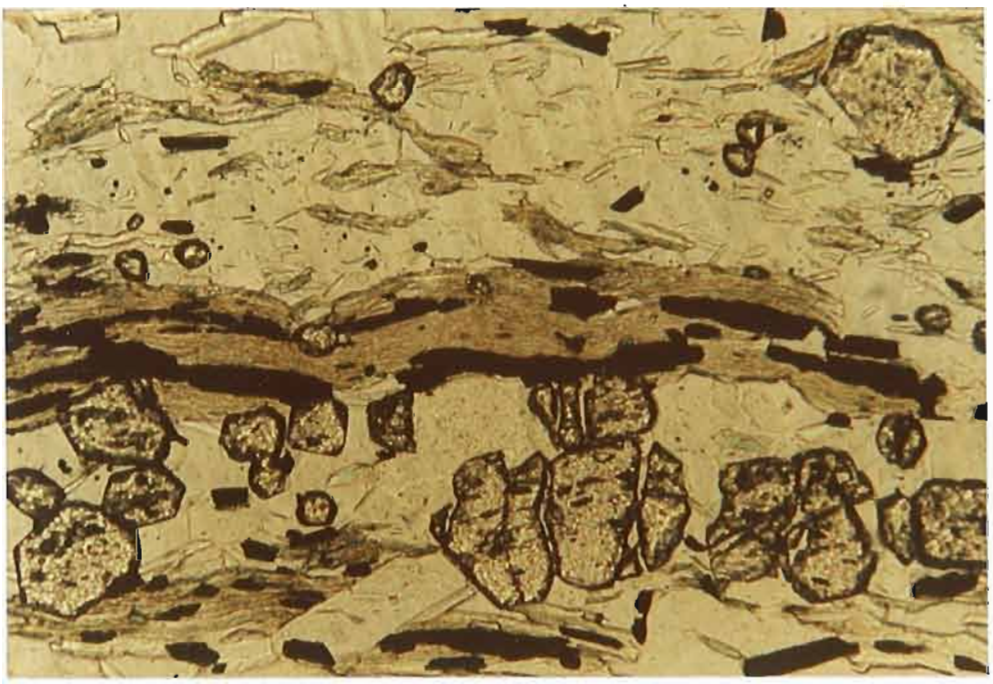

24. A mineralogically complex quartz-sillimanite-garnet-sericite-hematite-chlorite-tourmaline-zircon schist characteristic of the uppermost parts of the Buffards Formation (sample D-60, X150).

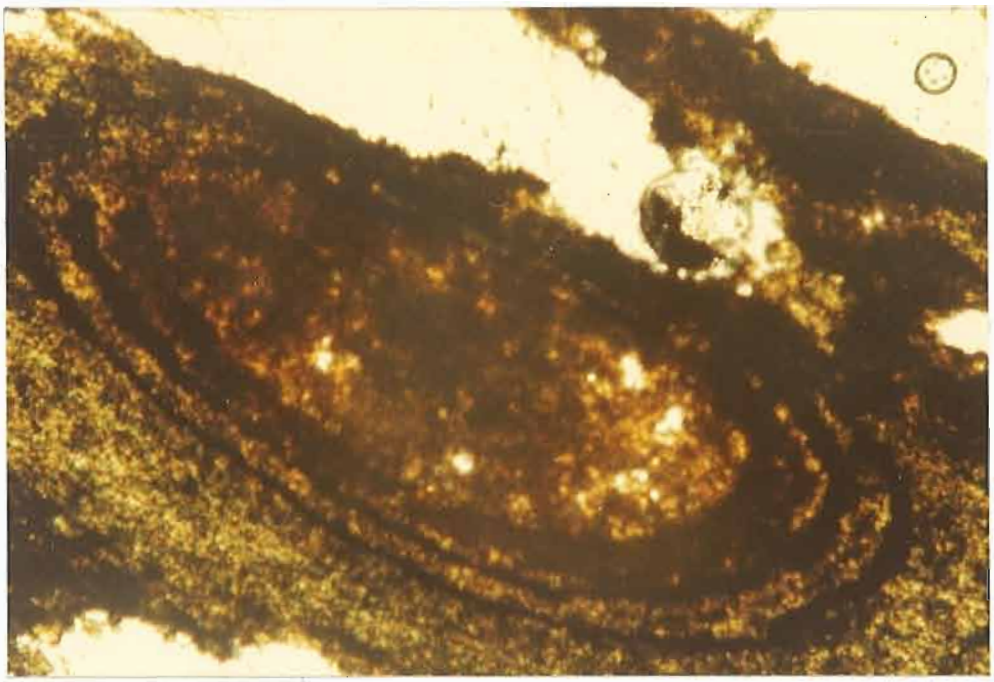

25. Basal shale silicate iron formation: Oolitic chloritite occurring below the almandine isograd. The oolites are defined by concentric layering of chamositic chlorite and goethite (sample A-50, ppl, X50).

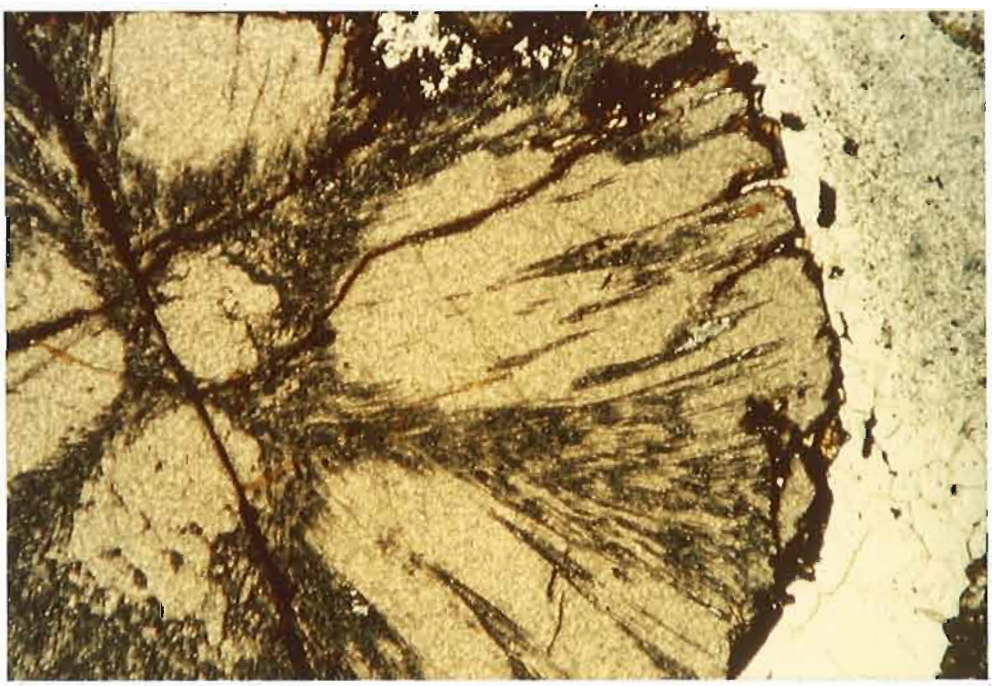

26. Characteristic radial inclusion patterns in garnet porphyroblasts growing in the oolitic chloritite above the almandine isograd (sample A-27, ppl, X75).

As such rock types as these have never been geochemically investigated on the systematic basis that the intrusive and extrusive rocks have, it is difficult to generalize about the connections to be made between geochemical signatures and the features of a hypothetical hydrothermal event. Without comparative data the petrochemical nature of this group can only be noted and petrogenetic implications speculated upon. As with the preceding section, the following discussion is not partitioned into separate subsections for each of the different hydrothermal deposit facies. Rather, the geochemical data for all the various facies are plotted together. Because of their apparent petrographic convergence with volcanic rocks, some plots also show fields occupied by the latter in order to demonstrate how these different lithofacies overlap.

As illustrated on the AFM diagram (Figure 22), most of the various facies of hydrothermal deposit have very specific compositional limits. Those that do not occupy restricted fields are very highly siliceous types which because of their very low iron, alkali, and magnesian contents have overly sensitive ratios among these components. Nevertheless, although the compositional fields of siliceous types are broad, several petrochemical features are of note. The kyanite quartzites show iron enrichment and locally plot near the iron corner of the diagram. Significantly, they share this iron-enriched aspect with the closely affiliated Buffards quartz mica schists. In contrast to the kyanite quartzites, metacherts from both the Mineral and Palmyra metavolcanic assemblages prove to be enriched in alkalies and locally plot near the alkali corner.

All other facies of the hydrothermal deposits show far more restricted compositional fields. As expected, the iron formations generally plot as a tight grouping near the iron corner and generally on the FeO-MgO tie-line,

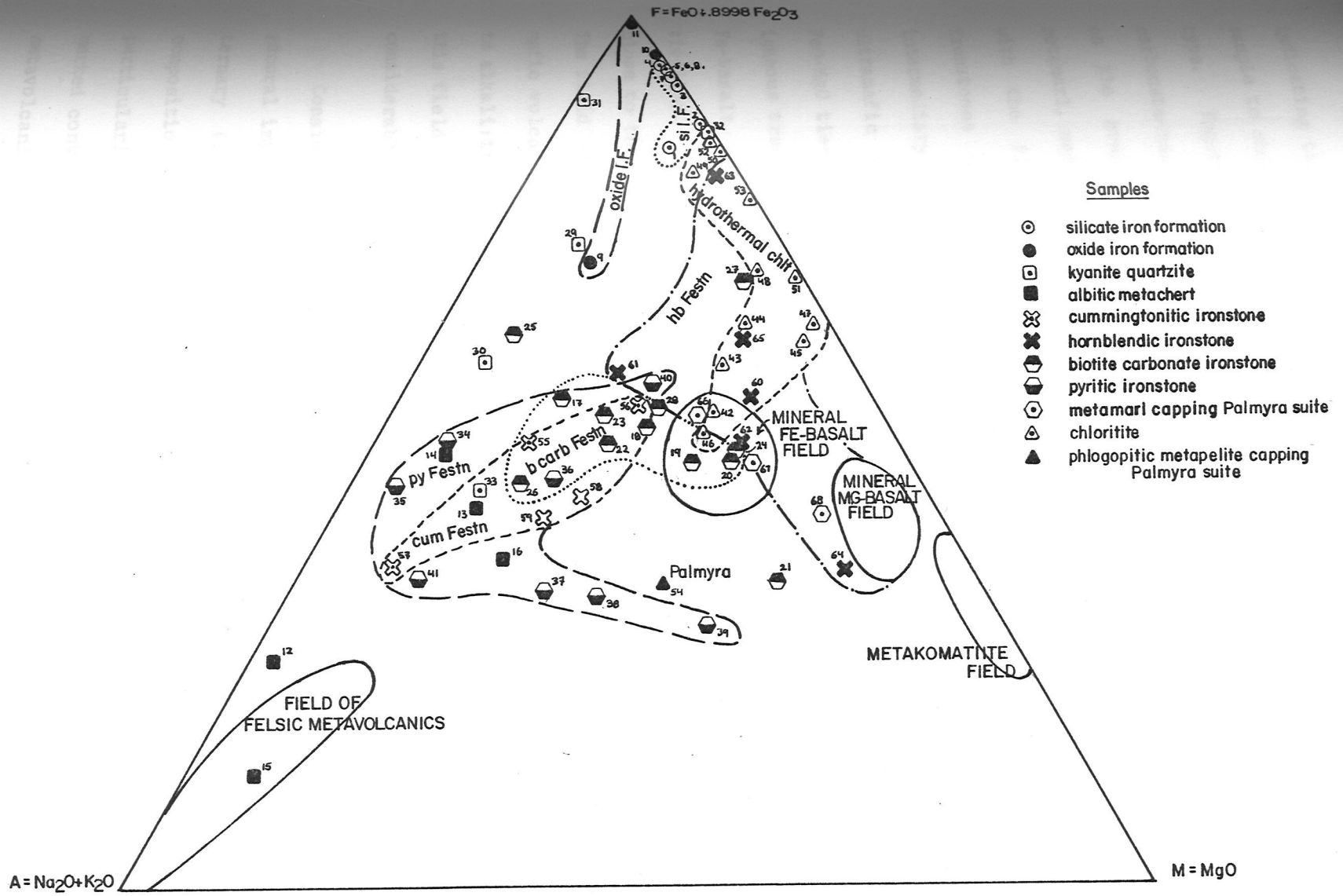

Figure 22: AFM Ternary for Hydrothermal Deposits in the Chopawamsic Metavolcanic Belt

indicating their extremely low alkali contents. The only iron formation sample to show notable alkali content was of a mixed oxide silicate facies type. Together the compositional fields of the hornblendic, biotitic carbonate-bearing, and cummingtonitic ironstones occupy a compositional tract on the graph that broadly mimics an igneous trend. Many samples of the metamarl, mafic ironstone, and biotitic carbonate-bearing ironstone overlap with the field of Fe-basalt, and locally the metamarls and hornblendic ironstones also encroach on the field of Mg-basalt. This field occurs intermediary between that of Fe-basalt and the rather tight cluster of ultramafic amphibolite (metakomatiite?) towards the magnesian end of the FeO-MgO tie-line. The hydrothermal chloritites depart markedly from any such igneous trend, occupying a rather narrow trough originating in the field of Fe-basalt and finishing up in a rather broad field along the FeO-MgO tie-line. Interestingly, the chloritites from the New Canton trend plot very close to the most magnesian samples of the silicate facies iron formation. The field of pyritic ironstones would seem also to overlap the area where mafic volcanics plot, but this facies comprises a relatively broad field due to alkali:iron variation. The samples of pyritic ironstone that do not occupy this field are of the chloritic subfacies; these particular samples show considerable magnesian enrichment.

Considering that the various facies of the hydrothermal deposits are in general impoverished in alkalies, it is unexpected that on a Na_2O-CaO-K_2O ternary (Figure 23) the alkali ratios should define quite restricted compositional fields for the various members. Even more surprisingly, this is particularly evident in the most siliceous types -- a geochemical feature in marked contrast to the previously discussed alkali scatter of the siliceous metavolcanics. The metacherts define a striking narrow tract leading directly

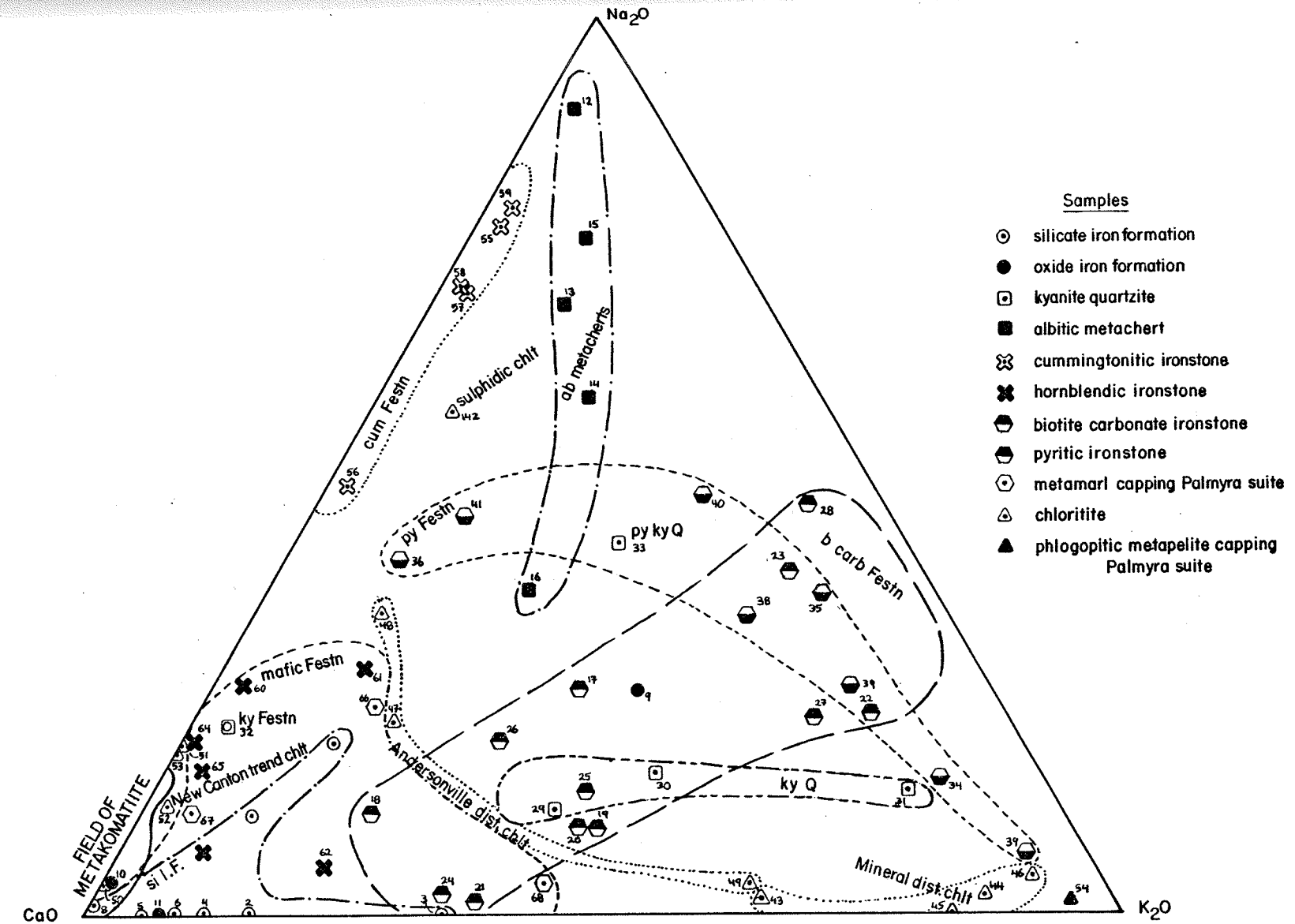

Figure 23: Na_2O-CaO-K_2O Ternary for Hydrothermal Deposits in the Chopawamsic Metavolcanic Belt

away from the Na_2O corner, due to their variable albite contents. The cummingtonitic ironstones occupy a narrow band along the Na_2O-CaO tie-line, indicating that they have considerable modal albitic plagioclase and are transitional with the more calcic hornblende-rich ironstone facies. Both the kyanite quartzite and the biotite carbonate ironstone are enriched in K_2O over Na_2O, and define trends towards CaO enrichment. The hornblendic ironstones, silicate iron formation, and magnesian amphibolites plot close to the CaO corner, showing very low Na_2O and K_2O contents. The fact that there is one sample of metamarl from the Palmyra assemblage with K_2O enrichment over other mafic types suggests that the K_2O can be selectively partitioned into some bands. Of all the various lithofacies, the hydrothermal chloritites show the broadest compositional differences in their alkali contents. It is interesting, however, that this scatter is broadly correlative to the different geographic areas where these rocks were collected. The New Canton chloritites plot near the CaO corner of the NaO-CaO tie-line; the chloritites from the Andersonville district show significant increases in their ratio of K_2O and Na_2O over the New Canton chloritites; the Mineral district chloritites plot with the single sample of phlogopitic metapelite capping the Palmyra assemblage very near the K_2O corner.

The SiO_2, FeO^T+MgO+MnO, Al_2O_3 diagram (Figure 24) generally includes between 85-95% of the rock constituents. Again relatively tight compositional fields are demonstrated by the various hydrothermal types. Collectively these samples occupy a tract lying subparallel to the SiO_2-FeO^T+MgO+MnO tie-line. Along the extent of the tract there is a general differentiation into SiO+FeO^T+MgO+MnO-rich and Al_2O_3-rich facies. The kyanite quartzites are enriched in Al_2O_3 over albitic metachert and cummingtonitic ironstone. The sericitic pyritic ironstones appear transitional between the high Al_2O_3 and

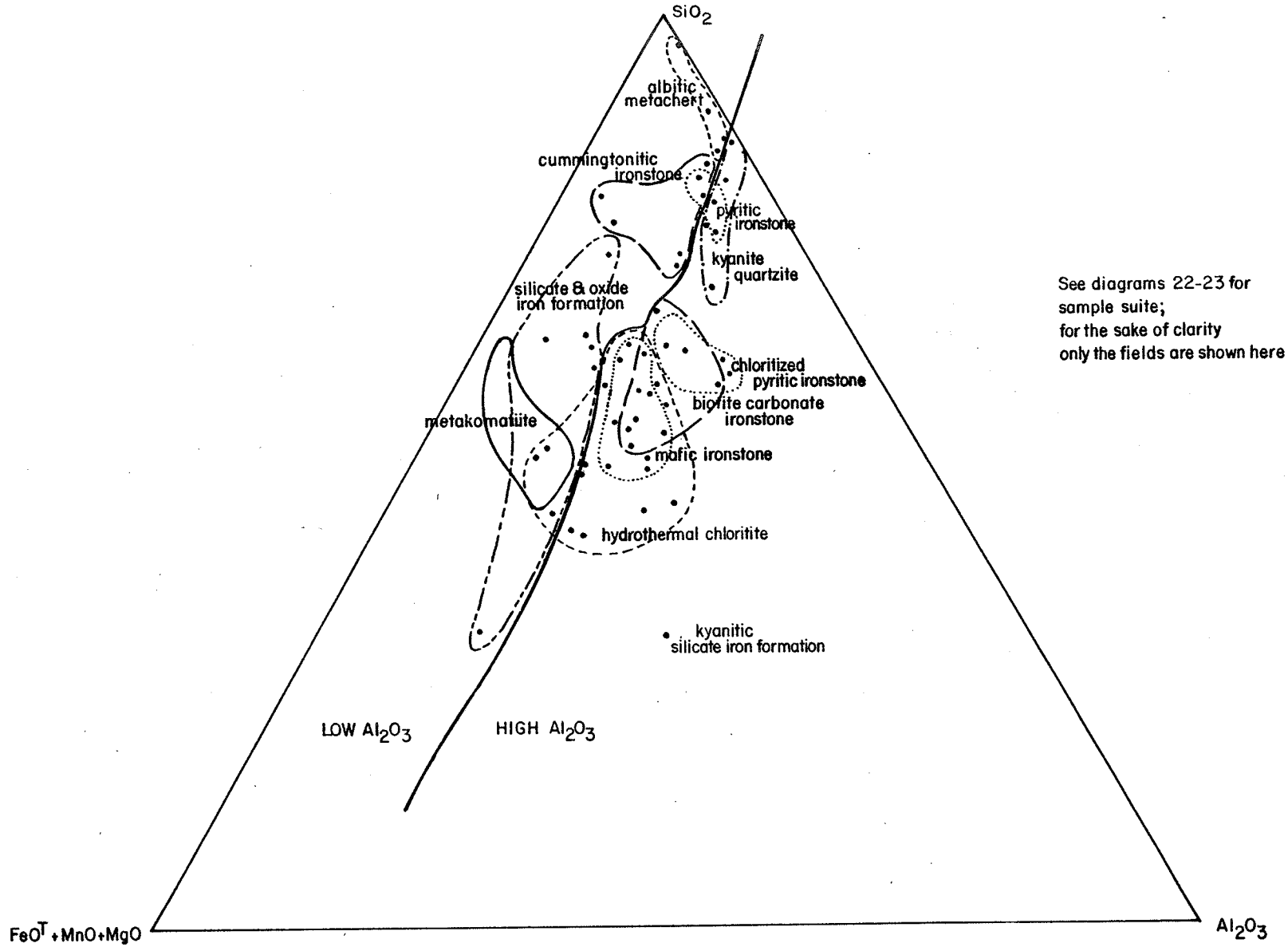

See diagrams 22-23 for sample suite; for the sake of clarity only the fields are shown here.

Figure 24: SiO_2-FeO^T+MgO+MnO-Al_2O_3 Ternary for Hydrothermal Deposits in the Chopawamsic Metavolcanic Belt

low Al_2O groups, but the chloritized subfacies broadly overlaps with the biotite-carbonate ironstone facies in the Al_2O_3-rich field. The broad differentiation into low and high Al_2O_3 types also occurs within silicate facies iron formation with the local occurrence of the kyanite-bearing member. The ultramafic amphibolite field broadly overlaps with silicate facies iron formation in the low Al_2O_3 field.

Two further diagrams are presented to illustrate the compositional variation among the species MgO, CaO, FeO^T, and Al_2O_3 in the various hydrothermal deposits. As demonstrated on the MgO-CaO-Al_2O_3 diagram (Figure 25), by far the greatest number of samples plot near the MgO-Al_2O_3 tie-line, indicating that the group as a whole is depleted in CaO over MgO. Significantly, even the samples that do reflect an appreciable CaO content, such as the biotite carbonate, mafic, and cummingtonitic ironstones, all belong to groups which are dominantly magnesian. This compositional feature would seem to indicate a general bias towards either a petrogenetic system geochemically enriched in MgO over CaO or environmental conditions favouring precipitation of the MgO component while CaO stayed in solution. Also of note on the MgO-CaO-Al_2O_3 ternary is the fact that all of the various deposits identified as being of hydrothermal origin on petrographic evidence tend to mutually overlap, while the magnesian amphibolites are quite distinct. This suggests that the latter rocks had an origin quite different from the hydrothermal one advocated for the group as a whole, and indeed are probably pyroxenitic komatiites as was previously suggested.

The last diagram (Figure 26) illustrates the chemical variation of MgO-FeO-Al_2O_3 in the suite. As on other plots, each type of hydrothermal deposit occupies a unique position in this field; this is interpreted to signify that rather than deriving haphazardly and purely coincidentally from

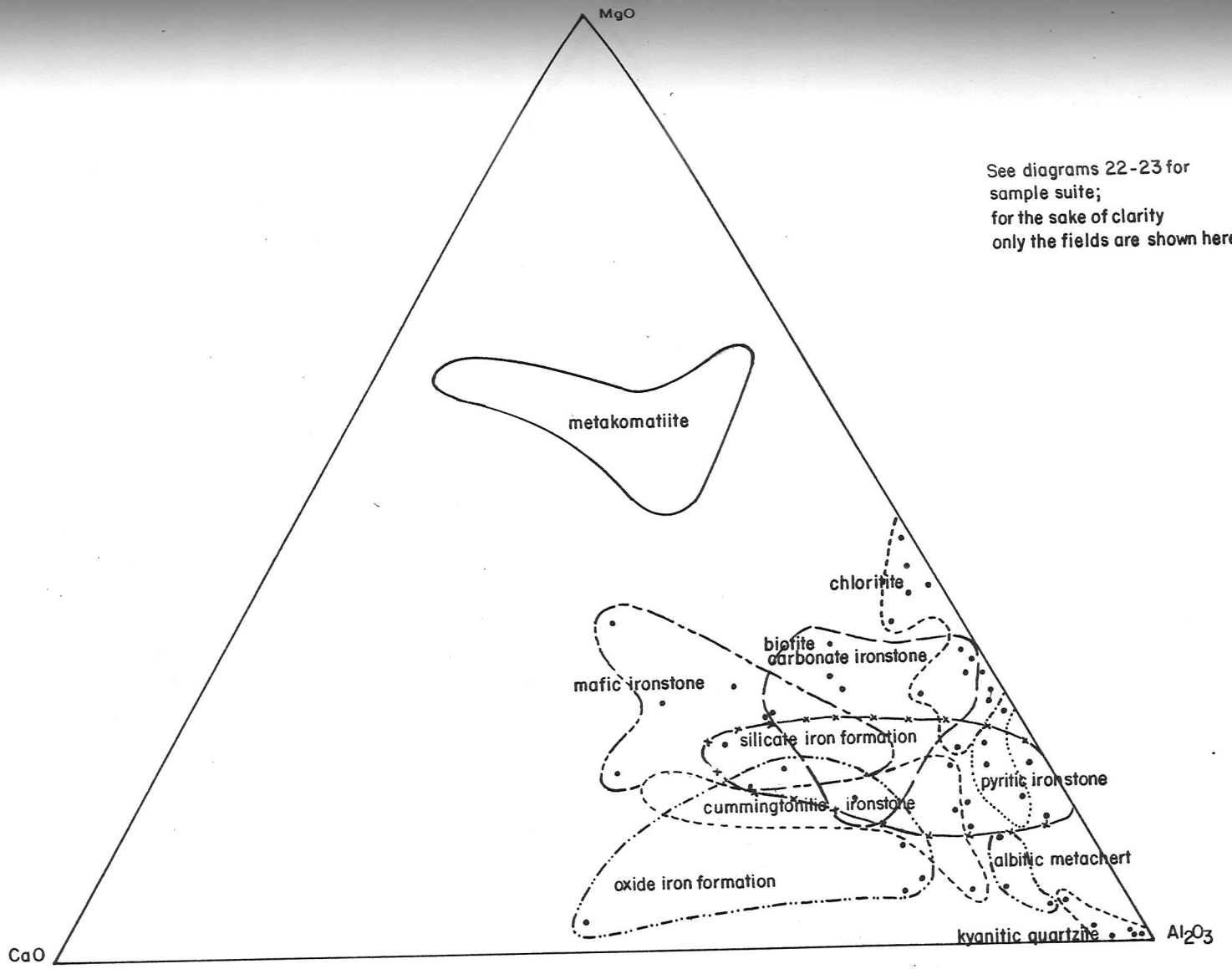

Figure 25: $MgO-CaO-Al_2O_3$ Ternary for Hydrothermal Deposits in the Chopawamsic Metavolcanic Belt

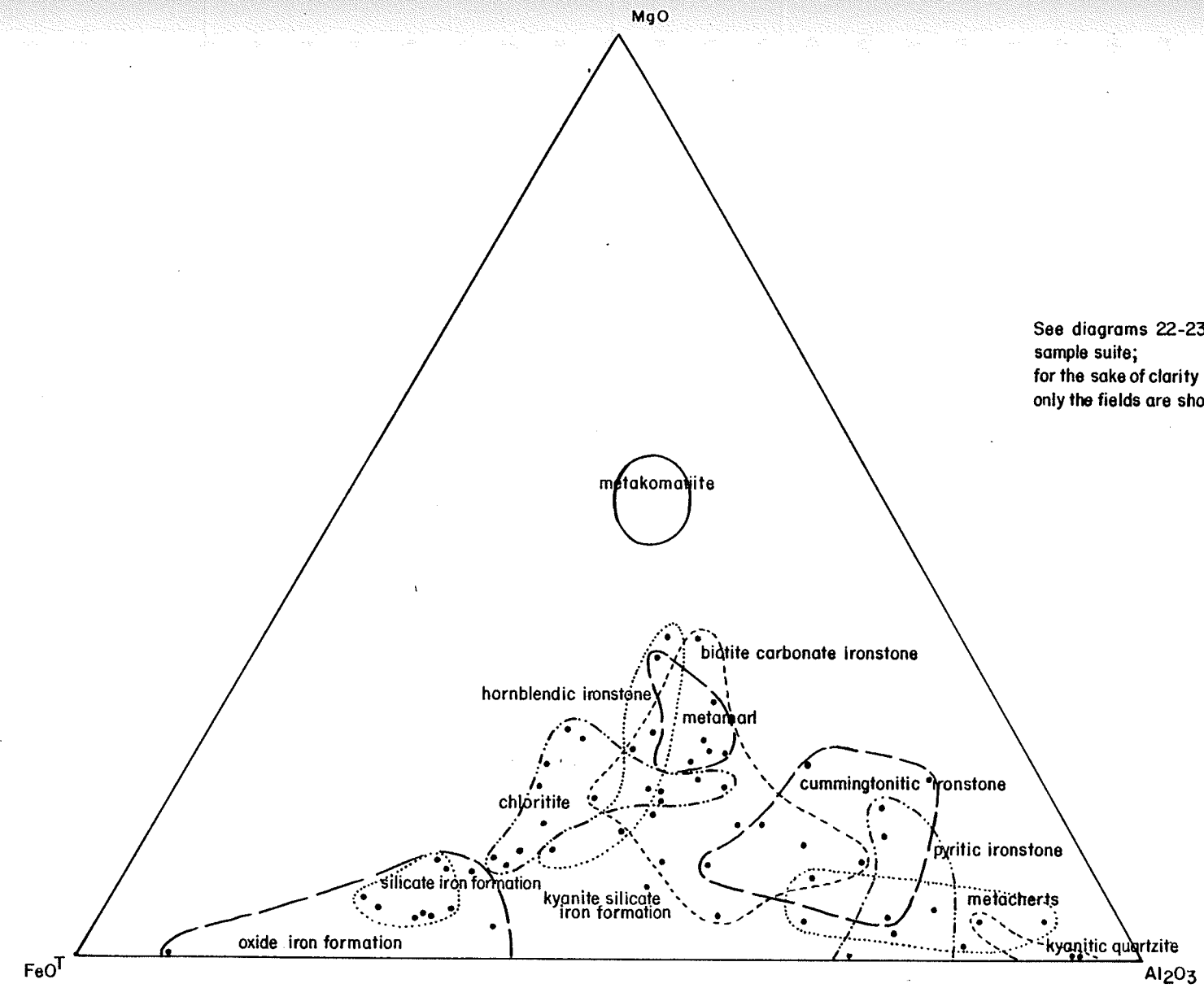

Figure 26: MgO-FeO^T-Al_2O_3 Ternary for Hydrothermal Deposits in the Chopawamsic Metavolcanic Belt

random events, these various rock types stem from petrogenetic processes which had a critical control on their resultant petrochemical features. Here again the suite is broadly differentiated into aluminous and iron-rich types. Also, the various lithofacies tend to converge in a tract centered on the highest MgO content located in the field occupied by the hornblendic ironstones and compositionally similar metamarls which cap the Palmyra metavolcanic suite. It is particularly noteworthy that hornblendic ironstones here define a very narrow trend with more magnesian and iron-enriched members at nearly constant Al_2O_3 contents. The two samples of hornblendite (64 and 65) in this group, which were included for comparison on plots with magnesian amphibolites in the discussion on ultramafic-mafic intrusive rocks and discoverd to have many whole rock compositional similarities to magnesian and iron tholeiitic basalt respectively, here plot in the more magnesian end of the mafic ironstone spectrum. The more magnesian members of the mafic ironstones compositionally overlap with the biotite-carbonate ironstones, while the more iron-rich members overlap with the chloritites. The chloritites, however, show even further iron enrichment and encroach on the field of silicate iron formation. It is also noteworthy that the fields of hornblendic and cummingtonitic ironstones, which converged in other plots, here are isolated due to the proportionately higher Al_2O_3 in the cummingtonitic facies; mineralogically this is accounted for by the considerable albitic plagioclase. Once again the magnesian amphibolites plot as an isolated group, supporting the interpretation that they had a separate igneous origin.

In general the petrochemical features of the hydrothermal deposits, as illustrated on the foregoing graphical plots, indicate that the various facies identified on petrographic criteria are characterized by unique but mutually overlapping geochemistry. Furthermore, the inherent chemical expression of

any particular type generally transcends geography and in specific cases even holds between different volcanic assemblages. The upper Chopawamsic metamarls, carbonate-bearing metapelites, and metacherts capping the Palmyra suite, for instance, compare well respectively with the Mineral assemblage mafic ironstones, biotite carbonate ironstones, and metacherts. On the other hand, there is also some suggestion that within any given facies samples from particular areas may show geochemical idiosyncracies; this aspect is well illustrated by the alkali content of the Mineral district, New Canton, and Andersonville district chloritites.

In contrast to the siliceous volcanic rocks, the siliceous hydrothermal deposits show much more restricted alkali contents; this is interpreted to be a result of partitioning of the alkalies into differing facies. On the whole, the group is much more magnesian than calcic, and there is evidence that K_2O is partitioned into the more magnesian types while Na_2O is partitioned with iron (as in cummingtonitic ironstones) or, on occasion, with high-silica rocks (as in albitic metacherts). One of the more striking geochemical aspects evident particularly among the more mafic variants is the fact that the common overlapping of some facies tends to define trends that mimic igneous ones, while the compositional fields of other types depart quite radically from such trends. This is shown especially well on the AFM diagram, where the mafic ironstones, biotite-carbonate ironstones, cummingtonitic ironstones, and metacherts collectively lie along a trend paralleling that defined by the differentiated volcanic suite. Even the kyanite quartzites, though not lying on any common igneous trend, bear the same iron enrichment signature as the Buffards ash flow tuffs, a lithology with which it shows a close stratigraphic association. Alternately, although some samples of chloritite overlap in the area of mafic volcanics, the composition of this particular facies encroaches

on that of silicate iron formation, thus departing radically from any igneous signature.

The general compositional similarity of mafic ironstones and biotitic carbonate ironstones with mafic volcanics, and of cummingtonitic ironstone, pyritic ironstone, and metacherts with felsic metavolcanics, strongly suggests convergence of magmatic and hydrothermal fluid compositions or, conversely, that volcanic emanations in the submarine environment may have taken the form of peculiar thin-banded lithologies of extremely variable composition from one band to another. Whatever the specific associations are between hydrothermal metasomatic fluid and primary magma/rock components (this is discussed in greater detail in the following section), the apparent igneous affinity of these particular types of ironstone indicates that they are closely related to volcanism and do not perforce reflect on sedimentational conditions.

Hydrothermal deposit types in which an overlap with igneous suites is not a major characterizing feature include the silicate facies iron formation, chloritite, and the chloritic facies of the pyritic ironstones. As the fields of the latter two facies do show some encroachment on the igneous field, however, these species could conceivably have originated through the progressive intensification of hydrothermal activity that gave rise to other ironstone types. The chloritic pyritic ironstones show strong magnesian enrichment over the more common sericitic pyritic ironstones, while the chloritites demonstrate alkali depletion and iron enrichment over mafic biotite carbonate ironstones. The fact that the chloritites from New Canton reveal particularly close compositional similarity to the basal shale silicate facies iron formation could be interpreted to suggest a petrogenetic link between more localized hydrothermal processes and the formation of this regionally extensive silicate facies iron formation unit. What would seem to

be suggested by such a link is that syndepositional hydrothermal regimes have more and less focused counterparts, a feature which in this case is expressed lithologically by the formation of proximal chloritite and distal silicate iron formation. From this point of view the New Canton chloritite might be considered intermediary between the basal shale silicate facies iron formation and the chloritites of the Mineral and Andersonville districts.

3.5 Magma Genesis and Regional Hydrothermal Metasomatism

The petrogenetic interpretations offered throughout the foregoing discussion on whole rock geochemical signatures of the various intrusive, extrusive, and hydrothermal lithologies need to be considered collectively in order to clarify which specific petrogenetic processes have played significant roles in determining the lithological character of this terrane. Although brief mention has already been made of the apparent source magma affinity for the intrusive and extrusive igneous rocks, the many ramifications of repeated mafic to ultramafic injections overlapping with more centralized early tonalitic-trondhjemitic and later granodioritic-granite magma types and of the possible petrological ties between the various extrusive suites and their intrusive counterparts have not yet been considered in any detail. Furthermore, although the compositional similarities shown by a number of hydrothermal deposits with extrusive volcanic counterparts have been pointed out and general hydrothermal metasomatic processes invoked to account for such compositional overlaps as are evident, a more critical discussion of these hydrothermal metasomatic processes is necessary before this particular petrogenetic phenomenon may be adequately elucidated.

A full investigation of magma genesis including detailed petrological modelling of mantle compositions and primary melts utilizing "immobile" trace elements is beyond the scope of the present investigation. Nevertheless, it is evident from the general compositional difference between differentiated mafic sill complexes and stock-like felsic intrusives and from the strong bimodality of the volcanic suites that these primary melts probably did not all emanate from a common source. However, the fact that the sill complexes include intrusive phases which overlap with compositions in the more stock-like intrusives indicates that the magmas from different sources were spatially associated. It is hence hypothesized that although the ultamafic-mafic spectrum almost certainly derived from partial melting of mantle material, since there is no evidence for the volume of original mafic to ultramafic material needed to produce the preponderant felsic fraction here, the more stock-like intermediate to felsic intrusives were possibly produced through crustal anatexis. Under this schema the various intrusive and extrusive rocks that are considered to derive from primary mantle magmas would include the strongly differentiated mafic sills of the Buckingham and Diana Mills complexes, the bordering greenstone volcanic suites, the small but widespread trondhjemitic intrusives peripheral to the sill complexes and in the Mineral assemblage, the small composite peridotite-gabbro-diorite bodies along the Long Island and Columbia structures, and the komatiitic units interlayered with the ironstone-iron formation of the diverse upper Chopawamsic group. The various intrusive-extrusive rocks that are considered to reflect (at least in part) crustal anatexis include the Green Springs tonalite-granodiorite stock, the Palmyra assemblage felsic metavolcanics, the Ellisville granodiorite-granite stock, and the Buffards ash flow tuff deposits. These two magmatic lineages are broadly differentiated in K_2O contents, the former komatiite-tholeiite-trondhjemite lineage being a low-K

suite and the latter calc-alkaline lineage a high-K suite. A general discussion of the theoretical background to, and the practical implications of, this general regional genetic interpretation follows.

Investigations of the genesis of komatiitic magmas (Nesbitt & Sun 1976, 1979) indicate that these represent large-percentage (30%) partial melts of the mantle requiring very high temperatures (1700°C) in the source area for generation. To achieve these high temperatures, these magmas must therefore originate very deep -- possibly below 400 km -- in the mantle, rising as a result of their thermal instability as diapiric plumes. In many cases (Bickle et al 1975, Schwartz & Fujiwara 1977, Nesbitt & Sun 1979) the komatiite is held to have erupted onto sialic crust, indicating the initial stages of crustal rifting over plume sites.

In most areas of occurrence the komatiitic volcanism is preceded and succeeded by tholeiitic basalt, an association suggesting that komatiites and tholeiites may be genetically linked. Nesbitt and Sun (1979) suggest that the essential difference between the two resides in the greater degree of partial melting needed to achieve komatiitic magma. According to this, komatiite may be a simple extension of tholeiite into more highly magnesian compositions. In the case of the present investigation such a petrogenetic overlap is suggested by the magnesian metabasalts of the Mineral assemblage which have intermediary compositions between tholeiite and komatiite.

Although the ultramafic intrusive material along the belt is compositionally comparable to komatiite, since no quenched textures were observed it is questionable whether any of this magmatic fraction was ever extruded. The cumulate textures evident in the main gabbroic parts of the westerly sill complexes indicate that there was deep enough intrusion and thus

slow enough cooling of the thick sills to allow for the strong fractional crystallization necessary to derive dunitic cumulate, pyroxenitic gabbros, hornblendic gabbros, feldspathic gabbros, and dioritic differentiates. None of the composite peridotite-gabbro-diorite bodies emplaced along the Long Island and Columbia structures were well enough exposed to reveal internal relationships among dunitic, gabbroic, and dioritic phases, but their remnant igneous textures again suggest that strong crystal fractionation was operative. The complete lack of igneous textures in the magnesian amphibolites interlayered with the diverse Chopawamsic group together with the uniform composition of these particular bodies indicates that the pyroxenitic komatiite in this instance either was extruded or intruded near enough to surface to be cooled before fractional differentiation could proceed. It seems entirely possible that these metakomatiites were in fact extruded and that any quench textures signifying their ultramafic flow origin have been eradicated by the relatively high metamorphic overprint. Regardless of their specific mode of origin, the evidence of repeated injections and/or ejections of komatiitic-tholeiitic magma implies that an atypically hot mantle anomaly persisted throughout the formative period of the Chopawamsic metavolcanic belt.

The fractionation of hornblende is also thought to have played an important role in the formation of corundum-normative calc-alkaline magmas. Cawthorn and Brown (1976) show that the extent to which normative corundum increases in calc-alkaline compositions depends in part apon the Na/Na+K ratio of a magma. With a ratio greater than .6, there is a large compositional stability field of hornblende, while at lower ratios micas crystallize. As the micas are typically corundum-normative themselves, their crystallization buffers the increase in normative corundum in residual liquids. On this

basis, the origin of corundum-normative magmas may be explained in terms of sodic primary magma compositions which favour amphibole formation over micas in order to produce a calc-alkaline trend towards high SiO_2, corundum-normative liquids.

Although shallow level fractional crystallization of hornblende from gabbroic magma may be invoked as a generative source for the tonalite-trondhjemitic rocks affiliated with the mafic intrusive complexes along the western border of the Chopawamsic belt, this petrogenetic model cannot as readily explain the occurrence of the trondhjemites in the Mineral metavolcanic suite since these occur as isolated intrusive bodies. The melting experiments on primitive tholeiites carried out by Dixon and Rutherford (1979) in an attempt to account for the occurrence of similarly isolated trondhjemitic bodies in ophiolite suites affords a more plausible mechanism here. These melting experiments show that after 95% crystallization, the residual liquid of primitive tholeiite is an iron-enriched basalt. This basalt breaks down at a temperature of about 1010 C to two immiscible fractions, an even more iron-enriched basaltic liquid and a granitic liquid of trondhjemitic composition. On this evidence, Dixon and Rutherford conclude that silicate liquid immiscibility provides a viable explanation for the generation of trondjemitic bodies, adding that if sodic residuals are formed in this fashion there should also be evidence of the iron-enriched basaltic conjugate magma. Considering the affiliation of the Mineral suite trondhjemites with iron tholeiite and mafic ironstones of poorly understood origin, it is very possible that here we could have both immiscible fractions predicted by Dixon and Rutherford.

Bringing together all these various lines of research bearing on the petrogenesis of the komatiite-tholeiite-trondhjemite lineage, an hypothesized

petrogenetic model for the rocks is as follows. The repeated injection of komatiitic-tholeiitic liquids resulted from diapiric upwelling of high partial melt fractions derived at very high temperatures deep in the mantle. The komatiitic liquids probably represented an extension of tholeiite to more magnesian compositions by higher partial melting. The lower degrees of partial melting accompanying lower temperatures higher in the mantle (though derived from the same mantle melting anomaly) gave rise to voluminous primitive tholeiite with a rather broad range of compositions from magnesian to iron-rich variants. Together the komatiitic-tholeiitic magmas were injected into high crustal levels, at an early stage forming strongly differentiated sill complexes and subsequently creating small isolated compositite peridotite-gabbro-diorite bodies. Late in this magmatic episode, the tholeiitic fraction was largely extruded to produce the metabasalts of the Mineral assemblage, and in the terminal stages uniform pyroxenitic komatiite was injected-ejected near or at the surface. On its rise to the surface the mantle-derived magmas commonly collected in shallow level magma chambers. It seems likely that intrinsically high water and sodic contents in this dominantly gabbroic magma determined a large field of amphibole stability, which gave rise through early hornblende fractionation to tonalite and through later plagiclase fractionation to trondhjemite. This fractionation probably accounts for the affiliation of the tonalitic-trondjemitic intrusive facies with the westerly mafic sill complexes. However, in the case of the Mineral assemblage trondjemite, where there is no evidence for such a fractional crystallization scheme, liquid immiscibility resulting (as detailed above) in the splitting off of conjugate iron-rich basalt and sodic granite liquids is considered a more feasible petrogenetic model.

Although such an igneous scenario accounts well for the low-K

komatiite-tholeiite-trondhjemite lineage, the high-K calc-alkaline suite is, of course, quite another matter. Certainly the minor affiliation of higher-K phases with the tonalitic fractions of the westerly sill complexes and the tonalitic-granodioritic Green Springs intrusive is indicative that the low-K and high-K suites are spatially associated. Since, however, as mentioned above there is no evidence of nearly enough mafic material to account for the quantity of felsic material evident in the Green Springs body and, particularly, the Ellisville granodiorite-granite stock through fractional crystallization -- and since the mantle magmas are typified by low-K contents in any case -- it seems that other petrogenetic factors must have played a dominating role in the formation of the high-K calc-alkaline suite. On present, rather skimpy evidence (the petrochemistry of the calc-alkaline intrusives has not yet been well studied), the most plausible origin for the higher-K magmas is, as noted, provisionally considered to be crustal anatexis. Details, however, must remain vague. Whether the hypothetical anatectic fractions derived from older sialic basement or from the remelting of the early products of the same lithotectonic assemblage, for instance, is a question entirely open to speculation. One thing that is clear at this point, though, is that the rise of buoyant granodiorite-granite magma occurred late in the development of the belt as a whole, as these bodies appear to intrude to the base of the metashales. The relationship between these rocks and the volcanics has been considered previously, but to facilitate the present attempt to formulate a more holistic picture it is perhaps worth reviewing the significant aspects of this relation once more with specific reference to the question of volcanic petrogenesis.

Difficulties arise in petrogenetic investigations of eugeoclinal spilite-keratophyre-quartz keratophyre suites as a result of their tendency to

lose primary igneous compositions during equilibration to hydrous low-temperature conditions. Judging by academic interest, by far the most critical question posed by the spilite-keratophyre-quartz keratophyre associations is how their low temperature hydrous mineralogy evolved, and a survey of the literature reveals numerous schools of thought on this issue. Many Europeans (Amstutz 1974, Lehman 1974) postulate special hydrous magmatic conditions, while those studying similar rocks in Australia and New Zealand (Vallance 1960, 1965, 1969, Coombs 1969, Smith 1968) generally favour burial metamorphic adjustments. More recent work on spilitic rocks dredged from the sea floor (Cann 1969, Miyashiro et al 1971, Aumento et al 1976) demonstrates that low temperature equilibrium can also result from hydrothermal metasomatic adjustment on or near the ocean floor. Without attempting any definitive resolution of these differing views, this writer would merely point out that if nothing else the general petrographic-petrochemical features of these rocks indicate that they have been readily susceptible to open and/or closed system metasomatism. In this regard, recent studies of sea floor hydrothermal metasomatism (Spooner & Fyfe 1973, Humphries & Thompson 1977, Hutchinson et al 1980, Fyfe & Lonsdale 1981) suggest this regime as one which is particularly congenial to open system chemical exchange due to interaction between volcanic lithologies and oceanic brines.

Aside from this particular line of research, there has been surprisingly little attention directed towards the more fundamental petrogenetic problems concerning the tectonic setting and origin of parental magmas for spilite-keratophyre-quartz keratophyre suites. This association typifies early eugeclinal successions where the volcanics occur interlayered with pre-flysch successions rich in pelagic and chemical sedimentary components (Auboin 1965). Although alteration masks the identity of source magma(s) to a

considerable degree, there is meager evidence (Herman et al 1974, Tanaka 1975) to suggest that transitional basalt is a common parent for eugeoclinal spilites and that keratophyre-quartz keratophyre generally relates to a trondhjemitic (sodic) trend within the calc-alkaline series (Arth & Hanson 1975, Whitney et al 1978, Barker 1979).

The geochemical results of the present investigation (which are supported to a considerable extent by Pavlides' 1981 geochemical study of the metavolcanics of the Fredericksburg area) suggest that the Chopawamsic metavolcanics constitute a spilite-keratophyre-quartz keratophyre suite derived from multiple source magmas. The greenstones along the western border and the mafic-silicic metavolcanics of the Mineral suite are both low-K tholeiitic volcanic types which in all likelihood stem from the mantle-derived komatiitic-tholeiitic-trondhjemitic magma lineage cited above. The Palmyra metavolcanic assemblage and Buffards ash flow tuffs are high-K calc-alkaline volcanic types probably deriving from the anatectic tonalite-granodiorite magmas.

The broadly correlative compositions demonstrated by the extrusive and intrusive facies indicate that the volcanism along the Chopawamsic belt was a surface expression of the magmatism which gave rise to the intrusive bodies. On the basis of the lithological descriptions in Appendix B, it is considered most likely that the magma generally emanated from non-centralized fissure systems. It is further postulated that differing fissure systems across the belt tapped differing source magmas: i.e., the westerly greenstones and easterly Mineral assemblage volcanics tapped high level tholeiitic magma chambers which, through fractional crystallization or late stage liquid immiscibility, gave rise to sodic differentiates, while the Palmyra assemblage metarhyolites and more intermediate metadacitic-metaandesitic facies tapped

anatectic pockets of more and less evolved calc-alkaline magma respectively. The high-K Buffards ash flow tuffs, alternately, are considered to have derived through volcanic tectonic collapse over very high level Ellisville-age granodiorite-granite bodies. This terminal pyroclastic event could possibly have been initiated in part by the last phase of very high level komatiite intrusions. The injection of much hotter mafic material into felsic magma chambers has been suggested as a mechanism responsible for violent pyroclastic eruptions by Chapin and Elston (1979). The fact that the Buffards tuffs/quartz mica schists occupy the same stratigraphic position as the pyroxenitic komatiites, their unusually high Cr values (in the order of 200 ppm), and their local affiliation with fuchsite-bearing lithologies (a feature noted both by this writer and by Brown, 1969) all testify in different ways to the possibility that this simple, albeit particularly dramatic model provides a viable explanation for the present case.

The petrogenetic characteristics of the Chopawamsic rocks provide evidence, then, for such processes as (1) repeated high-temperature komatiitic-tholeiitic magma injections, (2) the formation of shallow magma chambers collecting liquids derived either by partial melting of mantle or through crustal anatexis or both, and (3) the individual tapping of these magmas by surface fissures, resulting in chemically correlative eruptions; collectively all this suggests that the belt originated as a volcanically active extensional zone over a thermally anomalous mantle rise. The anomalous geothermal conditions accompanying the volcanism would seem to have intensified in the near-surface environment in the late volcanic stage concomitant with the high level migration of the more quartzo-feldspathic of the melts owing to their buoyancy and thermal instability. If the transitional contact relationships between the quartz mica schists and

Ellisville-age granodiorite have been interpreted correctly, it would seem that the granitic melts on occasion must have nearly breached the surface. Regionally, however, the anomalously high geothermal conditions at the time of the more localized ash flow tuff eruptions are reflected in the lithologically varied ironstone-iron formation-quartzite suite. It seems evident that we are here looking at the surface products of voluminous discharged hydrothermal fluid resulting from intensified geothermal-hydrothermal conditions. This, of course, brings us back to the synintrusive-synmetamorphic depositional regime hypothesized in Chapter 2 to explain the paradoxical occurrence of locally more complex deformation fabrics in the metavolcanics along with regionally conformable contacts between the Chopawamsic and younger metashale formations. This particular depositional setting may now be more specifically identified as signifying a relatively long time interval during which hydrothermal metasomatism intensified due to abnormally high geothermal conditions relating to buoyant plutonism and resulting in voluminous surface discharge of hydrothermal fluid along the belt. Chemical precipitation from the discharged hydrothermal fluids produced the typically thin-banded ironstone-iron formation-quartzite deposits now concentrated at the metavolcanic-metashale contact.

At the beginning of the present chapter a case was made for differentiating syndepositional hydrothermal metasomatic effects from later regional metamorphic overprints on petrographic criteria. In the light of the foregoing observations it now begins to seem as if syndepositional hydrothermal metasomatic processes and metamorphic processes might converge petrogenetically after all. Both are associated with elevated temperatures. Hydrothermal discharge of siliceous hydrous fluids, moreover, may be broadly compared to metamorphic dehydration-desilication. Such apparent convergence

would seem to indicate that syndepositional hydrothermal metasomatism could in fact evolve into a late metamorphic regime as hydrothermal systems dry up. In this author's opinion, however, the critical point for deciding this ticklish question is the role played by wholesale fluid migration which, as discussed earlier, is not typically characteristic of a late metamorphic overprint. On this single but important criterion, identification of the syndepositional overprint as a hydrothermal metasomatic one rather than a late metamorphic one is still considered to offer the best means of accounting for all features present.

Unfortunately, it proves somewhat more difficult to differentiate metasomatic processes from orthomagmatic ones, as these occur synchronously throughout the generative stages of development. The forementioned controversy over the origin of the hydrous low temperature mineral assemblages in spilite-keratophyre suites is particularly relevant here, but considerably more research will be needed before this long outstanding petrological problem (i.e., how magmas equilibriate to hydrous conditions) is finally resolved. Judging by the diversity of opinion expressed, about the only thing one may conclude with assurance is that the answer will not be a simple one. Certainly the interaction of magma and hydrothermal fluids under hot geothermal conditions would seem to be a more complex process than hydration of volcanic rocks under the more normal much lower temperature conditions. The considerable research on spilites has even led some investigators (such as Amstutz, 1974) to postulate special hydrous magmas that rather than differentiating along classical trends tend to fractionate into mineralogically simple mineral assemblages, thus stimulating the generation of carbonates, epidotites, and metalliferous chloritites, albitites, and quartzites. Whether or not spilitic and, by analogy, keratophyric and

quartz-keratophyric rocks derive from such magmas -- whether in fact the classic concepts of closed system magmatism might prove to be inapplicable for hot, wet, geothermal regimes given to high chemical reactivity between magma/rock and hydrothermal fluids -- are, however, questions that remain entirely unresolved.

The present study area is not a particularly suitable one for carrying out the critical petrological work necessary to clarify magma/rock-hydrothermal fluid interactions. The late metamorphic overprint has not only masked original volcanic textures but also, predictably, upset the more subtle geochemical aspects such as isotopic ratios, oxidation states, and so on, which could help unravel original cooling histories of the magmatic rocks in hot hydrous geothermal regimes. Metamorphic overprint notwithstanding, though, the petrographic and petrochemical convergence of volcanics with hydrothermal deposits in this area does afford a unique opportunity for examining the petrogenetic results of overlapping orthomagmatic and hydrothermal metasomatic processes.

As a point of departure it is considered particularly significant that the effects of hydrothermal metasomatism are more or less restricted here to volcanic rocks. Neither the epiclastic sedimentary nor the deeper seated igneous intrusive lithologies manifest petrographic features which would suggest pervasive hydrothermal alteration. It thus seems that the extrusives and near-surface sills have by far the greatest propensity for metsomatization. This is interpreted to signify (1) that the volcanics were out of equilibrium in a geochemical environment that readily facilitated the chemical exchange necessary for them to equilibriate to the ambient conditions, (2) that the epiclastic sediments interlayered with the volcanics were not nearly so much in disequilibrium with the ambient hydrothermal

conditions as the volcanics, and (3) that the deeper intrusives were for one reason or another not susceptible to hydrous alteration at lower temperature conditions. Collectively these differing lithological responses to hydrothermal metasomatism suggest that the process is pervasive in rocks of high temperature origin and likely restricted to very hydrous near-surface environments. The fact that the interlayered epiclastic sediments were more or less in equilibrium with the ambient hydrothermal conditions further suggests that their formational brines were a likely source for the hydrothermal fluid which pervaded the volcanic lithologies. Due to the high chemical reactivity of this fluid with these lithologies, the compositions of both might subsequently be expected to converge in their attempt to reach mutual equilibrium. Such a supposition, though as yet not explicitly supported by experimental work, would at least explain the otherwise enigmatic petrographic and petrochemical similarities already noted between the volcanics and the well-banded hydrothermal deposits.

A general proclivity for chemical exchange between magma/rock and fluids under high prevailing geothermal conditions also explains the regional nature of hydrothermal metasomatic processes. The discharge products of this interaction, however, would seem to range from entirely unfocused to much more centralized types. Such features as the regional spilitization of mafic volcanics, alkali metasomatism of felsic volcanics, and deposition of thin but persistent ferruginous quartzites on mafic horizons or kyanitic quartzites over felsic volcanics could very possibly be products of laterally extensive hydrothermal metasomatic processes in the course of which hydrothermal emanations merely migrated upward to the sea floor to precipitate out as blanket deposits. Alternately, it is equally conceivable that such regionally extensive deposits as ferruginous quartzites, kyanite quartzites, oxide iron

formation, and two-amphibole ironstones could represent leached cap rocks developed at the water/rock interface over geothermal anomalies on rocks of variable composition at times of non-deposition. In contrast to both these possiblities, other hydrothermal deposits reflect more intense hydrothermal activity in areas of highly focused discharge. The crosscutting vein systems observed in rhyolite flows suggest that felsic volcanic vent areas represented one such locus of more active fluid expulsion.

The fluctuating intensity of the hydrothermal discharge evinced by such variations in apparent petrogenetic derivation is also implicit in the nature of the hydrothermal deposits themselves. Because of their inherent duplicity of character, such facies as the hornblendic, cummingtonitic, biotitic carbonate-bearing, and sericitic pyrite-bearing ironstones can best be explained in terms of unusually intense hydrothermal metasomatism of volcanic forerunners. Although these particular rock types have geochemical vestiges of igneous precursors, the thin banding produced by variation in iron mineral content obviously has to derive from some process such as precipitation from hydrothermal emanations. In this regard one may postulate either that magmas are directly hydrothermally modified or that pervasively altered volcanic rock constituents are remobilized intact within a fluid phase. Alternately, and perhaps most plausibly, these rocks may have originally been water-laden volcanic tuffs and the hydrothermal metasomatism an <u>in situ</u> chemical exchange between ferruginous formational water and rock components.

Where hydrothermal emanations have been most intense, the products depart radically from volcanic rock compositions. This aspect is well demonstrated by the hydrothermal chloritites which encroach compositionally on silicate facies iron formation. As the hydrothermal deposits at focused discharge centres include the massive sulphide occurrences along the belt, this specific

aspect of the syndepositional hydrothermal regime is considered more fully in the following chapter on metallogeny.

4. METALLOGENY

The majority of the numerous pyritic massive sulphide and lode gold deposits hosted in the Chopawamsic metavolcanics have been known since Colonial times. Indeed, it was due to the occurrence of these deposits that the metavolcanic host rocks were initially labelled as the Virginian gold-pyrite belt (Lonsdale 1927). The long history of mining activity along the belt has not been particularly well documented, but fragmentary information can be found in reports by Adams (1884), Holden (1905), Watson (1905), Taber (1913), Barton (1933), Currier (1935), Park (1936), Pardie and Park (1948), Katz (1961), Luttrell (1966), Sweet (1971, 80, 81), Poole (1974), Good et al (1977), and Young (1981). The following brief historical review of the mining effort is a synopsis of this material.

Mining began in the early 1700s with the roasting of gossans in the Mineral district for iron. This activity continued until the mid-1800s, the largest producers being the Arminius, Sulphur, and Boyd Smith deposits in the Mineral district. Other locales where less extensive gossan mining was carried out included limonitic gossans along the New Canton trend and, to a lesser extent, in the Andersonville district.

Subsequent to the removal of the gossan caps as an iron ore, a zone of high grade supergene copper ore was encountered between gossan and fresh sulphide mineralization. Extraction of this began as early as 1847 at the Arminius deposit and soon thereafter at the nearby Boyd Smith and Sulphur mines. No information is available as to how much copper in all was produced

from this source, but the high grade material was soon exhausted.

Mining of the non-weathered pyritic massive sulphide for sulphuric acid manufacture began at the Arminius in 1865 and at the Boyd Smith and Sulphur in the 1880s. At the height of production in the 1890s the mines of the Mineral district accounted for more than 50% of the U.S. output of pyrite. Pyrite mining continued until 1922, when the development of economical ways of extracting sulphur from the Gulf Coast salt domes made pyrite-based sulphuric acid non-economic (Hickman 1947). During the nearly continuous production between 1834 and 1922 the Arminius mine produced over two million tons of pyritic ore (Kazda & Hodder 1978). There are no records available of the base and precious metal content of the mined massive sulphide. However, copper, lead, and zinc were reportedly recovered as by-products (Currier 1935) during this phase.

The first reference to gold in Virginia is attributed to Thomas Jefferson (1782), who mentions a four pound lump he discovered near the Rappahannock River that yielded 17 ounces of metal possessing "extreme ductility." Real interest in gold mining was not, however, aroused until 1829 when the first production was recorded from the Collins property in Goochland County (Brown 1937). A peak in placer mining was reached in 1833-34; the greatest activity in lode gold mining occurred over the period from 1838 until the beginning of the Civil War. Many mines being operated prior to the California gold rush in 1849 were abandoned at that time due to the greater allure of western fortunes. The recorded value of gold mined between 1830 and 1856 amounts to nearly $55,000 calculated on the then-current price of $20.67 per troy ounce (Sweet 1971). Since the Civil War there has been only a brief revival of interest in gold. During the Great Depression of the 1930s several of the larger mines were reopened, but these were again abandoned by 1938. The total

reported gold production between 1804 and 1947 is 98,609 troy ounces (Sweet 1980).

Very little attention was paid to either the pyritic massive sulphides or the lode gold mineralization in the period between the Great Wars. From 1909 to 1918 a little high grade ore from the Valzinco deposit (about 8 kilometers north of the Mineral district) and, in 1915-16, from the Allah Cooper deposits was mined for lead, zinc, and precious metals, while the rise in copper prices during World War I initiated some prospecting of old gossan zones, such as at New Canton, for this metal. Such activity, however, was of short-term duration only. Following World War II interest was renewed in base metal mining and several of the pyrite deposits were evaluated for their base metal contents by the U.S. Bureau of Mines in the 1940s. As a result of exploratory drilling the Valzinco deposit was reopened and mined for base metals by Panaminos Co. between 1942 and 1945 (Luttrell 1966). Under further Defence Minerals Exploration Administration contracts, drilling was also carried out at the London & Virginia gold mine near Dillwyn at the north end of the Andersonville district in 1953 and along the New Canton trend in 1950 and again over the interval 1954-56 (Poole 1974). The Andersonville massive sulphides were discovered in the mid-1950s; early exploration in this area was carried out by the Virginia Mining Corp. between 1954-58. The Andersonville massive sulphide zones saw the most extensive investigation by North American Exploration over the period 1968-71 (Young 1981). Most recently this district has also been explored in a rather cursory manner by Conoco, 1976-77, and Callahan Mining Corp, 1979-81.

New Jersey Zinc acquired the Julia, Arminius, Boyd Smith, and Sulphur deposits in 1953, leased the Valzinco deposit in 1955, and carried out extensive regional exploration along the belt throughout the 1950s and 1960s.

On the basis of this, in mid-decade the Cofer area was concluded to be anomalous in base metals but not in sufficient abundance to warrant much exploratory work. In 1973 New Jersey Zinc Co. and Callahan Mining Corp formed Piedmont Mineral Associates, a limited partnership with Callahan as the operator, which proceeded between 1973 and 1976 to outline the reserves at the Cofer deposit by surface drilling and exploratory underground development of a decline and drifts on -160' and -340' levels. Callahan Mining Corp. has persisted with both detailed exploration in the Mineral District and regional exploration along the belt through the late 1970s, and since 1980 has been in partnership with Boliden in the ongoing effort. During this most recent spate of exploration both Callahan and Phelps Dodge have discovered further base metal mineralization along the Long Island isocline south of the James River.

Notwithstanding the long history of exploration of the lode gold and massive sulphide deposits none are currently known to be economic. Virginia, however, is presently the leading state in the production of kyanite. The Kyanite Mining Corp. has developed two sites on the kyanite quartzite unit forming Willis Mountain and the East Ridge located northeast of the Andersonville district. Open pit mining of this mineral at Willis Mountain began in 1957 and has continued since that time (Sweet 1981). In 1975 Potter estimated 65 million tons of 25% kyanite ore at this location. The current rate of production is about 90,000 tons per year (Jean Dixon, personal communication 1981).

The numerous occurrences of massive sulphide and lode gold discovered regionally over the years are shown on Plate 2 in the rear folder. To facilitate the following metallogenic discussion these clustered deposits have been consolidated into five main groups herein designated as the Mineral district at the north end of the area of investigation, the Columbia-Tellurium

gold camp north of the James River, the New Canton trend on the eastern limb of the Arvonia synclinorium, the Long Island trend coring the Palmyra assemblage, and the Andersonville district at the south end of the study area. Small scattered copper(-gold) occurrences known to accompany the westerly greenstone will also be discussed.

The primary objective of this chapter is, first, to consider the distribution of the known mineralization from the vantage of the regional structural-stratigraphic framework, and second, to elucidate the origins of these occurrences in terms of the characterizing petrogenetic processes elaborated upon in the previous chapter. As detailed study of individual deposits was beyond the scope of the present study the information concerning specific ore-host rock relationships presented in the text is largely based on extant work by other investigators as supplemented and reinterpreted on the basis of this writer's regional experience. The metallogenic discussion is partitioned into two main parts focusing respectively on (1) the regional geological setting of the various deposits, and (2) the genesis of massive sulphides and lode gold deposits as indicated by mineral chemistry.

4.1 Regional Geological Setting of the Mineral Deposits

4.1.1 The Mineral District

The Mineral district coincides with a doubling in width over a strike length of roughly twelve kilometers of the linear aeromagnetic anomaly that was recognized by Pavlides et al (1974) to delineate the Chopawamsic metavolcanic belt regionally. The several mineral deposits in the district

(Figure 27) are divisible into three separate trends aligned parallel to the regional strike at N30°E. The west and major trend is a more or less continuous belt of basemetal-bearing massive pyrite deposits including, from north to south, the Sulphur, Boyd Smith, Arminius, and Julia deposits. The central trend is a more discontinuous series of basemetal-bearing massive pyrite occurrences of which the largest known is the Cofer deposit. The most easterly trend, known as the Fisher Lode (Luttrell 1966), comprises a series of gold-pyrite-bearing vein prospects.

4.1.1.1 Western Arminius Trend

The northern end of the major westerly trend of massive pyritic sulphide occurrences has been recently nearly continuously drilled on 500' intervals over the length from the old Sulphur to Arminius deposit sites. A generalized longitudinal section along this segment of the mineralized zone is shown in Figure 28. As illustrated, although there is a continuous marker chloritite bed footwall to the massive sulphide, the hangingwall sequence is quite variable. The continuous, low grade to barren, massive sulphide interval favours the upper contact of the marker chloritite from the Sulphur deposit through to the Boyd Smith site, a strike length of over 2400 meters. The footwall chloritite shows a varied porphyroblastic suite including magnetite, garnet, staurolite, and chalcopyrite over this same length. Slightly reworked felsic tuffs and lapilli tuffs immediately overlie the sulphide mineralization at Sulphur North, while a lithologically complex succession of various sulphide, oxide, and silicate facies of siliceous ironstone prevails in the immediate hangingwall over the segment from Sulphur South to the Arminius deposit.

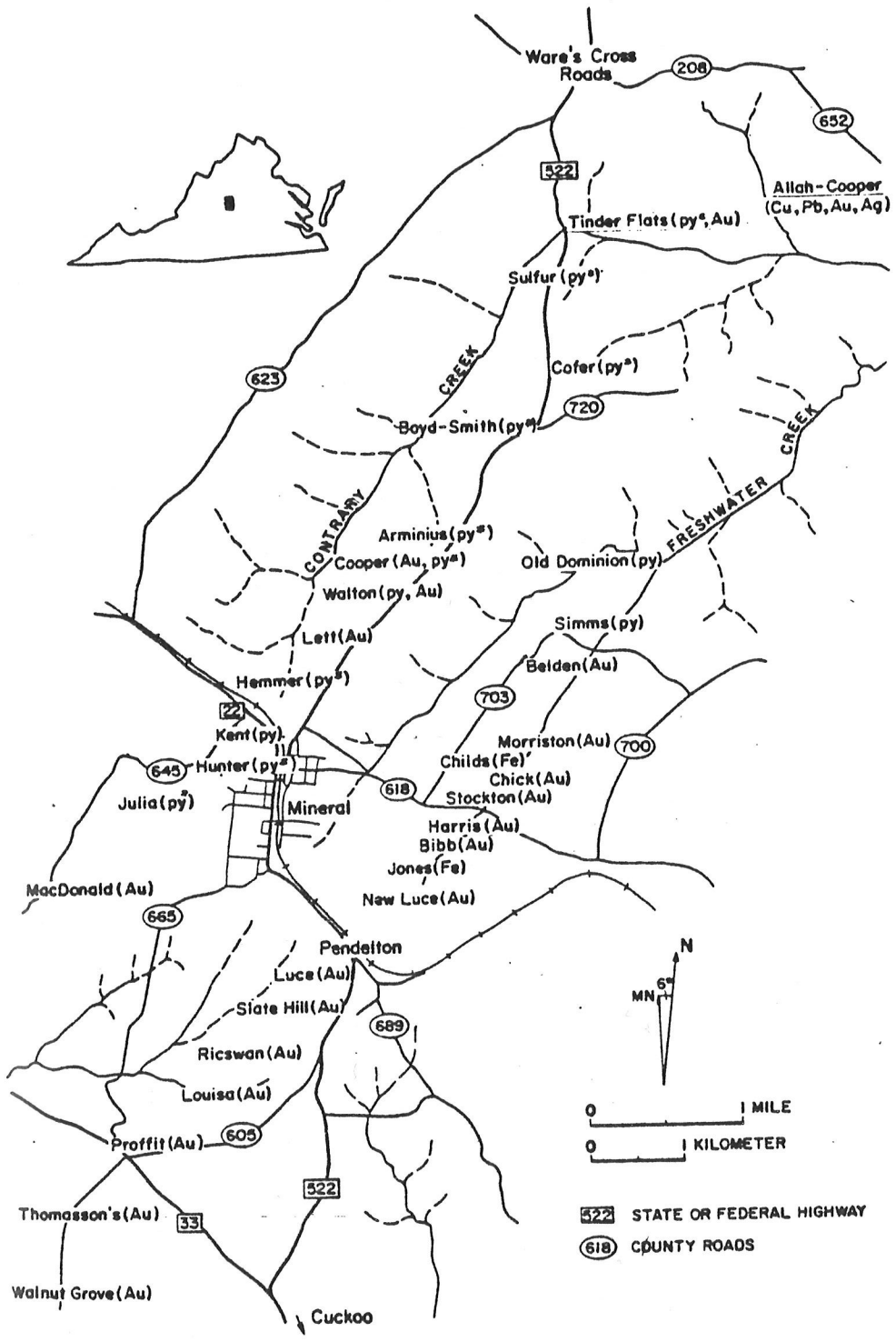

Figure 27: General setting of the mines of the Mineral District, Louisa County, Virginia. KEY: (Au)-gold deposit, (py)-massive pyritic deposit, (py*)-massive pyritic deposit with base metals, (Fe)-gossan iron deposit. (Craig, 1978)

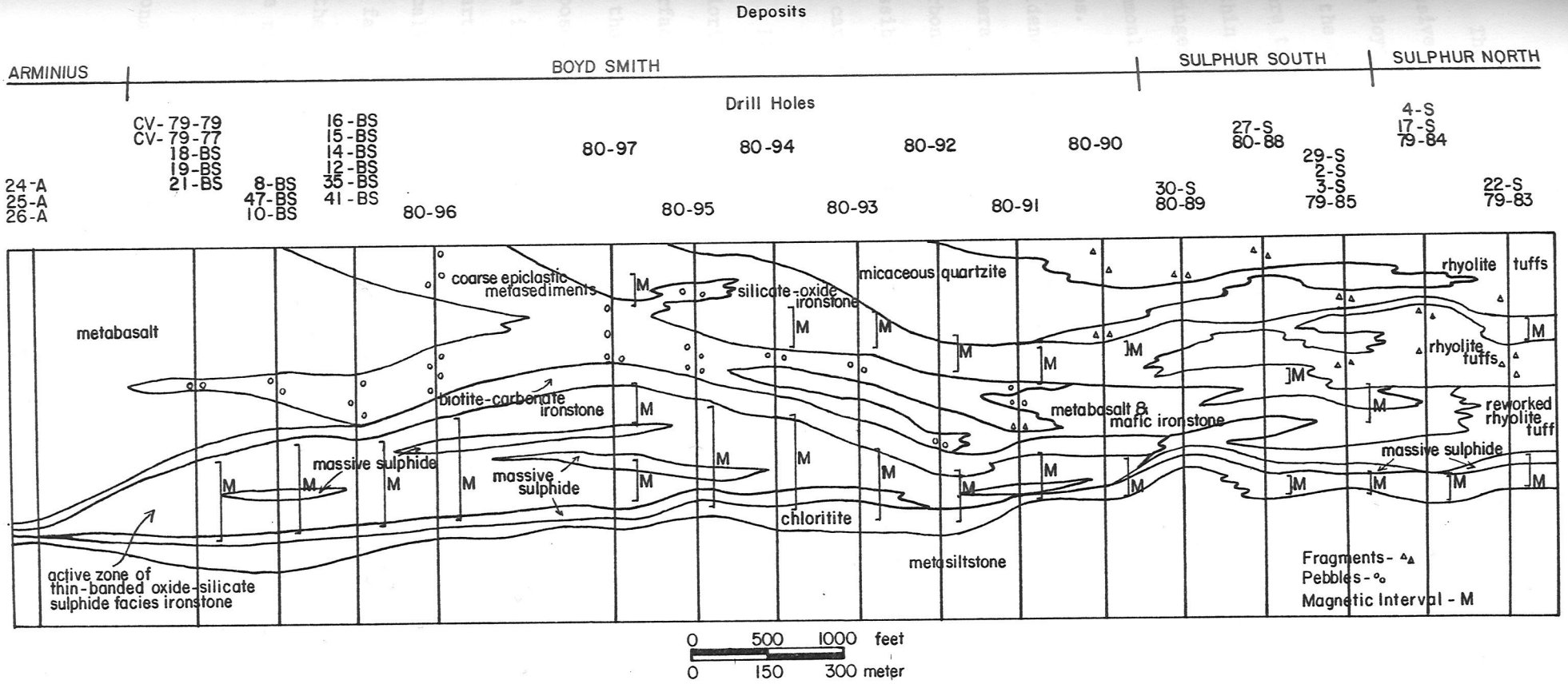

Figure 28:
Geological Longitudinal Section Arminius North to Sulphur North, Mineral District
(modified from Callahan Mining Corp. data)

The pyritic ironstone in the hangingwall may also host isolated lenses of massive sulphide mineralization. The largest known hangingwall lens, found at the Boyd Smith, has about 750,000 tons of massive sulphide comparable in grade to the Arminius deposit. Significantly, this massive sulphide lens occurs where there is the thickest development of the productive ironstone package. Within this thickened part, heavy sulphide disseminations and massive sulphide stringers are associated with magnetite-hornblende quartzite beds which commonly have amphibolitic (mafic ironstone-metabasalt) bases and metachert caps. The characteristic lithological zonation is here interpreted to be evidence for chemical cyclicity within the active zone for sulphide mineralization. Of considerable significance is the fact that the biotitic carbonate ironstone facies occurs at the outer limit of the active zone. This possibly suggests that the sulphide-bearing hydrothermal fluids changed facies to carbonate-bearing fluids.

Little is known of the detailed geology below the footwall marker chloritite, as drilling was discontinued once this rock type was penetrated. Surface mapping indicates that a thick continuous unit of metasiltstone occurs in the distant footwall along the whole western side of this zone. However, exposures on Contrary Creek reveal a thin interval of felsic lapilli tuff in the immediate footwall of the Sulphur North mineralization, and sericitic quartzite -- which possibly derives through silicification -- was intersected locally (CV 79-84, 80-94) along the segment. Notwithstanding these features, by far the most consistent lithology footwall to the marker chloritite is a rather monotonous quartz biotite sericite schist which is characteristic of the regional epiclastic sedimentary facies.

The hangingwall to the active zone capped by the biotite carbonate ironstone shows complex interdigitation of more northerly felsic metavolcanics

sequentially bordered by a quartzite-mafic ironstone association and more southerly atypically coarse epiclastic (turbiditic) sediment. Significantly, the coarse sedimentary facies appears to be more or less restricted to the area immediately overlying the active zone with sulphide mineralization. Southwards both the turbiditic sediments and the ironstones within the active zone pick up appreciably in chlorite; further south in the vicinity of the Arminius deposit banded amphibolite forms the dominant hangingwall lithology.

The largest known massive sulphide deposit in the Mineral district, the Arminius deposit (Figure 29), occurs centrally to the other known deposits along the westerly trend of sulphide ocurrences. The probable reserves of this mine are about four million tons at 4.08% Zn, .5% Pb, .48% Cu, .62 oz/ton Ag, .018 oz/ton Au, 33.84% Fe, and 35.56% S (Kazda & Hodder 1978). The deposit consists of four parallel aligned lenses peneconfromable with footwall quartz sericite schists and quartzites (a slightly reworked rhyolite tuff-sericitic pyritic ironstone-chert assemblage) and hangingwall banded amphibolite (a metabasalt-mafic ironstone assemblage).

As noted by Cox (1979), the mineralization here comprises both massive and disseminated pyrite. Where massive it occurs in well developed equilibrium mosaic textures; this particular facies has only minor grain boundary sited sphalerite and trace chalcopyrite, galena, and tetrahedrite-tennanite. Where disseminated the pyrite occurs as buckshot porphyroblasts in a matrix of sinusoidal sphalerite intergrown with minor chalcopyrite and galena. The pyrite may also be heavily disseminated in a "chloritite" matrix of biotite, garnet, chlorite, amphibole, epidote, quartz, sericite, and magnetite. This latter facies has not been well differentiated but it is common where the hangingwall metabasalt-mafic ironstone is in contact with the sulphide lens. The immediate contact between massive

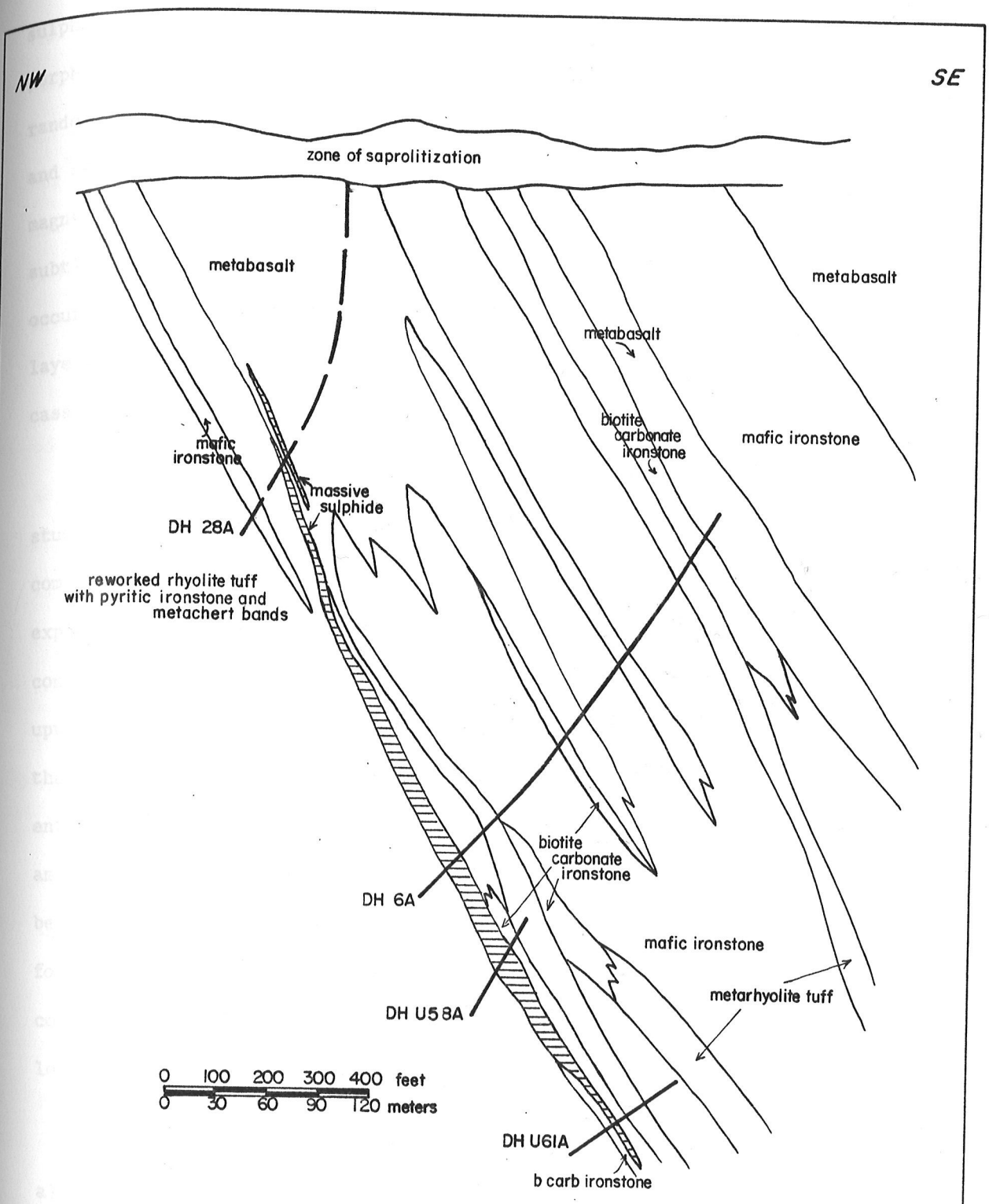

Figure 29: Geological Crossection of the Arminius Deposit, Mineral Deposit
(modified from Callahan Mining Corp. data)

sulphide and amphibolite is sometimes a site for the development of coarsely porphyroblastic hornblende, staurolite, garnet, gahnite, magnetite, and pyrite randomly oriented in a matrix of chlorite, biotite, chalcopyrite, pyrrhotite, and sphalerite. Notably, the intervening fringe zone is typically enriched in magnetite, pyrrhotite, and chalcopyrite over the massive sulphide itself. A subtle compositional banding is generally evident in the ore due to the occurrence of pyritic, polymineralic pyrite-sphalerite-quartz, and sphalerite layering. Cox (1979) observed that where sphalerite is most enriched, cassiterite is commonly present.

The Arminius deposit is the only one in which metal zoning has been studied in any detail. Both Cox (1979) and Zymela (1979) define striking compositional zoning within the Arminius lens. The zoning occurs along the explored 1100' strike length of its plunge at 023°-60° N. Copper is concentrated at the lower northerly end, and both zinc and lead increase upward from the area of copper enrichment. Cox draws attention to the fact that the metal zoning correlates with the lithological variation in the enveloping lithologies, i.e., the high Zn/Cu ratios correspond to an amphibolitic hangingwall and quartzitic footwall while the Cu-rich zone lies between a biotite-sericite schist hangingwall and quartz sericite schist footwall. Zymela interprets this as a primary depositional feature due to copper precipitating out of hydrothermal fluids at greater depth than zinc and lead in a fracture sited fluid conduit.

Detailed petrological investigations of the southernmost Julia deposit along the major western mineralized trend have not yet been undertaken. Also, as this deposit is very poorly exposed, its geological setting is known only from relatively minor drilling. The drilling completed to date, however, indicates that the sulphide mineralization here is hosted in an anomalously

thick section of hydrothermally silicified and chloritized rhyolite quartz-feldspar porphyry. The known mineralization comprises a massive lens (725,000 tons of 8.26% Zn, 2.43% Pb, .24% Cu, 1.28 oz/ton Ag, and .03 oz/ton Au) that trails off along strike to the northeast into a series of small massive sulphide pods. At its southern end this sulphide lens is related to a poorly defined footwall stringer zone of sphalerite and galena mineralization.

The massive sulphide mineralization appears to be restricted in occurrence within and above a 10-50' interval rich in chlorite, biotite, and sericite, and hosting porphyroblastic garnet and kyanite in its upper part and staurolite in the most chloritic sections of its lower part as well. This marker occurs between hangingwall chloritized and silicified rhyolite solution breccia, which appears to thin rapidly away from sulphide mineralization, and footwall silicified quartz feldspar porphyry hosting stringer sphalerite and galena mineralization. Where the hangingwall rhyolite breccia is most highly altered this lithology includes iron carbonate and pyrite veinlets. The distal hangingwall is made up of an unknown thickness of ironstone which is atypically rich in carbonate and magnetite and also hosts thin intervals rich in fuchsite mica.

What is known of the geological setting of the Julia deposit to date supports the interpretation that it derives from hydrothermal fluid discharge proximal to a small rhyolite centre. The stringer mineralization footwall to the major massive sulphide lens may have the shape of a flattened pipe; this has been interpeted as a conduit for ascending hydrothermal solutions by Sauer (1980).

4.1.1.2 Central Cofer Trend

The Cofer deposit lies on a trend of old occurrences of pyritic schist and gossan which from north to south includes the Old Dominion, Morriston, Childs, and Jones prospects. These deposits are centrally located with respect to the apparent convergence of the westerly "Arminius" trend and easterly Fisher Lode in the northern part of the Mineral district. The considerable work carried out in recent years -- including fence drilling, exploratory underground drifting, and studies by Hodder et al (1977), Miller (1978), Feuer (1980), and Allen (1980) -- has defined the geological setting of the Cofer deposit as well as any in the district. Since this is the only deposit along the central trend for which there is much information, it is the only one considered in the present discussion.

As illustrated in Figure 30, the Cofer mineralization occurs within a thick (<150 meter) section of sericite-pyrite ironstone structurally capped by a distinct fragmental unit identified as a mongenetic rhyolite breccia in a detailed petrological study by Rymph (1980). The mineralized section structurally overlies the major amphibolite (metabasalt-mafic ironstone) unit that occurs between the westerly Arminius trend and central Cofer trend of sulphides. The distal hangingwall to the mineralized zone comprises a rather monotonous section of non-pyritic, moderately reworked felsic volcanic material. Interestingly, a porphyroblastic chloritite interval, showing considerable lithological similarity to the footwall chloritite of the Sulphur-Boyd Smith sulphides, was intersected in the drill hole collared furthest in the hangingwall succession.

The active zone for sulphide mineralization includes continuous strataform-stratabound beds as well as numerous lenses of massive sulphide,

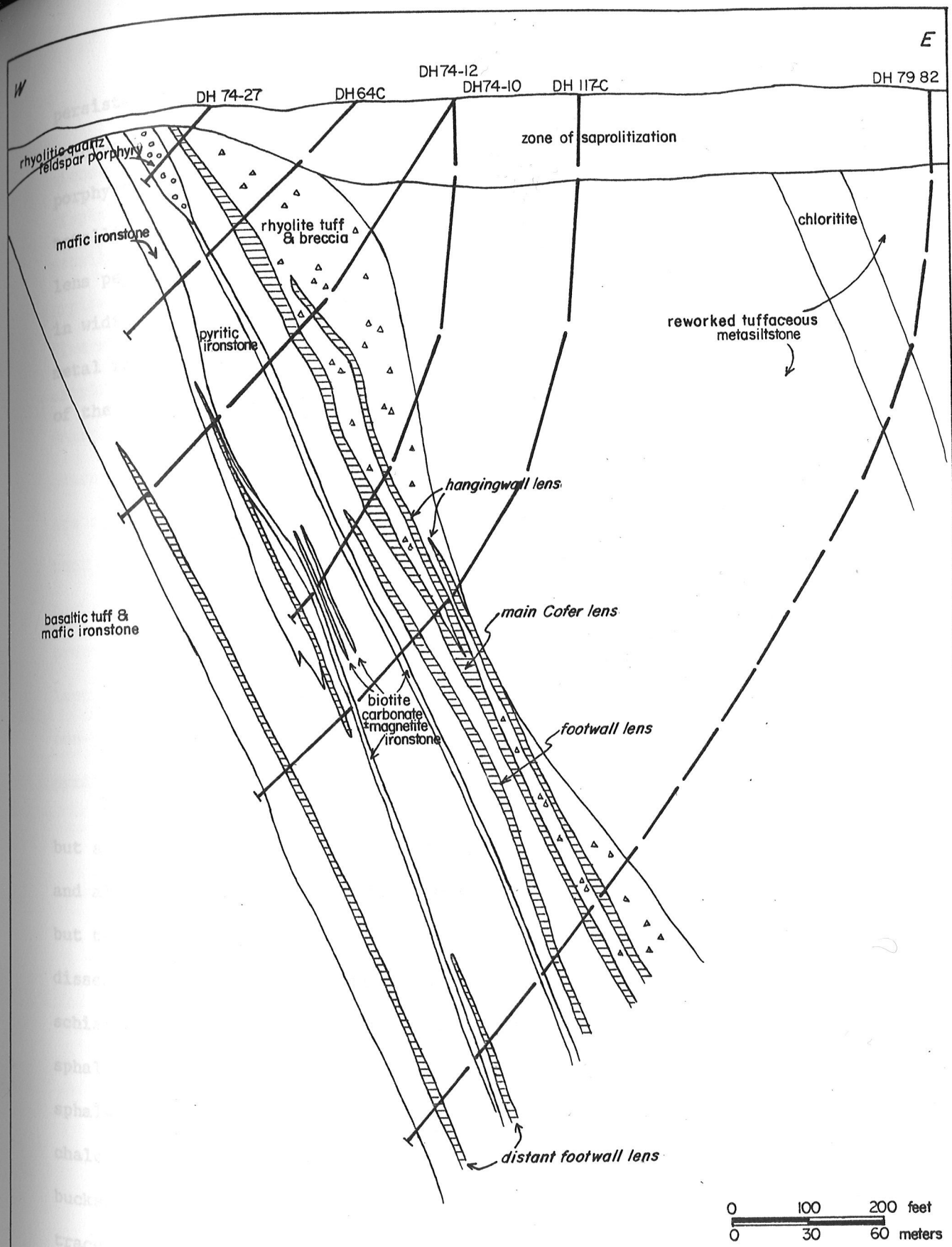

Figure 30: Geological Crossection of the Cofer Deposit, Mineral District
(modified from Callahan Mining Corp. data)

persistent magnetite-bearing biotite-carbonate ironstone, and minor but thicker lenses of amphibolite (mafic ironstone) and rhyolitic quartz feldspar porphyry. The Cofer ore essentially consists of four en echelon lenses totalling about 1.5 million tons of 7% combined base metals. The main Cofer lens persists for 515 meters along strike, varies from .5 to over ten meters in width, and has a known downdip extension of several hundred meters. The metal ratios determined from drill core assays by Hodder et al (1977) for each of the four lenses are listed in Table 9 below.

Table 9: Metal Ratios in the Various Massive Sulphide Lenses of the Cofer Deposit

	Zn:Pb:Cu	Ag:Au
(1) Hangingwall Lens	27:12:1	125:1
(2) Main Cofer Lens	10:2:1	50:1
(3) Footwall Lens	18:8:1	140:1
(4) Distant Footwall Lens	6:0.6:1	70:1

Not only are the evident metal ratios variable from one lens to another, but sulphide textures and mineralogy are quite variable both between lenses and along strike within any given lens. Miller (1978) notes four differing but transitional types of mineralization including: (1) weak to moderate disseminations of pyrite, sphalerite, chalcopyrite, and galena in siliceous schist; (2) massive granoblastic pyrite with grain boundary sited xenoblastic sphalerite, chalcopyrite, galena, and quartz; (3) massive sinusoidal sphalerite hosting 5-10% buckshot pyrite porphyroblasts and minor chalcopyrite, galena, and silicate gangue; and (4) heavy disseminations of buckshot pyrite in a lobate granoblastic matrix of chalcopyrite including trace sphalerite, arsenopyrite, molybdenite, and a variety of sulpho-salts. Notably, pyrrhotite has not yet been identified at the Cofer deposit.

The hangingwall lens is dominantly massive pyrite. Although it is microscopically featureless, Miller discovered that the pyrite grains often display undistorted concentric growth zoning when etched with nitric acid, attributing this to static metamorphic recrystallization of primary colloform pyrite. The main Cofer lens is the most texturally and mineralogically diverse and also the most chalcopyrite-rich. While typically forming the matrix and/or hosting other sulphide species the chalcopyrite also occurs as monomineralic fracture fillings up to several centimeters in width in crosscutting quartz veins. Most of the trace sulpho-salts and arsenopyrite are affiliated with chalcopyrite-rich ore. Significantly, Miller estimated that over 90% of the silver in the deposit comes from members of the tennantite-tetrahedrite-friebergite (fahlerz) series. Feuer (1980) notes that breccia ore occurs locally in the main lens with 1-5 cm lenticular shaped lapilli and rounded quartz fragments in either coarse recrystallized non-banded pyrite-sphalerite-chalcopyrite matrix or a laminated fine-grained pyrite matrix.

The footwall lens is characterized by distinctly banded pyritic, sphaleritic, and, more rarely, galena-rich layers interpreted by both Feuer and Miller to be a primary bedding feature. An interesting fact noted by Miller is that while exsolved bismuth accompanies the trace galena in both the overlying main Cofer and hangingwall lenses, the galena in the footwall lens is free of such inclusions. The distal footwall includes all the various types of ore recognized by Miller and is characterized by the absence of members of the fahlerz series.

Although each of the lenses is to some extent compositionally unique, there is no consistent vertical zonation pattern evident. This was considered

by Feuer to be due to complex lateral variation along strike interfering with the vertical zonation. As Miller points out, however, in general zinc-lead-rich ore is dominant at the south end of the deposit and copper-rich ore at the north end. Interestingly enough, as mentioned above, this is roughly the same zonation as is evident at the Arminius deposit.

The Cofer massive sulphide lenses are believed to be volcanic exhalites precipitated from hydrothermal brines deposited in deeps within a subsiding trough during a lapse in active volcanism and clastic sedimentation (Hodder et al 1977, Feuer 1980). Miller (1978) draws attention to numerous petrological similarities with the Japanese Kuroko and Besshi-type deposits. The structual-stratigraphic relationship between this occurrence and the Arminius trend to the west has been an ongoing target for speculation, but the lack of outcrop makes it difficult to come up with definitive answers. Rymph considers the Cofer deposit to be overturned on the basis that rhyolite breccia is a common footwall lithology to massive sulphide deposits generally. If this interpretation were correct it would imply that the Arminius and Cofer deposits are probably related structurally, the former occupying the upright limb and the latter the overturned limb of a major isoclinal synform cored by the amphibolitic unit that is central to the mineralization. Due to the apparent absence of such features as graded bedding and vertical metal zoning in the sulphide deposits themselves, however, any such interpretation remains problematic. Indeed, on present evidence depositional cyclicity seems to offer just as reasonable an explanation as structural repetition.

4.1.1.3 Eastern Fisher Lode Trend

These numerous (fourteen documented by Luttrell, 1966) old workings comprise a series of pits and semi-continuous trenches that extend from the southern shores of Lake Anna to well south of Pendleton (Figure 27). Little geological data can be gleaned from the old pits, though, as these were not cut into bedrock but rather originated with oldtimers excavating auriferous quartz veins in saprolite. In most cases, moreover, the pit walls are now caved in and the sites generally overgrown with heavy underbrush. Apart from this, the trend is very sparsely exposed in any case -- the outcrop situation along the whole eastern side of the Mineral district is quite poor. The specific host rock setting to the lodes is consequently still not well understood. The following brief resume is based essentially on this writer's regional work in this part of the belt.

All these gold occurrences are coincident with the intense magnetic ridge along the eastern side of the Chopawamsic belt regionally. The old workings occur very near or at the contact between the two amphibole ironstones-ferruginous quartzite-oxide iron formation assemblage capping the Mineral metavolcanics (and responsible for the magnetic high) and the Columbia metashales. The work to date has not succeeded in demonstrating the existence of a persistent basal shale garnet-grunerite facies of iron formation along this contact. However, a number of key features -- i.e., the fact that a few areas with over 50% garnet in a more chloritic than normal metashale facies have been noted, that a sample of such garnet-rich rock hosted trace grunerite, and that oolites were noted in one sample of chloritic metashale -- collectively suggest that the base of the metashale over this length is at least a more iron-enriched variety of metashale if not a true silicate facies

iron formation.

The ironstone-iron formation assemblage west of the metashales shows considerable variation along strike over the length of the Fisher Lode deposits. At the north end in the area immediately south of Lake Anna, metakomatiite units occur near or at the shale base. Significantly, the best development of oxide iron formation was also found to accompany the ultramafic rocks. One of the old pits exposes a thick (1.5 meter) bed of semi-massive to massive magnetite with lesser specularite bordered on both sides by ultramafic amphibolite.

Further south, opposite the town of Mineral, an anomalously magnetite-rich two-amphibole ironstone persists almost to the metashale contact but is separated from the latter by a thin stratum of pyrite-bearing kyanite quartzite. South of Pendleton this same stratigraphic position is occupied by a fragmental quartzite unit, tentatively identified as a quartz pebble metaconglomerate, hosting disseminated fuchsite and pyrite. The old workings at this southerly end commonly expose the lower contact of the overlying metashale. The very basal part observed in the saprolitic walls of the pits appears to be thinly bedded ferruginous quartzite of clastic origin. This particular facies is interpreted to indicate local reworking of the west-bordering ironstones prior to the onset of pelagic sedimentation.

According to descriptions of the old gold occurrences by Luttrell (1966), most of the gold production came from the southerly end of the Fisher Lode trend. Although the material mined is reported to be quartz veins, it seems that these were very much restricted to such lithologies as the "conglomeratic" fuchsite-bearing quartzite and the ferruginous metasiltstone base to the metashale that is evident at this end of the trend. Further north

the less productive quartz veins were apparently hosted within the two-amphibole ironstone, oxide iron formation, and metakomatiite flow assemblage.

4.1.2 The Columbia-Tellurium Gold Camp

Approximately fifty old gold prospects cluster along the western limb and within the core of the Columbia synclinorium near its closure north of the James River. There has been essentially no modern exploration carried out on this old gold camp. The only recent studies comprise an evaluation of geochemical prospecting methods for gold mineralization in the area by Good et al (1977) and brief descriptions of the sites of the old workings by Sweet (1980).

Only scant assay information is available on the grade of the historically productive veins. As summarized by Good et al the Tellurium mine had some of the richest veins, averaging 119 ppm during the years 1832-46. In the 1800s the Moss vein averaged 24 ppm gold and during the later work in 1936 the same vein averaged 19 ppm gold. The vein at the Young American prospect averaged 16.5 ppm gold. The distribution of gold in these veins was reportedly erratic and rich shoots often changed abruptly into barren quartz. The most productive of them were granular in texture, reddish in colour above the water table and typically a blue-grey below, indicating finely disseminated magnetite-specularite. The barren veins, which cut both the gold-bearing veins and the country rock, consisted mainly of white, coarsely crystalline bull quartz. Disseminated auriferous pyrite in mica schist sometimes formed haloes up to thirty meters thick around the auriferous veins.

As illustrated in Plate 2, most of these old occurrences lie along trends paralleling the regional strike, a distributional feature this gold mineralization shares with the mineralization in the Mineral district. For the purposes of the following brief discussion of the geological setting of these deposits, they are considered to comprise a westerly Tellurium trend, a central Moss trend, and an easterly Grannison tract.

4.1.2.1 Western Tellurium Trend

The numerous old gold prospects along the Tellurium trend are situated near and at the contact between the easterly Columbia metashales and the westerly ironstone-iron formation assemblage capping the Mineral assemblage. Notably a rather large, late, composite gabbro-diorite sill with affiliated ultramafic differentiate shares this same contact zone but appears to be separated from the actual shale contact by a thin band of ferruginous quartzite, at least over its southern extension. All the old pits occur in either the intervening zone of ferruginous or feldspathic quartzite or, on occasion, the most basal part of the metashale.

Although not well exposed, the very base of the metashale here comprises a thin two meter zone of brown garnetiferous phyllite which is locally talc, phlogopite, and, more rarely, sideritic and fuchsite-bearing. The immediately underlying rocks may comprise either fine-grained ferruginous quartzite or very feldspathic (albitic) quartzite of igneous appearance. Thin beds (5-50 cm) of the albitic quartzite persist into the base of the overlying metashale. From descriptions given by Luttrell (1966), most of the gold production would seem to have come from a one to two meter thick quartzite

unit known as the Big Sandstone containing coarsely granular quartz and kaolinized feldspar with minor pyrite and trace free gold, sphalerite, tetradymite, selenium, silver, chalcopyrite, covellite, pyromorphite, vanadanite, and tourmaline. This particular lithology -- which was not identified by the present writer -- was reportedly traceable for several miles and crosscut by numerous quartz veins up to 20 cm in width.

4.1.2.2 Central Moss Trend

The numerous old prospects along the Moss trend are located in the immediate hangingwall of the basal shale silicate facies iron formation that occurs along the eastern contact of the Columbia metashale. These gold showings occur in ankerite, pyrite, chalcopyrite, and arsenopyrite-bearing quartz veins conformable to layering in enveloping pyritic and occasionally fuchsitic quartzite. Further east the host quartzite is bordered by largely undifferentiated ironstones, feldspathic quartzites, and quartz mica schists of the diverse upper Chopawamsic group.

4.1.2.3 Eastern Grannison Tract

The geological setting of the numerous deposits in the core of the Columbia synclinorium cannot be identified with any degree of certainly due not only to the very poor outcropping conditions but also to the general lack of detailed exploration. As with the Tellurium and Moss trends, some of these deposits occur on the same vein system, and hence would appear to have some basic stratigraphic control. The Young American, Belzoro, and Morgan occur along one such system in magnetite-rich hornblendic ironstone, interlayered

with feldspathic and ferruginous quartzite. In this system the en echelon lenses of mineralized quartz range up to about one meter thick and six meters long, and contain chalcopyrite, sphalerite, gold, silver, and tetradyrite. At the Belzoro the quartz veins are paralleled by narrow discontinuous lenses of auriferous pyrite. The Grannison, Atmore, and Kent comprise a similar gold-bearing quartz vein system but in quartz mica schist. The Bertha and Edith mine contains auriferous pyrite and free gold with magnetite and kaolin in quartz veins hosted in interlensing quartz mica schist, hornblendic ironstone, and feldspathic and gahnite-bearing quartzite. Interestingly, Good et al (1977) noted common gahnite in heavy mineral suites from streams in the vicinity of both the Grannison and the Bertha and Edith.

Recent work by Sauer (1981) indicates that most of the past production from the core of the Columbia structure came from a ferruginous quartzite series with common magnetite, muscovite, and garnet porphyroblasts, as well as numerous quartz eyes. This series is bordered by structurally lower carbonate-bearing amphibolite and structurally overlying magnetite-bearing quartz mica schists and quartzites. It is here hypothesized that this is a contact zone or facies break between ironstones capping the Mineral assemblage and Buffards age pyroclastic-epiclastic lithologies. As reported by Luttrell (1966), some of the deposits in the core of the Columbia synclinorium also demonstrate a spatial association with intrusive rocks. The writer has observed float samples of Mineral assemblage granophyre in the vicinity of the Bertha and Edith workings. Another possibility suggested by the relatively shallow attitudes in the core of this synclinorium due to F interference is that the Columbia granodiorite could be exposed locally. Not enough is yet known of the specific geological setting of these particular deposits to establish definitively whether or not the veining may be related to igneous

intrusive bodies. However, ferruginous quartzite units seem to constitute the favoured host rock; it is possible that these are concentrated at facies changes between the regionally extensive diverse upper Chopawamsic ironstones and the more restricted pyroclastic-epiclastic deposits.

4.1.3 New Canton Trend

The New Canton, Johnson, Margaret, McKenna, and Hodgins mines are located along a five kilometer segment of the east contact of the east limb of the Arvonia metashale immediately south of the James River. During the 1830s, as noted above, limonitic gossans along this trend were mined for iron. According to available information (quoted in Barnes 1963) the main easterly gossan was traced for about ten kilometers along strike with the northern three kilometers forming a tactite iron ore which ran about 50% iron. Sulphide mineralization was observed to be associated with the unoxidized chlorite-garnet schist precursor to the gossan, but it was not until the turn of this century that the sulphide mineralization was prospected for base metal potential. A second, smaller, westerly gossan was also worked to a more limited extent for iron during the early period but this had no affiliated sulphide mineralization. On the basis of work carried out by the author, these two gossans are respectively identified as (1) an easterly hydrothermal chloritite footwall to sulphide mineralization and (2) a westerly basal shale garnet-grunerite silicate facies iron formation.

The detailed stratigraphic setting of the New Canton mineralization is illustrated in Figure 31. The massive sulphides are restricted to the near-vertical contact between the westerly Arvonia metashale and the easterly Mineral assemblage of bimodal mafic-felsic metavolcanics interbedded with

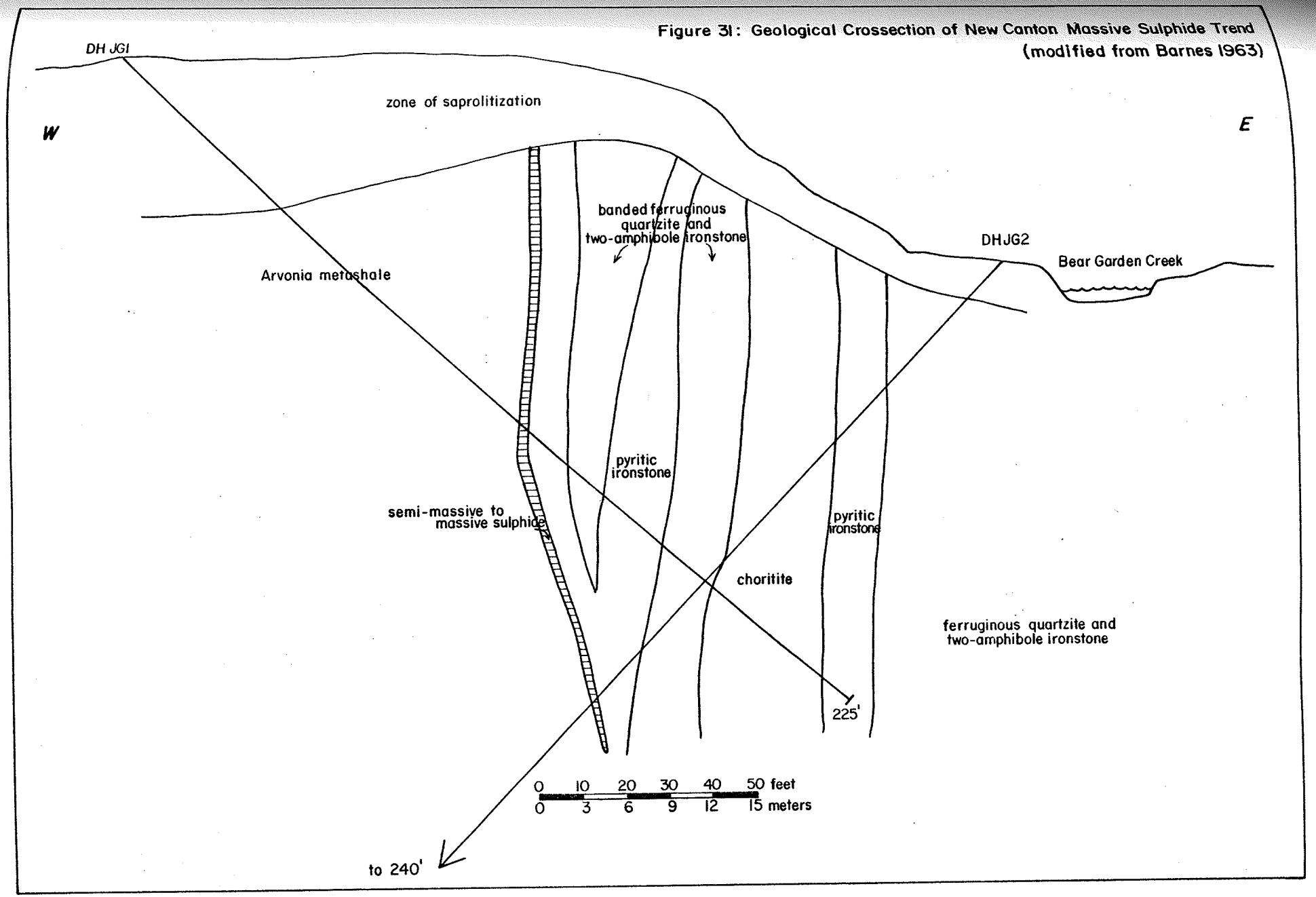

Figure 31: Geological Crossection of New Canton Massive Sulphide Trend (modified from Barnes 1963)

thin-banded ferruginous quartzites, hornblende-cummingtonite ironstones, and more restricted hornblendic amphibolites with coarsely radiating textures. The immediately adjacent chloritite east of the sulphide mineralization intertongues with ferruginous quartzite and as a result shows considerable variation in thickness along strike.

The massive sulphide here, which reaches a maximum thickness of two meters, is a coarsely granular pyrrhotitic ore hosting minor chalcopyrite and trace sphalerite. Assay values quoted in Barnes (1963) indicate an average grade of 1-2% Cu, .5% Zn, .2-2 oz/ton Ag, and trace Au. High grade zinc ore averaging between 5-12% Zn occurs locally within the lower grade pyrrhotite ore; these high grade shoots are oriented parallel to the regional minor fold plunges at 030°- 10-15°N. The massive sulphide mineralization is hosted in a narrow zone of pyrite-sericite schist intercalated with ferruginous quartzite bands occasionally hosting varied minor amounts of staurolite and gahnite besides disseminated pyrite, chalcopyrite and sphalerite. Peculiarly enough, while the textures of the massive pyrrhotite mineralization reflect coarse metamorphic recrystallization of the sulphides, well preserved framboidal textures are sometimes evident in restricted near-massive pyrite concentrations in the host sericite schist-quartzite package.

The geological setting of the New Canton sulphide mineralization shows numerous similarities to the setting for the sulphides in the Mineral district. Hydrothermal chloritite occurs footwall to the sulphide mineralization and this mineralization is hosted in an active zone of sericitic schist and ferruginous quartzite comprising a complex package of sulphide, oxide, and silicate facies ironstone. The main difference lies in the fact that the Mineral district sulphides are hosted within the metavolcanic assemblage while the New Canton sulphide mineralization occurs at

the younger metashale contact.

It is interesting to speculate on the structural-stratigraphic relationship between the basal shale silicate facies iron formation on the western contact and the garnetiferous chloritite and the active zone of sulphide mineralization on the east. As noted previously, geochemical studies of the New Canton chloritite and the basal shale garnet-grunerite indicate that both of these broadly qualify as silicate facies iron formation. Although the two lithologies are petrographically distinct it is considered more than coincidental that such an unusual rock type should border on either side of an inferred syncline. The mere occurrence of silicate iron formation in such a manner is thought to support the hypothesis that the shale limb here is indeed an infold. The difference in rock type between the garnet-grunerite iron formation and the garnetiferous chloritite is interpreted as a facies change relating to variations in the depositional setting prior to shale sedimentation. As the garnet-grunerite facies can be traced northward into an oolitic Fe-chloritite precursor between crossbedded Bremo sands and Arvonia shale, it is considered a near-shore facies of iron formation. The garnet chloritite, on the other hand, is considered a deeper water facies deposited in a geothermal setting given to syndepositional hydrothermal processes.

4.1.4 Mineral Deposits Along the Long Island Trend

The Long Island trend of mineralization occurs near or within the Long Island syncline, the most westerly infold of metashale and/or ferruginous upper Chopawamsic lithologies capping the Palmyra assemblage. Too little exploratory work has been carried out along this trend to allow a detailed assessment of the geological setting of the various mineral showings in the

area. However, diverse types of deposit are known to occur along its length. These include: well developed oxide and silicate facies iron formation, with the best known development just south of Louisa at the north end where the trend is truncated by the Ellisville granodiorite; lode gold mineralization near Palmyra, coincident with the thickest development of metashale; base metal sulphide mineralization near Penlan; and the London & Virginia trend of auriferous base metal sulphide mineralization just west of Dillwyn at the north end of the Andersonville district. The brief reviews following are based on the author's regional work supplemented by extant information where available. The Long Island trend mineral occurrences are discussed sequentially from north to south.

4.1.4.1 Louisa Iron Formation

The town of Louisa is located at the western contact of the Ellisville granodiorite where this intrusive changes form from the southern sill to the northern stock-shaped parts. South of Louisa the strongly developed interbedded oxide and silicate facies iron formation of the Long Island trend persists southwards along the western border of the sill to near Ferncliffe. The area immediately west of this segment of iron formation is underlain by Palmyra assemblage felsic pyroclastics.

Both the Long Island iron formation and the Palmyra assemblage metavolcanics appear to be sharply crosscut by the Ellisville granodiorite stock, indicating that the northerly part of this body postdates the deposition of the iron formation. In contrast to this, the southerly Ellisville sill hosts bands of iron formation, a feature suggesting that this part of the granodiorite intruded coevally with the stage of iron formation

generation. Significantly, the most northerly exposure of the silicate facies iron formation near the border of the Ellisville stock is a coarsely porphyroblastic garnet chlorite ± grunerite rock lithologically similar to the basal shale silicate facies iron formation above the almandine isograd. The presence of such a coarsely recrystallized rock suggests that a narrow thermal aureole bordering the northerly stock overprinted the basal shale iron formation at this locale.

The iron formation comprises massive magnetite-specularite bands up to about .5 meters thick interlayered with heavy disseminations of these same iron oxides in granular quartzite and densely chloritic beds. The iron, manganese, and gold content of several samples collected by the writer are listed in Table 10 below. The considerable variation in iron reflects primarily on the variability of the modal quartz content in the different facies. Although not highly enriched in manganese, the few analysed samples reveal that this element is quite active in the 100-400 ppm range. Significantly, all the various facies have generally high backgrounds (up to 200 ppb) in gold.

Table 10: The Metal Content in Long Island Iron Formation

	% Fe	ppm Mn	ppm Au
LI 2-2 ferruginous quartzite	6.10	300	.02
LI 3-0 oxide silicate Fe Fm	16.00	188	.20
LI 3-1 silicate Fe Fm	20.00	128	.05
LI 3-2 silicate Fe Fm	13.00	133	.05
LI 3-3 silicate oxide Fe Fm	6.00	120	.03
LI 3-4 silicate Fe Fm	23.00	190	.06
LI 5-1 oxide Fe Fm	12.00	350	.06
LI 5-2 silicate oxide Fe Fm	19.00	375	.02

4.1.4.2 Gold Prospects Near Palmyra

The Old Stockton Tunnel and Page gold prospects respectively occur near the west and east contacts of the thickest development of metashale in the core of the Long Island syncline east of Palmyra. As reported by Luttrell (1966), production here came from quartz veins containing free gold, pyrite, and, at the Page, argentiferous galena as well.

The old pits at the eastern Page deposit occur in interbedded silicate-oxide facies iron formation; here specularite is preferentially partitioned into the Fe-chloritite facies while both magnetite and specularite form fine but heavy disseminations in blue-grey quartzite bands. Oolitic structures were observed in the Fe-chloritite. The basal shale silicate-oxide facies iron formation at this location overlies massive buff to cream colour metarhyolite which locally transits into a rhyolite breccia with angular fragments up to about 4 cm hosted in chloritic epiclastic material. Both massive and brecciated facies of the footwall metrhyolite commonly show a rusty weathering due to trace disseminated pyrite. The host iron formation facies transits upward into normal metashale through a zone where it is interlayered with chloritic metasiltstone. Occasional graded intraformational conglomerates with ferruginous quartzite clasts up to about 5 cm in a matrix of chloritite are observed in this zone, indicating that the iron formation was locally reworked prior to the onset of shale deposition.

Most of the work carried out at the Stockton Tunnel site on the western border of the metashale appears to have been placer activity along Long Island Creek. However, a few old pits occur in a thin interval of interbedded quartz mica schist and ferruginous quartzite that persists between the Long Island metashale and a bordering composite diorite-gabbro-peridotite body. This

pod-like intrusive is here situated between the quartz-mica schist border to the metashale and the Ellisville granodiorite further east. Notably, a few of the productive quartz veins exposed by the old pits in the basal part of the westerly metashale were found to contain tourmaline and ankerite.

4.1.4.3 Penlan Massive Sulphide Mineralization

Massive sulphide mineralization on the Long Island trend was discovered by Callahan Mining Corp. in 1977 through routine ground followup of an airborne EM anomaly. As illustrated in Figure 32, this mineralization occurs within a banded succession of pyrite and siderite-bearing metacherts, magnetite iron formation, and chloritic carbonate+epidote-bearing metamarls. This succession is interlayered with pelitic (dust) tuff, while coarser lapilli tuff underlies the metashale.

The ore zone here comprises heavily pyritized (up to about 25%) sericite schist (sericitic pyrite ironstone) and a massive pyritic sulphide unit, varying in thickness up to about three meters, sandwiched in a magnesian chlorite ± talc facies of the metamarl (chloritite). The massive sulphide mineralization consists of laminated fine-grained pyrite with visible chalcopyrite and sphalerite. As indicated by core assays, typical grades of massive ore with 40% Fe and 47% S are 1.25-4.35% Zn, 1.75-2.65% Cu, 0-0.2%Pb, .20-.45 oz/ton Ag, and .01-.02 oz/ton Au.

The best development of the thin magnetite iron formation lithology occurs adjacent to contacts with metamarl. Notably, the magnetite dissemination generally persists into the bordering facies and may even occasionally concentrate enough to form oxide-rich bands within the metamarl.

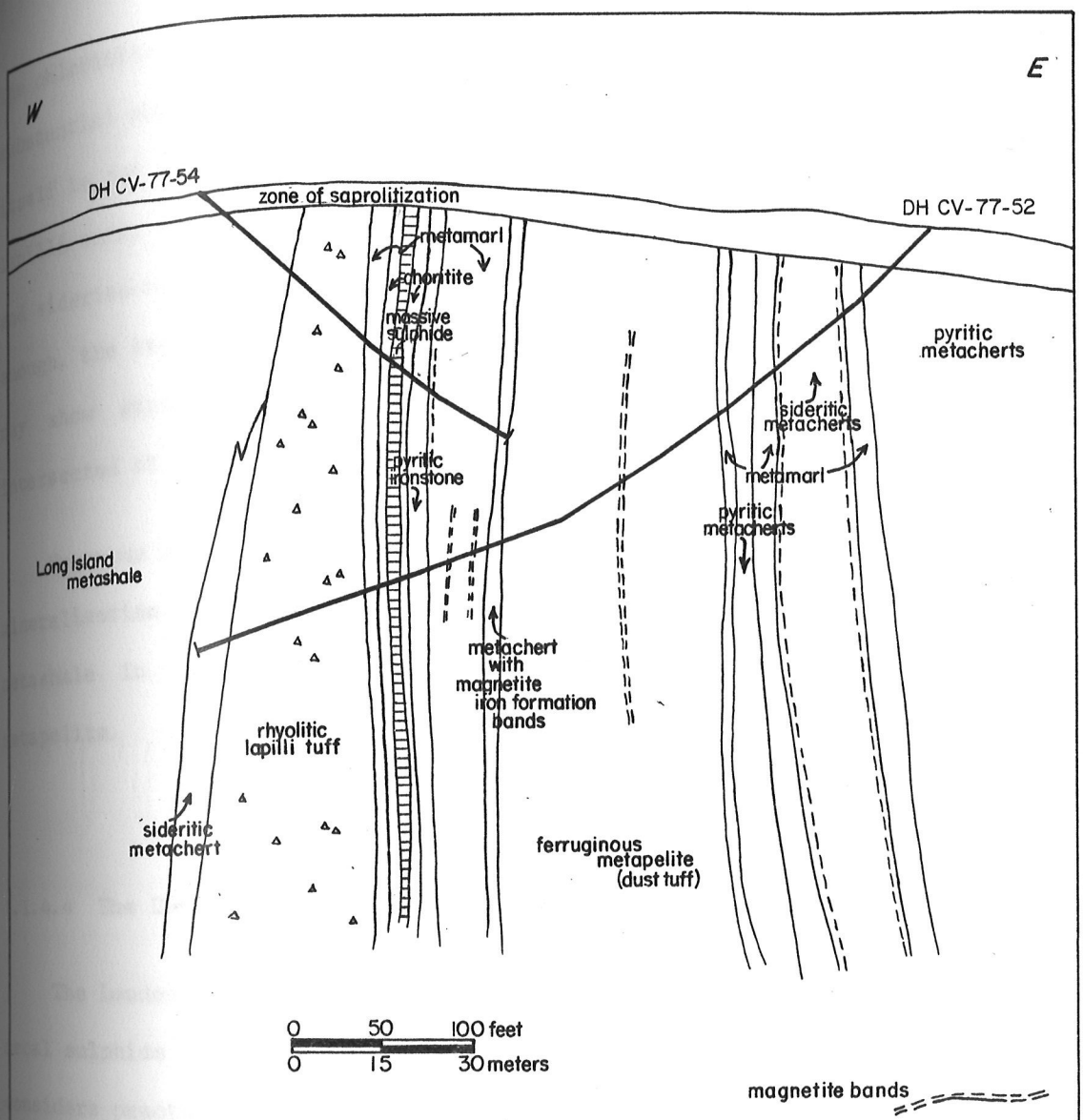

Figure 32:
Geological Crossection of the Penlan Massive Sulphide Mineralization, Long Island Trend

(modified from Callahan Mining Corp. data)

The chloritite immediately adjacent to the massive sulphide also demonstrates substantial amounts of disseminated magnetite, although the massive sulphide itself is not magnetite-bearing. The mineralization is capped by a silicified lapilli tuff, and this in turn overlain locally by a zone of mixed magnetite and siderite-bearing metachert at the base of the metashale. Interestingly enough, the iron formation bands in proximity to the sulphide mineralization may show significant enrichments in manganese. For instance, a band intersected at CV 77-60-357' proved to have 2.61% MnO.

Numerous old gold pits are known to occur along strike from the sulphide mineralization. These gold-bearing quartz veins are located at the base metashale in pyritic and carbonate-bearing metachert and carbonate-rich metapelite.

4.1.4.4 The London & Virginia "Vein" System

The London & Virginia "vein" system comprises a series of gold and base metal sulphide prospects hosted within a quartzite unit that Taber (1913) considers practically continuous over some fifteen kilometers. This rather massive, sugary textured quartzite regionally hosts disseminated magnetite and specularite. The oxides commonly show varied concentrations defining a subtle banding. Massive bands of magnetite with lesser specularite are rare but do occur to about 5 cm. thick.

Over its length this lithology hosts pod-like masses of disseminated to semi-massive (2-60%) to massive pyrite with associated chalcopyrite, sphalerite, galena, and tennantite. Free gold occurs disseminated in the quartzite and in quartz veins transecting the sulphide mineralization. Other

minerals that have been identified (reported by Luttrell, 1966) include barite, chalcopyrite, and pyromorphite, while native silver is associated with the free gold.

This mineralized interval is bordered on the west at least locally by dense green chloritite with up to 15% disseminated garnet and moderate disseminations of magnetite. This is identified as the basal shale silicate facies iron formation, here occurring on the western border of the Long Island syncline. To the east the mineralized quartzite unit appears to be intercalated with and bordered by quartz mica schists of the Buffards type. This lithology commonly has a fragmental texture and weathers red to rusty due to the trace to minor pyrite and common discontinuous lenticles of magnetite-specularite-bearing quartzite.

The lithological setting of the London & Virgina trend supports an interpretation of sulphide and gold mineralization being generated during silicic exhalation in the waning stages of felsic pyroclastic volcanism and prior to the deposition of the basal shale silicate facies iron formation. The London & Virginia mine is the largest zone of mineralization known to date in this locale. Its drill-indicated reserves as established by the Virginia Mining Corp. and reported by Brown (1969) are approximately 723,000 tons of .58% Cu, 3.20% Zn, .92% Pb, .73 oz/ton Ag, and .012 oz/ton Au in ore averaging 20% pyrite.

4.1.5 The Andersonville District

The Andersonville district broadly coincides with the extensive zone of mafic metavolcanics at the south end of the study area. Geophysically this

general area has anomalously high gravity (it is known as the mid-Piedmont gravity high), a feature supporting the thesis that the amphibolites coring the district may comprise an exposure of oceanic crust (Johnson 1981). This amphibolite core is rimmed sequentially by a ferruginous quartzite-iron formation-ironstone assemblage which transits through epiclastic sedimentary facies to quartz mica schists. Metakomatiitic sills are rather commonly interbedded with the peripheral iron formation-epiclastic sedimentary-ash flow tuff assemblage and at the north end of the district these also occur near or at the base of the overlying Arvonia metashale

Several gold prospects known since the early 1800s are located near the western border of the Arvonia synclinorium west of the Andersonville district; these have a similar geological setting to, and may even be coextensive with the London & Virginia trend previously discussed. As the old Morrow and Seay gold prospects at the northern end of the Andersonville district occur well to the east of the London & Virginia trend, however, the geological setting of these particular deposits is discussed below prior to that of the sulphide mineralization.

Although sulphide gossans were known and mined for iron in the mid-1880s, it was not until the 1950s that these were actively explored for their base and precious metal potential. Since that time six sulphide bodies have been evaluated and two of them, Zone 18 and Zone 24, found to contain a significant amount of zinc and copper, minor silver, and trace gold. Recent mapping by Marr (1981) demonstrates that all of the major massive sulphide occurrences lie on a single horizon which is traceable magnetically as regionally extensive ferruginous quartzite. In the following discussion of this productive interval only the sulphide mineralization at Zone 3 (Atkins), Zone 9 (Nixon & Benedict), and Zone 24 (Morris), all of which occur near the nose

of an isoclinal fold on the eastern side of the district, and Zone 18 on the western side are considered.

4.1.5.1 The Morrow Gold Mine

According to Sweet (1981) the Morrow mine was one of the first properties in Virginia on which underground mining was attempted. It was also the largest producer, with over $60,000 in gold (valued at $20.67 per troy ounce) recovered initially from placer operations near the veins, plus 257.77 troy pounds -- including one 9-lb. nugget as well as many masses of a few ounces each -- produced by lode mining between 1850-52. The mines were shut down during the Civil War but were worked briefly in the 1880s and again in 1938 when five shafts and 120 meters of drifts were developed. There has been essentially no modern detailed exploration to evaluate the remaining gold potential at this property but Tongue-Quarter Creek running through the general area of the old workings has become a favoured stream for weekend panners. The following brief resume of the geological setting of the gold mineralization here is based essentially on regional work carried out by this writer.

The mineralization here occurs in an area where broad anticlinal folding terminates the eastern limb of the Arvonia synclinorium through gross intertonguing of the metashale to the northeast with the Mineral assemblage metavolcanics to the southwest. This structural situation has been particularly favourable for exposure of the metashale-metavolcanic contact, and a variety of unusual lithologies are encountered.

Towards the base the metashale is atypically sulphidic and graphitic,

comprising a finely laminated black argillite. Near or at the contact these laminations are locally disrupted by quartz-siderite stockwork vein systems, the borders of which are occasionally lined with fuchsite. At the base the argillite changes from sulphide to carbonate facies, producing well banded siderite iron formation with massive siderite bands alternating with argillite. Below the thin siderite interval is a quartz eye-bearing mica schist-ferruginous quartzite assemblage locally hosting pink felsite and cherty rhyolite flow material with common trace tourmaline and local tourmaline veining. A coarsely porphyroblastic pistachio-green fuchsite-siderite schist with red garnet porphyroblasts up to about 1 cm in diameter locally forms a transitional lithology between the iron formation and the quartz mica schist assemblage.

Other lithologies observed near or at the metashale contact include rather restricted magnesian amphibolites (metakomatiite flows?), coarse-grained hornblendic amphibolites (Mg-basalt flows?), and more extensive thin-banded hornblendic and cummingtonitic ironstones hosting a varied porphyroblastic suite including garnet, kyanite, and staurolite. This two-amphibole ironstone facies is commonly interlayered with and transits into biotitic carbonate (sideritic) ironstone. At one location the contact between the two-amphibole ironstone and magnesian amphibolite also appeared transitional with appreciable anthophyllite occurring in the bordering ironstone. The various facies of the extensive ironstone assemblage are thought to transit downward into a dominantly mafic volcanic assemblage that characterizes the core of the Andersonville district.

Most of the old workings at the Morrow mine occur at the contact between the fuchsite mica schist-sideritic iron formation association and overlying black pyritic argillite. According to Luttrell (1966), most of the old

production here came from free gold affiliated with pyrite, chalcopyrite, and tetradymite hosted in quartz veins within this host rock package. Considerably more exploratory and detailed petrological reasearch will be required before the specifics of the gold metallogenic processes can be delineated definitively, but the following schemata is considered as offering a useful provisional interpretation. The co-presence of veined rhyolitic flow material, siderite±fuchsite-bearing iron formation, and pyritic argillite suggests a zone of focused hydrothermal discharge of early carbonate-rich and later sulphide-bearing fluids at a small volcanic center. The occurrence of tourmaline vein stockworks in cherty rhyolite flows and carbonate breccia in sideritic-pyritic argillite indicates further that this discharge was at times quite dynamic. That carbonate and pyritic bands continue well into the basal shale suggests a long-lived hydrothermal system strong enough to modify sedimentation at the onset of shale deposition. The heat for driving such a local convection cell may well have been derived from late high level injection of komatiite-Mg basalt magma. The siderite iron formation fuchsite-siderite schist exposed in the old pits would seem to be a likely source for syngenetic gold initially liberated through pervasive hydrogen ion metasomatism of the ultramafic material. Remobilization of gold during sweating out of quartz into dilatent zones along an anticlinal hinge zone during the late regional metamorphism is thought to account for the gold now being hosted in quartz veins.

4.1.5.2 Zone 3 Sulphide Mineralization (Atkins Property)

Zone 3 or the Atkins property occurs on the southeast limb of the isoclinal closure of the productive horizon at the southeastern side of the

Andersonville district. The zone comprises massive to disseminated sulphide mineralization of which the largest known lens is a minimum of 427 meters long and up to five meters thick, extending down-dip beyond the current limit of drilling in the vicinity of 60 meters below surface. This particular body, which dips ~35°NW, is exposed as gossan on the surface. Additional small gossans are known to occur along the southwest to westerly strike.

The semi-massive to massive sulphide comprises pyrite-pyrrhotite mixtures with a minor variable chalcopyrite and sphalerite content. Chalcopyrite generally dominates over sphalerite, although Young (1981) reports that sphalerite dominates in the southeastern part. Where richest in chalcopyrite, the ore tends to be pyrrhotitic and to host large (up to 2 cm) buckshot pyrite porphyroblasts. As noted by Young, both base and precious metal contents are uniformly low; the sulphide mineralization here is subeconomic in grade.

As illustrated in Figure 33, the mineralization occurs in an active zone of ferruginous quartzite, chloritite, and garnetiferous quartzite within banded amphibolites. Variable biotite and chlorite contents within the bordering amphibolites suggest moderate reworking of mafic volcanic precursors interlayered with non-reworked mafic flows. Young notes that the mineralized zone as a whole is richer in magnetite than the country rock amphibolites to the extent that the stratum can be traced magnetically by ground geophysics. This magnetic expression is primarily due to a thick section of biotite-magnetite-bearing quartzite structurally overlying the sulphide mineralization. The heavily disseminated to massive sulphide is hosted within a coarsely porphyroblastic garnet-cummingtonite chloritite (silicate iron formation) bed. Thin-banded impure quartzite hosting garnet, muscovite, and minor magnetite and biotite structurally underlies the massive sulphide-chloritite association, isolating it from reworked biotitic

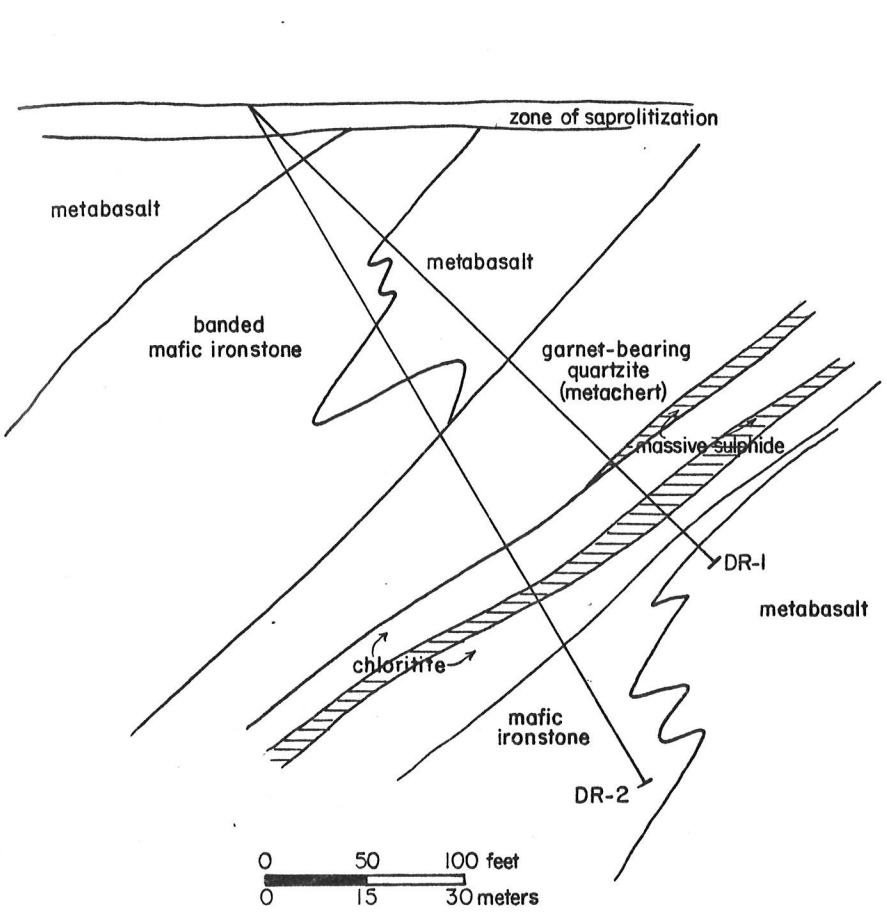

Figure 33:

Geological Crossection of Zone 3 (the Atkins property)
Andersonville District

(modified from Young 1981)

amphibolite (metabasalt) further in the footwall.

4.1.5.3 Zone 9 Sulphide Mineralization (Nixon-Benedict Property

Zone 9 or the Nixon-Benedict Property occurs on the northwestern limb of the isoclinal fold in the host lithology at the southeastern side of the Andersonville district. As reported by Young (1981), surface geophysics and drilling in this vicinity have outlined a massive sulphide bed which is a minimum of 1220 meters long and up to seven meters thick, extending beyond the current depth of drilling. This unit has very low base and precious metal contents, comprising 90% pyrrhotite with minor pyrite and trace (less than 2%) chalcopyrite.

As illustrated on Figure 34, the sulphide mineralization here again occurs in banded metabasalt with variable quartz-chlorite-biotite contents indicative of local reworking. As with the Atkins property, the active zone is richer in magnetite than the bordering reworked mafic volcanics. Banded biotite-magnetite-garnet-bearing quartzite concentrates peripheral to the sulphide, which is hosted in a coarsely porphyroblastic garnetiferous chloritite. The mineralogical assemblage of this chloritite typically includes only cummingtonite and staurolite besides the garnet, though andalusite was tentatively identified at its outer margin. The oxide-sulphide mineral zoning associated with the occurrence of sulphides is transitional, with decreasing magnetite and increasing sulphide. As a result, magnetite is virtually absent from the massive sulphide facies. The trace chalcopyrite typically occurs as inclusions in pyrite. Where sulphides are heavily disseminated in chloritite, subtle compositional layering is discernible. Here the trace chalcopyrite and sphalerite occur mostly in silicate-rich

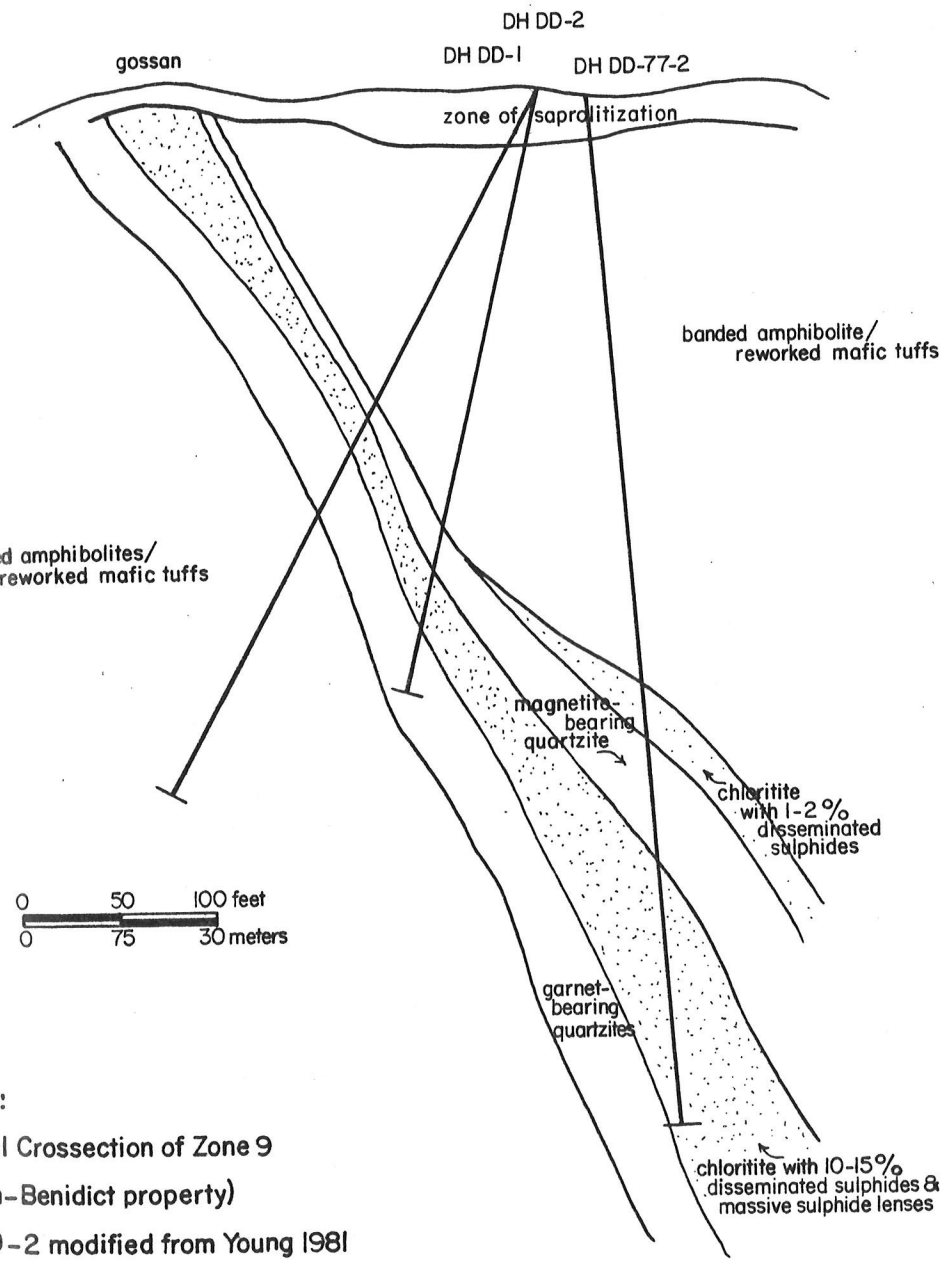

Figure 34:
Geological Crossection of Zone 9
(the Nixon-Benidict property)
DD-1, DD-2 modified from Young 1981
DD-77-2 drilled by Conico 1977

layers.

4.1.5.4 Zone 24 (Morris Property)

The showing known as Zone 24 or the Morris property outcrops as an extensive zone of gossan near the nose of the isoclinal fold in the ore-bearing lithology at the southeastern side of the Andersonville district. This gossan, covering an area about 550 meters by 275 meters, is developed over a sulphide unit dipping shallowly to the northwest. As reported by Young (1981), drilling to date has outlined a reserve of 550,000 tons with an average grade of 4.8% Zn and .98% Cu.

As illustrated on Figure 35, there are three subparallel sulphide bodies here, dipping 20-30°NW. Only the upper lens, however, shows consistent significant zinc and copper values. Where massive the ore is typically medium-grained and granular, constituted largely of pyrite, although where chalcopyrite is most enriched, pyrrhotite predominates and pyrite occurs as porphyroblasts. The middle and lower lenses are everywhere pyritic and in general have only very restricted zones enriched in sphalerite. As reported by Young (1981), one of the highest grade shoots intersected in the upper lens comprises 18.47% Cu, 8.2% Zn, and 7.2 oz/ton Ag over a .9 meter interval.

The host rock to the sulphide mineralization here is a moderately reworked mafic metavolcanic characterized by a variably biotitic, garnetiferous, and quartzitic banded amphibolite succession. The sulphides are specifically hosted in garnetiferous chloritite, with heavy disseminations transiting into local massive sulphide lenses. Although not noted in Young's core logs, mineralogically complex garnet, staurolite, and gahnite-bearing

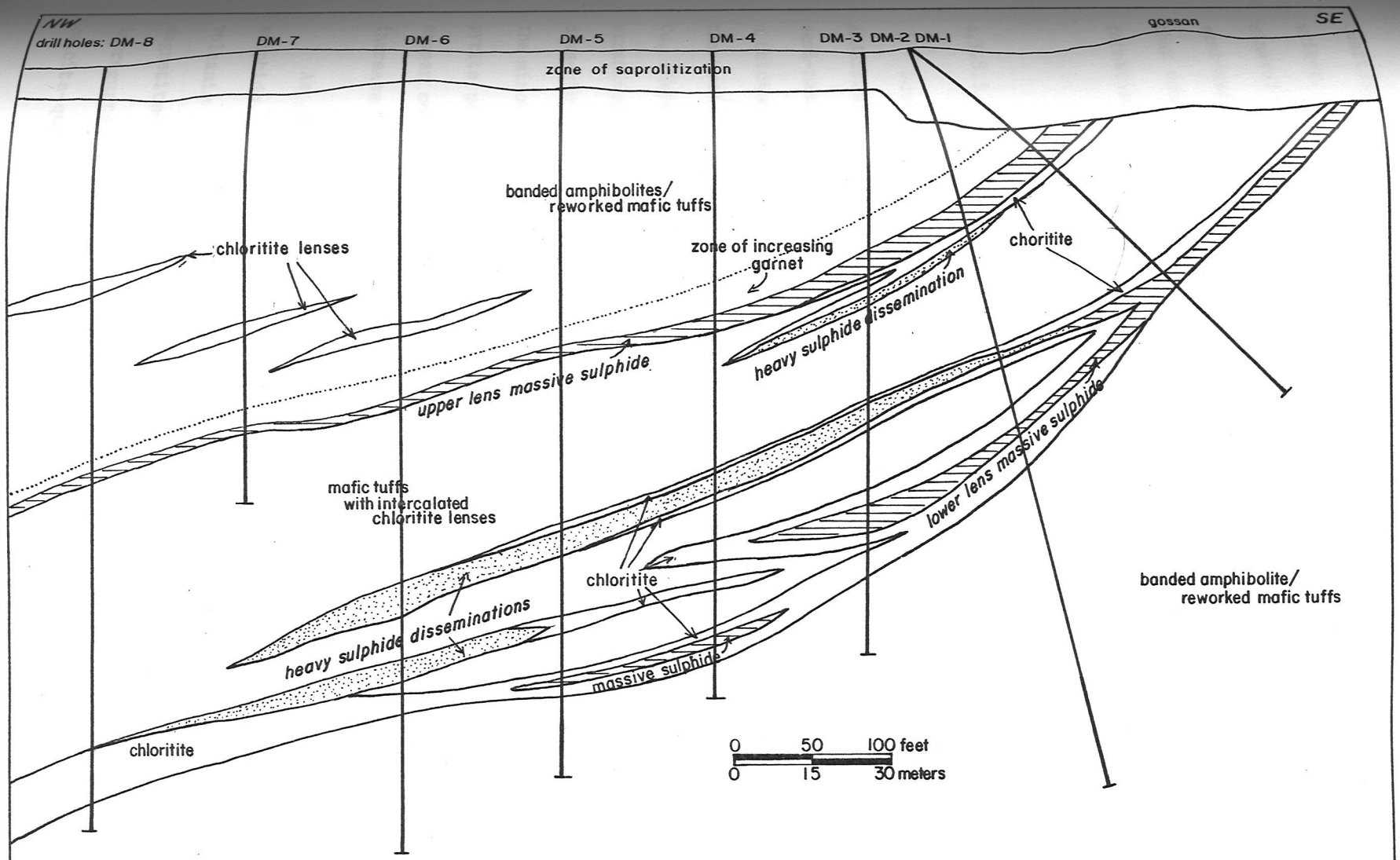

Figure 35: Geological Crossection of Zone 24 (the Morris property), Andersonville District
(modified from Young 1981)

quartzites have been observed affiliated with the surface gossan by the writer. Also, porphyroblastic kyanite was observed to be a common gangue mineral (up to about 20 modal %) in gossan boulders after massive and semi-massive sulphide. The occurrence of these alumino-silicates suggests that complex lateral facies changes may accompany the silicate-sulphide iron formation at this location.

4.1.5.5. Zone 18

Occurring on the same productive horizon on the western side of the Andersonville district, this showing, as reported by Young (1981), comprises a semi-massive to massive sulphide lens with a minimum length of 305 meters and a thickness up to fifteen meters. As such, it is the largest known deposit in the area, with a drill-indicated reserve of 794,000 tons of 4.68% Zn and .60% Cu. Extensive drilling (Young reports 67 holes) defines the ore as a strataform elongate body dipping 50-55°NW and pinching out down-dip and down-plunge. Medium-grained granular pyrite predominates, serving as host to the minor sphalerite, pyrrhotite, and chalcopyrite and trace galena. Buckshot pyrite porphyroblasts up to 2.5 cm are rather common. Subtle bands of higher copper concentration are evident, and here pyrrhotite may be observed to increase in abundance as well.

As illustrated in Figure 36, the host rock assemblage to the massive sulphide comprises little reworked metabasalt interlayered with minor felsic volcanic material. The mineralization is hosted in a garnetiferous magnetite-bearing chloritite iron formation which is commonly heavily impregnated with disseminated sulphide as well as being crosscut by stockwork calcite-quartz veining and sulphide stringers. Irregular contortions and

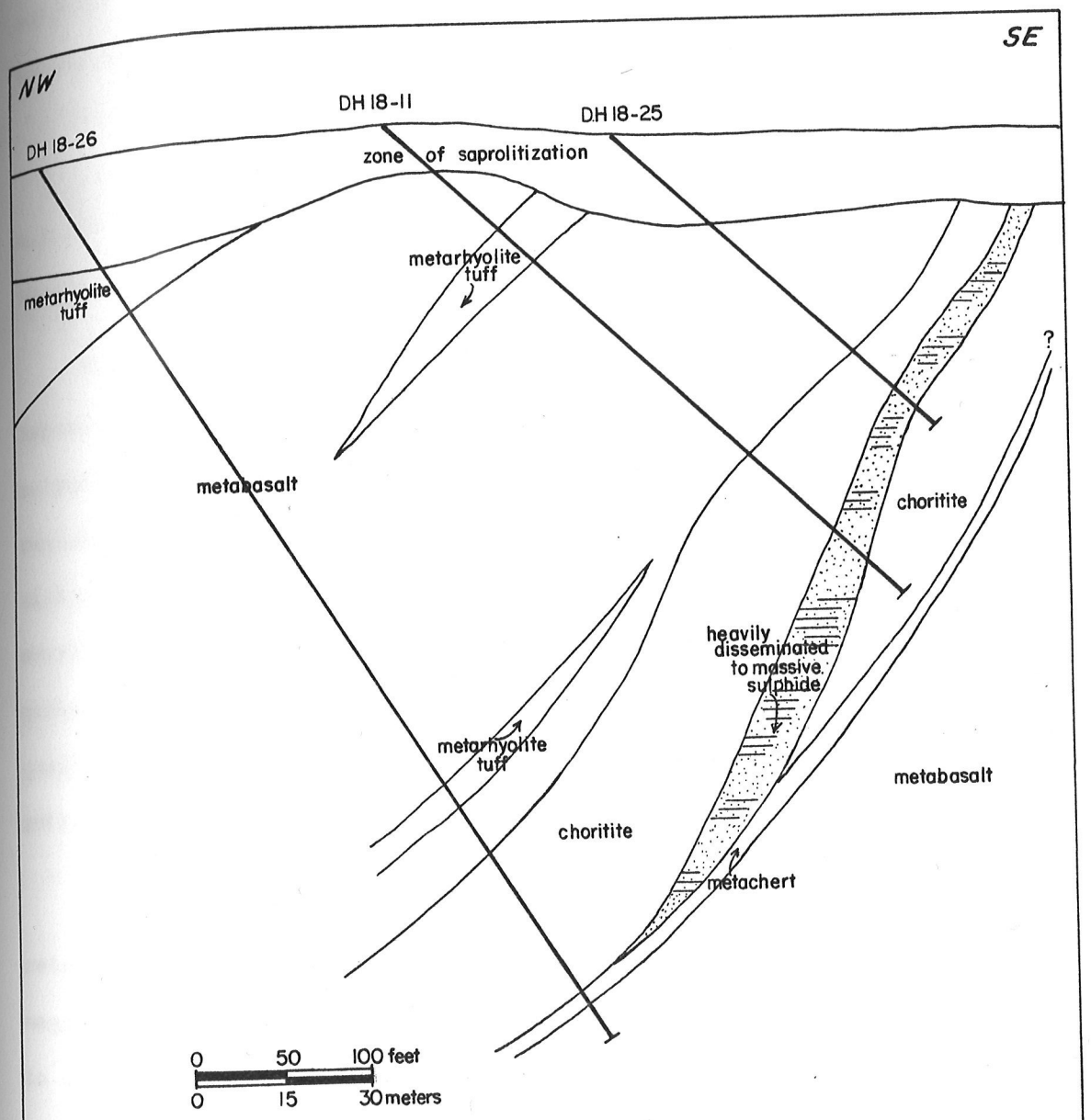

Figure 36: Geological Crossection Zone 18, Andersonville District
(modified from Young 1981)

fragmental zones both in bordering chloritite schist and in the massive sulphide itself suggest that there was likely syndepositional slumping prior to the metamorphic overprint.

4.1.5.6 Geological Setting of the Andersonville District

Massive Sulphides

The regional and detailed geological work carried out in the Andersonville district to date supports the interpretation that all the known sulphide mineralization is hosted on one stratigraphic horizon represented regionally by ferruginous quartzite-oxide iron formation and more locally by silicate-sulphide iron formation. The interval is usually isolated from overlying and underlying reworked mafic volcanics by ferruginous and garnetiferous quartzite. Locally, such as at Zone 24, the bordering quartzites include mineralogically complex staurolite and gahnite-bearing units as well.

The massive sulphide mineralization here shows very intimate relationships with the host chloritite. Complete transitions from magnetite-bearing chloritite through sparse to heavily disseminated sulphide to massive sulphide mineralization are commonly observed. The chief gangue minerals associated with the sulphides include a variety of ferruginous and aluminous silicates: garnet, staurolite, cummingtonite, and, more locally, kyanite and possibly andalusite. Which type of porphyroblast occurs in any given spot is presumably determined by subtle chemical variations in the precursor chloritite iron formation.

Collectively, then, the Andersonville massive sulphides appear to be

related to a blanket iron formation deposited near the top of a slightly to moderately reworked mafic metavolcanic succession. Regionally, lean oxide iron formation-ferruginous quartzite was developed, while more locally silicate-sulphide iron formation at least in part replaced the oxide faces. The origin of the iron formation is attributed to a period of generally diffuse hydrothermal discharge in the waning stages of Mineral suite volcanism and prior to Buffards type ash flow effusion. This will be discussed further in the regional metallogenic synthesis below.

4.1.6 Copper-Gold Mineralization Affiliated with Greenstone

For the sake of completeness one further type of mineralization comprising several small copper showings in the greenstone beds at the base of the Palmyra assemblage should be noted in brief. At the old Lightfoot prospect in the Shores greenstone south of the James River, heavily chloritized and magnetite-bearing spilite with a stockwork of chlorite, epidote, quartz, and calcite veining hosts disseminated and stringery chalcopyrite and pyrite. Luttrell (1966) points out that a .5-1 meter quartz vein hosting auriferous pyrite and chalcopyrite at this site was worked first for gold prior to the Civil War and later for copper at the turn of this century. This writer observed that trace copper disseminations commonly occur with the chlorite and epidote-rich facies of the host greenstone. At the Anaconda prospect similar copper-gold mineralization is hosted in a series of thin spilite flows showing extreme segregation of the chlorite-actinolite-albite-epidote-quartz assemblage into mineralogically simple and often near-monomineralic facies. Disseminated minor chalcopyrite commonly accompanies quartz-epidote segregations, while the more massive chlorite-

actinolite-albite schist facies only rarely hosts trace amounts of this same mineral. Stringer pyrite and chalcopyrite were also observed to be affiliated with the quartz vein stockworks which appear to pervade all the various facies.

The copper-gold mineralization hosted in vein systems within the greenstone is interpreted to result from the partitioning of these elements into hydrothermal phases during the spilitization process. The chlorite-rich and epidote-rich facies of the spilite seem to be the favoured ones for hosting disseminated copper mineralization. It is not known, however, whether the host quartz veins relate to early late stage hydrothermal silicification or to later metamorphism.

4.2 Metallogenic Processes as Indicated by Mineral Chemistry

Because most minerals, metallics and silicates alike, are complex solid solutions, the specific elemental relationships between given ores and their host rocks -- which are, of course, critical to an understanding of metallogenic processes -- can only be determined through a systematic study of mineral chemistry. This is particularly true when one is dealing with metamorphosed mineral deposits. The coexisting mineral assemblages and mineral compositions in such cases, though constrained by bulk chemistry, are also determined by sulphide-silicate-oxide-carbonate equilibria reactions occurring during the metamorphic overprint. With respect to the present study area, the investigation of mineral chemistry is still in its infancy. The recent theses of Miller (1978), Cox (1979), Feuer (1980), and Sandhaus (1981) have documented the compositions of a number of ore and gangue minerals at the

Arminius and Cofer deposits in the Mineral district, however, and collectively their findings provide a useful starting place for discussion of this aspect. Additional mineralogical data have been generated through an investigation of the regional variation in garnet and amphibole chemistry. In particular, a series of microprobe analyses was carried out at the University of Western Ontario (R.L. Barnett, analyst) on a suite of surface handsamples and drill core specimens selected by this writer primarily to reflect any chemical variation in these particular mineral species with proximity to known sites of massive sulphide and gold mineralization.

Although chemical data exist for a number of specific mineral species, there has as yet been no systematic investigation of coexisting mineral assemblages; this precludes for the present any definitive documentation of the specific metamorphic mineral reactions which have occurred. Nevertheless, since all samples for which mineral chemical data are available derive from the Mineral metavolcanics which, as previously discussed, lie at or above the low to medium grade transition in metamorphic rank, it is considered that the analytic results presented here generally reflect on low amphibolite facies metamorphic conditions. No mineral chemical investigations have yet been carried out on the lower grade (greenschist), fine-grained, pelitic lithologies occurring in the west to central parts of the belt.

Metamorphic overprint notwithstanding, the primary objective of the present discussion is to utilize known mineral compositional data as a means of unraveling the metallogenic processes through which the above noted massive sulphide and lode gold mineralization were produced. Towards this end, an effort has been made to determine the manner in which metamorphic crystallization of various mineral species occurred, as this has significant bearing on the question of how given mineral compositions reflect on the

chemical nature of any pre-metamorphic precursor. The discussion begins with a brief review of the mineralogical data presented in other studies. The results of the regional garnet and amphibole investigations are then considered sequentially with the aim of establishing what particular metallogenic processes are signified by the apparent composition changes evident in these mineral species.

4.2.1 Mineral Chemical Data Reported in Other Studies

The mineralogical data reported in the aforementioned theses collectively cover numerous mineral species including sulphide, carbonate, oxide, and silicate types; the individual members of these respective groups for which data are available are considered sequentially below.

4.2.1.1 Sulphides

Pyrite: As yet there has been no systematic investigation of pyrite. However, both Miller and Cox have noted that this mineral is here compositionally uniform and characteristically contains only trace (.3-.4 wt %) As besides Fe and S.

Pyrrhotite: The pyrrhotite from the Arminius deposit analysed by Cox for Fe and S proved to comprise homogeneous grains with their iron content dependent on the presence or absence of pyrite in the assemblage. The pyrrhotite compositions range from 47.65 to 46.45 atomic % Fe, with many falling in the compositional gap 47.4-46.8 atomic % Fe that has been determined by various investigators (Gronvold & Haraldson 1952, Arnold 1962,

Yond & Hall 1969 -- all quoted by Cox) to mark the boundary between higher iron hexagonal and lower iron monoclinic pyrrhotite. Compositionally most of the pyrrhotite would seem to result from homogenization of original two-phase mixtures of hexagonal and monoclinic types. Such mixtures are observed to be commonplace in many natural pyrrhotite-bearing assemblages (Arnold 1969). As noted by Cox, higher iron (hexagonal) pyrrhotite is found alone in samples in which pyrite is absent while lower iron (monoclinic) pyrrhotite occurs occasionally as inclusions in pyrite within pyritic assemblages.

Sphalerite: Microprobe analyses of sphalerite from the Cofer deposit reported by Miller and from the Arminius deposit reported by Cox generally show Cu and Mn below .2 wt % respectively and Cd content below .3 wt %. In the more systematic study carried out by Cox, the FeS content of sphalerite was found to vary considerably depending on the coexisting mineral assemblage. As summarized in Table 11, the FeS content in sphalerite in polymineralic assemblages (other than those comprising sphalerite-pyrite-pyrrhotite) shows a broad range of values. Cox, however, found that although the mole % FeS varies considerably from one sample to another, there is only a limited divergence from grain to grain within any given sample, the greatest variation within any one specimen being 3.9 mole %. This would seem to indicate that the equilibrium domains for sphalerite are quite small. Within these domains the sphalerite composition is essentially controlled by the local bulk chemistry while the much more limited grain to grain variation is probably accounted for by modal fluctuation in the immediately bordering mineral assemblage. Interestingly, Cox also found that sphalerite coexisting only with pyrite shows a consistent FeS increase from hangingwall to footwall. This particular compositional feature may be evidence for a cryptic vertical zonation with Zn-enrichment towards the structural top of the Arminius lens.

Table 11: FeS Variation of Sphalerite in Differing Mineral Assemblages (Cox 1979)

Mineral Assemblage	Mole % FeS
sph + py + po	14-16
sph + py	12-14
sph + py + mt	7-14
sph + gal	9-11
sph + py + aspy	6-10
sph + py + cpy	5-17
sph + py + tet-ten + gal	4-10

Cox also explored the use of sphalerite compositions as a geobarometer. In the presence of both pyrrhotite and pyrite, the FeS content of sphalerite has been found to be fixed essentially by the pressure conditions existing during the metamorphic overprint (Toulmin & Barton 1964, Scott 1973-76). Assuming that the Fe-rich composition of sphalerite coexisting with pyrite and pyrrhotite (approximately 15.1 mole % FeS) is representative of equilibrium at the metamorphic maximum, this indicates that a pressure of 4.6 + 0.1 kbar was attained.

Arsenopyrite: The microprobe analyses of arsenopyrite reported by Miller and Cox reveal that this sulphide species is characterized by an S-As ratio 1 and all grains contain a small (<.1 wt %) amount of Ni. Most grains (except those bordering on sphalerite) show a slight zonation with S-enriched cores and As-enriched rims. This zoning is reverse to that observed by Kretshmer and Scott (1976) to be most common in natural arsenopyrites. Cox suggests that either an isobaric pressure decrease occurred during growth or the zoning may simply reflect local variation in As and S activity. By utilizing the composition of arsenopyrite in arsenopyrite-pyrite pairs as a sliding scale geothermometer as proposed by Kretshmer and Scott, Cox determines a metamorphic temperature maximum of 420 ± 13° C.

Tetrahedrite-Tennantite: A complete spectrum of this fahlerz solid solution series has been identified in both the Arminius and Cofer deposits by Cox and Miller respectively. The reported analyses show that the Ag content varies directly with Sb, while As and Sb vary inversely. The tetrahedrite end members occur in pyritic assemblages with associated trace galena. The compositionally intermediate fahlerz grains generally show a marked increase in Sb content adjacent to galena and a marked decrease in Sb adjacent to chalcopyrite. The tennantite end members occur in polymineralic assemblages devoid of galena. Sphalerite coexisting with fahlerz shows anomalously low FeS content with grains adjacent to tetrahedrite having >3 mole % FeS and those adjacent to tennantite <1 mole % FeS.

4.2.1.2 Carbonates

There has as yet been no systematic investigation of the composition of carbonate species. Most of the analyses reported by Feuer from the Cofer deposit show that the carbonate here is ankeritic with a Ca:Mg:Fe ratio of 2:1:1. However, Feuer also notes that Ca-Mg, Mg-Fe, and Fe carbonates are present in some samples as well.

4.2.1.3 Oxides

Magnetite: The few microprobe analyses of magnetite reported by Cox reveal that this mineral typically contains only iron. However, where coexisting with staurolite, the magnetite contains trace amounts of Zn, Al, Ti, Mn, Cd, and Si.

Ilmenite: This mineral is quite rare but has been reported by Cox to be included in magnetite and/or garnet in sulphide-poor samples from the Arminius deposit. When included in garnet the ilmenite is sometimes associated with gahnite and in addition to Fe and Ti contains 1-2% Mn and trace V and Mg. The magnetite coexisting with ilmenite, on the other hand, is notably Ti-free; as a result this mineral pair cannot in this instance be utilized for determining the temperature or oxygen fugacity at which these minerals attained equilibrium.

Gahnite: Sandhaus (1981) investigated gahnite chemistry in the Sulphur, Arminius, Julia, and Cofer deposits in the Mineral district; his main results are summarized in Table 12. As shown, the gahnite has a fairly narrow compositional range (between 70.5-81.9 mole %) in gahnite end member but varies considerably in both hercynite (7.5-21.9 mole %) and spinel (4.7-21.9 mole %) end members. All the gahnites analysed have less than 1 mole % galaxite. Also, as shown in Table 12, there is only minor variation evident in the average wt % Zn content in gahnite from the differing sulphide deposits. In general the grains of this mineral demonstrate no compositional zoning. At the Sulphur deposit, however, the gahnites have very slightly Zn-enriched cores and Mg + Fe-enriched rims.

Table 12: Compositional Variation in Gahnite (from Sandhaus 1981)

	Max Modal%	Mole% Spinel Phase of Spinel $MgAl_2O_4$	Hercynite $FeAl_2O_4$	Galaxite $MnAl_2O_4$	Gahnite $ZnAl_2O_4$	Avg Wt% Zn in Gahnite
Sulphur	14.9	5.7-21.9	13.7-21.9	1.0	70.5-77.1	34.77
Arminius	--	6.0-8.5	14.2-21.0	.5	71.5-79.4	34.57
Julia	3.9	4.7-12.7	11.5-17.4	1.0	74.5-80.9	35.63
Cofer	5.0	6.1-16.9	7.5-16.6	1.0	71.6-81.9	36.02

Although the gahnite appears compositionally uniform, the modal abundance does vary significantly from one deposit to another. Also, Sandhaus notes that the gahnite content increases towards the margins of any one ore lens. Although Sandhaus found no evidence for any gross compositional trends in any of the ore zones he studied, such a feature was observed by Cox at the Arminius deposit. Here the Zn/Fe ratio in gahnite increases regularly from hangingwall to footwall in the few samples analysed. This evident iron enrichment towards the structural top is an inversion of the compositional trend observed by Cox in sphalerite. Interestingly, Cox also demonstrates an inverse relationship between Fe and Zn contents of coexisting gahnite and staurolite and an increase in the Zn/Fe ratio in staurolite towards the structural top (paralleling the Zn enrichment trend in sphalerite). The absolute iron and zinc content in both gahnite and staurolite, moreover, is found to be dependent on the presence or absence of sphalerite. These compositional features very definitely suggest that these zinc-bearing minerals partook in sulphide-silicate-oxide equilibrium reactions during the metamorphic overprint.

With respect to gahnite metallogenesis, Cox hypothesizes that original sulphur undersaturation resulted in the initial deposition of zinc oxide and/or hydrates which during subsequent metamorphism converted to gahnite and zincian staurolite. A similar mechanism has also been proposed by Plimer (1979) to account for gahnite at the Broken Hill deposit in Australia. Significantly, Bischoff (1969) reports that ZnO is a rather common constituent in the metalliferous muds of the Red Sea. On this basis it would seem feasible that primary zinc oxide could well have been the source of the zinc now found in gahnite. Against this, Sandhaus argues that that at least in the present study area he finds essentially no petrological basis for favouring this

latter thesis over the postulate that the mineral originated through desulphidization of sphalerite during the metamorphic overprint. Notably, such a strictly metamorphogenetic schema has also been proposed by Wall and England (1979) for the origin of the Broken Hill gahnite. As this theory would have it, rather than signifying the occurrence of original sulphur-deficient zinc mineralization, the gahnite resulted through a net flux of zinc outwards and aluminum inwards during the metamorphic overprint, thus explaining its tendency to be concentrated near the margins of the ore lenses.

4.2.1.4 Silicates

The silicate mineral species for which there are chemical data include staurolite, chlorite, biotite, garnet, and amphibole. Because compositional variation in the latter two are discussed at considerable length in subsequent sections, however, only staurolite, chlorite, and biotite will be noted here.

Staurolite: The microprobe analyses of staurolite presented by Miller, Cox, and Feuer all indicate not only that zinc is the most variable component but that it varies inversely with iron. In the analyses reported by Cox the highest Zn and lowest Fe are 7.0 wt % Zn and 9.4 wt % Fe, while the lowest Zn and highest Fe are .51 wt % Zn and 14.5 wt % Fe. This investigator points out further that the high-Zn staurolites are found coexisting with pyrrhotite and magnetite while low-Zn staurolite occurs in pyrite quartzite. These relationships would seem to indicate that high-zinc staurolite developed in a metal-rich but sulphur-undersaturated source rock while low zinc staurolite developed in a sulphur-saturated but metal-poor source rock. It seems likely that readily available sulphur and metals were not everywhere coincident.

According to Plimer (1978), the condition of sulphur undersaturation would leave zinc, a normally chalcophile element, to form oxide (gahnite) and silicate (zircian staurolite) phases. Also, it is possible that the presence of non-sulphur-complexed zinc may in fact stabilize the assemblage gahnite-quartz-staurolite in pelitic rocks (Frost 1973). That the high-zinc staurolite occurs with low-Zn gahnite indicates that the former may derive its zinc content in reactions with gahnite as postulated by Beach (1973).

Biotite and Chlorite: Although numerous biotite and chlorite analyses have been reported by Feuer, Cox, and Sandhaus, there has as yet been no systematic investigation of these particular mineral species. The analyses that exist do show, however, that there is considerable compositional variation, with both iron and magnesium-rich members present. An example of this variability is the striking fluctuation in Mg/Fe ratios in biotites and chlorites in the Cofer deposit reported by Feuer. As demonstrated in Table 13, the compositions of both these species change radically from one host rock to another. The Mg enrichment evident in the matrix of the fragmental metarhyolite unit structurally overlying the mineralized zone at the Cofer deposit suggests that this was likely a focus for hydrothermal Mg-metasomatism. Although the magnesian character of the biotite and chlorite in amphibolite can be accounted for in terms of bulk chemisty, the magnesian biotite occurring in pyritic quartzite would seem to be anomalous in this respect; it is likely that silicate-sulphide equilibria reactions of the type investigated by Hammarbuck and Lindquist (1972) and Bachinski (1976) whereby iron is preferentially partitioned into the sulphide phase may play an important role here. The low Mg/Fe ratios in non-mineralized metavolcanics and in the carbonate ironstones probably do, however, reflect more on the basic bulk chemical control.

Table 13: Variation in the Mg/Fe Ratio in Biotite and Chlorite Occurring at the Cofer Deposit (from Feuer 1980)

Lithology	Mg/Fe in Biotite	Mg/Fe in Chlorite
fragmental schist		
- matrix	1.3-7.7	1.7-9.3
- fragment	.96-1.05	.82-1.00
pyritic quartzite	26	--
amphibolite	2.4	3.00
biotitic carbonate ironstone	1.4	1.7
quartz feldspar porphyry	.75	.87

The compositions of numerous coexisting biotite-garnet pairs were investigated by Cox in order to establish a temperature of metamorphic equilibrium by the method of Ferry and Spear (1978). The distributional coefficients evident between these minerals for five of the six analyses reported give a metamorphic temperature of 465° ± 35°C. The one remaining sample gave an unexplained aberrantly high value of 587°C.

4.2.2 Regional Variation in Garnet Chemistry

This investigation of the regional variation in garnet chemistry is based on microprobe analyses of garnet in 43 separate specimens with an average of approximately ten spot analyses per sample. The cumulative results are listed in table form in Appendix D. The essential compositional features collectively revealed by this body of data are demonstrated graphically on a plot of end member components (Figure 37) and numerically in the listing of the core-to-rim zonation patterns observed in MnO, FeO , MgO, and CaO (Table 14).

A shown on Figure 37, garnets from the metashale and basal shale silicate facies iron formation typically comprise over 75% almandine end member and

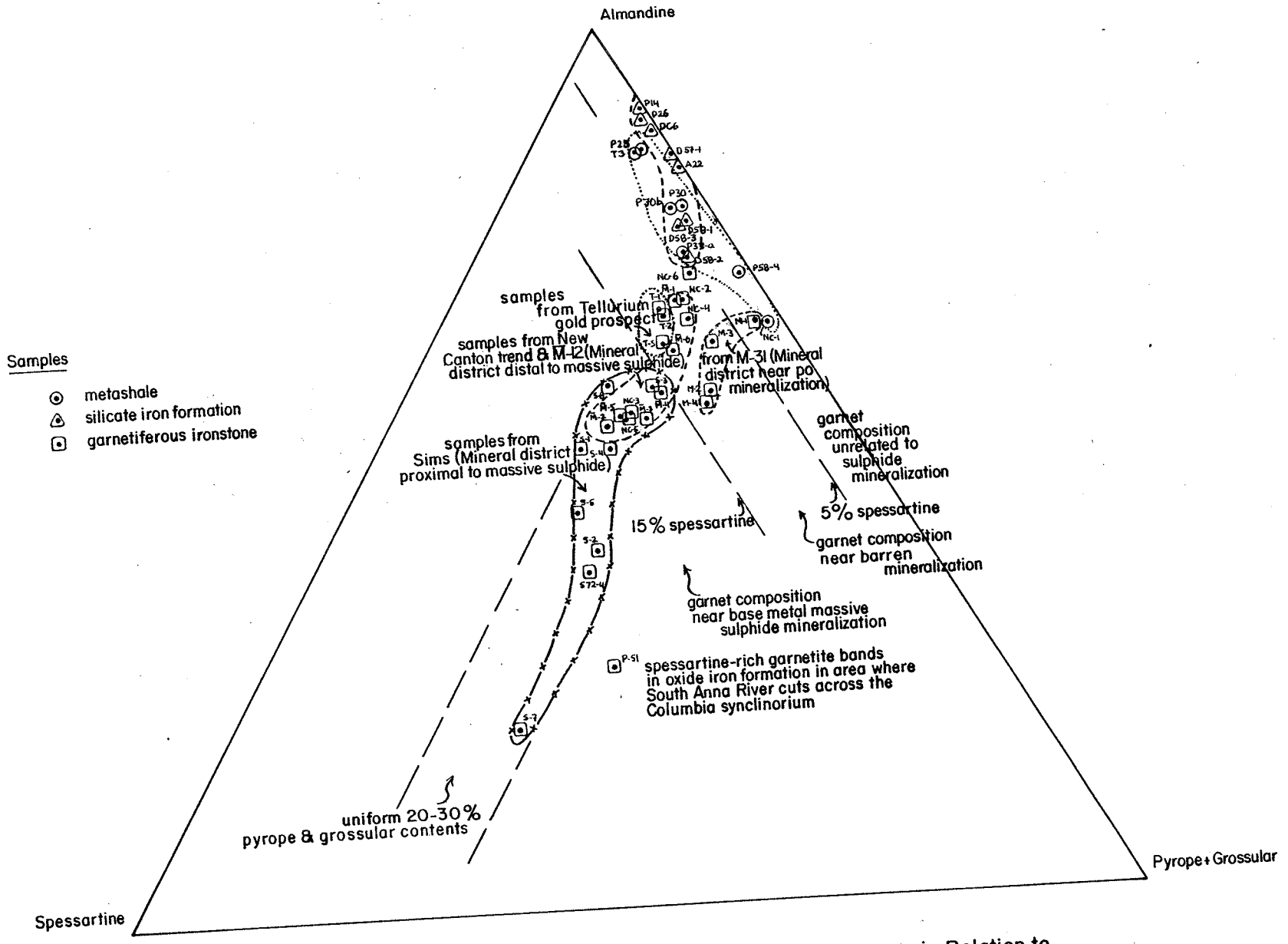

Figure 37: Almandine - Spessartine - Pyrope + Grossular Content of Garnets in Relation to Massive Sulphide Mineralization

Table 14: Core-to-Rim Elemental Zonation in Garnet
Values in Wt % (FeO = total iron)

CORE RIM

Garnet in Metashale

1. P30 (sparse isolated idioblasts)

	1	2	3	4	5	6	7
MnO	4.06	4.05	3.60	2.05	.65	.11	.15
FeO	31.23	30.69	31.57	34.48	36.62	37.13	37.53
MgO	1.21	1.26	1.11	1.61	2.21	3.28	3.40
CaO	5.48	5.40	5.01	3.64	2.05	.57	.63

2. P33A (sparse isolated idioblasts)

	5	6	7	8
MnO	4.94	4.09	2.21	.43
FeO	29.63	30.99	32.48	35.46
MgO	1.14	1.17	1.32	1.84
CaO	6.08	5.99	5.72	4.00

Garnets Near Base Metal Sulphide Mineralization

Sims Prospect

3. S2-77-62-206.5' (abundant small idioblasts with sulphides)

	4	5	6
MnO	19.50	14.12	8.60
FeO	13.55	17.58	22.03
MgO	.89	1.63	2.70
CaO	.30	.24	.09

4. S4-77-65-529' (abundant small idioblasts with sulphides)

	2	3	4
MnO	15.64	12.53	7.59
FeO	17.77	21.38	28.34
MgO	1.36	2.18	4.34
CaO	7.18	6.21	1.61

(Table 14 cont.)

CORE RIM

5. S5-77-65-711' (massive glomeric patches)

	11	12	13
MnO	17.34	15.82	12.64
FeO	15.98	17.89	22.76
MgO	.98	1.27	2.68
CaO	7.86	6.66	3.21

6. S6-M128 (abundant small isolated idioblasts with sulphides)

	1	2	3
MnO	9.47	8.39	7.82
FeO	25.19	27.57	28.09
MgO	3.11	3.82	3.52
CaO	3.84	1.09	1.16

7. S7-P152 (abundant small isolated idioblasts with sulphides)

	1	2	3
MnO	24.29	22.26	20.70
FeO	7.18	9.76	12.04
MgO	.17	.46	.68
CaO	10.86	9.45	8.00

New Canton Trend

8. NC2-A189-1 (sparse isolated subidioblasts in two-amphibole ironstone)

	1	2	3	4
MnO	5.88	3.37	2.17	1.67
FeO	28.32	30.86	30.23	31.85
MgO	2.12	2.99	3.42	4.54
CaO	4.72	3.61	3.97	2.17

9. NC6-A191-10 (sparse isolated idioblasts in two-amphibole ironstone)

	1	2	3
MnO	4.09	.80	.76
FeO	29.67	34.30	34.25
MgO	1.60	2.62	2.61
CaO	5.72	3.14	3.08

(Table 14 cont.)

CORE RIM

M12 Prospect

10. M2-78-66-331.5' (sparse isolated subidioblasts in amphibole-rich mafic ironstone)

	6	7	8
MnO	12.74	12.14	5.79
FeO	22.60	22.39	28.54
MgO	1.58	1.48	2.63
CaO	4.61	5.32	3.78

11. M3-77-66-417' (sparse isolated subidoblasts in biotite and chlorite bearing mafic ironstone)

	4	5	6
MnO	10.69	9.50	8.47
FeO	23.41	23.90	24.34
MgO	2.48	2.98	3.24
CaO	5.03	4.41	4.89

Tellurium Prospect

12. Ca2b-4 (sparse isolated subidioblasts in two-amphibole ironstone)

	6	7	8
MnO	7.99	5.22	2.88
FeO	26.58	28.36	31.91
MgO	1.86	2.41	3.22
CaO	5.16	5.50	3.20

13. Ca2b-2 (sparse subidioblasts in two-amphibole ironstone)

	1	2	3
MnO	5.55	4.93	3.40
FeO	31.09	30.44	32.10
MgO	2.82	2.94	3.47
CaO	2.32	3.38	3.10

contain only minor (<5%) spessartine. The combined pyrope and grossular content of garnets in these particular lithologies is considerably depleted over that in garnet occurring in the metavolcanics. The grossular content typically dominates over pyrope in the silicate iron formation; conversely, pyrope dominates over grossular in the normal metashale.

The garnet analyses from the underlying metavolcanic assemblage were carried out, as mentioned above, on samples selected to show variation in garnet composition with proximity to sulphide mineralization. These specimens fall into the following groups:

(1) Drill core and surface samples of mafic ironstones known to host base metal sulphides at the Sims prospect at the south end of the Mineral district;

(2) Drill core of mafic ironstones at the M-12 anomaly occurring in the distal hangingwall of the Arminius trend but with no immediately associated sulphide mineralization;

(3) Drill core from a mafic ironstone-metabasalt assemblage at the M-31 anomaly occurring east of the Columbia metashale in Caledonia quadrangle, known to host disseminated magnetite and pyrrhotite mineralization;

(4) Surface samples collected from the New Canton trend where amphibolitic and pyritic ironstones host low grade massive pyrrhotite sulphide mineralization;

(5) Surface samples collected of a brown garnetiferous schist at the base of the Columbia metashale and from the immediately underlying mafic ironstones at the Tellurium gold prospect where trace to minor disseminated pyrite accompanies gold-bearing quartz veins.

As illustrated on Figure 37 there is a tremendous variation in spessartine content demonstrated with proximity to base metal-bearing sulphide mineralization. The highest recorded value (sample S7) indicates a spessartine content of over 50%. Garnet compositions in samples from the Sims as well as from the M-12 and the New Canton trend taken in the vicinity of sulphides cluster in the 15-25% spessartine range. Samples from the New

Canton trend taken more distal to known mineralization, conversely, have much lower (about half) spessartine; these overlap in composition with M-12 garnet poorest in MnO.

It is interesting that all the garnets analysed from mafic ironstones show very little variation (20-30%) in their combined grossular and pyrope contents, indicating that the spessartine content here increases at the expense of almandine. The garnets from the metabasaltic amphibolites at M-31 show a slight increase in the combined grossular and pyrope content, running between 28-33% in these latter mineral components. The garnets from the basal shale garnetiferous interval at the Tellurium gold prospect plot with other metashale-basal shale silicate facies iron formation samples, while garnets in bordering ironstones that host the gold mineralization plot with the New Canton and M-12 garnets poorest in MnO.

All the analysed garnets except those in samples from the basal shale silicate facies iron formation and the higher grade metamorphic terrane east of the Columbia metashale (M-31) are characterized by decreasing core-to-rim Mn-Fe ratios. The manganese content of the basal shale silicate facies iron formation is generally below 1.5% MnO, and even those samples that are slightly more manganiferous (up to 5% spessartine in D58-2) from the Hatcher complex are homogeneous. Interestingly, an example of a spessartine-rich garnetite interbanded with magnetite iron formation from the area of the South Anna feldspathic quartzite on the east limb of the Columbia synclinorium in southern Pendleton quadrangle is also homogeneous, even though the garnet in this particular rock has over 35% spessartine. As is illustrated in Table 14, however, a core-to-rim zonation with decreasing MnO and increasing FeO is characteristic for the garnet occurring in the lower metamorphic conditions west of the Columbia metashale. Another feature associated with this

core-to-rim compositional pattern is the tendency for MgO to vary directly with FeO, increasing noticeably towards the rim. The CaO contents, alternately, may be seen to vary with MnO, attaining their highest values in core areas. The strongest core-to-rim zonation found among all the oxides occurs in samples with a high modal abundance of small isolated spessartine-rich idioblasts.

Numerous studies (Hollister 1966, Woodsworth 1977, Trzcienski 1977) interpet manganese-zoned almandine at medium metamorphic grades to be a result of Rayleigh fractional depletion. Two factors come into play in this model: (1) manganese is strongly partitioned into garnet in preference to other manganese-bearing phases in a rock, and (2) because garnet is highly refractory, as each infinitesmal garnet layer grows the immediately preceding layer is effectively removed from the system. The continuous depletion of the constituent elements in garnet from a homogeneous non-refractory matrix as the garnet grows thus changes the bulk composition of the remaining matrix. The zonation so derived persists to about the biotite-staurolite isograd; at higher metamorphic conditions either pre-existing zoning is homogenized by volume diffusion within the garnet or else the garnet ceases to be a refractory mineral due to the fact that, along with the staurolite, it becomes implicated in alumino-silicate producing reactions (Trzcienski 1977). This explains why, as Woodsworth notes, the garnet with staurolite typically shows slight core-to-rim zonation while garnet with cordierite generally has uniform composition.

Because manganese is strongly partitioned into garnet over other manganese-bearing phases, bulk composition is the main factor in determining how strongly zoned the garnet becomes. This influence of bulk chemistry on zoning profiles is well demonstrated on Figure 38 (from Trzcienski 1977).

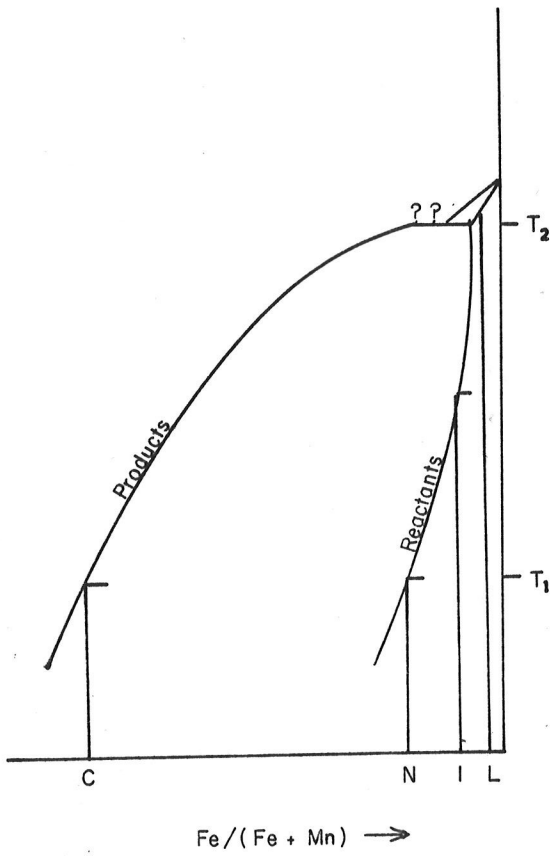

Figure 38: Schematic Representation of Product (Garnet)–Reactant (Chlorite) Equilibria T-X Space

(after Trzcienski 1977)

Based on the assumption that chlorite is the primary MnO-bearing reactant and garnet the major MnO-bearing product, the equilibria expressed between these two phases define a divariant loop leading to a general decrease in MnO in the chemically interacting matrix assemblage. It is evident from this that the initial Fe/Fe+Mn ratio of a rock essentially controls the zoning and can even dictate whether or not garnet will be present. As illustrated on Figure 38, for instance, a rock with an initial Fe/Fe+Mn ratio of N will be more highly zoned than one of ratio I, and rocks with very low Fe/Fe+Mn ratios such as L may not produce garnet at all. Atherton (1968) notes, further, that not only is the concentration of MnO in garnet dependent on the amount available but the FeO content is dependent specifically on the MnO content. An increase in available MnO, that is, automatically decreases a garnet's affinity for FeO, and probably for MgO as well, considering the direct relationship noted above between these particular oxide species.

There have been other correlations drawn between the maximum range in Mn zoning with the modal abundance of garnet in the analysed sample. Woodsworth (1977), for instance, found the strongest developed zoning in specimens with a high modal abundance of garnet. Presumably this occurs because the high effective volume of the growing garnet rapidly depletes the matrix reservoir of manganese. It would seem evident that such specimens must have been particularly favourable for widespread garnet nucleation and growth due to their original considerable MnO content. Atherton (1968) suggests that small size and large number per unit area in garnets imply widespread nucleation prior to the main growth stage. In this particular type of garnet crystallization the core-to-rim zonation would be expected to prove consistent in all grains. In more complex crystallization sequences, on the other hand, the garnet compositions will be the same at the periphery of the early

crystals as in the cores of later nucleii. Detailed microprobe analysis in the latter case should determine the specifics of the nucleation and growth history of the various garnet species present.

Stanton (1976) and Stanton and Williams (1978) counter the general assumption that garnet grows from a chemically interacting matrix reservoir with the hypothesis of closed system recrystallization on the scale of the individual grains. This argument is based on these authors' findings that the garnet chemistry in some small garnetite bands at Broken Hill, Australia, appears to reflect precisely the initial chemical composition of the domain now occupied by the garnet, thus implying that the constituents of the garnet were wholly derived in situ. In explanation of this phenomenon Stanton postulates the existence of an initial precursor with a near-perfect composition for nucleation and growth of garnet without the necessity of interaction among various mineral species in a matrix assemblage. A similar genetic model may be suggested by the more or less homogeneous garnets of the basal shale silicate iron formation of the present investigation and by the lone sample of spessartine-rich garnetite interbanded with oxide iron formation on the eastern limb of the Columbia synclinorium. In general, however, where garnet growth is controlled by preexisting primary bedding features in this study area, the garnet bands are typically slightly wider than the initial chlorite ± biotite assemblages; this would indicate that at least minor material from the bordering quartz-rich domains is also consumed by the growing garnet.

From the point of view of metallogeny, the most significant feature demonstrated by the evident regional variation in garnet chemistry is the striking enrichment in spessartine content in the vicinity of sulphide mineralization. The marked increase in manganese content is attributed by

this writer to the existence of primary manganese haloes peripheral to the sulphides. The pioneering work of Krauskopf (1957) first brought attention to the geochemical bases for the gross separation of iron and manganese under naturally occurring Eh-pH conditions due to the fact that iron compounds are uniformly less soluable than manganese compounds. More recently, however, it has become recognized that manganese haloes are formed peripheral to many massive sulphide deposits. In a study of the Heath Steele mine in the Bathurst camp of New Brunswick, Whitehead (1973) formulated a specific geochemical model (Figure 39) for the distribution of Mn/Fe ratios in areas of massive sulphide deposition; his schema has been validated by numerous studies since that time.

Fryer and Hutchinson (1976) demonstrate that iron and manganese are effectively separated at sites of Cyprus-type massive sulphides. Russell (1974) shows that a manganese aureole exists over a seven kilometer radius beyond the Tynagh deposit in Ireland which comprises over 100 ppm manganese at the periphery of the aureole increasing by a factor of 100 above the sulphide mineralization. Gwosdz and Krebs (1977) demonstrate a manganese dispersion halo of similar dimension to that bordering the Tynagh mine in the pelagic limestones along strike from the strataform sulphide-barite body at Meggan, Germany. Around the immediate ore body the ore-equivalent limestone is distinctly anomalous with above 2000 ppm manganese, while a halo of 1000-2000 ppm is detectable for about two kilometers southwest and five kilometers northeast of the deposit. Gwosdz and Krebs note further that the shales underlying both the Meggin and Rammelsburg deposits are also manganese-rich.

More applicable to the present investigation is the fact that the combined studies by Stanton (1976) and Stanton and Williams (1978) of the Broken Hill deposit in New South Wales, Australia; by Addy and Ypma (1978) of

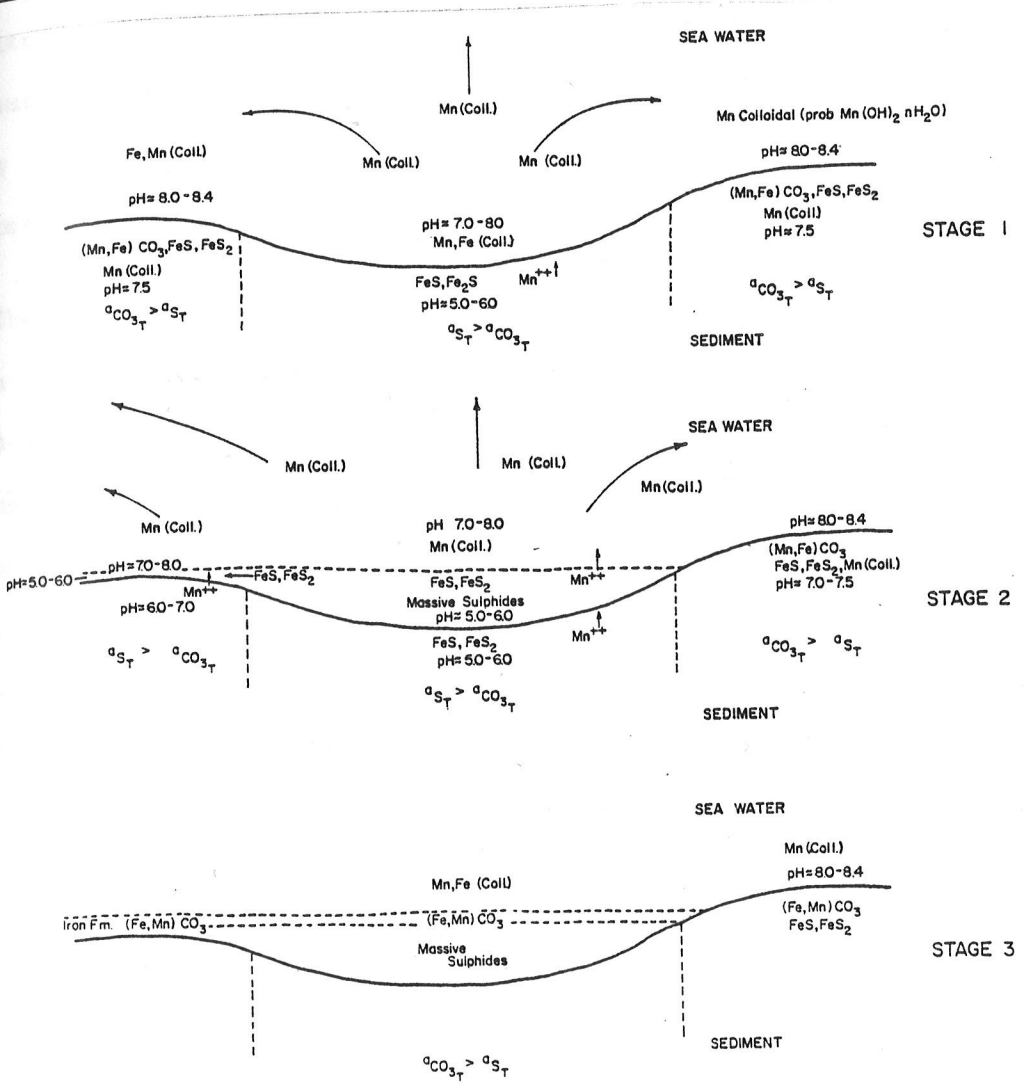

Figure 39: Schematic Representation of the Conceptual Model for the Distribution of Mn:Fe Ratios in Sedimentary Rocks at Heath Steele Mines Massive Sulphide Deposits

(after Whitehead 1973)

the Ducktown deposit in Tennesee, U.S.A.; by Stumpfl (1979) of the sulphide deposits in Namaqualand, South Africa; and by Valliant and Barnett (1982) of the Bousquet deposit in Quebec collectively illustrate that primary manganese haloes survive medium to high grade regional metamorphic overprints. Within such terranes the manganese is invariably concentrated in garnet.

The significance of these haloes becomes manifest if they are viewed within the context of presentday hydrothermal systems. Bischoff and Manhein (1969) note that the base metal-laden muds of the Red Sea deeps are rimmed by manganese haloes extending over a radius of ten kilometers from active vent systems. The manganese concentrations on the Mid-Atlantic Ridge (Scott et al 1974), on the Galapagos Ridge (Edmond 1979, and in the lakes of the East African Rift Valley (Degens & Stoffers 1977) further demonstrate that manganese, together with sulphide mineralization, originates from hydrothermal emanations. The discovery of the manganese enrichments accompanying the sulphide mineralization of the present study area strongly supports the metallogenic interpretation put forth above; i.e., that these rocks originated under similar sea floor hydrothermal conditions.

4.2.3 Regional Variation in Amphibole Chemistry

This investigation of the regional variation in amphibole chemistry entails microprobe analysis on 30 separate specimens. Most of the samples selected contained coexisting amphibole pairs and on the average approximately five spot analyses were completed on each species. This data is listed in table form in Appendix D. The average composition computed for individual amphibole species occurring in a given sample is utilized in the following discussion of the essential compositional features demonstrated by the

amphiboles.

In the final report by the international subcommittee on the amphibole group, Leake (1978) proposed that amphibole nomenclature should be based primarily on crystal chemistry, with further subdivision between orthorhombic and monoclinic members. All the amphibole species analysed in the present study were accordingly plotted on the appropriate discriminant diagrams as proposed by Leake. As illustrated in Figure 40, a and b, the various iron-magnesium-manganese amphibole species include both orthorhombic anthophyllite and gedrite and monoclinic cummingtonite and grunerite. As illustrated in Figure 41, the various calcic amphibole species include actinolite, actinolitic hornblende, magnesio-hornblende, tschermakitic hornblende, and both alumino and ferro-tschermakite. It should be noted that the duplicate sample numbers appearing on the various discriminant plots are of coexisting amphibole species in given samples.

Figure 42 reveals that coexisting cummingtonite-tschermakitic hornblende pairs from the two-amphibole ironstones each form relatively restricted groupings. The large miscibility gap between these calcium-poor and calcium-rich monoclinic species is well demonstrated here; the near parallelism of the tie lines between coexisting pairs indicates that these minerals are more or less in equilibrium. The slight divergence, evident particularly in the total alkali versus Fe/Fe+Mg plot, is probably due to bulk compositional variations, as there would seem to be a subtle steepening in slope with increase in iron in the amphibole pairs. In the more magnesian rocks there was apparently a greater degree of partitioning of magnesian into cummingtonite and of the iron into the tschermakitic hornblende.

Occasionally, as shown on Figure 42a, both the low-Ca and high-Ca

Figure 40: Classification of Iron Magnesium - Manganese Amphiboles
(after Leake 1978)

a) Orthorhombic

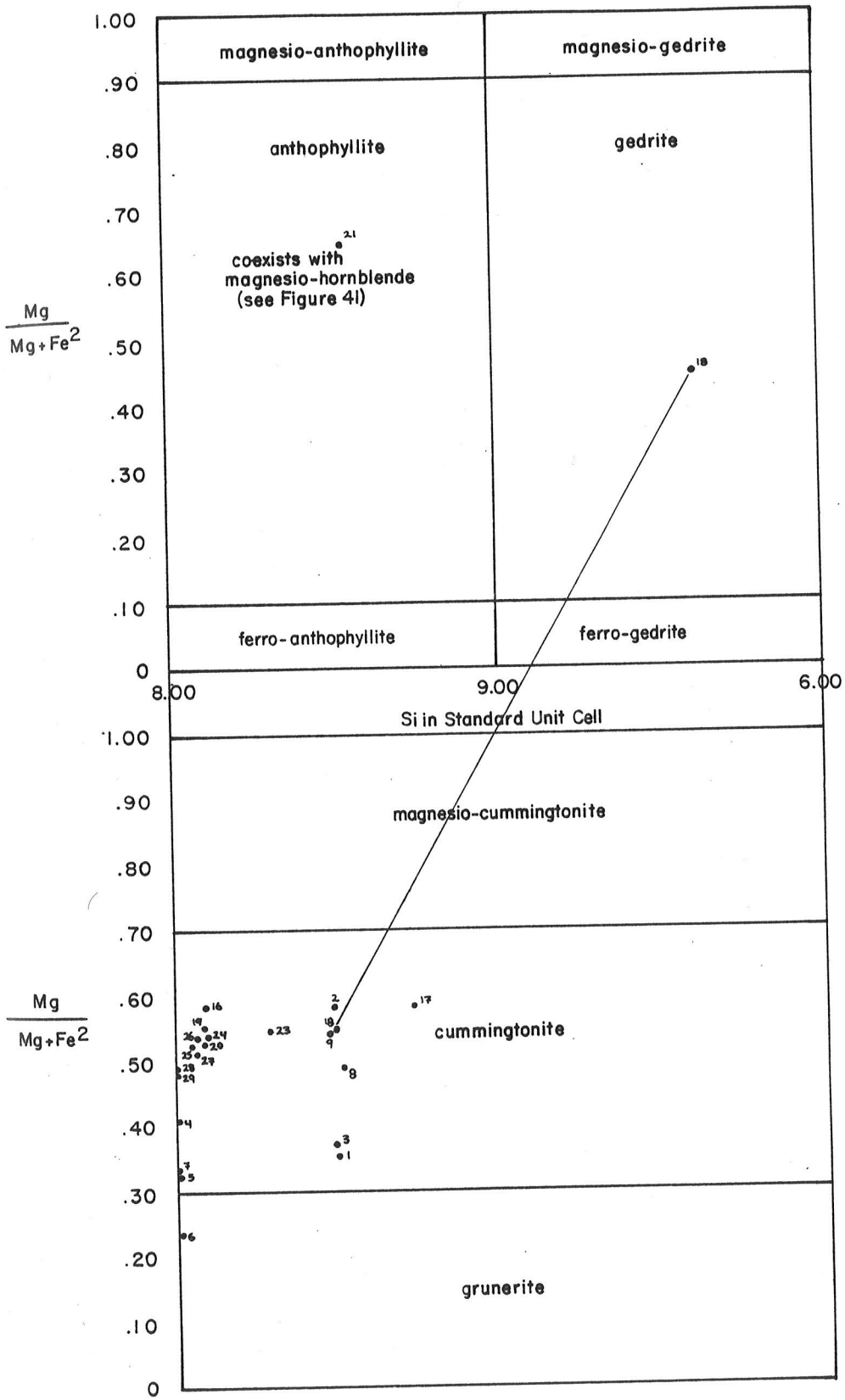

b) Monoclinic

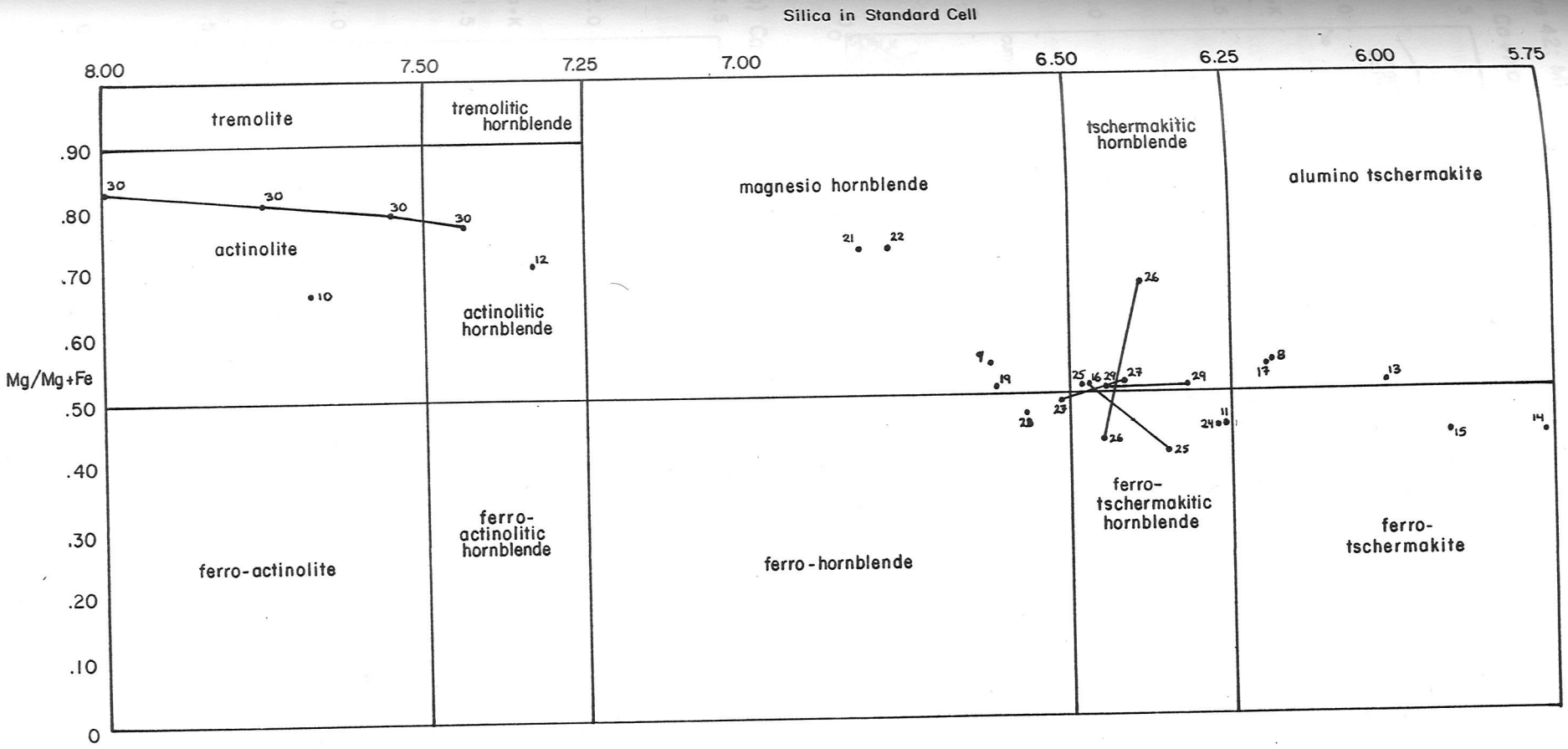

Figure 41: Classification of Calcic Amphiboles (after Leake 1978)

Figure 42: Miscibility Gap Between Coexisting Amphiboles

a) Ca+Na+K vs Al^{vi} Binary

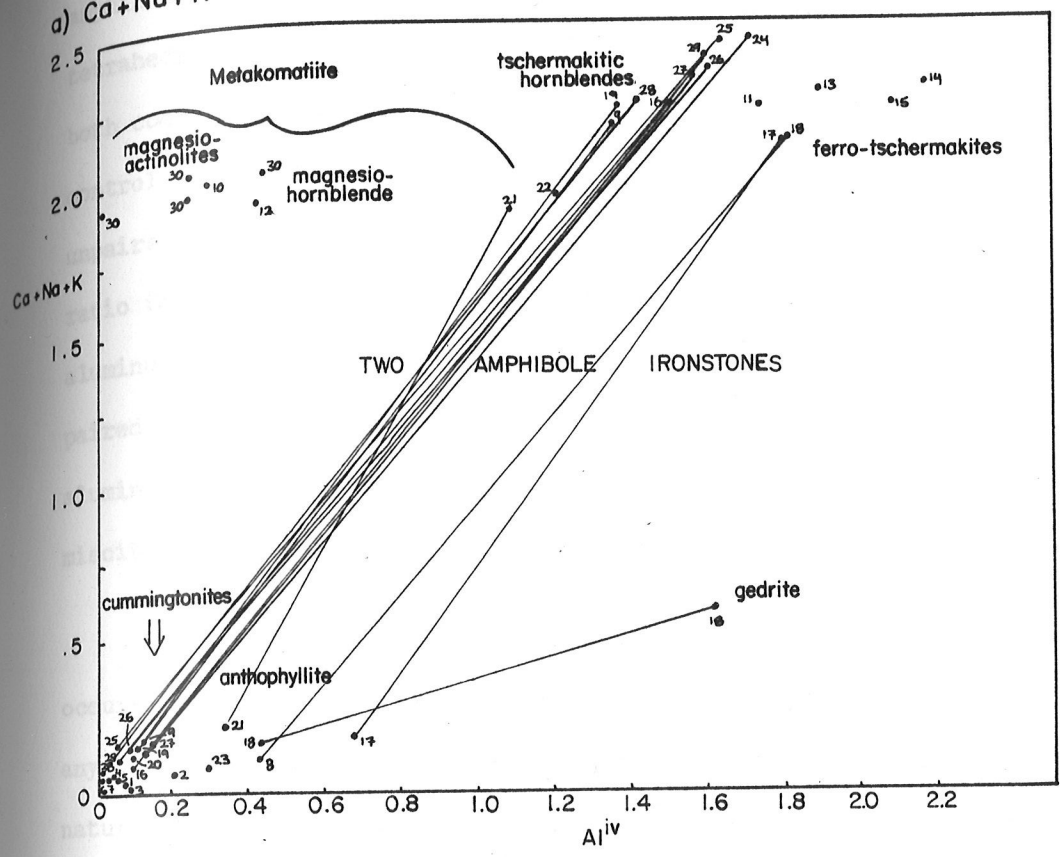

b) Ca+Na+K vs Fe/(Fe+Mg) Binary

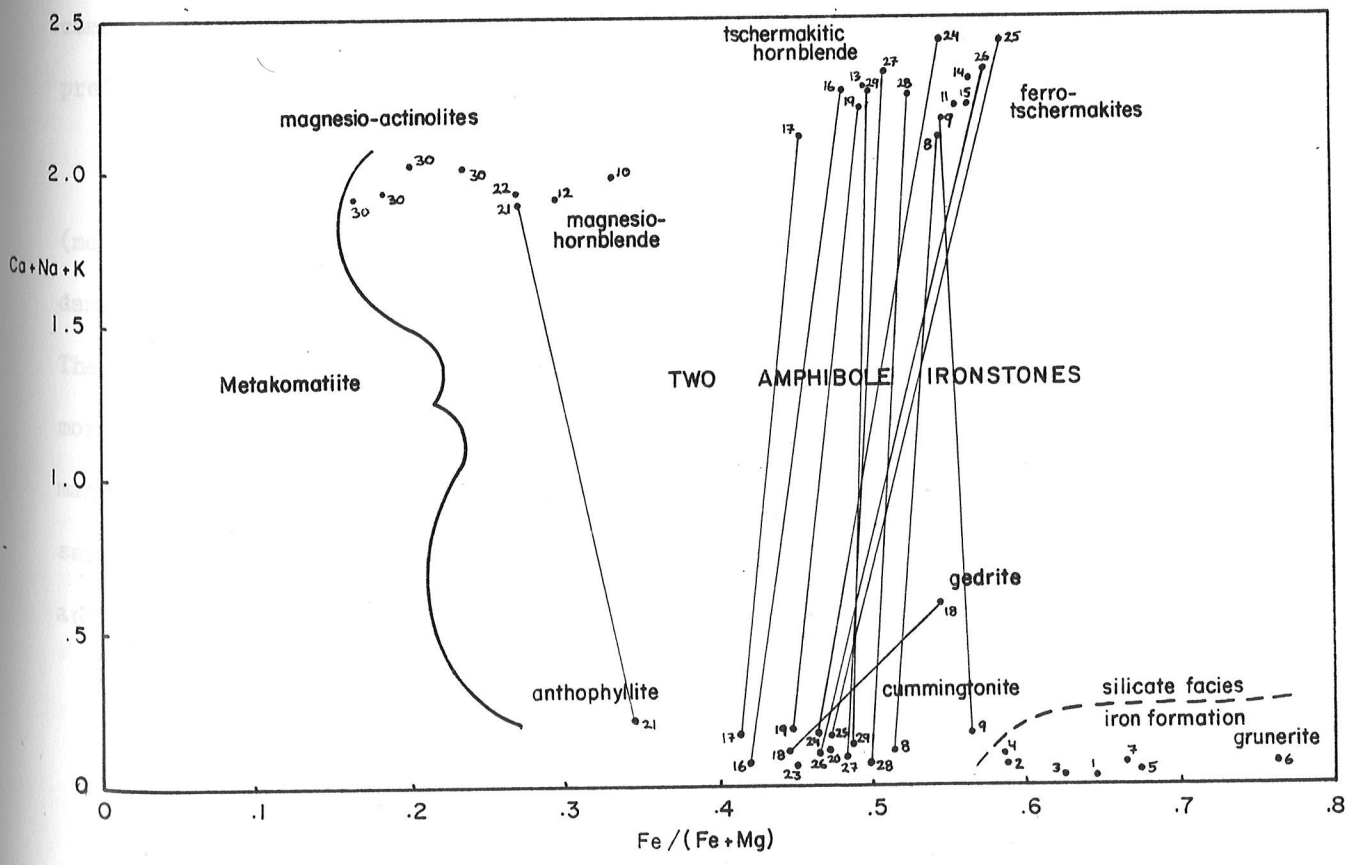

amphiboles in the two-amphibole ironstone show aluminum enrichment in the tetrahedral site. It is interesting that this enrichment is demonstrated by both coexisting amphibole pairs, which again reflects on a bulk chemical control. Rather commonly the most aluminous ferro-tschermakite occurs unpaired with any Ca-poor species, suggesting that the host rock Ca:Fe:Al ratio favoured crystallization of a single Ca-amphibole abnormally rich in aluminum and iron. More rarely, moderately aluminous cummingtonite may be paired with degrite. The shorter tie-line between coexisting alumino-cummingtonite and gedrite for sample 18 indicates a more restrictive miscibility gap between these particular amphibole species.

Figure 42b demonstrates that iron-rich cummingtonite-grunerite amphiboles occurring in the basal shale silicate facies iron formation are unpaired with any Ca-rich amphibole species; this again reflects on the generally Ca-poor nature of the host rock. Interestingly, as noted previously, the coexisting garnets in these particular samples are slightly enriched in grossular component, indicating that the CaO component in this instance was preferentially partitioned into garnet rather than amphibole.

Not enough microprobe work was carried out on magnesian amphibolites (metakomatiite) to allow for generalizations about the chemical features demonstrated by the amphibole species present in this particular rock type. The few analyses completed indicate that the calcic species may comprise a more or less continuous spectrum from magnesio-actinolite through magnesio-hornblende with increasing aluminum and iron contents. The only sample in which coexisting iron-magnesium amphibole was analysed showed anthophyllite coexisting with magnesio-hornblende.

One further chemical feature revealed by the microprobe investigation of

coexisting amphiboles is a tendency for MnO to be strongly partitioned into cummingtonite over the tschermakitic hornblende (see Table 15). Although the manganese content of the amphiboles is generally low as a whole (in the order of .5% MnO), some enrichments in this component may be observed in the former species without any corresponding changes in the latter. Only one exception to this general pattern was noted. A sample of banded spessartine-rich garnetite affiliated with oxide iron formation on the eastern limb of the Columbia synclinorium proved to host a calcic amphibole enriched in manganese. The trace actinolite coexisting with the spessartine garnet in this particular sample has 1.57% Mn.

Table 15:
Preferential Partitioning of MnO into Cummingtonite over Ca-Amphibole
(MnO values in wt %)

	Tschermatkitic Hornblende	Cummingtonite
9 (P53)	.14	1.17
16 (A191-8)	.35	1.29
19 (A190-3)	.47	1.65
24 (A189-4)	.40	1.11
27 (Ca2b3)	.16	.80
28 (Calf)	.29	.97

Note: 10 (P51) actinolite shows 1.57% MnO coexisting with spessartine-rich garnet; manganese may help stabilize actinolite at higher metamorphic conditions or perhaps this rock formed above the cummingtonite-actinolite solvus.

While garnet growth during metamorphism is exemplary for refractory minerals, the amphiboles are equally exemplary for equilibrium crystallization. All the amphibole species are homogeneous and non-zoned. Even where coexisting Ca-poor and Ca-rich species occupy parts of the same grain there is no ostensible zonation from one species to another; the contacts are optically and chemically sharp. From a metallogenic standpoint,

of course, the important question to be addressed is why divergent species should have arisen in tandem like this in the first place. Although the stability relationships among coexisting amphibole species are still not completely unravelled, the work which has been done throws considerable light on the determining factors for the growth of more than one type of amphibole in a given rock.

As we have already implied, two-amphibole assemblages depend essentially on the presence of miscibility gaps between coexisting species. Of particular relevance to the present case of coexisting Ca-poor and Ca-rich monoclinic amphiboles is the work of Cameron (1975) on the pseudo-binary between actinolite and cummingtonite-anthophyllite. As illustrated in Figure 43, the phase relationship along this particular join between the calcic amphiboles and the iron-magnesium-manganese amphiboles is dominated by an asymetric solvus. The near-vertical cummingtonite limb occurs at about 10 mole % actinolite; the temperature-dependent actinolite limb shows that the Ca content of the actinolite field decreases regularly from about 96 mole % actinolite at 500°C to about 85 mole % actinolite at 600°C. Above this temperature the actinolite amphibole begins reacting to Cum+Cpx+Qtz -- the ultimate breakdown assemblage of the actinolite.

In this particular study, Cameron further notes that only anthophyllite can be synthesized in Ca-free runs. Apparently the presence of Ca facilitates nucleation of cummingtonite. The amount of cummingtonite relative to anthophyllite appears to increase regularly with increasing Ca content irrespective of temperature, and at a bulk composition of 10 mole % actinolite (1.27 wt % CaO) cummingtonite alone is present. It therefore seems likely that any CaO present in a rock would have the effect of stabilizing cummingtonite over anthophyllite. This could well explain, in at least

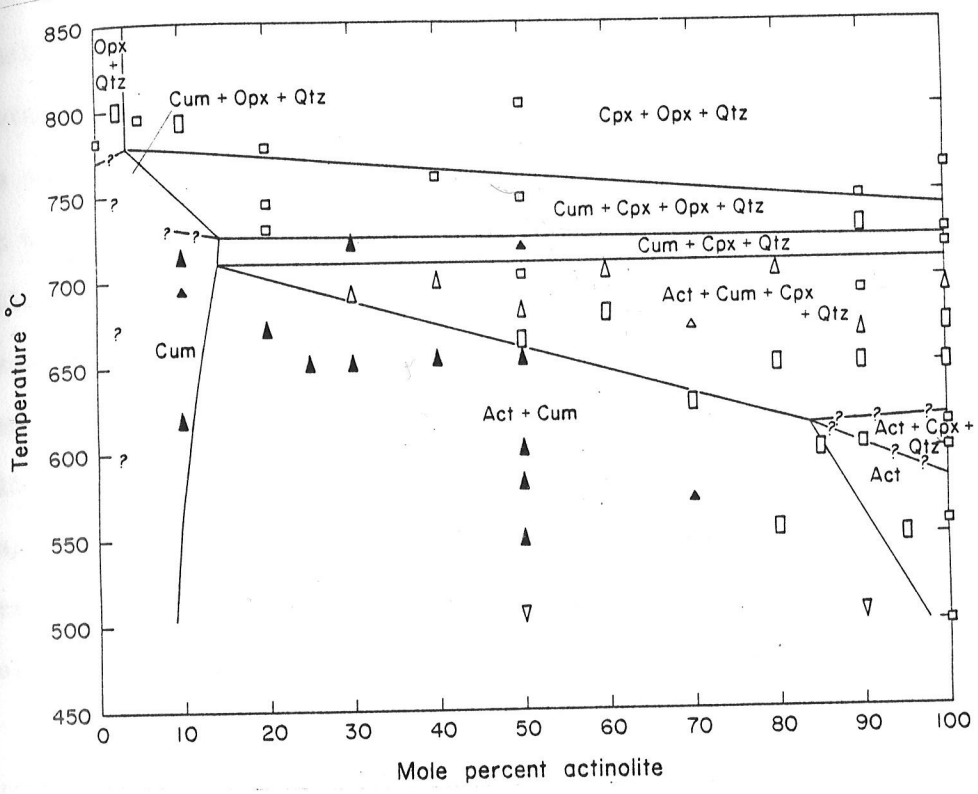

Figure 43: Phase Diagram for the Pseudobinary Join, $Mg_{3.5}Fe_{3.5}Si_8O_{22}(OH)_2$ - $Ca_2Mg_{2.5}Fe_{2.5}Si_8O_{22}(OH)_2$ + excess H_2O, at P_{fluid} = 2000 bars and at oxygen fugacities defined by the FMQ buffer

(after Cameron 1975)

general terms, the observed coexistence of cummingtonite with calcic amphiboles.

In the present case, of course, we are not dealing specifically with actinolite-cummingtonite pairs but rather with cummingtonite-tschermakitic hornblende. No direct experimental work on the stability relationships of these particular species is known to the writer. Fortunately, studies do exist that have at least indirect bearing here. An understanding of the stability relationships in the anthophyllite-gedrite system, for instance, may be expected to cast important light on the nature of stability relations between the roughly analogous pair of Ca-rich and Ca-poor monoclinic amphiboles yielded by the present investigation. In this respect, one may perhaps consider the findings of Robinson et al (1971) and Spear (1980) as offering a useful provisional model. These researchers demonstrate that the compositional discontinuity between anthophyllite and gedrite can be ascribed to gaps in the edenite (NaAl Si) and tschermakite ($Al^{iv}Al^{vi} \gtrless MgSi$) substitutions. Through such substitutions gedrite is enriched in Al^{iv}, Al^{vi}, Fe^{2t}, Ti, Ca+Mn, and anthophyllite enriched in Si+Mg. If similar substitutions occurred as well in the case of the monoclinic amphibole pairs we are considering, it would account for the fact that the cummingtonite is typically more highly enriched in Si and Mg and the calcic amphibole in Al, Fe, Na, and Ca. The orthoamphibole model can obviously not be directly applied for all components. In the case of the clinoamphiboles Mn is, as previously noted, correlative with Mg in being partitioned into cummingtonite, while in the orthoamphiboles this particular component is apparently correlative with iron, being partitioned preferentially into gedrite over anthophyllite. Notwithstanding such departures from the documented pattern, the main substitutions are still considered by this writer to offer a reasonable

explanation for the rise of coexistent cummingtonite-tschermakite hornblende compositions in the study area.

It seems evident from the experimental work cited here that under certain PTX conditions broad miscibility gaps can be expected in both the anthophyllite-gedrite series and in the actinolite-cummingtonite series. Klein (1969) shows that a similar compositional gap probably exists in the actinolite-hornblende system at relatively low temperatures. Under conditions where both calcic and iron-magnesium-manganese amphiboles coexist, Robinson et al (1971) note that anthophyllite could coexist with hornblende but actinolite would not occur with gedrite. Such miscibility gaps may thus be utilized to explain the coexistence of the magnesio-hornblende-anthophyllite assemblages in the magnesian amphibolites (metakomatiites) of the present study area as well.

The study of tremolite-hornblende relationships by Misch and Rice (1975) is also germane here because of the common coexistence of highly magnesian actinolite and magnesio-hornblende in the metakomatiites. As illustrated in Figure 44, these workers found that tremolite and aluminous hornblendes form a continuous solid solution in the sillimanite grade of regional metamorphism. At a slightly lower grade of amphibolite facies a large compositional gap exists between tremolite and moderately aluminous hornblendes. The apparent complete transition from magnesio-actinolites through actinolitic hornblende to magnesio-hornblende in metakomatiites along the eastern side of the belt supports the existence of such a continuous solid solution series at the higher metamorphic conditions.

The apparent enrichment in aluminum in the hornblende of the present study can also be attributed to the relatively high ambient metamorphic

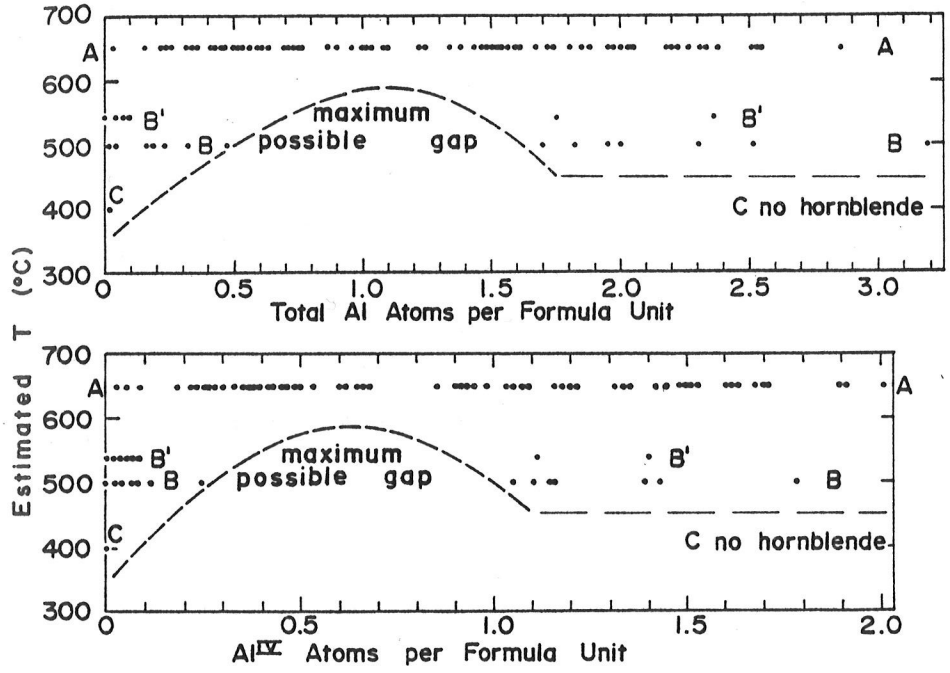

Figure 44: Tremolite–Hornblende Miscibility in Progressive Skajit Metamorphic Suite (after Misch & Rice 1975)

conditions along the eastern side of the belt. Aluminum enrichment within the hornblende structure with increasing metamorphic grade has been noted by Misch and Rice (1974), Raase (1974), and Fleet and Barnett (1978). Figure 45 demonstrates that the tschermakitic amphiboles coexisting with cummingtonite in the two-amphibole ironstones do show compositions that overlap the 5 kbar boundary of Raase (1974). Significantly, not all the amphiboles show such high aluminum enrichment, though. Enrichments in this component, as in others, depends to a large extent on the available aluminum in the bulk rock. The amphiboles occurring in the metakomatiites, for instance, generally show a far lower aluminum content even though these were subject to the same metamorphic conditions. The extent to which amphibole compositions reflect ambient conditions is as yet incompletely understood due to the basic overriding compositional control on amphibole chemistry by the bulk composition of the specific host.

Although the origin of the various amphibole species can be adequately accounted for by the interplay of bulk composition, ambient metamorphic conditions, and crystal chemical effects within and between the differing amphibole solid solution series, from a metallogenic standpoint the most significant and problematic aspect of the amphibole picture for this study area is the fact that the basal shale silicate facies iron formation - two-amphibole ironstone - metakomatiite lithological association we have been dealing with here basically comprises the host rock assemblage for much of the lode gold mineralization along the belt. The phenomenon is not likely coincidental. Judging from studies such as those conducted by Krank (1961), Leake (1972), Immega and Klein (1976), Bostock (1977), and Gole and Klein (1981), the natural occurrence of members of the cummingtonite-grunerite series and perhaps even the coexistence of cummingtonite and tschermakite

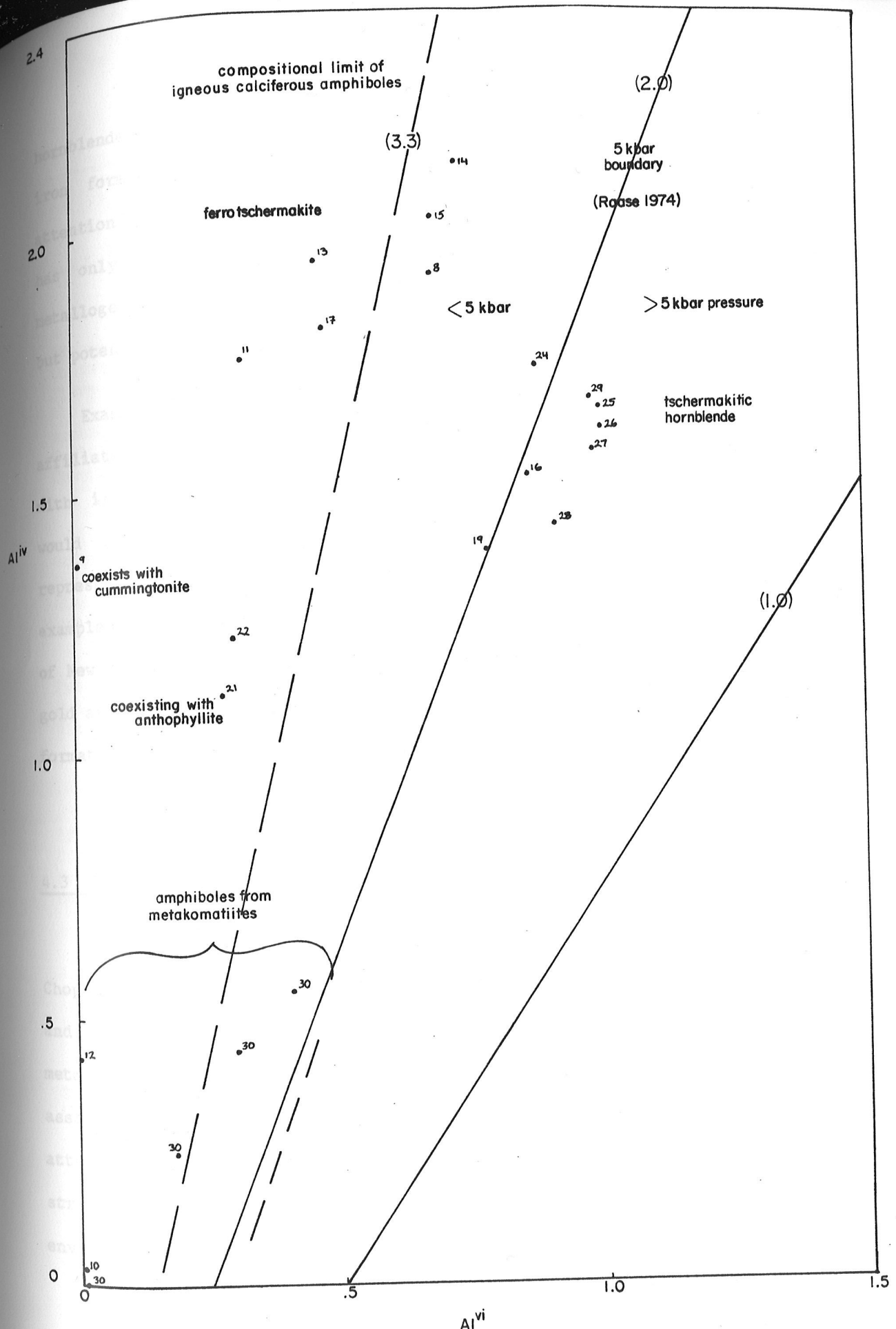

Figure 45: Al^{iv} vs Al^{vi} Diagram for Calcic Amphibole Field Boundaries (from Fleet & Barnett 1978)

hornblende might be considered as diagnostic of metamorphosed silicate facies iron formation. Although such lithologies have historically caught the attention of metamorphic petrologists because of their peculiar mineralogy, it has only recently come to be recognized that they have considerable metallogenic significance, particularly with respect to gold mineralization but potentially for basemetal mineralization as well.

Examples of gold and/or basemetal-bearing sulphide mineralization affiliated with iron formation environments similar to the one we are dealing with in the current study are listed in Table 16. The pattern revealed here would seem to indicate that this specific metallogenic association is best represented in earlier Precambrian times. However, numerous Proterozoic examples do occur, and if the present area and the Bathurst-Newcastle district of New Brunswick can be considered as grossly analogous, the occurrence of gold and/or massive sulphide mineralization in settings of multi-facies iron formation may be held to have recurred throughout much of geological time.

4.3 Regional Metallogenic Synthesis

The foregoing establishes that the central Virginian segment of the Chopawamsic metavolcanic belt is a metallotect for pyritic massive sulphide and lode gold mineralization. It now only remains to determine which specific metallogenic processes were instrumental in bringing about such a gold-pyrite association. As both an aid to and a by-product of this task we will also attempt to clarify how such processes could relate to the regional structural-stratigraphic framework on the one hand and the petrogenetic environment on the other.

Table 16: Examples of Multi-Facies Iron Formation Hosting Gold and/or Sulphide Mineralization

Age & Occurrence	Deposit Setting	Reference
	NORTH AMERICAN DEPOSITS	
Archaean, Contwoyto Lake, Slave Province	gold with sulphides in almandine cummingtonite gneiss within a greywacke-argillite succession	Bostock 1977-80 Boyl 1979
Archaean, Cullaton Lake Churchill Province	gold with sulphide facies interlayered with oxide-carbonate-silicate facies iron formation within a greywacke-argillite succession	Page 1981
Ordovician, Bathurst-Newcastle, district of New Brunswick	polymetallic massive sulphide lenses in sulphide-oxide-silicate facies iron formation in volcaniclastics flanking a felsic volcanic centre	Jambor 1979
Proterozoic, Homestake Mine, Black Hills	gold in chloritized and sulphidized cummingtonitic schists within wacke-type sediments	Sawkins & Rye 1974 Boyl 1979
	SOUTH AMERICAN DEPOSITS	
Archaean, Quadrilatero Ferifero, Minas Gerais, Brazil	gold in dolomitic subfacies of carbonate iron formation horizons affiliated with oxide-silicate and sulphide iron formation in a greywacke argillite sequence	Tolbert 1964 Boyl 1979
	AFRICAN DEPOSITS	
Archaean, Vubachikwe, Zimbabwe	gold in multifacies iron formation interlayered with mafic-felsic tuffs	Fripp 1976
Archaean, Lake Victoria Goldfield, Tanzania	gold with sulphide facies of banded ironstones interlayered with ferruginous quartzites and mafic-felsic volcanics	Pelletier 1964 Kondakov & Perunov 1973
Archaean, Moto area, Zaire	gold in multi-facies iron formation in graphitic sediments	Woodtli 1961 Boyl 1979
mid-Proterozoic, Gamsberg, S. Africa	zincian massive sulphide in the multi-facies Gams iron formation	Rozendaal 1978 Stumpfl 1979

(Table 16 cont.)

Age & Occurrence	Deposit Setting	Reference
	AUSTRALIAN DEPOSITS	
Archaean, Yilgarn Goldfield, Western Australia	gold in dolomitic subfacies (Copperhead) and in oxide facies iron formation (Nevaria) interlayered with laminated greenstone and argillite	Williamson & Barr 1970
lower Proterozoic, Tennant Creek, Northern Territory	gold in iron-oxide silicate replacement bodies in hematite shale	Boyl 1979
lower Proterozoic, Golden Dyke Dome, Northern Territory	base metal sulphide, precious metal, and tin mineralization associated with multi-facies iron formation interlayered with mudstones, greywacke, tourmalinite	Nicholson 1980
	INDIAN DEPOSITS	
Archaean, Kolar Goldfield, Southern India	gold with disseminated sulphides in cummintonitic hornblende amphibolite interlayered with cherty carbonate facies iron formation and graphitic argillite	Sawkins & Rye 1974
Archaean, Ramagiri Goldfield, Southern India	gold hosted in carbonate facies iron formation and in phyllites intercalated with greenstone and oxide iron formation	Sawkins & Rye 1974
mid-Proterozoic, Saladipura, Northern India	ferruginous massive sulphide bound between overlying phyllite and underlying silicate-carbonate facies ironstone interlayered with metabasalt	Sarker, Bhattacharyya, & Mukherjee 1980
	GREENLAND DEPOSITS	
(pre-3760 m.y.) Isua belt, West Greenland	cupreous massive sulphide hosted in silicate-carbonate-oxide facies iron formation interlayered with quartzite and amphibolite and minor lense-shaped ultramafic bodies	Appel 1979

It is difficult to generalize about the specific structural-stratigraphic associations demonstrated by either the pyritic massive sulphide or the gold mineralization, since at times these deposits occur within the same geological setting while at others each type may be found in quite different environments. Notwithstanding, it is possible to say that the known sulphide and gold deposits seem broadly to fall into two distinct (though not mutually exclusive) groups with the sulphide mineralization generally hosted within the metavolcanics and the gold mineralization favouring the contact between the metavolcanics and the younger metashales. Such a division as this not only reflects on the differential metallogenic processes operative in this belt but also brings into focus the interesting metallogenic problem posed by exceptions to the rule. In general the deposits in the metavolcanics of the Mineral and Andersonville districts would seem to be normative, while the sulphides along the New Canton and Long Island trends should be considered as part of the same metallogenic picture as the gold.

Both the intravolcanic and basal shale-sited types of mineralization are thought to be derived through syndepositional hydrothermal activity. It is of prime importance, however, that one critically consider both the synchronous and diachronous variation evident in the syndepositional hydrothermal metasomatic process. The Mineral district sulphide deposits, for instance, cluster in an area of bimodal volcanism. The largest buildups of rhyolite identified to date occur at the centrally located Cofer deposit and at the Julia deposit at the south end of the main Arminius trend of massive sulphides. Mineralized footwall breccias at the Julia attest that this particular rhyolite centre was also a focus for hydrothermal fluid discharge. More laterally, though, the mineralization along the Arminius trend is closely allied with a marker chloritite unit which would seem to have originated as a

metalliferous mud. This lithology thus not only shows compositional similarities to footwall chlorite alteration zones commonly occupying volcanogenic massive sulphide deposits (Hutchinson 1973), but also demonstrates the stratigraphic nature of a silicate facies iron formation.

At the north end of the Arminius trend, massive sulphide mineralization occurs as well in overlying ironstones, and there is a suggestion in the longitudinal section (Figure 28) that the lenses formed in such cases may relate to local thickening in the active zone for mineralization. One might consider such a feature as stemming from the development of an original hydrothermal mound over the main silicate-sulphide facies "iron formation." The repetitive amphibolite - sulphidic amphibolitic quartizite - quartzite cycles observed within the mound and the occurrence of the biotite-carbonate facies of ironstone overlying the mound give evidence of striking hydrothermal fluctuations and evolving fluid chemistry over the period during which hydrothermal discharge was active. That this particular mound is covered by atypically coarse epiclastic material suggests that it probably grew in a topographic low.

In contradistinction to this type of hydrothermal activity accompanying an area given to bimodal volcanism, the Andersonville district sulphides appear to be affiliated with a persistent iron formation capping little reworked metabasalts. As no evidence of focused hydrothermal discharge has as yet been discovered, it would seem most plausible to conclude that this extensive iron formation developed essentially through unfocused hydrothermal emanations which precipitated out regionally as ferruginous quartzite-oxide facies iron formation and locally as silicate-sulphide facies iron formation. Just why the oxide facies gave way locally to silicate-sulphide facies remains enigmatic. One might, however, speculate that the geothermal condition of the

sea floor was perhaps not completely uniform here. If the productive iron formation were in this case laid down rather passively as a crust on top of the mafic volcanics, hotter spots could have been responsible for stimulating the localized preferential development of sulphidic strata. Adding to the plausibility of such an explanation, the distribution of the mineralization seems to be more or less random within the silicate facies of this crust, with common transition from minor through heavy disseminations to massive sulphide in evidence.

When the hydrothermal settings of the Mineral and Andersonville districts are viewed comparatively, it seems self-evident that the hydrothermal activity accompanying the main stage of volcanism differed from one area to another. Nevertheless, these diverse fluid discharge regimes produced mineral deposits demonstrating considerable similarity; i.e., massive sulphide mineralization intimately associated with silicate facies iron formation. There are differences, of course -- the fact that the sulphides occurring proximal to small rhyolite buildups in the Mineral district are polymetallic-pyritic and the Andersonville ones low grade basemetal-bearing pyrite-pyrrhotite types, for instance -- but these are relatively incidental and readily accounted for by the variance in original setting. The hydrothermal activity concomitant with the bimodal volcanism in the Mineral district quite naturally resulted in both a more varied deposit setting and a more complex metal signature. Such features notwithstanding, however, it must be emphasized that both these districts were characterized during the main stages of volcanism by the kind of hydrothermal system which produces massive sulphide-type mineralization.

In upper Chopawamsic times there was a general change in the nature of the hydrothermal activity in this area such that it no longer produced restricted sulphide-silicate iron formation but now facilitated the

development of the regionally extensive two-amphibole ironstone - ferruginous quartzite - oxide iron formation assemblage. Facies relationships within the the upper Chopawamsic hydrothermal deposits are not well understood but it seems that here again there is considerable lateral variation, ranging from the regional two-amphibole ironstone-oxide iron formation to more localized multi-facies oxide-sulphide-carbonate-silicate iron formation deposits. Much of this lateral variation is attributed by this writer to the high level or surface injection-ejection of komatiite into the iron formation environment at various sites along the belt. These particular sites subsequently became loci for the development of the multi-facies iron formation which -- most significantly for the present discussion -- would seem to be the favoured setting for the gold mineralization. Just such a coincidence of metakomatiite and multi-facies iron formation-ironstone characterizes the Fisher lode, the Tellurium trend, and the Morrow mine; notably, the latter two were historically the greatest gold producers in the study area. Ultramafic material is also known to occur along strike from both the multi-facies sulphide-carbonate-silicate-oxide iron formation near Penlan and the Dillwyn gold mines, both of which are situated on the Long Island trend.

Recent work by Spooner et al (1977), Kerrich (1980), Kerrich and Fryer (1981), and Kerrich and Fyfe (1981) elucidating the importance of water-rock ratios as a main determining factor in hydrothermal fluid compositions may well afford an elegant explanation for the diachronous variation evident in the hydrothermal regime. Hydrothermal systems characterized by high water/rock ratios (in the order of 100-1000:1 according to Spooner et al) lead to basemetal sulphide mineralization, while systems characterized by much lower water/rock ratios (1:20 according to Kerrich) concentrate gold. Many of the metallogenic features observed in the present study area may well attest

to just such a water-related basis of differentiation. The intravolcanic activity leading to massive sulphide mineralization here would seem to have been characterized at least initially by high water/rock systems -- though inasmuch as the above cited studies demonstrate that K and Ca are enriched in fluids originating in low water/rock environments, the occurrence of the biotite-carbonate ironstone facies at the periphery of the active zone at the Arminius quite possibly indicates the drying up of this particular hydrotherm. The geochemical expression generally characteristic of the numerous sites of gold mineralization, on the other hand, would seem to be diagnostic of low water/rock hydrothermalism across the board. Not only is there a general affiliation of gold with carbonate-bearing iron formation-ironstones, but many prospects show a conspicuous buildup of potassium micas; i.e., phlogopite at the the Tellurium and Penlan, fuchsite at the Tellurium and the Morrow. One might also take note of the fact that many trace minerals reported from the various gold showings testify to significant enrichments in such metals as do not go easily into solution. As noted by the above investigators, this is a further characteristic of fluid compositions in low water/rock environments.

It is instructive to view this particular metallogenic schema in the context of the regional petrogenetic framework outlined at the end of Chapter 3. Not only is the broader perspective useful in pointing up the significance of all these individual data, but the crucial extra evidence afforded by our explication of these metallogenic processes in turn facilitates greatly our as-yet tentative elucidation of the more enigmatic features of the syndepositional hydrothermal metasomatic regime. Utilizing the thesis of differentially hydrous environments, for example, it would seem that we may now plausibly infer two phases of regional hydrothermal metasomatic activity

for this area, an earlier stage typified by high water/rock ratios and a later stage typified by low ones. Using this insight as a jumping off point, we might then go on to speculate that the former conditions could well have resulted from dynamic convective overturn accompanied by the expulsion of considerable amounts of formational water, while the latter likely signify a prolonged period of rather static hydrothermal "cooking" culminating in pervasive mineralogical hydration and a progressively diminished rate of dewatering. Such a program could well account for the peculiarities of the depositional pattern to be observed in this area. During the active earlier stage the relatively soluable base metals would tend to be liberated; during the secondary, more quiescent stage the more insoluable elemental species, including gold, would be released.

These two types of hydrothermal metasomatism are obviously transitional one to the other, of course, and cannot therefore be wholly differentiated on a temporal basis. Just as there is evidence that the high water/rock hydrotherms of the main volcanic stage dried up to produce biotitic carbonate ironstone, in some places -- such as at the New Canton trend and the Penlan massive sulphide deposit -- the characteristically low water/rock upper Chopawamsic hydrothermal systems would seem to have had local access to greater amounts of water which faciliated deposition of multi-facies iron formation including basemetal-bearing massive sulphide. If we allow that the postulated two-stage hydrous regime has at least general validity, however, we may speculate further that the transition from earlier to later types of hydrothermal activity occurred at the time of the deposition of the regionally extensive two-amphibole ironstone. As earlier discussions intimated, this stratum was laid down more or less concurrently with the emplacement of late granodiorite-granite melts which characteristically intruded very near to

surface, locally venting to give rise to Buffards-type quartz-mica schists. With such widespread igneous activity in evidence, it would seem probable that the two-amphibole ironstone may regionally reflect the thermal maximum for the syndepositional metasomatic regime. Inasmuch as Kerrich et al postulate that the environment most likely to favour gold-producing over basemetal-producing hydrothermal activity is one in which "metamorphically" derived fluids debouching onto the sea floor finally precipitate out as carbonate facies exhalite, such ambient conditions as we may infer for this transitional period seem quite consistent with the proposed metallogenic model.

The hydrothermal activity relating more specifically to the actual areas of late pyroclastic volcanism is not as yet well documented. It is considered metallogenically significant, however, that the contact zone between the two-amphibole ironstones and the more restricted upper Chopawamsic pyroclastic-epiclastic deposits is a favoured setting for gold-bearing ferruginous and occasionally staurolite and/or gahnite-bearing quartzites (see previous discussion on the Columbia-Tellurium gold camp). Equally interesting, the fact that the disseminated pyrite in the kyanite quartzite capping the Buffards ash flow deposits has recently been discovered to be auriferous (the pyrite concentrate from the kyanite mining operation runs about .2 oz/ton Au; J. Dixon, personal communication 1981) indicates that gold was an active component in these more restricted hydrothermal environments as well. A third feature of note is the observed tendency for tourmalinite to occur locally in association both with the kyanite quartzites and with the basal shale garnet-grunerite iron formation which, significantly enough, shows its thickest development in the areas of late pyroclastic volcanism. Although neither the tourmalinite nor the garnet-grunerite lithology has as yet proven to be gold-bearing, one might well reason from analogy that closer examination

of these rocks is likely to turn up at least minor enrichments in this metal. A significant gold-tourmalinite association has been reported in areas such as the Golden Dyke Dome in Australia. The garnet-grunerite iron formation, on the other hand, shows considerable petrological similarity to the gold-bearing silicate facies iron formation that has been discovered at Contwoyto and Cullaton lakes (see Table 16).

It is noteworthy with respect to the question of the longevity of the hydrothermal activity that the fluid discharge evidently overlapped locally with pelagic shale deposition. This is particularly well demonstrated at the Morrow mine, where there is interlayering of atypically sulphidic and graphitic argillite with sideritic iron formation at the shale base, but interbedding of graphitic argillite with the multi-facies iron formation may be observed as well near Penlan on the Long Island trend. These sites are thought to demark the areas where hydrothermal discharge was the most prolonged. Soon after the beginning of pelagic sedimentation, however, all hydrothermal activity appears to have ceased. Where the younger shales have been laid down on locally reworked epiclastic material -- as is the case at the southern end of the Fisher Lode in the Mineral district and at the Page mine on the Long Island trend -- the underlying epiclastic facies may also be host to lode gold mineralization. On present data it would be premature to make generalizations about this setting considered as a "type" or to expound too broadly on the role played by hydrothermal processes in its genesis, but with respect at least to these particular occurrences one might plausibly consider paleo-placer beneficiation as a possible generative mechanism.

5. CONCLUSION

Considerable effort was made over the course of this project to integrate all data generated by various means on an ongoing basis such that each stage of the investigation would both subsume and modify the results of all preceding stages. The regional geological schema formulated in Chapter 2 provides a framework for the detailed petrogenetic and metallogenic investigations of chapters 3 and 4 respectively. The implications -- both specific and cumulative -- of the author's findings, rather than being reserved for separate consideration at the end of the study, have thus for the most part been discussed and evaluated progressively throughout the whole text. What remains for this conclusion, therefore, is merely to provide a broad general summary of what has already essentially been covered. After reviewing briefly (1) the main geological events hypothesized to have effected the formation of the Chopawamsic metavolcanic belt, (2) the principle results of the varied petrogenetic and metallogenic investigations carried out with respect to this area, and (3) the depositional model inferred from all extant data for such a volcani-sedimentary terrane, the chapter concludes with an assessment of the viability of this type of regional geological analysis as a methodology in geological studies.

5.1 Historical Review

The Chopawamsic metavolcanic belt appears to have originated as a zone of

extensional volcanism between a westerly Iapetus ocean and an easterly cratonic terrane in Late Precambrian-Lower Paleozoic times. There is considerable question, however, as to what this proto-environment actually comprised. In particular it would seem misleading to put too much emphasis on the analogy of a modern mature ocean basin. At the western boundary of the Chopawamsic belt, the rocks exposed along the Hardware arch comprise mafic sill complexes hosted in part in a magnesian schist tectonite and in part in an assemblage of greenstone flows interlayered with basinal pelitic sediment. This lithological association, while consistent enough with ocean basement-type terranes, clearly implies an immature species; more specifically, it suggests that these intrusives were probably not generated at a mature oceanic spreading ridge. On both petrological and structural-stratigraphic evidence, in fact, extensional tectonic conditions seem here rather to have been relieved through widespread mafic-intrusive-extrusive igneous activity overlapping with surface sedimentation. As a result of this sedimentational interference with the igneous system -- or perhaps simply because the crust so generated was not thick or rigid enough to focus igneous activity along a single centralized vent -- the full ophiolitic successions diagnostic of mature ocean basins apparently never formed. Despite such disqualifiers, the fact that many of the components of an oceanic crust can be recognized, albeit interlayered with basinal sediment, still strongly argues that the assemblage as a whole was basically oceanic in derivation. The lithologies exposed along the Hardware arch at the west side of the Chopawamsic metavolcanic belt might be considered as broadly similar to the ophiolitic melange which has been reported from subduction complexes (Myashiro 1977).

The nature of the easterly cratonic terrane is poorly known due to the

lack of geological study in the outer Piedmont. It is evident that it includes Grenvillian-age sial exposed in gneiss domes flanked by younger ortho and paragneiss, but the age and nature of the younger gneisses is at this point open to speculation. The Sabot amphibolite immediately overlying the Grenvillian State Farm gneiss may signify that plateau basalt volcanism occurred during the initial stages of fragmentation of the Grenvillian supercraton, while the Maidens quartzite-calc-silicate gneiss association overlying the Sabot amphibolite possibly reflects shelf-type sedimentation. The much more regionally extensive Po River paragneiss structurally juxtaposed against the eastern side of the Chopawamsic metavolcanics along the Spotsylvania lineament, on the other hand, is much more immature, plausibly suggesting a thick accumulation of greywacke-type sediments. Collectively, at least to the extent they are currently known, the lithologies comprising the easterly cratonic terrane would seem to indicate that long-lived tectonic instability, accompanied by mafic igneous activity and varying sedimentational regimes, persisted throughout much of the post-Grenvillian but pre-Chopawamsic times.

The tectonic setting of the Chopawamsic metavolcanic belt would seem to be in many ways analogous to a modern continental margin island arc environment. Although it is entirely a point of conjecture whether or not the volcanism was initiated by subduction, the occurrence of ophiolitic melange along the western border, as well as the fact that the belt itself can be broadly partitioned into a "frontal arc" Palmyra assemblage and a "back arc" Mineral assemblage could be interpreted to support such a possibility. Nevertheless, on the more basic lithological level numerous aspects of the Chopawamsic belt depart radically from those demonstrated by island arcs. Most significantly, the style of physical volcanism to be inferred from

regional relationships would seem to suggest regional fissure systems rather than any centralized volcanic activity. Evidence for a major volcanic buildup or even for the type of crosscutting relationship that might signify centralized volcanic feeder systems appears to be completely lacking. As mentioned above, the igneous material generated across this belt seems to have been everywhere intercalated with varying amounts of sedimentary material. Since there is no extant trace of conduits, the fissures themselves must have been fairly ephemeral; alternately they may have become foci for shale deposition and as a result are now covered. That the younger shales do in fact occur at major facies breaks in the volcanics supports the latter contention.

An even more critical factor militating against any strict island arc analogy is the occurrence of considerable hydrothermally derived chemical precipitate both interlayered with and capping the metavolcanic assemblage. As far as this writer is aware, no regionally extensive iron formation-type deposit has been documented in any modern island arc terrane. On the other hand, there are numerous reports of this general type of lithology from modern rift settings. Accordingly, the widespread occurrence of iron formation-type rocks along the Chopawamsic belt is here deemed to signify that this volcani-sedimentary terrane had more in common with a modern rift-setting than a typical island arc one. Postulation of an original rift setting would also better account for the volcanism being characteristically bimodal in nature and for eruptions taking place along laterally extensive fissure systems.

The deposition of extensive iron formation-type lithologies is considered to reflect significant syndepositional hydrothermal metasomatism, particularly in the latter stages of volcanism. It seems evident that the maximal geothermal conditions within the rift floor were attained during late but

widespread intrusive activity which included the near-surface emplacement of granodiorite-granite melts and the injection or ejection of pyroxenitic komatiite. Local pyroclastic eruptions, possibly initiated where komatiitic injections encountered near-surface granitic melts, terminated Chopawamsic volcanism. Following these local eruptions, the setting evolved as a successor shale basin; pelagic sedimentation during mid to upper Ordovician times completed the formative stage of development.

Subsequent to the formative stage, the terrane was highly foreshortened by regional metamorphic events culminating in the later Paleozoic. The metamorphic overprinting was probably episodic in nature; as a result, the Chopawamsic belt now demonstrates a polyphase style of deformation. Early F isoclinal folding, accompanied by varying intensities of axial planar transpositional shearing, controls structural patterns along the western side of the belt. Alternately, later F broad coaxial warping appears to be the main control of structural patterns along the eastern margin. The major synclinoria along the core of the belt show the effects of interference between these two deformation styles. The metamorphic overprint itself is everywhere above the biotite isograd and increases in intensity from west to east across the belt. The low to medium grade transition occurs in the core of the belt, with higher amphibolite facies conditions existing in the easterly gneiss terrane. Subsequent to the regional metamorphic overprint, the belt lay dormant until the Mesozoic, when tensional conditions set up during the opening up of the Atlantic in Triassic-Jurassic times led to widespread diabase dyking and the development of restricted molasse-filled graben. This Mesozoic rejuvenation concluded the geological history of the belt.

5.2 Petrogenetic and Metallogenic Summary

The petrogenetic investigation of the intrusive and extrusive rocks in this area indicates that multiple source magmas were involved in the generation of the igneous suite present in the Chopawamsic belt. In general these would seem to have comprised two overlapping but differing magmatic lineages. A low-K komatiite-tholeiite-trondjemite lineage gave rise to the strongly differentiated mafic sill complexes along the western side of the Chopawamsic belt, the westerly greenstone suite basal to the Palmyra assemblage, the small isolated composite diorite-gabbro-peridotite bodies in the core of the belt, the small but widely occurring granophyric bodies in the Mineral assemblage, the strongly bimodal Mineral assemblage volcanics, and, in the terminal stages, a uniform pyroxenitic komatiite that was injected or ejected near or at the surface in upper Chopawamsic times. This particular magmatic lineage is considered to have resulted from diapiric upwelling of high partial melt fractions derived at very high temperatures deep in the mantle. On their rise to the surface, these mantle-derived magmas commonly collected in shallow level magma chambers where they underwent strong crystallization differentiation. Intrinsically high water and soda contents determined a large field of amphibole stability and give rise through early hornblende fractionation and later plagioclase fractionation respectively to the tonalite and trondhjemite which occur in association with the westerly sill complexes. In contrast to this, in the case of the Mineral assemblage trondhjemite bodies, and perhaps of the bimodal volcanic assemblage as well, because there is no evidence for such a fractional crystallization scheme, liquid immiscibility resulting in the splitting of conjugate iron-rich basaltic and trondhjemitic liquids from a primitive tholeiitic parental magma is considered a more plausible petrogenetic model.

A high-K calc-alkaline lineage gave rise to parts of the Green Springs and to all of the Ellisville and the compositionally similar unnamed granitic body in the Appomattox River area, the Palmyra assemblage rhyolites and more intermediate pyroclastics, and the Buffards-type quartz mica schist deposits. This particular magmatic suite is thought to be derived largely through crustal anatexis, though such an interpretation needs further petrochemical investigation before it may be definitively substantiated. Because of their gross spatial restrictions, it seems likely that such broadly calc-alkaline volcanic types as the Palmyra assemblage metarhyolites west of the Long Island syncline, the Palmyra assemblage metadacites and meta-andesites east of the Long Island syncline, and the Buffards-age metarhyolites in the core and along the east flank of the Arvonia synclinorium and again in the core of the Columbia synclinorium, stemmed from compositionally distinct source magmas. In some instances the origins may have been exceedingly complex. If, for example, the Buffards pyroclastic eruptions in fact originated where late stage komatiitic magmas encountered near-surface anatectic granitic melts, as has been previously postulated, this would explain a number of anomalous features in these rocks which make them difficult to account for under conventional, more simplistic schemata.

Repeated komatiitic-tholeiitic injection, formation of shallow magma chambers, and occurrence of lateral fissure systems collectively suggest that Chopawmasic volcanism occurred in response to a thermally anomalous mantle rise. The geothermal conditions accompanying the volcanism would seem to have peaked in the near-surface environment at the time of the late stage igneous activity, giving rise to the lithologically diverse upper Chopawamsic ironstone-iron formation-quartzite association. The alterations effected by this syndepositional hydrothermal metasomatic regime seem to be more or less

restricted to the volcanic lithologies. The mafic volcanics were pervasively spilitized, while the felsics suffered considerable redistribution of alkalies. Much of the fluid for such hydrothermal metasomatic processes likely derived from the formational brines held in intercalated epiclastic and pyroclastic deposits. Interacting with primary volcanics it led, on a regional scale, to the development of a suite of ironstones showing remnant volcanic compositional signatures and locally, where hydrothermal activity was more intense, to multi-facies iron formation-type deposits. The extent to which the various facies of ironstone-iron formation reflect (1) hydrothermal alteration of primary volcanics and (2) chemical precipitation from hydrothermal fluids is not fully understood; this particular petrogenetic dichotomy will need considerable further research before it may be explicated definitively.

The metallogeny of the gold-pyrite mineralization can be broadly modelled with reference to synchronous and diachronous variations in the syndepositional hydrothermal metasomatic regime. The earlier high water/rock hydrothermal system operative during dynamic convective discharge of considerable amounts of formational brine resulted in massive pyritic sulphide mineralization closely affiliated with silicate facies iron formation in areas where hydrothermal discharge was most intense. In areas of bimodal volcanism, such as in the Mineral district, the massive sulphide so generated tends to have a polymetallic signature. Where hydrothermal activity was enhanced over hot spots in basins floored by mafic volcanics, as in the Andersonville district, it is iron-dominated and characteristically shows only a modest basemetal expression. In contrast to both these types, as the hydrous conditions changed, so did the metallogenic picture. In particular, after a significant proportion of the formational brine had been expelled, a low

water/rock system operative over a prolonged period at heightened geothermal conditions resulted in a metal expression characterized most notably by gold mineralization hosted preferentially within local zones of multi-facies iron formation-ironstones at the base of the shales.

Many of the specific mineralogical features observed in relation to mineralization reflect not only original compositional aspects, of course, but also the effects of the late metamorphic overprint. As a result, interpretation of some of the mineralogical data is ambiguous. For instance, the question of whether the increase in gahnite and zincian staurolite towards the margins of the ore lenses in the Mineral district is due to original sulphur deficiency or to metamorphic desulphidization processes must remain at this point unresolved. Such ambiguity notwithstanding, the study of mineral chemistry is undoubtedly a key to unravelling many of the more subtle metallogenic processes. Through investigation of regional variation in garnet chemistry, the occurrence of affiliated manganese enrichments with sulphide mineralization was brought to light, allowing a number of critical analogies to be drawn linking the massive sulphide deposits of the Chopawamsic belt not only with numerous other sulphide deposits but, most significantly, with currently active sea floor hydrothermal systems where such manganese haloes have been recognized. The study of amphibole chemistry, on the other hand, draws attention to the metallogenic significance of multi-facies iron formation environments with respect not only to gold but, potentially, to base metal sulphide mineralization as well.

The metallogenic processes in these particular settings have not yet been studied thoroughly enough to allow for generalizations. One point in particular might be noted, however. In the present study area the spatial association of mineralization with metakomatiitic units seems far too

fortuitous to be considered as purely coincidental. Considering the pervasive hydration demonstrated by these rocks, and especially considering their abnormally low Au contents (consistently below a .2 ppm detection limit), this lithology in fact seems to be a prime candidate for the source of the gold. Presumably partitioned into the fluid phase during the peak geothermal period of the terminal volcanic stage when the amount of hydrous fluid left subsequent to convective dewatering was quite low, this metal precipitated out preferentially in potassium mica and carbonate-enriched iron formation-ironstone deposits. Later, during the subsequent metamorphic overprint, it was commonly remobilized into quartz veins within these auriferous lithologies.

5.3 Depositional Environment

When one is considering original depositional sites within an active volcanic setting, multiple environmental influences must be born in mind: the control effected by physical conditions (subareal, intertidal, subtidal, deep basin floor); the control effected by proximity to loci of active volcanism; in the present instance, the control effected by the varying intensity of hydrothermal activity as well. With all these contemporaneous and mutually interfering petrogenetic determinants to account for, it is obvious that layer cake stratigraphic models can only be of marginal use. No schema is going to be adequate to explain such an area, in fact, unless it can accommodate an intercalation of primary volcanics, clastic sedimentary, and hydrothermally derived lithologies typified by rapid lateral as well as vertical facies changes. Despite the problems inevitably entailed by such complexities, on the basis of the petrogenetic work carried out some of the hydrothermal facies

in addition to several of the volcanic and sedimentary rock types can be provisionally identified as diagnostic of specific depositional environments. The most useful of these indicators are as follows:

(1) Indicators of subareal deposition:

(a) The accretionary lapilli tuffs flanking the Ellisville may signify air fall pyroclastic activity;

(b) The aluminous facies of the basal shale silicate iron formation developed between Buffards quartz mica schists and Arvonia metashale has a generally "lateritic" chemical composition and thus could be interpreted to suggest that subareal conditions existed locally over Buffards pyroclastics prior to the onslaught of shale deposition.

(2) Indicators of intertidal deposition:

(a) The conglomeratic and crossbedded Bremo quartzite signifies a deltaic depositional regime with riverine feldspathic sands debouching into a shale basin;

(b) The basal shale silicate facies iron formation evidently originated as an oolitic chloritite and is therefore interpreted to outline the near-shore settings along the margins of the successor basins (that this is the only shale facies occurring along the eastern limb of the Columbia synclinorium and in the Whispering Creek anticline indicates that it marks the eastern extent of shale deposition).

(3) Indicators of subtidal deposition:

(a) The general lack of evidence for current action together with the regular banding demonstrated by the diverse upper Chopawamsic ironstone-iron formation-quartzite association implies deposition below wave base;

(b) The interlayered bimodal volcanics, silty epiclastic sediments, and ironstones of the Mineral suite are considered collectively to signify a relatively deep water depositional setting, with the local occurrence of coarser clastic fractions being due to turbiditic sedimentation into topographic lows in volcanically active areas.

(4) Indicators of basin floor deposition:

(a) The delicately laminated and carbonaceous nature of the regional shales may be interpreted as evidence of a reduced, near starved, sedimentary basin;

(b) The characterizing paper phyllites and occasional interbedded siltstone wacke units of the Candler metasedimentary assemblage suggest a basinal environment receiving a distal terrigenous supply.

(5) Indicators of proximity to volcanic centres:

(a) The rhyolite flows of the Palmyra suite, quartz feldspar porphyry bodies of the Mineral suite, and the quartz eye porphyry facies of the Buffards quartz mica schist deposits are considered to be the most proximal volcanic deposits recognized to date;

(b) The intermediate pyroclastic deposits flanking the Ellisville sill are atypically coarse in comparison with other tuffaceous units and may signify that an original fissure is now occupied by the Ellisville sill;

(c) By and large, the physical characteristics of both mafic and felsic members of the Mineral metavolcanic suite indicate that they were deposited distally with respect to a volcanic centre.

(6) Indicators of intensity of hydrothermal activity:

(a) The hydrothermal chloritite-massive sulphide association,

observed at all known major sulphide occurrences, is considered to have developed under anomalously high geothermal conditions;

(b) The restricted occurrence of multifacies iron formation-ironstone locally interbedded with basal shale graphitic and sulphidic argillite is thought to reflect enhanced long-lived geothermal zones in the post-volcanic stage;

(c) The laterally extensive oxide iron formation, two-amphibole ironstone, ferruginous quartzite and kyanite quartzite units are considered to have developed during hiatuses in active volcanism and clastic sedimentation, and are interpreted as signifying the passive generation of "hydrothermal crusts" over lithologies of varying character in areas peripheral to the anomalous hot spots of (a) and (b).

When all these environmental indicators are taken into account, much light is shed on the question of how this paleo-volcanic setting evolved through time. Over the main period of volcanism the setting was evidently dominantly submarine. The only evidence for possible subareal conditions so far recognized is the occurrence of accretionary lapilli in the intermediate pyroclastics of the Palmyra assemblage flanking the Ellisville sill; the much more common laminated dust tuffs of the Palmyra assemblage signify that deposition was primarily subaqueous. The Mineral assemblage as a whole is thought to signify a deep water active volcanic rift setting.

Following the main stage of volcanism, there apparently occurred a prolonged period dominated regionally by hydrothermal metasomatic petrogentic processes. The long-lived geothermal conditions responsible for this hydrothermal activity may have been produced by a shift from the extensional tectonics which initiated the volcanic rift to epierogenic tectonics related to the rise of buoyant granitic melts. The tectonic instability accompanying

the late intrusive activity would seem to have resulted in a general shoaling. The localized Buffards-type pyroclastic eruptions occurring at this time were more or less confined to volcani-tectonic sinks, while bordering highs became sites for Bremo-type sedimentational regimes. Subareal conditions may even have existed locally and caused the development of thin lateritic intervals. More generally, however, the terrane remained submerged. Due to the proclivity of the ash flows for hydrothermal alteration, thick clay-chert (kyanite-quartzite) cap(s) were generated on these deposits regionally. The basal shale oolitic chloritite iron formation accumulated in near-shore environments more or less as a time equivalent to the kyanite quartzite.

Interestingly, the basal shale silicate facies iron formation had greater extent than the overlying normal pelagic shales. This would seem to indicate that the prolonged period of subsidence necessary to maintain the relatively starved successor basin(s) was likely focused primarily along the more internal of the facies boundaries between the differing volcanic assemblages and/or in the areas of the late pyroclastic activity. Such original control of the shale deposition would seem also to have had considerable influence during later deformation, as the regional structures along the belt are now essentially dominated by the shale synclinoria at facies breaks in the underlying metavolcanic assemblage.

5.4 Assessment of the Effectiveness of the Methodology

This study of the central Virginian segment of the Chopawamsic metavolcanic belt was, as mentioned in the introduction, conceived at least partly as a means of testing and demonstrating the utility of regional

geological analysis as a tool for mineral exploration. To briefly review the theoretical rationale for selecting such an approach, we may perhaps begin by saying that the writer's preferred methodology is based on the assumption that at least in economically oriented field investigations, optimum results will be obtained if any given tectonic setting is treated as a functional whole, viewed as comprising not merely a series of discrete, mutually exclusive temporal-spatial events but a complexly structured almost-organism which must be explicated in terms of the relations between, not merely the physico-chemical characteristics of, its individual parts. This does not mean that gross phenomena cannot or should not be analysed into their constituent members but it does mean that the naturally occurring regional geological framework must be considered as providing a necessary context within which all data must be interpreted and against which every provisional model must be tested. In the simplest terms, an appreciation of the dynamic interplay among the varying lithological aspects of any geological environment is critical for unravelling petrogenesis. This in turn is essential for determining the signficance of the specific features which emerge from either meso or micro-scale examination of individual rock species.

One must, of course, keep in mind the critical qualification cited above, "at least in economically oriented field investigations." Geological studies have traditionally subsumed both scientific and historical approaches. With the technological and theoretical advances of the last two decades, however, not only industry but also the academic establishment -- attracted perhaps as much by the mystique of hardware as by the ease of dealing with quantifiable data -- has inclined increasingly toward the former. This poses something of a problem. It might be said that scientific enquiry aims at understanding the general while historical enquiry addresses itself to what is unique. With

this critical divergence in ends, the necessity arises of making some kind of distinction in means. Where the "pure" scientist, whether in the laboratory or in the field, is quite properly concerned with the ideal -- with inferring the normative features of a rock type, say, rather than describing the specifics of any given outcrop -- the more practically inclined field researcher is constrained to focus on the real, that is, on the peculiarities of an essentially unduplicatable phenomenon existing at one and only one location in space and time. The only way to do this is by employing an historical perspective. This is not to say that the practical investigator may not make use of the fruits of scientific endeavour in pursuing his own particular ends. Indeed, as the present study attempts to demonstrate with its synthesis of widely diverse types of approach, inasmuch as they provide not merely increasingly sensitive analytic techniques but, more important, the interpretive models necessary to elucidate given sets of data, a knowledge of current developments in the geo-sciences is an invaluable resource for the field researcher. It is only when these are employed in conjunction with -- and indeed, toward the specific end of achieving -- an adequate historical reconstruction of a unique temporal/spatial phenomenon, though, that such aids really become useful in practical field programs. Though much may be gained by taking advantage of the insights offered by the numerous specialties currently flourishing in the geo-sciences, in other words, it is this author's firm conviction that as long as these are divorced from a specific geological context, there is no way of evaluating how relevant they are -- and how far they may be applied -- in any given case.

The present study attests in many ways to the advantages of this stance. From a purely practical standpoint, it is evident that the methodology employed provides a highly efficient means of approaching reconnaissance. One

of the problems with high-budget, high-technology exploration programs is that they are very often geared more to amassing facts than to interpreting them. It is obviously useful to have a framework for synthesizing on an ongoing basis the copious and diverse data yeilded by combined geological, geophysical and geochemical investigations at varying scales if only because the capacity to test an evolving model while still on site makes it possible to modify and refine the thrust of a field program, perhaps even redefining its targets, while it is still in progress, thus effecting a considerable savings in both time and money. Beyond this, however, this writer's findings make it clear that the approach also offers qualitative advantages -- that it has ramifications not merely for the efficiency but for the accuracy of the interpretive process -- which may in the long run be even more important for the exploratory function. If nothing else, when the regional structural-stratigraphic interplay is kept consistently in view, the significance of individual features is brought into higher relief. In the present case the facies change from metashale to basal shale garnet-grunerite iron formation along the east limb of the Columbia synclinorium provides a simple explanation for the fact that the normal metashale is not found in this locale. Similarly, identification of the basal shale silicate facies iron formation as a regional stratigraphic marker occurring in each of the major shale infolds as well as in the easterly gneiss terrane establishes a crucial stratigraphic correlative across the belt.

Many aspects of petrogenesis and metallogenesis presented in this thesis also depend largely on regional observations. The inferences that multiple source magmas played a role in generating the igneous suite, that the volcanism was dominantly submarine and overlapped with various sedimentational

regimes, and that the ongoing syndepositional metasomatism intensified in the late volcanic stage to give rise to regional iron formation-type deposits collectively derive from the petrogenetic signature of the belt as a whole. These geological processes would have been considerably harder, perhaps impossible, to grasp had each been considered only in isolation. Nor does the regional approach lend itself only to an elucidation of general or broad-based phenomena. In establishing an interpretive framework which is both transcendent and specific, it can also cast light on more narrowly specialized aspects of the environment that would almost certainly remain enigmatic if one were to attempt explanations in terms solely of either local features or idealized models. Perhaps the most striking example yielded by the present study of the kind of insight to be gained on this level is the writer's recognition that synchronous high level intrusion of anatectic granitic melts and komatiite resulting in local pyroclastic eruptions provides an eminently plausible explanation for the occurrence of fuchsitic mica in these pyroclastic deposits.

Most important of all, perhaps, regional analysis is in a sense propaedeutic to any detailed study of more specific aspects of geology. The dual perspective is particularly critical when one attempts to explicate those more elusive genetic controls which, though subtle, may assume considerable significance in metallogeny. Knowing the appropriate context within which to set specific metallogenic problems is an absolute prerequisite for deriving adequate explanatory schemata. In this present case, for instance, the recognition that syndepositional hydrothermal processes played an important petrogenetic role within this regional setting provides a key for understanding the origin of the pyritic massive sulphide and gold

mineralization -- hence facilitating the selection of likely targets for subsequent phases of exploration. This alone would be enough to make regional geological analysis a preferred methodology for economically oriented reconnaissance.

6. REFERENCES

Adams, W.H., 1884, The pyrites deposits of Louisa County, Virginia: Am. Inst. Mining Engineers Trans., v. 12, p. 527-35.

Addy, S.K., and Ypma, P.J.M., 1978, Chemical zoning in garnets from rocks around the massive sulfide deposits at Ducktown Tennesee and its implications: Jour. Geol., v. 86, p. 385-92.

Allen, R.M., Jr., 1963, Geology and mineral resources of Greene and Madison counties: Virginia Div. Min. Resources Bull. 78, 102 p.

Allen, N.E., 1980, The 1979-80 Mineral district drilling program: Callahan Mining Corp. unpub. rpt., 15 p.

Amstutz, G.C., 1974, Spilites and spilitic rocks, in Amstutz, G.C., ed., Spilites and spilitic rocks: New York, Springer Verlog, p. 737-53.

Appel, P.W.U., 1979, Stratabound sulphides in a banded iron-formation and in basaltic tuffs in the early Precambrian Isua supercrustal belt, west Greenland: Econ. Geol., v. 74, p. 45-52.

Arnold, R.G., 1962, Equilibrium relations between pyrrhotite and pyrite from 325 to 743 C: Econ. Geol., v. 57, p. 72-90.

_____ 1969, Pyrrhotite phase relations below 304 $\pm$ 6°C at less than 1 atm. total pressure: Econ. Geol., v. 64, p. 405-19.

Arndt, N.T., Naldrett, A.J., and Pyke, D.R., 1977, Komatiite and iron-rich tholeiite lavas of Munro Township, northeast Ontario: Jour. Petrol. 18, p. 319-26.

Arth, J.G., 1979, Some trace elements in trondhjemites -- Their implications to magma genesis and paleotectonic setting, in Barker, Fred, ed., Trondjemites, dacites, and related rocks: Amsterdam, Elsevier, p. 123-32.

_____ and Hanson, G.N., 1972, Quartz diorite derived by partial melting of eclogite or amphibolite at mantle depths: Contrib. Mineral. & Petrol., v. 37, p. 161-74.

Atherton, M.P., 1968, The variations in garnet, biotite, and chlorite composition in medium grade pelitic rocks from the Dolradion, Scotland, with particular reference to the zonation of garnet: Contrib. Mineral. & Petrol., v. 18, p. 347-71.

Auboin, J., 1965, Geosynclines, in Developments in geotectonics: Amsterdam, Elsevier, 33 p.

Aumento, F., Mitchell, W.S., and Fratta M., 1976, Interaction between sea water and oceanic layer two as a function of time and depth -- I field evidence: Cdn. Mineral. 14, p. 269-90.

Bachinski, D.J., 1976, Metamorphism of cupriferous iron sulfide deposits, Notre Dame Bay, Newfoundland: Econ. Geol., v. 71, p. 443-52.

Barnes, R.C., 1963, Geological and geophysical investigation of sulphide deposits near New Canton, Virginia: unpub. MSc. diss., U.Va.

Barker, Fred, ed., 1979a, Trondhjemites, dacites, and related rocks: Amsterdam, Elsevier, 659 p.

_____ 1979b, Trondhjemite: Definition, environment, and hypotheses of origin, in Barker, Fred, ed., Trondjemites, dacites and related rocks: Amsterdam, Elsevier, p. 1-12.

Barton, J.C., 1933, Memorandum on the Goochland gold mines, Holding Corp. of Goochland Co., Va: Open-File Rpt., Virginia Div. Min. Resources.

Beach, A., 1973, The mineralogy of high temperature shear zones at Scourie, NW Scotland: Jour. Petrol., v. 14, p. 231-48.

Bickle, M.J., Ford, C.E., and Nisbet, E.G., 1975, Basaltic and peridotitic komatiites and stromatolites above a basal unconformity in the Belingwe greenstone belt, Rhodesia: Earth Planet Sci. Lett., v. 27, p. 155-62.

Bird, J.B., Dewey, J.F., and Kidd, W.S.F., 1971, Proto-Atlantic ocean crust and mantle: Appalachian Caledonian ophiolites: Nature Phys. Sci., v. 231, p. 28-33.

Bischoff, J.L., 1969, Red Sea geothermal brine deposits: Their mineralogy, chemistry, and genesis, in Degens, E.T., and Ross, D.A., eds., Hot brines and heavy metal deposits in the Red Sea: New York, Springer, p. 368-401.

_____ and Manheim, F.T., 1969, Economic potential of the Red Sea heavy metal deposits, in Degens, E.T., and Ross, D.A., eds., Hot brines and recent heavy metal deposits in the Red Sea: New York, Springer, p. 535-41.

Bland, A.E., 1978, Trace element geochemistry of volcanic sequences of Maryland, Virginia and North Carolina and its bearing on the tectonic evolution of the central Appalachians: unpub. PhD. diss., U. Kentucky.

Bostock, H.H., 1977, The composition of hornblende, grunerite, and garnet in Archean iron formation of the Itchen Lake area, District of Mackenzie, Canada: Cdn. Jour. Earth Sci. 14, p. 1740-52.

_____ 1980, Geology of the Itchen Lake area, District of Mackenzie: Geol. Surv. of Canada Mem. 391, p. 1-99.

Bourland, W.C., and Glover, L., III, 1979, The Columbia metagranite, in Glover, L. III, and Tucker, R.D., eds., Guides to fieldtrips 1-3: SE Sect. Geol. Soc. Am., Blacksburg, Va., p. 14-16.

Boyle, R.W., 1979, The geochemistry of gold and its deposits: Cdn. Geol. Surv. Bull. 280, 584 p.

Brown, C.B., 1937, Outline of the geology and mineral resources of Goochland County, Virginia: Va. Geol. Surv. Bull. 48, 68 p.

Brown, W.R., 1958, Geology and mineral resources of the Lynchburg quadrangle, Virginia: Va. Div. Min. Resources Bull. 74, 99 p.

_____ 1969, Geology of the Dillwyn quadrangle, Virginia: Va. Div. Min. Resources Rpt. Inv. 10, 77 p.

_____ 1976, Tectonic melange (?) in the Arvonia slate district of Virginia (abs.): Geol. Soc. Am. Abs. w/ Programs, NE & SE sect., v. 8, no. 2, p. 142.

Cady, J.G., 1951, Rock weathering and soil formation in the North Carolina region: Soil Soc. Am. Proc., v. 15, p. 337-42.

Cameron, K.L., 1975, An experimental study of actinolite-cummingtonite phase relations with notes on the synthesis of Fe-rich anthophyllite: Am. Min., v. 60, p. 375-90.

Cameron, W.E., Nisbet, E.G., and Dietrich, V.J., 1979, Boninites, komatiites, and ophiolitic basalt: Nature, v. 280, p. 550-53.

Cann, J.R., 1969, Spilites from the Carlsberg Ridge Indian Ocean: Jour. Petrol., v. 10, p. 1-19.

Card, K.D., 1982, Progress report on regional geological synthesis, central Superior Province: Geol. Surv. Can. Pap. 82-1A, p. 23-28.

Carroll, D., 1970, Rock weathering: New York, Plenum Press, 325 p.

Carter, J.B., and Wills, J.W., 1972, Soils of Louisa County, Virginia: Rpt. no. 16 Va. Polytechnic Inst. & State U.

Cawthorn, R.G., and Brown, P.A., 1976, A model for the formation and crystallization of corundum-normative calc-alkaline magmas through amphibole fractionation: Jour. Geol., v. 84, p. 467-76.

_____ and O'Hara, M.J., 1976, Amphibole fractionation in calc-alkaline magma genesis: Am. Jour. Sci., v. 276, p. 309-29.

_____, R.G. Strong, D.F., and Brown, P.A., 1976, Origin of corundum-normative intrusive and extrusive magmas: Nature, v. 259, no. 5539, p. 102-104.

Chapin, C.E., and Elston, W.E., 1979, Ash flow tuffs: Geol. Soc. Am. Spec. Pap. 180, 211 p.

Clifford, P.M., 1968, Flood basalts, dike swarms and subcrustal flow: Cdn. Jour. Earth Sci., v. 5, p. 92-96.

Cline, J.H., Watson, T.L., and Wright, F.J., 1921, A geologic map of the pyrite-gold belt in Louisa and Spotsylvania counties, Virginia: Va. Geol. Surv., scale 1 inch to 1 mile.

Coleman, R.G., and Peterman, Z.E., 1975, Oceanic plagiogranite: Jour. Geophys. Research, v. 80, no. 8, p. 1099-1108.

Conley, J.F., 1978, Geology of the Piedmont of Virginia -- Interpretations and

problems, in Contributions to Virginia geology -- III: Va. Div. Min. Resources Pub. 7, p. 115-49.

_____ and Marr, J.D., Jr., 1979, Reinterpretation of the Arvonia syncline central Virginia (abs.): Geol. Soc. Am. Abs., vol. II, no. 4, p. 174-75.

Cook, F.A., Brown, L.D., and Oliver, J.E., 1980, The southern Appalachians and the growth of continents: Scientific American, v. 243, no. 4, p. 156-68.

Coombs, D.S., 1960, Lower grade mineral facies in New Zealand: Rep. 21st Int. Geol. Congr., pt. 13, p. 339-51.

_____ 1974, On the Mineral facies of spilitic rocks and their genesis, in G.C. Amstutz, ed., Spilites and spilitic rocks: New York, Springer Verlog, p. 373-85.

Corliss, J.B., Dymond, J., Gordon, L.I., Edmond, M.E., von Herzon, R.P., Ballard, R.D., Green, K., Williams, D., Bainbridge, A., Crane, K., and van Andel, T.H., 1979, Submarine thermal springs on the Galapagos rift: Science, v. 203, p. 1073-1083.

Cox, L.J., 1979, Mineralogy and petrogenesis of the Arminius deposit, Louisa County, Virginia: unpub. MSc. diss., Va. Polytech. Inst. & State U.

Craig, J.R., Miller, J.W., Cox, L.J., and Kazda, R.F., 1978, Ores of the Mineral district: U.S. Geol. Surv. Open-File Rpt. 78-1068, p. 26-31.

Currier, L.W., 1935, Zinc and lead region of southwestern Virginia: Va Geol. Surv. Bull. 43, 122 p.

Davis, P.A., Jr., 1977, Trace element model studies of late Precambrian - Early Paleozoic greenstones of Virginia, Maryland and Pennsylvania: unpub. PhD. diss., U. Kentucky.

Davis, P.A., Jr., Blackburn, W.H., and Brown, W.R., 1978, Genesis of Catoctin volcanic rocks by a mantle-driven magma plume (abs): Geol. Soc. Am. Abs. w/ Prog., vol. 10, no. 4, p. 166.

Davis, R.G., 1974, Pre-Grenville ages of basement rocks in central Virginia -- A model for interpretation of zircon ages: unpub. MSc. diss., Va. Polytech. Inst. & State U.

Degens, E.T., and Stoffers, P., 1977, Phase boundaries as an instrument for metal concentration in geological systems, in Klem, D.D., and Schneider, H.J., eds., Time- and strata-bound ore deposits: New York, Springer, p. 25-45.

Dewey, J.F., 1969, The evolution of the Appalachian-Caledonian orogen: Nature, v. 222, p. 124-29.

_____, and Bird, J.M., 1971, Origin and emplacement of the ophiolite suite: Appalachian ophiolites in Newfoundland: Jour. Geophys. Research, v. 76, p. 3179-3206.

Dickinson, W.R., 1975, Potash-depth (K-h) relations in continental margin and intraoceanic magmatic arcs: Geol., v. 3, p. 53-56.

and Rich, E.I., 1972, Petrologic intervals and petrofacies in the Great Valley Sequence, Sacramento Valley, California: Geol. Soc. Am. Bull., v. 83, p. 3007-3024.

Dixon, S., and Rutherford, M.J., 1979, Plagiogranites as late-stage immiscible liquids in ophiolite and mic-ocean ridge suites: An experimental study: Earth Planet Sci. Lett., v. 45, p. 45-60.

Drake, A.A., Jr., and Morgan, B.A., 1981, The Piney Branch Complex -- a metamorphosed fragment of the central Appalachian ophiolite in northern Virginia: A. Jour. Sci., v. 281, p. 414-508.

Edmond, N.M., 1979, The chemistry of hot springs on the Galapagos spreading ridge: Metallogenesis in and on new oceanic crust: Proceedings IAVCEI Ophiolite Symp., Nicosia, Cyprus.

Ern, E.H., 1968, Geology of the Buckingham quadrangle, Virginia: Va. Div. Min. Resources Rpt. Inv. 15, 45 p.

Espenshade, G.H., and Potter, D.B., 1960, Kyanite, sillimanite, and andalusite deposits of the southeastern states, U.S. Geol. Surv. Prof. Pap. 336, 121 p.

Ferry, J.M., and Spear, F.S., 1978, Experimental calibration of partitioning of Fe and Mg between biotite and garnet: Contrib. Mineral. & Petrol., v. 66, p. 113-17.

Feuer, W.J., 1980, Origin of the fragmental mica schist, Cofer deposit, Virginia: unpub. MSc. diss, U. Western Ontario, 154 p.

Finlow-Bates, T., and Stumpfl, E.F., 1979, The copper and lead-zinc-silver orebodies at Mount Isa Mine, Queensland: Products of one hydrothermal system: Ann. Soc. Geol. Belgique, T. 102, p. 497-517.

Fleet, M.E., and Barnett, R.L., 1978, Al /Al Partitioning in calciferous amphiboles from the Frood mine, Sudbury, Ontario: Cdn. Min., v. 16, p. 527-32.

Fripp, R.E.P., 1976, Stratabound gold deposits in Archean banded iron formation, Rhodesia: Econ. Geol., v. 71, p. 58-75.

Frost, B.R., 1973, Ferroan gahnite from quartz-biotite-almandine schist, Wind River Mountains, Wyoming: Am. Min., v. 58, p. 831-34.

Fryer, B.J., and Hutchinson, R.W., 1976, Generation of metal deposits on the sea floor: Cdn. Jour. Earth Sci., v. 13, p. 126-35.

Fullagar, P.D., 1971, Age and origin of plutonic intrusions in the Piedmont of the southeastern Appalachians: Geol. Soc. Am. Bull., v. 82, no. 10, p. 2845-62.

Fyfe, W.S. and Lonsdale, P., 1981, Submarine hydrothermal activity, in Emiliani, C., ed., The seas: New York, Wiley-Interscience.

Gair, J.E., and Slack, J.F., 1980, Stratabound massive sulfide deposits of the

U.S. Appalachians: Geol. Surv. Ireland Spec. Pap. no. 5.

Gale, G.H., 1973, Paleozoic basaltic komatiite and ocean-floor type basalts from northeastern Newfoundland: Earth Planet Sci. Lett., v. 18, p. 22-34.
Gill, J.B., and Stork, A.L., 1979, Miocene low-K dacites and trondhjemites of Fiji, in Barker, Fred, ed., Trondhjemites, dacites, and related rocks: Amsterdam, Elsevier, p. 629-49.

Glover, Lynn, III, 1974, Speculations on the relations between eastern and western Piedmont vulcanism (abs): Geol. Soc. Am. Abs. w/ Prog., v. 6, no. 7, p. 757.

_____, Mose, D.G., Poland, F.B., Bobyarchick, A.R., and Bourland, W.C., 1978, Grenville basement in the eastern Piedmont of Virginia: implications for orogenic models: Geol. Soc. Am. Abs. w/ Prog., v. 10, no. 4, p. 169.

_____, and Sinha, A.K., 1973, The Virgilina deformation - a late Precambrian to early Cambrian orogenic event in the central Piedmont of Virginia and North Carolina: Am. J. Sci. Cooper v. 273-A, p. 146-63.

_____, Sinha, A.K., and Higgins, M.W., 1971, Virgilina phase (Precambrian and Early Cambrian?) of the Avalonian orogeny in the central Piedmont of Virginia and North Carolina (abs.): Geol. Soc. Am. Abs. w/ Prog., v. 3, no. 7, p. 581-82.

Gole, M.J., and Klein, C., 1981, High-grade metamorphic Archean banded iron-formations, Western Australia: Assemblages with coexisting pyroxene ± fayolite: Am. Min, v. 60, p. 87-99.

Good, R.S., Fordham, O.M., Jr., and Halladay, C.R., 1977, Geochemical reconnaissance for gold in the Caledonia and Pendleton quadrangles in the Piedmont of central Virginia: Va. Minerals, v. 23, no. 2, p. 14-22.

Grieve, R.A.A., and Fawcett, J.J., 1974, The stability of chloritoid below 10 kb Ph O: Jour. Petrol., v. 15, p. 113-39.

Gronvold, F., and Haraldson, H., 1952, On the phase relations of synthetic and natural pyrrhotites (Fe 1-X)S: Acta Chem. Scand., v. 6, p. 1452-69.

Gross, G.A., 1965, Geology of the iron deposits in Canada: General geology and evaluation of iron deposits: Geol. Surv. Can. Econ. Geol. Rpt. 22(1), 181 p.

_____ 1970, The depositional environment of principal types of Precambrian iron formation: Proceedings, Kiev Symp. Genesis of Precambrian iron and manganese deposits, UNESCO, p. 15-20.

_____ 1980, A classification of iron formation based on depositional environments: Cdn. Min., v. 18, p. 215-22.

Gwosdz, W., and Krebs, W., 1977, Manganese halo surrounding Meggen ore deposits, Germany: Trane Inst. Mining Metall. 86, B73-B77.

Hammarback, S., and Lindquist, B., 1972, The hydrothermal stability of annite in the presence of sulfur: Geol. Foren. Forh., 94, p. 549-564.

Harper, C.T., et al, 1973, The Arvonia Slate -- A useful standard for K-Ar dating (abs.): Geol. Soc. Am. Abs. w/ Prog., v. 5, no. 5, p. 402.

Hatcher, R.D., Jr., 1972, A development model for the southern Appalachians: Geol. Soc. Am. Bull, v. 83, p. 2735-60.

_____ 1978, Tectonics of the western Piedmont and Blue Ridge, southern Appalachians: Review and speculation: Am. Jour. Sci., v. 278, p. 276-304.

Hayman, R.M., and Kastner, M., 1981, Hot spring deposits on the East Pacific Rise at 21 N: Preliminary description of mineralogy and genesis: Earth Planet Sci. Lett., v. 53, p. 363-81.

Hellman, P.L., and Henderson, P., 1977, Are rare earth elements mobile during spilitization?, Nature, v. 267, p.38-40.

Henika, W.S., 1969, Geology of the Buckingham injection complex, Virginia: unpub. MS thesis, U. of Virginia.

_____ 1977, Geology of the Blairs, Mount Hermon, Danville, and Ringgold quadrangles, Virginia, with sections on the Triassic System by Thayer, P.A.: Va. Div. Min. Resources Pub. 2, 45 p.

Hermann, A.G., Potts, M.J., and Knake, D., 1974, Geochemistry of the rare earth elements in spilites from oceanic and continental crust: Contrib. Mineral. & Petrol., v. 44, 1-16.

Hickman, R.C., 1947, Pyrites, Mineral, Louisa County, Virginia: U.S. Bur. Mines Rpt. Inv. 4116, 3 p.

Higgins, M.W., 1972, Age, origin, regional relations, and nomenclature of the Glenarm Series, central Appalachian Piedmont -- A reinterpretation: Geol. Soc. Am. Bull., vol. 83, no. 4, p. 989-1026.

_____ et al, 1971, Correlation of the metavolcanic rocks in the Maryland, Delaware, and Virginia Piedmont (abs.): Geol. Soc. Am. Abs. w/ Prog., v. 3, p. 320-21.

_____ et al, 1977, U-Pb Zircon dates from the central Appalachian Piedmont -- A possible case of inherited radiogenic lead: Geol. Am. Bull., v. 88, no. 1, p. 25-32.

Hill, R.E.T., and Boettcher, A.L., 1970, Water in the earth's mantle: Melting curves of basalt-water and basalt-water-carbon dioxide: Science, v. 167, p. 980-81.

Hobbs, B.E., Means, W.D., and Williams, P.F., 1975, An outline of structural geology: New York, John Wiley & Sons, 571 p.

Hodder, R.W., Kazda, F.F., and Bojtos, P., 1977, A base metal massive sulphide deposit within a turbidite succession of the Virginia Piedmont: Callahan Mining Corp. unpub. rpt., 8 p.

Holden, R.J., 1905, The brown ores of the New River - Cripple Creek District, Virginia: U.S. Geol. Surv. Bull. 285, p. 190-93.

Hollister, L.S., 1966, Garnet zoning: An interpretation based on the Rayleigh fractionation model: Science, v. 154, p. 1647-51.

Hopkins, H.R., 1960, Geology of western Louisa County, Virginia: unpub. PhD. thesis, Cornell University.

Hughes, C.J., 1973, Spilites, keratophyres, and the igneous spectrum: Geol. Mag., v. 109, p. 513-27.

Humphries, S.E., and Thompson, G., 1978, Hydrothermal alteration of oceanic basalts by sea water: Geochem. Cosmochim. Acta 42, p. 107-24.

Hutchinson, R.W., 1973, Volcanogenic sulfide deposits and their metallogenic significance: Econ. Geol. 68, p. 1223-46.

_____, Fyfe, W.S., and Kerrich, R., 1980, Deep fluid penetration and ore deposition: Min. Sci. Eng., v. 12, no. 3, p. 107-20.

Immega, J.P., and Klein, C., Jr., 1976, Mineralogy and petrology of some metamorphic Precambrian iron-formation in southwestern Montana: Am. Mineral. 61, p. 1117-44.

Irvine, T.N., and Baragar, W.R.A., 1971, A guide to the chemical classification of the common volcanic rocks: Cdn. Jour. Earth Sci., v. 8, p. 523-47.

Ishizaka, K., and Yanagi, T., 1977, K, Rb, and Sr abundances and Sr isotopic composition of the Tonzowa granitic and associated gabbroic rocks, Japan: Low-potash island arc plutonic complex: Earth Planet Sci. Lett. 33, p. 345-52.

Jambar, J.L., 1979, Mineralogical evaluation of proximal-distal features in New Brunswick massive sulfide deposits: Cdn. Min., v. 17, pt. 3, p. 649-65.

Jefferson, Thomas, 1787, Notes on the State of Virginia, v. 6, p. 2.

Jensen, L.S., 1976, A new cation plot for classifying subalkalic volcanic rocks: Ontario Dept. Mines Misc. Pap. 66, 22 p.

Johnson, R.W., Mackenzie, D.E., and Smith, I.E.M., 1978, Volcanic rock association at convergent plate boundaries: Reappraisal of the concept using case histories from Papua, New Guinea: Geol. Soc. Am. Bull., v. 89, p. 96-106.

Johnson, S.S., 1981, Regional geophysics, in Geologic investigations in the Willis Mountain and Andersonville quadrangles, Virginia: Va. Div. Min. Resources Pub. 29, p. 9-16.

Jolly, W.T., 1972, Degradation (hydration) - aggradation (dehydration) and low-rank metamorphism of mafic volcanic sequences: 24th IGC sect. 2, p. 11-18.

Jonas, A.I., 1932, Geology of the kyanite belt of Virginia: Va. Geol. Surv. Bull. 38, p. 5-38.

Karig, D.E., 1971, Origin and development of marginal basins in the western Pacific: Jour. Geophys. Res., v. 76, p. 21-29.

Katz, A.S., 1961, The mineralogy of the Sulfur mine, Mineral, Virginia: unpub. MSc. diss., U.Va.

Kazda, R.F., and Hodder, R.W., 1978, Arminius mine, Louisa County, Virginia: Callahan Mining Corp. unpub. rpt.

Kerrich, R., 1980, Archean gold-bearing chemical sediments and veins: A synthesis of stable isotope and geochemical reactions, in Roberts, R.G., ed., Archean volcanic hosted gold deposits: Symp. March 1980, U. Waterloo, Ontario, p. 137-211.

_____ and Fryer B.J., 1981, The separation of rare elements from abundant base metals in Archean lode gold deposits: Implications of low water/rock source regions: Econ. Geol., v. 76, no. 1, p. 160-66.

_____ and Fyfe, W.S., 1981, The gold-carbonate association: Source of CO_2 and CO_2 fixation reactions in Archean lode deposits: Chem. Geol., 33, p. 265-94.

Kerrick, D.M., 1968, Experiments on the upper stability limit of pyrophyllite at 1.8 kb and 3.9 kb H_2O pressure: Am. Jour. Sci., v. 226, p. 204-14.

King, P.B., 1959, Tectonic framework of southeastern United Stated: Am. Assoc. Petrol. Geol. Bull., v. 34, p. 635-71.

Klein, C., 1969, Two-amphibole assemblages in the system actinolite-hornblende-glaucophane: Am. Min., v. 54, p. 213-37.

Kondakou, L.A., and Perunov, V. I., 1973, Origin of Tanzanian ferruginous quartzites illustrated by the Lupa gold field: Akad. Nauk. USSR Izv. Ser. Geol., no. 12, p. 136-38.

Krank, S.H., 1961, A study of phase equilibria in a metamorphic iron formation: Jour. Petrol., v. 2, pt. 2, p. 137-84.

Krauskopf, K., 1957, Separation of magnanese from iron in sedimentary processes: Geochim. Cosmochim. Acta, v. 12, p. 62-84.

Kretschmar, U., and Scott, S.D., 1976, Phase relations involving arsenopyrite in the system Fe-As-S and their application: Cdn. Min., v. 14, p. 364-86.

Kuno, H., 1960, High-alumina basalt: Jour. Petrol., v. 1, p. 121-45.

_____ 1966, Lateral variation of basaltic magma across continental margins and island arcs: Geol. Surv. Can. Pap. 66-15, p. 317-36.

_____ 1968, Differentiation of basaltic magmas, in Hess, H., and Poldervaart, A., eds., Basalts, v. 2, New York, Interscience John Wiley & Sons, p. 623-85.

Laird, J., 1980, Phase equilibria in mafic schist from Vermont: Jour. Petrol., v. 21, pt. 1, p. 1-37.

Lambert, I.B., and Wyllie, P.J., 1974, Melting of tonalite and crystallization of andesite liquids with excess water to 30 kilobars: Jour. Geol., v. 82, p. 88-97.

Leake, B.E., 1972, Garnetiferous striped amphibolites from Connemara, western Ireland: Min. Mag., v. 38, no. 298, p. 649-65.

_____ 1978, Nomenclature of amphiboles: Am. Min., v. 63, p. 1023-52.

Lehman, E., 1974, Spilitic magma: Characteristics and mode of formation, in Amstutz, G.C., ed., Spilite and spilitic rocks, New York, Springer Verlog, p. 23-38.

Lonsdale, J.T., 1927, Geology of the gold-pyrite belt of the northeastern Piedmont, Virginia: Va. Geol. Surv. Bull. 30, 110 p.

Lonsdale, P., and Lawver, L.A., 1980, Immature plate boundary zones studied with a submersible in the Gulf of California: Geol. Soc. Am. Bull., pt. 1, v. 91, p. 555-96.

Luttrell, G.W., 1966, Base and precious-metal and related ore deposits of Virginia: Min Res. Rpt. 7, 165 p.

Mack, T., 1965, Characteristics of the Everona Formation in Virginia: Va. Div. Min. Resources Circ. 10, 16 p.

Marr, J.D., Jr., 1981, Stratigraphy and structure, in Geologic investigations in the Willis Mountain and Andersonville quadrangles, Virgina: Va. Div. Min. Resources Pub. 29, p. 3-8.

McCollum, M.B., 1981, Triassic system, in Geologic investigations in the Willis Mountain and Anderrsonville quadrangles, Virginia: Va. Div. Min. Resources Pub. 29, p. 17-23.

Middleton, R.C., 1976, The geology of the Prieska copper mines: Econ. Geol., v. 71, p. 328-50.

Miller, J.W., 1978, The ore mineralogy of the Cofer property, Louisa County, Virginia: A volcanogenic massive sulphide deposit: unpub. MSc. diss., Va. Polytech. Inst. & State U.

Misch, P., and Rice, J.M., 1975, Progressive Skagit metamorphic suite, North Cascades, Washington: Jour. Petrol., v. 16, pt. 1, p. 1-21.

Mitchell, A.H.G., and Garson, M.S., 1976, Mineralization at plate boundaries: Min. Sci. Eng., v. 8, p. 129-69.

Miyashiro, A., 1975, Classification, characteristics, and origin of ophiolites: Jour. Geol. 83, p. 249-81.

_____, Shido, F., and Ewing, M., 1971, Metamorphism in the mid-Atlantic Ridge near 24 and 30 N: Phil. Tran. R. Soc. A268, p. 589-603.

Mueller, R.F., and Saxena, S.K., 1977, Chemical petrology; with application to the terrestrial planets and meteorites: New York, Springer-Verlog, 394 p.

Munha, J., Fyfe, W.S., and Kerrich, R., 1980, Adularia, the characteristic mineral of felsic spilites: Contrib. Mineral. & Petrol. 75, p. 15-19.

Naldrett, A.J., and Goodwin, A.M., 1977, Volcanic rocks of the Blake River Group Abitibi greenstone belt, Ontario, and their sulfur content: Cdn. Jour. Earth Sci., v. 14, p. 539-50.

Nason, F.L., 1894, Origin of the iron pyrites deposits in Louisa County, Virginia: Eng. Mining Jour., v. 57, 414-16.

Nelson, W.A., 1962, Geology and mineral resources of Albemarle County: Va. Div. Min. Resources Bull. 77, 92 p.

Nesbitt, R.W., and Sun, S.S., 1976, Geochemistry of Archean spinifex-textured peridotites and magnesium and low-magnesium tholeiites: Earth Planet Sci. Lett. 31, p. 433-53.

_____ and Purvis, K., 1979, Komatiites: Geochemistry and genesis: Cdn. Min: v. 17, p. 165-86.

Neuschel, S.K., 1970, Correlation of aeromagnetics and aeroradioactivity with lithology in the Spotsylvania area, Virginia: Geol. Soc. Am. Bull., v. 81, no. 12, p. 3575-82.

Nicholls, G.D., 1959, Autometasomatism in the lower spilites of the Builth volcanic series: Q. Jour. Geol. Soc. London, v. 114, p. 137-62.

Nicholson, P.M., 1980, The geology and economic significance of the golden dyke dome, Northern Territory: Proceedings Interntl. Uranium Symp. on the Pine Creek geocsyncline, p. 319-33.

Ntiamoah-Agyakwa, Y., 1979, Relationship between gold and manganese mineralization in the Birimian of Ghana, West Africa: Geol. Mag. 116(5), p. 345-52.

O'Connor, J.T., 1965, A classification for quartz-rich igneous rocks based on feldspar ratios: U.S. Geol. Surv. Prof. Pap. 525-B, p. B79-B84.

Odom, A.L., and Fullagar, P.D., 1973, Geochronic and tectonic relationships between the Inner Piedmont, Brevard Zone, and Blue Ridge belts, North Carolina: Am. Jour. Sci., v. 273-A, p. 133-49.

Page, C.E., 1981, B-zone deposit, Cullaton Lake district of Keewatin, NWT, in R.D. Morton, ed., Proceedings of the Gold Workshop, Yellowknife NWT, Dec. 1979.

Pardee, J.T., and Park, C.F., Jr., 1948, Gold deposits of the southern Piedmont: U.S. Geol. Surv. Prof. Pap. 213, 156 p.

Park, C.F., Jr., 1936, Preliminary report on gold deposits of the Virginia Piedmont: Va. Geol. Surv. Bull. 44, 42 p.

Papunen, H., Hakli, T.A., and Idman, H., 1979, Geological, geochemical and mineralogical features of sulphide-bearing ultramafic rocks in Finland: Cdn. Min., v. 17, p. 217-32.

Pavlides, Louis, 1976, Piedmont geology of the Fredericksburg, Virginia, area and vicinity, in Geol. Soc. Am. Guidebook for field trips 1 and 4, 44 p.

1980a, Revised nomenclature and stratigraphic relationships of the Fredericksburg Complex and Quantico Formation of the Virginia Piedmont: U.S. Geol. Surv. Prof. Pap. 1146, 29 p.

1980b, Piedmont tectonic features in Virginia, in Geological Survey Research: U.S. Geol. Surv. Prof. Pap. 1150, 258.

1981, The central Virginian volcanic-plutonic belt: An island arc of Cambrian (?) age: U.S. Geol. Surv. Prof. Pap., 1231-A, 34 p.

, Pojeta, John, Jr., Gordon, Mackenzie, Jr., Parsley, R.L., and Bobyarchick, A.R., 1980, New fossil and stratigraphic evidence for the Ordovician age of the Quantico Formation of Virginia and its regional implications: Geol. Soc. Am. Abs. w/ Prog., v. 12, no. 4, p. 204.

, Stern, T.W., Arth, J.G., Muth, K.G., Newell, M.F., and Cranford, S.L., 1979, Middle and Late Paleozoic plutonic suites in the Piedmont near Fredericksburg, Virginia: Geol. Soc. Am. Abs. w/ Prog., v. 11, no. 4, p. 208.

, Sylvester, K.A., Daniels, D.L., and Bates, R.G., 1974, Correlation between geophysical data and rock types in the Piedmont and Coastal Plain of northeast Virginia and related areas: U.S. Geol. Surv. Jour. Research, v. 2, no. 5, p. 569-80.

Pelletier, R.A., 1964, Mineral resources of south central Africa: Capetown, Oxford U. Press, 277p.

Perdery, W.V., 1979, Relationship of ultramafic amphibolites to metavolcanic rocks and serpentinites in the Thompson belt, Manitoba: Cdn. Min., v. 17, no. 2, p. 187-200.

Pereira, J., and Dixon, C.J., 1971, Mineralization and plate tectonics: Mineralium Deposita, v. 6, p. 404-405.

Plimer, I.R., 1977, The mineralogy of the high-grade metamorphic rocks enclosing the Broken Hill orebodies, Australia: N. Jb. Miner. Abh. 131, p. 115-39.

1978, Proximal and distal stratabound ore deposits: Mineralium Deposita, v. 13, p. 345-53.

Poole, J.L., 1974, Notes on some abandoned copper, lead and zinc mines in the Piedmont of Virginia: Va. Minerals, v. 20, no. 2, p. 9-14.

Popolitov, E.I., Filisofova, T.M., and Selivanova, G.I., 1973, Geochemical characteristics and genesis of plagiogranite intrusives in the western Sayan geosyncline: Geochem. Intntl, v. 10, no. 6, 1209-14.

Potter, M.J., 1975, Kyanite and related minerals, in Mineral facts and problems: U.S. Bur. Mines Bull. 667, p. 579-90.

Raase, P., 1974, Al and Ti contents of hornblende, indicators of pressure and

temperature of regional metamorphism: Contrib. Mineral. & Petrol. 45, p. 231-36.

Rankin, D.W., 1975, The continental margin of eastern North America in the southern Appalachians, the opening and closing of the proto-Atlantic Ocean, in Tectonics and mountain ranges: Am. Jour. Sci., v. 273-a, p. 298-336.

_____ et al, 1971, From the Blue Ridge anticlinorium to the Sauratown Mountains anticlinorium -- A major synclinorium and the Brevard fault zone: Geol. Soc. Am. Abs. w/ Prog., v. 3, no. 5, p. 343, and no. 7, p. 677.

Ridge, J.D., 1973, Volcanic exhalation and ore deposition in the vicinity of the sea floor: Mineralium Deposita, v. 16, p. 332-48.

Ridler, R.H., 1971, Analysis of Archean volcanic basins in the Canadian Shield using the exhalite concept (abs.): Cdn. Inst. Min. & Met. 64 (714), p. 20.

_____ 1973, Exhalite concept: a new tool for exploration: Northern Miner, Nov. 29, p. 59-61.

Robinson, P., Ross, M., and Jaffe, H.W., 1921, Composition of the anthophyllite-gedrite series, comparisons of gedrite-hornblende, and the anthophyllite-gedrite solvus: Am. Min. 56, p. 1005-41.

Rozendaal, A., 1978, The Gamsberg zinc deposit, Namaqualand, in Verwoerd, W.J., ed., Mineralization in metamorphic terranes: Pretoria, J.L. van Schiek, p. 235-65.

Russell, M.J., 1974, Manganese halo surrounding the Tynagh ore deposit, Ireland: A preliminary note: Trans. Instn. Min. Metall. 83, p. B65-66.

Rye, D.M., and Rye, R.O., 1974, Homestake gold mine, South Dakota, I. Stable isotope studies: Econ. Geol. 69, p. 293-317.

Sandhaus, D.J., 1981, Gahnite in metamorphosed volcanogenic massive sulfides of the Mineral districts, Virginia: unpub. MSc. diss., Va. Polytech. Inst. & State U.

Sarkar, S.E., Battacharyya, P.K., and Mukherjee, A.D., 1980, Evaluation of the sulphide ores of Saladipura Rajasthan, India: Econ. Geol., v. 75, p. 1152-67.

Sauer, R.T., 1980, Reevaluation of the Julia mine, Mineral District, Louisa County, Virginia: Callahan Mining Corp. unpub. rpt. 8 p.

_____ 1981, Field investigation of Virginian Piedmont gold occurrences: Callahan Mining Corp. unpub. rpt., 31 p.

Sawkins, F.J., 1976, Massive sulphide deposits in relation to geotectonics, in Strong, D.F., ed., Metallogeny and plate tectonics: Geol. Assoc. Can. Pec. Pap. 14, p. 221-40.

_____ and Rye, D.M., 1974, Relationship of Homestake-type gold deposits to iron-rich Precambrian sedimentary rocks: Trans. Inst. Mining & Metall. 83, p. B56-59.

Schwartz, E.J., and Fujiwara, Y., 1977, Komatiitic basalts from the Proterozoic Cape Smith Range in northern Quebec, in W.R.A. Baragar, L.C. Coleman, and J.M. Hall, eds., Volcanic regimes in Canada: Geol Assoc. Can. Spec. Pap. 16, p. 193-201.

Schmidt, R., 1981, Descriptive nomenclature and classification of pyroclastic deposits and fragments: Recommendations of IUGS Subcommission on the systematics of igneous rocks: Geol. v. 9, p. 41-43.

Scott, S.D., 1973, Experimental calibration of the sphalerite geobarometer: Econ. Geol., v. 68, p. 466-74.

_____ 1976, Application of sphalerite geobarometry to regionally metamorphosed terranes: Am. Min., v. 61, p. 661-70.

_____ 1980, Sulphide ironstones as a guide to massive sulphide ores: U. of Toronto Rpt. no. 12.

Scott, M.R., Scott, R.B., Rona, P.A., Butter, L.W., Nalwalk, A.J., 1974, Rapidly accumulating manganese deposit from the median valley of the Mid-Atlantic Ridge: Geophys. Res. Lett. vi, p. 355-62.

Seiders, V.M., and Wright, J.E., 1977, Geology of the Carolina volcanic slate belt in the Asheboro, North Carolina area: Geol. Soc. Am. Field Guide, Winston-Salem, NC, p. 1-34.

Simonian, O., and Gass, I.G., 1978, Arakapos fault belt, Cyprus: A fossil transform fault: Geol. Soc. Am. Bull., v. 89, p. 1220-30.

Smith, J.W., Milici, R.C., and Greenberg, S.S., 1964, Geology and mineral resources of Fluvanna County: Va. Div. Min. Resources Bull. 79, 62 p.

Smith, R.E., 1968, Redistribution of major elements in the alteration of some basic lavas during burial metamorphism: Jour. Petrol., v. 9, p 191-219.

Sohl, N.F., 1977, Stratigraphic Commission: Note 45 - Application for amendment concerning terminology for igneous and high-grade metamorphic rocks: Am. Assoc. of Petroleum Geol., v. 61, p. 248-52.

Southwick, D.L., Reed, J.C., Jr., and Mixon, R.B., 1971, The Chopawamsic Formation -- A new stratigraphic unit in the Piedmont of northeast Virginia: U.S. Geol. Surv. Bull. 1324-D, p. D1-D11.

Spear, F.S., 1980, The gedrite-anthophyllite solvus and the composition of orthoamphibole from the Post Pond volcanics, Vermont: Am. Min., v. 65, p. 1103-18.

Spooner, E.T.C., and Fyfe, W.S., 1973, Sub-seafloor metamorphism, heat and mass transfer: Contrib. Mineral. & Petrol. 42, p. 287-304.

Spooner, E.T.C., Beckinsale, P.D., English, P.C., and Senior, 1977, Hydration, ^{18}O enrichment and oxidation during ocean floor metabasic rocks from East Liguria, Italy: Geochim. Cosmochim. Acta, v. 41, p. 857-72.

Stanton, R.L., 1976, Petrochemical studies of the ore environment at Broken Hill, New South Wales: 3 - Banded iron formation and sulphide orebodies:

Constitutional and genetic ties: trans. Inst. Min. Metall. 85, p. B132-41.

Williams, K.L., 1978, Garnet compositions at Broken Hill, New South Wales, as indicators of metamorphic processes: Jour. Petrol., v. 19, p. 514-529.

St. Jean, Joseph, 1973, A new Cambrian trilobite from the Piedmont of North Carolina, in The Byron N. Cooper Volume: Am. Jour. Sci., v. 273-A, p. 196-216.

Stose, G.W., and Stose, A.J., 1948, Stratigraphy of the Arvonia Slate, Virginia: Am. Journ. Sci., v. 246, no. 7, p. 393-412.

Stumpfl, E.F., 1979, Manganese haloes surrounding metamorphic stratabound base metal deposits: Mineralium Deposita, v. 14, p. 207-17.

Sun, S.S., and Nesbitt, R.W., 1978, Petrogenesis of ultrabasic and basic volcanics: Evidence from rare earth elements: Contrib. Mineral. & Petrol. 65, p. 301-308.

Sweet, P.C., 1971, Gold mines and prospects in Virginia: Va. Min., v. 17, no. 3, p. 25-33.

____ 1980, Gold in Virginia: Va. Div. Min. Resources Pub. 19, 77 p.

____ 1981, Selected mineral resources, in Geologic investigations in the Willis Mountain and Andersonville quadrangle, Va. Div. Min. Resources Pub. 29, p. 70-75.

Taber, S., 1913, Geology of the gold belt in the James River basin: Va. Geol. Surv. Bull. 7, 271 p.

Tanaka, T., 1975, Geological significance of rare earth elements in Japanese geosynclinal basalts: Contrib. Mineral. & Petrol., v. 52, p. 77-106.

Tillman, C.G., 1970, Metamorphosed trilobites from Arvonia, Virginia: Geol. Soc. Am. Bull., v. 81, p. 1189-1200.

Tilton, G.R., Doe, B.R., and Hopson, C.A., 1970, Zircon age measurements in the Maryland Piedmont, with special reference to Baltimore Gneiss problems, in Fisher, G.W., et al, eds., Studies of Appalachian geology -- Central and southern: New York, Interscience, p. 429-34.

Thompson, A.B., 1976a, Mineral reactions in pelitic rocks: I. Predictions of T-T-X (Fe-Mg) phase relations: Am. Jour. Sci., v. 276, p. 401-24.

____ 1976b, Mineral reactions in pelitic rocks: II. Calculation of some P-T-X (Fe-Mg) phase relations: Am. Jour. Sci., v. 276, p. 425-54.

Tolbert, G.E., 1964, Geology of the Raposas gold mine, Minas Gerais, Brazil: Econ. Geol. v. 59, no. 5, p. 775-98.

Toulmin, P., III, and Barton, P.B., Jr., 1964, A thermodynamic study of pyrite and pyrrhotite: Geochim. Cosmochim. Acta, v. 28, p. 641-71.

Tremblay, L.P., 1976, Geology of the northern Contwoyto Lake area, District of Mackenzie: Geol. Surv. Can. Mem. 381, p. 1-54.

Trzcienski, W.E., Jr., 1977, Garnet zoning - a product of a continuous reaction: Cdn. Min., v. 15, p. 250-56.

Vallance, T.G., 1960, Concerning spilites: Proc. Linn. Soc. N.S.W. 85, p. 8-52.

_____ 1965, On the chemistry of pillow lavas and the origin of spilites: Mineral. Mag., v. 34, p. 471-81.

_____ 1969, Spilites again: Some consequences of the degradation of basalts: Proc. Linn. Soc. N.S.W. 94, p. 8-51.

_____ 1974, Spilitic degradation of a tholeiitic basalt: Jour. Petrol., v. 15, pt. 1, p. 79-96.

Valliant, R.I., and Barnett, R.L., 1982, Manganiferous garnet underlying the Bousquet gold orebody, Quebec: Metamorphosed sediment as a guide to gold ore: Cdn. Jour. Earth Sci., v. 19, no. 5, p. 993-1010.

Viljoen, M.J., and Viljoen, R.P., 1969, The geology and geochemistry of the lower ultramafic unit of the Overwacht Group and a proposed new class of igneous rocks, in The upper mantle project: Geol. Soc. S. Africa Spec. Pub. 2, p. 245-74.

Viljoen, R.P., and Viljoen, M.J., 1970, The geology and geochemistry of the layered ultramafic bodies of the Kaapmuiden area, Barberta Mountain Land: Geol. Soc. S. Africa Spec. Pub. 1, p. 661-93.

Wall, V.J., England, R.N., 1979, Zn-Fe spinel-silicate-sulphide reactions as sensors of metamorphic intensive variables and processes (abs.): Geol. Soc. Am. Abs. w/ Prog., v. 11, no. 7, p. 534.

Watson, T.L., 1905, Lead and zinc deposits of Virginia: Va. Geol. Surv. Bull. 1, 156 p.

_____ and Powell, S.L., 1911, Fossil evidence of the age of the Virginia Piedmont slates: Am. Jour. Sci., v. 31, p. 33-44.

Whitehead, R.E., 1973, Environments of strataform sulphide deposition: Variation in Mn:Fe ratio in host rocks at Heath Steele Mine, New Brunswick: Mineralium Deposita 8, p. 148-60.

Whitney, J.A., Paris, T.A., Carpenter, R.H., and Hartley, M.E., III, 1978, Volcanic evolution of the southern slate belt of Georgia and South Carolina: A primitive oceanic island arc: Jour. Geol., v. 86, no. 2, 173-192.

Williams, Harold, compiler, 1978, Tectonic lithofacies map of the Appalachian orogen: Newfoundland Memorial U. Map 1, 2 sheets, scale 1:1,000,000.

_____ and Hatcher, R.D., Jr., 1982, Suspect terranes and accretionary history of the Appalachian orogen: Geology, v. 10, p. 530-36.

Williamson, H.C., and Barr, D.J., 1970, Gold mineralization in the Yilgarn goldfield, in McAndrew, J., ed., Geology of Australian Ore Deposits, 2nd ed.: 8th Commonwealth Mining and Metallogeny Congress, p. 87-94.

Wilson, J.T., 1966, Did the Atlantic close and re-open?: Nature, 211, p. 676-681.

Winkler, H.G.F., 1976, Petrogenesis of metamorphic rocks (rev. 4th ed.): New York, Springer-Verlag, 334 p.

Wolery, T.J., and Sleep, N.H., 1976, Hydrothermal circulation and geochemical flux at mid-ocean ridges: Jour. Geol., v. 84, p. 249-75.

Woodsworth, G.J., 1977, Homogenization of zoned garnets from pelitic schists: Cdn. Min., v. 15, p. 230-42.

Woodtli, R., 1961, Gold impregnation deposits in the Moto area (central Africa): Econ. Geol., v. 56, p. 603-607.

Wright, J.E., and Seiders, V.M., 1980, Age of zircon, from volcanic rocks of the central North Carolina Piedmont and tectonic implications for the Carolina volcanic slate belt: Geol. Soc. Am. Bull., v. 91, pt. 1, p. 287-94.

_____, Sinha, A.K., Glover, Lynn, III, 1975, Age of zircons of the Petersburg Granite, Virginia, with comments on belts of plutons in the Piedmont: Am. Jour. Sci., v. 275, no. 7, p. 848-56.

Yoder, H.S., and Tilley, C.E., 1962, Origin of basalt magmas: An experimental study of natural and synthetic rock systems: Jour. Petrol., v. 3, p. 342-69.

Young, R.S., 1981, Sulfide zones, in Geologic investigations in the Willis Mountain and Andersonville quadrangles, Virginia: Va. Div. Min. Res. Pub. 29, p. 17-47.

Yund, R.A., and Hall, H.T., 1969, Hexagonal and monoclinic pyrrhotites: Econ. Geol., v. 64, p. 420-23.

Zymela, S., 1979, Location of ore shoots in tabular massive sulphide bodies -- primary or secondary?: unpub. BSc diss., U. Western Ontario.

7. APPENDIX A

Nomenclature System Used for Classifying Schists

A.1 Terminology

It is difficult to classify schists in volcanic-sedimentary terranes not only because the metamorphic overprint masks precursor lithologies to varying degrees but also because the classification of lithology of mixed volcanic-sedimentary parentage is inherently problematic. The terminology for mixed pyroclastic-epiclastic rocks has historically received considerable attention by volcanologists, and the recent report by Schmidt (1981) on the recommendations of the IUGS subcommission well summarizes the current consensus on the descriptive nomenclature and classification of volcaniclastic deposits. In contrast to this, the significant role that may be played by syndepositional hydrothermal activity not only in effecting widespread alteration but also in chemically modifying surface environments over volcanic-related geothermal zones has only relatively recently become recognized. A formal descriptive nomenclature for rocks derived wholly or in part through chemical precipitation from hydrothermal brines -- and therefore unclassifiable in terms of traditional volcanic or chemical sedimentary categories -- has consequently not yet received any sort of official sanction.

Since the early seventies, hydrothermal rocks have popularly been known as volcanic exhalites (Ridler 1971, 1973), a strictly genetic designation emphasizing their origin through exhalative volcanic processes. Unfortunately, exhalative volcanism has itself never been formally defined. Presumably it broadly encompasses all hydrothermal emanations whether or not these occur in terranes given to actual volcanic extrusive activity. On strictly semantic grounds there is nevertheless some question about the appropriateness of applying an essentially volcanogenic classification to what could just as easily be considered a special class of chemical sediment. Judging by recent usage, the controversy is far from resolved. Inasmuch as work on these rocks to date has generally shown or assumed a close genetic association with volcanism, however, this author favours adoption of the "exhalite" label at least on a provisional basis.

The problems do not end here. As there is no formal subdivision of exhalites in existence, differentiation of varying types can only be done on an ad hoc basis by adding such adjectives as cherty, pyritic, etc. Also, the specific relationship between exhalites and the long-recognized iron formation class of deposits has not yet been adequately elucidated. Before one can even approach the problem of exhalite classification, in fact, it is necessary to critically assess the genetic processes involved.

Disregarding such complexities as the source and composition of the hydrothermal fluids which on discharge comprise exhalative volcanism,

exhalite deposits may be defined as those that form by direct precipitation from such fluids. The main limiting factor for exhalite formation is thus the amount of interaction that can take place between any given exhaled fluid and seawater before the former loses identity. If chemical precipitation occurs immediately on expulsion prior to dilution or if there is little chemical communication between the hydrothermal brines and the seawater due to such physiochemical variants as density and/or temperature contrasts, then the resultant precipitation would form an exhalite deposit. If, on the other hand, there is wholesale dilution, the resultant precipitate, deriving from a hydrothermally modified marine environment rather than stemming directly from hydrothermal fluid, is not strictly speaking an exhalative precursor. Such precipitates as the latter type could be expected to comprise lithologies transitional in nature between exhalites and normal chemical sedimentary rocks. In cases where there has been a great deal of dilution or, conversely, where a large volume of seawater has been modified by the hydrothermal fluid, they could also be expected to have the broad lateral extension characteristic of chemical sediments. The best known examples of this transitional-type lithology are those broadly recognized as belonging to the iron formation family.

For the purposes of the present investigation the definition of "iron formation" is deemed to be that adopted by Gross (1965, p 83): "all stratigraphic units of layered, bedded, or laminated rock that contains 15 percent or more iron, in which the iron minerals are commonly interbanded with quartz, chert, or carbonate, and where the banded structure of the ferruginous rocks conform in attitude with the structure of adjacent sedimentary, or volcanic rocks." Following Scott (1980), rocks lithologically similar to this but containing lower percentages of iron -- those conventionally designated as "lean iron formation" -- have herein, for ease of reference, been labelled as "ironstones." Both iron formation and ironstone in the present study area are, however, considered to be genetically linked. According to Gross's strictly descriptive formula, iron formation may be volcanic or sedimentary in origin -- derived through chemical precipitation, clastic deposition, or wholesale replacement of originally layered rocks by iron minerals during diagenesis or during a later period in their history -- but unless there is evidence to the contrary all ironstone-iron formation deposits cited in this thesis are assumed to be products of chemical precipitation. Although not genetically delimited by definition, in other words, these particular ironstone-iron formation lithologies are considered to be specifically intermediary between volcanic exhalites and normal chemical sediments.

Stipulating a continuous spectrum like this not only aids petrogenetic interpretation but also solves some of the terminological problems posed by the study area. Assuming a link between exhalites and ironstone-iron formation, one may also assume the propriety of applying the same subdivisional principles to both classes. Iron formations have traditionally been differentiated generally according to facies (oxide, carbonate, silicate, and sulphide) and specifically according to mineralogical content and textural criteria. For present purposes exhalites are deemed to be meaningfully subdividable along exactly the same lines.

In practice, of course, application of this rule is somewhat more difficult than it sounds in theory. In many cases, origin is enigmatic. Hydrothermal systems not only modify chemical environments on the surface but may effect varying intensities of alteration in the subsurface setting as well. Whether a given species of rock was produced through hydrothermal

alteration of a pre-existing lithology or through hydrothermal emanation may be impossible to determine, particularly where exposure is poor. Indeed, subsurface alteration and surface exhalation may actually overlap at the rock/water interface to give rise to a lithology that stems in part from a presursor and in part from primary exhalative elements. Such a convergence might be most apt to occur during diastemes in surface volcanic and sedimentary activity when the rock/water interface would remain at the same statigraphic position for a considerable time. In the present study in cases where such a complex genesis is a possibility or where the specific origin of a rock is in doubt, a general descriptive terminology such as chloritite, marl, ferruginous pelite, aluminous quartzite, and so on, has been utilized in preference to the term "exhalite."

Aside from the categorization of chemical precipitates, there is one other aspect of the nomenclature used in this thesis that would seem to require some explanation. Because of their rarety, classification systems for ultramafic volcanics have not yet been well worked out. Although the term "komatiite" has long been used in reference to the ultramafic lavas of Archaean greenstone belts (Viljoen and Viljoen 1969, 1970); more recently, other varieties of ultramafic lava, especially those from Phanerozoic ophiolite terranes, have also been referred to as komatiites in the literature (Gale 1973, Simonian & Gass 1978). Although one might argue with Sun and Nesbitt (1978) that the geochemical differences between ultramafic lavas from ophiolitic complexes and greenstone belts militates against using the komatiite label for the former, the objection is in practical terms counterproductive inasmuch as no other terminology exists for ultramafic compositions. The term "boninite" is unhelpful since this rock type, which is generally recognized as having the chemistry of a high magnesian andesite (Cameron et al 1979), only overlaps compositionally with the basaltic end of the ultramafic spectrum. In any case the recent work of Cameron et al (1979) indicates that the terms boninite and basaltic komatiite are essentially synonymous. Accordingly, due to the lack of alternatives, just as basalt is used as a blanket term for mafic volcanics, komatiite is used herein as a general cognomen for ultramafic members of any volcanic suite.

A.2 Classification System

In order to classify rocks of mixed pyroclastic-epiclastic-exhalative parentage the terminology for mixed pyroclastic-epiclastic rocks advocated by Schmidt (1981) was extended to include chemical precipitates. A classification system with these three components as end members is shown in Figure A-1. The subdivision of the pyroclastic-epiclastic spectrum is essentially that of Schmidt with the additional differentiation of tuffite into dominantly pyroclastic and dominantly epiclastic types. Like the pyroclastic and epiclastic deposits, exhalites are restricted to less than 25% impurity; lithology comprising 25-50% impurity is designated as tuffaceous exhalite. A more detailed general classification for mixed pyroclastic-epiclastic-chemical precipitates, again a modified version after the scheme of Schmidt, is shown in Table A-1.

Other terminological problems had to be dealt with more informally. Metamorphic rocks posed particular difficulties. Since the primary aim of this study was the accomplishment of a specifically genetic interpretation, it was considered necessary that the names adopted for lithological subdivision should as far as possible reflect the original character of the

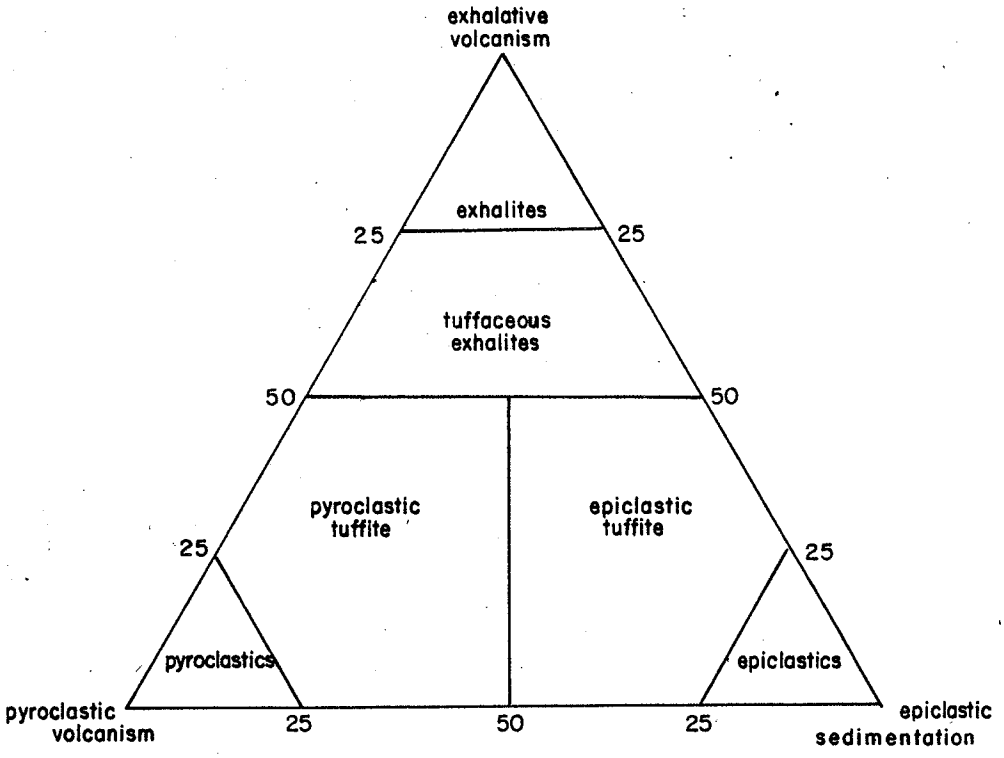

Figure A-1: Subdivision of Mixed Pyroclastic- Epiclastic- Exhalative Deposits

Table A-1: Nomenclature for Rocks of Mixed

Pyroclastic-Epiclastic-Chemical Precipitate Origin

Chemical Precipitates

exhalite (Ex) iron formation (Fe fm) ironstone (Festn) chemical sediment

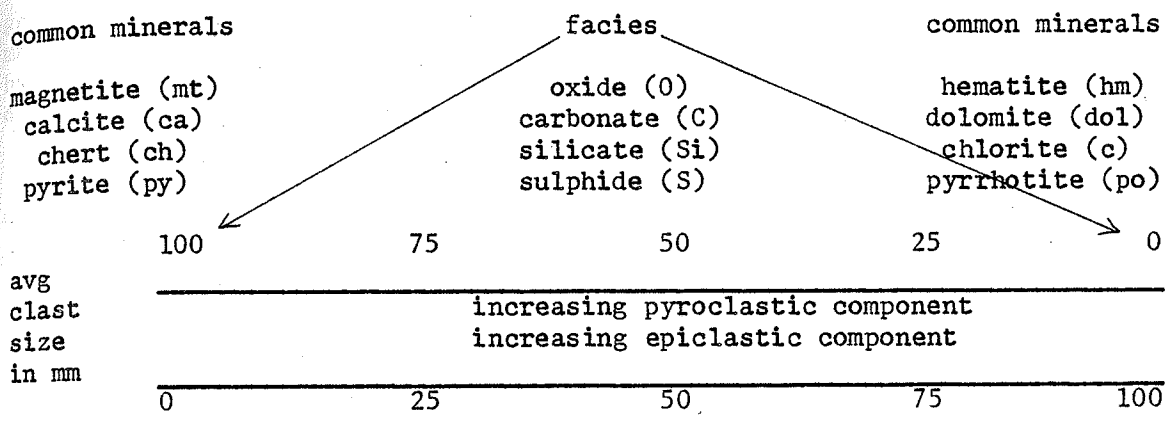

1/256 dust tuff (dt) shaley tuff (Sht) tuffaceous shale (tSh) shale (Sh)

1/16 fine tuff (t) silty tuff (stt) tuffaceous siltstone (tSt) siltstone (St)

2 coarse tuff (t) sandy tuff (Art) tuffaceous arenite (tAr) arenite (Ar)

64 lapilli tuff (lt)

agglomerate (agl) volcanic conglomerate (vCgl) conglomerate (Cgl)
breccia (bx)

terranes under examination. This, however, is a question that conventional metamorphic terminology quite fails to address. Different members assigned to given species on the basis of similar mineralogy may in fact be derived from decided different progenitors. A single primary rock type, conversely, can form numerous differing metamorphic lithologies depending on the conditions to which it is subjected. The resultant ambiguities render "blanket" classifications -- like "gneiss" or "schist" -- singularly inadequate for the full elucidation of metamorphic terranes. During the field stages of the current project an effort was therefore made to identify rock types not only in terms of conventional metamorphic categories but -- utilizing all available evidence from bedding characteristics through remnant textures to petrographic and petrochemical data -- according to original pre-metamorphic lithology as well. These complex preliminary determinations were then selectively simplified to provide a concise, sensitive, genetically-oriented system of notations suitable for regional-scale mapping. Under this system a facies of quartz-sericite schist identified as having had a rhyolitic precursor (qsS/Rt) will, for instance, be designated on the map simply as metarhyolite tuff, or Rt.

8. APPENDIX B

Systematic Description of Lithologies

		Page
B.1	Candler Formation	8-1
B.2	Hardware Magnesian Schists	8-2
B.3	Mafic Intrusive Complexes	8-3
	a) Buckingham Complex	8-3
	b) Diana Mills Complex	8-5
	c) Green Springs Complex	8-7
B.4	Greenstones	8-8
B.5	The Palmyra Metavolcanic Suite	8-10
	a) Metarhyolites	8-10
	b) Felsite Sills	8-12
	c) Metadacites	8-13
	d) Meta-andesites	8-13
B.6	The Mineral Metavolcanic Suite	8-14
	a) Epiclastic Metasediments	8-15
	b) Metavolcanics	8-15
	c) Ironstones	8-21
	d) Hydrothermal Chloritite	8-27
	e) Intrusive Bodies	8-30
B.7	The Diverse Upper Chopawamsic Group	8-32
	a) Lithologies Capping the Palmyra Assemblage	8-32
	b) Regionally Extensive Lithologies Capping the Mineral Metavolcanic Suite	8-37
	c) Regionally Restricted Lithologies Capping the Mineral Metavolcanic Suite	8-41
	d) The Diverse Upper Chopawamsic Intrusive Facies	8-50
B.8	Post-Volcanic Metashale Formations	8-54
	a) Basal Silicate Facies Iron Formation	8-54
	b) Metashales	8-57
B.9	The Eastern Plutonic Terrane	8-58
	a) Amphibolitic Orthogneiss	8-59
	b) Feldspathic Paragneiss	8-61
	c) Granitic Orthogneiss and Associated Granitoid Intrusive Material	8-62
B.10	Triassic Rocks	8-63
	a) Farmville Basin	8-63
	b) Diabase Dykes	8-63

B.1 Candler Formation

Along its eastern margin this formation is characterized by monotonous thinly layered (mm to cm scale) micaceous paper schists. These schists are locally interbedded with thin (meter scale) layers of fine-grained micaceous quartzite and, more rarely, medium-grained feldspar-bearing schist with remnant clastic textures. The dominating micaceous paper schists are particularly susceptible to chemical weathering and outcrops are virtually lacking except along deeper creek gorges. Where fresh the paper schists are lustrous, fissile, very fine-grained, light grey to green coloured rocks. The common mineral assemblages include sericite + chlorite + quartz $\pm$ albite $\pm$ calcite. The uniform sized (.05 mm in the a-direction) sericite and chlorite form well aligned phyllosilicate-rich layers that alternate with very fine (.02 mm polygonal quartz laminae. Smith et al (1964) discovered that submicroscopic biotite is evident in most x-ray scans, indicating a greenschist facies metamorphic overprint near the biotite isograd. Pyrite and magnetite form common 1-2 mm idioblasts that preferentially occur along chlorite-rich laminae.

The thin impure quartzite beds show gradational contacts with bordering paper schist, and these occur where there is a marked increase in quartz over phyllosilicate. These siliceous units are generally slabby, very fine-grained, grey-green to cryptocrystalline light grey rocks. Quartz overgrowths on detrital quartz and feldspar clasts were noted by Smith et al (1964). Subtle grading within 2-5 cm beds was observed by Henika (1969) and noted by Conley (1978). The characterizing minor well aligned sericite and chlorite ranges from .01-.1 mm in the a-direction and slight modal variations define a subtle compositional layering. Pyrite idioblasts up to 2 mm and trace to minor amounts of patchy calcite accompanies the most siliceous layers.

Very occasionally medium-grained, poorly sorted (1 to 3 mm sized grains), clastic textured, grey-green to olive green chlorite + feldspar + quartz $\pm$ sericite $\pm$ calcite schists form massive moderately foliated beds up to a few meters thick. Brown (1969) noted that this lithology is characterized by a discrete quartz, plagioclase (An 5-15) and rare microcline grains embedded in a matrix of fine chlorite, sericite, and quartz. The matrix chlorite and minor sericite grains are less than .5 mm in their a-direction, and both are moderately well aligned even where dispersed along grain boundaries of polygonal quartz $\pm$ calcite. Pyrite idioblasts (.05-.5 mm) occur occasionally as a trace constituent.

The provenance of the Candler schists poses a major problem as no lithic clasts have yet been discovered even in the coarser grained facies. The dominating chloritic and sericitic paper schists and the transitional impure quartzite could possibly stem from montmorillonitic, illitic, and siliceous pelite respectively. Although there is little ostensible grading apart from the micrograding observed in fine-grained quartzose schist by Henika (1969) and Conley (1978), such fine grading of pelitic precursors could easily be lost during metamorphic recrystallization. The medium-grained clastic textured

schist lithology has been broadly identified as metagreywacke by Hopkins (1960), Brown (1969), and Ern (1968). It therefore seems likely that much of the succession probably had a turbiditic mode of deposition. However, a distal volcanic source for very sericite-rich and chlorite-rich facies of paper schist cannot be ruled out (Conley 1980, personal communication). If volcanic, the impure quartzite intervals transitional with the paper schists could conceivably reflect periods of diminished tuffaceous supply resulting in siliceous shale. Considerable more study will be needed to definitively document the origin of the Candler schists but at present the general lithological constitution along the eastern margin suggests basinal sediments deposited distally from a terrigenous source area which may or may not have been volcanically active.

B.2 Hardware Magnesian Schists

The magnetite-bearing magnesian schists coring the Hardware arch have been deeply weathered; thick red lateritic soils prevail over most of the area this schist facies underlies. Where freshest the rock typically comprises non-stratified, silvery grey to dark grey-green, multiply foliated talc + chlorite + mica schist. The characteristic red weathering is due to omnipresent fine disseminations and occasional idioblasts (up to 1 cm) of magnetite. The common quartz veins hosted in the Hardware schists typically define tight minor fold noses, and granulated and boudinauged quartz stringers demonstrate intense shearing along fold limbs subsequent to quartz vein generation. The quartz veins are locally bordered by massive pale yellow-blue serpentine hosting glomeric knots of muscovite.

Modal analyses of several typical examples of the magnesian schist are given in Table B-1. As indicated, the Hardware schists are mineralogically variable but dominantly consist of a talc - Mg chlorite - white mica - magnetite assemblage with local enrichments in phlogopite and accessory porphyroblastic tremolite and epidote. Characteristically these rocks exhibit crisscrossing wavy foliae of talc, Mg-chlorite and/or phlogopite bounding 1-3 mm lensoidal microdomains that have striking variations in both composition and texture. Domains consisting of a finely (.1 mm) foliated talc - white mica matte dominate and these occasionally demonstrate delicate microfolding outlined by very fine (.05 mm) magnetite laminae. In the area of microfold noses so defined the micaceous minerals have locally recrystallized to slightly coarser (.5 mm) lepidoblastic textures. Domains rich in pale brown phlogopite and pale green chlorite are more restricted and these typically host disseminated magnetite. Chlorite commonly defines discrete 1-2 mm chaotically deformed (2-4 mm) lenticules. Talc and chlorite occasionally form .5-2 mm rounded polycrystalline masses which could possibly stem from retrogressive breakdown of original olivine or pyroxene. Very rarely chlorite forms a near-monomineralic lithology consisting of a homogenous matte of .02-.1 mm feathery chlorite hosting well aligned 1 mm acicular tremolite porphyroblasts. Finely schistose quartz - white mica domains occasionally intercalated within mafic mineral dominated domains could indicate the sites of original feldspar. Epidote occurs occasionally as patchy disseminations that tend to concentrate along chloritic laminae.

Quartz constitutes more than 10 percent of most handsamples but generally occurs as microveining or as cataclastic grains derived from granulation of original quartz veins. In thin section finely polygonized quartz stringers can be observed to transit into domains where granulated quartz clasts are

Table B.1 : Modal Analysis of Hardware Schists

	Fe 2-6	Fe 7-1	Fe 11-7	Fe 17-2	Zc - 15	D32
talc	-	30	30	40	50	-
Mg-chlorite	95	10	-	10	8	-
white mica	-	25	-	20	10	5
phlogopite	-	5	25	-	-	-
tremolite	3	-	-	-	-	-
serpentine	-	-	-	10	-	95
epidote	-	5	-	-	2	-
chromite	-	tr	-	tr	-	-
magnetite	2	5	20	10	10	-
quartz	-	15	25	10	20	tr
zircon	-	-	-	-	tr	-

intercalated within mafic schist domains. This indicates that at least one episode of cataclastic deformation postdated quartz vein generation. The phlogopite content is slightly greater in domains where quartz vein material is mixed with mafic schist, suggesting that phlogopite may have also originated during deformation. Interestingly, both the phogopite and chlorite in these domains commonly show pleochroic haloes, indicating included zircon. Pale yellow serpentine locally forms near-monomineralic masses along the borders of the larger quartz veins. These masses consist of 1 cm globular segregations of ultra-fine serpentine with minor included white mica. These globules rimmed by coarser (.2-1.5 mm) platy aggregates of muscovite and lesser serpentine hosting scattered angular 5-15 mm quartz vein fragments. The occurrence of near-monomineralic serpentine segregations on quartz vein borders might point to a generation of quartz veins during desilication with the massive serpentine being residual material left after extreme silica removal into veins.

There is no readily apparent textural evidence remaining to reveal the initial parentage of the Hardware magnesian schist in the limited number of thin sections studied. The ultra-fine talc - Mg chlorite - white mica - magnetite paragenesis is interpreted to be phyllonitic in origin and considering the composition most likely to result from the breakdown of original mafic to ultramafic igneous rock.

B.3 Mafic Intrusive Complexes

Three intrusive complexes occur just west of that part of the Chopawamsic metavolcanic belt covered by this investigation. The southerly Buckingham complex and northerly Green Springs complex are only partially within the map area but the central Diana Mills complex, occurring along the crest of the Hardware arch, lies wholly within the map area, and this particular body recieved the most attention by the writer. All three intrusions from gently rolling little dissected upland typified by dendritic drainage systems. The characterizing mafic igneous rock decomposes to brown-grey granular soils that are easily distinguished from the red-coloured micaceous soils developed over country rock schists. Saprolitic exposures along stream valleys retain their igneous textures and even subtle lithological changes are often accentuated by weathering. Because of their homogenous nature the igneous bodies have weathered spheroidally, resulting in the widespread occurrence of large rounded boulders which afford relatively fresh rock for petrological study.

a) Buckingham Complex

The southerly Buckingham complex, underlying a 100 square km area about 10 km west of Dillwyn, has been the best studied of the these complexes to date. Previous investigations by Ern (1968) and Henika (1969) delineated two adjacent hornblende metagabbro bodies, each consisting of numerous thin (10-100 meter scale) mafic sills intruded conformably with primary layering in the country rock schist. Both sills and bordering schist have been subject to the same structural deformation during the regional metamorphic overprint. The sills consequently provide useful marker horizons in the otherwise monotonous schist series. Despite the overprinting, however, the primary igneous layering and textures in these rocks are generally well preserved. Pervasive metamorphic fabrics are restricted to sill borders and to crosscutting shear zones. The igneous mineralogy, on the other hand, has undergone considerable modification,

Table B.2: Modal Compositions of Representative Samples of the Various Facies in the Buckingham Complex (selected from Henika 1969)

	1	2	3	4	5	6
quartz	-	-	-	1	1	26
plagioclase	-	-	4	2	14	35
K-fedspar	-	-	-	-	-	4
olivine	30	-	-	-	-	-
hypersthene	60	20	-	1	-	-
augite	-	42	1	1	-	-
hornblende	-	35	85	65	25	-
biotite	-	-	-	5	21	19
chlorite	-	2	7	-	-	-
talc	-	-	tr	-	-	-
muscovite	-	-	-	1	10	-
epidote	-	-	1	12	31	7
allanite	-	-	-	tr	tr	6
sphene	-	tr	tr	2	1	tr
apatite	-	-	-	tr	tr	tr
zircon	-	-	tr	-	tr	tr
opaques	10	tr	2	tr	tr	2

1. Metaperidotite
2. Metapyroxenite
3. Hornblende Metagabbro
4. Metagabbro
5. Metadiorite
6. Biotite Quartz Diorite

making specific classification of original rock types difficult. Ultramafic compositions occur both as individual sills up to several hundred meters in width and as thin (1-10 m) basal layers to rythmically layered (cm to m scale) metagabbro. Volumetrically, metagabbro constitutes the primary igneous facies and typically forms the main zones of well differentiated sills grading from basal metapyroxenite through hornblendic metagabbro to upper hornblendic metadiorite. Leucocratic granophyre segregations occur locally within the upper parts of many sills. Biotite quartz diorite occurs as thin (1-10 m) discontinuous dykes that crosscut all other igneous facies as well as migmatic injection zones peripheral to the main complex. Modal variations, summarized from Henika (1969), for these various intrusive facies are listed in Table B-2; the main petrographic features shown by each are briefly outlined below.

The ultramafic facies includes well foliated talc - Mg chlorite - actinolite - magnetite $\pm$ carbonate schist devoid of igneous textures but is typified by medium to coarsely granular metaperidotite and hornblende metapyoxenite. The metaperidotite exhibits well preserved 1-10 mm rounded completely serpentinized cumulus olivine grains outlined by magnetite and poikilitically enclosed in intercumulus uralitized hypersthene. The coarsest olivine grains occasionally demonstrate reaction rims now altered to talc. The orthopyroxene has been more or less completely replaced by fibrous amphibole but remnant grains have the optical properties of hypersthene. The metapyroxenites, which constitutes the more abundant ultramafic rock type, also demonstrate cumulus textures. The more ultramafic compositions characteristically have euhedral clinopyroxene and rounded serpentinized olivine suspended in uralitized intercumulus pyroxene now consisting of platy hornblende, fibrous amphibole, and chlorite mixtures. The large (2-10 mm) hornblende grains preserve relict Schiller structure and the compositional zoning from original hypersthene, but a few grains have remnant augite cores. It is impossible to discern the original proportion of clinopyroxene to orthopyroxene, as both have contributed to the hornblende content. The less ultramafic compositions commonly have euhedral hypersthene forming an interlocking crystal mesh with angular interstices filled with augite and plagioclase. Feldspar-bearing metapyroxenites are also difficult to classify as the calcic plagioclase has been pervasively saussuritized during the metamorphic overprint. Remnant normally zoned laboradorite with core-to-rim variation from An63 to An54 was the most calcic plagioclase observed. Accessory minerals in the ultramafic compositions include apatite, sphene, and magnetite. An apparent increase in the abundance of granular sphene typically accompanies the intensification of chloritization of original pyroxene.

Compositional layering on the cm-m scale is characteristic of the main metagabbro zones of the sills. Crystal grading (15-5 mm over 2 m in extreme cases) commonly accompanies layering and is indicative of gravitational settling. The main zones commonly show the transition from a thin (1-10 m) layer of metapyroxenite at the base through mesocratic medium to coarse-grained metagabbro to hornblende metadiorite near the top. The most abundant rock type consists of plagioclase and amphibole occurring in well developed subophitic textures defined by 4-8 mm saussuritized andesine laths crosscutting the boundaries of interlocking uralitized pyroxene. With increase in plagioclase (andesine, oligoclase, and albite species are all present) textures become hypidiomorphic granular. Primary igneous hornblende occurs in coarsely granular to pegmatitic layers where 1-1.5 cm hornblende grains poikilitically encloses plagioclase and relict pyroxene. The uppermost parts of well differentiated sills become increasingly feldspathic, giving rise to hornblende metadiorite compositions consisting of tabular hornblende intergrown with subhedral plagioclase and anhedral biotite. The well defined hypidiomorphic

textures transit into gneissic textures near the upper contact with country rock schist. The main metagabbro - metadiorite fractions are noticeably richer in minor and accessory minerals compared to the ultramafic facies. Epidote, clinozoisite, calcite, and chlorite accompany the albitization of plagioclase and trace minerals include apatite, zircon, ilmenite, and magnetite.

Granophyric segregations are widespread in the uppermost parts of well differentiated sills and where most concentrated, granophyre forms net veins and zones of intrusive breccia. The granophyre consists of fine (1 mm) sugary textured albite, muscovite, microcline, orthoclase, and quartz with accessory fibrous amphibole, epidote, and magnetite. The most volumetrically significant concentration of late acid fractions, however, occurs as lit-par-lit injections into country rock schist peripheral to the mafic sills. Biotite quartz diorite dominates. Zones and layers of granodiorite do occur, although these have never been differentiated during mapping. The igneous textures manifested by late differentiates vary with rock composition from hypidiomorphic granular biotite quartz diorite rich in normally zoned andesine to allotriomorphic granular granodiorite rich in quartz and alkali feldspar. The feldspar-rich quartz diorite concentrated along the southern margin is commonly flow banded, with the andesine and microcline laths oriented during injection. The dominant mafic phase, brown pleochroic biotite, increases in abundance towards the contacts with bordering schist. As a result, quartz biotite gneiss is a common intermediary lithology developed between the igneous injections and country rock schists. The accessory minerals occurring in the late felsic fractions include epidote, clinozoisite, and allanite; zircon and magnetite are also present locally.

b) Diana Mills Complex

The central Diana Mills complex, underlying a 30 square km area 8 km west of Arvonia south of the James River, is the smallest of the three complexes. Inasmuch as it has never been investigated in the detail which the Buckingham complex has, its lithological makeup remains poorly defined. Its elliptical shape was defined by Brown (1969), and its outside borders are broadly concordant with the dominant foliation in the enveloping Hardware schist. The complex was identified by Brown as being a rootless hornblende metadiorite intrusive including undifferentiated hornblendite, metaperidotite, serpentinite and aplite subfacies. Individual sills have not yet been delineated but the writer observed that the Diana Mills complex has many features in common with the Buckingham complex. Although composed primarily of intrusive material the area as mapped includes large screens and interlayers of Hardware magnesian schist which could be septa between different sills. Rythmic layering is not as pronounced in the main hornblende metadiorite facies as it is in the metagabbro of the Buckingham complex, but widespread layering due to modal variation in plagioclase and hornblende is evident. Although no well differentiated sills with ultramafic bases and feldspathic tops were observed, an ultramafic facies is dominant at the north and south ends of the complex, and late acid fractions occur both as local aplitic segregations and as quartz diorite injection gneisses east of the main intrusive body. Modal analyses of several samples from the Diana Mills complex are listed in Table B-3; the petrographic features of the various subfacies are outlined below.

The ultramafic facies is typically a drab green, medium to coarse-grained (3 mm-1 cm) metaperidotite composed of coalescing rounded serpentinized olivine clusters poikilitically enveloped in interlocking, moderately chloritized

Table B.3: Modal Analyses of Samples From the Diana Mills Complex

	1	2	3	4	5	6	7
	A124-1	A124-6	A127-1	A127-2	A127-3	D22	A144-3
plagioclase	25	20	50	25	10	65	-
albite	5	-	-	-	-	10	-
epidote/zoisite	15/	4/	8/	15/	10/8	-	-
white mica	20	3	7	3	3	tr	-
hornblende	25	70	25	-	10	10	-
pyroxene	-	-	-	15	50	-	20
olivine	-	-	-	-	-	-	75
uralite actinolite/ tremolite	-	-	-	20/15	50	-	/5
chlorite	5	2	10	-	-	3	5
talc	-	-	-	-	3	-	-
serpentine	-	-	-	-	-	-	63
sphene	-	-	-	1	tr	-	-
quartz	5	-	-	-	4	10	-
biotite/ phlogopite	-	1/	-	/2	/2	-	-
chromite	-	-	-	-	tr	-	5
magnetite	-	-	-	-	-	2	2
zircon	-	-	-	tr	-	-	-

☐ mineral completely pseudomorphed by alteration products

1. porphyritic metadiorite
2. hornblende metagabbro
3. metadiorite
4. orbicular metagabbro
5. uralized pyroxene metagabbro
6. metadiorite
7. metaperidotite

augite and hypersthene. The olivine grains are pseudomorphed by radiating antigorite and minor patchy tremolite, and original grain boundaries are everywhere outlined by magnetite. platy talc occasionally occurs at the boundaries between olivine and the intercumulus pyroxene, perhaps signifying original reaction rims.

The dominant intrusive facies is a modally variable, green-white spotted, inequigranular to porphyritic textured rock with a medium-grained (2-4 mm) hypidiomorphic granular groundmass of subhedral interlocking plagioclase (An30) and dark green hornblende hosting coarse (to 1 cm), normally zoned (An30-40) rounded plagioclase phenocrysts. Locally the groundmass plagioclase and hornblende manifests a graphic texture that may indicate that it crystallized near a eutectic composition. Quartz occurs as a trace to minor component interstitial to the plagioclase and hornblende. The groundmass plagioclase shows incipient alteration to sericite and epidote, and locally exhibits vermiform quartz intergrowths near grain margins. The andesine phenocrysts are pervasively altered to sericite, epidote (concentrated at the cores) and patchy albite. Though typically dark green, the hornblende grains occasionally have yellowish rims, indicating that rim compositions were modified during the metamorphic overprint.

Although a subtle layering is generally discernible in the dominant porphyritic metadiorite due to modal variation in plagioclase and hornblende contents much more striking compositional layering on the cm to m scale is evident locally. Melanocratic layers consisting of coarse (8 mm), rounded hornblende grains bordered by fine-grained (.2-.4 mm) subhedral to anhedral plagioclase (An33) can be quite common. Near monomineralic layers consisting of .5 mm subhedral hornblende with minor interstitial dark brown biotite are much less common. Rarely, original pyroxene cleavage can be discerned in these amphibole-rich facies but no remnant pyroxene was identified. Locally the mafic and felsic minerals have more or less completely segregated. In these areas orbicular structured uralite is crosscut by white aplite stringers and veins. The 1-3 cm orbicules are typically zoned with Schiller-textured hypersthene cores and sieve-textured actinolite-chlorite rims that host droplet inclusion trains of albite and epidote. Tremolite locally forms a patchy cleavage-controlled replacement within the core pyroxene and occasionally these same centers have also been replaced by epidote. The white aplite vein material is a fine-grained (1 mm) sugary textured rock composed of plagioclase (An15) with minor quartz and accessory muscovite.

Sills of metaperidotite, metagabbro and quartz metadiorite occur well east of the main Diana Mills complex where the effects of the regional metamorphic overprint are more evident. The ultramafic facies here is generally intensely sheared and typically consists of a dense fine-grained talc - actinolite - chlorite - magnetite schist devoid of remnant igneous textures. The metagabbro is moderately well foliated, consisting typically of a heteroblastic polygonal assemblage of plagioclase, hornblende, and trace to minor quartz. Two generations of plagioclase are generally discernible: (1) primary .5-1 mm lobate grains of andesine (An35) with common deformation twins and crossgrain microfractures, and (2) secondary .5-.8 mm sinusoidal-shaped grains of albite (An5) with polysynthetic albite twins free of deformation effects. The green-brown pleochroic hornblende occurs as .2-.5 mm inclusion-free idioblasts. The felsic quartz diorite facies which is a common lithology assocated with the peripheral sills is typically a white, fine to medium-grained, hypidiomorphic granular rock composed essentially of 1-3 mm lath-shaped plagioclase (andesine, oligoclase and albite are all present) and minor anhedral quartz. Biotite, epidote, clinozoisite, and muscovite occur as

common accessories. The amount of biotite increases markedly in gneissic-textured border zones developed near contacts with country rock schists.

c) Green Springs Complex

The northern Green Springs intrusive complex, underlying an 80 square km area east of Louisa is a massive triangular igneous body that for the most part occurs northwest of the map area. To date this body has been neither mapped nor studied in much detail, and the only information available on it is contained in Hopkins' thesis (1960). Hopkins identifies it as a metadiorite intrusive stock composed dominantly of leucocratic hornblende diorite and syenodiorite but noted that more mafic hypersthene-bearing and more acid granodiorite facies were present as well. The hypersthene-bearing melanocratic facies occupies local interior zones while the more granitic fractions comprise the northeastern part of the intrusion and form sills along the eastern margin. Modal analyses of the various rock types are listed in Table B-4, and the petrographic features of the main intrusive facies are outlined below.

The dominant buff to green-white mottled, medium-grained (2-3 mm) metadiorite consists of approximately equal proportions of subhedral hornblende and plagioclase (An15) and these minerals form a strongly interlocking hypidomorphic granular texture. Occasionally this even-grained lithology constitutes the groundmass to 5-10 mm hornblende phenocrysts, thereby giving rise to a porphyritic textured subfacies. The original igneous mineralogy is commonly prevasively overprinted by a fine (.05 mm), sericite - chlorite - epidote - sphene alteration assemblage but original igneous textures are generally discernible. With the loss of hornblende and increase in microcline and orthoclase content dioritic compositions transit into syenodiorite composed dominantly of lath-shaped plagioclase (An12) that may be either randomly oriented or well aligned. The strong crystal alignment demonstrated locally is indicative of primary magma flowage at an advanced crystal mush stage of crystallization. The minor interstitial material in the syenodiorite comprises anhedral quartz with trace amounts of associated epidote, sphene, chlorite, apatite and zircon.

Volumetrically less important facies closely associated with the main diorite-syenodiorite facies includes both more mafic and more granitic compositions. Coarse-grained dark green biotite hypersthene metagabbro consists of allotriomorphic granular hornblende, hypersthene, brown biotite, and trace feldspar. This facies forms localized zones within the intrusion as well as 5-20 cm-thick schlieren within hornblende-rich and porphyritic metadiorite. Fine-grained leucogranodiorite composed of subhedral plagioclase (An 10), anhedral quartz, and microcline with minor biotite and muscovite, and trace pyrite occurs as white bands in medium-grained syenodiorite. The medium to coarse, inequigranular to porphyritic granodiorite facies comprising the northeastern part of the intrusion (outside the map area) as well as sills along the eastern edge consists of 4-10 mm grains of euhedral albite and microcline togheter with hetergeneously distributed aggregates of anhedral black biotite and hornblende in a medium-grained (2-3 mm) allotriomorphic granular feldspathic groundmass rich in quartz. Minor minerals in the porphyritic granodiorite facies include epidote, chlorite, and muscovite, and traces include apatite, sphene, and pyrite.

Table B.4: Modal Analyses of Samples From the Green Springs Complex 1 - 6 from Hopkins (1960)

	1	2	3	4	5	6	7	8
hornblende	40	48	75	20	36	5	15	50
hypersthene	-	-	-	30	-	-	-	30
plagioclase	48	32	12	15	26	55	45	-
K-feldspar	1	9	-	5	18	20	-	-
quartz	1	2	6	20	13	18	-	-
epidote	6	2	4	2	2	1	8	-
biotite	tr	-	-	1	2	1	-	10
chlorite	2	tr	-	-	2	-	15	3
muscovite	tr	3	1	-	tr	tr	15	2
apatite	1	tr	tr	1	tr	tr	-	-
zircon	-	tr	-	-	-	-	-	-
sphene	tr	1	1	1	tr	-	2	tr
pyrite	tr	tr	3	5	tr	-	tr	tr

1. coarse-grained metadiorite
2. even-grained syenodiorite
3. metadiorite
4. hypersthene metadiorite
5. granodiorite
6. granodiorite
7. metadiorite (ZC-37-9)
8. biotite metagabbro (ZC-37-13)

B.4 Greenstones

Greenstone bodies cluster near the borders of the mafic intrusive complexes and along the contacts between Hardware magnesian schist with westerly Candler metasediment and easterly Chopawamsic metavolcanics. The latter contact is the site of the large Shores greenstone striking the length of Palmyra quadrangle. Occasionally greenstone beds occur well within Candler metasediments, however. As they also form the basal units and thin members within the Chopawamsic metavolcanics it seems evident that the mafic volcanism which gave rise to the greenstones overlapped with both Candler sedimentation and Chopawamsic volcanism.

The greenstones are mainly composed of fine-grained to aphanitic dark green-yellow mottled, massive but heterogeneous, spilitized metabasalt. The more mafic compositions are moderately to well foliated. Amygdaloidal facies are occasionally observed, and these have quartz - epidote - calcite filled vesicles but are otherwise much like the dominating massive non-amygdaloidal type. Though pillow structures were tentatively identified at one location in the large greenstone unit east of Shores, such features are extremely rare. Some of the greenstone bodies are decidedly more siliceous (keratophyric) but apart from this aspect appear to be petrographically similar to the more common mafic variety. Rather thick units of tough well-banded, light yellowish green epidosite (an apidote - albite - quartz assemblage) are occasionally affiliated with the more siliceous keratophyric facies. Locally, as in the Shores body, pods and vein stockwork segregations of massive albitite (an albite-quartz assemblage) is hosted within massive greenstone. Only very rarely does this latter facies form discrete interlayers.

Modal analysis of several representative samples of the greenstone suite are listed in Table B.5. As shown by their respective modal compositions the metaspilites are essentially composed of actinolite, epidote, and albite, with minor quartz. The metakeratophyres are modally variable, particularly in epidote and quartz, and also show a significant decrease in the amount of modal actinolite relative to the metaspilites. The albitites consist mainly of albite and quartz but show minor epidote and chlorite impurity.

The metaspilites are dense, dark green-yellow mottled, moderately well foliated, fine-grained (.5 mm) to aphanitic rocks consisting of parallel oriented (.2-1 mm) columnar actinolite and minor (.1-.2 mm) lepidoblastic flakes of biotite interleaved with .3 mm granular epidote and finely (.1 mm) polygonal albite and minor quartz. The common occurrence of biotite indicates metamorphic conditions near the biotite isograd; the garnet observed in one sample is considered due to local growth of a spessartine-rich species well below the almandine isograd. A subtle compositional banding (mm scale) is locally evident with modal variation in actinolite and epidote, and the bands richer in epidote are also commonly richer in polygonal albite and quartz. Minor pale grey birefringent chlorite and anomalous blue zoisite and trace white mica are characteristically disseminated throughout. The actinolite occurs as slightly larger (1-1.2 mm) tabular porphyroblasts subparallel to foliation, and pale green chlorite develops in pressure shadows where actinolite crosscuts foliation at a high angle. The epidote distribution is everywhere heterogeneous and sphene and iron-titania oxides occur where the patchy epidote disseminations are more concentrated. Commonly the epidote concentrations have annealed to form coarsely crystalline nodules which may have ilmenitic cores and/or occur as radial epidote - sphene - ilmenite clusters. Rarely such clusters adjoin along foliation to give rise to peculiar

Table B.5: Modal Analysis of Greenstone Suite

	1	2	3	4	5	6	7	8
	A158-1	Sh-6	D36-3	D36-1	D176-2	D173-3	Sh-4	A-51
albite	15	25	25	5	20	15	83	60
actinolite	30	45	50	15	20	-	-	-
quartz	5	5	5	20	55	15	15	30
epidote	35	20	15	50	4	55	2	1
zoisite	5	-	-	8	-	-	-	-
chlorite	10	-	tr	-	-	10	-	8
biotite	-	5	5	-	-	2	-	-
white mica	-	-	-	-	-	2	-	.5
garnet	-	-	-	1	-	-	-	-
sphene	tr	tr	tr	-	-	1	tr	-
ilmenite	-	-	tr	-	-	-	-	-
magnetite	-	-	-	1	1	-	-	-
calcite	-	-	-	-	-	-	-	.5

1 spilite
2 spilite
3 spilite
4 keratophyre
5 keratophyre
6 epidosite
7 quartz keratophyre
8 quartz keratophyre

bead-like chains. Numerous epidote veinlets, which are sometimes bordered by albite and quartz, transect the foliated assemblage.

The metakeratophyres are typically grey-green, fine-grained (.5-1 mm) rocks which generally show a subtle compositional layering defined by 1-2 mm bands variously rich in actinolite, epidote, albite, and quartz. Typically, decussate-textured actinolitic laminae alternate with polymineralic heteroblastic polygonal domains of epidote, albite, quartz, and magnetite. Equilibrium textures are developed locally between albite and quartz. The albite (An5-8) exhibits both pericline and albite twinning. The actinolite also forms columnar poikiloblasts including quartz and chlorite. Minor epidote granules (2 mm) and fine (1 mm) magnetite grains are disseminated throughout but show a preference for the laminae richer in actinolite. The metakeratophyres are very heterogeneous in places, comprising intertonguing lenses of granular epidote and polymineralic domains of actinolite, quartz, albite, and magnetite. The polymineralic domains are typically finer grained (.2 mm) and appear to be invaded by coarser epidote.

Locally, massive yellow-mottled epidosite forms discrete beds which demonstrate a remarkable heterogeneity in both texture and mineral distribution. This heterogeneity results primarily from the segregation of epidote into rounded masses (up to 1 cm) within a heteroblastic polygonal matrix of quartz, chlorite, zoisite, biotite, muscovite, and sphene. These segregations may be pure or include varying amounts of quartz and albite; all types show epidote-depleted coronas. The polymineralic matrix is typified by microdomainal clustering of the various constituents within a finely (.1 mm) polygonized quartz-albite matrix. Chlorite forms .5 mm sheaves, epidote forms .1 mm granular clusters (commonly with associated sphene), and muscovite and biotite form lepidoblastic knots. In domains where foliation fabrics prevail chlorite laths and dimensionally oriented quartz interleave.

Where least metamorphosed the albitites are massive, white, fine to medium-grained (1-1.5 mm), allotriomorphic granular rocks consisting almost solely of alkali-feldspar and quartz myrmekite. More typically, however, this lithofacies occurs as a strongly polygonized albite-quartz assemblage exhibiting strongly sutured grain boundaries, indicating that these minerals were highly reactive during the metamorphic overprint. The original feldspars include albite (An5) and patch antiperthite. The polygonal albite grains commonly show both albite and pericline twinning, often contain strain-induced subgrains, and are generally incipiently altered to sericite along cleavage. Minor chlorite and sericite form spotty segregations. Epidote granules (.1-.3 mm) commonly occur intergranular to albite and quartz, locally forming aggregates with sphene and zoisite or, like calcite, discontinuous microveinlets.

The various lithologies comprising the greenstones collectively constitute a metamorphosed spilite - keratophyre - quartz keratophyre volcanic suite. The textures and mineralogy reflect a mid-greenschist metamorphic overprint near the biotite isograd, and this has eradicated original igneous textures. Notably, the metamorphic fabric has also overprinted preexisting microdomainal mineralogical heterogeneity, indicating that this feature is pre-metamorphic in origin.

B.5 The Palmyra Metavolcanic Suite

Modal analyses of samples representative of the various facies of the Palmyra metavolcanics are listed in Table B.6. As demonstrated, the various extrusive facies include metarhyolitic pyroclastics and flows, felsite sills, metadacitic pyroclastics, and meta-andesitic pyroclastics and flows. The greenstone units are most common near and at the western border, but these also occur interlayered with metadacites from Dillwyn quadrangle southward. As this particular facies is lithologically similar to the greenstones described in the last section, however, they are henceforth not separately treated. Apart from this, the petrographic characteristics of the Palmyra metavolcanics are covered facies by facies in the subsections that follow.

a) Metarhyolites

The Palmyra assemblage is primarily constituted of a thinly (1-10 cm scale) layered succession of weakly metamorphosed, fine to very fine-grained felsic tuffs. Along the western border the series is composed dominantly of well foliated sericitic phyllites commonly interlayered with thin (10-100 m), massive, blocky, bone white to pink, aphanitic felsite beds. Where most fine-grained the phyllitic facies is megascopically not unlike the sericitic metapelite of the Candler metasediments to the west. However, regularity of banding, absence of interlayered metasedimentary material of more diverse composition, and association with the felsite sills are considered to signify a volcanic derivation.

The only area demonstrating appreciable rhyolitic flow material discovered during the mapping occurs in the vicinity of Mountain Hill 5 km. southwest of the town of Palmyra. This area is typified by a series of low monadnocks caused by the physical resistance of these dense, white, conchoidally fracturing aphanites to weathering. The flows exhibit subtle light and dark grey flow banding, and locally moderate hydrothermal alteration has resulted in the occurrence of dark green chlorite as incipient patches and as coatings on fracture surfaces. The rhyolitic flow material commonly interfingers with grey-green crystal tuffs which show evidence of moderate reworking prior to lithification.

Petrographically the metarhyolite tuffs comprise a texturally varied group of uniformly banded to laminated, weakly porphyritic, pink-buff-weathering, light grey-green aphanites with common microphenocrysts. The matrix is consistently composed of a cryptocrystalline to very fine-grained (.01-.05 mm) quartz-alkali feldspar mosaic in which the feldspars are pervasively sericitized and occasionally epidotized. This assemblage is host to both alkali feldspar and quartz phenocrysts as well as polycrystalline feldspar-quartz phenocryst clusters. The alkali feldspar phenocrysts typically occur as rounded .5-1 mm tabular grains consisting of patch perthite and antiperthite with the latter generally dominating. The quartz phenocrysts are of a similar size and are always anhedral, commonly occurring as polycrystalline quartz eyes. Both the alkali feldspars and quartz phenocrysts may show embayments indicative of magmatic resorption. Typically the alkali feldspar phenocrysts are incipiently saussuritized with albite (An5) and occasionally microcline occurring as patchy remnants in the ultrafine epidote alteration.

The polycrystalline phenocrystic clusters occasionally coalesce to form relatively discrete, 2-4 mm monogenetic lithic inclusions which may be as common as isolated phenocrysts in some samples. The clusters are consistently

Table B.6: Modal Analysis of Palmyra Metavolcanics

	1	2	3	4	5	6	7	8	9	10	11	12	13	14	15	16	17	18	19	20	21	22	23	24
	C-1	LI-2	A74-1	A80-1	Co27b	C48	A56-1	A56-2	A171	D37	Fe13-1	Zc-2	Zc-32	Co2b	Co32a	Co32b	Pa5	A40	A42	A43-1	CV55-133'	CV58-324'	Zc24a	Zc19d
plagioclase	-	50	30	30	60	63	-	-	-	-	-	-	-	-	-	-	-	-	-	-	-	-	-	-
albite	35	-	-	-	-	-	-	-	-	-	-	-	-	-	-	-	-	-	-	-	-	-	-	-
alkali feldspar	-	-	-	-	-	-	40	50	40	72	65	65	20	45	40	25	55	27	55	55	50	70	-	-
amphibole	40	40	40	65	22	30	-	-	-	-	-	-	-	-	-	-	-	-	-	-	-	-	-	-
epidote	3	5	20	2	3	3	25	25	20	8	-	-	-	15	-	30	5	-	tr	-	-	5	-	-
quartz	20	5	-	-	10	3	35	25	30	15	35	32	75	25	40	20	27	63	40	30	45	20	60	70
sericite	-	-	30	-	-	-	-	-	15	10	-	3	4	7	20	15	3	10	2	10	5	5	39	30
chlorite	-	-	5	3	-	-	-	-	2	-	-	-	-	7	-	10	-	-	-	5	-	-	-	-
uralite	-	-	5	-	-	-	-	-	-	-	-	-	-	-	-	-	-	-	-	-	-	-	-	-
biotite	-	-	-	-	-	-	-	-	1	-	-	-	-	-	-	-	-	-	3	-	-	-	-	-
sphene	-	tr	tr	-	-	-	-	-	1	-	-	-	-	-	-	-	-	-	-	-	-	-	-	-
zircon	-	tr	-	-	-	-	-	-	-	-	-	-	-	-	-	-	-	-	-	tr	tr	-	-	-
calcite	-	-	-	-	-	-	-	-	-	-	-	-	-	1	-	1	-	-	-	-	tr	-	-	-
ilmenite	-	-	tr	-	-	-	-	-	1	-	-	-	-	-	tr	tr	-	-	-	-	-	-	-	-
hematite	-	-	-	-	-	-	-	-	-	tr	-	-	1	-	-	-	-	-	-	tr	-	-	-	-
magnetite	2	-	-	-	5	1	-	tr	-	-	-	-	-	-	-	-	-	-	-	-	-	-	-	-
pyrite	-	-	-	-	-	-	-	-	-	-	tr	-	-	-	-	-	-	-	-	-	-	-	1	tr

Greenstone
1 spilite

Mafics
2 amphibolite basalt
3 basaltic andesite
4 basaltic andesite
5 porphyritic andesite crystal tuff
6 andesite accretionary lappilli tuff

Dacites
7 dacite crystal tuff (25% Ph)
8 dacite crystal tuff (20% Ph)
9 dacite crystal tuff (12% Ph)

Felsites
10 porphyritic felsite (10% Ph)
11 felsite
12 sericitized felsite
13 siliceous felsite

Rhyolites
14 rhyolite crystal tuff (12% Ph)
15 rhyolite flow (1% Ph)
16 rhyolite flow (2% Ph)
17 rhyolite crystal lithic tuff (7% Ph, 8% lith)
18 porphyritic rhyolite flow (10% Ph)
19 reworked rhyolite crystal lithic tuff (20% clst, 10% Ph, 10% lith)
20 reworked rhyolite crystal tuff (20% clst, 10% Ph)
21 rhyolite tuff (5% Ph)
22 rhyolite lithic lappilli tuff (5% Ph, 5% lith)
23 rhyolite dust tuff
24 rhyolite dust tuff

☐ mineral pseudomorphed by alteration products

composed of antiperthite laths intergrown with anhedral quartz. Significantly, although relatively discrete, these clusters never show well defined fragment outlines, which indicates that they originated through coalescing of phenocrysts in the magma prior to eruption rather than by fragmentation of precrystallized rock. The feldspathic component of the clusters is typically pervasively sericitized and epidotized.

The occasional .2 mm euhedral zircon grains in some samples might also represent a microphenocryst phase. More generally, however, this characterizing accessory occurs as very fine (.05 mm) rounded grains sparsely scattered throughout, appearing to have crystallized at the same time as the matrix alkali feldspar-quartz assemblage.

The coarser metarhyolite crystal tuffs commonly bear evidence of moderate sedimentary reworking. Where reworked the matrix material is subtly layered with slightly finer (.05 mm) and coarser (1 mm) grained bands. The matrix hosts moderate amounts of unsorted .1-.5 mm angular quartz and alkali feldspar crystal fragments with the quartz clasts typically making up about twice the modal amount of feldspar. The matrix hosts moderate amounts of sericite aligned parallel to the compositional layering, and near-monomineralic sericite laminae, interleaved with quartz seams, occur between coarse and fine fractions.

Light grey, delicately laminated sericite phyllites are more regionally extensive than the crystal tuffs and dominate along the most westerly part of the Palmyra assemblage. It is difficult to assess the degree to which this particular facies has been reworked subsequent to eruption. These phyllites exhibit .5-.8 mm laminae variously rich in quartz and sericite. The quartzose laminae are composed of .2 mm granoblastic polygonal quartz grains and the sericite laminae of well aligned sericite microlites interleaved with polygonal quartz. Generally there is a compositional transition between adjacent laminae such that the two variants are completely gradational one to the other. This petrographic feature is interpreted to signify that the lamination resulted from the settling of very fine pyroclastic debris in an aqueous medium. Alkali-feldspar or quartz phenocrysts are observed very occasionally, but where they occur these .5-1 mm anhedral grains disrupt the regular lamination-foliation fabric. Trace amounts of fine (.5-1 mm) pyritic cubes are characteristically disseminated throughout this water-lain dust-tuff facies.

The areally restricted rhyolitic flow facies comprises dense pink to greenish white aphanites composed essentially of a cryptocrystalline alkali feldspar-quartz groundmass. The subtle flow lamination observed megascopically is best defined in thin section by delicate saussurite laminae. The cryptocrystalline groundmass is host to common euhedral to subhedral alkali feldspar and subhedral to anhedral quartz phenocrysts. The alkali feldspar phenocrysts are most typically an antiperthite species hosting subgrain domains of patch perthite. Locally the alkali feldspar phenocrysts have secondary perthite overgrowths, indicating that the potassium component of the original high temperature Na-K feldspar species was susceptible to metamorphic recrystallization. The subhedral quartz phenocrysts commonly exhibit embayments indicative of igneous resorption; the few anhedral types, which are generally eye-shaped, may be polycrystalline with subgrain boundaries intricately sutured. As with the crystal tuffs, the alkali-feldspar and quartz phenocrysts tend to cluster, but well defined fragments were not observed.

Both tuffs and flows show the effects of a moderate metamorphic overprint. The quartzo-feldspathic groundmass may show strong optical orientation, and

both sericite microlites and very fine (.1 mm) ragged albite laths hosted in the groundmass lie in the plane of optical layering. Sericite may form discrete foliae, thereby imparting a spaced foliation fabric. This mineral also concentrates locally in the pressure shadow of phenocrysts. In the massive flows sericite foliae bound lenticular quartzo-feldspathic domains, indicating that the flows deformed rather brittly. Where such foliae are most intense, quartz forms discontinuous, finely (1 mm) polygonal quartz vein stockworks within the sericite. The alkali feldspar phenocrysts in most samples exhibit strain-induced recrystallization, and the quartz phenocrysts characteristically exhibit strain shadows and microfracturing. Minor green biotite accompanies sericite defining foliation fabrics in the reworked crystal tuffs. Calcite was observed forming large (2 mm) sieve poikiloblasts including polygonized quartz and alkali-feldspar in one sample.

Further petrographic aspects affecting the massive flows and, though less commonly and to a lesser degree, the tuffaceous units are those resulting from hydrothermal alteration. The effects of such alteration are particularly evident in outcrops where the light coloured metarhyolite is transected by a stockwork of rusty-weathering dark green chlorite, epidote, and quartz veinlets. Thin sections of hydrothermally altered rock show fine (.5 mm) curvilinear hairline fractures coated variably with mono or polycrystalline chlorite, epidote, quartz, and, more rarely, calcite transecting the quartzo-feldspathic groundmass. Where this same hydrothermal paragenesis has pervaded the rock mass, the fine-grained alkali feldspar-quartz assemblage may be partly or wholly replaced by a very delicate spherulitic textured matte of chlorite - epidote - sericite and pyrite. More commonly, the alteration results in patchy disseminations of chlorite and/or epidote, and locally these have further aggregated to form poorly developed nodular segregations with central chlorite sheaves rimmed by granular epidote or, more rarely, with intimately intergrown epidote and pyrite rimming quartz cores. The alkali feldspar phenocrysts in hydrothermally altered domains are incipiently kaolinized and have chlorite altered rims. Notably, pyrite is a ubiquitous trace constituent in altered domains, most typically affiliated with chlorite, but also accompanying the discontinuous quartz stringers that both crosscut and parallel the weak foliation fabrics defined by sericite.

b) Felsite Sills

Thin (10-100 m), blocky-fractured, buff-weathering, white felsitic sills are commonly interlayered within the westerly phyllitic dust tuff facies of the Palmyra assemblage. These felsitic units are lithologically quite distinct from the extrusive lithologies just described. The felsites comprise ultrafine (.01 mm) cryptocrystalline quartz and alkali feldspar which only rarely hosts microphenocrysts (.1-.5 mm) of equant to rounded microcline with diagnostic crosshatched twinning, simple twinned orthoclase, tabular albite, and, very rarely, .5 mm euhedral quartz phenocrysts and/or anhedral quartz eyes. Both the euhedral quartz and quartz eyes may show groundmass embayments indicative of magmatic resorption. Where the metamorphic overprint has been least intense both the feldspathic groundmass and the feldspar phenocrysts demonstrate incipient alteration to randomly oriented sericite microlites and patchy epidote. Where the metamorphic overprint has been stronger the sericite microlites align to define foliation fabrics. Where strongly deformed the felsites are saccharoidal in handspecimen and consist of a fine (.3 mm) granoblastic polygonal assemblage of quartz and untwinned alkali feldspar. Polygonized quartz microveinlets, hosting disseminated hematite and border by

hematite-stained sericite, accompany pervasively polygonized assemblages.

c) Metadacites

East of the Long Island isocline the Palmyra pyroclastics show a marked change in facies to a more intermediate composition. Metarhyolite tuffs similar to those just described are in the minority, giving way to more chloritic and/or biotitic compositions and more coarsely porphyritic textures. These metadacites are typically massive, thickly banded (metre scale), yellowish grey-green to buff porphyritic aphanites consisting of a fine (.05-.1 mm) mosaic of anhedral albite and quartz with varying minor amounts of platy chlorite as matrix materal. The matrix feldspar shows varying degrees of saussuritization, and the alteration epidote has a tendency to segregate into rounded polycrystalline aggregates. This assemblage commonly hosts a bimodal phenocryst population. The larger (1-4 mm) phenocrysts are rather uniform (typically 1-2.5 mm) within any given band and the largest sizes are restricted in occurrence. The large oligoclase (An 8-15) phenocrysts occur as broken euhedrons showing moderate normal zonation. Their cores are altered to epidote and in rare cases the epidote alteration shows delicate concentric rings, indicating initial oscillatory zoning. These oligoclase grains also often exhibit strain-induced exsolution to patch antiperthite. The larger anhedral quartz grains are typically broken fragments of original eye-shaped forms, and these are moderately polygonized with subgrain boundaries typically sutured. The micro-phenocrysts (.3-.5 mm) are more commonly not broken and occur homogeneously scattered throughout the matrix. The plagioclase here is slightly more albitic (An8-12), and tends to form laths which sometimes show a crude alignment. No eye-shaped quartz microphenocrysts were observed, the quartz tending to form slightly columnar subhedrons.

Where foliated the metadacite crystal tuffs commonly reveal evidence of concomitant cataclastic deformation with lenticular microdomains outlined by laminae of finely (.01-.04 mm) polygonal quartz and albite, aligned chlorite platelets, and granular epidote. Within lenses thus defined, the original textures are variably masked by metamorphic recrystallization, and where pervasive this has resulted in .1-.2 mm polygonal quartz-untwinned albite - sericite - epidote assemblage hosting 1-1.5 mm rounded and microfractured albite (An5-8) phenocrysts. These show incipient alteration to epidote and sericite, and sometimes have chlorite altered rims and chlorite concentrated in pressure shadows. The original quartz phenocrysts in such domains are generally so polygonized as to be indistinguishable from the matrix material.

d) Meta-andesite

Outside of the few "basal" greenstone members, lithologies more mafic than dacite are rare within the Palmyra suite. There is, however, a striking lithological difference demonstrated between the metaspilites and the meta-andesites which form a minor facies intercalated with the Palmyra assemblage felsic pyroclastics flanking the sill-shaped part of the Ellisville granodiorite. This meta-andesite commonly forms very homogeneous, fine-grained lithologies exhibiting relict igneous textures. Significantly, although a minor facies these lithologies comprise the thickest (2-30 m) individual volcanic units observed in the Palmyra assemblage.

Petrographically the meta-andesites are homogeneous buff-green, fine-grained (1 mm), equigranular rocks which show remnant igneous textures and relict pyrogenic mineralogy. Modal analyses of several typical samples are listed in Table B6; these indicate a considerably more plagioclase-rich parentage than is evident for the metaspilites. It is on the basis of the high model andesine contents demonstrated on this table that these rocks are identified as metamorphosed andesites.

The remnant fine (.1 mm) hypidiomorphic granular texture is most evident in sawn handspecimens. In a few cases thin section study reveals an interlocking network of subhedral hornblende and plagioclase (An30-35). Much more commonly, however, the igneous textures apparent in handspecimens prove to be modified by metamorphic recrystallization in thin section. Metamorphic textures range from heteroblastic polygonal with 1-1.5 mm columnar-shaped hornblende intergrown with granular plagioclase to decussate with diamond-shaped hornblende occurring with polygonal plagioclase, quartz, and granular epidote. Commonly both the plagioclase and hornblende grains mutually include one another. Even where moderately polygonized the plagioclase shows moderate zonation (An30-35), indicating that it stems from original igneous feldspars. Occasionally the plagioclase occurs with larger (2 mm) actinolitic hornblende poikiloblasts riddled with quartz and epidote inclusions. Locally pervasive saussuritization and sericitization of plagioclase and uralitization of hornblende give rise to domains with remnant hornblende in an alteration assemblage of epidote - sericite - chlorite - tremolite where original textures are obliterated. Pale green (.5 mm) platelets of low order grey chlorite often occur as a minor constituent. Epidote typically occurs as .1-.2 mm granules that tend to cluster and, where concentrated, commonly show affiliated trace sphene and ilmenite. Magnetite is a characterizing trace mineral disseminated throughout. Very rarely epidote and quartz microveinlets transect the main paragenesis.

The matrix material in tuffaceous, grey-green to olive green lithologies is typically aphanitic and, where least metamorphosed, may consist of randomly oriented (.2 mm) plagioclase (An10-15) laths and poorly aligned (.3 mm) columnar hornblende grains. Where more strongly overprinted this lithology generally comprises a heteroblastic polygonal assemblage of the same mineralogy, but may be locally enriched in actinolite, epidote, and magnetite. This assemblage is host to 1-3 mm, rounded to lath-shaped, normally zoned plagioclase (An25-30) phenocrysts plus a few polycrystalline quartz eyes of the same size. Locally the plagioclase-hornblende matrix also hosts 1-2 mm. rounded concretionary structures cored by interlocking subhedral plagioclase (An27) rimmed by concentric zones of epidote and opaques; these structures are identified as accretionary lapilli. Within lapilli the groundmass oligoclase is incipiently sericitized, while the zoned phenocrysts are saussuritized with epidote concentrated at cores.

B.6 The Mineral Metavolcanic Suite

The Mineral metavolcanic suite forming the central part of the Chopawamsic metavolcanic belt is much more lithologically diverse than the Palmyra suite. The differing lithologies characterizing the Mineral suite include metasediments, metavolcanics, ironstones, and intrusives; these are described separately below.

a) Epiclastic Metasediments

Monotonous quartz - sericite - biotite schist forms intervals up to 2 kilometers wide with several kilometers of strike length, concentrating in the northern segments of the map area. This lithology is typically a medium grey, streaky layered silicic schist characterized by alternating discontinuous 3 mm quartzose and 1 mm micaceous laminae concordant with well developed foliation fabrics defined by the micaceous minerals. Modally the lithology varies considerably but an average specimen consists of about 60% quartz, 20% sericite, 15% biotite, with accessory feldspar, zircon, carbonate, garnet, and pyrite comprising about 5% of the rock. The garnet porphyroblasts sometimes show rotational distortion of included quartz trains, indicating that they are syntectonic in origin. Larger (2 mm) biotite laths occasionally parallel a poorly developed crenulation cleavage up to 35° to the dominant foliation. The trace carbonate occurs in spongy patches, while the pyrite occurs as trains of fine (.3-1 mm) rounded grains. The grey quartz-rich laminae comprises more than 95% quartz in fine (.1 mm) mosaics commonly exhibiting sutured boundaries but with occasional 120° grain boundary intersections. Rounded fractured quartz and feldspar porphyroclasts, patchy olive coloured biotite, carbonate, and twinned feldspar occur as accessories scattered within these layers. The occasional quartz veins which occur interlayered with the schist lithology are generally conformable and restricted to definite zones. In section these consist essentially of coarse mosaics of jagged quartz crystals showing undulose extinction but trace amounts of carbonate, chlorite, and fine (.2 mm) rounded pyrite grains are scattered throughout.

Where the Palmyra and Mineral metavolcanic suites intertongue east of the Ellisville granodiorite sill, the epiclastic component changes character to drab olive green, fine-grained (.1-.3 mm) quartz-chlorite schist which in rare instances exhibits preserved graded bedding. This metasiltstone facies may host trace amounts of disseminated magnetite and occasionally the iron oxide concentrates in 1-4 mm nodular aggregates of epidote.

b) Metavolcanics

In contrast to the Palmyra metavolcanics those of the Mineral suite are strongly bimodal and much more intensely overprinted by metamorphism. This lithology typically forms thin (10-100 m) discontinuous units, interlayered with epiclastic sediment or ironstone, which congregate along particular intervals. The mafic amphibolitic metabasalts and siliceous metarhyolite schists shown on the regional map bound the intervals where mafic or siliceous metavolcanics dominate rather than discrete lithological units. The metabasalts typically dominate thicker and more continuous sections than do the metarhyolites, and commonly the mafic and siliceous metavolcanic intervals are spatially paired. Neither facies shows any centralized buildup other than the zone of amphibolite gneisses coring the Andersonville district.

i) Mafic Metavolcanics

Modal analysis of several samples of amphibolitic "basalt" of the Mineral assemblages are listed in Table B7. As demonstrated, these rocks are essentially composed of hornblende and plagioclase. There is considerable

Table B.7: Modal Analysis of Mineral Mafic Metavolcanics

	CV78 193	NB1 187	NB2 326	Law 5	Pe6 Pe12		Pe25 Pe31		Al95 D55		D123 D120		Ar72	Ar7 10a	Ar7 10b	P37 K
plagioclase	-	30	30	25	28	15	-	25	20	20	15	50	32	8	20	20
hornblende	75	55	45	35	60	25	85	35	75	75	75	15	55	80	60	35
actinolite	10	-	-	25	-	30	-	20	-	-	-	-	-	-	-	-
epidote	9	-	-	5	-	3	13	5	-	tr	5	20	-	-	-	-
quartz	-	-	10	5	5	25	2	15	-	5	3	10	5	10	5	20
chlorite	3	4	-	4	5	-	-	-	4	-	tr	1	8	2	-	3
calcite	3	2	-	-	-	-	-	-	-	-	-	-	-	-	7	5
biotite	-	4	5	-	-	-	-	-	-	-	-	-	-	-	-	15
muscovite	-	2	-	-	-	-	-	-	-	-	-	-	-	-	-	2
garnet	-	2	5	-	2	-	-	-	-	-	-	3	-	-	8	-
sphene	-	-	1	1	tr	2	-	tr	-	-	1	-	-	-	-	-
zircon	-	-	tr	-	-	-	-	-	-	-	tr	-	-	-	-	tr
magnetite	-	tr	4	-	-	tr	tr	tr	1	tr	1	1	-	tr	-	-
pyrite	-	-	-	-	tr	-	-	-	-	-	-	-	tr	-	tr	tr
pyrrhotite	-	tr	-	tr	-	-	-	-	-	-	-	-	-	-	-	-

modal variation in these constituents as well as in the amount of associated actinolite, epidote, and quartz. Chlorite and garnet are the most consistent minor minerals while sphene and magnetite are characterizing traces.

Petrographically the metabasalts are dark green, rather uniform, fine to medium-grained (1-3 mm) amphibolites exhibiting moderately foliated, heteroblastic, polygonal metamorphic textures. Only one sample studied in thin section demonstrated a relict isogranular igneous texture in which polycrystalline aggregates of hornblende pseudomorph originally equant mafic minerals (pyroxene?) and the original plagioclase laths are pervasively epidotized. In all other sections metamorphic recrystallization has completely destroyed original igneous textures.

Where hornblende dominates, well developed decussate textures are defined by oriented .5-1 mm idioblastic amphibole grains. Specimens richer in plagioclase (An25-35) show a typifying heteroblastic polygonal texture with the hornblende tending to be slightly larger (1-2 mm) and better formed than the plagioclase (.5-1 mm) in any given rock. These two minerals commonly mutually include one another, and occasionally the hornblende forms large (2-5 mm) xenoblastic sieves including (less than .3 mm) polygonal plagioclase and quartz. Granoblastic growth textures prevail where the plagioclase forms near-monomineralic microdomains in the most feldspathic amphibolite. Significantly, even where such textures are in evidence the plagioclase sometimes shows moderate normal zonation (An30-35) which is interpreted to be relict from primary igneous compositions.

Slightly lighter green and better foliated lithologies exhibit oriented heteroblastic polygonal textures overgrown by aligned (.2-2.5 mm) columnar to acicular actinolite and lath-shaped chlorite porphyroblasts. The largest of the actinolite porphyroblasts tend to lie subparallel to the foliation and may locally crosscut it at high angles. The minor pale green chlorite typically occurs as aligned laths sited at the triple points of amphibole grains but locally aggregates into polycrystalline sheaves that are also oriented parallel to the plane of foliation. The plagioclase in these more foliated samples tends to be untwinned, but where twinned indicates a more albitic composition (An17-25) which is interpreted to result from readjustment to metamorphic conditions. A few of the intensely foliated samples are devoid of plagioclase but show hornblende interleaved with lenticles of .1 mm polygonal quartz, cuspate calcite, and granular epidote presumably stemming from complete breakdown of the original plagioclase component. Trace biotite occurs in many of the foliated samples, and where foliation is intense enough to define schistosity, lepidoblastic biotite may replace hornblende as the chief mafic mineral. Biotitic samples are typically transected by numerous calcite veinlets. The strong schistosity and lenticular fabrics exhibited by the samples devoid of plagioclase and rich in biotite indicate that shear deformation was a major factor in the stability of both amphibole and plagioclase.

Both massive and foliated types show a variety of trace minerals. Garnet is common as small 1-2 mm idioblasts which typically include .1 mm polygonal quartz. These porphyroblasts occasionally show retrograde breakdown to dark green chlorite on rims. The sphene occurs as patchy disseminations and local xenoblastic sieves including iron-titanian oxide. Zircon was only observed in samples relatively rich in sphene. Magnetite is the characteristic trace opaque and is typically disseminated throughout as fine (.1 mm) cubes. Rarely pyrrhotite or pyrite replaces magnetite as the chief opaque. The sulphides generally show more heterogeneous dissemination than the magnetite.

A few of the metabasalts show relict amygduloidal features. Calcite forms 1-2 mm oblate nodules bordered by radial chlorite and exhibiting polygonal quartz pressure shadows. Rarely the nodules are perfectly round. These are composed of polygonal quartz and granular epidote; alternately they may consist essentially of radial and/or concentric epidote growths with a thin outer rim of quartz. Pyrrhotite commonly concentrates near the rims of these epidote amygdules.

ii) Silicic Metavolcanics

Silicic metavolcanics in the Mineral assemblage range from very fine-grained sericitic schists hosting scattered quartz and feldspar phenocrysts to dense aphanitic quartz feldspar porphyries which have to a large extent escaped the penetrative metamorphic overprint. Fragmental units have only been observed in the Mineral district and even in this area they are very restricted. South of the Mineral district the more typical sericitic schist facies is speckled with minor biotite; this unit is shown as metarhyodacite on the map.

Modal analyses of several silicic metavolcanic samples are listed in Table B.8. As demonstrated, these rocks are essentially composed of quartz and alkali feldspar with considerable modal variation in these minerals correlating inversely to the amount of sericite present. Calcite is the characterizing minor mineral, and zircon and pyrite the most common accessories. The hydrothermally altered facies are rich in biotite $\pm$ chlorite, and these commonly show a varied porphyroblastic suite as well. The rhyodacite facies has slightly lower modal feldspar and higher modal biotite contents.

Metarhyolite

The most widespread metarhyolite in the Mineral suite occurs as white sericite schist that bears little evidence for its primary volcanic derivation. Except for being slightly coarser textured, these schists have considerable petrographic similarity to the Palmyra assemblage dust tuffs and indeed may well be correlative as they are most commonly interlayered with the previously described epiclastic biotite schists that favour the western part of the Mineral suite. In thin section the sericitic schist facies exhibits finely foliated textures with laminae of acicular sericite interleaved with dimensionally and optically oriented polygonal quartz and feldspar. The finely foliated fabric is occasionally disrupted by the occurrence of small (.3-.5 mm) rounded albite and eye-shaped quartz phenocrysts. More rarely the sericitic schists are intercalated with light grey aphanite with megascopic (1 mm) kaolinized white feldspar phenocrysts. Occasionally the sericite forms 1-2 mm monomineralic lensoidal domains which conceivably derive from original pumice fragments.

Quartz Feldspar Porphyry

The silicic metavolcanic showing the best preserved igneous textures are observed in drill core from the mineralized trend within the Mineral district. However, even here these typically massive, light grey-white, porphyritic aphanites with megascopic (1 mm) phenocrysts of quartz and feldspar are restricted to thin (10 cm - 3 m) intersections which escaped the normal penetrative schistosity developed in bordering quartz-sericite schists. In

Table B.8: Modal Analysis of Silicic Metavolcanics from the Mineral Assemblage

	C43	CV78 416	Pel4	CV89 1284	CV85 1700	CV87 383	CV87 214	1035 806	P31 A	55J 332	CV78 1622	CV78 1618	102J 398	PA1	P37H	P37I	P37J
	1	2	3	4	5	6	7	8	9	10	11	12	13	14	15	16	17
alkali feldspar	-	-	[5]	55	50	-	-	-	-	-	50	65	-	-	-	-	-
albite	30	35	-	-	-	23	25	15	30	20	-	-	51	36	28	16	20
microcline	-	-	-	-	-	-	-	8	-	-	1	-	-	2	12	-	-
quartz	50	30	60	40	22	75	60	70	40	20	17	20	24	45	46	59	60
epidote	tr	-	-	-	-	-	-	-	5	-	-	-	-	-	-	-	-
chlorite	-	-	-	1	-	-	-	-	7	-	1	tr	-	5	2	-	2
calcite	-	-	-	1	3	2	5	4	3	-	-	2	10	-	-	-	-
sericite	20	35	40	2	20	-	10	2	8	45	15	3	4	4	3	10	tr
biotite	-	-	-	-	-	-	-	1	-	7	3	5	9	8	8	15	18
cordierite	-	-	-	-	-	-	-	-	-	2	-	-	2	-	-	-	-
garnet	-	-	-	-	-	-	-	-	2	2	4	3	-	tr	-	-	-
chloritoid	-	-	-	-	-	-	-	-	-	tr	-	2	-	-	-	-	-
staurolite	-	-	-	-	-	-	-	-	-	-	1	-	-	-	-	-	-
zircon	-	-	-	tr	-	tr	-	-	-	tr	-	-	-	-	-	-	-
rutile	-	-	-	-	-	tr	-	-	-	-	-	-	-	-	-	-	-
ilmenite	-	-	-	-	-	-	-	-	-	2	-	-	-	-	-	-	-
magnetite	-	-	-	1	-	-	-	-	-	-	-	-	-	-	-	-	-
pyrite	-	tr	tr	-	-	-	tr	-	5	2	-	tr	-	tr	1	-	tr

1 rhyolite tuff 2% Ph, 1% ab, 1% q
2 rhyolite tuff 2% Ph, 1% ab, 1% q
3 rhyolite tuff 3% Ph, 7% lith frgm ?
4 quartz-feldspar porphyry 15% Ph (10% q, 5% f)
5 quartz-feldspar porphyry 15% Ph (5% q, 5% f) cognate incl. 15%
6 rhyolite flow 5% Ph (4% q, 1% f)
7 tectonic brecciated quartz feldspar porphyry
8 altered quartz feldspar porphyry 15% Ph (7% q, 4% ab, 4% mica) 5% cognate incl.
9 altered rhyolite
10 altered rhyolite
11 altered quartz feldspar porphyry 5% q Ph, 5% cognate incl.
12 altered quartz feldspar porphyry q Ph 5%
13 hydrothermally brecciated quartz feldspar porphyry 80% frg, 5% Ph
14 rhyodacite tuff 5% Ph (2% f, 2% ab, 1% q)
15 tectonically brecciated rhyodacite tuff 12% frg, 8% Ph (3% ab, 2% f, 3% q)
16 rhyodacite tuff 5% Ph (4% q, 1% ab)
17 reworked rhyodacite tuff

[ ] completely pseudomorphed by alteration products

thin sections the porphyritic aphanites exhibit a very fine (.02 mm) polygonal groundmass of quartz and alkali feldspar with indistinct sutured grain boundaries. This assemblage is host to .2-1 mm tabular antiperthite and anhedral (commonly eye-shaped) quartz phenocrysts and more rarely to polycrystalline perthite - albite - patch perthite - quartz clusters. The alkali feldspar phenocrysts show occasional groundmass embayments. The rare 2-4 mm polycrystalline feldspar-quartz clusters sometimes have arms extending well into bordering groundmass, suggesting the aggregation of phenocrysts in the magma prior to eruption rather than the fragmentation of preexisting rock. The more feldspathic clusters are commonly transected by a fine stockwork of calcite and are generally more intensely sericitized than single grain feldspar phenocrysts. This implies that the primary ternary feldspar phase(s) in the clusters were possibly richer in both Ca and K components which exsolved to form patch perthite and calcite microveinlets during subsolidus cooling and/or metamorphic recrystallization.

With intensification of metamorphic overprinting, these little-deformed porphyritic rhyolite flows (?) lose their original textures. The groundmass changes to a fine (.5 mm) schistose assemblage of polygonal quartz and untwinned alkali feldspar interleaved with parallel aligned sericite. There is considerable modal variation in the sericite, and where most abundant the groundmass may be completely devoid of feldspar, indicating that this mineral is readily broken down during formation of intense schistosities. Both the alkali feldspar and quartz phenocrysts, as well as the polycrystalline feldspar quartz clusters, show all stages of polygonization to the point where they are no longer discernible from the polygonized and foliated groundmass. Where phenocrysts are observed in the resulting finely foliated sericite schists, they contain only small ($\leq$1 mm) rounded albite (AN3-5) and polycrystalline quartz eyes, indicating that the original potassium feldspar components were most readily altered to sericite.

Although the metarhyolites are modally variable in quartz and alkali feldspar (or sericite where schistose), they characteristically have very little in the way of minor or trace mineral constituents -- unless, of course, they have been hydrothermally altered. In unaltered facies, discontinuous calcite microveinlets comprise the most common minor constituent while occasional zircon forms the characterizing trace mineral. Opaque minerals are not characteristic; however, rutile was noted as an inclusion in a few of the quartz phenocrysts and, on rarer occasions, trace patchy disseminations of both hematite and pyrite were observed.

Hydrothermally Altered and/or Fragmented Quartz Feldspar Porphyry

Where hydrothermally altered, these porphyritic metarhyolites transit into mineralogically complex assemblages and where alteration has been pervasive the original lithology is unrecognizable. The effect of hydrothermal alteration is readily recognizable in places where original porphyritic aphanite occurs as remnants, with primary textures intact, bordered by mineralogically complex "hydrothermal vein" assemblages. However, the lithological distinction between pervasively hydrothermally overprinted rhyolite from the occurrence of slightly more intermediate (rhyodacitic) rocks as well as from a variety of "exhalative" lithologies proves to be one of the most difficult petrological problems to unravel in the Mineral district. A further petrological problem arises in differentiating primary mechanically brecciated rhyolite, which, because of its greater porosity and permeability, would tend to channel hydrothermal fluids, from breccias resulting from chemical dissolution of originally massive

rhyolite by the corrosive activity of the hydrothermal fluid phase. This particular petrological problem is exacerbated by the possibility of tectonic fragmentation during the metamorphic overprint. A full explication of this petrological nexus (defined by, first, the converging lithological similarity of hydrothermally altered rhyolite to either originally more intermediate primary volcanics or exhalite formed through chemical precipitation from discharged hydrothermal brines, and second, the textural convergence of primary mechanical and/or solution brecciation and tectonic fragmentation) is beyond the scope of the present investigation. However, the essential petrological features demonstrated by the main members of this lithological grouping may be briefly summarized as follows.

Primary rhyolite breccias were only observed in the areas of sulphide mineralization in the Mineral district; the best exposure of rhyolite fragmental to date was revealed by the underground exploration at the Cofer deposit. Angular fragments up to ten centimeters in the median dimension occur on occasion, but typically they range up to about two centimeters. These breccia deposits are always unsorted with the matrix-supported monolithic fragments comprising 50-75% of a given rock. The fragments consist of unfoliated light grey porphyritic aphanite with quartz and albite (An8-12) phenocrysts scattered evenly in a fine (.01-1 mm) polygonal quartz-alkali feldspar groundmass. The bleached rims observed bordering many fragments are formed by very fine (.01 mm) polygonal quartz and could be evidence for subaqueous quenching of lava. The matrix material consists of well foliated quartz and sericite with variable amounts of a varied accessory suite including biotite, chlorite, carbonate, untwinned alkali feldspar, zircon and pyrite; quartz and feldspar phenocrysts (1 mm) are also rare matrix constituents.

Hydrothermal solution breccias are as restricted as primary mechanical breccias and are best exposed in drill core from the Julia deposit located at the south end of the main mineralized trend in the Mineral district. At this location massive rhyolitic units show the effect of chemical dissolution which has resulted in the formation of coarse breccia zones. Significantly, complete transitions are observed from massive unaltered porphyritic aphanite to diffusely light grey-dark grey mottled zones to "wispy" fragmentals and thence to definite breccias. No clear boundary exists between mottled zones or even between these and the wispy fragmental textures, and therefore these rocks cannot be products of active mechanical fragmentation. Even in the case of the zones where fragment borders are well developed, the adjoining fragments generally show mirror image boundary configuration, indicating that they result from fragmentation in place. Passive hydrothermal alteration processes must be invoked over active explosive fragmentation to account for these particular features.

In thin section the incipiently mottled zones are more quartz-rich and the light to dark grey mottling is interpreted as primarily due to bleaching during hydrothermal silicification. As the hydrothermal dissolution gets progressively more intense, less and less of the darker grey unsilicified porphyritic aphanite remains, and the cores of the silicified zones are in turn replaced by diffuse glomeroporphyroblastic knots formed by metamorphic recrystallization of chlorite. The porphyroblastic assemblage includes biotite, calcite, muscovite, chlorite, garnet, cordierite, magnetite, and pyrite, and rarely, where these types are abundant, chloritoid and staurolite as well. In a few cases a noticeable metamorphic mineral zonation can be observed within the glomeroporphyroblastic knots as well, with extremities rich in micas and cores rich in garnet and opaque minerals. Central porphyroblasts sometimes exhibit coronas of fine (.01-1 mm) polygonal quartz devoid of other

mineral species, indicating that the former grew at the latter's expense.

Where most intense the hydrothermal alteration has given rise to stringery breccia zones. These range from massive, silicified, light grey, porphyritic aphanite transected by rusty quartz veins bordered by chlorite-calcite rims to "cherty" fragments occurring in a biotite matrix rich in the same porphyroblasts as mentioned above. In thin section the remnant fragments consist of fine (.05 mm) quartz $\pm$ untwinned alkali feldspar groundmass hosting a few scattered 1 mm quartz and patch antiperthite phenocrysts. The quartz veins are made up of coarse (2 mm) polygonal quartz hosting minor heterogeneously disseminated pyrite. The fragments lie in a polymineralic assemblage characterized by decussate textured biotite, cuspate calcite, and polygonal quartz and cordierite. This biotite carbonate-bearing alteration assemblage commonly hosts a variety of porphyroblasts including large (1-4 mm) lepidoblastic muscovite, xenoblastic sieves of garnet, staurolite, and chloritoid, and smaller (1-2 mm) garnet and magnetite idioblasts. The garnet occasionally shows biotite-chlorite retrogression on grain rims. The skeletal chloritoid sieves were only observed in domains unusually rich in calcite, which may occur not only as typical cuspate grains but in xenoblastic patches and microveinlets. Where this biotitic metasomatic assemblage is rich in garnet and staurolite porphyroblasts, it is characteristically accompanied by patchy sulphide disseminations.

Differentiating primary breccias from tectonic breccias can be very subtle. For instance, some well foliated samples exhibit ostensible cataclastic textures with thin (.5 mm) wavy laminae of aligned sericite interleaved with very fine (.05 mm) granulated quartz that bounds coarser (.5 mm) lensoidal domains consisting of a granoblastic polygonal quartz-alkali feldspar assemblage. However, in some rocks of the same composition, the granoblastic quartz-alkali feldspar assemblage is partially or completely replaced by a very fine sericite matte with biotite along the outer margin of complete alteration. The latter texture indicates that the sericite mattes result from hydrothermal sericitization rather than being generated during metamorphic overprinting. That such sericitic domains sometimes exhibit intense crenulations with lepidoblastic biotite and occasionally small (1 mm) garnet idoblasts accompanied by patchy sulphide disseminations clustering along the axial planes of the crenulations further supports a pre-metamorphic origin for the latter sericite.

Metarhyodacites

The task of differentiating hydrothermally altered rhyolites from slightly more intermediate primary volcanic lithologies and/or slightly reworked rhyolitic tuffaceous material also relies on relatively subtle petrographic distinctions. Where massive rhyolite has been hydrothermally altered the resulting biotite typically shows a heterogeneous patchy distribution. However, difficulty arises when one attempts to determine whether the regionally extensive, uniformly biotitic, buff to light grey units particularly common immediately south of the Mineral district may (1) be due to less active but more pervasive hydrothermal alteration of original rhyolite, (2) stem from a slightly more intermediate parental magma, or (3) arise from slight reworking of rhyolitic pyroclastics.

In thin sections this lithology consists of a uniform heteroblastic polygonal quartz - alkali feldspar - biotite - sericite assemblage with well oriented biotite and sericite interleaved with dimensionally elongate quartz and untwinned feldspar grains. Compositional layering (cm scale) is evident

due to modal variation particularly in biotite. Many samples are devoid of phenocrysts, but 1-2 mm slightly rounded, polysynthetically twinned albite (An8-10) and, more rarely, simple twinned, incipiently kaolinized orthoclase in 1-3 mm grains do occur. Significantly, quartz eyes sometimes form trains along the same horizon. Also, .3-.5 mm polygonal quartz seams with trace pyrite sited at triple point junctions sometimes occur between bands of differing composition; this could suggest that these stem from original pyritic chert. Significantly, these uniform units are relatively free of minor minerals, though ragged flakes of chlorite and muscovite lepidoblasts occur locally and biotite commonly shows pleochroic haloes, implying included zircon.

At Yancyville, located fifteen kilometers southwest of Mineral, the rhyodacitic units appear fragmental, with aphanitic, white, rodded fragments devoid of biotite occurring in a biotitic schist matrix similar to the uniform lithologies just described. In thin section the fragments consists of very fine (.05 mm) polygonal quartz and untwinned feldspar hosting rare euhedral (1 mm) patch antiperthite phenocrysts and polygonized quartz eyes. Annealing of quartz in the cores of these fragments has given rise to microdomains of .3-.4 mm granoblastic quartz with common 120° triple point junctions. The matrix to the fragments is more biotitic than is typical of the uniform unfragmented facies, as well as being richer in porphyroblasts including muscovite, chlorite, garnet, and pyrite.

In general, the detailed petrographic characteristics of the "rhyodacitic" units suggest that they comprise an intermediate lithology between rhyolitic tuffs and the biotitic epiclastics. Compositional layering, defined primarily by modal variation in biotite, sorting of phenocrysts, and interlaminated chert, may be attributed to sedimentary processes. General uniform appearance, quartzo-feldspathic composition, scattered phenocrysts, and local siliceous rhyolitic crystal tuff intervals, locally fragmented during metamorphic overprinting, indicate that these rocks had a direct siliceous pyroclastic source.

c) Ironstones

Ironstones are commonly interlayered with the Mineral mafic and silicic metavolcanics, concentrating in the eastern part of the suite. It cannot be overemphasized that this facies comprises an enigmatic group of highly variable and mineralogically complex lithologies that do not readily fit into existing rock classifications. Their origins are problematic. Because they are characterized by various minerals including oxide, silicate, carbonate, and sulphide species, and show petrological similarities to iron formation (i.e., in being thinly banded) they are considered to have been generated at least in part through chemical precipitation, albeit precipitation that overlapped with active volcanism.

The massive metabasalts transit into banded (cm to m scale mafic ironstones with modal increase in quartz and magnetite. This particular lithology was colloquially named transitional amphibolite inasmuch as the resulting rocks are compositionally intermediate between amphibolite and ferruginous hornblende magnetite-bearing quartzite. The silicic metavolcanics transit into extensive beds of quartz sericite pyrite schist. Thin (cm scale) well banded biotitic and carbonate-bearing strata comprise a more lithologically distinctive ironstone facies. With intensification of chloritization both the pyritic and iron carbonate-bearing facies further transit into a dense chloritic lithology

with abundant porphyroblasts.

In the following discussion three particular species -- mafic amphibolitic ironstone, sericitic pyritic ironstone, and biotitic-iron carbonate ironstone -- are described in detail. Subsequent to this, the petrography of the affiliated "hydrothermal chloritite" will be examined.

i) Mafic Ironstones

Modal analyses of several samples of mafic ironstone are listed in Table B.9. As demonstrated, these rocks are mainly composed of a modally variable assemblage including plagioclase, hornblende, quartz, chlorite, and biotite. All samples tend to be mineralogically complex -- three differing amphibole species may occur in the same rock -- and many host aluminous minerals (garnet, staurolite, kyanite) as porphyroblasts. Notably, zircon is the characterizing accessory silicate, while magnetite is the characterizing minor mineral and may achieve major proportions in some bands.

The prevailing fine (.5 mm) heteroblastic polygonal texture is essentially defined by quartz-plagioclase mosaics. The plagioclase may be untwinned or show both albite and pericline twinning in any given slide. Twin measurements show compositions ranging from An5 to An30, but albitic compositions dominate. Significantly, the An content of the plagioclase tends to be uniform in any given band. The assemblages rich in quartz and albite exhibit lobate heteroblastic polygonal texture with sinusoidal boundaries developed between these minerals. The rarer calcic compositions sometimes show moderate normal zonation (An25-30) inherited from original igneous plagioclase. Sometimes the plagioclase grains are pervasively altered with the albitic varieties tending to be incipiently sericitized and the more calcic types altered to an assemblage of chlorite, biotite, epidote, and calcite. In some samples a few grains of rounded strained quartz up to 1.5 mm are present; these are likely of detrital origin. In the most siliceous bands, coarser (.3 mm) granoblastic quartz occasionally forms thin (1-3 mm) lenses parallel to banding. As these may also host iron carbonate or, more rarely, disseminated pyrite, they likely represent original carbonate-bearing and/or sulphidic chert layers.

The more mafic bands tend to be either hornblendic or biotitic, and these typically demonstrate .5-2.5 mm decussate textures with either the hornblende or the biotite interleaved with minor polygonal quartz and plagioclase. Occasionally the hornblende forms radial porphyroblasts on the plane of foliation, producing Garbenschiefer textures. The mafic bands generally host a variety of porphyroblasts and the growth morphology of these porphyroblasts controls textures to a considerable extent. The mineralogically complex assemblages in particular have many unique textural features. Interestingly, these samples show a direct relationship between the size of porphyroblasts and their shape. The smaller ($<$.5 mm) varieties tend to be idioblastic and inclusion-free, while the larger ($\geq$1.5 mm) ones are typically xenoblastic sieves. A further textural feature generally demonstrated is a tendency for isolated porphyroblasts to be idioblastic while glomeroporphyroblastic aggregates of the same mineral in the same slide are xenoblastic. Doubtless these porphyroblastic textural features relate to availability of nucleation sites and to variable growth rates, which in turn must have depended to a large extent on the accessibility and immediacy of the ingredients necessary to form particular varieties of porphyroblast.

Table B.9: Modal Analysis of Mineral Mafic Ironstones

	1	2	3	4	5	6	7	8
	CV76 361'	NB77-1 229'	NB77-1 567'	NB77-2 349'	CV89 1170'	D110 1	D59 1	D94 1
plagioclase	-	65	-	50	-	35	36	15
albite	25	-	53	-	-	-	-	-
alkali feldspar	-	-	-	-	-	5	-	-
hornblende	25	10	-	-	10	30	5	15
actinolite	-	-	-	-	-	-	40	-
cummingtonite	-	3	-	-	-	-	2	5
quartz	25	5	30	30	70	15	5	15
epidote/zoisite	5/	-	-	-	-	/10	-	-
chlorite	10	3	-	-	7	tr	10	-
biotite	-	5	10	13	10	-	-	25
white mica	-	-	-	-	-	tr	-	-
garnet	2	2	2	-	-	3	-	2
calcite	5	2	-	-	1	-	-	-
siderite	-	-	-	-	-	-	-	5
staurolite	-	-	-	-	-	-	-	15
kyanite	-	-	-	-	-	-	-	1
sphene	-	-	-	-	-	tr	-	-
zircon	tr	tr	tr	-	-	tr	-	tr
tourmaline	-	-	-	-	-	-	-	tr
magnetite	1	-	5	12	-	2	2	2
pyrite	2	-	-	-	2	-	-	-

The unique textural relationships observed in individual mineral species are as follows. The .5 mm decussate hornblende sometimes coalesces to form large (1-2 cm) xenoblastic sieves including polygonal quartz and plagioclase. The smaller (.2-1 mm) subidioblastic columnar hornblende grains are often intergrown with cummingtonite along twin boundaries. Cummingtonite rarely forms isolated porphyroblasts, whereas actinolite occurs as isolated columnar porphyroblasts restricted to the biotitic bands. Corona textures are sometimes evident, with pale green actinolite rimming coarse (5 mm) dark green hornblende poikiloblasts which include .2 mm magnetite idioblasts with polygonal quartz rims. Where pale brown biotite dominates the assemblage it forms decussate textures with biotite grains interleaved with dimensionally oriented quartz and feldspar. Where biotite is isolated, the grains are lepidoblastic, but large (1-3 mm) biotite porphyroblasts have lath shapes.

Garnet occurs both as small (.5 mm) idioblasts and as large (1-3 mm) xenoblastic sieves including quartz and magnetite. Rarely, small (.3 mm) subidioblasts of garnet coalesce to form necklace trains at the contacts between adjoining bands of differing composition. Chlorite shows a variety of textures including .05 mm acicular microlites, .5 mm laths, and radial sheaves that sometimes cluster to form 1-2 mm buttons. The columnar actinolite porphyroblasts locally exhibit chlorite intergrowths along twin boundaries. The carbonate in any given slide tends to form monomineralic domains with well developed equilibrium textures. Occasionally siderite forms dimensionally oriented lepidoblasts parallel to layering. Epidote occurs as patchy disseminations of fine (.1 mm) granules, while zoisite typically forms isolated stubby subidioblastic laths.

Large (1-3 mm) xenoblastic sieves of staurolite are hosted in biotitic bands which include quartz and magnetite trains paralleling the compositional layering. The smaller (1 mm) staurolite grains are idioblastic and inclusion-free. Kyanite was only observed in one sample (D94-1), where it occurred as bluish grey blades paralleling primary layering defined by quartz inclusion trains within bordering xenoblastic hornblende sieves. Trace sphene was observed in a few sample as scattered subidioblastic grains. Zircon is the characterizing accessory, giving rise to pleochroic haloes in biotite, chlorite, and, more rarely, even in hornblende. Trace small (.1 mm) idioblasts of tourmaline are rare. Magnetite, the characterizing minor mineral, generally occurs as a heavy dissemination of .2 mm idioblastic grains which is uniform within given bands but shows considerable modal variation from one band to the next. The larger (1 mm) magnetite grains are subidioblastic. Pyrite was observed only in the most siliceous of the mafic ironstones studied in thin section, where it was found to be concentrated along quartz-carbonate laminae or included within staurolite and garnet porphyroblasts forming trains parallel to the compositional layering.

ii) Pyritic Ironstones

The pyritic ironstones have their thickest (up to 100 m) development along the mineralized trends in the Mineral district. However, thinner beds do occur over the strike length of the segment, bordering on the western limb of the Columbia synform and again along the New Canton trend. This lithology has not been observed to date in the Andersonville district.

Modal analyses of several samples of pyritic ironstones are listed in Table B.10. As demonstrated, this ironstone facies essentially comprises a quartz -

Table B.10: Modal Analysis of Pyritic Ironstones of the Mineral Assemblage

	CV85 153'	CV89 841'	CV89 900'	CV89 1184'	CV89 1293'	CV76 1101'	Ar7-4
albite	10	5	-	10	5	50	-
quartz	65	64	60	23	45	15	70
sericite	25	25	7	50	30	5	25
chlorite	-	1	20	-	15	8	-
biotite	-	2	8	15	5	12	3
cordierite	-	-	-	-	tr	-	-
garnet	-	tr	3	-	-	5	-
staurolite	-	-	-	-	-	2	-
chloritoid	-	-	-	-	tr	-	-
calcite	3	-	-	-	-	-	-
tourmaline	-	-	-	-	-	-	1
zircon	-	-	tr	tr	tr	tr	-
pyrite	2	2	2	2	2	3	1

sericite - albite - pyrite assemblage. Chlorite and/or biotite may constitute major proportions in some specimens. Although the modal porphyroblast content of these rocks is minor, a surprising number of differing mineral species do occur. Zircon is a common trace mineral in rocks including minor biotite. Pyrite is omnipresent and is the characterizing minor mineral in all the samples.

Typically the pyritic ironstones are laminated (mm scale), light grey to white, fine-grained schists. In thin section these rocks demonstrate strong foliation fabrics defined by the interlensing of fine (.2 mm) parallel aligned sericite microlites and dimensionally elongate polygonal quartz and cloudy untwinned albite. The subtle compositional layering evident in handspecimen is a result of delicate interbanding of 1-3 mm quartz - sericite - albite - pyrite assemblages with 1 mm near-monomineralic sericite laminae. The latter are disrupted by a few rounded 1 mm grains of partially polygonized alkali feldspar (antiperthite) that could possibly be relict phenocrysts. Occasionally the sericite laminae host 1-5 mm polycrystalline quartz lenticles that exhibit equilibrium textures. Sometimes .5 mm grains of dimensionally elongate quartz form seams of single grain thickness parallel to the lamination, and these are occasionally accompanied by calcite and may be bordered by pyrite trains. More rarely the calcite forms similar seams also accompanied by pyrite.

The more quartz-rich intervals tend to have near-monomineralic quartz laminae interlayered with micaceous laminae poor in quartz. The quartz layers typically show development of equilibrium textures. Occasionally quartz-rich facies also demonstrate effects of cataclastic deformation with lenticulated quartzose domains bordered by sericite or biotite laminae. The former sometimes show extreme chevron crenulation, while the latter comprise coarse (1 mm) oriented lepidoblastic biotite rich in garnet poikiloblasts. Locally the garnet may be partially or completely pseudomorphed by pyrite. The ubiquitous pyrite in these rocks occurs both as uniform disseminations of fine (.02 mm) rounded to larger (.1 mm) idioblastic grains and as heavier disseminations along some laminae. occasionally it forms near monomineralic laminae.

In the Mineral district the light grey to white sericitic ironstones sometimes transit into lithology with a distinct green cast due to an increase of modal chlorite. In these pale green lithologies chlorite is intimately interleaved with the sericite, but otherwise the subfacies is petrographically similar to those without chlorite. However, generally the chloritic facies has been more favourable for the growth of porphyroblasts, resulting in megascopic spotted schist lithologies. Pale green-brown biotite forms the most modally significant porphyroblasts which occur as 1-1.2 mm lepidoblasts within sericite-chlorite laminae. Occasionally biotite may replace both sericite and chlorite as the chief micaceous mineral, producing more pronounced compositional layering with lepidoblastic biotite intergrown with sheaves of acicular sericite and acicular to tabular chlorite forming laminae separating layers of heteroblastic polygonal quartz and minor alkali feldspar interleaved with chlorite. The biotitic faces are richest in porphyroblasts, including isolated .2-.4 mm idioblastic (hexagonal) cordierite, garnet, and chloritoid within the polymineralic domains and xenoblastic garnet and staurolite within biotite laminae. In a few cases the delicate biotite laminae have controlled garnet growth morphology, as massive garnet may totally replace the biotite, resulting in discontinuous garnet bands. Where this occurs the garnet bands are slightly thicker than original biotite laminae, indicating that garnet growth consumed ingredients from the bordering assemblages. Trace zircon gives rise to ubiquitous pleochroic haloes in biotite.

Probably because of their micaceous composition the pyritic ironstones are one of the most highly deformed lithologies observed within the Mineral suite. Both the lamination and the parallel foliation may be broadly to tightly crenulated, and where crenulation is intense the quartz and alkali feldspar are more finely polygonized with .5 mm lepidoblastic muscovite, chlorite, and, occasionally, 1 mm lath-shaped biotite poikiloblasts occurring along a transpositional cleavage formed axial planar to the crenulations. Where the chloritic facies is crenulated the larger (up to 3 mm) randomly oriented biotite poikiloblasts hosted in these more intensely deformed zones may also show mechanical disruption with remobilized quartz healing microfractures. These features indicate that further tectonism occurred subsequent to the growth of the porphyroblasts.

iii) Biotitic Carbonate Ironstones

The carbonate-bearing ironstones form thin (1-2 m) strata that were only observed in drill core and as float samples in the old mine dumps in the Mineral district. This particular ironstone facies comprises one of the most outstanding lithologies in the Mineral assemblage, however, first because it is typically strikingly thin-banded (cm scale) to laminated in dark brown to buff colours where fresh (an effect which is accentuated by the fact that the buff carbonate bands weather rapidly to a rusty orange-brown colour due to their high iron content), and second, because it demonstrates a common flow folding deformation style which makes it petrographically distinct. Mineralogically the carbonate ironstones show similarity to the mafic ironstones with which they are often spatially associated. This petrographic overlap is particularly evident where the mafic ironstones show an appreciable increase in biotite content. The mafic ironstones form thicker sections and, being on the whole more thickly banded, are generally distinct from the thin carbonate-rich units considered here.

Modal analyses of several samples of the biotitic carbonate ironstone are listed in Table B.11. As demonstrated, this facies is essentially composed of a quartz - biotite - carbonate - cordierite assemblage. Ferroan calcite makes up the majority of the carbonate content in all samples; however, siderite is also commonly present. Most of the samples host a rather varied suite of ferro-aluminous silicate porphyroblasts. Zircon is the characterizing trace silicate mineral and trace tourmaline was observed in two of the samples. Pyrite is common in many samples, suggesting a further petrological tie between the pyritic and carbonate ironstone facies.

In thin section the well developed compositional layering is defined primarily by the pronounced modal variation among quartz, biotite, and carbonate, with the boundaries between adjoining layers ranging from knife sharp to indistinct and gradational. The polymineralic assemblages tend to be heteroblastic polygonal where dominated by quartz and carbonate or to show well developed foliation fabrics where biotite-rich. Fine (.2 mm) heteroblastic quartz + carbonate + cordierite + biotite $\pm$ albite is a common polymineralic assemblage. However, the individual constituents of this assemblage also often form bands of simpler and even monomineralic compositions. The quartz-carbonate assemblages are most common, ranging from lobate heteroblastic with sinusoidal grain boundaries developed where both minerals are modally significant to granoblastic polygonal in cases where either one or the other dominates. Both monomineralic quartz and calcite bands are typically slightly coarser grained (.5 mm) than polymineralic bands and show 120° triple point

Table B.11: Modal Analysis of Biotite Carbonate Ironstones of the Mineral Suite

	CV89 91'	CV85 1610'	CV87 1190'	CV78 1934'	CV78 1944'	CV78 1945'	CV65 1610'	103J 908'	CV73 113'	D112
albite	-	-	-	-	-	-	15	-	5	5
hornblende	-	-	-	-	2	20	-	-	-	-
actinolite	-	-	-	-	-	-	-	-	25	-
quartz	65	65	50	25	45	10	25	15	20	-
chlorite	1	2	-	5	tr	2	-	-	1	-
biotite/ phlogopite	25/	15/	15/	25/	25/	50/	35/	25/	20/	/10
white mica	-	10	3	-	-	-	5	-	-	6
dolomite	-	-	-	-	-	-	-	-	-	10
Fe-calcite	8	8	10	25	10	3	8	40	25	65
siderite	-	-	-	5	5	-	-	10	-	-
garnet	-	-	-	-	2	2	2	-	-	2
cordierite	-	-	10	15	10	10	5	10	4	-
chloritoid	-	-	-	tr	-	-	-	tr	-	-
staurolite	-	-	3	-	1	2	-	-	tr	-
kyanite	-	-	8	-	-	-	-	-	-	-
sphene	-	-	-	-	-	-	-	-	-	tr
zircon	-	-	tr	tr	tr	tr	tr	tr	tr	tr
tourmaline	-	-	-	-	-	-	-	-	tr	tr
pyrite	1	-	1	-	-	1	-	1	-	-
magnetite	-	-	tr	-	-	-	-	-	-	2

junctions and straight grain boundaries. Near the borders of monomineralic quartz bands hexagonal quartz grains occasionally host droplet carbonate inclusions. Similarly, the carbonate grains may host polygonal quartz near the borders of carbonate bands. Sometimes the calcite forms lepidoblastic sieves, creating an optically continuous matrix around polygonal quartz. Generally there are two carbonate species present on the same slide with ferroan calcite predominating and comprising the monomineralic carbonate bands while the lesser siderite favours the biotitic domains.

The biotitic bands tend to be bimineralic with biotite-quartz, biotite-carbonate, and biotite-cordierite assemblages interlayered with more polymineralic bands of the same mineralogy. The biotitic bands typically exhibit well developed foliation fabrics, but with carbonate or cordierite heteroblastic polygonal textures prevail. In the biotite-cordierite assemblages, for instance, .2 mm scaly lepidoblasts of biotite border on puffy rounded to hexagonal cordierite grains. Occasionally the brown pleochroic biotite forms fine 1-3 mm monomineralic laminae exhibiting well developed decussate textures.

The biotitic compositions are the most favourable for the growth of porphyroblasts. Biotite itself, however, is by far the most common porphyroblast in quartz-carbonate domains, where it forms large (1-5 mm) xenoblastic sieves including polygonal quartz and calcite. Also, a few large (1-5 mm) xenoblastic sieves of garnet and hornblende are scattered throughout, seemingly unrelated to any particular host assemblage. Nevertheless, biotitic domains are on the whole far more porphyroblastic than the quartz-carbonate-rich assemblages. The near-monomineralic biotite bands host common 2-5 mm subidioblastic actinolite sieves and more rarely small (1 mm) idioblastic garnet, staurolite, and kyanite sieves including polygonal quartz. The staurolite in these biotitic laminae commonly forms interpenetrating twins. Massive xenoblastic garnet occasionally totally replaces the biotite laminae and the resulting garnet bands typically show cross band tension gashes filled with quartz. Peculiar sector twinned cordierite occasionally forms 2-4 mm porphyroblasts within the biotite laminae and these are rimmed by fine sericite.

Locally 1-5 mm subidioblastic actinolite and lesser garnet and staurolite totally replace biotite - cordierite - quartz assemblages with the poikiloblasts including polygonal quartz. The trace porphyroblastic chloritoid typically occurs as scattered 1 mm idioblasts in biotitic domains and on rare occasions forms .2 mm xenoblastic sieves that coalesce to bead stringers on the margins offthe monomineralic biotite laminae. The chlorite forms .2 mm sieves that coalesce to bead stringers on the margins of the monomineralic biotite laminae. The chlorite forms .2 mm laths that favour biotitic domains but also occur in quartzose domains, and these often transect the foliation at high angles. Interestingly, the minor muscovite shows the same textural features as biotite even to the extent that they occasionally occur as near-monomineralic laminae of well aligned sericite microlites which may be transected by 1 mm tabular books of either biotite or muscovite. The characterizing accessory zircon is evidenced by pleochroic haloes in biotite and, less commonly, in hornblende. Blue-grey zoisite laths are rare and are spatially related to the occurrence of the zircon. Trace pyrite typically forms patchy disseminations of .1 mm rounded grains, but this mineral shows numerous other textural associations as well, including: (1) glomeric aggregates rimmed by lepidoblastic biotite, (2) occasional large (1-2 mm) idioblastic cubes, (3) heavy disseminations along some sericite laminae, and (4) inclusion trains in garnet and staurolite porphyroblasts which are commonly at odd angles to the

compositional layering, indicating that these porphyroblastic species were rotated during growth (i.e., syntectonic in origin).

A further rock type noted here because it is thought to have an affinity to the biotitic-carbonate ironstones is a well-banded metacarbonate observed only at one spot location (D 112) in the Hatcher complex. In thin section this rock exhibits a well developed compositional layering with cyclic repetition between nearly monomineralic granoblastic carbonate bands (2-5 mm) and polymineralic heteroblastic carbonate - quartz - biotite bands to 10 mm. The carbonate bands consist essentially of calcite with minor dolomite and quartz. Pale brown biotite and minor white mica sometimes form foliae within the polymineralic bands, and here the micas can be interleaved with finely (.2 mm) polygonal zones of quartz and alkali feldspar. These foliae also host trace sphene. The biotite shows numerous pleochroic haloes, indicative of trace zircon. Magnetite is disseminated throughout as a fine dusting, while larger (.2 mm) idioblasts are concentrated along the boundaries between carbonate and the polymineralic bands.

d) Hydrothermal Chloritite

A peculiar, quartz-poor, densely porphyroblastic chloritic lithofacies forms the immediate footwall to sulphide mineralization in the Mineral district, along the New Canton trend, and again in the Andersonville district. The origin of this "chloritite" entails a considerable petrological problem as surface mapping complemented by detailed magnetic surveys and drilling in every area has demonstrated that although they may be of irregular thickness (as appears to be the case in the Mineral district and along the new Canton trend), they do nevertheless form continuous intervals with regional strike length (thousands of meters). The regional dimension and strataform nature of this particular rock type suggest a primary lithofacies laid down prior to sulphide deposition, while lithologically the rock bears evidence for having been produced by intense hydrothermal alteration. Needless to say, the genesis of this "hydrothermal chloritite" is an important key for unravelling sulphide metallogenesis.

Modal analyses of several samples of the hydrothermal chloritite from the Mineral district, New Canton trend, and Andersonville district are listed together in Table B.12. The first two samples listed demonstrate the mineralogy of transitional rocks showing affinity for both the chloritic subfacies of the pyritic ironstone-chloritite and the biotitic carbonate ironstone-chloritite. The remaining samples listed in this table show that the hydrothermal chloritite demonstrates a distinct mineralogical signature in each of the three respective areas: the chloritites from the Mineral district are typified by quartz - Mg chlorite - biotite - staurolite assemblages and are the only sample to host margarite, kyanite, and chloritoid; the chloritites from the New Canton trend are typified by Mg chlorite - garnet - quartz assemblages; the Andersonville chloritites are typified by garnet - phlogopite - staurolite assemblages and are the only samples to host actinolite - cummingtonite amphiboles. Zircon is the characterizing trace silicate in all areas, and most samples contain appreciable opaques with both magnetite and sulphides commonly occurring together.

Drill core intersections in the Mineral district illustrate that with increasing porphyroblastic content the pyritic and carbonate-bearing ironstones transit into the hydrothermal chloritite. The transition from pyritic

Table B.12: Modal Analysis of Hydrothermal Chloritite of the Mineral Assemblage

	1 CV87 781'	2 CV89 850-5'	3 CV89 1312'	4 CV89 1323'	5 CV88 1412'	6 ST	7 PE33	8 NC35	9 NC12	10 NC43	11 NC4	12 A191-10	13 NB77-1 397'	14 NB77-1 604'	15 NB77-2 416'	16 NB77-2 458'
plagioclase	-	-	-	-	-	-	-	-	-	-	-	-	2	10	-	-
albite	5	-	-	-	-	-	-	-	-	-	-	-	-	-	-	-
actinolite	-	-	-	-	-	-	-	-	-	-	-	-	2	65	-	5
cummingtonite	-	-	-	-	-	-	-	-	-	-	-	-	7	-	-	-
quartz	10	55	25	5	30	2	20	8	27	12	1	65	2	5	tr	10
Mg-chlorite	-	30	20	20	20	75	47	45	40	42	4	20	20	-	10	5
biotite/ phlogopite	60/	/6	20/	15/	/10	/10	-	-	-	-	-	-	/5	/3	/10	/5
green sericite	-	-	12	15	-	-	-	5	3	-	-	2	-	-	-	-
talc	-	-	-	14	10	-	8	5	-	5	-	-	-	5	-	-
serpentine	-	-	-	-	-	2	-	-	-	-	-	-	2	-	10	2
sillimanite	-	-	3	2	-	-	1	2	-	-	-	-	-	-	-	-
margarite	-	-	2	5	4	-	-	-	-	-	-	-	-	-	-	-
garnet	-	1	-	5	-	-	23	33	25	38	95	5	50	5	55	65
staurolite	15	-	8	6	20	8	1	2	4	-	-	2	8	5	5	5
cordierite	-	-	-	-	-	-	-	-	-	-	-	-	-	2	-	-
kyanite	-	-	10	8	-	-	-	-	-	-	-	-	-	-	-	-
chloritoid	2	-	-	2	-	1	-	-	-	-	-	-	-	-	-	-
calcite	5	1	-	-	-	-	-	-	-	-	-	-	-	-	tr	-
zircon	tr	tr	tr	tr	1	1	-	-	tr	-	-	-	tr	tr	tr	tr
gahnite	1	-	-	-	-	-	-	-	-	-	-	-	-	-	-	tr
magnetite	1	1	-	2	1	1	-	-	-	2	-	1	2	5	tr	3
ilmenite	-	-	-	-	-	-	-	-	1	1	tr	-	-	-	-	-
sulphides	1	1	-	1	1	1	tr	tr	tr	-	tr	-	-	-	10	tr

1-6 Mineral District 7-12 New Canton Trend 13-15 Andersonville District

ironstone to chloritite is particularly evident with the typical white sericitic lithology transiting first to the drab green chloritic subfacies and thence to dense green spotted chloritic schist with intensification of chlorite and concomitant growth of porphyroblasts. Sample CV 89-850.5 typifies the weakly porphyroblastic transition zone. In thin section this massive, well foliated, medium green rock shows a finely (.1-.3 mm) foliated assemblage of chlorite and quartz that hosts 1-2 mm biotite, garnet, magnetite, and pyrite porphyroblasts. The biotite forms lepidoblastic flakes that typically lie subparallel but occasionally crosscut the foliation. The garnet and magnetite occur as scattered idioblasts, while pyrite tends to be xenoblastic and confined to laminae rich in chlorite. Sample CV 87-781 represents a transition lithology between the carbonate-bearing ironstones and hydrothermal chloritite. This specimen was collected from a dark brown biotitic band particularly rich in porphyroblastic staurolite. In thin section it shows .5 mm decussate biotite hosting large (to 4 mm) glomeroporphyroblastic clusters of xenoblastic sieve staurolite which characteristically includes polygonal quartz, calcite, and pyrite. Notably, gahnite forms small (.2 mm) idioblastic grains that tend to cluster near staurolite. Magnetite forms isolated 1-2 mm cubes scattered throughout.

In the Mineral district the prototypical hydrothermal chloritite is a massive, spotted, pale bluish green, densely porphyroblastic schist. Thin sections reveal that the matrix to the porphyroblasts varies from a near-monmineralic finely foliated matte of .5 mm fibrous Mg chlorite to a relatively uniform polymineralic matte of well aligned .3 mm Mg chlorite, talc, and sericite with occasional minor sillimanite. This assemblage hosts 1-3 mm porphyroblasts of lepidoblastic to acicular phlogopite, 1-2 mm acicular kyanite, stubby .5 mm staurolite sieves, and 2-10 mm idioblasts of garnet. Minor margarite and muscovite sometimes occurs as fine (.3 mm) tabular porphyroblasts subparallel to or sharply crosscutting the foliation. The quartz typically occurs as a few scattered polygonal grains but occasionally forms discrete heteroblastic polygonal laminae with the quartz interleaved with parallel oriented sericite and chlorite; these particular laminae may be partially or wholly replaced by large (3 mm) xenoblastic chloritoid sieves hosting polygonal quartz.

The most quartzose of the chloritites exhibit marked compositional heterogeneity primarily due to variability in the quartz - chlorite - sericite distribution. This microdomainal heterogeneity is manifested in discontinuous lenticles of heteroblastic to granoblastic polygonal quartz hosting variable amounts of Mg chlorite and bordered by wavy foliar mattes of intimately intergrown chlorite and sericite. In these samples the porphyroblastic suite shows remarkable compositional specificity. The chlorite-sericite mattes host .2 mm microporphyroblasts of acicular muscovite, tabular margarite, and bundles of acicular sillimanite. Where the micaceous matte is most chloritic the assemblage is overgrown by large (5-10 mm) xenoblastic sieves of biotite/phlogopite and 2-10 mm idioblasts of garnet. The garnet tends to occur in the thickest part of these laminae. The polygonal quartz chlorite domains are overgrown by xenoblastic sieves of staurolite. Locally the staurolite sieves that typically host well preserved polygonal quartz laminae occasionally form nearly continuous bands (to 1 cm thick), suggesting local areas where the precise composition was ideal for staurolite growth. Where there is interlensing of polygonal quartz and sericite assemblages, kyanite is selectively overgrown on sericitic domains. The lepidoblastic biotite/phlogopite hosts up to 5% included zircon. The magnetite is typically scattered throughout as isolated 2-10 mm idioblasts with no apparent affinity

for any particular composition. The sulphides are disseminated throughout, but tend to aggregate in chlorite-quartz assemblages or in the more rare quartz-calcite assemblages. Locally these sulphides form semi-continuous cuspate masses within polygonal quartz laminae and may show this same habit within staurolite. Rarely, idioblastic magnetite may core some of the larger pyrite grains, suggesting sulphidization of original magnetite grains.

Along the New Canton trend the hydrothermal chloritite comprises very uniform, dense, phacoidal foliated, silvery green chlorite schist with variable amounts of quartz and porphyroblastic red garnet. Occasionally the garnet content intensifies to the extent of forming discontinuous massive red garnetite bands up to about 10 cm thick. In thin section the most chloritic lithology consists of a uniform crenulated matte of .3 mm parallel aligned chlorite intimately intergrown with minor pale green sericite and lesser talc; sometimes these minerals occur as laminae within the chlorite. The garnet typically occurs as 2.5 mm idioblasts that tend to cluster at the noses of microfolds.

The more quartz-rich assemblages show evidence of original compositional layering (mm-cm scale), but this is typically disrupted by microfolding and porphyroblastic growth of garnet. Notably, the microfold traces are sometimes preserved by polygonal quartz trains included in garnet. Normally the quartz occurs as .1-.5 mm heteroblastic polygonal grains interleaved with subparallel aligned chlorite. Where chlorite forms discrete laminae in the more quartz-rich lithologies these are rich in iron oxide and also host occasional subidioblastic staurolite sieves. The presence of spiral inclusion trains of polygonal quartz within the staurolite sieves indicates that these were rolled during growth. Very tight intrafolial microfolds are sometimes defined by interleaved chlorite-sericite laminae bordered by intensely polygonized quartz; the foliation fabric here may be sharply crosscut by idioblastic staurolite. Occasionally similar microfolds are defined by wormy bundles of sillimanite.

Where the chloritic facies has been intensely crenulated the garnet porphyroblasts tend to coalesce and, interestingly, to retain their idioblastic shapes to the point where adjoining grains give rise to domains of massive garnetite within the crenulated chloritite wherein minor included chlorite reveals the outlines of original idioblastic garnet.

Magnetite is the characteristic opaque in the New Canton chloritites where it is disseminated evenly throughout as .5-1.5 mm slightly rounded cubes. Less commonly, it forms spongy aggregates. Lath-shaped ilmenite locally replaces magnetite as the chief opaque, typically paralleling the foliation fabric defined by chlorite. Hematite was only noted in association with the monomineralic chlorite laminae in quartz-rich lithologies. Trace disseminated pyrite was observed within quartz-rich domains, but is not characteristic.

In the Andersonville district the hydrothermal chloritites form thick (up to about 50 m) beds of considerable strike length that are affiliated with the extensive ferruginous quartzite-oxide iron formation developed at the facies change from the central zone of amphibolite gneiss to the peripheral epiclastic sediment - mafic-felsic volcanic - ironstone assemblage. In this area the chloritite is a uniform varicoloured spotted schist with only minor blue-green fine-grained chloritic matrix remaining between coalescing 1-5 cm red garnet, 1-5 cm resinous brown staurolite, 4-6 cm dark green actinolite, and 1 cm chocolate brown phlogopite porphyroblasts.

Thin section textures are determined by the growth morphology of the various species. The shape of given porphyroblasts depends in turn on several variables including (1) attained size, (2) whether or not individual species are isolated from other porphyroblasts, (3) whether or not adjacent grains have interfered during growth, and (4) location in the crystalloblastic series. The smaller (3 mm) garnet idioblasts occur disseminated in matrix domains consisting of randomly oriented but intimately intergrown Mg chlorite-phlogopite and talc. These are typically inclusion-free and rimmed by pale brown phlogopite. The larger (greater than 1 cm) garnet porphyroblasts are xenoblastic sieves which occasionally are made up of coalescing subidioblastic subgrains. Staurolite exhibits idioblastic borders against the micaceous matrix assemblage but when in contact with garnet, the garnet morphology prevails. Actinolite forms 1-2 mm decussate prisms in chloritic domains and large (up to 6 cm) inclusion-free idioblastic blades that may be observed projecting through xenoblastic garnet -- a feature which suggests that actinolite has the strongest propensity to form idioblastic facies within this particular porphyroblastic assemblage. Colourless cummingtonite typically forms 1-2 mm acicular bundles of frequently bent grains in matrix domains of dark green granular biotite. Cordierite forms cloudy (incipiently sericitized) grains that accompany the rare heteroblastic polygonal quartz-albite (An8) matrix domains. Zircon forms numerous pleochroic haloes in phlogopite.

Magnetite is the most common opaque mineral and is typically disseminated throughout as small (1 mm) porphyroblasts with grain shapes determined by bordering minerals. In micaceous domains magnetite occurs as idioblasts, but against garnet forms oblong grains. The hematite is restricted to local granular dark green biotite masses. The sulphide minerals range from subidioblastic (pyrite only) to xenoblastic shapes and occur throughout as inclusion trains in garnet or staurolite porphyroblasts or as cuspate grains along porphyroblast borders. Notably, the sulphides concentrate in the domains richest in garnet, and here form glomeropoikiloblastic aggregates. Locally, sulphide masses replace the micaceous matrix assemblage and, rarely, may be observed partially or completely pseudomorphing original garnet and actinolite porphyroblasts.

e) Intrusive Bodies in the Mineral Assemblage

Intrusive material forms only a minor part of the Mineral assemblage but despite being quite localized nevertheless seems widespread along the segment of the Chopawamsic belt covered by this investigation. The largest known body occurs on the northwest flank of the Columbia synformal structure bridging southern Ferncliffe and northern Columbia quadrangles. Similar lithology was observed at one spot location in the poorly exposed core of this same structure, and again at a few spot locations within the Mineral assemblage bordering the atypical mafic metavolcanic core to the Andersonville district.

Megascopically the intrusive facies ranges from buff to mottled grey-green, uniform fine to medium-grained lithologies. Modal analyses of several typical samples are listed in Table B.13. As demonstrated, these lithologies fall into two groupings: very acid granophyres consisting essentially of albite and quartz with variable minor microcline, sericite, and chlorite; and quartz diorite consisting of albitic plagioclase, antiperthite intergrowth, and

Table B.13: Modal Analysis of Intrusive Facies in the Mineral Assemblage

	1 A113-23	2 A171-1	3 D70	4 D143-1	5 D155	6 D173	7 D134-2	8 D136-6	9 D138-2	10 D172-1	11 D172-2	12 D173-3
plagioclase	-	-	-	-	-	-	25	-	30	-	-	-
albite	65	45	50	20	50	25	-	20	-	10	30	10
alkali feldspar	-	-	-	-	-	58	20	-	20	-	15	10
potassium feldspar	20	-	8	-	-	-	-	-	-	-	-	-
hornblende	-	-	-	-	-	-	20	-	-	-	-	-
quartz	10	35	35	65	45	20	20	20	20	35	30	30
epidote	-	5	tr	-	3	2	-	10	15	25	2	5
chlorite	-	3	-	-	2	tr	-	15	5	10	2	10
sericite/muscovite	5/	/2	/5	/15	-	/tr	15/	/20	10/	-	/15	/22
biotite	-	-	1	-	-	-	-	2	-	15	5	8
garnet	-	-	tr	-	-	-	-	-	-	-	-	-
sphene	-	tr	-	-	-	tr	-	-	-	-	-	-
calcite	-	-	-	-	-	-	-	-	-	-	-	2
zircon	-	-	-	tr	tr	-	-	tr	-	-	-	-
magnetite	-	-	tr	-	-	-	-	3	-	5	1	3

1-6 trondhjemite

7-12 quartz diorite

quartz, with lesser epidote, chlorite, and muscovite. Notably, the one sample with modal hornblende was devoid of epidote and chlorite, indicating that these latter minerals within the quartz diorite may result from hornblende breakdown. Magnetite is a characterizing accessory of the quartz diorite facies.

i) Metatrondhjemite

Megascopically the trondhjemite forms a massive, non-banded, buff to medium grey, very fine-grained lithology which in thin section invariably shows the effects of intense cataclastic deformation. Where cataclasis has been extreme, streaky mylonitic textures prevail with a finely (.05 mm) granulated and optically oriented polygonal quartz-alkali feldspar assemblage hosting trains of annealed quartz bordering on lithic fragments with original allotriomorphic granular textures defined by interlocking alkali feldspar and quartz. When cataclastic deformation has been less extreme the 1-2 mm quartz-alkali feldspar grains exhibit rounded and polygonized grain boundaries, and the feldspars bent and wedge-shaped twins. A variety of alkali feldspar species including albite (An5), patch antiperthite, and minor microcline perthite coexist. The albite commonly shows both polysynthetic albite and pericline twinning. The antiperthite shows spindle-shaped exsolution lamellae of microcline.

Muscovite occurs as randomly oriented anhedral grains where igneous textures are preserved but is oriented parallel to the lithic fragments in cataclastic domains. Biotite and chlorite occur sporadically as minor constituents showing the same habit as muscovite. Minor very fine (.1 mm) granular epidote accompanies most feldspar grains and rarely the albite is totally replaced by intergrown epidote aggregates and chlorite sheaves. Rare xenoblastic garnet sieves are overgrown on such chlorite-epidote aggregates. The trace sphene and ilmenite also occur intergrown with epidote. The trace magnetite occurs as .2 mm euhedra inhomogeneously disseminated throughout, favouring domains rich in chlorite and muscovite.

ii) Meta-Quartz Diorites

Megascopically the quartz diorites are mottled, grey-geen-white, medium-grained rocks which in thin section also exhibit very disrupted igneous textures. Typically polysynthetically twinned plagioclase (An15-30) and lesser microcline occur as spongy rounded and incipiently sericitized remnants (up to 4 mm) in a finely (.02 mm) granulated groundmass of pervasively sericitized feldspar. Occasionally the remnant feldpars are rimmed by polygonal quartz and granular epidote. Where cataclastic deformation has been extreme these rocks may show streaky mylonitic textures defined by polygonal feldspar domains bordered by polymineralic foliae of chlorite, biotite, sericite, and quartz. The mylonitic assemblage is locally overprinted by metamorphic porphyroblastic growth of subidioblastic hornblende sieves, chloritic laths, lepidoblasts of muscovite and biotite, and occasionally idioblastic clinozoisite and xenoblastic aggregates of magnetite. Iron oxide forms the cores of many of the biotite porphyroblasts. Notably, even where both cataclastic deformation and metamorphic overgrowths has been intense, feldspar still occurs as occasional large (.8-2 mm), rounded, incipiently altered and somewhat polygonized

porphyroclasts.

Quartz epidote veining commonly crosscuts both feldspathic and mylonitic assemblages. Lenticular aggregations of annealed quartz are sometimes localized along thin, intensely polygonized (<.02 mm) cataclastic laminae. Locally quartz appears to have been secondarily introduced as a wholesale replacement of the feldspathic assemblage, primarily along microfractures but also by metasomatic engulfment. Where silica metasomatism has been intense the most prevalent feldspar occurring in the remnant feldspathic assemblages is the antiperthite with spindle-shaped exsolution lamellae. Interestingly, the most mylonitized rocks are accompanied not only by silicification but by increased modal chlorite and biotite and the appearance of calcite as well.

B.7 The Diverse Upper Chopawamsic Group

The rock types occurring along the contact between the Chopawamsic metavolcanic complex and the metashale formations occupying the cores of regional synformal folds are so diverse that they would defy any sort of group classification if it were not for the fact that regionally they occur at the same stratigraphic position. Indeed, it is on this criterion alone that they are treated as a group here. The differentiation of this group as a group is advantageous, however, if only because it focuses attention on regional contact relationships between the Chopawamsic metavolcanic complex and the younger metashale deposits.

In the following presentation the diverse upper Chopawamsic group is treated in the following manner. First, the rock types capping the Palmyra metavolcanic suite and basal to the metashales coring the Long Island and western limb of the Arvonia structure are discussed as a subgroup. As these particular units are at a lower metamorphic rank, they show a different petrographic signature than do the types occurring along the eastern side of the belt. Secondly, rocks capping the Mineral metavolcanic suite and regionally underlying the metashales of the western limb of the Columbia structure and eastern limb of the Arvonia structure are discussed together. A third subgroup comprises areally more restricted lithologies -- although differentiation of this particular assemblage from the previous subgroup is difficult (especially in the core of the Columbia structure and in the core of the Whispering Creek anticline) in that the restricted facies locally replaces the more regional lithology along the strike of the metashale formations. Finally, the last subgroup to be considered comprises an intrusive suite along the metavolcanic-metashale contact.

a) Lithologies Capping the Palmyra Assemblage

Regionally the contact between the Palmyra metavolcanics and overlying metashales is a focus for the development of ferruginous quartzite and oxide iron formation. Typically these lithologies transit through interbanding into a silicate facies iron formation basal to the metashales. More locally, however, peculiar chemical sedimentary lithologies occur at the interface between the Palmyra pyroclastics and metashales, and in this case these chemical sedimentary strata interband with a densely graphitic argillite facies

that forms the basal facies of the metashales. Near the nose of the Arvonia structure graphitic argillite onlaps the Palmyra pyroclastics; in this area reworked tuffite deposits formed at the contact and no chemical sedimentary deposits were observed.

Modal analyses of several samples collected near or at the contact between the underlying Palmyra pyroclastic series and overlying metashale are listed in Table B.14. As demonstrated, there is a tremendous variety of lithologies present. The first two samples listed illustrate the quartz-rich composition of tuffite developed in areas with no intermediary chemical sedimentary deposits. The remaining samples comprise mixed clastic and chemical sediments which may broadly be broken down into two transitional types showing mineralogical affinity with felsic and mafic volcanics respectively. The ferruginous sericitic metapelites show petrographic similarities to the Palmyra assemblage dust tuffs, but transit into siliceous ironstones with increase in quartz and magnetite or siderite. The chlorite-epidote metamarls show petrographic similarities to the Palmyra assemblage metaspilites, and these transit into carbonate-rich metamarls with increasing calcite or siderite. Biotite comprises a significant proportion of the chloritic metamarls and forms a more restricted facies which ranges from biotitic quartz-carbonate metapelite to near-monmineralic phlogopitic metapelite, both of which characteristically have minor talc. Tourmalinites consisting of quartz, tourmaline, and hematite form a further restricted facies.

i) Quartz Porphyry Tuffites

South of Palmyra near Little Mountain, an area which shows the greatest buildup of rhyolitic extrusives within the Palmyra assemblage, rhyolitic pyroclastics border directly on the regional metashales. The rhyolitic lithologies immediately adjacent to the metashales are typically much more rich in quartz phenocrysts than are the Palmyra rhyolite tuffs generally, and local reworking has given rise to a quartz eye tuffite base to the metashale in this area. In thin section the quartz porphyries exhibit a very fine (.05 mm) cryptocrystalline quartz-alkali feldspar groundmass which includes only very minor fine (.1 mm) granular epidote, acicular chlorite, and trace biotite. The assemblage hosts minor euhedral patch perthite microphenocrysts and a high modal percentage (over 40% was observed in outcrop) or coarse (to 8 mm) euhedral quartz phenocrysts. The latter are commonly polygonized and occasionally show .5-1 mm droplet-shaped inclusions of groundmass material. These quartz porphyries commonly reveal variable hydrothermal alteration effects including: (1) pervasive stockworks of quartz - chlorite - epidote veins which are commonly discontinuous and, where thickest (up to 1 cm), exhibit chlorite rims on .2 mm polygonal quartz-epidote cores, (2) 1-2 mm chlorite - epidote - opaque mineral segregation intergrowths, and (3) patchy chloritization. Where the rock is strongly chloritized, the chlorite often rims quartz phenocrysts.

The coarsely clastic tuffites derived by reworking of quartz-porphyry lithology are typically drab brownish grey lithologies with a phyllitic matrix supporting quartz eye clasts. As evident in thin section, the unsorted .5-8 mm subrounded quartz clasts lie in a very fine (.01 mm) sericitic matrix consisting essentially of aligned sericite and angular quartz. Graphite and pyrite locally replace sericite as the chief matrix minerals, and where these

Table B.4: Modal Analysis of the Diverse Upper Chopawamsic Group Capping Palmyra Assemblage

	1	2	3	4	5	6	7	8	9	10	11	12	13	14	15	16	17	18	19
	Pa6-1	Pa6-2	ZC24C	CV56-264'	CV53-184'	D146-1	D146-3	CV55-230'	Fe12-5	CV54-158'	Pa-1	CV52-148'	CV52-302'	CV55-285' (2 thin sections)	CV54-178'	CV56-175'	CV60-369'	CV55-135'	ZC-25
alkali feldspar	50	-	-	-	-	-	-	-	-	-	-	-	-	-	-	-	-	-	-
albite	-	-	-	-	-	-	-	-	-	3	20	-	-	-	-	-	-	-	-
quartz	40	85	20	75	70	92	95	55	80	45	20	30	15	35 - 30	30	25	60	2	60
epidote	5	tr	-	-	-	-	-	-	-	-	5	10	30	5 - 20	10	-	-	-	-
chlorite	5	-	-	3	-	-	-	-	-	-	25	35	50	12 - 30	20	35	-	-	-
actinolite	-	-	-	-	-	-	-	-	-	-	10	-	-	-	-	-	-	-	-
sericite	-	10	75	20	5	tr	4	10	-	20	-	-	-	-	-	-	-	-	-
biotite	tr	-	-	-	-	-	-	-	-	-	5	10	-	45 - 10	10	15	25	-	-
phlogopite	-	-	-	-	-	-	-	-	-	-	-	-	-	-	-	-	-	90	-
talc	-	-	-	-	-	-	-	-	-	-	5	-	-	-	-	-	-	5	-
garnet	-	-	-	-	-	-	-	-	3	-	-	-	-	-	-	-	2	-	-
calcite	-	-	-	-	15	-	-	-	-	-	5	10	5	-	15	25	13	-	-
siderite	-	-	-	1	5	-	-	2	-	30	-	-	-	3 - 10	15	-	-	-	-
dolomite	-	-	-	-	-	-	-	-	-	-	5	-	-	-	-	-	-	3	-
zircon	-	tr	-	-	-	-	-	-	-	-	-	-	-	-	-	-	-	-	-
tourmaline	-	tr	-	-	-	-	-	-	-	-	-	-	-	-	-	-	-	-	30
magnetite	-	-	5	-	5	8	1	33	5	-	-	-	-	tr - tr	-	5	tr	-	-
hematite	tr	-	-	-	-	-	-	-	10	-	-	-	-	-	-	-	-	-	10
rhodonite	-	-	-	-	-	-	-	-	2	-	-	-	-	-	-	-	-	-	-
graphite	-	4	-	-	-	-	-	-	-	1	-	-	-	-	-	-	-	-	-
pyrite	-	tr	-	1	-	-	-	-	-	1	-	5	-	-	-	-	-	-	-
chalcopyrite	-	-	-	-	-	-	-	-	-	-	-	tr	-	-	-	-	-	tr	-

1 rhyolite quartz porphyry (30% Ph, 5% f, 25% q)
2 quartz eye tuffite (80% clasts)
3 rhyolite dust tuff w/ magnetite lam
4 chert-clay pelite
5 ferruginous clay - carbonate chert
6 ferruginous chert
7 ferruginous pelite
8 iron formation
9 iron formation
10 pelitic siderite iron formation
11 tuffaceous marl
12 tuffaceous marl
13 marl
14 banded pelitic marl
15 carbonate marl
16 sideritic marl
17 siliceous clay-carbonate ooze
18 phlogopitic pelite
19 tourmalinite

define laminae the included quartz clasts are commonly bordered by dusty graphite rims. Very rarely fine (.3 mm) epidote and zircon clasts are also present. Trace brown coloured euhedral tourmaline grains are considered an authigenic constituent.

ii) Ferruginous Metapelites - Ironstone - Iron Formation

Sericitic metapelites are much more regionally extensive along the metavolcanic-metashale contact than are coarse pyroclastic-epiclastic lithologies. These rocks show considerable petrographic similarity with the Palmyra assemblage rhyolitic dust tuffs but there is also evidence that pelitic deposition overlapped with chemical precipitation of silica, Mg-Ca carbonate, and iron in oxide, carbonate, and sulphide mineral species. As a result of the overlapping clastic and chemical sedimentary processes there is a complete transition from sericitic metapelite through ferruginous mixed chemical clastic metapelites to ferruginous metacherts and iron formation.

The typical sericitic pelites are laminated pale green-grey to white phyllites consisting of 1 mm laminae of parallel aligned sericite interleaved with minor chlorite and polygonal quartz interbanded with discontinuous fine (.05 mm) heteroblastic polygonal quartz seams. Very delicate magnetite laminae, often consisting of .1-.2 mm subidioblastic single grain trains are commonly hosted within near-monomineralic sericite laminae. Disseminated idioblastic pyrite and siderite typically accompany quartz laminae, and where this occurs the latter are slightly coarser grained (.5-1 mm). In samples where there is considerable magnetite and carbonate (both calcite and siderite often coexist) the carbonate sometimes has a patchy distribution along the borders of both quartz and magnetite laminae. In the latter case, the carbonates locally rim discrete 1 mm quartz nodules. They also form 1 mm granoblastic polygonal laminations which may host delicate (<.4 mm) bands of sooty magnetite and minor quartz.

With further increase in quartz and iron content the sericitic metapelites transit into ferruginous quartzites and iron formation. Sample CV 55-230 is an excellent example of oxide iron formation within sericitic metapelite. This lithofacies is a very delicately laminated, dark grey to black argillite comprising a flaser laminated assemblage of magnetite and quartz. Minor sericite occurs as fine (.1 mm) aligned muscovite, while trace siderite occurs as 1 mm porphyroblasts hosting rotated magnetite laminae, indicating that these grew syntectonically. Occasional chaotic soft sedimentary slump structures occur in 1-4 mm intervals but, significantly, these are bordered by undeformed laminations. Minor quartz stringers also locally disrupt the laminations and may signify further disturbances during dewatering.

Ferruginous quartzites hosting bands of oxide iron formation characterize the contact between the Palmyra metavolcanics and metashale regionally. The pale grey, fine-grained ferruginous quartzite, which typically consists of uniform .3 mm polygonal quartz with cuspate and sutured grain boundaries, hosts homogenous disseminations of ultra fine (.02 mm) iron oxide (both magnetite and specularite may be present in the same rock) and minor to trace sericite occurring as .01 mm aligned microlites. These rocks generally show a very subtle layering (cm-m scale) due to modal variation in iron oxide content, and occasionally the iron oxide trains define fine lamination. Locally the iron oxide together with minor rhodonite comprises iron formation, with 1-10 cm

bands of over 80% metal oxide interlayered with ferruginous quartzite. A polished thin section of such iron formation (Fe 12-5) shows .1-.5 mm idioblastic magnetite grains intergrown with lath-shaped specularite grains and polygonal quartz. Interestingly, both minor rhodonite and garnet were found to be affiliated with this particular example of iron formation.

iii) Tourmalinite

Tourmalinite forms a restricted subfacies affiliated with feruginous quartzite. The tourmaline-bearing rocks may look quite similar to typical streaky banded grey ferruginous quartzites but in thin section they are observed to consist of heterogeneous granular masses of blue-green tourmaline in .2 mm polygonal quartz. Where the tourmaline masses are near-monomineralic the 1-3 mm tourmaline grains host polygonal quartz inclusion trains and show varying amounts of intergranular hematite cement. Occasionally these tourmaline masses appear rounded (1 mm scale), suggesting an oolitic origin. Locally the granular tourmaline has recrystallized to 1 mm randomly oriented idioblasts.

iv) Metapelite - Metamarl Transitions

Locally the sericitic metapelites also transit into sideritic metapelites and metamarl lithologies (this transition was only observed in drill core which, incidentally, also intersected the metashale contact and revealed interbanding of sericitic metapelite, metamarl, and graphitic meta-argillite at the base of the metashale). With increase in siderite (up to 30%) the light grey sericitic lithologies become a cream colour which quickly turns to a buff brown on weathering. Similar to the typical sericitic metapelite, these buff phyllites are also thinly (mm scale) laminated. The sericite-siderite bands consists of aligned .2 mm sericite interleaved with minor .05 mm polygonal quartz, and this assemblage is overprinted by 1-3 mm spongy xenoblasts of siderite with rotated inclusion trains of carbonaceous matter. The quartzose laminae consist of .3 mm quartz grains with common equilibrium textures developed; where these host minor sericite, siderite, and albite (An3), heteroblastic polygonal textures prevail. The trace pyrite commonly associated with the sideritic faces occurs as .2 mm cubes which favour the quartz-rich laminae.

v) Metamarl

Although siderite does occur as bands within sericitic metapelites, this mineral together with calcite is a more common constituent of the chloritic metamarl facies. Just as the sericitic metapelites show a petrological association with the Palmyra assemblage dust tuffs, the chloritic metamarls demonstrate an association with the Palmyra greenstones. Indeed, except for their consistently high carbonate content and characteristically sharply defined green-buff-yellow banding, the metamarls have considerable lithological overlap with the metaspilites, and in specific cases the differentiation of these respective rock types is very difficult.

The most enigmatic lithologies with respect to their derivation from mafic

flows or marly sediment comprise rather massive, medium green, fine-grained chlorite-carbonate schists. In all cases but one (Pa-1), however, these rocks show no plagioclase content or any textural characteristics indicative of a derivation through overlapping chemical-clastic sedimentation. In thin section Pa-1 reveals petrographic features strikingly similar to the metaspilites with their diagnostic patchy compositional heterogeneity. In this rock fine (.01 mm) polygonal quartz-albite domains border on mafic domains consisting of parallel oriented platy chlorite overgrown by columnar actinolite and ragged aggregates of very fine (.05) granular epidote. Locally the platy chlorite gives way to deep brown biotite and trace talc. The chlorite and biotite sometimes coexist as cleavage laminae of the same mineral grain. Calcite and dolomite form 1-1.5 mm xenoblasts randomly distributed throughout.

The metamarls range from uniform, medium green, finely foliated aphanites to thin-banded (cm scale) to laminated (mm scale) green-yellow-white, fine-grained schists. However, even where ostensibly megascopically uniform these rocks exhibit delicate laminations in thin section. This lamination is most commonly defined by interlayering of chloritic and quartzose laminae which consist of .02 mm dimensionally oriented chlorite interleaved with varying amounts of finely (.01 mm) polygonal quartz. The chlorite is typically accompanied by olive green biotite, and the quartz, more rarely, by polygonal albite (An2), polycrystalline blebs of clacite, and granular epidote. A subtle compositional layering is also often evident between carbonate-enriched laminae and chloritic laminae.

Where thin lenticular banding is most evident there is a tendency for the constituent minerals to partition into simpler bimineralic assemblages or, on occasion, monomineralic layers. The chloritic lenses are generally polymineralic and consists of aligned bundles of chlorite intergrown with biotite and interleaved with finely (.1 mm) polygonal quartz and minor stubby (.2 mm) epidote granules. The quartz and carbonate tend to form modally variable bands: where quartzose the texture is heteroblastic and the carbonate distribution patchy; where the modal carbonate content is highest the calcite and siderite form relatively pure granoblastic to heteroblastic polygonal mixtures.

Of the essential minerals, epidote shows the most varied distribution and textures. Although minor, fine (.1 mm) epidote granules are common in polymineralic assemblages. This mineral, together with lesser quartz and calcite, commonly forms discrete lensoidal bands. Within the epidote-rich bands, the epidote tends to form 1 mm nodular segregations which occasionally show concentric zones of epidote and quartz or, less often, radial epidote rimming quartz-iron oxide cores. Occasionally the epidote nodules are rimmed by carbonate. Epidote granules (.4 mm) are also common in chloritic laminae and locally the epidote and chlorite form .5 mm knots which may be bordered by biotite foliae. A few laminae are composed essentially of decussate biotite and granular epidote.

Where most iron-rich the metamarls show considerable modal carbonate and magnetite. These green-buff phyllites typically comprise very delicately laminated, modally variable chlorite-quartz-biotite assemblages interlayered with 1-2 mm bands of massive, finely (.05 mm) polygonal siderite with variable amounts of associated quartz. Also, siderite porphyroblasts to 1-2 mm in size are often scattered throughout. Tension gashes commonly crosscut the sideritic bands and these are filled with polygonal quartz. The magnetite in these rocks typically forms discrete but discontinuous laminae focused along the interfaces between chloritic and siliceous layers; occasionally these magnetite laminae

terminate crosscutting magnetite stylolites, suggesting that the magnetite precipitated from solutions expelled during dewatering.

Although biotite is a characteristic constituent of most metamarl assemblages, biotitic phyllites devoid of chlorite form a more restricted metamarl subfacies. This lithology occurs as a very delicately laminated dark grey phyllite with very regular (.5-.7 mm) polymineralic laminae consisting of .1 mm polygonal quartz with minor calcite and biotite bound by biotite foliae. Occasionally biotite laminae thicken (.5 mm) to become interleaved with dimensionally oriented quartz; such thickened domains host small (.2 mm) garnet idioblasts. Slightly coarser (.3 mm) polygonized quartz seams occur in quartzose bands, and these host trace disseminations of fine (.2 mm) idioblastic magnetite.

A very restricted (only one 10 cm interval was observed in drill core) variant of the biotitic subfacies comprises a uniform, very fine-grained, chocolate brown phyllite constituted by a near-monomineralic matte of parallel oriented microlites (.01 mm) of pale brown phlogopite. In thin section very subtle colour banding (mm scale) is evident, due to the presence of finely intergrown talc in the lighter coloured bands. Minor amounts of dolomite and quartz and trace pyrite in this lithology are observed forming discontinuous microveinlets and discrete 1 mm blebs scattered throughout the phlogopitic matte.

b) Regionally Extensive Lithologies Capping the Mineral Metavolcanic Suite

Regionally the contact between the Mineral metavolcanic suite and overlying metashales is a focus for the development of interbanded two-amphibole ironstones, ferruginous quartzite, and iron formation. The two amphibole ironstones show considerable petrographic similarity to the previously described mafic ironstones observed interlayered with the Mineral mafic metavolcanics, and these lithologies are considered to have close genetic ties. The two-amphibole ironstones are, however, far more quartz and magnetite-rich generally, and with increase in these minerals towards the metashale contact form a lean iron formation basal to the metashales. The contact between lean iron formation and metashales is very poorly exposed but appears to be sharp with both the Columbia and Arvonia metashale formations.

Modal analyses of several samples of the most regionally distributed of the diverse upper Chopawamsic group of rocks observed capping the Mineral metavolcanic suite are listed in Table B.15. As demonstrated, this regional assemblage includes hornblende-cummingtonite ironstones, ferruginous quartzite, oxide iron formation, and tourmalinites. The latter lithology is more restricted but was observed in numerous spot locations along the contact between the Mineral metavolcanics and overlying metashale formation.

i) Two-Amphibole Ironstone

The two-amphibole ironstones are characterized by striking compositional banding which most commonly comprises fine-grained blue-grey quartz - cummingtonite - magnetite assemblages interlayered with coarser grained dark green hornblendic bands. Completely transitional compositions between these

Table B.15: Modal Analysis of Regionally Extensive Lithologies of the Diverse Upper Chopawamsic Group

	1	2	3	4	5	6	7	8	9	10	11	12	13	14	15	16	17	18	19	20
	Mi3a	Mi3b	Pe20	Ca2c	Ca6b	Ar 1-1	Ar-6	Ar1901	A188	D107-1	P57	C13	Calb	P52-11	Law-6b	P51	A-14	D57-4	D102	D113
							q-f bnd / contact / hb bnd									gn bnd / q bnd				
plagioclase	-	tr	-	-	-	-	-	-	-	47	-	-	-	-	-	-	-	-	-	-
albite	50	30	-	20	20	50	45-1-20	40	-	-	-	-	-	-	-	-	-	-	-	-
hornblende	4	20	30	2	7	1	7-70-50	tr	5	20	-	-	-	-	-	-	-	-	-	-
cummingtonite	6	10	5	12	20	4	10-10-10	15	1	15	15	-	-	-	-	-	-	-	-	-
quartz	32	32	60	65	30	40	35-10-15	40	75	5	80	95	90	97	75	80-40	75	50	40	92
epidote	-	-	-	tr	-	-	-	-	-	-	-	-	-	tr	-	-	-	-	-	-
chlorite	-	-	-	-	20	2	- 2 -	-	2	-	-	-	-	-	-	-	-	-	-	-
sericite	-	-	-	-	-	-	-	-	-	-	-	-	tr	-	-	-	-	-	-	-
garnet	-	-	-	-	tr	-	-	3	15	8	3	-	-	tr	8	10-40	-	-	-	-
staurolite	-	-	-	-	-	-	-	tr	1	tr	-	-	-	-	-	-	-	-	-	-
sphene	-	-	-	-	tr	1	-	-	-	-	-	-	-	-	-	-	-	-	-	-
calcite	-	-	-	-	-	-	-	-	-	-	-	-	-	tr	-	-	-	-	-	-
zircon	-	-	-	-	-	-	-	-	-	-	-	-	-	-	-	-	-	tr	-	-
tourmaline	-	-	-	-	-	-	-	-	1	5	-	tr	-	-	-	-	25	45	60	8
magnetite	8	8	5	1	3	2	3-10-5	2	-	-	2	5	10	3	5	10-20	-	-	-	-
specularite	-	-	-	-	-	-	-	-	-	-	-	-	-	-	12	-	-	-	tr	-
graphite	-	-	-	-	-	-	-	-	-	-	-	tr	-	-	-	-	-	4	tr	-
pyrite	-	-	-	-	-	-	-	-	-	-	-	-	-	tr	-	-	-	-	-	-

1-10 2-amphibole ironstones
11-16 ferruginous quartzite - iron formation
17-20 tourmalinite

two species are evident, but the contacts between adjacent bands are still generally sharp and commonly accentuated by magnetite concentrations (a petrographic feature shown by banded oxide iron formation, though in this case much of the iron is tied up in silicate mineralogy). Rarely, both the hornblendic and cummingtonitic end-members form strikingly massive unbanded lithologies even at outcrop scale.

The hornblendic facies ranges from siliceous grey-green aphanites to coarse-grained (to 1 cm) near-monomineralic hornblendites. Very well developed Garbenschiefer textures are occasionally evident where coarse (1-2 mm) hornblende blades form radial stars on foliation planes parallel to banding. Massive cummingtonite lithologies are distinct, dense, white to buff rocks with notably high specific gravity. On surfaces sawn perpendicular to foliation these exhibit a diagnostic "chicken track" texture as a result of randomly oriented cummingtonite within the fine-grained light bluish coloured quartz-magnetite matrix.

Predictably, thin section textures vary considerably with modal variation. Although many specimens are feldspar-free, many of the samples studied proved to be unexpectedly rich albitic plagioclase. The typical polymineralic asssemblage comprises an inequigranular (.03-.5 mm) heteroblastic polygonal quartz-albite-magnetite pargenesis hosting .5-.3 mm subidioblastic hornblende sieves and 1-2 mm idioblastic cummingtonite blades generally free of inclusions. Quartz occasionally forms large (1-2 mm) polycrystalline grains that are typically slightly flattened parallel to banding. The albite (An0-5) typically forms corroded and cloudy grains showing the same polygonization as the quartz, but also occasionally appears as clear, often untwinned, amoeboid grains elongate parallel to the foliation. Both the larger polycrystalline quartz grains and amoeboid albite are interpreted to be a result of annealing during metamorphic recrystallization. Very occasionally, however, the plagoclase bears a primary igneous signature, as shown by 1 mm polycrystalline feldspar aggregates in which albitic plagioclase may be moderately normally zoned (an8-15). The most calcic plagioclase (An25) observed occurs as well formed polygonal grains intergrown with decussate hornblende; this very restricted paragenesis has the most mineralogical similarity to the mafic ironstone within the Mineral assemblage. Within these polymineralic bands the magnetite is uniformly disseminated throughout as very fine (.01 mm) dust and occasionally as .1 mm idioblasts.

Compositional layering is most accentuated between quartzo-feldspathic and hornblendic compositions; however, striking compositional layering is also evident between the hornblendic and cummingtonitic subfacies. Significantly, there is often a concentration of magnetite along the typically sharp contacts between bands where trains of 1 mm idioblastic magnetite grains are connected by thin (.4 mm) seams of polygonal quartz. The commonly near-monomineralic hornblendic bands may be constituted essentially by 2-4 mm decussate hornblende grains but where there is moderate quartz present the hornblende typically forms large (2-10 mm) radiating poikiloblasts with quartz inclusion trains preserving original bedding planes. Where the hornblendic bands are richer in quartz than in hornblende and have moderate magnetite dissemination, the hornblende tends to form smaller (.5-1 mm) well developed columnar grains that are often well aligned and define a foliation fabric parallel to the banding. Lepidoblastic flakes of chlorite locally accompany the hornblende facies, and where there is chlorite the hornblende is typically a paler green (actinolitic), forming 1-2 mm randomly oriented columnar sieves.

The cummingtonite bands are everywhere dominated by finely polygonal

quartz. These tend to be poorer in albite than the polymineralic bands but consistently richer in magnetite. The cummingtonite typically forms small (1-2 mm) radiating bundles and sheaves, but sometimes appears as near-monomineralic crosshatched splays with included polygonal quartz. The heavier disseminations of magnetite in the cummingtonitic facies tend to be heterogeneous in distribution, and glomeropophyroblastic aggregates consisting of .2 mm idioblasts are rather common.

In some bands both amphibole species are intergrown; the textural relationship between them depends on which is modally in excess of the other. In hornblende-rich bands the hornblende may host rare cummingtonite twin lamellae and sometimes shows cummingtonite rims. In cummingtonite-rich bands the cummingtonite blades commonly have hornblende terminations. In the latter case the boundary between cummingtonite and hornblende is knife sharp but cleavage is continuous across the boundary line. Notably, where hornblende and cummingtonite are both present the hornblende grains are more riddled by inclusions. The cummingtonite always tends to be relatively inclusion-free, but where inclusions are present these tend to be idioblastic magnetite grains.

There is surprisingly little in the way of accessory minerals associated with the two-amphibole ironstones. Porphyroblastic garnet is the most common trace mineral, and this occurs both in the hornblendic and cummingtonitic facies. In hornblendic facies, particularly in those bands with minor chlorite, the garnet tends to form slightly larger (2-4 mm, but in rare cases to 1 cm) subidioblastic sieves including quartz and magnetite. In the cummingtonite facies the garnet typically occurs as 1-2 mm inclusion-free idioblasts with finely polygonal quartz coronas free of cummingtonite, albite, and iron oxide. Occasionally the garnets show minor patchy retrogression to chlorite. Trace sphene is a rare constituent of hornblendic bands and fine (.05 mm) epidote granules very occasionally accompany the polygonal quartz-albite matrix assemblage.

ii) Ferruginous Quartzite - Oxide Iron Formation

With modal increase in quartz at the expense of plagioclase and amphibole, the ironstones transit into ferruginous quartzite and, with increase in iron oxide, thence to iron formation. Ferruginous quartzite intervals are common throughout the amphibole ironstones but are concentrated at the contact with the overlying metashales. A general increase in iron oxide occurs concomitant with the buildup of more highly siliceous units towards the metashales, and the thin (50 m) units of thin-banded (cm scale) oxide iron formation are more or less restricted to a position immediately basal to the metashales. The iron oxide buildup accounts for the striking regional magnetic ridge along the metashale contact.

The ferruginous quartzites, typically a red-weathering, sugary, grey-white, subtly thin-banded (2-5 cm) lithology, are commonly quite magnetic when the main iron oxide present is magnetite but also often non-magnetic and composed of quartz and specularite. In thin section these rocks typically exhibit equilibrium granoblastic textures with straight grain boundaries developed between .5-1 mm hexagonal quartz grains. Magnetite occurs as a very fine (<.05 mm) soot included in quartz or as .05-.2 mm idioblasts commonly sited at triple point junctions. Hematite occurs as .1 mm tabular grains that occur along the grain boundaries of the quartz. Occasionally the iron oxides concentrate into

diffuse patches bordered by iron oxide-free quartz. Both magnetite and hematite commonly show single grain trains defining lamination within the granoblastic polygonal quartz, and even in relatively iron oxide-poor lithologies these minerals occasionally form thin (.3 mm) laminations of massive iron oxide.

Only very occasionally do the ferruginous quartzites show impurities other than garnet. In rare cases there may be significant modal epidote which forms granoblastic polygonal grains with the quartz. In the sample with accessory epidote studied in thin section (P 33-11), the epidote, accompanied by trace calcite, garnet, and pyrite, forms a few small (.3 mm) grains which include magnetite. Trace calcite also occurs disseminated throughout, and typically forms hexagonal grains bound by quartz. The garnet in this same sample shows a very unusual disequilibrium texture, occurring as it does in laminae of massive hematite wherein it rims included pyrite. Significantly, the garnet here shows a yellowish brown colouration adjacent to the pyrite core but has colourless rims, indicating a core-to-rim compositional variation.

More typically the garnet is a significant component only where there has been such an intensification of iron oxide as to make oxide iron formation. In these rocks the distribution of iron and quartz is surprisingly heterogeneous, with clusters of .2 mm granoblastic quartz hosting 1 mm magnetite idioblasts bordered by massive sooty hematite-magnetite which may be intergrown with very fine (.05 mm) pale yellow garnet. In a few cases the granoblastic quartz grains have annealed to form coarse (2-3 mm) amoeboid grains hosting scattered aggregates of magnetite; these same coarse grains appear to be partially engulfed by the massive hematite - magnetite $\pm$ garnet assemblage.

Regularly banded (cm scale) iron formation with garnet-rich bands is not as widely distributed as the oxide iron formation, but does form a subfacies. In thin section (P 51) this facies shows 1-2 mm garnet-rich laminae interlayered with quartz-rich bands; the garnet-rich strata comprise minute ($<$.2 mm) garnet aggregates occurring along the grain boundaries of polygonal quartz grains or, where garnet is most enriched, define spongy overgrowths. The quartz-rich bands exhibit polygonal grains with curvilinear boundaries that only occasionally form 120° triple point junctions. Magnetite, which is concentrated in the garnet-rich intervalss, shows the same textural association as the garnet, though generally this latter mineral is better formed with most grains being subidioblastic and inclusion-free. Lesser magnetite and trace garnet are also disseminated in the silicic bands, and here both minerals generally occur at triple point junctions.

iii) Tourmalinites

Tourmalinites were observed at several spot locations within the ironstone - ferruginous quartzite - iron formation assemblage. However, the extent of this lithofacies at any given location is at present unknown. The tourmalinites range from black cryptocrystalline metacherts to sooty black massive tourmaline which is usually accompanied by earthy carbon and hematite. Some samples appear similar to bull quartz veins hosting fine tourmaline ribbons. In thin section the black tourmaline-rich metacherts comprise cryptocrystalline to massive strained quartz hosting a heavy dissemination of .1 mm idioblastic tourmaline, and very fine (.08 mm) granular tourmaline defines monomineralic laminae. Occasionally the tourmaline laminae broaden considerably into oriented bomb-burst microlites within adjacent quartz.

Rarely the sooty tourmaline concentrates into rounded structures along the laminae.

In thin sections of massive sooty tourmalinite, the tourmaline grains show a considerable variation in size (.05-1.5 mm) and shape (granular to idioblastic). Where very fine-grained the tourmaline forms a monomineralic matte with indistinct grain boundaries. When included in polygonal quartz, the recrystallized tourmaline typically tends to be idioblastic (may have either triagonal or hexagonal outline). These idioblasts commonly show blue cores and green rims, and are inclusion-free. The hematite and graphite accompanying the tourmaline in the sooty tourmalinite generally forms minor cement between adjoining tourmaline grains or, occasionally, where the amount of hematite - earthy carbon matrix increases, completely surrounds individual grains that show very ragged borders.

In thin sections the massive bull quartz hosting ribbon tourmaline comprises large (1-5 mm) polygonal grains with intense strain shadows and sutured grain boundaries. Here the tourmaline occurs in 5 mm heteroblastic polygonal quartz-tourmaline assemblages which form distinct but irregular parallel laminae. The quartz intergrown with tourmaline is more highly polygonized. lepidoblastic muscovite grains are sometimes interleaved with tourmaline along the laminae richest in granular tourmaline.

c) Areally Restricted Lithologies Capping the Mineral Metavolcanic Suite

The contact between the Mineral assemblage and overlying metashales is also a locus for more areally restricted deposits that occur locally along the length of the belt covered by this investigation. In the following discussion, the various rock types are subdivided on lithological grounds into two broad categories: (1) the quartzo-micaceous schists which make up Brown's (1969) Buffards Formation and Marr's (1981) Lower Arvonia micaceous schist unit as well as the slightly coarser muscovite schists that comprise the core of the Whispering Creek anticline and also occur within the core of the Columbia structure, and (2) quartzites, including mineralogically simple feldspathic and kyanitic variants plus a mineralogically complex type which hosts garnet, staurolite, gahnite, and commonly sulphide minerals as well. Of the quartzites the feldspathic types, including Brown's Bremo Formation as well as unnamed feldspathic quartzites in the Columbia structure, form the thickest and most localized deposits. The kyanite quartzites are the most regionally extensive of the group, showing their thickest development in the Willis Mountain area and along the western limb of the Columbia structure. The mineralogically complex quartzites are the most restricted, but may be observed in association with the other quartzite types at numerous spot locations near the base of both the Columbia and Arvonia metashales.

Modal analyses of several samples of these areally restricted lithofacies of the diverse upper Chopawamsic group are listed in Table B-16. As demonstrated, the quartzo-micaceous schists range from simple to complex mineral assemblages that include quartz - sericite - sillimanite - hematite, alkali feldspar - quartz - sericite - chlorite, and quartz - sericite - chlorite - biotite - garnet - magnetite. Margarite is a common member of all these assemblages but is not omnipresent. Zircon and tourmaline are characterizing trace minerals. The quartzites include the mineralogically simple feldspathic and kyanitic variants, while the mineralogically complex

Table D-15: Modal Analysis of Restricted Lithologies of the Diverse Upper Chopawamsic Group

	1	2	3	4	5	6	7	8	9	10	11	12	13	14	15	16
	D116-3	A152-6	A192	D117-2	A194	D61-1	D2	Buff	D112-1	Ca35a	D60-1a	D60-1b	D60-3	D140-6	A11-48	P8b
albite	-	-	-	-	-	15	tr	-	-	-	-	-	-	-	8	25
alkali feldspar	-	-	-	-	-	30	10	-	-	-	-	-	-	-	-	-
potassium feldspar	-	-	-	-	-	-	-	-	-	-	-	-	-	-	-	10
quartz	50	40	50	50	14	15	50	85	75	70	60	50	70	78	82	55
epidote	-	-	-	-	-	-	2	5	-	-	-	-	-	-	tr	-
chlorite	-	-	-	-	-	4	10	-	-	-	10	8	7	-	1	1
sericite	40	40	48	25	85	10	10	-	5	30	10	24	-	20	7	-
biotite	-	-	-	-	-	4	-	-	-	-	-	-	-	-	-	-
garnet	tr	tr	-	-	-	5	-	-	-	-	1	2	2	-	-	-
sillimanite	9	3	-	-	-	-	10	6	5	-	10	-	5	-	-	-
kyanite	-	-	-	-	-	tr	-	-	-	-	-	2	1	-	-	-
chloritoid	-	1	-	-	-	-	-	-	5	-	-	5	-	-	-	-
margarite	-	-	-	23	-	8	-	-	5	-	-	-	-	-	-	-
muscovite	-	1	-	-	-	-	-	6	-	-	-	-	10	-	2	8
calcite	-	-	-	-	-	-	-	-	-	-	-	-	tr	-	-	-
zircon	tr	-	-	-	-	1	-	-	-	-	-	-	tr	-	-	-
tourmaline	tr	-	-	-	-	-	-	tr	-	-	tr	1	-	-	-	-
magnetite	-	-	-	-	-	-	-	3	5	-	4	4	2	2	-	-
hematite	1	5	2	-	1	3	10	-	-	-	4	4	3	-	tr	-
pyrite	tr	-	-	2	-	-	-	-	-	-	-	-	-	-	tr	1

	17	18	19	20	21	22	23	24	25	26	27	28	29	30	31	32
	P52-1 P52-2	P52-3b CV73-51'			Ca5a	Law-1	D127-3	D130	D131	D130-23/	D131	D131-24-1/D131-34-1 D131-24-2/D131-34-2			Mi9a	Mi10g
albite	22	20	5	20	40	8	-	-	-	-	-	-	-	-	-	-
alkali feldspar	-	-	-	-	-	-	-	-	-	-	-	-	-	-	-	-
potassium feldspar	5	15	-	10	-	-	-	-	-	-	-	-	-	-	-	-
quartz	60	65	85	55	20	85	85	50	60	20	50	-	55	60	85	85
zoisite	1	-	-	-	-	-	-	-	-	-	-	-	-	-	-	-
chlorite	-	-	-	4	-	-	-	-	-	-	-	-	-	-	-	-
sericite	-	-	-	-	-	7	-	-	-	-	-	-	-	-	-	3
biotite/phlogopite	-	-	-	3/	/30	-	-	-	-	-	-	-	-	-	-	-
garnet	-	-	-	1	-	-	-	-	-	-	-	-	-	-	-	-
kyanite	-	-	-	-	-	-	10	45	25	15	40	95	30	15	15	12
clay	-	-	-	-	-	-	-	-	-	60	-	tr	-	-	-	-
pyrophyllite	-	-	-	-	-	-	2	-	2	3	-	2	-	5	-	-
muscovite	5	-	10	5	-	-	3	tr	3	2	2	3	5	10	-	-
calcite	-	-	-	1	-	-	-	-	-	-	-	-	tr	-	-	-
magnetite	-	-	-	1	10	-	-	-	-	-	-	-	-	-	-	-
pyrite	2	-	-	-	-	tr	tr	5	10	-	8	-	10	10	tr	tr

1-14 quartz mica schists

1-5 quartz mica schist
6-7 feldspathic mica schist
8 5% quartz eye mica schist
9 10% quartz eye mica schist
10 30% quartz eye schist
11-14 laminated quartz schist

15-23 feldspathic quartzite

23-32 kyanite quartzite

26 clay altered kyanite pegmatite
28 kyanite pegmatite

assemblage hosts variable amounts of quartz - sericite - staurolite - gahnite and sulphide minerals. Notably this particular quartzite subfacies may host accessory chalcopyrite, sphalerite, and graphite.

i) Buffards-Type Quartz-Mica Schists

By far the best exposures of the quartz-mica schist occur in the core of the Arvonia structure where, because of resistance to weathering, this lithology forms prominent ridges. In outcrop these schists are strikingly uniform and due to pervasive phacoidal foliations typically show a slightly knobby weathered surface. Significantly, except for the earlier described magnesian schists exposed along the Hardware arch, the quartz-mica schists show the most intense development of multiple schisosity of any lithology in the map area. Within the core of the Arvonia structure, outcrops along the western metashale-micaceous schist boundary show a sharp vertical contact typified by a streaky mylonitic fabric and coarsely fragmental textures accentuated by the common occurrence of rounded vein quartz clasts. The outcrops further east reveal moderate to shallow 15-30° easterly dips, and schists here lack the coarse fragmental appearance. In handspecimen the typical lithology is a mottled to streaky laminated, light green-silvery grey schist with interlensing 1-3 mm micaceous and quartzose domains bound by intersecting curvilinear sericitic laminae which produce the characterizing spindle-shaped foliation fabrics. Significantly, the lithology is slightly more greenish in colour along the eastern border, and here the schists are laminated in appearance. The subtle colour and textural changes occur in response to a change from relatively simple mineralogy to the more complex assemblages noted above.

The quartz-mica schists occurring east of the Arvonia metashales show several lithological variations. The correlative lithology which comprises a major part of the core of the Whispering Creek anticline is noticeably coarser in texture and typically consists of a simple quartz-rich mineralogy. Variation in the quartz:muscovite ratio gives rise to subtle 1-2 meter scale compositional banding of quartz-mica schist and muscovite quartzite. These coarsely recrystallized variants are occasionally interbedded with compact buff to pink porphyritic felsites; this particular lithofacies was not observed to accompany the quartz-mica schists outside of the Whispering Creek anticline. Quartz-mica schists rich in 2-8 mm quartz eyes comprise one further facies variant. This species has its greatest development along the thin zone of quartz-mica schist separating the western limb of the Arvonia metashale from the thickened part of the Ellisville intrusion north of the James River. Megascopically it appears as a very uniformlight grey-green schist with up to 35 modal % white to pale blue quartz eyes. Notably, the muscovite-rich, quartz-eye-poor lithology associated with the quartz eye schists in this location commonly hosts coarse (2.5 mm) porphyroblastic chloritoid.

In thin section typical micaceous schists from the core of the Arvonia structure show wavy mylonitic textures with fine (1mm) quartz-sericite laminae enclosing discontinuous (5-8 mm long and 1-2 mm thick) quartz laminae and/or monocrystalline quartz eyes. The dominant foliation is a curvilinear transpositional schistosity developed along microshears on the limbs of tight asymetric microfolds. Significantly, the lensoidal fabric predates the development of the tranpositional schistosity as the lenticular domains are themselves microfolded and further disrupted by offsets along the transpositional schistosity.

The wavy transpositional schistosity consists of .05 mm well aligned sericite interleaved with variable amounts of polygonal quartz. These laminae bound lenses of: (1) granoblastic polygonal quartzite which may or may not host very fine (.01 mm) aligned sericite and/or disseminated iron oxide(up to 20 % hematite and lesser magnetite were observed in some lenses), and (2) sericitic lenses which may or may not host sillimanite, chlorite, margarite, and iron oxide. Laminae with sillimanite bundles interleaved with sericite are generally the richest in iron oxide which, where most concentrated, forms semi-massive impregnations. The micaceous laminae richest in chlorite may host .2-.4 mm hematite laths oriented parallel to the foliation. The margarite and pale green chlorite typically occur interleaved with sericite but occasionally these minerals together with muscovite form .3 mm randomly oriented lepidoblastic porphyroblasts. Where garnet occurs it typically forms 1-2 mm idioblasts but very occasionally this mineral appears as xenoblastic sieves (to 1 cm) bordered by .1-.5 mm rims of interleaved dark brown biotite and chlorite. The rare chloritoid forms tabular porphyroblasts to 2 mm in the long dimension, and the even rarer clinozoisite occurs as 1-1.5 mm iron oxide rimmed poikiloblasts. Trace zircon is observed in the form of small (.1 mm) discrete grains that occasionally have idioblastic shapes.

Most samples have the foliation disrupted by 1.5 mm mono or polycrystalline quartz eyes and rounded untwinned orthoclase. The quartz eyes sometimes show embayments and very rarely have squarish shapes which suggest that they are relict phenocrysts. Significantly, the samples which have considerable modal feldspar do not show the extreme transpositional fabric evident in highly sericitic schists. This indicates that at least some of the sericite derives from feldspar breakdown. The feldspathic samples typically comprise a fine (.1-.3 mm) heteroblastic polygonal alkali feldspar-quartz assemblage interleaved with variable amounts of sericite and margarite. When associated with alkali feldspar, the polygonal quartz typically appears as strained lobate grains which locally have annealed to form cuspate grains to 1 mm in maximum diameter. The alkali feldspar generally forms untwinned oscillating zoned grains with occasional secondary twinned albite overgrowths. The feldspars are also commonly polygonized, with subgrains showing intricately sutured grain boundaries.

The very quartz-eye-rich lithologies typically have a yellowish grey muscovite as groundmass to the smoky to pale blue quartz eyes. In thin section they exhibit a porphyritic texture with large (2-4 mm) polycrystalline quartz eyes occurring in a well foliated sericite matte. Generally the quartz eyes show strongly polygonized terminations trailing off into the sericitic matrix. Inclusion of the sericitic groundmass within quartz eyes is quite common. These quartz eye porphyry samples typically show inhomogeneous disseminations of trace pyrite throughout the sericitic groundmass.

The mineralogically complex facies of quartz-mica schist occurring along the eastern inside limb of the Arvonia structure is characterized by lenticular laminations ranging from granoblastic polygonal quartz to subtly laminated heteroblastic polygonal quartz - sericite - magnetite - hematite - epidote - chlorite - garnet assemblages. In polymineralic assemblages adjoining quartz grains have sinusoidal grain boundaries. Where chlorite occurs in quartzose domains it is often intimately intergrown with white mica. Sillimanite is generally confined to sericitic laminae bordering the quartzose lenses. The garnet typically appears as small (1.5 mm) colourless idioblasts that form trains parallel to microfolding and locally concentrate near fold noses. The few isolated kyanite microporphyroblasts (.1-.2 mm) favour micaceous domains. Trace tourmaline is preferentially concentrated among sillimanite-rich sericite

laminae. Magnetite forms .1 mm cubes disseminated throughout, while hematite occurs as .2 mm laths concentrated along sillimanite-rich laminae.

The mineralogically simple coarse-grained quartz-mica schists of the Whispering Creek anticline are characterized by 1-2 mm granoblastic polygonal quartz with variable amounts of interleaved, parallel oriented (2-4 mm) muscovite laths typically sited along grain boundaries of appropriate orientation. Where there is very little white muscovite present equilibrium textures are pervasive, with adjoining quartz grains having straight boundaries meeting at 120° triple point junctions. The occasional quartz eye schists observed in the Whispering Creek anticline comprise variable amounts (up to 80 modal %) of 3-8 mm polygonized quartz eyes bordered by coarse muscovite foliae. A pale yellowish green muscovite is noticeable in the muscovite-rich samples, and very rarely thin (10 cm) bands of nearly monomineralic apple green fuchsite occur between muscovite quartzite intervals. In thin section the green muscovite-rich schists demonstrate subparallel aligned 3-5 mm lepidoblasts interleaved with minor polygonal quartz. Notably, the muscovite-rich schists are characterized by trace disseminated tourmaline and hematite.

In thin section the compact pink to buff porphyritic felsite lithology which is occasionally interlayered with the coarse quartz-muscovite schists of the Whispering Creek anticline comprises a very finely (.02 mm) foliated matte of polygonal quartz and untwinned alkali feldspar interleaved with sericite. This groundmass assemblage hosts scattered 1 mm rounded albite (An5), microcline, and quartz phenocrysts. The microcline phenocrysts are incipiently sericitized, while the albite phenocrysts are rimmed by sericite but free of internal alteration. The quartz eyes may be either monocrystalline or polygonized with sutured subgrain boundaries. Trace disseminations of hematite and acicular tourmaline are characterizing accessories. Significantly, isolated grains of randomly oriented idioblastic kyanite were observed in one sample.

The origin of the quartz-mica schist lithofacies is problematic. Brown (1969) interprets the Buffards Formation as having originally been a pyroclastic deposit, while more recently Marr (1981) identifies the quartz-muscovite schists at the south end of the map area as unconformity-related sediments at the base of the Arvonia metashale, interpreting the quartz eye schists as "jelly bean gravels." The present author favours the earlier pyroclastic interpretation. The quartz-mica schist is on the whole a very monotonous uniform lithology with marked compositional layering at a scale larger than the fine lamination generally characteristic of the most easterly coarse quartzose muscovite schists of the Whispering Creek anticline. The fine lenticular lamination predates the develoment of the strong transpositional schistosity and is reminiscent of the welded textures of subaereal ash flow deposits. Where the rocks are least deformed there can be considerable alkali feldspar present; the scattered distribution of 1 mm alkali feldspar and quartz porphyroclasts in the feldspathic variant suggests that these were originally phenocrysts.

The fact that the more common quartz eyes sometimes show embayments and sericitic inclusions is considered indicative of magmatic resorption, again supporting a primary igneous origin. The association of porphyritic felsites of undoubted igneous origin in the Whispering Creek anticline, moreover, provides a virtually unquestionable link with volcanism. Collectively these features are interpreted to substantiate a thesis of generation by pyroclastic ash flow eruption. The characteristic interleaving of micaceous and quartzose

domains hosting minor to heavy disseminations of iron oxide together with ubiquitous trace tourmaline suggests further that these flows were deposited subaqueously. This would also explain why the quartz-mica schists host minerals high in aluminum, since the original volcanic glass would be readily susceptible to hydrous breakdown.

ii) Feldspathic Quartzites

The feldspathic quartzites occurring near the nose of the Arvonia structure comprise the thickest deposit of feldspathic quartzite known along the segment of the Chopawamsic belt covered by the investigation. By far the best exposures of this particular lithofacies are found along the bluffs on both the north and south banks of the James River where it cuts through the Arvonia synclinorium at the village of Bremo Bluffs (Brown named this occurrence the Bremo Formation). Feldspathic quartzite is by no means restricted to the Arvonia structure, however, as this lithofacies is also observed in the core and on both limbs of the Columbia synformal structure. The most extensive development related to the Columbia structure occurs in the area where the South Anna River transects the east limb. Other locales with feldspathic quartzite include the core near the nose just north of the village of Columbia, in the vicinity of the Tellurium gold mine in Caledonia quadrangle, and again in the Mineral district.

The Bremo Feldspathic Quartzite

This feldspathic quartzite is characterized by conglomeratic lenses consisting of quartz pebbles and sometimes shale chips in festoon crossbedded arenite with shaly partings. Top directions indicated by the crossbedding and grading in the conglomeraitc lenses are variable and indicate that the Bremo is exposed in a series of anticlinal folds in the core of the Arvonia structure. A well developed axial planar cleavage is evident in most outcrops and locally this cleavage may be broadly warped. More locally, shaly compositions have further failed; these sometimes show small scale intrafolial folds defined by rather chaotic flow deformation.

Megascopically the Bremo feldspathic quartzite is a buff quartzite with slightly more whitish coloured feldspar clasts and pale green argillaceous matrix. The conglomeratic lenses are typically poorly sorted with open framework subangular 5-10 mm quartz granules and, in some lenses, common 1 cm shale chips hosted in a 2-3 mm arenaceous matrix. Microscopically the typical crossbedded arenite shows well sorted, moderately recrystallized, 1-2 mm polygonal quartz and incipiently sericitized alkali feldspar (patch antiperthite interleaved with variable amounts of dimensionally oriented sericite). Significantly, trace amounts of pyrite are characteristically disseminated throughout. The original crossbedding is best demonstrated by argillaceous laminae consisting of sericite with minor chlorite and graphite; these terminate against the quartz-alkali feldspar assemblage.

In the conglomeratic facies the matrix material is similar to the typical arenite but commonly shows higher admixed sericite and pyrite. The sericite is sited at the grain boundaries of the polygonal quartz and alkali feldspar, as well as being commonly concentrated in the pressure shadows of the quartz granules. These are finely polygonized and sometimes host trace disseminated opaque minerals, suggesting that they may have originated from chert. The shale chips comprise indistinct domains of feathery sericite interleaved with

very fine (.05 mm) polygonal quartz, and are rich in fine graphite and pyrite disseminations. The conglomeratic facies shows a slightly more varied trace mineral content with scattered grains of epidote, calcite, and chlorite; the calcite sometimes forms amoeboid grains including pyrite.

Feldspathic Quartzites of the Columbia Structure

A lithology strikingly similar to the Bremo feldspathic quartzite was observed near the nose in the poorly exposed core of the Columbia synclinorium. Megascopically this lithology is a buff massive feldspathic quartzite with subtly graded beds on the .5-1 meter scale. No crossbedding structures were observed. In thin section this occurrence demonstrates a more pervasive metamorphic overprint and exhibits a heteroblastic polygonal texture with 1.5 mm hexagonal shaped quartz grains and lobate alkali feldspar. Two species of feldspar are present: the albite (An5) grains are similar in size to the quartz, but the lesser microcline tends to form slightly larger (2 mm) amoeboid grains. Parallel aligned cleavage flakes of muscovite, biotite, and chlorite define a moderately well developed foliation fabric; the chlorite and muscovite also form a few lepidoblastic laths which strongly crosscut the foliation. Trace amounts of .5 mm subidioblastic magnetite and 1-2 mm xenoblastic garnet are disseminated throughout. Both chlorite and biotite show common pleochroic haloes indicative of accessory zircon. Calcite was observed as rare microveinlets.

In the vicinity of the Tellurium gold mine on the west limb of the Columbia structure feldspathic quartzite occurs as uniform buff units with white-weathering feldspar grains. These strata occur immediately below and interbed with the Columbia metashale. A transitional, both feldspathic and phyllitic lithology marks the first appearance of metashale, but this rapidly (over 2 m) transits into the grey non-feldspathic phyllite that typifies the metashale regionally. Except for the presence of significant modal feldspar these units are petrographically similar to ferruginous quartzites which are also common in this locale. In thin section the typical feldspathic quartzites at the Tellurium comprise a heteroblastic polygonal assemblage of quartz and remarkably fresh appearing albite (An0-3). The quartz grains are often annealed and have sutured grain boundaries with albite. The albite grains are commonly sited at the triple points of annealed quartz grains. Subparallel aligned minor muscovite and chlorite impart a poorly developed foliation. Rarely 2-3 mm xenoblastic knots of garnet intergrown with chlorite amd magnetite disrupt the uniform polygonal assemblage. Magnetite is the characterizing opaque, typically occurring as uniformly subidioblastic cubes sited at grain boundary junctions. The transitional phyllitic lithology shows the typical feldspathic quartzites interbanded with coarse (1-2 mm) biotite laminae. The biotite is a very pale brown (phlogopitic) and is locally replaced by hematite along cleavage planes.

The feldspathic quartzites observed near or at the base of the metashale at the north end of the Mineral district form the distinct topographical ridges but rarely outcrop. Megascopically the feldspathic quartzite at this locale is a buff saccharoidal quartzo-feldspathic semi-schist. In thin section the rock exhibits a finely foliated texture with .2 mm sericite needles strongly oriented within a .1 mm polygonal matrix of quartz and untwinned, incipiently sericitized alkali feldspar. Occasionally the quartz grains have annealed to form .3 mm lobate grains that sometimes have sericite rims. In the rare cases where the annealed quartz grains that sometimes border on one another, triple point junctions are developed between adjoining grains. Pyrite is the characterizing opaque, occurring both disseminated throughout and concentrated

along fine (1-2 mm) laminae parallel to the foliation fabric.

The most extensive deposit of feldspathic quartzite known to date in the Columbia structure occurs along its east limb in the South Anna River area. This particular occurrence differs from all others in that the feldspathic quartzite here is very fine-grained and has extremely regular thin (cm scale) banding. In outcrop the lithofacies shows a striking buff to rusty brown striping due to weathering of variable feldspathic and pyrite-bearing quartzite bands. In thin section the rock exhibits a subtle compositional banding defined primarily by variation in modal feldspar and quartz. A fine (.2 mm) heteroblastic polygonal assemblage of quartz and both twinned and untwinned alkali feldspar prevails, but the near-monomineralic quartzose bands have near-equilibrium granoblastic textures developed. On occasion -- particularly in the monomineralic bands -- the quartz has annealed to form slightly larger .5 mm grains. Both albite and crosshatched microcline are present and in the most feldspathic bands occasional two-feldspar myrmekite results from vermiform exolution of perthite in albite. Rarely, larger (1 mm) pervasively sericitized feldspar grains with cuspate borders are observed; these are identified as porphyroclasts after original phenocrysts. Fine (.05-.1 mm) sericite microlites may either lie subparallel and define a crude foliation paralleling the compositional layering or occur in random orientation controlled by the orientation of quartz-feldspar grain boundaries. Larger (to 1 mm) lepidoblastic muscovite grains sharply crosscutting the foliation fabric are not uncommon. Notably, near muscovite porphyroblasts the near-equilibrium textures defined by the quartz and feldspar change to a markedly more disequilibrium texture of cuspate grains with sutured contacts.

The feldspathic quartzite in the South Anna area is richer in trace minerals than that in other locations. Trace chlorite shows the same texture as the muscovite. Straw yellow bundles of acicular sillimanite, blue-grey kyanite blades, zoisite laths, and garnet porphyroblasts all occur as isolated .1-.2 mm microporphyroblasts in domains richest in pyrite. The pyrite is disseminated throughout as a fine dusting but also forms heavier disseminations along the more quartzose and most sericitic bands. In domains hosting porphyroblastic muscovite, the pyrite may occur in .3 mm subidioblastic cubes.

iii) Kyanite Quartzite

Kyanite quartzites are most extensively developed in the Whispering Creek anticline; within this area the greatest known thickness occurs at Willis Mountain where it is presently being actively quarried by the Kyanite Mining Corp. The resistance of the kyanite quartzite to weathering has given rise to the most persistent ridges in this part of the Piedmont and these form excellent regional markers. Outside of the Whispering Creek anticline the most prominent kyanite quartzite units were observed both north and south along strike from the South Anna feldspathic quartzite on the eastern limb of the Columbia synclinorium. A thin stratum was also observed immediately adjacent to the metashale contact in the Mineral district.

Megascopically the kyanite quartzites are everywhere white granular rocks with quartz hosting random to well-oriented, light blue-grey kyanite blades. Even megascopically, however, they show extreme variation in granularity and range from near-amorphous translucent quartzite to coarsely (2-5 mm) granular kyanitic schists. This variation in granularity and kyanite content defines thick (2-10 m) planar bedding in the quarries of Willis Mountain. Here the

lithology is notably free of accessory minerals other than the unusual amount of associated pyrite which comprises up to 10 modal %. On weathering the most pyritic lithologies develop distinct red hematite cemented caps in which the kyanite is also pervasively hematized to a brick red colour. Significantly, the most pyritic of the beds exposed in the Willis Mountain quarries often develop a pale green coating of secondary calcanthite. Pods of massive pegmatitic (blades to 8 cm) kyanite and knots of chalky white pyrophyllite are not uncommon in the kyanite schists.

In thin section the textures of the kyanite quartzites are determined by the porphyroblastic growth habit of kyanite and the degree of polygonization shown by the quartz. Typically the kyanite occurs as crudely aligned subidioblastic blades with slightly cuspate sides and dentate terminations. The individual grains are sometimes twinned and are often bent and microfractured. The largest (1-2 cm) kyanite porphyroblasts occur in the most quartz-rich facies. The quartz generally shows straight contacts against kyanite but cuspate to sinusoidal contacts between adjoining quartz grains. Where polygonization is most intense the kyanite forms 1-2 mm xenoblastic sieves with quartz and occasionally pyrite inclusions oriented along cleavage planes. It must be emphasized that there is no textural evidence to suggest an original clastic origin for the quartz in the thin sections studied.

The trace to minor amounts of muscovite and pyrophyllite that accompany the kyanite quartzite occur as .5-1.5 mm lepidoblasts oriented parallel to the kyanite; often these minerals forms intergrowths in the pressure shadows of the larger kyanite porphyroblasts. The pyrite occurs as .2-.5 mm subidioblastic pyritohedrons which tend to cluster in the most kyanite-rich domains. The kyanite and pyrite may mutually include one another. Notably, granular zircon was observed as an accessory in a few samples.

The kyanite schists have a decussate texture with 1-2 mm stubby kyanite laths intergrown with .5-1.2 mm polygonal quartz. Adjacent quartz grains in schists have sinusoidal borders while the kyanite laths exhibit straight sides and slightly dentate terminations. In most schists kyanite may also form larger (3 mm) subidioblastic blades which lie subparallel to the schistosity. Muscovite and pyrophyllite are typically enriched in schists over quartzite; these minerals form lepidoblasts oriented subparallel to the foliation fabric defined by the kyanite. Within schists the pyrite often shows a thin (.01 mm) muscovite rim and occasionally the pyritohedrons coalesce into amoeboid masses.

Pegmatitic kyanite knots within the kyanite schists are composed of coarse kyanite blades that abut and interpenetrate in random orientation. Pyrophyllite and muscovite intergrowths occur intergranular to the kyanite. These knots are sometimes incipiently altered to clay with remnant kyanite occurring in a boxwork of clay alteration, but the intergranular pyrophyllite and muscovite intergrowths are free of alteration.

The kyanite quartzites observed north and south along strike from the laminated South Anna feldspathic quartzites are petrographically similar to the coarsely granular kyanite quartzite at Willis Mountain except for the fact that they are devoid of pyrite. Where observed in the Mineral district, however, the kyanite quartzite has a different petrographic character. Here this lithofacies is a striking, bone white, very fine-grained to aphanitic quartzite with fibrous kyanite splays on a spaced foliation. Pyrite occurs as ultra-fine glomeric aggregations along light grey kyanite-enriched laminations and forms a well developed lineation. In thin section these rocks exhibit a

near-equilibrium texture with .5 mm granoblastic quartz grains forming straight boundaries intersecting at 120° triple point junctions. The kyanite is restricted to semi-continuous irregular laminae, and where these are thickest decussate textures are developed by the interleaving of subidioblastic kyanite with granoblastic quartz. The trace pyrite occurs as disseminated microporphyroblasts (very rarely to .4 mm) throughout, but shows appreciable increases within kyanitic domains.

iv) Mineralogically Complex Quartzites

Perhaps the most unusual and certainly the most mineralogically complex of the diverse upper Chopawamsic group lithologies is a species comprising staurolite and gahnite-bearing quartzite. This particular lithology was observed in numerous spot locations near the regional metashale contacts along the entire length of the belt covered: in the Mineral district, in the area of the South Anna feldspathic quartzites, in the vicinity of the the Tellurium gold mine, in the core of the Columbia structure, along the New Canton trend, and along the trend of ferruginous quartzites in the Andersonville district.

Megascopically this lithofacies forms a dense masssive grey quartzite with unevenly distributed varicoloured porphyroblasts of which the most striking include brown staurolite, green gahnite, and red garnet. In thin section these mineralogically complex quartzites exhibit .2-.3 mm granoblastic polygonal textures with common 120 triple points developed by adjoining quartz veins. Subparallel oriented microlites of sericite occur along the grain boundaries and project into adjoining grains. Rare .3-.5 mm lepidoblastic grains of muscovite and even rarer margarite of the same habit sometimes accompany the sericite; these slightly coarser grains occasionally have cleavage laminae of hematite. Very fine iron oxide is common and heavy disseminations may crudely define discontinuous laminae which are sometimes continuous through polygonal quartz grains.

Porphyroblasts are heterogeneously distributed in the quartzite and where modally high their growth forms to a large extent determine the local textures. The gahnite and staurolite typically occur as 1-2 mm patchy xenoblastic sieves in .2-.4 mm heteroblastic polygonal quartz. Notably, the former minerals not only show the same habit but commonly border on one another, on rare occasions forming parts of the same poikiloblast. Very occasionally they appear as subidioblastic grains which are free of included quartz. The garnet sometimes occurs as subidioblastic sieves but more often forms idioblasts that tend to be free of inclusions. Where these porphyroblastic minerals are concentrated minor brown biotite, chlorite, and, somewhat more rarely, sillimanite often accompany the typical host quartz-sericite assemblage. The biotite has common pleochroic haloes indicative of included zircon.

Significantly, these staurolite-gahnite-bearing quartzites characteristically host trace to minor amounts of sulphide. Pyrite is by far the most common sulphide mineral, typically occurring as .5 mm subidioblastic cubes in quartz-sericite assemblages but tending to form xenoblastic grains that cluster in monomineralic quartz domains. Where the pyrite is more heavily disseminated it defines diffuse laminations; locally it combines with chalcopyrite and sphalerite to form fine (1 mm) massive sulphide laminae. Where sulphides are abundant, intergrowths with garnet, gahnite, and staurolite are also rather common.

d) The Diverse Upper Chopawamsic Group Intrusive Facies

Not uncommonly the overlying metashale formations border almost directly on intrusive rocks; this is the primary reason why these latter have been classified as members of the diverse upper Chopawamsic group. It is significant that although the intrusive material is near or at the base of the metashales, in no case were these bodies ever found within the metashale. This would seem to indicate that shale deposition postdated the intrusive activity. Several regional relationships, however, suggest that the timing of this latter activity was late with respect to the Chopawamsic metavolcanic assemblages. Both the large Ellisville and the unnamed granodiorite bodies exposed at the north and south ends of the map area respectively show lithological relationships that tie them to the age of deposition of the quartz-mica schists. In the case of the Ellisville body, for instance, intrusive plagioclase porphyry is separated from the Arvonia metashale by a thin but persistent interval of massive, non-bedded, presumably extrusive "porphyritic" quartz eye mica schist. In the case of the Appomattox River body the connection is even more convincingly evinced by the fact that it is bordered entirely by quartz-mica schist with a transitional facies developed at the interface. The thin diorite sills with locally associated peridotite differentiate also demonstrate relationships tying them to the late Chopawamsic period. These occur along the margins of the Ellisville sill and of the Long Island and Columbia structures, in the latter case hugging the outside contact with metashales on the western limb and nose and continuing along the eastern limb at the same approximate structural location, where they separate upper Chopawamsic quartzites from the high grade gneissic terrane further east. Notably, the only peridotite sill that was observed unassociated with diorite occurs on the eastern limb.

One further regional lithological relationship suggesting that the intrusions are of late Chopawamsic age is an affiliation of intrusive material with ferruginous quartzite and iron formation. Screens of iron formation can be found in the Ellisville sill, while the areas with diorite along the margins of both Long Island and Columbia structures are typically the focus for the best development of ferruginous quartzite - iron formation deposition at the shale base. This association is best demonstrated, however, by the highly magnesian amphibolites which occur interbanded with oxide iron formation at the base of the metashale in the Mineral district, at facies changes from basal metashale silicate iron formation to ferruginous and kyanitic quartzites in the Whispering Creek anticline, and interlayered with the extensive ferruginous quartzite units in the Andersonville district.

Modal analyses of several samples of this diverse upper Chopawamsic intrusive suite are listed in Table B.17. As demonstrated, the granodiorite consists essentially of plagioclase with variable amounts of asociated alkali feldspar and quartz, and minor epidote, muscovite, and biotite. The diorites contain plagioclase and hornblende with minor quartz; alteration of plagioclase and hornblende gives rise to moderate to considerable modal epidote, chlorite, and sericite in this facies. Lithologies more mafic than diorite are pervasively altered, containing variable amounts of magnesian silicates including hornblende, tremolite, Mg-chlorite, talc, and serpentine; anthophyllite was observed in one sample. Significantly, the magnesian amphibolites interlayered with iron formation are nearly monomineralic in amphibole or Mg-chlorite.

Table B.17: Modal Analysis of the Diverse Upper Chopawamsic Intrusive Suite

	1	2	3	4	5	6	7	8	9	10	11	12	13	14	15
	Fe-10	ZC-10	GD-E	ZC37-3	ZC-29	ZC-28	Co-3	Ca-1d	Ca-1e	Co-12	Law-3	Law-9	Ca-1	Ar190-1	D26-6
plagioclase	70	50	30	-	50	40	25	70	-	5	-	-	-	-	-
albite	-	-	5	30	-	-	-	-	-	-	-	-	-	-	-
alkali feldspar	-	20	20	30	-	-	-	-	-	-	-	-	-	-	-
potassium feldspar	5	-	20	10	-	-	-	-	-	-	-	-	-	-	-
hornblende	-	-	tr	3	20	30	70	27	-	40	20	80	-	-	-
tremolite	-	-	-	-	-	-	-	-	10	10	75	19	40	60	-
anthophyllite	-	-	-	-	-	-	-	-	-	-	-	-	-	9	99
quartz	13	10	15	10	10	5	5	3	-	-	-	-	-	-	-
epidote	4	2	tr	3	10	5	-	-	-	-	-	-	tr	-	-
chlorite	1	-	2	2	-	5	-	-	30	15	5	-	30	30	-
sericite/ muscovite	2	10	3	5	10	10	-	-	-	-	-	-	-	-	-
talc	-	-	-	-	-	-	-	-	30	15	-	-	-	-	-
serpentine	-	-	-	-	-	-	-	-	30	15	-	-	30	-	-
biotite	5	5	5	6	5	5	-	-	-	-	-	-	-	-	-
sphene	-	tr	-	-	3	tr	-	-	-	-	tr	-	tr	-	-
zircon	-	-	tr	tr	-	-	-	-	-	-	-	-	-	-	-
magnetite	-	-	-	-	-	-	-	-	-	-	tr	1	-	1	-
ilmenite	-	3	-	-	2	-	-	-	-	-	-	-	-	-	-
chromite	-	-	-	-	-	-	-	-	-	-	tr	-	tr	-	1
pyrite	-	-	tr	tr	-	-	-	-	-	-	-	-	-	-	-

1-2 plagiogranite porphyry
3 porphyritic granodiorite
4 granite
5-8 diorite-gabbro
9-10 peridotite
11-15 magnesian amphibolite

i) Granodiorite

The Ellisville granodiorite body consists of a large northern stock (only partially lying in the map area) and a central sill which thickens considerably at its southern end to underlie much of the area between the noses of the two major Arvonia and Columbia synformal structures. Although the southern and sill-shaped parts of this body show lithological relationships indicating that they are pre-shale in age, the northern stock may well have had a longer-lived active intrusive history. Certainly no iron formation or metashale was observed bordering the Ellisville stock northwest of Louisa, which suggests that both these lithologies pinch out where the Ellisville changes from a sill to a stock-shaped body. Furthermore, it was noted that although the sill and southern parts have a well developed foliation fabric much of the northern stock is unfoliated; most notably a non-foliated granitic facies comprises a significant part of its core. It is therefore quite probable that the Ellisville body is in fact a composite intrusive entailing facies of differing ages, i.e. earlier foliated plagiogranite and later porphyroblastic granodiorite-granite.

In outcrop the sill and southern parts of the Ellisville granodiorite form a uniform porphyry consisting primarily of rounded 5-8 mm white plagioclase phenocrysts hosted in well foliated biotitic groundmass. In thin section the original porphyritic texture is obscured by strong metamorphic overprinting. Original oligoclase (An12-15) phenocrysts have rounded shapes and indistinct borders due to intensification of both polygonization and sericitization at the rims which results in a transition into an assemblage of polygonal feldspar interleaved with aligned sericite. The sericite locally intensifies to the point of forming wavy laminae. The groundmass quartz has been both polygonized and annealed to form amoeboid grains. The inhomogeneously distributed sericite is interleaved with the polygonal quartz and is generally aligned so as to produce a streaky foliation fabric. Chlorite, quartz, epidote, and hematite occasionally form discontinuous polymineralic veinlets paralleling oriented biotite and sericite laminae. The accessory sphene forms 1 mm subhedral grains that are locally intergrown with ilmenite. Trace zircon occurs as a part of the interstitial groundmass assemblage and also gives rise to pleochroic haloes in biotite.

Near the western contact with the thin quartz eye mica schist zone which in turn borders on the Arvonia metashale, the southern thickened part of the Ellisville becomes far more compositionally heterogeneous and locally coarsely porphyroblastic. Both albite and microcline are observed as phenocrysts up to 4 cm in the long dimension, and these are sometimes accompanied by polycrystalline massses of bluish quartz 2.5-18 mm in diameter. The micaceous groundmass minerals form wavy laminae wrapping around both the quartz and alkali feldspar metacrysts.

The northern stock of the Ellisville is a massive porphyritic granodiorite with randomly oriented pink microcline megacrysts (up to 2 cm) occurring in a 2-4 mm allotriomorphic groundmass of oligoclase (An12-15), biotite, quartz, and, locally, hornblende, and microcline. Although this lithology does not have the penetrative foliation fabric evident in the porphyritic sill and southern part, the effects of a metamorphic overprint are evident in the rounding and granulation of grain borders and cross-grain microfracturing. The large microcline phenocrysts are euhedral in shape but show some grain boundary

dissolution, often hosting albite and vermiform quartz near rims. The minor hornblende is generally chloritized.

A uniform pink equigranular 2-4 granitic subfacies forms a significant subfacies in the central part of the northern stock. In thin section this lithology exhibits an allotriomorphic assemblage of albite, patch perthite, microcline quartz and biotite. On rare occasions 3-5 mm subhedral green hornblende is present. These grains show igneous reaction texture, with the hornblende being rimmed by biotite, indicating that the early crystallizing hornblende was unstable when the allotriomorphic assemblage crystallized. All of the alkali feldspar species are incipiently sericitized, particularly along cleavage planes. The minor epidote is commonly intergrown with quartz and at times these intergrowths appear myrmekitic, perhaps having originated through autometasomatic epidotization of late quartz-feldspar myrmekite. The epidote and biotite both show common pleochroic haloes indicative of included zircon.

The Appomattox River body was not studied in any detail. However, megascopically this intrusive is lithologically similar to the sill and southern part of the Ellisville. As reported by Marr (1981), the rock is light grey to white, medium to coarse-grained, and moderately foliated. it is chiefly composed of plagioclase (An25), with lesser quartz, muscovite, biotite, and microcline.

ii) Composite Diorite-Gabbro-Peridotite Bodies

The mafic to ultramafic sills are typically small but are widespread in their occurrence. Although observed at numerous spot locations none of these intrusives are well enough exposed to reveal relationships between the mafic and ultamafic facies. However, a uniform saussuritized diorite with unfoliated igneous textures is by far the most frequently observed rock type, and this facies almost certainly dominates most of the occurrences.

Megascopically, the dioritic facies forms a uniformly textured, fine to medium-grained, green-white mottled lithology. In thin section it exhibits primary hypidiomorphic granular textures defined by strongly interlocking 2-3 mm subhedral plagioclase laths and equant hornblende (the shape of the hornblende suggests that this mineral may pseudomorph original pyroxene; however, no pyroxene remnants were observed). The plagioclase (An35) is almost always pervasively epidotized, while the hornblende typically shows a patchy breakdown to chlorite. Slight inhomogeneity is occasionally observed, with local microdomains consisting predominantly of coarse (4-5 mm) chloritized hornblende hosting minor plagioclase laths in subophitic textural relationships. The minor quartz is anhedral and occurs interstitial to the plagioclase and hornblende. The sporadic minor microcline is also anhedral and quartz sometimes forms thin rims between the microcline and plagioclase. The occasional ragged muscovite, exhibiting a habit similar to the patchy alteration chlorite, is restricted to domains where the saussurite from plagioclase breakdown has recrystallized to coarse .5 mm radiating sheaves of epidote. The epidote occasionally forms veinlets that randomly transect the rock. The accessory sphene forms large (2 mm) anhedral masses which appear to be primary.

The more mafic facies affiliated with the diorite bodies are massive, melanocratic, coarse-grained (to 1 cm), uralitic rocks that may be totally devoid of plagioclase. In thin section the samples that do have plagioclase

exhibit a coarse (4-8 mm) hypidiomorphic inequigranular texture with equant poikilitic hornblende (pseudomorphing original pyroxene) forming a strongly interlocking network with minor, pervasively saussuritized anhedral plagioclase occurring interstitially. Two varieties of amphibole are typically present: a high order birefringent pargasitic (?) hornblende and tremolite. The former sometimes exhibits a peculiar vermiform to droplet replacement by talc and in places is completely replaced by fine-grained talc-serpentine aggregates. The droplet texture possibly suggests original pyroxene intergrowths with the more magnesian phases most readily retrograded to the talc-serpentine alteration product.

Samples devoid of plagioclase exhibit a coarse (3-5 mm) cumulate texture with rounded primary olivine grains (completely pseudomorphed by fine serpentine-talc aggregates) hosted by a felted matte of tremolite intergrown with patchy talc. Odd zonation textures within this matte suggest that it may have originally consisted of coarse intercumulus pyroxene. Rarely, coarse (5 mm) anhedral augite, with original exsolution lamellae preserved by talc-tremolite alteration, occurs as strongly interlocking grains hosting minor rounded olivine. The remnant igneous textures are sometimes completely destroyed by foliation fabrics; the foliated domains comprise a fibrous talc - chlorite - serpentine matte overgrown by .5 mm acicular tremolite porphyroblasts.

iii) Magnesian Amphibolites (Metakomatiite?)

Peculiarly magnesian amphibolites are widely distributed along the entire segment of the belt covered by this investigation. Significantly, in every case this particular lithology shows a close spatial relationship with well developed oxide iron formation, and the amphibolitic lithology itself is generally weakly to moderately magnetic. Megascopically the magnesian amphibolites are uniform, medium green, finely foliated to coarsely fibrous textured rocks which are schistose only where there is considerable modal talc. Even specimens consisting almost solely of chlorite typically do not have schistosities developed.

No remnant igneous textures were observed in any of the numerous specimens studied in thin section. The textures vary according to the types of amphibole present and the modal variation between amphibole and chlorite. In samples almost wholly composed of amphibole, coarse (up to 1.5 cm), randomly oriented, simple twinned porphyroclasts of tremolite locally abut one another to form coarse mosaics. Typically these show the effects of postcrystalline deformation with common microfolding, bending of grains, and local development of foliation fabrics. Where deformation has been extreme, amphibole metacrysts occur as remnants in a fibrous matte of .1-1.2 mm anthophyllite. Within this recrystallized assemblage the amphibole grains are commonly zoned with pale green cores and colourless rims. Those grains that have the highest birefringence here often reveal moderate lavender blue pleochroism, suggesting a crossitic component. Sometimes the fibrous recrystallized assemblage comprises laminae that penetrate earlier amphibole metacrysts; where such deformation laminae crosscut preexistent cleavages, reticulate textures develop, and with the common incipient breakdown of the amphibole metacrysts to anthophyllite this results in remnant boxes of the original tremolitic metacrysts in an anthophyllite matrx.

Trace magnetite and chromite are disseminated throughout and are diffusely

included in both early and late crystallizing amphibole. Rarely, a deep yellowish red trace mineral with both high relief and birefringence occurs in .2 mm patchy disseminations; this is tentatively identified as sphene heavily impregnated with iron-titanian oxide.

The more mineralogically complex samples generally show a slightly heterogeneous distribution of the constituent minerals. Most commonly, fibrous bundles of anthophyllite intimately intergrown with Mg-chlorite host patchy tremolite and occasionally polygonal quartz. The fibrous anthophyllite in this instance commonly forms folded splays, but as this happens where there is no evident penetrative foliation it would appear to be a growth habit of anthophyllite in this medium. Where the rock is chlorite-rich, on the other hand, a foliation fabric prevails, defined by a .05 mm matte of well oriented chlorite sheaves, scaly talc, spherulitic serpentine, and small (.2 mm) platelets of tremolite. This foliated matte assemblage hosts occasional (1-2 mm) columnar anthophyllite porphyroblasts oriented subparallel to the foliation.

In one sample (D-26-6) nearly monomineralic Mg-chlorite was observed to occur as .5-1 mm polygonal grains defining non-foliated near-equilibrium metamorphic textures. The chlorite here was colourless to very pale green in plain light and showed low order birefringence; most grains were characterized by schiller structure. In this sample trace chromite (.2 mm) formed inclusion trains and local glomeric knots in chlorite.

B.8 Post-Volcanic Metashale Formations

The affiliation of regional iron formation with the metavolcanic-metashale contact zone results in one of the most unique lithological relationships to be found in the area of investigation. In everycase where metashale is preserved in the regional synformal infolds one limb of the metashale shows the development of an irregular, thin (in the order of 50 m), but regionally persistent basal silicate iron formation. This iron formation is not only the best regional marker in the map area, thus proving invaluable as an aid to deciphering the regional stratigraphic and stuctural framework, but is also an excellent indicator of peleoenvironmental conditions at the onset of shale deposition.

Modal analyses of both the basal silicate iron formation and overlying metashale are listed in Table B.18. As demonstrated, below the garnet isograd, the silicate iron formation comprises a modally variable Fe chlorite - quartz - iron oxide assemblage. Above the almandine isograd this same lithology comprises a striking, coarsely porphyroblastic garnet - quartz - grunerite assemblage. The several samples of metashales demonstrate a modally uniform quartz - sericite - biotite - garnet assemblage with variable amounts of chlorite; an inverse relationship is apparent between the amounts of modal chlorite and biotite-garnet, indicating that the latter grew largely at the expense of the original chlorite content. Characteristically, the metashales have trace amounts of zircon, tourmaline, graphite, and pyrite.

a) Basal Silicate Facies Iron Formation

Where exposed along the western border of the Long Island metashales the

Table B.18: Modal Analysis of Representative Samples of Regional Metashale Formations

	1	2	3	4	5	6	7	8	9	10	11	12	13	14	15	16	17	18
	Co-8	Co-9	Co-19	Co-20	Co-24	Co24-d	CV71-133'	C-8	D58-1	A-22	A-50	D60-c	A-9	A11-48	A19-1	Pe-33	Pe33-d	Co-7
albite	-	-	-	-	-	-	5	-	-	-	-	-	-	8	-	-	-	-
grunerite	-	-	-	-	-	-	-	10	10	20	-	-	-	-	-	-	-	-
quartz	40	70	90	40	80	35	25	35	5	25	20	15	10	80	77	50	50	40
epidote	-	-	-	-	1	-	-	-	-	-	-	-	-	tr	-	-	-	-
chlorite	40	10	-	-	11	20	3	-	5	-	45	8	15	1	-	5	5	30
chamosite	-	-	-	45	-	15	-	-	-	-	-	-	-	-	-	-	-	-
margarite	-	-	-	-	-	-	-	-	-	-	-	1	-	-	-	-	-	-
sericite	10	10	-	-	-	5	-	-	-	-	-	7	-	8	15	25	30	25
biotite	-	-	-	-	-	-	10	-	-	-	-	-	-	-	5	10	10	5
garnet	-	-	-	-	-	-	50	45	80	50	-	3	10	-	3	5	1	3
staurolite	-	-	-	-	-	-	-	-	-	-	-	-	1	-	-	-	-	-
chloritoid	-	-	-	-	-	-	-	-	-	-	-	-	-	-	-	-	1	-
kyanite	-	-	-	-	-	-	-	-	-	-	-	62	55	-	-	-	-	-
calcite	-	-	-	-	-	-	5	-	-	-	-	-	-	3	-	-	-	-
apatite	-	-	-	-	-	-	tr	tr	-	-	-	-	-	-	-	-	-	-
zircon	-	-	-	-	-	-	tr	-	-	-	-	1	tr	-	tr	-	tr	tr
tourmaline	-	-	-	-	-	-	-	tr	-	1	-	1	1	-	tr	-	-	tr
magnetite	10	10	10	15	8	20	-	-	-	-	15	4	tr	-	-	-	-	-
hematite	-	-	-	-	-	5	-	10	-	1	20	4	1	tr	-	-	-	-
graphite	-	-	-	-	-	-	1	-	-	3	-	-	-	tr	-	3	3	-
pyrrhotite	-	-	-	-	-	-	1	-	-	-	-	-	-	-	tr	-	-	tr
pyrite	-	-	-	-	-	-	-	-	-	-	-	-	-	tr	-	2	2	-

1-3 ferruginous siltstones; 4 oolitic chamositic iron formation; 5-6 clastic iron formation; 7-11 silicate facies iron formation; 12-13 kyanitic silicate facies iron formation; 14 sandy shale base; 15-18 metashale

silicate facies iron formation shows its lowest metamorphic overprint. Here, iron formation forms numerous thin beds in a clastic succession dominated by thin (10 cm-2 m scale) olive green chloritic metasiltstones that occasionally show grading into coarsely mottled, brown-green metaconglomerate containing intraclasts (typically 1-2 cm but occasionally up to 10 cm in the long direction) of magnetite quartzite in a phyllitic matrix of quartz, chlorite, magnetite, and sericite. The metasiltstones generally show delicate layering defined by the distribution of iron oxide and chlorite, and occasionally chloritic laminae define cross-ripple lamination structures. The intensely chloritic silicate iron formation bands form massive, non-bedded, drab green chloritite consisting of uniformly distributed chlorite, quartz, and magnetite. Notably, these silicate iron formation bands were observed to be recrystallized to a porphyroblastic garnet - chlorite - magnetite $\pm$ grunerite lithology in the area immediately adjacent to the Ellisville granodiorite south of Louisa. As this is well below the regional almandine isograd, the metamorphic recrystallization of the unit here possibly suggests that it was thermally metamorphosed at the time of intrusion.

In thin section the ferruginous clastics and silicate iron formation at the base of the Long Island metashales exhibit clastic textures which vary according to grain size and composition. The siliceous metasiltstones are composed of well sorted .2-.4 mm subangular chlorite and sericite. The more quartz-rich domains appear to be the most susceptible to metamorphic recrystallization; these comprise polygonal quartz and magnetite cubes. The massive non-bedded chloritite has an open framework texture with fine (.1 mm) angular quartz detritus hosted in an ultrafine chloritic matrix. Fine (.5 mm) oolitic structures are not uncommon, and these have chromositic cores and iron oxide-rich rims. The conglomeratic facies also has open framework sedimentary textures with fine (.1-.2 mm) granoblastic polygonal quartzite clasts, hosting glomeric aggregates of idioblastic magnetite, occurring within a matrix of chlorite interleaved with 1 mm angular quartz, iron oxide, and minor sericite.

Where exposed in the nose of the Arvonia synclinorium the basal silicate iron formation occurs as an oolitic chloritite. Megascopically this is a dark blue-green phyllite with well preserved oolites up to about 1 cm. In thin sections much of this lithology consists of a dense foliated matte formed by parallel oriented scaly chlorite grains hosting a few isolated quartz clasts. The oolites exhibit concentric growth rings defined by bands of goethite and possibly graphite interlayered with chlorite. The oolites typically show a 2:1 flattening ratio parallel to the foliation fabric defined by chlorite.

Well defined oolitic structures are also present in remnant low grade patches in specimens collected where the garnet isograd transects the Arvonia structure. At this location the silicate iron formation occurs as a thin (approx. 10 m) interbed in silty metashale at the contact with the Bremo quartzite. It is characterized by xenoblastic garnet masses to 2.5 cm in a deep green chloritic matrix of foliated chlorite and detrital quartz. The original bedding plane laminae defined by quartz grains in the remnant chlorite patches are parallel to inclusion trains in adjacent garnet areas, demonstrating that bedding is preserved by the inclusion fabric in garnet. In the rare cases where oolitic structures are preserved in garnet, the chlorite rings have reacted to garnet while the delicate iron oxide and graphite rings are faithfully preserved. Where bedding plane foliations are disrupted by garnet prophyroblasts, radiating sheaves and platy grains of grunerite often border on the garnet. However, grunerite is not abundant ($<$3 modal %), its sparsity being accounted for by the occurrence of remnant unreacted chlorite.

Compositional variation in the low grade chloritite precursor to quartz-graphite domains gives rise to a unique garnet textural variant. Here the garnet forms dodecahedral idioblasts with feather graphite inclusion trains radiating outward from the grain centers in a pattern controlled by the {111} crystal form. Occasionally triangular inclusion configurations near margins of these porphyroblasts are conrolled by the {200} form. At the margin between chloritic and quartz-graphite domains the garnets typically exhibit a number of radiating growth sectors, and in this case both sooty tourmaline and graphite parallel the sides of each sector. Cleavage cracks are developed parallel to the elongation direction of some sectors, resulting in a strong radial growth sector cleavage. Occasionally this particular garnet textural variant is bordered by .3-.5 mm radiating columnar grunerite aggregates.

A very peculiar lithology considered correlative with the silicate facies iron formation occurs interbedded with Buffards quartz-mica schist along the inner side of the eastern limb of the Arvonia structure in the vicinity of Buffards Mountain. This is a dark green chloritic lithology rich in porphyroblastic kyanite and garnet; its texture is controlled by the growth morphology of these particular constituents. The .2-2 mm kyanite occurs as stubby columnar blades which have random orientations where isolated but show weakly radial orientations where clustered. Where the kyanite aggregates the matrix areas consist of lepidoblastic chlorite interleaved with polygonal quartz. In the rare instances where polygonal quartz dominates the matrix, the chlorite forms idioblastic laths to 1.5 mm. This matrix assemblage is interrupted by patchy bands of small (.2 mm) garnet idioblasts intergrown with minor polygonal quartz and muscovite. Microdomains poor in both kyanite and garnet consist of decussate chlorite - muscovite - margarite mixtures; these areas host the majority of the trace idioblastic tourmaline and zircon. Zircon also occasionally gives rise to pleochroic haloes in chlorite. Two species of iron oxide are present in this rock: subidioblastic magnetite cubes and lath-shaped specularite. Locally massive iron oxide replaces quartz and chlorite as matrix material to the kyanite porphyroblasts.

The thickest development of the garnet-grunerite lithology known to date occurs in the Tower Hill area of the Whispering Creek anticline east of the Arvonia synclinorium. Here the silicate facies iron formation is interbedded with coarse quartz-muscovite schist and locally occurs in contact with the kyanite quartzite. The garnet-grunerite shows both quartz-rich, quartz-poor, and tourmaline-rich subfacies. The quartz-rich layers commonly display fine (.2-2 cm) bands of idioblastic garnet sheathed by light green to colourless grunerite within coarsely (.5 mm) polygonal quartz. Minor amounts of finely disseminated iron oxide, sooty tourmaline, and graphite generally accompany the quartzose layers. The tourmaline-rich facies is similar to the quartz-rich facies but here 1-1.5 mm granular tourmaline replaces polygonal quartz as the chief mineral in an assemblage hosting scattered garnet and grunerite porphyroblasts. The quartz-poor facies comprises a matrix of decussate grunerite intergrown with polygonal quartz. This hosts coarse (up to 1 cm) inclusion-free radiating sheaves of grunerite as well as acicular grunerite rimming typically idioblastic and inclusion-free garnet which locally shows retrogression to chlorite along rims and microfractures.

The ten meter thick interval of silicate facies iron formation intersected in drilling on the east side of metashale on the west limb of the Columbia structure ranges from massive garnet to thin-banded (.5-5 cm) layers of very fine-grained grunerite-bearing quartzite hosting large (1 cm) idioblastic garnets. The garnet here shows identical growth morphology to the specimens from above the almandine isograd in the Arvonia synclinorium and ranges from

massive poikiloblastic bands, with quartz inclusion trains preserving original bedding laminae, to idioblasts showing radiating inclusion trains and sector growth patterns. The grunerite typically forms acicular grains in a fine polygonal quartz matrix but also forms platy sheaves bordering on garnet porphyroblasts.

Notably, the modal percentage of both grunerite and garnet increases perceptibly toward the center of the interval. Although the core of the silicate iron formation is free of biotite, this mineral does occur in bordering zones, and its occurrence here is anomalous. The 2-4 mm biotitic laminae define a very delicate layering within quartzose domains and these biotite laminae may be partially or wholly replaced by massive garnet. Significantly, the biotite characteristicaly shows pleochroic haloes indicative of included zircon. The occurrence of minor calcite and pyrrhotite is also anomalous for the silicate iron formation regionally; both these minerals fill tension gashes crosscutting massive garnet bands and sometimes the sulphides replace the biotite laminae in the same fashion that the garnet does.

The garnet-grunerite is thicker and more regionally extensive along the east limb of the Columbia structure and here, as at Tower Hill, there is no evidence for overlying metashale. Along the east limb this lithology is typically quartz-rich and well banded (1-10 cm scale) with layers of granoblastic quartz overgrowing delicate (.2 mm) laminations of magnetite and hosting variable amounts of idioblastic garnet interbanded with massive garnet. The latter are often boudinaged, with grunerite aggregates forming xenoblastic sieves including quartz in the areas between boudins. Very fine (1 mm) laminae of decussate grunerite intergrown with polygonal quartz sometimes occur between adjacent garnet bands. Locally both garnet and grunerite are heavily impregnated with iron oxide. Trace tourmaline and rare apatite are included in quartzose bands.

b) Metashales

The regional metashale formations comprise a distinctly uniform, medium grey lithology that varies from slate (actively being quarried at Arvonia) below the garnet isograd to a porphyroblastic semi-schist above it. The basal parts transit into the silicate iron formation where this is present. Where it is not, there is generally a thin (2-3 m) development of intermediate lithology. For instance: graphitic quartz eye tuffites occur where shale overlies the Palmyra assemblage rhyolitic pyroclastics. The Bremo quartzites host shale chips in its conglomeratic facies and the immediately overlying shale is more quartz-rich and arenaceous than is typical. Where the shale overlies feldspathic quartzite a brown tuffaceous phyllite with 40% albite forms a thin (5 m) base.

The metashales exposed in the thickened part of the Long Island structure are typically laminated phyllites which are atypically quartz and chlorite-rich with respect to the Arvonia and Columbia metashale formations. Notably, these grey-green phyllites demonstrate more intense deformation, indicating that they lie in the core of a tightly compressed isocline. In thin section subtle 2-5 mm compositional bedding is shown by modal variation between quartz-rich and chlorite and sericite-rich layers. In sections these rocks demonstrate a kinked transpositional cleavage axial planar to tight crenulation of the bedding.

The metashales of the Arvonia structure are typically uniform dark grey slates to phyllites that are thinly laminated with fine silty layers. Comprising local zones along the base and observed as shaly seams within the Bremo quartzite is a black graphite - pyrrhotite - pyrite -bearing phyllite indicative of more euxenic conditions. If the upper part of the shale series is identified with the core of the western and major isocline of the Arvonia structure, the top of the shale may also be a locus of more euxenic conditions as quite pyritic bands are observed in the slate quarries; the slates currently being profitably exploited in the Arvonia area are a product of extremely uniform axial planar cleavage developed along the core of the western isocline.

The greater part of the Arvonia metashales lies above the garnet isograd and occurs as dark greenish grey porphyroblastic phyllites. In thin section these phyllites exhibit fine mm scale compositional laminations with .1-.2 mm polygonal quartz laminae interlayered with finely foliated sericite interleaved with .05 mm polygonal quartz. Spongy 1 mm biotite xenoblasts accompany the sericite laminae and these commonly show pleochroic haloes indicative of included zircon. The garnet porphyroblasts also favour the sericitic laminae, typically appearing as 1-2 mm idioblasts that may or may not be inclusion-free. Fine (.01 mm) tourmaline, lath-shaped pyrrhotite, and graphite are characterizing trace minerals disseminated throughout.

The Columbia metashale is lithologically similar to the Arvonia metashale, but is everywhere above the almandine isograd. Where exposed near the nose of the synform and along the Columbia to Mineral segment the rock is a uniform, fine-grained, slaty grey semi-schist with garnet, twinned biotite, occasional staurolite, and rare chloritoid porphyroblasts. Pegmatite stringers are fairly common, increasing in frequency to the east. The eastern border of the Columbia shales was not observed along the northern extension of the Columbia structures due to extreme scarcity of outcrop; east of the Mineral district the shales are thought to transit directly into high grade gneiss.

In thin section the typical Columbia metashale comprises .2-1.2 mm granoblastic polygonal quartz with grain boundary sited sericite microlites interlayered with sericitic laminae with dimensionally oriented sericite interleaved with minor polygonal quartz. Biotite forms 1-2 mm cuspate xenoblasts in quartzose domains but commonly twinned idioblastic laths which transect the foliation in sericitic laminae. Both textural variants show common pleochroic haloes indicative of included zircon. In quartzose domains garnet forms elongate xenoblastic sieves including trains of polygonal quartz that parallel the compositional layering. Within sericite laminae the garnet forms 2-3 mm inclusion-free idioblasts. The uncommon staurolite and rare chloritoid are confined to sericitic laminae; both these minerals show intimate textural relationships with biotite, suggesting metamorphic conditions near the upper stability limit of the latter. A few isolated green-brown chlorite sheaves were observed but do not appear to be a retrograde mineral. Pyrite and graphite are disseminated throughout, and heavy disseminations of these minerals occasionally impregnate sericite laminae.

B.9 The Eastern Plutonic Terrane

The lithofacies which are indigenous to the eastern plutonic terrane can be broadly differentiated into amphibolitic orthogneiss, feldspathic paragneiss, and "granitic" orthogneiss with associated post-metamorphic intrusive

material. As only cursory fieldwork was conducted in the area underlain by these various gneisses during the course of the present investigation, the lithological distribution demonstrated on the regional map relies heavily on sparse existing geological data and interpretations based on aeromagnetic and aeroradiometric signatures.

The occurrence of amphibolitic gneiss and granitic intrusive material immediately east of the Columbia metashales at the north end of the map area is based directly on the recent work by Pavlides (1981) in the Fredericksburg area which overlaps the northern extension of the area covered by the present study. The correlation of Pavlides' Spotsylvania lineament with the western border of the Triassic Farmville basin in the southeastern corner of the map is supported by both magnetic and radiometric geophysical data. The undifferentiated feldspathic-amphibolitic gneiss terrane occurring east of this major lineament has a similar geophysical signature to Pavlides' Po River biotitic gneisses, and these lithologies are considered correlative. The prominent tract of amphibole gneiss lying east of the Columbia structure but west of the Spotsylvania lineament is inferred from a correlation of Brown's (1937) Elkhill gneisses with the mafic Ta River gneisses recognized by Pavlides to the north. The identification of similar amphibole gneisses which interfinger with the Mineral metavolcanics east of the Columbia structure and with upper Chopawamsic lithologies north of the Whispering Creek anticline stems from field observation supported by aeromagnetic data in addition to Brown's (1969) and Marr's (1981) mapping. The granitic gneiss occurring along the east limb and at the nose of the Columbia structure and interfingering with amphibolite gneiss at the north end of the Hatcher complex is derived from a correlation of the "Columbia granodiorite" recognized both in early mapping by Brown (1937) and in more recent mapping by Smith, Milici, and Greenberg (1964) with the "granitic" gneisses differentiated by Brown in 1969. The distribution of feldspathic paragneiss and granitic orthogneiss within the core of the Columbia structure is based on the mapping carried out during the present investigation; the inference of similar lithology in the Hatcher complex and in the Andersonville district is based respectively on Brown's (1969) and Marr's (1981) mapping of "biotitic" gneiss in these areas.

Even aside from the limitations implied by the largely synthetic nature of the present interpretation, it must be emphasized that the differentiation of the eastern plutonic gneiss terrane into amphibolitic, feldspathic, and granitic facies, as illustrated on the regional map, is both speculative and oversimplified. Certainly there is more interbanding of the various facies than is indicated; the broad tracts depicted are, however, considered to grossly delineate the areas wherein given facies predominate. Part of the reason why the geology of this area is not well understood is rooted in the fact that outcrop is poor and part simply in the fact that it has not attracted much geological attention. The brief comments which follow are consequently put forth as provisional rather than definitive, being largely limited to notations of gross characteristics exhibited by each of the gneiss variants and a few speculations about their apparent lithological relationships.

a) Amphibolitic Orthogneiss

The amphibolitic gneiss facies includes a considerable range of lithologies ranging from mottled green-white to black in colour, fine to medium (and very rarely coarse) in grain size, weak to strongly foliated and/or lineated in textural fabric, and massive non-banded to thin (cm scale) banded in structural

aspect. The lithology is everywhere constituted essentially of modally variable hornblende and plagioclase (An15-35) and lesser quartz. In thin section textures range from decussate where hornblende-rich (over 60 modal %) to heteroblastic polygonal where plagioclase-rich (over 40 modal %). The strongly foliated and/or lineated facies are always hornblendic and typically consist of well aligned .5-2.5 mm columnar to acicular hornblende grains interleaved with polygonal plagioclase. Both hornblende and plagioclase tend to be poikiloblastic and mutually include one another. The ubiquitous but modally variable (2-20 modal %) quartz shows the same texture as plagioclase. Both epidote and sphene are characterizing minor minerals that occur as small (.2 mm) granules disseminated throughout or sometimes forming glomeric aggregates in which these minerals are occasionally intergrown. Notably, light yellowish grey epidosite composed of granoblastic polygonal epidote and quartz forms discrete 5-20 cm discontinuous schlieren that commonly occur interlayered with the amphibolitic gneiss bands. Other trace minerals occasionally observed in amphibolitic gneiss include muscovite, garnet, chlorite, hematite, pyrrhotite, and pyrite. The 1-2 mm subidioblastic garnet sieves are most common in thin-banded lithology; these porphyroblasts occasionally host snowball inclusion trains of quartz and pyrite, indicating that they have been rolled during growth.

Not enough work has been carried out on the amphibolitic gneisses to show any definitive along-strike variation. However, considering Pavlides' (1981) discussion of the Ta River gneisses, the northerly tract bordering on the Spotsylvania lineament is thought to comprise more massive non-banded lithology than the tract interfingering with the Mineral metavolcanics and in the Hatcher complex. It is also noteworthy that "metagabbro" was observed to accompany the amphibolitic gneiss east of the Columbia structure and that similar lithology was noted by Pavlides as a restricted component of the Ta River gneisses further north.

Although biotite is not characteristically present in the amphibolitic gneisses, distinct bands rich in this mineral (10-30 modal % biotite) are rather commonly interlayered within the amphibolitic gneisses. Marr (1981) notes that biotite gneiss interlayers within the amphibole gneiss in Andersonville and Willis Mountain quadrangles range from less than one to more than a hundred meters thick. This particular subfacies forms an intermediary facies between the amphibolitic and feldspathic gneisses.

The amphibolitic orthogneisses are considered to stem primarily from mafic volcanics; the more massive beds possibly signify thick basaltic flows, the thin-banded units basaltic pyroclastics or reworked flow material. The occurrence of a restricted coarse-grained metagabbroic facies in the amphibolitic gneiss tract bordering on the Spotsylvania lineament indicates that the minor mafic intrusive material is markedly different from the dominating amphibolitic gneiss and therefore further substantiates an extrusive origin for much of the original mafic material. The geochemical work carried out by Pavlides (1981) broadly identifies the mafic Ta River gneisses as stemming from tholeiitic basalts. The interfingering of the amphibolitic gneisses with both the Mineral assemblage and upper Chopawamsic lithologies in the Hatcher complex strongly supports Pavlides' interpretation that this particular gneiss facies is an eastern, more highly metamorphosed, mafic temporal equivalent of the Chopawamsic metavolcanics proper.

b) Feldspathic Paragneiss

The feldspathic gneisses form rather monotonous buff to light grey, medium-grained, well foliated lithologies with gneissosity primarily defined by thin (2-20 cm) dark grey biotitic bands. The biotite distribution in the bordering quartzo-feldspathic layers is often heterogeneous, as glomeroporphyroblastic aggregates of this mineral sometimes define a strong linear fabric which occasionally results in the main rock mass having the fabric of a pencil gneiss. Plagioclase (An17-30) is the most abundant constituent, typically comprising over 50 modal % of the feldspathic bands, where it occurs in equilibrium granoblastic textures with quartz, and forming (as does quartz) heteroblastic lobate grains in the biotitic domains. Biotite is the characteristic mafic mineral, constituting in the order of 20-25 modal % of the rock where hornblende is absent. Where hornblende is present -- which is not uncommon -- the combined hornblende and biotite make up about 50 modal % but biotite content falls to below 10 modal %. Quartz typically comprises 1-20 modal % in both feldspathic and mafic bands. Microcline is a characteristic minor (2-8 modal %) mineral, tending to form amoeboid grains slightly larger relative to the polygonal plagioclase and quartz. Muscovite is present locally but reaches signficiant (20 modal %) contents only in the most biotitic bands. Sphene and epidote are common trace minerals, particularly in hornblende-bearing bands. Garnet porphyroblasts are most common in micaceous bands, where they occur as 1-5 mm idioblasts more or less free of inclusions. The feldspathic gneisses are typically free of opaques; however, small (1 mm) idoblastic pyrite cubes are observed occasionally in micaceous bands.

At present any regional variation in the feldspathic gneiss facies, even between those portions occurring east and west of the Spotsylvania lineament, remains unknown. Also, the relationship of the feldspathic gneisses to the Chopawamsic metavolcanic belt is at present only speculative. Pavlides (1981) believes the Po River biotitic gneisses to the north to be an older basement underlying the Ta River gneisses, and it is tempting to consider that this may be older crustal material exposed in structural highs. The geophysical expression over the anticlinal structure in south central Andersonville quadrangle is considered by Johnson (1981) to support the possibility of such a basement in this particular locale. Here magnetic lows frequently occur over areas where amphibolites, which regionally have relatively high magnetic signatures, have been mapped on the surface; such amphibolites could overlie a bulk of feldspathic gneiss with relatively low magnetic signatures. However, in other instances gross lithological similarities with lithologies indigenous to the Chopawamsic belt proper argue against a blanket assumption that all feldspathic gneisses are older basement exposures. The feldspathic gneisses occurring within the core of the Columbia synform, for instance, locally appear very similar lithologically to the thick sections of reworked metarhyodacites which form a major facies of the Mineral assemblage immediately west of the Columbia metashale through Pendleton quadrangle. More specifically, the fact that both the metarhyodacite lithology west of the metashales and the feldspathic gneisses east of the metashale are characteristically magnetite-bearing supports a contention that this particular occurrence of feldspathic gneiss is a higher rank equivalent to the metarhyodacite units of the Mineral assemblage. At the present state of knowledge neither a more precise differentiation of the feldspathic gneisses nor a more definitive delineation of their relationship with the Chopawamsic metavolcanics is possible. It seems probable that the feldspathic gneisses in the core of the Columbia structure and at least some of this lithology in the Hatcher complex are higher rank Chopawamsic equivalents, while roughly similar lithology east of the Spotsylvania lineament may well, as Pavlides (1980) postulates, be older.

c) Granitic Orthogneiss and Associated Granitoid Intrusive Material

Of all the lithofacies that have been differentiated in the area of investigation, the "granitic" plutonic group undoubtedly is the most varied in both lithological types and age. Collectively the group comprises a surprising amount of the easterly plutonic terrane; "granitic" othogneiss is thought to dominate the Hatcher complex and pegmatitic granitoids at least locally devoid of gneissosity truncate the eastern limb of the Columbia structure at the north end of the map area. This twofold differentiation into gneissic and non-gneissic "granitic" terranes is depicted on the regional map; however, both of these subdivisions entail subfacies of differing composition.

According to the work carried out by Pavlides (1981), the granitoid rocks in the Lake Anna area at the end of the project area are monzogranitic and, less commonly, granodioritic in composition. The lithology is perceptibly foliated but exhibits a primary fine to medium-grained allotriomorphic granular texture defined by interlocking anhedral grains of plagioclase, quartz, and microcline, which in a typical specimen runs about 40, 30, and 20 modal % respectively. Biotite is the only mafic mineral present, and averages about 10 modal %. The orientation of biotite imparts the non-penetrative foliation fabric. Minor and trace minerals include epidote and pyrite; myrmekite is also present as a trace.

Alaskitic granite bodies devoid of any metamorphic overprint were observed at two locations along the east side of the Columbia synform, an area which also has a considerable amount of pegmatite injecta. Megascopically both occurrences are leucocratic, almost white, coarse-grained, and composed essentially of albite and quartz, with lesser microcline and muscovite. The estimated modal percentages of these minerals on slabbed handsamples are albite 45%, quartz 35%, microcline 20%, and muscovite 5%. This rock was not studied in thin section. Significantly, the irregularly shaped pegmatitic bodies in the same area have roughly the same mineralogy, with large pegmatoid albite crystals being the most abundant essential mineral and imparting the characteristic white colour.

The "granitic" gneiss facies includes the Columbia granodiorite at the nose of the Columbia synform, and compositions range from quartz diorite and monzonite to granite. According to Brown (1969), these rocks are variable in colour, texture, fabric, and gneissosity. For the most part they are medium to light grey, medium-grained, and have a moderately well developed gneissic structure and strong mineral lineation. In thin section textures are predominantly xenomorphic-granular. Biotite is the characteristic dark mineral, but hornblende is common near hornblende gneiss. Pegmatitic and aplitic bodies devoid of dark minerals locally accompany the gneisses. Porphyroblastic varieties are not unusual. Augen gneiss east of the Spotsylvania lineament shows the effects of strong granulation. The augens, ranging from 2-15 mm in the long dimension, are chiefly of plagioclase (An30-39) but locally are also microcline. In thin section many of the augens have granulated borders and show strain effects such as bent twin laminae. Matrix material is mainly a foliated matte of biotite and finely granulated quartz, feldspar, and muscovite. Trace minerals include epidote, clinozoisite, garnet, sphene, chlorite, apatite, zircon, carbonate, and iron oxide.

B.10 Triassic Rocks

Finally, to complete this lithological overview, two Triassic lithologies are present in the study area, including, first, the molassic sediments of the Farmville basin, and second, the numerous diabase dykes. Interestingly, the age of these rocks coincides with the beginning of the rifting which eventually led to the opening up of the Atlantic (Clifford 1968), and both graben formation and dyke emplacement likely resulted from tensional tectonic conditions set up by this event.

a) The Farmville Basin

Recent work by M.B. McCollum (1981) has demonstrated that two major depositional regimes are represented by the sedimentary rocks of the Farmville basin. A gravity flow regime, in which metamorphic rocks northwest of the basin were eroded and transported to the southwest, is represented by a fanglomerate sequence along the western margin of the basin. The average grain size of the fanglomerate facies progressively decreases eastward from boulder conglomerate to fine-grained arkose. To the southeast running water played an increasing important role in the detrital process, and the arkose beds in this locale commonly contain heavy mineral-accentuated cross-beds and coarse pebbles in channelfill deposits. The sediments along the southeast border formed under fluvial-lacustrine conditions resulting in a sequence of siltstone, shale, and mudstone.

b) Diabase Dykes

Diabase dykes are particularly numerous in the southern end of the map area, diminishing in frequency northward. This distribution, together with the development of the Farmville graben, suggests that the southern part of the map area was more affected by Triassic extensional tectonism than was the north. The dykes range from 1-100 meters in width and up to ten kilometers in strike length. Most have nearly vertical dips and strikes of 160 $\pm$ 10 , although a few of the larger ones have more northerly attitudes. Significantly, some of the largest dykes crosscut the sediments of the Farmville basin, indicating that the intrusive period ranged into late Triassic to early Jurassic times.

The diabase is dark olive-grey to black and fine to medium-grained. Well developed subophitic textures characterize the lithology away from chill margins. The very fine-grained margins are commonly intergranular and microporphyritic in texture. Plagiclase (An65) normally comprises 40-60 modal %. The almost equally abundant pyroxene occurs in two species, augite and pigeonite. Where olivine is present it generally consitutes less than 5 modal % and shows moderate serpentinization along microfractures. Micropegmatite is typically present where the olivine is absent. Magnetite, ilmenite, and apatite are characterizing accessories.

9. APPENDIX C

Bulk Rock Major and Trace Element Data

Sample Groupings

Basal Shale Silicate Faces Iron Formation
Manganiferous Oxide Iron Formation
Metachert
Biotitic Carbonate Ironstones
Kyanite Quartzite
Sericitic Pyritic Ironstones
Hydrothermal Chloritite
Cummingtonitic Ironstones
Hornblendic Ironstones
Metamarl
Metarhyolites
Metadacites
Meta-andesites
Metabasalts
Metakomatiites
Granophyre - Granite - Monzonite
Granodiorite - Diorite
Gabbro
Peridotite - Hardware Schist

Basal Shale Silicate Facies Iron Formation

	1 71-133'	2 P-54-1	3 A-50	4 A-22	5 A-58	6 C-8	7 Th-30	8 Li-3-3
SiO_2	50.60	71.40	29.61	46.60	41.40	58.50	58.00	58.70
TiO_2	00.38	00.30	00.40	00.54	00.52	00.43	00.78	00.77
Al_2O_3	08.80	07.51	16.70	10.30	14.70	09.30	11.70	10.20
Fe_2O_3	01.53	03.40	16.88	15.98	05.53	10.26	02.28	02.27
FeO	19.72	12.04	23.04	13.10	26.92	11.96	20.50	19.43
MnO	00.22	00.10	00.14	00.14	00.40	00.06	00.31	00.07
MgO	03.28	02.43	03.88	02.00	02.40	01.45	01.82	01.64
CaO	04.68	00.65	00.34	01.26	02.92	01.26	00.47	01.96
Na_2O	00.68	00.00	00.00	00.00	00.00	00.00	00.10	00.03
K_2O	00.62	00.12	00.18	00.16	00.16	00.12	00.14	00.00
P_2O_5	00.64	00.07	00.34	00.80	00.44	00.20	00.43	00.52
H_2O	00.67	00.82	04.53	03.06	01.73	02.18	00.63	01.49
CO_2	06.35	00.12	01.75	03.47	00.25	00.89	00.07	00.05
Total	98.17	98.96	97.78	97.41	97.43	96.61	97.23	97.13
trace elements in ppm								
Ni	58	14	84	11	17	13	28	25
Cu	130	39	24	21	86	47	65	12
Co	27	3	37	8	9	4	11	8
Zn	57	9	560	25	47	26	68	59
Cr	400	640	160	440	560	560	380	410
Rb	40	40	0	0	0	130	30	0
Sr	200	0	10	20	0	20	0	10
Ag	1.6	0	2.0	0.5	0.5	0	0	0
Cd	2	1	11	4	4	3	0	1
Pb	56	8	47	18	15	15	8	12
Zr	60	40	60	60	140	50	170	160
Mo	14	2	8	3	13	2	0	0

Manganiferous Oxide Iron Formation

	9 60-357'	10 NC-4	11 P-51
SiO_2	68.40	46.20	58.80
TiO_2	00.32	01.11	00.10
Al_2O_3	05.81	15.40	02.48
Fe_2O_3	03.67	02.61	22.40
FeO	07.28	22.29	05.52
MnO	02.16	04.06	04.64
MgO	01.68	01.38	00.16
CaO	01.59	03.56	02.68
Na_2O	01.14	00.17	00.00
K_2O	01.90	00.01	00.18
P_2O_5	00.26	00.10	00.04
H_2O	01.55	00.62	00.33
CO_2	02.92	00.07	00.13
Total	98.68	97.58	97.46
trace elements in ppm.			
Ni	63	7	20
Cu	107	110	12
Co	50	3	11
Zn	79	9	36
Cr	280	310	400
Rb	90	20	40
Sr	80	0	20
Ag	3.0	0	0.8
Cd	2	1	6
Pb	89	4	16
Zr	20	0	0
Mo	12	0	3

Metachert

	12 89-1284'	13 1-567'	14 Ca-3b	15 55-133'	16 53-184'
SiO_2	77.20	67.60	91.50	80.90	66.40
TiO_2	00.17	00.48	00.28	00.18	00.38
Al_2O_3	11.30	13.00	03.11	08.93	11.60
Fe_2O_3	02.08	02.30	00.61	00.36	01.60
FeO	00.38	03.38	00.86	00.44	02.68
MnO	00.04	00.10	00.06	00.06	00.08
MgO	00.22	01.78	00.22	00.42	01.86
CaO	00.57	01.40	00.38	00.77	03.20
Na_2O	06.29	04.80	00.94	04.27	02.62
K_2O	00.22	00.92	00.34	00.68	01.88
P_2O_5	00.04	00.14	00.06	00.04	00.08
H_2O	00.08	01.06	00.59	00.04	02.30
CO_2	00.49	00.11	00.15	01.16	02.21
Total	99.08	97.07	99.10	98.25	96.95

trace elements in ppm

Ni	7	10	20	7	32
Cu	27	7	16	21	45
Co	2	9	6	2	12
Zn	42	160	27	37	42
Cr	180	240	400	160	100
Rb	20	0	30	0	60
Sr	10	0	30	20	100
Ag	0	1.1	0	0	0.5
Cd	2	0	4	0	0
Pb	7	9	11	10	13
Zr	140	140	130	90	80
Mo	2	3	2	5	14

Biotitic Carbonate Ironstone

	17	18	19	20	21	22	23	24
	89-91'	89-1190'	78-1944'	78-1945'	103J-980'	Pe-7	Ca-5e	Mau-1
SiO_2	55.60	48.60	49.70	45.00	44.80	49.70	50.50	55.20
TiO_2	00.54	00.65	01.00	01.08	00.38	01.21	01.42	00.76
Al_2O_3	13.20	15.60	16.00	17.20	12.00	14.90	16.60	14.40
Fe_2O_3	04.04	06.43	02.11	03.49	01.33	01.91	02.71	02.26
FeO	07.26	02.84	09.00	09.96	06.04	11.38	11.56	07.11
MnO	00.22	00.21	00.41	00.47	00.18	01.13	00.27	00.13
MgO	03.07	04.20	07.23	09.70	10.10	06.03	05.60	06.67
CaO	03.90	08.04	04.00	04.28	06.80	01.11	01.08	05.65
Na_2O	02.41	01.33	00.83	00.88	00.13	01.79	03.09	00.20
K_2O	03.47	02.65	03.95	03.86	04.07	05.35	04.09	02.91
P_2O_5	00.06	00.08	00.12	00.10	00.04	01.10	00.04	00.06
H_2O	01.78	01.22	01.89	02.07	01.98	00.56	01.82	03.88
CO_2	01.64	05.83	02.21	02.19	10.04	00.62	00.81	00.43
Total	97.19	97.68	98.45	100.28	98.49	96.79	99.59	99.66
trace elements in ppm								
Ni	18	27	29	45	290	18	16	50
Cu	82	240	51	100	76	91	33	68
Co	45	32	50	43	64	59	43	22
Zn	160	179	240	130	110	600	190	21
Cr	160	200	160	140	1200	140	140	910
Rb	90	300	310	100	270	100	100	50
Sr	100	100	40	30	80	40	110	40
Ag	2.7	2.0	4.1	3.5	3.5	3.0	2.5	0
Cd	9	7	11	9	11	22	7	0
Pb	62	41	120	140	52	40	40	16
Zr	0	10	0	10	10	0	10	0
Mo	8	9	9	6	12	7	4	4

(Biotitic Carbonate Ironstones cont.)

	25 Mau-2	26 Th-17-2	27 NC-44	28 54-158'
SiO_2	45.00	48.10	57.90	44.30
TiO_2	00.56	00.81	00.82	00.90
Al_2O_3	20.40	20.10	12.80	13.20
Fe_2O_3	02.06	02.31	02.32	01.89
FeO	11.39	06.34	11.82	11.20
MnO	00.11	00.17	00.53	00.46
MgO	01.55	03.99	05.47	06.03
CaO	05.33	06.41	00.27	00.40
Na_2O	01.60	02.47	00.32	02.54
K_2O	04.99	03.91	00.89	02.64
P_2O_5	00.06	00.16	00.10	00.08
H_2O	02.77	02.29	03.33	01.09
CO_2	00.81	00.25	00.37	12.09
Total	96.81	96.31	97.94	96.82
trace elements in ppm				
Ni	150	8	6	17
Cu	24	18	260	74
Co	24	16	12	48
Zn	65	120	830	600
Cr	2520	110	320	120
Rb	110	110	20	80
Sr	100	250	0	30
Ag	0	0	0	1.1
Cd	1	0	14	5
Pb	8	20	16	95
Zr	10	110	50	30
Mo	4	0	0	7

Kyanite Quartzite

	29 Mi-9a	30 Mi-10g	31 D-131	32 NC-61	33 Th-19
SiO_2	82.70	86.10	61.70	28.80	77.80
TiO_2	00.19	00.16	00.52	01.85	00.28
Al_2O_3	12.60	10.10	18.20	30.30	14.20
Fe_2O_3	00.63	00.74	10.07	03.35	01.78
FeO	00.24	00.04	00.18	22.91	00.75
MnO	00.03	00.02	00.01	00.78	00.09
MgO	00.10	00.08	00.09	04.71	00.70
CaO	00.21	00.22	00.18	00.22	00.87
Na_2O	00.05	00.12	00.18	00.06	01.29
K_2O	00.17	00.31	00.96	00.01	01.01
P_2O_5	00.04	00.03	00.06	00.09	00.05
H_2O	00.96	00.18	00.99	03.46	01.53
CO_2	00.08	00.41	07.52	00.39	00.17
Total	98.00	98.24	100.66	96.93	100.52
trace elements in ppm					
Ni	8	8	13	53	10
Cu	6	6	110	23	7
Co	1	2	9	21	3
Zn	5	3	16	77	3
Cr	280	260	330	520	210
Rb	0	0	20	70	10
Sr	40	10	40	20	120
Ag	0	0	0.7	0	0
Cd	2	0	5	0	0
Pb	5	10	21	12	4
Zr	120	130	140	460	70
Mo	0	1	23	4	0
Au	-	-	-	.05	0

Sericitic-Pyritic Ironstone

	34	35	36	37	38	39	40	41
	89-841'	85-153'	89-1170'	89-1184'	89-1293'	89-1312'	85-900'	73-51'
SiO_2	75.60	73.60	49.80	68.10	72.20	53.50	58.80	74.20
TiO_2	00.23	00.17	00.46	00.23	00.18	00.31	00.42	00.21
Al_2O_3	11.60	10.90	15.90	14.70	11.90	23.30	14.90	11.60
Fe_2O_3	03.65	04.42	06.53	02.76	01.14	01.78	04.24	00.58
FeO	00.20	00.28	04.22	01.36	02.16	03.68	06.88	01.94
MnO	00.02	00.04	00.19	00.06	00.07	00.14	00.34	00.08
MgO	00.46	00.43	07.95	02.80	02.95	07.51	04.38	00.77
CaO	00.34	00.60	04.23	00.78	00.88	00.32	00.82	02.69
Na_2O	00.51	01.93	03.33	01.44	01.52	00.37	02.18	03.00
K_2O	02.55	02.94	00.91	03.52	02.19	04.70	01.70	01.00
P_2O_5	00.06	00.03	00.02	00.04	00.03	00.03	00.05	00.07
H_2O	01.42	01.00	02.44	00.77	01.08	01.18	00.55	00.71
CO_2	01.99	04.02	04.02	00.93	00.22	00.08	01.36	00.96
Total	98.63	100.36	100.00	97.49	96.52	96.90	96.62	97.81
trace elements in ppm								
Ni	6	7	80	9	10	9	32	24
Cu	24	5	58	17	13	110	210	22
Co	6	3	55	6	2	3	34	11
Zn	60	90	48	39	155	280	220	37
Cr	220	120	740	240	140	60	280	380
Rb	280	60	50	70	40	140	60	20
Sr	0	30	80	20	20	0	40	150
Ag	0	1.5	0.8	0.4	0	1.4	0.7	0
Cd	5	4	10	8	3	7	7	4
Pb	30	30	25	19	29	120	33	22
Zn	20	110	0	180	150	280	0	60
Mo	3	5	5	3	3	5	3	4

Hydrothermal Chloritite

	42 89- 850.5	43 89- 1323'	44 88- 1412'	45 ST	46 87-781'	47 1-597'	48 2-416'	49 2-458'
SiO_2	56.70	46.70	58.20	26.80	41.00	27.60	38.40	48.30
TiO_2	00.88	00.25	00.21	00.28	01.31	01.78	01.40	01.54
Al_2O_3	15.80	19.00	15.70	19.80	22.40	21.00	16.70	15.00
Fe_2O_3	02.93	05.42	04.62	09.61	04.51	08.68	03.37	06.57
FeO	08.06	10.42	08.44	17.24	10.04	16.68	20.36	18.68
MnO	00.48	00.08	00.15	00.14	00.29	00.32	00.86	00.28
MgO	06.25	07.75	05.62	14.90	08.10	14.10	09.34	04.87
CaO	01.83	01.78	00.25	00.30	00.31	00.90	01.92	00.76
Na_2O	02.79	00.24	00.05	00.00	00.23	00.32	01.18	00.07
K_2O	00.44	03.13	01.77	01.52	04.58	00.30	00.44	01.38
P_2O_5	00.09	00.04	00.03	00.04	00.11	00.18	00.12	00.12
H_2O	02.50	01.32	02.56	03.73	02.27	03.41	02.95	00.09
CO_2	00.45	01.21	01.47	01.86	01.65	01.55	00.86	02.42
Total	99.20	97.34	99.07	96.22	96.80	96.82	97.50	100.08
trace elements in ppm								
Ni	24	29	11	10	38	17	24	21
Cu	104	140	250	670	670	18	95	470
Co	42	22	11	33	10	25	33	12
Zn	210	140	56	640	660	36	91	19
Cr	220	40	220	10	180	180	280	420
Rb	40	120	110	560	280	0	20	100
Sr	50	0	0	0	0	0	0	0
Ag	0.7	0.9	0.7	2.9	6.8	0.9	1.1	2.0
Cd	10	7	8	16	23	3	2	3
Pb	64	50	54	130	3200	18	23	26
Zr	10	220	170	260	140	80	60	20
Mo	4	4	6	8	6	8	5	4

(Hydrothermal Chloritite cont.)

	50 NC-35	51 Pe-33	52 NC-12	53 NC-43	54 55-135'
SiO_2	39.40	45.00	60.10	55.00	41.20
TiO_2	00.87	01.50	00.95	01.22	01.08
Al_2O_3	18.10	15.30	11.90	13.60	18.80
Fe_2O_3	02.37	03.00	02.45	02.72	01.73
FeO	24.99	17.72	16.44	16.05	19.14
MnO	00.42	00.49	00.62	00.43	00.14
MgO	05.87	09.47	03.37	05.48	11.40
CaO	01.59	00.89	01.25	00.27	00.46
Na_2O	00.08	00.21	00.18	00.06	00.18
K_2O	00.00	00.00	00.03	00.00	09.69
P_2O_5	00.04	00.22	00.11	00.12	00.08
H_2O	03.26	04.97	01.59	03.19	02.01
CO_2	00.36	00.51	00.18	00.35	00.98
Total	97.35	99.28	99.17	98.49	96.89

trace elements in ppm

Ni	24	6	8	6	250
Cu	120	71	36	120	4
Co	16	14	17	14	82
Zn	75	130	46	20	560
Cr	480	250	270	200	780
Rb	10	0	0	10	370
Sr	0	0	0	0	0
Ag	0	0	0	0	6.7
Cd	1	0	0	0	4
Pb	8	12	8	8	34
Zr	10	0	20	10	10
Mo	4	4	0	4	8

Cummingtonitic Ironstones

	55 Mi-3a	56 Mi-3b	57 Ar-1-7	58 A-190-1	59 Ca-2c
AlS_2	65.50	54.70	75.40	65.60	70.30
TiO_2	00.97	01.15	00.29	00.54	00.24
Al_2O_3	13.00	13.80	11.50	13.20	11.70
Fe_2O_3	04.54	04.84	01.83	01.19	01.64
FeO	04.50	07.18	01.46	05.72	04.54
MnO	00.11	00.20	00.09	00.30	00.13
MgO	02.49	05.08	00.76	03.70	03.06
CaO	01.71	05.04	01.97	02.07	01.36
Na_2O	06.03	04.67	04.74	05.08	05.39
K_2O	00.17	00.18	00.14	00.14	00.15
P_2O_5	00.18	00.14	00.05	00.08	00.04
H_2O	00.85	00.65	00.16	00.65	00.67
CO_2	00.20	00.06	00.16	00.10	00.14
Total	99.29	97.69	98.55	98.37	99.36
trace elements in ppm					
Ni	7	8	6	8	9
Cu	8	43	9	15	36
Co	6	15	1	3	9
Zn	33	20	11	15	18
Cr	160	120	180	200	220
Rb	20	30	10	10	40
Sr	80	80	70	50	30
Ag	0	0	0	0	0
Cd	0	0	1	2	3
Pb	5	7	3	5	7
Zr	20	0	100	60	120
Mo	3	4	2	0	1

Hornblendic Ironstones

	60 Pe-6	61 P-37K	62 73-113'	63 A-188	64 Th-36	65 NC-47
SiO_2	46.30	52.40	43.50	77.40	50.60	50.30
TiO_2	00.70	01.22	00.24	00.32	01.12	01.40
Al_2O_3	15.10	13.86	14.10	06.16	11.50	15.10
Fe_2O_3	04.53	03.43	02.26	02.44	02.62	02.90
FeO	09.72	09.03	09.66	05.84	05.20	10.27
MnO	00.53	00.30	00.18	00.16	00.18	00.29
MgO	08.44	04.15	08.32	01.87	11.50	06.32
CaO	07.69	07.18	10.40	01.39	10.50	08.52
Na_2O	02.71	03.28	00.73	00.12	02.61	01.77
K_2O	00.30	01.58	02.83	00.13	00.13	00.32
P_2O_5	00.15	00.11	00.03	00.05	01.42	00.13
H_2O	01.81	01.41	00.72	01.38	00.97	01.32
CO_2	00.08	01.92	04.15	00.15	00.11	00.15
Total	98.06	99.87	97.12	97.41	98.46	98.85
trace elements in ppm						
Ni	35	24	220	24	16	6
Cu	4	55	42	53	18	6
Co	8	15	60	7	2	7
Zn	53	109	80	21	11	30
Cr	900	50	1400	600	730	130
Rb	40	30	80	20	10	0
Sr	150	11	60	0	140	70
Ag	0	0	0	0	0	0
Cd	0	0	0	1	0	0
Pb	11	0	36	9	4	12
Zr	10	0	0	0	320	20
Mo	10	0	10	2	0	0

Metamarl

	66 52-148'	67 52-178'	68 55-285'
SiO_2	48.70	37.30	42.70
TiO_2	01.33	00.59	00.74
Al_2O_3	14.10	15.60	15.60
Fe_2O_3	04.02	04.87	04.02
FeO	07.78	04.52	08.38
MnO	00.28	00.19	00.12
MgO	06.47	07.00	13.50
CaO	05.88	14.50	03.86
Na_2O	02.26	02.07	00.24
K_2O	01.66	01.82	03.06
P_2O_5	00.13	00.08	02.04
H_2O	03.21	03.15	02.90
CO_2	02.00	05.52	00.64
Total	97.82	97.21	98.80

trace elements in ppm

Ni	29	78	190
Cu	98	84	130
Co	48	37	70
Zn	110	62	100
Cr	100	680	1400
Rb	40	20	90
Sr	180	310	180
Ag	2.9	2.0	3.3
Cd	3	0	2
Pb	26	18	23
Zr	40	20	10
Mo	14	16	9

Metarhyolites

	69	70	71	72	73	74	75	76
	87-383'	Law-1	Ca-1a	P-52	Buff	D-60-3	Co-35	85-1900'
SiO_2	80.70	81.50	93.70	79.60	77.05	71.55	72.90	74.50
TiO_2	00.14	00.18	00.07	00.24	00.51	00.51	00.54	00.25
AL_2O_3	09.06	08.69	01.25	09.81	10.98	11.95	16.66	12.50
Fe_2O_3	00.29	00.29	00.34	01.55	05.18	07.20	01.14	00.70
FeO	00.52	00.10	00.02	00.14	00.97	01.74	00.36	00.92
MnO	00.03	00.02	00.03	00.02	00.01	00.09	00.01	00.04
MgO	00.33	00.11	00.17	00.22	00.47	01.42	00.35	00.60
CaO	00.32	00.30	00.27	01.04	00.01	00.44	00.45	00.37
Na_2O	05.16	02.21	00.09	02.79	00.26	00.43	00.27	03.95
K_2O	00.19	03.54	00.16	01.58	02.72	02.12	05.13	03.15
P_2O_5	00.03	00.03	00.02	00.05	00.06	00.13	00.17	00.07
H_2O	00.18	00.38	00.33	00.40	02.00	02.31	02.10	02.41
CO_2	00.80	00.06	00.16	02.37	00.04	00.05	00.00	00.87
Total	97.75	97.40	96.61	99.81	100.26	99.94	100.08	100.33
trace elements in ppm								
Ni	21	7	10	20	24	36	23	7
Cu	18	5	8	8	12	16	9	8
Co	3	1	2	6	11	16	0	2
Zn	44	4	4	16	55	64	19	100
Cr	220	160	360	220	180	238	-	200
Rb	40	30	0	30	82	64	79	100
Sr	10	40	0	170	10	9	67	30
Ag	0	0	0	0	0	0	0	0
Cd	3	0	2	3	-	-	-	2
Pb	8	9	4	11	-	-	.5	13
Zr	130	120	40	70	-	-	-	140
Mo	1	3	1	5	-	-	-	1

(Metarhyolites cont.)

	77 78-1622'	78 C-43	79 P-37h	80 A-40	81 A-42-3	82 A-42-2	83 A-194	84 Co-32
SiO_2	77.70	80.00	81.20	85.05	78.10	76.95	56.70	69.75
TiO_2	00.20	00.52	00.17	00.10	00.14	00.16	00.69	00.30
Al_2O_3	12.10	11.41	09.30	08.33	11.66	12.76	24.11	16.20
Fe_2O_3	00.74	00.10	02.18	00.67	00.56	00.25	02.38	01.63
FeO	00.40	00.08	00.31	00.33	00.91	00.12	00.70	00.08
MnO	00.03	00.00	00.01	00.01	00.02	00.00	00.01	00.01
MgO	00.33	00.15	00.15	00.24	00.10	00.02	02.22	00.40
CaO	00.58	01.02	00.34	00.05	00.02	00.02	00.01	00.14
Na_2O	01.38	02.65	03.74	00.57	02.18	02.64	00.23	03.28
K_2O	02.30	02.88	00.92	03.74	05.45	06.70	08.57	06.80
P_2O_5	00.04	00.01	00.01	00.00	00.01	00.01	00.08	00.02
H_2O	01.34	01.56	00.59	00.67	00.60	00.32	04.06	01.44
CO_2	00.15	00.08	000.27	00.06	00.09	00.09	00.14	00.02
Total	97.29	100.46	99.19	99.82	99.84	100.04	99.90	100.07
trace elements in ppm								
Ni	8	10	0	0	11	0	14	11
Cu	14	0	0	11	13	0	23	11
Co	2	10	0	0	0	0	0	13
Zn	16	0	0	15	35	0	19	119
Cr	180	0	88	110	119	115	41	-
Rb	30	21	11	55	109	87	107	28
Sr	70	4	4	8	3	5	4	50

(Metarhyolites cont.)

	85 Pa-4	86 Pa-5	87 D-37	88 Sh-4	89 A-51-1	90 Co-2	91 ZC-2
SiO_2	76.70	72.80	71.20	76.10	75.50	70.35	87.40
TiO_2	00.18	00.24	00.06	00.16	00.31	00.14	00.08
Al_2O_3	10.89	13.08	15.86	14.54	13.06	15.96	06.06
Fe_2O_3	00.85	01.97	01.35	00.20	00.26	01.74	00.68
FeO	01.25	02.60	00.12	00.12	01.04	00.22	00.72
MnO	00.09	00.07	00.14	00.01	00.02	00.02	00.01
MgO	00.75	01.38	00.36	00.05	00.34	01.25	00.70
CaO	00.80	00.73	02.05	00.72	00.78	01.95	00.13
Na_2O	04.18	04.95	04.06	07.60	05.40	04.97	00.10
K_2O	00.26	00.25	02.04	00.25	00.32	01.86	03.50
P_2O_5	00.06	00.10	00.04	00.17	00.03	00.03	00.00
H_2O	04.16	01.55	02.78	00.33	00.46	01.26	00.51
CO_2	00.04	00.21	00.07	00.08	00.14	00.06	00.15
Total	100.21	99.93	100.11	100.33	97.66	99.79	100.04

trace elements in ppm

Ni	10	14	13	13	12	76	114
Cu	19	41	11	13	46	9	36
Co	0	5	0	0	0	6	4
Zn	29	37	22	0	10	9	19
Cr	58	-	49	178	143	-	-
Rb	0	5	64	0	0	39	90
Sr	10	97	44	9	10	295	35
Pb	-	13	-	-	-	49	26

Metadacite

	92 A-56-1	93 A-171	94 D-36-3
SiO_2	71.10	64.65	48.50
TiO_2	00.36	01.14	01.68
Al_2O_3	12.93	14.12	12.42
Fe_2O_3	04.13	03.21	06.35
FeO	00.12	03.85	07.33
MnO	00.04	00.07	00.27
MgO	00.03	02.25	07.65
CaO	06.85	02.16	10.15
Na_2O	02.76	04.96	02.34
K_2O	00.10	00.87	00.19
P_2O_5	00.08	00.30	00.19
H_2O	00.76	02.09	03.34
CO_2	00.04	00.06	00.06
Total	99.30	99.73	100.47
trace elements in ppm			
Ni	0	24	83
Cu	0	12	106
Co	0	13	64
Zn	0	20	126
Cr	90	63	114
Rb	0	25	0
Sr	62	13	11

Meta-andesites

	95 Pe-12b	96 Ar-5	97 A-74-1	98 A-80-2	99 Co-27
SiO_2	53.80	49.10	50.35	49.65	56.35
TiO_2	00.64	00.87	00.74	00.58	01.68
Al_2O_3	15.30	14.90	14.74	15.47	14.72
Fe_2O_3	02.82	04.40	04.48	03.48	05.94
FeO	05.80	07.86	04.83	06.49	04.92
MnO	00.22	00.40	00.23	00.30	00.17
MgO	06.32	07.61	07.50	08.55	03.55
CaO	08.02	07.54	08.40	09.95	04.77
Na_2O	04.08	03.96	01.88	03.24	06.05
K_2O	00.25	00.27	02.63	00.19	00.20
P_2O_5	00.07	00.06	00.14	00.11	00.29
H_2O	00.09	01.72	03.45	01.78	01.07
CO_2	00.59	00.08	00.05	00.04	00.03
Total	98.00	98.77	99.42	99.83	99.74
trace elements in ppm					
Ni	9	9	98	71	290
Cu	22	66	63	55	13
Co	4	9	31	35	21
Zn	12	20	63	53	32
Cr	200	140	216	78	-
Rb	40	30	54	0	3
Sr	180	130	15	11	117
Ag	0	0	-	-	-
Cd	0	2	-	-	-
Pb	5	6	-	-	59
Zr	50	20	-	-	-
Mo	4	2	-	-	-

Metabasalts

	100 78-192'	101 1-187'	102 Pe-25	103 D-55-6	104 P-27i	105 Pe-31
SiO_2	47.40	48.40	50.50	51.35	50.45	53.60
TiO_2	00.61	01.16	00.40	00.21	00.36	00.38
Al_2O_3	12.60	16.00	13.40	11.89	15.42	14.38
Fe_2O_3	02.43	02.89	02.30	02.84	03.28	04.26
FeO	06.36	08.50	05.82	06.24	05.45	05.96
MnO	00.17	00.38	00.18	00.20	00.17	00.18
MgO	14.10	07.50	10.70	12.25	08.85	08.70
CaO	08.39	07.10	02.00	11.65	13.00	09.65
Na_2O	02.19	03.96	00.68	01.24	00.96	01.27
K_2O	00.19	00.39	00.28	00.49	00.22	00.18
P_2O_5	00.06	00.09	00.04	00.10	00.09	00.07
H_2O	02.82	01.25	01.56	01.72	01.57	01.41
CO_2	00.70	00.70	00.13	00.00	00.00	00.04
Total	98.02	98.32	97.99	100.17	99.82	100.08
trace elements in ppm						
Ni	61	14	28	147	67	125
Cu	82	57	20	63	69	94
Co	15	16	4	49	41	40
Zn	30	40	10	53	47	65
Cr	1500	160	1100	770	286	-
Rb	10	20	40	0	0	8
Sr	110	30	90	5	13	167
Ag	0	.7	0	-	-	-
Cd	3	0	0	-	-	-
Pb	7	9	7	-	-	0
Zr	0	40	0	-	-	-
Mo	2	70	6	-	-	-

(Metabasalts cont.)

	106 NC-7-7	107 NC-20	108 Pa-1	109 A-158-1	110 Sh-6
SiO_2	56.40	52.10	49.70	51.80	50.10
TiO_2	00.58	00.82	00.83	00.87	01.33
Al_2O_3	14.20	15.60	11.20	13.32	14.36
Fe_2O_3	02.08	02.32	03.21	07.01	05.17
FeO	09.02	08.22	07.28	03.15	04.89
MnO	00.28	00.20	00.16	00.15	00.17
MgO	06.24	06.23	11.55	05.05	07.30
CaO	05.03	08.08	06.31	13.45	09.75
Na_2O	02.94	04.08	02.38	02.16	03.30
K_2O	00.30	00.17	00.39	00.03	00.76
P_2O_5	00.06	00.13	00.09	00.13	00.13
H_2O	01.66	00.42	04.13	01.82	02.64
CO_2	00.19	00.05	02.84	00.07	00.05
Total	98.98	98.42	100.05	99.01	99.95
trace elements in ppm					
Ni	7	6	270	152	73
Cu	30	5	83	35	42
Co	9	5	47	43	43
Zn	17	8	57	40	63
Cr	160	160	-	480	322
Rb	10	0	11	0	14
Sr	110	170	87	30	18
Ag	0	0	-	-	-
Cd	0	0	-	-	-
Pb	4	8	0	-	-
Zr	10	40	-	-	-
Mo	0	0	-	-	-

Metakomatiites

	111 Law-9	112 A-190-9	113 Th-25	114 Th-26	115 D-212
SiO_2	52.30	44.40	46.40	42.00	42.20
TiO_2	00.25	00.40	00.20	00.26	00.32
Al_2O_3	12.03	12.30	10.10	12.80	11.40
Fe_2O_3	01.32	01.84	01.70	01.76	01.82
FeO	05.56	08.94	07.11	08.84	08.59
MnO	00.14	00.17	00.11	00.11	00.16
MgO	20.10	17.20	20.90	24.10	22.40
CaO	11.30	07.61	06.99	02.00	06.22
Na_2O	00.06	00.31	00.66	00.36	00.49
K_2O	00.13	00.16	00.08	00.02	00.04
P_2O_5	00.01	00.04	00.06	00.03	00.02
H_2O	02.30	03.94	03.95	06.65	05.06
CO_2	01.05	00.11	00.44	00.74	00.56
Total	96.55	97.12	98.70	99.67	99.64
trace elements in ppm					
Ni	23	140	66	66	140
Cu	5	35	24	8	15
Co	4	23	10	10	14
Zn	7	32	17	12	12
Cr	2700	2000	2250	2930	2320
Rb	0	30	0	0	0
Sr	0	10	30	10	10
Ag	0	0	0	0	0
Cd	1	2	0	0	0
Pb	4	9	8	8	8
Zr	0	10	20	0	0
Mo	0	1	0	0	0

(Metakomatiites cont.)

	116 D-0	117 Law-3a	118 Law-6a	119 C-42
SiO_2	44.90	47.70	46.40	44.85
TiO_2	00.76	00.41	00.29	00.46
Al_2O_3	12.30	09.10	11.40	09.07
Fe_2O_3	02.26	02.56	04.40	02.70
FeO	07.83	06.22	06.84	07.46
MnO	00.17	00.20	00.79	00.20
MgO	18.30	16.30	14.10	22.60
CaO	08.44	11.00	09.47	08.00
Na_2O	00.59	00.96	01.23	00.47
K_2O	00.07	00.22	00.24	00.02
P_2O_5	00.07	00.12	00.02	00.08
H_2O	02.84	01.60	00.92	04.27
CO_2	00.32	01.03	00.08	00.02
Total	98.85	97.42	96.18	100.20

trace elements in ppm

Ni	69	40	57	710
Ci	26	32	61	115
Co	9	6	11	80
Zn	11	17	21	77
Cr	1730	2300	2300	1388
Rb	30	0	10	0
Sr	10	20	20	3
Ag	0	0	0	0
Cd	0	0	0	0
Pb	4	6	6	-
Zr	10	10	0	-
Mo	0	3	3	-

	Granophyres			Granites		Monzonite
	120 D-155	121 P-70	122 NC-21	123 ZC-29	124 ZC-37-1	125 ZC-28
SiO_2	77.75	77.20	73.90	76.20	75.05	52.60
TiO_2	00.21	00.20	00.78	00.24	00.10	00.66
Al_2O_3	11.74	12.16	12.60	12.66	14.44	14.62
Fe_2O_3	00.91	01.18	01.78	01.34	00.81	04.33
FeO	00.58	01.18	02.34	00.92	00.98	02.60
MnO	00.02	00.02	00.04	00.02	00.01	00.12
MgO	00.47	00.38	00.43	00.83	00.35	08.95
CaO	02.85	00.50	01.09	01.83	00.65	08.85
Na_2O	04.54	06.14	05.44	04.90	03.25	02.05
K_2O	00.06	00.14	00.33	00.17	04.25	01.28
P_2O_5	00.04	00.02	00.05	00.09	00.01	00.05
H_2O	00.59	00.62	00.49	00.72	00.36	03.08
CO_2	00.07	00.10	00.05	00.06	00.27	00.09
Total	99.83	99.84	98.82	99.98	100.52	99.78
trace elements in ppm						
Ni	11	13	7	16	0	101
Cu	0	0	34	19	14	26
Co	0	0	4	5	5	37
Zn	0	0	15	11	16	45
Cr	183	200	200	-	-	-
Rb	0	0	10	7	51	31
Sr	21	7	90	80	555	125
Ag	-	-	0	-	-	-
Cd	-	-	0	-	-	-
Pb	-	-	4	45	0	44
Zr	-	-	60	-	-	-
Mo	-	-	0	-	-	-

	Granodiorite	Diorites		
	126 EP-0	127 Ca-1b	128 A-118-1	129 ZC-37-9
SiO_2	71.30	48.30	53.10	54.30
TiO_2	00.23	00.22	00.30	00.94
Al_2O_3	15.22	15.90	21.64	12.64
Fe_2O_3	00.77	01.96	03.53	04.15
FeO	01.24	03.84	01.00	04.18
MnO	00.04	00.18	00.07	00.14
MgO	00.71	10.70	03.42	08.85
CaO	02.33	13.00	07.08	07.48
Na_2O	03.22	01.64	04.68	01.82
K_2O	04.06	00.32	02.22	03.14
P_2O_5	00.09	00.03	00.14	00.25
H_2O	00.54	01.75	02.62	01.74
CO_2	00.09	00.24	00.01	00.29
Total	99.84	98.08	99.81	99.92
trace elements in ppm				
Ni	11	16	69	230
Cu	0	140	31	27
Co	0	6	20	9
Zn	34	7	25	69
Cr	184	520	149	-
Rb	104	20	50	40
Sr	35	200	195	797
Ag	-	0	-	-
Cd	-	1	-	-
Pb	-	4	-	35
Zr	-	0	-	-
Mo	-	2	-	-

Gabbros

	130 ZC-37-13	131 A-124-6	132 Co-12	133 A-124-1	134 A-127-1	135 Co-3
SiO_2	50.40	49.35	48.95	54.50	52.20	49.90
TiO_2	00.52	00.63	00.36	00.49	00.58	00.37
Al_2O_3	07.04	11.51	08.32	17.08	13.40	12.56
Fe_2O_3	03.35	03.80	02.50	03.82	04.36	04.45
FeO	04.56	05.12	06.92	02.88	04.66	05.24
MnO	00.12	00.17	00.20	00.11	00.14	00.19
MgO	20.00	12.05	17.15	05.78	08.51	11.10
CaO	08.88	10.85	10.65	05.53	09.15	10.15
Na_2O	00.68	01.76	00.70	04.52	03.00	01.18
K_2O	01.80	00.85	00.79	02.51	01.67	01.12
P_2O_5	00.03	00.08	00.06	00.17	00.26	00.05
H_2O	02.08	02.74	03.31	01.56	01.94	03.61
CO_2	00.30	00.03	00.07	01.06	00.03	00.04
Total	99.76	98.94	99.98	100.01	99.89	99.96
trace elements in ppm						
Ni	615	159	850	126	63	330
Cu	91	47	39	16	102	33
Co	61	46	65	28	26	49
Zn	68	58	83	41	59	60
Cr	-	760	-	298	390	-
Rb	33	14	8	38	36	19
Sr	412	36	97	48	54	287
Pb	5	-	5	-	-	0

	Peridotite				Hardware Schists		
	136 Ca-1e	137 LI-24	138 LI-25	139 LI-11-6	140 A-144-3	141 D-26-6	142 Fe-2
SiO_2	48.10	39.70	43.70	41.90	41.35	32.30	28.70
TiO_2	00.13	00.20	00.18	00.08	00.09	01.82	00.42
Al_2O_3	08.03	05.33	10.00	02.14	02.74	16.65	18.94
Fe_2O_3	01.70	01.70	01.68	01.58	11.20	03.63	05.04
FeO	07.94	08.82	07.10	07.33	02.32	02.23	09.63
MnO	00.30	00.13	00.16	00.12	00.15	00.41	00.18
MgO	18.90	32.70	23.10	34.80	32.00	30.70	27.50
CaO	09.60	01.11	07.29	00.18	03.94	00.34	00.02
Na_2O	00.35	00.11	00.25	00.16	00.31	00.03	00.28
K_2O	00.15	00.02	00.02	00.03	00.08	00.00	00.01
P_2O_5	00.02	00.01	00.01	00.01	00.02	00.04	00.29
H_2O	01.96	09.40	05.13	09.70	05.84	09.17	09.17
CO_2	00.11	01.00	00.57	01.10	00.03	00.03	00.02
Total	97.29	100.23	99.19	99.13	100.13	97.35	99.93
trace elements in ppm							
Ni	99	640	390	500	975	1150	1970
Cu	100	15	6	11	12	16	10
Co	24	32	20	20	100	90	17
Zn	43	14	18	27	65	97	218
Cr	100	3870	3830	3760	762	924	-
Rb	30	0	0	10	0	0	3
Sr	0	0	0	0	8	8	22
Ag	0	0	0	0	-	-	-
Cd	2	0	0	0	-	-	-
Pb	7	8	12	12	-	-	-
Zr	0	0	0	0	-	-	-
Mo	0	0	0	0	-	-	-
Au(ppb)	-	1	1	1	-	-	-

10. APPENDIX D

Microprobe Analyses of Garnets and Amphiboles

Garnet Analyses (pp. D-1 to D-45)

a) Regional Samples of Metashale and Silicate Facies Iron Formation

Metashales

(1) P-25, (2) P-30, (3) P-33a, (4) P-58-4, (5) P-70-b

Garnet-Grunerite Iron Formation

(6) P-14, (7) A-22, (8) P-29, (9) DC-6, (10) D-57-1, (11) D-58-1, (12) D-58-2, (13) D-58-3

Garnet-Bearing Oxide Iron Formation

(14) P-51, (15) C-72-4

b) Garnet Analyses From Mineral Prospects

Sims

(16) 62-109', (17) 62-206.5', (18) 62-378', (19) 65-529', (20) 65-711', (21) M-128, (22) P-152

M-12

(23) 66-131', (24) 66-331.5', (25) 66-417', (26) 67-397', (27) 67-431.5', (28) 68-192'

M-31

(29) 47-393'-455', (30) 48-86'-98', (31) 48-136'-151', (32) 48-186'-196'

Tellurium

(33) Ca-2-b2, (34) Ca-2-b4, (35) Ca-3a-1, (36) Ca-4-b3, (37) Ca-6d

New Canton Trend

(38) A-188-5, (39) A-189-1, (40) A-190-3, (41) A-190-4, (42) A-191-8, (43) A-191-10

Amphibole Analyses (pp D-45 to D-80)

(1) P-14, (2) P-58-4, (3) CD-6, (4) D-57-1, (5) D-58-1, (6) D-58-2, (7) D-58-3, (8) A-22, (9) P-53, (10) P-51, (11) P-137, (12) P-66, (13) P-46, (14) P-27a, (15) P-27b, (16) A-191-8, (17) A-188-5, (18) A-190-4, (19) A-190-3, (20) A-190-8, (21) A-190-2, (22) A-190-9, (23) A-189-1, (24) A-189-4, (25) Ca-2b-6, (26) Ca-2b-4, (27) Ca-2b-3, (28) Ca-1f, (29) Ca-6b-2, (30) Ca-1e

SUPER RECAL — GARNET SAMPLES

SUB GROUP SI AL / AL TI MG CA MN FE / O /

SUB GROUP CA / MN / FE / MG /

	1	2	3	4	5	6	7	8
SIO2	37.66	37.93	37.63	37.50	37.74	37.45	37.59	37.91
A203	20.85	20.57	20.70	20.57	20.61	20.50	20.55	20.66
TIO2	.06	.06	.07	.06	.04	.04	.04	.05
FEO	37.42	37.88	38.22	37.64	38.17	37.93	38.05	37.73
MGO	1.75	1.79	1.71	1.66	1.68	1.79	1.73	1.82
MNO	1.48	1.38	1.14	.97	1.14	1.16	1.15	1.19
CAO	1.38	1.18	1.25	1.30	1.13	1.12	1.12	1.20
SUM	100.60	100.79	100.72	99.70	100.51	99.99	100.23	100.56
SI	6.070 *	6.105 *	6.070 *	6.096 *	6.096 *	6.082 *	6.090 *	6.107 *
AL	0.000 6.070	0.000 6.105	0.000 6.070	0.000 6.096	0.000 6.096	0.000 6.082	0.000 6.090	0.000 6.107
AL	3.960 *	3.902 *	3.935 *	3.941 *	3.923 *	3.923 *	3.923 *	3.922 *
TI	.007 *	.007 *	.008 *	.007 *	.005 *	.005 *	.005 *	.006 *
MG	.420 *	.429 *	.411 *	.402 *	.404 *	.433 *	.418 *	.437 *
CA	.238 *	.204 *	.216 *	.226 *	.196 *	.195 *	.194 *	.207 *
MN	.202 *	.188 *	.156 *	.134 *	.156 *	.160 *	.158 *	.162 *
FE	5.044 9.871	5.099 9.829	5.156 9.882	5.117 9.828	5.156 9.840	5.152 9.867	5.155 9.853	5.083 9.817
O	24.000 *	24.000 *	24.000 *	24.000 *	24.000 *	24.000 *	24.000 *	24.000 *
GROS	4.04	3.44	3.64	3.85	3.31	3.28	3.28	3.52
SPES	3.42	3.19	2.62	2.27	2.64	2.69	2.66	2.76
ALM	85.42	86.13	86.82	87.04	87.21	86.74	87.01	86.31
PYRP	7.12	7.25	6.92	6.84	6.84	7.30	7.05	7.42
F/M	12.478	12.312	12.919	13.054	13.133	12.257	12.718	12.003
F/FM	.926	.925	.928	.929	.929	.925	.927	.923

1 SAMPLE P25 GARNET
2
3 AT ONE END
4 ANOTHER AREA NOTE PPL BY HM
5
6
7
8

SUPER RECAL — GARNET SAMPLES

	9	10	11	12
SIO2	37.65	37.66	37.82	37.50
A203	20.59	20.62	20.72	20.52
TIO2	.11	.06	.08	.04
FEO	37.06	37.79	38.14	37.44
MGO	1.70	1.74	1.79	1.69
MNO	1.69	1.26	1.46	1.05
CAO	1.26	1.22	1.30	1.13
SUM	99.96	100.34	101.31	99.37
SI	6.090 *	6.090 *	6.068 *	6.112 *
AL	0.000 6.090	0.000 6.090	0.000 6.068	0.000 6.112
AL	3.935 *	3.929 *	3.917 *	3.941 *
TI	.013 *	.007 *	.010 *	.005 *
MG	.411 *	.419 *	.428 *	.409 *
CA	.219 *	.211 *	.223 *	.197 *
MN	.232 *	.172 *	.199 *	.145 *
FE	5.027 9.837	5.110 9.847	5.117 9.894	5.102 9.799
O	24.000 *	24.000 *	24.000 *	24.000 *
GROS	3.72	3.56	3.75	3.37
SPES	3.94	2.91	3.33	2.47
ALM	85.36	86.45	85.76	87.15
PYRP	6.98	7.08	7.17	6.99
F/M	12.796	12.620	12.432	12.819
F/FM	.928	.927	.926	.928

9 GARNET P25
10 AVERAGE
11 AVERAGE PLUS SIGMA
12 AVERAGE MINUS SIGMA

SUPER PECAL — GARNET SAMPLES

	1	2	3	4	5	6	7	8
SIO2	37.20	38.03	37.80	37.30	37.62	36.97	36.99	37.20
A2O3	20.46	20.70	20.64	20.32	20.76	20.77	20.59	20.60
TIO2	.07	.11	.09	.10	.07	.05	.02	.10
FEO	31.23	30.69	31.57	34.48	36.62	37.13	37.53	36.85
MGO	1.21	1.26	1.11	1.61	2.21	3.28	3.40	2.27
MNO	4.06	4.05	3.60	2.05	.65	.11	.15	.71
CAO	5.46	5.40	5.01	3.64	2.05	.57	.63	1.97
SUM	99.71	100.24	99.82	99.50	99.98	98.88	99.31	99.70
SI	6.036	6.102	6.101	6.067	6.071	6.020	6.012	6.037
AL	0.000 6.036	0.000 6.102	0.000 6.101	0.000 6.067	0.000 6.071	0.000 6.020	0.000 6.012	0.000 6.037
AL	3.912	3.914	3.925	3.895	3.948	3.985	3.943	3.939
TI	.009	.013	.011	.012	.008	.006	.002	.012
MG	.293	.301	.267	.390	.532	.796	.824	.549
CA	.953	.928	.866	.634	.354	.099	.110	.343
MN	.558	.550	.492	.282	.089	.015	.021	.098
FE	4.238 9.961	4.118 9.825	4.261 9.823	4.690 9.904	4.942 9.873	5.056 9.959	5.101 10.001	5.001 9.942
O	24.000	24.000	24.000	24.000	24.000	24.000	24.000	24.000
GROS	15.77	15.74	14.72	10.58	5.99	1.67	1.81	5.72
SPES	9.24	9.33	8.36	4.71	1.50	.25	.34	1.63
ALM	70.15	69.82	72.39	78.21	83.52	84.74	84.24	83.49
PYRP	4.84	5.11	4.54	6.51	8.98	13.34	13.60	9.17
F/M	16.788	15.493	17.801	12.740	9.464	6.370	6.218	9.286
F/FM	.942	.939	.947	.927	.904	.864	.861	.903

1 SAMPLE P30 GRAIN CENTER
2 NEARBY
3 TOWARD EDGE
4 CLOSER
5 CLOSER
6 EDGE
7 EDGE
8 ANOTHER GRAIN CENTRAL

SUPER PECAL — GARNET SAMPLES

	9	10	11	12	13
SIO2	37.40	37.88	37.44	37.79	37.08
A2O3	20.68	20.84	20.64	20.78	20.49
TIO2	.07	.05	.07	.10	.05
FEO	36.27	36.66	34.90	37.47	32.33
MGO	2.69	3.46	2.25	3.13	1.37
MNO	.34	.15	1.59	3.20	-.02
CAO	1.91	.50	2.72	4.63	.81
SUM	99.36	99.54	99.60	107.11	92.10
SI	6.059	6.095	6.060	5.909	6.340
AL	0.000 6.059	0.000 6.095	0.000 6.060	.191 6.000	0.000 6.340
AL	3.946	3.951	3.936	3.572	4.128
TI	.009	.006	.009	.011	.006
MG	.650	.833	.543	.718	.348
CA	.332	.086	.471	.762	.148
MN	.047	.020	.218	.416	-.004
FE	4.914 9.898	4.933 9.827	4.725 9.901	4.816 10.296	4.623 9.248
O	24.000	24.000	24.000	24.000	24.000
GROS	5.58	1.47	7.91	11.35	2.89
SPES	.79	.35	3.65	6.20	-.07
ALM	82.70	84.05	79.32	71.75	90.38
PYRP	10.93	14.14	9.11	10.70	6.81
F/M	7.637	5.969	9.104	7.289	13.270
F/FM	.884	.857	.901	.879	.930

9 INT
10 OUTER EDGE
11 AVERAGE
12 AVERAGE PLUS SIGMA
13 AVERAGE MINUS SIGMA

SUPER RECAL — GARNET SAMPLES

	1	2	3	4	5	6	7	8
SIO2	38.59	38.00	37.68	38.17	37.69	37.80	38.02	37.75
A2O3	21.11	20.77	20.92	20.90	20.43	20.45	20.78	20.70
TIO2	.04	.02	.08	.13	.15	.11	.10	.07
FEO	35.14	35.28	29.95	29.55	29.63	30.99	32.48	35.46
MGO	3.64	3.58	1.03	1.06	1.14	1.17	1.32	1.84
MNO	.41	.36	5.07	5.21	4.94	4.09	2.21	.43
CAO	1.90	1.94	6.11	5.87	6.08	5.99	5.72	4.00
SUM	100.83	99.95	100.84	100.89	100.06	100.60	100.63	100.25

SI	6.103	*	6.081	*	6.033	*	6.088	*	6.075	*	6.070	*	6.081	*	6.070	*
AL	0.000	6.103	0.000	6.081	0.000	6.033	0.000	6.088	0.000	6.075	0.000	6.070	0.000	6.081	0.000	6.070
AL	3.934	*	3.917	*	3.947	*	3.928	*	3.880	*	3.869	*	3.916	*	3.922	*
TI	.005	*	.002	*	.010	*	.016	*	.018	*	.013	*	.012	*	.006	*
MG	.858	*	.854	*	.246	*	.252	*	.274	*	.280	*	.315	*	.441	*
CA	.322	*	.333	*	1.048	*	1.003	*	1.050	*	1.031	*	.980	*	.689	*
MN	.055	*	.049	*	.688	*	.704	*	.674	*	.556	*	.299	*	.059	*
FE	4.647	9.821	4.721	9.876	4.010	9.949	3.941	9.843	3.994	9.890	4.161	9.911	4.344	9.867	.766	9.888
O	24.000	*	24.000	*	24.000	*	24.000	*	24.000	*	24.000	*	24.000	*	24.000	*
GROS		5.47		5.58		17.49		17.00		17.52		17.09		16.51		11.57
SPES		.93		.82		11.48		11.93		11.25		9.23		5.04		.98
ALM		79.01		79.26		66.93		66.80		66.65		69.03		73.15		80.05
PYRP		14.59		14.34		4.10		4.27		4.57		4.65		5.30		7.40
F/M		5.481		5.586		19.112		18.434		17.046		16.848		14.757		10.946
F/FM		.846		.848		.950		.949		.945		.944		.937		.916

1 SAMPLE P33A LARGE GRAIN AT EDGE
2 ANOTHER
3 APPROX CENTER
4 OTHER

5 CENTRE
6 TOWARD EDGE
7
8

SUPER RECAL — GARNET SAMPLES

	9	10	11	12	13	14
SIO2	37.59	38.11	38.43	37.98	38.29	37.68
A2O3	20.98	20.77	21.29	20.83	21.07	20.58
TIO2	.06	.11	.04	.08	.12	.04
FEO	34.28	32.93	35.24	32.81	35.13	36.50
MGO	3.61	1.48	3.44	2.12	3.24	1.00
MNO	.38	1.91	.37	2.31	4.32	.29
CAO	2.05	5.55	1.79	4.27	6.13	2.41
SUM	98.95	100.86	100.60	100.41	108.31	92.50

SI	6.057	*	6.081	*	6.092	*	6.075	*	5.800	*	6.384	*				
AL	0.000	6.057	0.000	6.081	0.000	6.092	0.000	6.075	.200	6.000	0.000	6.384				
AL	3.984	*	3.905	*	3.977	*	3.925	*	3.560	*	4.110	*				
TI	.007	*	.013	*	.006	*	.010	*	.014	*	.006	*				
MG	.867	*	.352	*	.813	*	.505	*	.730	*	.253	*				
CA	.354	*	.949	*	.304	*	.732	*	.995	*	.438	*				
MN	.052	*	.268	*	.050	*	.313	*	.555	*	.042	*				
FE	4.620	9.884	4.394	9.871	4.672	9.820	4.389	9.874	4.449	10.304	4.321	9.169				
O	24.000	*	24.000	*	24.000	*	24.000	*	24.000	*	24.000	*				
GROS		6.01		15.94		5.21		12.33		14.79		8.66				
SPES		.88		4.34		.85		5.26		8.24		.83				
ALM		78.40		73.81		80.02		73.90		66.11		85.50				
PYRP		14.71		5.91		13.92		8.51		10.85		5.01				
F/M		5.388		13.217		5.809		9.306		6.951		17.228				
F/FM		.843		.930		.853		.903		.873		.945				

9
10 OTHER GRAIN CENTRAL
11 AT EDGE

12 AVERAGE
13 AVERAGE PLUS SIGMA
14 AVERAGE MINUS SIGMA

SUPER RECAL — GARNET SAMPLES

	1		2		3		4		5		6		7		8	
SIO2	38.14		39.35		39.16		39.05		38.77		38.95		39.05		38.96	
A2O3	21.35		21.03		21.22		21.06		21.11		21.20		20.62		20.97	
TIO2	0.00		0.00		0.00		0.00		0.00		0.00		0.00		0.00	
FEO	32.40		31.93		32.21		32.21		32.35		32.90		32.08		31.52	
MGO	5.96		5.95		6.01		6.15		5.69		5.70		5.09		5.27	
MNO	.80		.51		.67		.54		.70		.63		1.00		.88	
CAO	.86		1.33		1.29		.88		1.07		1.08		2.60		1.84	
SUM	99.51		100.10		100.56		99.89		99.69		100.46		100.44		99.44	
SI	6.038	*	6.160	*	6.115	*	6.132	*	6.116	*	6.106	*	6.141	*	6.154	*
AL	0.000	6.038	0.000	6.160	0.000	6.115	0.000	6.132	0.000	6.116	0.000	6.106	0.000	6.141	0.000	6.154
AL	3.983	*	3.879	*	3.905	*	3.897	*	3.924	*	3.916	*	3.821	*	3.903	*
TI	0.000	*	0.000	*	0.000	*	0.000	*	0.000	*	0.000	*	0.000	*	0.000	*
MG	1.406	*	1.388	*	1.399	*	1.439	*	1.338	*	1.332	*	1.193	*	1.241	*
CA	.146	*	.223	*	.216	*	.148	*	.181	*	.181	*	.438	*	.311	*
MN	.107	*	.068	*	.089	*	.072	*	.094	*	.084	*	.133	*	.118	*
FE	4.289	9.931	4.180	9.738	4.207	9.815	4.230	9.786	4.268	9.804	4.313	9.827	4.219	9.805	4.164	9.737
O	24.000	*	24.000	*	24.000	*	24.000	*	24.000	*	24.000	*	24.000	*	24.000	*
GROS		2.45		3.81		3.65		2.51		3.08		3.07		7.32		5.34
SPES		1.80		1.15		1.50		1.22		1.59		1.42		2.23		2.02
ALM		72.10		71.34		71.18		71.82		72.58		72.98		70.51		71.37
PYRP		23.64		23.69		23.67		24.44		22.75		22.54		19.94		21.27
F/M		3.126		3.060		3.070		2.988		3.260		3.301		3.648		3.451
F/FM		.758		.754		.754		.749		.765		.768		.785		.775

1 SAMPLE P58-4 ALMANDINE
2
3
4
5
6
7 CENTER
8 EDGE

SUPER RECAL — GARNET SAMPLES

	9		10		11	
SIO2	38.93		39.27		38.59	
A2O3	21.07		21.27		20.87	
TIO2	0.00		0.00		0.00	
FEO	32.20		32.57		31.83	
MGO	5.73		6.08		5.38	
MNO	.72		.87		.56	
CAO	1.37		1.92		.82	
SUM	100.01		101.98		98.04	
SI	6.120	*	6.070	*	6.172	*
AL	0.000	6.120	0.000	6.070	0.000	6.172
AL	3.904	*	3.876	*	3.932	*
TI	0.000	*	0.000	*	0.000	*
MG	1.342	*	1.400	*	1.282	*
CA	.231	*	.318	*	.140	*
MN	.095	*	.114	*	.078	*
FE	4.234	9.805	4.211	9.919	4.257	9.688
O	24.000	*	24.000	*	24.000	*
GROS		3.91		5.26		2.44
SPES		1.62		1.89		1.32
ALM		71.74		69.68		73.97
PYRP		22.74		23.17		22.27
F/M		3.225		3.089		3.380
F/FM		.763		.755		.772

9 AVERAGE
10 AVERAGE PLUS SIGMA
11 AVERAGE MINUS SIGMA

SUPER PECAL — GARNET SAMPLES

	1	2	3	4	5	6	7	8
SIO2	38.08	36.33	37.88	37.96	37.31	38.08	37.69	36.23
A2O3	21.35	20.78	21.21	21.00	20.69	21.23	21.15	20.67
TIO2	.07	.10	.04	.02	.08	.02	.04	.01
FEO	35.82	34.88	35.85	36.76	34.98	36.15	35.15	36.52
MGO	3.09	3.24	3.37	3.30	3.15	3.33	3.26	3.34
MNO	.54	1.50	1.05	.55	1.04	.53	.97	.51
CAO	2.02	1.98	1.61	1.51	1.84	1.44	1.61	1.45
SUM	100.97	100.81	101.01	101.10	99.09	100.78	99.87	100.73
SI	6.044 *	6.094 *	6.023 *	6.040 *	6.045 *	6.056 *	6.045 *	6.095 *
AL	0.000 6.044	0.000 6.094	0.000 6.023	0.000 6.040	0.000 6.045	0.000 6.056	0.000 6.045	0.000 6.095
AL	3.993 *	3.893 *	3.974 *	3.938 *	3.950 *	3.978 *	3.997 *	3.883 *
TI	.008 *	.012 *	.005 *	.002 *	.010 *	.002 *	.005 *	.001 *
MG	.731 *	.768 *	.799 *	.783 *	.751 *	.789 *	.779 *	.794 *
CA	.344 *	.337 *	.274 *	.257 *	.319 *	.245 *	.277 *	.248 *
MN	.073 *	.202 *	.141 *	.074 *	.143 *	.071 *	.132 *	.069 *
FE	4.755 9.904	4.638 9.850	4.767 9.960	4.892 9.946	4.740 9.923	4.808 9.895	4.715 9.904	4.869 9.864
O	24.000 *	24.000 *	24.000 *	24.000 *	24.000 *	24.000 *	24.000 *	24.000 *
GROS	5.82	5.67	4.59	4.29	5.36	4.15	4.69	4.14
SPES	1.23	3.40	2.36	1.23	2.39	1.21	2.23	1.15
ALM	80.56	78.01	79.70	81.45	79.49	81.30	79.88	81.43
PYRP	12.39	12.92	13.35	13.03	12.76	13.35	13.20	13.27
F/M	6.603	6.303	6.146	6.345	6.418	6.181	6.219	6.222
F/FM	.868	.863	.860	.864	.865	.861	.861	.862

1 SAMPLE P708 GRAIN CENTER
2 CENTER AGAIN
3 AGAIN
4 EDGE
5 ANOTHER CENTRE
6 EDGE
7 ANOTHER CENTRAL
8 EDGE

SUPER PECAL — GARNET SAMPLES

	9	10	11	12	13	14
SIO2	37.66	38.52	38.14	37.99	38.31	37.66
A2O3	21.18	21.22	21.04	21.05	21.27	20.82
TIO2	.05	.04	.10	.05	.08	.02
FEO	34.97	35.03	34.46	35.51	36.22	34.79
MGO	2.98	2.73	2.82	3.15	3.35	2.94
MNO	.98	.93	1.41	.91	1.24	.58
CAO	2.61	2.29	2.61	1.91	2.32	1.49
SUM	100.43	100.76	100.58	100.56	102.81	98.30
SI	6.019 *	6.113 *	6.076 *	6.059 *	6.002 *	6.118 *
AL	0.000 6.019	0.000 6.113	0.000 6.076	0.000 6.059	0.000 6.002	0.000 6.118
AL	3.989 *	3.968 *	3.956 *	3.956 *	3.927 *	3.988 *
TI	.006 *	.005 *	.012 *	.006 *	.010 *	.003 *
MG	.710 *	.646 *	.670 *	.748 *	.783 *	.711 *
CA	.447 *	.389 *	.446 *	.326 *	.390 *	.259 *
MN	.133 *	.125 *	.190 *	.123 *	.165 *	.079 *
FE	4.674 9.959	4.649 9.783	4.591 9.858	4.736 9.895	4.746 10.020	4.727 9.765
O	24.000 *	24.000 *	24.000 *	24.000 *	24.000 *	24.000 *
GROS	7.49	6.70	7.56	5.49	6.41	4.43
SPES	2.22	2.15	3.23	2.07	2.71	1.33
ALM	78.38	80.03	77.86	79.83	78.00	81.82
PYRP	11.90	11.12	11.36	12.61	12.88	12.32
F/M	6.771	7.393	7.140	6.496	6.269	6.756
F/FM	.871	.881	.877	.867	.862	.871

9 ANOTHER GRAIN CENTRAL
10 EDGE
11 ANOTHER CENTRAL
12 AVERAGE
13 AVERAGE PLUS SIGMA
14 AVERAGE MINUS SIGMA

SUPER RECAL — GARNET SAMPLES

	1	2	3	4	5	6	7	8
SIO2	38.18	38.03	38.20	37.52	37.56	38.11	37.84	37.09
A203	20.25	20.50	20.30	20.43	20.54	20.39	20.16	20.04
TIO2	.01	.02	0.00	.04	0.00	.02	0.00	.07
FEO	39.17	38.88	38.93	39.23	39.29	38.96	39.32	39.36
MGO	1.98	1.70	1.70	1.71	1.74	2.01	1.89	1.89
MNO	.26	.27	.29	.29	.30	.26	.26	.31
CAO	.23	.25	.23	.32	.27	.27	.20	.25
SUM	100.08	99.65	99.65	99.54	99.70	100.02	99.67	99.03

SI	6.176	*		6.172	*		6.200	*		6.119	*		6.114	*		6.164	*		6.159	*		6.097	*	
AL	0.000	6.176		0.000	6.172		0.000	6.200		0.000	6.119		0.000	6.114		0.000	6.164		0.000	6.159		0.000	6.097	
AL	3.860	*		3.920	*		3.882	*		3.926	*		3.940	*		3.886	*		3.866	*		3.882	*	
TI	.001	*		.002	*		0.000	*		.005	*		0.000	*		.002	*		0.000	*		.009	*	
MG	.477	*		.411	*		.411	*		.416	*		.422	*		.485	*		.458	*		.463	*	
CA	.040	*		.043	*		.040	*		.056	*		.047	*		.047	*		.035	*		.044	*	
MN	.036	*		.037	*		.040	*		.040	*		.041	*		.036	*		.036	*		.043	*	
FE	5.299	9.714		5.277	9.691		5.284	9.657		5.350	9.793		5.349	9.799		5.270	9.725		5.352	9.747		5.414	9.854	
O	24.000	*		24.000	*		24.000	*		24.000	*		24.000	*		24.000	*		24.000	*		24.000	*	
GROS		.68			.75			.69			.95			.80			.80			.59			.74	
SPES		.61			.64			.69			.68			.71			.61			.61			.72	
ALM		90.55			91.47			91.50			91.27			91.29			90.29			91.00			90.77	
PYRP		8.16			7.13			7.12			7.09			7.21			8.30			7.80			7.76	
F/M		11.174			12.922			12.946			12.968			12.767			10.949			11.751			11.784	
F/FM		.918			.928			.928			.928			.927			.916			.922			.922	

1 SAMPLE P14
2
3
4
5
6
7
8 SAMPLE P14

SUPER RECAL — GARNET SAMPLES

	9	10	11	12	13
SIO2	36.97	36.54	37.60	38.15	37.06
A203	20.23	20.46	20.33	20.48	20.18
TIO2	.01	0.00	.02	.04	-.00
FEO	39.39	39.25	39.18	39.36	39.00
MGO	1.98	1.95	1.86	1.98	1.73
MNO	.29	.26	.28	.30	.26
CAO	.25	.25	.25	.28	.22
SUM	99.12	98.71	99.52	100.59	98.45

SI	6.072	*		6.028	*		6.130	*		6.145	*		6.116	*		
AL	0.000	6.072		0.000	6.028		0.000	6.130		0.000	6.145		0.000	6.115		
AL	3.915	*		3.977	*		3.905	*		3.888	*		3.923	*		
TI	.001	*		0.000	*		.002	*		.005	*		-.001	*		
MG	.485	*		.480	*		.451	*		.475	*		.426	*		
CA	.044	*		.044	*		.044	*		.049	*		.039	*		
MN	.040	*		.036	*		.039	*		.041	*		.036	*		
FE	5.410	9.896		5.415	9.953		5.342	9.782		5.302	9.759		5.382	9.807		
O	24.000	*		24.000	*		24.000	*		24.000	*		24.000	*		
GROS		.74			.74			.75			.83			.67		
SPES		.67			.61			.66			.69			.62		
ALM		90.48			90.63			90.92			90.39			91.47		
PYRP		8.11			8.02			7.57			8.09			7.24		
F/M		11.245			11.369			11.936			11.255			12.713		
F/FM		.918			.919			.923			.918			.927		

9 LARGER GRAIN CENTRAL
10 AT EDGE
11 AVERAGE
12 AVERAGE PLUS SIGMA
13 AVERAGE MINUS SIGMA

SUPER RECAL — GARNET SAMPLES

	1	2	3	4	5	6	7	8
SIO2	36.57	36.79	36.57	37.45	36.84	36.84	37.17	36.52
A2O3	21.17	20.80	21.15	20.98	20.53	20.93	21.16	20.69
TIO2	.14	.14	.13	.13	.13	.13	.14	.13
FEO	36.20	35.89	35.27	35.47	35.99	35.76	36.11	35.42
MGO	.61	.87	.76	.63	.54	.68	.80	.56
MNO	.24	.11	.73	.60	.28	.39	.63	.16
CAO	4.39	4.29	3.86	4.26	4.55	4.27	4.50	4.04
SUM	99.32	98.89	98.47	99.52	98.86	99.01	100.50	97.52
SI	5.976 *	6.024 *	6.007 *	6.078 *	6.048 *	6.027 *	5.899 *	6.056 *
AL	.024 6.000	0.000 6.024	0.000 6.007	0.000 6.078	0.000 6.048	0.000 6.027	.101 6.000	0.000 6.056
AL	4.052 *	4.013 *	4.094 *	4.013 *	3.972 *	4.033 *	4.024 *	4.042 *
TI	.017 *	.017 *	.016 *	.016 *	.016 *	.016 *	.017 *	.016 *
MG	.149 *	.212 *	.186 *	.152 *	.132 *	.166 *	.192 *	.139 *
CA	.769 *	.753 *	.679 *	.741 *	.800 *	.748 *	.778 *	.718 *
MN	.033 *	.015 *	.102 *	.082 *	.039 *	.054 *	.086 *	.022 *
FE	4.947 9.967	4.915 9.926	4.845 9.921	4.815 9.819	4.941 9.900	4.892 9.911	4.873 9.970	4.912 9.849
O	24.000 *	24.000 *	24.000 *	24.000 *	24.000 *	24.000 *	24.000 *	24.000 *
GROS	13.03	12.77	11.69	12.79	13.54	12.77	13.12	12.40
SPES	.56	.26	1.75	1.42	.66	.93	1.44	.38
ALM.	83.88	83.37	83.36	83.15	83.57	83.47	82.19	84.81
PYRP	2.52	3.60	3.20	2.63	2.23	2.84	3.25	2.41
F/M	33.520	23.218	26.584	32.131	37.689	29.749	25.771	35.390
F/FM	.971	.959	.964	.970	.974	.967	.963	.973

1 SAMPLE A22
2
3
4
5
6 AVERAGE
7 AVERAGE PLUS SIGMA
8 AVERAGE MINUS SIGMA

SUPER RECAL

GARNET SAMPLES

	1		2		3		4		5		6		7		8	
SIO2	37.31		37.80		37.65		37.69		37.93		37.90		38.00		37.78	
A2O3	20.43		20.84		20.80		20.56		20.67		20.43		20.27		20.57	
TIO2	0.00		0.00		0.00		0.00		.11		.02		0.00		.02	
FEO	39.07		39.00		38.63		38.22		38.59		38.83		38.66		38.71	
MGO	1.94		1.98		1.89		1.91		1.85		1.93		1.90		1.91	
MNO	.55		.62		.66		.61		.61		.64		.61		.61	
CAO	.55		.51		.54		.57		.54		.65		.59		.56	
SUM	99.85		100.75		100.37		99.56		100.30		100.40		100.03		100.18	
SI	6.076	*	6.085	*	6.107	*	6.126	*	6.122	*	6.124	*	6.156	*	6.114	*
AL	0.000	6.076	0.000	6.085	0.000	6.107	0.000	6.126	0.000	6.122	0.000	6.124	0.000	6.156	0.000	6.114
AL	3.921	*	3.953	*	3.955	*	3.938	*	3.931	*	3.890	*	3.869	*	3.922	*
TI	0.000	*	0.000	*	0.000	*	0.000	*	.013	*	.002	*	0.000	*	.002	*
MG	.471	*	.475	*	.455	*	.463	*	.445	*	.465	*	.459	*	.462	*
CA	.096	*	.088	*	.093	*	.099	*	.093	*	.113	*	.102	*	.098	*
MN	.076	*	.085	*	.090	*	.084	*	.083	*	.088	*	.084	*	.084	*
FE	5.321	9.885	5.250	9.851	5.213	9.806	5.195	9.778	5.209	9.775	5.247	9.804	5.237	9.752	5.239	9.807
O	24.000	*	24.000	*	24.000	*	24.000	*	24.000	*	24.000	*	24.000	*	24.000	*
GPOS		1.61		1.49		1.60		1.70		1.60		1.90		1.74		1.66
SPES		1.27		1.43		1.54		1.47		1.43		1.48		1.42		1.43
ALM		89.22		89.02		89.09		88.94		89.34		88.75		89.04		89.06
PYRP		7.90		8.06		7.77		7.92		7.63		7.86		7.80		7.85
F/M	11.461		11.229		11.666		11.409		11.891		11.477		11.599		11.529	
F/FM	.920		.918		.921		.919		.922		.920		.921		.920	

1 SAMPLE P29
2 ANOTHER SMALL GRAIN
3 LARGE GRAIN CENTRAL
4 EDGE
5
6 LARGE GRAIN CENTRAL
7 EDGE
8 AVERAGE

SUPER RECAL — GARNET SAMPLES

	1	2	3	5	6	7	8
SIO2	37.97	37.62	37.56	37.52	37.39	37.74	37.56	37.33
A2O3	19.96	20.02	20.31	20.32	20.21	20.15	20.28	20.47
TIO2	.03	.04	0.00	.07	.04	.03	0.00	.01
FEO	37.24	37.97	38.67	38.73	37.25	37.95	38.32	38.56
MGO	1.91	2.06	1.88	2.00	1.63	1.85	2.24	2.44
MNO	.46	.41	.44	.54	.55	.46	.35	.28
CAO	2.13	1.01	.43	1.54	2.14	2.01	.39	.44
SUM	99.70	99.13	99.29	100.72	99.21	100.19	99.14	99.53
SI	6.160 *	6.144 *	6.132 *	6.062 *	6.108 *	6.112 *	6.129 *	6.076 *
AL	0.000 6.160	0.000 6.144	0.000 6.132	0.000 6.062	0.000 6.108	0.000 6.112	0.000 6.129	0.000 6.076
AL	3.816 *	3.853 *	3.907 *	3.868 *	3.890 *	3.845 *	3.900 *	3.926 *
TI	.004 *	.005 *	0.000 *	.009 *	.005 *	.004 *	0.000 *	.001 *
MG	.462 *	.501 *	.457 *	.482 *	.397 *	.447 *	.545 *	.592 *
CA	.370 *	.177 *	.075 *	.267 *	.375 *	.349 *	.068 *	.077 *
MN	.063 *	.057 *	.061 *	.074 *	.076 *	.063 *	.048 *	.039 *
FE	5.052 9.767	5.186 9.779	5.280 9.780	5.233 9.932	5.089 9.832	5.140 9.847	5.229 9.790	5.248 9.883
O	24.000 *	24.000 *	24.000 *	24.000 *	24.000 *	24.000 *	24.000 *	24.000 *
GROS	6.22	2.98	1.28	4.40	6.31	5.81	1.16	1.29
SPES	1.06	.96	1.04	1.22	1.28	1.05	.82	.65
ALM	84.95	87.59	89.89	86.42	85.72	85.69	88.77	88.12
PYRP	7.77	8.47	7.79	7.95	6.69	7.44	9.25	9.94
F/M	11.076	10.455	11.674	11.619	13.014	11.651	9.687	8.932
F/FM	.917	.913	.921	.917	.929	.921	.906	.899

1 SAMPLE DC-6
2 EDGE
3 SMALL GRAIN
4 CENTRE OF LARGE GRAIN
5 INT
6 TOWARDS EDGE
7 CLOSER
8 EDGE

SUPER RECAL — GARNET SAMPLES

	9	10	11
SIO2	37.59	37.77	37.40
A2O3	20.22	20.37	20.06
TIO2	.03	.05	.01
FEO	38.09	38.64	37.53
MGO	2.00	2.23	1.77
MNO	.44	.52	.35
CAO	1.26	2.00	.52
SUM	99.61	101.59	97.63
SI	6.115 *	6.149 *	6.184 *
AL	0.000 6.115	0.000 6.049	0.000 6.184
AL	3.876 *	3.844 *	3.908 *
TI	.003 *	.006 *	.001 *
MG	.485 *	.533 *	.436 *
CA	.220 *	.343 *	.093 *
MN	.060 *	.071 *	.049 *
FE	5.182 9.826	5.175 9.972	5.189 9.676
O	24.000 *	24.000 *	24.000 *
GROS	3.70	5.60	1.61
SPES	1.01	1.15	.85
ALM	87.13	84.53	89.98
PYRP	8.16	8.71	7.55
F/M	10.802	9.834	12.026
F/FM	.915	.908	.923

9 AVERAGE
10 AVERAGE PLUS SIGMA
11 AVERAGE MINUS SIGMA

SUPER PECAL GARNET SAMPLES

	1	2	3	4
SIO2	36.64	36.64	36.64	36.64
A2O3	20.13	20.13	20.13	20.13
TIO2	.12	.12	.12	.12
FEO	0.00	0.00	0.00	0.00
MGO	.63	.63	.63	.63
MNO	39.13	39.13	39.13	39.13
CAO	4.12	4.12	4.12	4.12
SUM	100.77	100.77	100.77	100.77

SI	5.960	*	5.960	*	5.960	*	5.960	*
AL	.040	6.000	.040	6.000	.040	6.000	.040	6.000
AL	3.818	*	3.818	*	3.818	*	3.818	*
TI	.015	*	.015	*	.015	*	.015	*
MG	.153	*	.153	*	.153	*	.153	*
CA	.718	*	.718	*	.718	*	.718	*
MN	5.391	*	5.391	*	5.391	*	5.391	*
FE	0.000	10.094	0.000	10.094	0.000	10.094	0.000	10.094
O	24.000	*	24.000	*	24.000	*	24.000	*
	GROS	11.47		11.47		11.47		11.47
	SPES	86.09		86.09		86.09		86.09
	ALM	0.00		0.00		0.00		0.00
	PYRP	2.44		2.44		2.44		2.44
	F/M	35.296		35.296		35.296		35.296
	F/FM	.972		.972		.972		.972

1 SAMPLE D-57-1 GARNET
2 AVERAGE
3 AVERAGE PLUS SIGMA
4 AVERAGE MINUS SIGMA

SUPER PECAL — GARNET SAMPLES

	1	2	3	4	5	6	7	8
SIO2	36.86	37.02	37.06	37.60	37.94	37.30	37.70	36.89
A2O3	20.24	20.97	21.07	20.52	20.61	20.74	21.04	20.45
TIO2	1.27	1.13	1.41	1.33	1.19	1.27	1.37	1.17
FEO	0.00	0.00	0.00	0.00	0.00	0.00	0.00	0.00
MGO	1.48	.91	1.16	1.20	1.29	1.21	1.39	1.02
MNO	33.09	34.79	34.19	33.82	33.66	33.91	34.47	33.35
CAO	5.60	5.03	4.61	5.30	5.25	5.20	5.46	4.93
SUM	98.54	99.85	99.70	100.07	99.94	99.62	101.44	97.80

SI	5.991	*	5.962	*	5.956	*	6.011	*	6.064	*	5.997	*	5.961	*	6.033	*
AL	.009	6.000	.038	6.000	.044	6.000	0.000	6.011	0.000	6.064	.003	6.000	.039	6.000	0.000	6.033
AL	3.868	*	3.941	*	3.946	*	3.922	*	3.881	*	3.927	*	3.861	*	3.941	*
TI	.155	*	.137	*	.170	*	.160	*	.143	*	.153	*	.162	*	.144	*
MG	.359	*	.218	*	.278	*	.286	*	.307	*	.290	*	.328	*	.249	*
CA	.975	*	.868	*	.828	*	.908	*	.899	*	.895	*	.926	*	.864	*
MN	4.556	*	4.745	*	4.654	*	4.579	*	4.556	*	4.618	*	4.617	*	4.619	*
FE	0.000	9.913	0.000	9.910	0.000	9.877	0.000	9.855	0.000	9.787	0.000	9.883	0.000	9.914	0.000	9.817
O	24.000	*	24.000	*	24.000	*	24.000	*	24.000	*	24.000	*	24.000	*	24.000	*
GROS		16.56		14.88		14.38		15.72		15.60		15.43		15.77		15.08
SPES		77.35		81.37		80.80		79.32		79.07		79.58		78.64		80.58
ALM		0.00		0.00		0.00		0.00		0.00		0.00		0.00		0.00
PYRP		6.09		3.75		4.82		4.95		5.33		4.99		5.59		4.35
F/M		12.795		21.725		16.749		16.016		14.828		15.952		14.060		18.530
F/FM		.927		.956		.944		.941		.937		.941		.934		.949

1 SAMPLE D-58-1
2
3 GARNET LATH
4
5
6 AVERAGE
7 AVERAGE PLUS SIGMA
8 AVERAGE MINUS SIGMA

SUPER PECAL — GARNET SAMPLES

	1	2	3	4	5	6	7	8
SIO2	37.35	37.29	36.64	36.69	37.44	37.08	37.43	36.74
A2O3	20.89	21.49	20.70	20.68	20.86	20.92	21.22	20.63
TIO2	4.45	4.52	4.68	4.68	4.70	4.61	4.71	4.50
FEO	0.00	0.00	0.00	0.00	0.00	0.00	0.00	0.00
MGO	.75	.80	.60	.89	.83	.81	.86	.77
MNO	31.66	31.73	31.99	31.40	32.24	31.80	32.09	31.92
CAO	4.84	4.78	4.30	4.32	4.13	4.47	4.76	4.19
SUM	99.94	100.61	99.11	98.66	100.20	99.70	101.06	98.35

SI	5.919	*		5.866	*		5.870	*		5.889	*		5.919	*		5.893	*		5.870	*		5.915	*	
AL	.081	6.000		.134	6.000		.130	6.000		.111	6.000		.081	6.000		.107	6.000		.130	6.000		.085	6.000	
AL	3.820	*		3.850	*		3.777	*		3.808	*		3.805	*		3.810	*		3.792	*		3.829	*	
TI	.530	*		.535	*		.564	*		.565	*		.559	*		.550	*		.555	*		.545	*	
MG	.177	*		.188	*		.191	*		.213	*		.196	*		.193	*		.201	*		.184	*	
CA	.822	*		.806	*		.738	*		.743	*		.700	*		.762	*		.799	*		.723	*	
MN	4.250	*		4.228	*		4.341	*		4.269	*		4.317	*		4.281	*		4.263	*		4.298	*	
FE	0.000	9.598		0.000	9.605		0.000	9.611		0.000	9.589		0.000	9.577		0.000	9.596		0.000	9.611		0.000	9.580	
O	24.000	*		24.000	*		24.000	*		24.000	*		24.000	*		24.000	*		24.000	*		24.000	*	
GROS		15.66			15.43			14.01			14.22			13.42			14.55			15.19			13.89		
SPES		80.97			80.98			82.37			81.71			82.83			81.77			80.99			82.57		
ALM		0.00			0.00			0.00			0.00			0.00			0.00			0.00			0.00		
PYRP		3.39			3.59			3.62			4.08			3.75			3.68			3.82			3.54		
F/M		23.988			22.539			22.723			20.049			22.073			22.203			21.209			23.316		
F/FM		.960			.958			.958			.952			.957			.957			.955			.959		

1 SAMPLE D-58-2
2
3
4
5
6 AVERAGE
7 AVERAGE PLUS SIGMA
8 AVERAGE MINUS SIGMA

SUPER PECAL — GARNET SAMPLES

	1	2	3	4	5	6	7	8
SIO2	37.56	37.78	37.69	37.63	37.25	37.58	37.76	37.40
A2O3	21.54	21.34	20.94	21.16	21.25	21.25	21.44	21.05
TIO2	2.02	1.95	2.12	2.08	1.94	2.06	2.17	1.96
FEO	0.00	0.00	0.00	0.00	0.00	0.00	0.00	0.00
MGO	1.37	1.32	1.30	1.32	1.50	1.36	1.43	1.29
MNO	37.41	37.80	34.01	33.78	33.75	33.75	33.94	33.56
CAO	4.07	4.59	4.55	4.56	4.96	4.55	4.83	4.26
SUM	100.17	100.78	100.61	100.53	100.65	100.55	101.58	99.51

SI	5.960	*		5.975	*		5.982	*		5.970	*		5.916	*		5.961	*		5.933	*		5.989	*	
AL	.040	6.000		.025	6.000		.018	6.000		.030	6.000		.084	6.000		.039	6.000		.067	6.000		.011	6.000	
AL	3.988	*		3.953	*		3.898	*		3.926	*		3.892	*		3.931	*		3.903	*		3.961	*	
TI	.265	*		.232	*		.253	*		.248	*		.232	*		.246	*		.256	*		.236	*	
MG	.324	*		.311	*		.308	*		.312	*		.355	*		.322	*		.336	*		.308	*	
CA	.692	*		.778	*		.774	*		.775	*		.844	*		.773	*		.813	*		.731	*	
MN	4.493	*		4.528	*		4.572	*		4.540	*		4.540	*		4.534	*		4.517	*		4.552	*	
FE	0.000	9.759		0.000	9.802		0.000	9.805		0.000	9.801		0.000	9.862		0.000	9.806		0.000	9.824		0.000	9.787	
O	24.000	*		24.000	*		24.000	*		24.000	*		24.000	*		24.000	*		24.000	*		24.000	*	
GROS		12.57			13.85			13.69			13.78			14.71			13.73			14.35			13.08		
SPES		81.55			80.61			80.87			80.68			79.11			80.55			79.72			81.41		
ALM		0.00			0.00			0.00			0.00			0.00			0.00			0.00			0.00		
PYRP		5.98			5.54			5.44			5.55			6.19			5.72			5.93			5.50		
F/M		13.858			14.551			14.867			14.542			12.786			14.081			13.444			14.731		
F/FM		.933			.936			.937			.936			.927			.934			.931			.937		

1 SAMPLE D58-3
2
3
4

5
6 AVERAGE
7 AVERAGE PLUS SIGMA
8 AVERAGE MINUS SIGMA

SUPER RECAL — GARNET SAMPLES

	1	2	3	4	5	6	7	8
SIO2	37.10	36.55	37.51	37.20	37.15	38.05	37.78	36.85
A203	17.86	17.89	18.27	18.05	17.79	18.42	18.22	18.14
TIO2	0.00	0.00	0.00	0.00	0.00	0.00	0.00	0.00
FEO	13.31	12.85	13.29	12.76	12.53	13.40	13.28	13.11
MGO	1.00	1.05	.95	1.04	1.08	1.03	1.02	.93
MNO	17.82	18.59	17.77	18.21	18.36	17.44	17.94	18.23
CAO	12.02	11.72	11.84	11.60	11.80	11.53	12.07	11.55
SUM	99.11	98.65	99.63	98.86	98.71	99.97	100.31	98.81

SI	6.083	*	6.035	*	6.100	*	6.099	*	6.105	*	6.144	*	6.105	*	6.060	*
AL	0.000	6.083	0.000	6.035	0.000	6.100	0.000	6.099	0.000	6.105	0.000	6.144	0.000	6.105	0.000	6.060
AL	3.451	*	3.481	*	3.501	*	3.487	*	3.445	*	3.505	*	3.469	*	3.515	*
TI	0.000	*	0.000	*	0.000	*	0.000	*	0.000	*	0.000	*	0.000	*	0.000	*
MG	.244	*	.258	*	.230	*	.254	*	.265	*	.248	*	.246	*	.226	*
CA	2.112	*	2.073	*	2.063	*	2.038	*	2.078	*	2.012	*	2.090	*	2.033	*
MN	2.475	*	2.600	*	2.447	*	2.529	*	2.556	*	2.385	*	2.455	*	2.539	*
FE	1.825	10.107	1.774	10.187	1.807	10.049	1.749	10.057	1.722	10.065	1.809	9.959	1.795	10.054	1.303	10.121
O	24.000	*	24.000	*	24.000	*	24.000	*	24.000	*	24.000	*	24.000	*	24.000	*
GROS		31.73		30.92		31.50		31.01		31.39		31.17		31.73		30.81
SPES		37.18		38.77		37.38		38.49		38.61		36.95		37.29		38.44
ALM		27.42		26.46		27.60		26.63		26.01		28.03		27.25		27.30
PYRP		3.67		3.85		3.52		3.87		4.00		3.84		3.73		3.45
F/M		17.594		16.927		18.479		16.834		16.170		16.921		17.300		19.049
F/FM		.946		.944		.949		.944		.942		.944		.945		.950

1 SAMPLE P51 RANDOM
2
3
4
5
6
7
8 GRAIN EDGE

SUPER RECAL — GARNET SAMPLES

	9	10	11	12	13
SIO2	37.66	37.86	37.37	37.83	36.92
A203	17.82	18.09	18.06	18.26	17.85
TIO2	0.00	0.00	0.00	0.00	0.00
FEO	13.50	13.64	13.17	13.50	12.83
MGO	.85	.96	.99	1.06	.93
MNO	18.07	17.21	17.96	18.36	17.56
CAO	12.23	12.03	11.85	12.07	11.63
SUM	100.13	99.79	99.40	101.07	97.73

SI	6.116	*	6.139	*	6.099	*	6.081	*	6.116	*
AL	0.000	6.116	0.000	6.139	0.000	6.099	0.000	6.081	0.000	6.116
AL	3.410	*	3.457	*	3.472	*	3.459	*	3.486	*
TI	0.000	*	0.000	*	0.000	*	0.000	*	0.000	*
MG	.206	*	.232	*	.241	*	.253	*	.229	*
CA	2.128	*	2.090	*	2.072	*	2.079	*	2.056	*
MN	2.485	*	2.364	*	2.483	*	2.501	*	2.465	*
FE	1.833	10.062	1.850	9.992	1.797	10.065	1.815	10.106	1.778	10.022
O	24.000	*	24.000	*	24.000	*	24.000	*	24.000	*
GROS		31.99		31.98		31.42		31.27		31.59
SPES		37.36		36.17		37.66		37.62		37.71
ALM		27.56		28.30		27.26		27.31		27.20
PYRP		3.09		3.55		3.66		3.81		3.50
F/M		20.992		18.159		17.756		17.052		18.559
F/FM		.955		.948		.947		.945		.949

9
10
11 AVERAGE

12 AVERAGE PLUS SIGMA
13 AVERAGE MINUS SIGMA

SUPER RECAL — GARNET SAMPLES

	1	2	3	4	5	6	7	8
SIO2	38.77	38.66	38.81	37.73	38.98	38.90	38.64	39.06
A2O3	20.48	20.58	20.87	20.67	20.21	20.54	20.58	20.78
TIO2	.11	.04	0.00	0.00	.10	.04	.05	.09
FEO	13.75	14.32	20.06	20.67	17.72	14.29	16.80	19.64
MGO	2.65	2.50	2.32	2.25	2.05	2.27	2.34	2.53
MNO	17.53	16.87	14.09	13.29	14.68	17.11	15.60	17.23
CAO	7.64	7.68	5.05	4.94	7.11	7.43	6.64	7.82
SUM	100.93	100.75	101.20	99.55	100.85	100.58	100.64	107.15

SI	6.105	*	6.098	*	6.124	*	6.069	*	6.164	*	6.143	*	6.117	*	5.927	*
AL	0.000	6.105	0.000	6.098	0.000	6.124	0.000	6.069	0.000	6.164	0.000	6.143	0.000	6.117	.073	6.000
AL	3.800	*	3.844	*	3.880	*	3.918	*	3.766	*	3.823	*	3.838	*	3.642	*
TI	.013	*	.005	*	0.000	*	0.000	*	.012	*	.005	*	.006	*	.010	*
MG	.622	*	.588	*	.546	*	.539	*	.483	*	.534	*	.552	*	.572	*
CA	1.289	*	1.298	*	.854	*	.851	*	1.205	*	1.257	*	1.127	*	1.271	*
MN	2.338	*	2.254	*	1.883	*	1.811	*	1.966	*	2.289	*	2.091	*	2.215	*
FE	1.811	9.874	1.889	9.876	2.647	9.810	2.761	9.900	2.343	9.775	1.887	9.795	2.224	9.838	2.492	10.203
O	24.000	*	24.000	*	24.000	*	24.000	*	24.000	*	24.000	*	24.000	*	24.000	*
	GEOS	21.27		21.53		14.40		14.23		20.09		21.07		18.79		19.41
	SPES	38.58		37.39		31.76		30.27		32.78		38.35		34.89		33.81
	ALM	29.88		31.33		44.64		46.48		39.07		31.63		37.11		38.04
	PYRP	10.26		9.75		9.20		9.02		8.06		8.95		9.21		8.74
	F/M	6.670		7.048		8.303		8.511		8.919		7.815		7.816		8.221
	F/FM	.870		.876		.893		.895		.899		.887		.887		.892

1 SAMPLE 072-4
2 ANOTHER CENTRAL
3 EDGE
4 ANOTHER AT END
5 OPP END
6
7 AVERAGE
8 AVERAGE PLUS SIGMA

SUPER RECAL — GARNET SAMPLES

	1	2	3	4	5	6	7	8
SIO2	36.92	36.00	36.83	37.54	36.68	36.48	36.54	36.50
A203	20.36	20.51	20.40	20.97	21.02	20.25	20.48	21.23
TIO2	.22	.18	.21	.07	.06	.21	.18	.05
FEO	21.45	20.30	20.83	27.79	26.28	22.20	22.93	28.47
MGO	2.01	1.56	2.01	3.88	3.56	1.99	2.45	3.89
MNO	14.80	15.50	15.84	8.29	9.38	13.83	12.25	7.71
CAO	4.61	4.96	4.42	1.65	2.54	4.37	4.06	1.54
SUM	100.37	99.01	100.54	100.39	99.52	99.33	98.89	99.39

SI	5.964	*		5.906	*		5.948	*		5.995	*		5.925	*		5.956	*		5.961	*		5.903	*	
AL	.036	6.000		.094	6.000		.052	6.000		.005	6.000		.075	6.000		.044	6.000		.039	6.000		.097	6.000	
AL	3.839	*		3.872	*		3.830	*		3.941	*		3.927	*		3.851	*		3.898	*		3.949	*	
TI	.027	*		.022	*		.026	*		.008	*		.007	*		.026	*		.022	*		.006	*	
MG	.484	*		.381	*		.484	*		.924	*		.957	*		.484	*		.596	*		.938	*	
CA	.796	*		.872	*		.765	*		.317	*		.440	*		.764	*		.710	*		.267	*	
MN	2.025	*		2.154	*		2.167	*		1.121	*		1.283	*		1.912	*		1.693	*		1.056	*	
FE	2.898	10.070		2.785	10.087		2.813	10.084		3.711	10.022		3.550	10.065		3.031	10.069		3.128	10.046		3.850	10.066	
O	24.000	*		24.000	*		24.000	*		24.000	*		24.000	*		24.000	*		24.000	*		24.000	*	
GROS		12.86			14.08			12.28			5.21			7.17			12.34			11.58			4.37		
SPES		32.64			34.78			34.79			18.46			20.94			30.89			27.63			17.28		
ALM		46.70			44.98			45.17			61.11			57.91			48.95			51.06			63.01		
PYRP		7.80			6.16			7.77			15.21			13.98			7.82			9.72			15.34		
F/M		10.172			12.947			10.293			5.233			5.639			10.209			8.093			5.233		
F/FM		.910			.928			.911			.840			.849			.911			.890			.840		

1 SAMPLE 77-62-109 CLOUDY GRAIN CENTRAL
2 ANOTHER CENTRAL
3
4 AT EDGE
5 ANOTHER GRAIN CENTRAL
6 VERY CHL RICH AREA
7 ANOTHER IN V DARK AREA
8

SUPER RECAL — GARNET SAMPLES

	9	10	11	12
SIO2	36.77	36.70	37.09	36.30
A203	20.08	20.59	20.96	20.22
TIO2	0.00	.13	.21	.05
FEO	22.14	23.60	26.51	20.69
MGO	2.23	2.62	3.47	1.77
MNO	14.20	12.42	15.41	9.43
CAO	3.46	3.53	4.73	2.34
SUM	98.88	99.59	108.37	90.81

SI	6.019	*		5.953	*		5.669	*		6.274	*	
AL	0.000	6.019		.047	6.000		.331	6.000		0.000	6.274	
AL	3.873	*		3.889	*		3.444	*		4.118	*	
TI	0.000	*		.016	*		.024	*		.007	*	
MG	.544	*		.634	*		.791	*		.455	*	
CA	.607	*		.614	*		.774	*		.434	*	
MN	1.969	*		1.707	*		1.996	*		1.381	*	
FE	3.031	10.024		3.202	10.061		3.389	10.417		2.993	9.384	
O	24.000	*		24.000	*		24.000	*		24.000	*	
GROS		9.87			9.98			11.14			8.25	
SPES		32.01			27.73			28.72			26.24	
ALM		49.28			52.01			48.76			56.85	
PYRP		8.85			10.29			11.38			8.66	
F/M		9.189			7.748			6.807			9.596	
F/FM		.902			.886			.872			.906	

9 NEAR MN MAX
10 AVERAGE
11 AVERAGE PLUS SIGMA
12 AVERAGE MINUS SIGMA

SUPER RECAL — GARNET SAMPLES

	1	2	3	4	5	6	7	8
SIO2	37.50	38.46	38.54	38.06	37.91	38.41	38.25	38.36
A2O3	20.34	21.77	20.96	19.60	19.83	20.66	20.21	20.26
TIO2	.34	.07	.20	.30	.24	.09	.17	.09
FEO	23.88	25.29	17.06	13.55	17.58	22.03	17.56	21.97
MGO	2.62	3.66	1.26	.89	1.63	2.70	1.50	2.65
MNO	8.94	8.51	14.46	19.50	14.12	8.60	14.56	9.96
CAO	5.86	3.27	8.60	8.62	6.46	7.11	8.18	7.45
SUM	99.68	101.03	101.08	100.52	99.77	99.60	100.43	100.74

SI	6.020	*		6.039	*		6.083	*		6.104	*		6.090	*		6.112	*		6.099	*		6.080	*	
AL	0.000	6.020		0.000	6.039		0.000	6.083		0.000	6.104		0.000	6.090		0.000	6.112		0.000	6.099		0.000	6.080	
AL	3.848	*		4.028	*		3.899	*		3.704	*		3.754	*		3.874	*		3.798	*		3.784	*	
TI	.041	*		.008	*		.024	*		.036	*		.029	*		.011	*		.020	*		.011	*	
MG	.575	*		.857	*		.296	*		.213	*		.390	*		.640	*		.357	*		.626	*	
CA	1.009	*		.550	*		1.454	*		1.481	*		1.456	*		1.212	*		1.398	*		1.269	*	
MN	1.218	*		1.132	*		1.933	*		2.649	*		1.921	*		1.159	*		1.967	*		1.337	*	
FE	3.206	9.993		3.321	9.897		2.252	9.858		1.817	9.901		2.362	9.912		2.931	9.827		2.342	9.880		2.912	9.935	
O	24.000	*		24.000	*		24.000	*		24.000	*		24.000	*		24.000	*		24.000	*		24.000	*	
GROS		16.51			9.39			24.50			24.04			23.76			20.40			23.05			20.60		
SPES		19.91			19.32			32.57			43.00			31.34			19.50			32.44			21.78		
ALM		52.52			56.68			37.94			29.50			38.53			49.33			38.63			47.43		
PYRP		11.05			14.62			4.99			3.46			6.37			10.77			5.88			10.20		
F/M		6.553			5.198			14.118			20.993			10.974			6.388			12.084			6.787		
F/FM		.868			.839			.934			.955			.916			.865			.924			.872		

1 SAMPLE 77-62-206.5 SMALL GRAIN CENTER
2 AT EDGE
3 ANOTHER GRAIN CENTRAL
4 ANOTHER GRAIN CENTRAL
5 INT SPOT
6 AT EDGE
7 ANOTHER GRAIN CENTRAL
8 EDGE

SUPER RECAL — GARNET SAMPLES

	9	10	11	12	13	14	15	16
SIO2	37.61	37.98	37.29	37.98	37.37	37.14	37.32	37.74
A2O3	20.09	20.86	19.97	21.01	19.81	19.75	19.57	20.05
TIO2	.20	.02	.19	.05	.23	.25	.27	.25
FEO	23.79	24.70	13.52	22.67	12.49	10.09	10.58	13.39
MGO	2.96	3.82	.63	2.73	.43	.24	.28	.55
MNO	8.79	8.51	19.43	8.65	21.04	23.50	22.75	19.36
CAO	6.31	8.23	8.82	6.19	8.85	8.55	8.93	8.60
SUM	98.75	99.12	99.85	99.28	100.22	99.52	99.70	99.94

SI	6.079	*		6.081	*		6.034	*		6.070	*		6.039	*		6.046	*		6.062	*		6.081	*	
AL	0.000	6.079		0.000	6.081		0.000	6.034		0.000	6.070		0.000	6.039		0.000	6.046		0.000	6.062		0.000	6.081	
AL	3.826	*		3.936	*		3.808	*		3.957	*		3.773	*		3.786	*		3.746	*		3.807	*	
TI	.024	*		.002	*		.023	*		.006	*		.028	*		.031	*		.033	*		.030	*	
MG	.713	*		.912	*		.152	*		.650	*		.104	*		.058	*		.068	*		.132	*	
CA	.920	*		.554	*		1.529	*		1.060	*		1.532	*		1.491	*		1.554	*		1.485	*	
MN	1.203	*		1.154	*		2.663	*		1.171	*		2.880	*		3.240	*		3.130	*		2.542	*	
FE	3.216	9.902		3.307	9.865		1.829	10.004		3.030	9.874		1.688	10.005		1.374	9.982		1.437	9.968		1.804	9.901	
O	24.000	*		24.000	*		24.000	*		24.000	*		24.000	*		24.000	*		24.000	*		24.000	*	
GROS		15.19			9.35			24.77			17.93			24.70			24.20			25.11			24.49		
SPES		19.88			19.47			+3.14			19.81			46.42			52.57			50.57			43.58		
ALM		53.14			55.80			29.64			51.26			27.21			22.23			23.22			29.76		
PYRP		11.78			15.38			2.46			11.00			1.67			.94			1.10			2.18		
F/M		6.197			4.894			29.567			6.460			44.103			79.231			67.372			33.663		
F/FM		.861			.830			.967			.866			.978			.988			.985			.971		

9 ANOTHER GRAIN CENTRAL
10 AT EDGE
11 ANOTHER GRAIN CENTRAL
12 AT EDGE
13 ANOTHER CENTRAL
14 ANOTHER V LARGE GARNET CENTRAL
15
16

SUPER PECAL — GARNET SAMPLES

	1	2	3	4	5	6	7	8
SIO2	37.69	37.20	37.41	37.99	37.29	36.84	37.30	37.46
A2O3	21.49	21.79	22.03	21.69	20.99	20.74	20.67	21.08
TIO2	.10	.07	.05	.09	.07	.03	.11	.05
FEO	26.79	26.80	26.56	26.15	27.89	26.29	25.60	27.80
MGO	4.00	3.85	3.88	3.81	4.55	3.93	3.64	4.76
MNO	7.70	8.19	8.37	7.81	6.90	8.50	7.97	6.09
CAO	2.68	2.81	2.78	3.67	3.00	3.13	3.63	3.11
SUM	100.65	100.71	101.08	101.21	100.69	99.26	99.12	100.35
SI	5.971 *	5.907 *	5.910 *	5.976 *	5.928 *	5.949 *	6.005 *	5.950 *
AL	.029 6.000	.093 6.000	.090 6.000	.024 6.000	.072 6.000	.051 6.000	0.000 6.005	.050 6.000
AL	3.982 *	3.965 *	4.012 *	3.997 *	3.861 *	3.895 *	3.921 *	3.895 *
TI	.012 *	.008 *	.006 *	.011 *	.008 *	.004 *	.013 *	.006 *
MG	.944 *	.911 *	.914 *	.893 *	1.078 *	.946 *	.921 *	1.127 *
CA	.489 *	.478 *	.471 *	.619 *	.511 *	.542 *	.626 *	.529 *
MN	1.033 *	1.102 *	1.120 *	1.041 *	.929 *	1.163 *	1.087 *	.819 *
FE	3.549 10.010	3.559 10.043	3.509 10.031	3.440 10.001	3.708 10.095	3.523 10.072	3.446 10.015	3.693 10.069
O	24.000 *	24.000 *	24.000 *	24.000 *	24.000 *	24.000 *	24.000 *	24.000 *
GROS	6.13	7.90	7.83	10.32	8.21	8.77	10.30	8.58
SPES	17.17	18.21	18.63	17.36	14.92	18.83	17.87	13.28
ALM	59.00	58.83	58.36	57.41	59.55	57.07	56.68	59.87
PYRP	15.70	15.06	15.19	14.91	17.32	15.32	15.15	18.27
F/M	4.852	5.115	5.067	5.016	4.301	4.954	4.920	4.004
F/FM	.829	.836	.835	.834	.811	.832	.831	.800

1 SAMPLE 77-62-378 CENTRAL
2 AT EDGE
3 ANOTHER SMALL GRAIN AT EDGE OF PY
4 ANOTHER GRAIN CENTRAL
5 SMALL GRAIN CENTRAL
6 AT EDGE
7 ANOTHER GRAIN CENTRAL
8 AT EDGE

SUPER PECAL — GARNET SAMPLES

	9	10	11	12	13	14	15	16
SIO2	36.72	37.67	37.09	36.52	37.04	37.05	36.58	37.19
A2O3	20.92	21.01	20.69	20.57	20.64	20.88	20.80	21.07
TIO2	.12	.04	.05	.07	.07	.11	.07	.07
FEO	26.25	26.95	27.02	25.97	26.82	27.73	26.62	26.74
MGO	4.06	4.38	4.57	3.85	4.16	4.88	4.11	4.18
MNO	7.94	6.89	6.47	8.41	7.63	5.79	7.46	7.47
CAO	3.68	3.21	3.31	3.77	3.12	3.15	3.05	3.22
SUM	99.72	100.11	99.20	99.16	99.48	99.59	98.69	99.93
SI	5.902 *	5.988 *	5.963 *	5.917 *	5.962 *	5.931 *	5.931 *	5.946 *
AL	.098 6.000	.012 6.000	.037 6.000	.083 6.000	.038 6.000	.069 6.000	.069 6.000	.054 6.000
AL	3.864 *	3.928 *	3.863 *	3.844 *	3.876 *	3.869 *	3.305 *	3.915 *
TI	.015 *	.005 *	.006 *	.009 *	.008 *	.013 *	.009 *	.009 *
MG	.980 *	1.039 *	1.095 *	.930 *	.998 *	1.164 *	.993 *	.996 *
CA	.634 *	.547 *	.570 *	.654 *	.538 *	.540 *	.530 *	.552 *
MN	1.081 *	.929 *	.881 *	1.154 *	1.040 *	.785 *	1.025 *	1.012 *
FE	3.528 10.101	3.587 10.035	3.633 10.069	3.519 10.109	3.610 10.071	3.712 10.085	3.610 10.071	3.575 10.058
O	24.000 *	24.000 *	24.000 *	24.000 *	24.000 *	24.000 *	24.000 *	24.000 *
GROS	10.18	8.97	9.23	10.46	8.70	8.71	8.61	8.99
SPES	17.37	15.22	14.26	18.44	16.81	12.66	16.64	16.50
ALM	56.70	58.78	58.79	56.24	58.36	59.86	58.62	58.28
PYRP	15.75	17.03	17.72	14.86	16.13	18.77	16.13	16.23
F/M	4.704	4.346	4.122	5.026	4.660	3.862	4.665	4.608
F/FM	.825	.813	.805	.834	.823	.794	.823	.822

9 ANOTHER GRAIN CENTRAL
10 AT EDGE
11 SAME SPOT AGAIN
12 ANOTHER GAI CENTRAL
13 AT EDGE
14 ANOTHER GRAIN CENTRAL
15 AT EDGE
16 AVERAGE

SUPER RECAL — GARNET SAMPLES

	1	2	3	4	5	6	7	8
SIO2	37.24	37.46	37.20	37.61	37.66	37.73	37.64	37.63
A2O3	21.06	21.20	20.77	21.86	21.27	21.81	21.26	21.61
TIO2	.21	.18	.18	.05	.11	.05	.14	.15
FEO	24.84	17.77	21.38	28.34	24.07	27.61	24.31	23.59
MGO	3.13	1.36	2.18	4.34	2.78	4.13	3.01	2.02
MNO	10.84	15.64	12.53	7.59	9.22	8.05	10.28	10.59
CAO	3.29	7.18	6.21	1.61	5.68	1.70	3.93	5.25
SUM	100.61	100.79	100.45	101.40	100.79	101.08	100.57	100.84
SI	5.951 *	5.974 *	5.960 *	5.928 *	5.975 *	5.958 *	5.990 *	5.980 *
AL	.049 6.000	.026 6.000	.040 6.000	.072 6.000	.025 6.000	.042 6.000	.010 6.000	.020 6.000
AL	3.917 *	3.957 *	3.882 *	3.988 *	3.952 *	4.016 *	3.976 *	4.026 *
TI	.025 *	.022 *	.022 *	.006 *	.013 *	.006 *	.017 *	.018 *
MG	.746 *	.323 *	.521 *	1.020 *	.657 *	.972 *	.714 *	.478 *
CA	.563 *	1.227 *	1.066 *	.272 *	.966 *	.288 *	.670 *	.894 *
MN	1.467 *	2.112 *	1.700 *	1.013 *	1.239 *	1.077 *	1.386 *	1.425 *
FE	3.320 10.038	2.370 10.011	2.865 10.055	3.736 10.034	3.194 10.021	3.646 10.005	3.235 9.998	3.135 9.977
O	24.000 *	24.000 *	24.000 *	24.000 *	24.000 *	24.000 *	24.000 *	24.000 *
GROS	9.24	20.34	17.33	4.50	15.94	4.81	11.16	15.07
SPES	24.07	35.02	27.64	16.78	20.46	18.00	23.07	24.03
ALM	54.46	39.29	46.57	61.84	52.74	60.95	53.88	52.84
PYRP	12.23	5.36	8.46	16.88	10.86	16.25	11.89	8.06
F/M	6.421	13.866	8.769	4.658	6.743	4.859	6.472	9.532
F/FM	.865	.933	.898	.823	.871	.829	.866	.905

1 SAMPLE 77-65-529 CLOUDY GRAIN CENTRAL
2 ANOTHER SPOT CENTRAL
3 INT SPOT
4 AT EDGE
5 ANOTHER GRAIN CENTRAL
6 AT EDGE
7 ANOTHER GRAIN CENTRAL
8 INT SPOT

SUPER RECAL — GARNET SAMPLES

	9	10	11	12	13	14	15	16
SIO2	38.06	37.65	37.35	37.27	36.77	37.96	37.52	37.84
A2O3	21.71	22.09	20.93	21.02	21.09	21.86	21.40	21.80
TIO2	.07	.03	.18	.18	.12	.04	.12	.18
FEO	27.46	27.18	18.35	18.41	20.23	27.39	23.64	27.30
MGO	4.20	4.30	.98	1.13	1.38	4.25	2.80	4.05
MNO	7.86	7.96	15.42	15.65	13.35	7.93	10.92	13.89
CAO	1.81	1.71	6.68	6.77	6.28	1.87	4.28	6.43
SUM	101.17	100.92	99.89	100.43	99.22	101.30	100.68	111.48
SI	5.992 *	5.940 *	6.016 *	5.980 *	5.962 *	5.970 *	5.970 *	5.883 *
AL	.008 6.000	.060 6.000	0.000 6.016	.020 6.000	.038 6.000	.030 6.000	.030 6.000	.395 6.000
AL	4.020 *	4.047 *	3.973 *	3.955 *	3.991 *	4.022 *	3.982 *	3.411 *
TI	.008 *	.004 *	.022 *	.022 *	.015 *	.005 *	.014 *	.020 *
MG	.986 *	1.011 *	.235 *	.270 *	.334 *	.996 *	.664 *	.894 *
CA	.305 *	.289 *	1.153 *	1.164 *	1.091 *	.315 *	.730 *	1.020 *
MN	1.048 *	1.064 *	2.104 *	2.127 *	1.833 *	1.056 *	1.472 *	1.743 *
FE	3.616 9.983	3.586 10.001	2.472 9.958	2.470 10.008	2.748 10.007	3.603 9.997	3.146 10.008	3.362 10.470
O	24.000 *	24.000 *	24.000 *	24.000 *	24.000 *	24.000 *	24.000 *	24.000 *
GROS	5.13	4.86	19.37	19.30	18.18	5.28	12.15	14.50
SPES	17.60	17.88	35.28	35.26	30.55	17.69	24.49	24.76
ALM	60.72	60.27	41.45	40.96	45.71	60.34	52.32	48.05
PYRP	16.55	16.99	3.95	4.48	5.56	16.69	11.04	12.70
F/M	4.732	4.598	19.447	17.011	13.722	4.676	6.955	5.735
F/FM	.826	.821	.951	.944	.932	.824	.874	.852

9 AT EDGE
10 OTHER AT EDGE
11 V LARGE GRAIN CENTRAL
12 ANOTHER SPOT CENTRAL
13 INT SPOT
14 AT EDGE
15 AVERAGE
16 AVERAGE PLUS SIGMA

SUPER RECAL GARNET SAMPLES

	1	2	3	4	5	6	7	8
SIO2	37.27	36.94	37.37	37.19	37.35	36.73	37.04	36.67
A2O3	21.31	20.77	20.63	21.07	21.39	20.48	20.82	21.51
TIO2	.12	.17	.26	.19	.11	.30	.16	.14
FEO	23.36	24.21	21.52	20.72	23.87	16.03	18.69	23.13
MGO	2.99	2.79	2.26	1.66	2.89	.75	1.22	2.78
MNO	10.67	11.81	12.45	14.38	11.90	17.04	15.62	12.37
CAO	3.02	2.94	5.31	5.49	2.86	7.90	6.32	3.46
SUM	98.74	99.63	99.80	100.70	100.37	99.23	99.87	99.96

SI	6.017	*		5.973	*		6.011	*		5.959	*		5.972	*		5.975	*		5.983	*		5.888	*	
AL	0.000	6.017		.027	6.000		0.000	6.011		.041	6.000		.028	6.000		.025	6.000		.017	6.000		.112	6.000	
AL	4.054	*		3.931	*		3.910	*		3.937	*		4.002	*		3.900	*		3.946	*		3.969	*	
TI	.015	*		.021	*		.031	*		.023	*		.013	*		.037	*		.019	*		.017	*	
MG	.719	*		.672	*		.542	*		.396	*		.689	*		.182	*		.294	*		.667	*	
CA	.522	*		.509	*		.915	*		.942	*		.490	*		1.377	*		1.094	*		.597	*	
MN	1.459	*		1.618	*		1.696	*		1.952	*		1.612	*		2.348	*		2.137	*		1.687	*	
FE	3.154	9.923		3.274	10.025		2.895	9.990		2.776	10.027		3.192	9.998		2.181	10.024		2.525	10.014		3.115	10.052	
O	24.000	*		24.000	*		24.000	*		24.000	*		24.000	*		24.000	*		24.000	*		24.000	*	
GROS		8.92			8.39			15.13			15.53			8.19			22.62			18.08			9.84		
SPES		24.92			26.63			28.05			32.17			26.94			38.57			35.33			27.81		
ALM		53.87			53.91			47.86			45.76			53.36			35.82			41.74			51.35		
PYRP		12.29			11.07			8.96			6.53			11.51			2.99			4.86			11.00		
F/M		6.411			7.274			8.473			11.926			6.974			24.903			15.871			7.197		
F/FM		.865			.879			.894			.923			.875			.961			.941			.878		

1 SAMPLE 77-65-711 VEINED GARNET
2 VERY DARK CENTRAL AREA
3 ANOTHER SPOT
4 CENTRAL AGAIN
5 EDGE
6 WIDE AREA OF VEINLET
7 INT SPOT ON THIS GRAIN
8 OUTER EDGE

SUPER RECAL GARNET SAMPLES

	9	10	11	12	13	14	15	16
SIO2	36.55	36.79	36.66	37.21	37.38	37.00	37.31	36.70
A2O3	20.64	20.57	20.48	20.50	20.90	20.85	21.20	20.50
TIO2	.23	.21	.21	.21	.13	.19	.24	.13
FEO	16.68	16.41	15.98	17.89	22.76	20.10	23.21	16.98
MGO	1.01	1.07	.98	1.27	2.68	1.87	2.71	1.04
MNO	16.14	16.60	17.34	15.82	12.64	14.21	16.44	11.99
CAO	7.55	7.57	7.86	6.66	3.21	5.40	7.37	3.42
SUM	98.80	99.22	99.51	99.56	99.70	99.62	108.48	90.77

SI	5.961	*		5.976	*		5.954	*		6.019	*		6.018	*		5.977	*		5.676	*		6.318	*	
AL	.039	6.000		.024	6.000		.046	6.000		0.000	6.019		0.000	6.018		.023	6.000		.324	6.000		0.000	6.318	
AL	3.928	*		3.913	*		3.873	*		3.907	*		3.965	*		3.946	*		3.477	*		-.159	*	
TI	.028	*		.026	*		.025	*		.026	*		.015	*		.023	*		.028	*		.017	*	
MG	.246	*		.259	*		.237	*		.306	*		.643	*		.451	*		.614	*		.267	*	
CA	1.319	*		1.317	*		1.368	*		1.154	*		.554	*		.934	*		1.202	*		.631	*	
MN	2.230	*		2.284	*		2.385	*		2.167	*		1.724	*		1.945	*		2.119	*		1.748	*	
FE	2.275	10.025		2.229	10.028		2.170	10.059		2.420	9.981		3.084	9.965		2.715	10.013		2.954	10.393		2.444	9.266	
O	24.000	*		24.000	*		24.000	*		24.000	*		24.000	*		24.000	*		24.000	*		24.000	*	
GROS		21.74			21.63			22.20			19.08			9.25			15.45			17.45			12.39		
SPES		36.73			37.59			38.72			35.84			28.80			32.17			30.76			34.34		
ALM		37.48			36.61			35.23			40.01			51.20			44.91			42.88			48.03		
PYRP		4.05			4.25			3.85			5.06			10.75			7.46			8.91			5.24		
F/M		18.347			17.421			19.204			14.982			7.445			10.332			8.264			15.717		
F/FM		.948			.946			.951			.937			.882			.912			.892			.940		

9 CENTRE OF ANOTHER GRAIN
10 ANOTHER SPOT CENTRAL
11 ANOTHER CENTRAL
12 INT SPOT
13 EDGE
14 AVERAGE
15 AVERAGE PLUS SIGMA
16 AVERAGE MINUS SIGMA

SUPER RECAL

GARNET SAMPLES

	1	2	3	4	5	6	7	8
SIO2	37.21	37.20	36.90	37.79	37.67	37.39	37.16	37.33
A2O3	20.41	21.21	20.94	21.11	20.72	21.21	20.73	20.90
TIO2	.29	.07	.05	.07	.27	.02	.24	.14
FEO	25.19	27.57	28.09	27.75	24.66	28.25	22.54	26.31
MGO	3.11	3.82	3.52	3.73	3.05	3.64	2.69	3.37
MNO	9.47	8.39	7.82	7.84	10.53	8.00	12.51	9.22
CAO	3.84	1.09	1.16	1.39	3.40	1.14	3.66	2.24
SUM	99.52	99.35	98.48	99.68	100.30	99.65	99.63	99.52

SI	6.002	*	5.991	*	6.004	*	6.050	*	6.023	*	6.008	*	5.994	*	6.010	*
AL	0.000	6.002	.009	6.000	0.000	6.004	0.000	6.050	0.000	6.023	0.000	6.008	.006	6.000	0.000	6.010
AL	3.880	*	4.015	*	4.015	*	3.983	*	3.904	*	4.016	*	3.934	*	3.966	*
TI	.035	*	.008	*	.006	*	.008	*	.032	*	.002	*	.029	*	.017	*
MG	.748	*	.917	*	.854	*	.896	*	.727	*	.872	*	.647	*	.808	*
CA	.664	*	.188	*	.202	*	.238	*	.582	*	.196	*	.632	*	.386	*
MN	1.294	*	1.144	*	1.078	*	1.063	*	1.426	*	1.069	*	1.709	*	1.256	*
FE	3.398	10.018	3.713	9.986	3.822	9.977	3.715	9.898	3.297	9.968	3.796	9.971	3.054	10.005	3.542	9.977
O	24.000	*	24.000	*	24.000	*	24.000	*	24.000	*	24.000	*	24.000	*	24.000	*
	GROS	10.87		3.15		3.40		4.04		9.65		3.30		10.47		6.45
	SPES	21.20		19.19		18.10		18.00		23.64		18.29		28.29		20.38
	ALM	55.68		62.27		64.18		62.90		54.66		63.77		50.54		59.10
	PYRP	12.25		15.38		14.33		15.07		12.05		14.64		10.70		13.48
	F/M	6.275		5.298		5.740		5.369		6.498		5.603		7.365		5.943
	F/FM	.863		.841		.852		.843		.867		.849		.880		.856

1 SAMPLE 128 M
2 ANOTHER CENTRAL
3
4
5
6 EDGE OF THIS GRAIN
7 LARGE CENTRAL
8 AVERAGE

SUPER RECAL — GARNET SAMPLES

	1	2	3	4	5	6	7	8
SIO2	36.89	37.45	37.48	37.35	37.16	37.37	37.70	37.40
A2O3	19.48	19.90	19.87	19.91	20.31	19.55	19.89	20.29
TIO2	.23	.36	.23	.17	.22	.37	.35	.24
FEO	7.18	9.76	12.04	8.38	13.14	7.34	10.14	11.59
MGO	.17	.46	.68	.25	.96	.20	.52	.72
MNO	24.29	22.26	20.70	24.31	20.17	23.50	22.57	20.71
CAO	10.86	9.45	8.00	9.63	7.38	11.45	8.91	8.67
SUM	99.10	99.64	99.00	100.00	99.34	99.78	100.08	99.62

SI	6.021	*	6.054	*	6.093	*	6.038	*	6.027	*	6.041	*	6.072	*	6.039	*
AL	0.000	6.021	0.000	6.054	0.000	6.093	0.000	6.038	0.000	6.027	0.000	6.041	0.000	6.072	0.000	6.039
AL	3.747	*	3.791	*	3.807	*	3.793	*	3.882	*	3.724	*	3.775	*	3.861	*
TI	.028	*	.044	*	.028	*	.021	*	.027	*	.045	*	.042	*	.029	*
MG	.041	*	.111	*	.165	*	.060	*	.232	*	.048	*	.125	*	.173	*
CA	1.899	*	1.637	*	1.393	*	1.668	*	1.282	*	1.983	*	1.538	*	1.500	*
MN	3.358	*	3.048	*	2.850	*	3.329	*	2.771	*	3.217	*	3.079	*	2.832	*
FE	.980	10.054	1.320	9.950	1.637	9.880	1.133	10.004	1.782	9.976	.992	10.010	1.366	9.924	1.565	9.960
O	24.000	*	24.000	*	24.000	*	24.000	*	24.000	*	24.000	*	24.000	*	24.000	*
GROS	30.25		26.77		23.05		26.95		21.14		31.77		25.18		24.71	
SPES	53.48		49.84		47.15		53.78		45.67		51.55		50.42		46.66	
ALM	15.61		21.58		27.08		18.30		29.37		15.90		22.36		25.78	
PYRP	.66		1.81		2.73		.97		3.82		.77		2.04		2.85	
F/M	104.892		39.404		27.233		74.065		19.619		87.363		35.606		25.377	
F/FM	.991		.975		.965		.987		.952		.989		.973		.962	

1 SAMPLE P 152
2 INT
3 EDGE
4 SMALLER GRAIN CENTRAL
5 EDGE
6 V LARGE GRAIN CENTRAL
7 ANOTHER LARGE CENTRAL
8 EDGE

SUPER RECAL — GARNET SAMPLES

	9	10	11	12	13	14	15	16
SIO2	36.87	37.55	37.45	37.25	37.52	38.01	38.06	37.88
A2O3	19.93	19.42	19.95	19.44	19.97	19.87	19.81	20.53
TIO2	.34	.29	.48	.43	.25	.29	.36	.16
FEO	6.89	7.64	7.35	7.75	7.89	7.82	8.70	12.85
MGO	.18	.18	.25	.25	.23	.23	.34	.87
MNO	24.23	23.66	23.89	23.09	23.75	23.77	22.77	20.94
CAO	11.05	10.78	10.88	11.48	10.55	10.22	10.02	7.12
SUM	99.49	99.52	100.25	99.69	100.16	100.21	100.06	100.35

SI	5.984	*	6.084	*	6.020	*	6.031	*	6.040	*	6.100	*	6.110	*	6.073	*
AL	.016	6.000	0.000	6.084	0.000	6.020	0.000	6.031	0.000	6.040	0.000	6.100	0.000	6.110	0.000	6.073
AL	3.795	*	3.708	*	3.779	*	3.709	*	3.788	*	3.757	*	3.748	*	3.878	*
TI	.041	*	.035	*	.058	*	.052	*	.030	*	.035	*	.043	*	.019	*
MG	.044	*	.043	*	.060	*	.060	*	.055	*	.059	*	.081	*	.208	*
CA	1.921	*	1.871	*	1.874	*	1.991	*	1.820	*	1.757	*	1.724	*	1.223	*
MN	3.331	*	3.247	*	3.253	*	3.167	*	3.238	*	3.231	*	3.096	*	2.843	*
FE	.935	10.067	1.035	9.940	.988	10.011	1.049	10.029	1.062	9.994	1.049	9.885	1.166	9.860	1.723	9.894
O	24.000	*	24.000	*	24.000	*	24.000	*	24.000	*	24.000	*	24.000	*	24.000	*
GROS	30.84		30.20		30.35		31.77		29.47		28.84		28.40		20.39	
SPES	53.46		52.40		52.68		50.52		52.44		53.03		51.02		47.41	
ALM	15.01		16.70		16.00		16.74		17.20		17.23		19.25		28.73	
PYRP	.70		.70		.97		.96		.89		.90		1.34		3.47	
F/M	97.971		98.510		70.799		69.878		77.927		77.805		52.414		21.965	
F/FM	.990		.990		.986		.986		.987		.987		.981		.956	

9 AT CONTACT WITH SULPH,CENTRE
10 ANOTHER CENTRAL
11 ANOTHER GRAIN CENTRAL
12 ANOTHER CENTRAL
13 ANOTHER GRAIN WITH SULPH,CENTRE
14 ANOTHER CENTRAL SAME GRAIN
15 INT
16 RIM

SUPER RECAL — GARNET SAMPLES

	17	18	19	20	21	22	23	24
SIO2	37.15	37.79	37.17	37.99	37.55	37.43	38.03	37.50
A2O3	19.71	20.44	20.16	20.42	20.04	20.63	19.89	19.97
TIO2	.15	.12	.30	.20	.27	.21	.29	.27
FEO	7.14	10.90	7.57	13.19	7.52	13.08	8.87	9.34
MGO	.23	.60	.36	.95	.27	.94	.47	.45
MNO	24.51	22.63	23.87	20.64	23.49	21.06	23.32	22.78
CAO	10.67	8.20	10.14	7.13	10.46	6.92	9.94	9.56
SUM	99.56	100.68	99.57	100.52	99.60	100.27	100.51	99.87

SI	6.029	*		6.052	*		6.012	*		6.080	*		6.059	*		6.019	*		6.088	*		6.051	*	
AL	0.000	6.029		0.000	6.052		0.000	6.012		0.000	6.080		0.000	6.059		0.000	6.019		0.000	6.088		0.000	6.051	
AL	3.769	*		3.957	*		3.842	*		3.851	*		3.810	*		3.909	*		3.752	*		3.798	*	
TI	.018	*		.014	*		.036	*		.024	*		.033	*		.025	*		.035	*		.033	*	
MG	.056	*		.143	*		.087	*		.227	*		.065	*		.225	*		.112	*		.108	*	
CA	1.855	*		1.407	*		1.757	*		1.223	*		1.308	*		1.192	*		1.709	*		1.653	*	
MN	3.369	*		3.070	*		3.270	*		2.798	*		3.210	*		2.868	*		3.121	*		3.113	*	
FE	.969	10.037		1.460	9.951		1.024	10.017		1.765	9.888		1.015	9.942		1.759	9.980		1.187	9.912		1.260	9.964	
O	24.000	*		24.000	*		24.000	*		24.000	*		24.000	*		24.000	*		24.000	*		24.000	*	
GROS		29.69			23.14			28.63			20.33			29.65			19.72			27.83			26.95		
SPES		53.91			50.49			53.28			46.53			52.64			47.45			50.95			50.75		
ALM		15.51			24.01			16.68			29.36			16.64			29.10			19.38			20.54		
PYOP		.89			2.36			1.41			3.77			1.06			3.73			1.83			1.76		
F/M		77.975			31.626			49.477			20.136			65.066			20.539			38.422			40.558		
F/FM		.987			.969			.980			.953			.985			.954			.975			.976		

17
18 EDGE
19 ANOTHER GRAIN CENTRAL
20 EDGE
21 CORE OF LARGEST GRAIN
22 EDGE
23 LAST TRY CENTRAL
24 AVERAGE

SUPER RECAL GARNET SAMPLES

	1	2	3	4	5	6	7	8
SIO2	38.20	37.17	38.06	38.48	38.23	37.61	38.12	38.38
A2O3	20.87	21.09	20.80	20.91	21.23	21.09	21.24	21.41
TIO2	.12	.10	.24	.19	.09	.11	.10	.11
FEO	29.83	30.38	30.45	29.62	30.43	29.45	29.95	30.33
MGO	2.73	2.84	2.95	2.78	2.91	2.93	2.90	2.86
MNO	4.01	3.96	3.71	3.39	3.71	4.18	4.20	3.70
CAO	3.78	3.67	3.64	4.89	3.92	3.91	3.82	4.21
SUM	99.54	99.21	99.85	100.26	100.52	99.28	100.33	101.00

SI	6.114	*	5.999	*	6.083	*	6.106	*	6.066	*	6.042	*	6.060	*	6.058	*
AL	0.000	6.114	.001	6.000	0.000	6.083	0.000	6.106	0.000	6.066	0.000	6.042	0.000	6.060	0.000	6.058
AL	3.936	*	4.010	*	3.917	*	3.910	*	3.969	*	3.992	*	3.979	*	3.982	*
TI	.014	*	.012	*	.029	*	.023	*	.011	*	.013	*	.012	*	.013	*
MG	.651	*	.683	*	.703	*	.558	*	.688	*	.702	*	.687	*	.673	*
CA	.648	*	.635	*	.623	*	.831	*	.666	*	.673	*	.651	*	.712	*
MN	.544	*	.541	*	.502	*	.456	*	.499	*	.569	*	.566	*	.495	*
FE	3.993	9.787	4.100	9.981	4.070	9.844	3.931	9.808	4.038	9.871	3.956	9.905	3.982	9.876	4.004	9.878
O	24.000	*	24.000	*	24.000	*	24.000	*	24.000	*	24.000	*	24.000	*	24.000	*
GROS		11.11		10.65		10.57		14.15		11.31		11.41		11.06		12.10
SPES		9.32		9.08		8.51		7.76		8.46		9.64		9.61		8.41
ALM		68.42		68.80		69.00		66.90		68.54		67.06		67.66		68.05
PYRP		11.16		11.46		11.91		11.19		11.68		11.89		11.68		11.44
F/M		6.965		6.794		6.506		6.671		6.592		6.450		6.618		6.685
F/FM		.874		.872		.867		.870		.868		.866		.869		.870

1 SAMPLE 78-66-131 CENTRE OF GRAIN
2 TOWARD EDGE
3 CLOSER TO EDGE
4 STILL CLOSER
5 CLOSER TO EDGE
6 OUTER EDGE
7 ANOTHER SPOT ON OUTER EDGE
8 SMALL GRAIN CENTRE

SUPER RECAL GARNET SAMPLES

	9	10	11	12	13	14	15
SIO2	37.64	38.01	37.94	37.76	37.97	38.32	37.61
A2O3	21.02	21.54	21.11	21.22	21.13	21.34	20.92
TIO2	.07	.07	.12	.14	.12	.17	.07
FEO	29.98	29.64	30.32	30.12	30.04	30.38	29.71
MGO	2.59	2.76	2.81	2.95	2.83	2.94	2.73
MNO	4.26	4.54	4.04	3.80	3.96	4.26	3.66
CAO	3.65	3.78	3.77	3.73	3.90	4.23	3.56
SUM	99.21	100.34	100.11	99.72	99.95	101.63	98.27

SI	6.063	*	6.041	*	6.055	*	6.039	*	6.061	*	6.029	*	6.093	*		
AL	0.000	6.063	0.000	6.041	0.000	6.055	0.000	6.039	0.000	6.061	0.000	6.029	0.000	6.093		
AL	3.990	*	4.034	*	3.970	*	3.999	*	3.974	*	3.955	*	3.993	*		
TI	.008	*	.008	*	.014	*	.017	*	.015	*	.020	*	.009	*		
MG	.622	*	.654	*	.668	*	.703	*	.674	*	.689	*	.660	*		
CA	.630	*	.644	*	.645	*	.639	*	.667	*	.713	*	.618	*		
MN	.581	*	.611	*	.546	*	.515	*	.535	*	.568	*	.562	*		
FE	4.038	9.869	3.940	9.891	4.046	9.890	4.029	9.902	4.010	9.875	3.997	9.942	4.024	9.807		
O	24.000	*	24.000	*	24.000	*	24.000	*	24.000	*	24.000	*	24.000	*		
GROS		10.73		11.01		10.92		10.86		11.32		11.96		10.65		
SPES		9.90		10.45		9.25		8.75		9.09		9.51		8.65		
ALM		68.78		67.36		68.52		68.45		68.13		66.99		69.34		
PYRP		10.59		11.18		11.32		11.95		11.46		11.54		11.36		
F/M		7.429		6.960		6.871		6.461		6.741		6.623		6.863		
F/FM		.891		.874		.873		.866		.871		.869		.873		

9 AT EDGE
10 ANOTHER VERY LARGE GRAIN AT EDGE
11 ANOTHER AT EDGE
12 INTERIOR OF GRAIN
13 AVERAGE
14 AVERAGE PLUS SIGMA
15 AVERAGE MINUS SIGMA

SUPER RECAL GARNET SAMPLES

	1	2	3	4	5	6	7	8
SIO2	37.68	36.90	37.45	37.50	37.58	36.79	37.13	37.25
A2O3	21.05	20.55	20.55	20.93	20.83	20.67	20.66	20.95
TIO2	.13	.19	.13	.05	.12	.18	.18	.08
FEO	23.56	21.75	25.67	28.55	21.90	22.60	22.39	28.06
MGO	1.77	1.66	2.11	2.65	1.59	1.58	1.48	2.63
MNO	10.81	13.11	7.91	5.60	13.17	12.79	12.14	5.79
CAO	5.42	5.05	5.18	3.73	4.58	4.61	5.32	3.78
SUM	100.42	99.21	99.00	99.21	99.77	99.22	99.30	98.54

SI	6.026	*	6.000	*	6.061	*	6.042	*	6.056	*	5.989	*	6.022	*	6.040	*
AL	0.000	6.026	.000	6.000	0.000	6.061	0.000	6.042	0.000	6.056	.011	6.000	0.000	6.022	0.000	6.040
AL	3.967	*	3.937	*	3.919	*	3.974	*	3.956	*	3.954	*	3.949	*	4.003	*
TI	.016	*	.023	*	.016	*	.006	*	.015	*	.022	*	.022	*	.010	*
MG	.422	*	.402	*	.509	*	.684	*	.382	*	.383	*	.358	*	.636	*
CA	.929	*	.880	*	.898	*	.644	*	.791	*	.804	*	.924	*	.657	*
MN	1.464	*	1.806	*	1.084	*	.764	*	1.798	*	1.764	*	1.668	*	.795	*
FE	3.151	9.948	2.958	10.006	3.474	9.901	3.847	9.920	2.952	9.893	3.077	10.004	3.037	9.957	3.805	9.906
O	24.000	*	24.000	*	24.000	*	24.000	*	24.000	*	24.000	*	24.000	*	24.000	*
GPOS		15.57		14.55		15.06		10.84		13.35		13.34		15.44		11.14
SPES		24.54		29.87		18.18		12.87		30.36		29.26		27.86		13.50
ALM		52.82		48.92		58.24		64.77		49.84		51.04		50.73		64.37
PYRP		7.07		6.66		8.53		11.52		6.45		6.36		5.98		10.79
F/M		10.939		11.839		8.956		6.737		12.435		12.626		13.149		7.237
F/FM		.916		.922		.900		.871		.926		.927		.929		.879

1 SAMPLE 78-66-331.5 CENTRAL
2 NOTHER SPOT CENTRAL
3 INTERMEDIATE SPOT
4 AT EDGE

5 ANOTHER GRAIN CENTRAL
6 ANOTHER SPOT CENTRAL
7 INTERMEDIATE SPOT
8 AT EDGE

SUPER RECAL GARNET SAMPLES

	9	10	11	12
SIO2	37.27	37.28	37.57	37.00
A2O3	20.60	20.75	20.93	20.58
TIO2	.12	.13	.18	.09
FEO	22.11	24.07	26.60	21.53
MGO	1.64	1.92	2.39	1.45
MNO	11.64	10.33	13.23	7.42
CAO	5.78	4.83	5.50	4.15
SUM	99.16	99.31	106.40	92.23

SI	6.038	*	6.031	*	5.805	*	6.279	*
AL	0.000	6.038	0.000	6.031	.195	6.000	0.000	6.279
AL	3.933	*	3.956	*	3.616	*	4.115	*
TI	.015	*	.016	*	.020	*	.011	*
MG	.396	*	.464	*	.551	*	.368	*
CA	1.003	*	.837	*	.911	*	.755	*
MN	1.597	*	1.415	*	1.732	*	1.067	*
FE	2.996	9.940	3.295	9.943	3.437	10.267	3.056	9.372
O	24.000	*	24.000	*	24.000	*	24.000	*
GPOS		16.74		14.01		13.74		14.40
SPES		26.66		23.70		26.12		20.34
ALM		49.99		54.52		51.83		58.25
PYRP		6.61		7.77		8.31		7.01
F/M		11.598		10.072		9.376		11.219
F/FM		.921		.910		.904		.918

9 ANOTHER GRAIN CENTRAL
10 AVERAGE

11 AVERAGE PLUS SIGMA
12 AVERAGE MINUS SIGMA

SUPER RECAL — GARNET SAMPLES

	1	2	3	4	5	6	7	8
SIO2	37.27	37.47	37.51	37.36	37.19	36.60	37.34	37.74
A203	21.17	21.18	21.45	21.46	21.12	20.55	21.38	21.37
TIO2	.13	.11	.08	.20	.20	.15	.12	.14
FEO	25.43	23.87	27.95	23.41	23.90	24.34	27.01	24.69
MGO	3.29	2.67	4.08	2.48	2.98	3.24	4.06	3.21
MNO	8.60	10.10	5.93	10.69	9.50	8.47	6.14	8.45
CAO	3.97	4.88	3.36	5.33	4.41	4.89	3.29	4.76
SUM	99.86	100.28	100.36	100.63	99.30	98.54	99.34	100.36
SI	5.966 *	5.984 *	5.956 *	5.950 *	5.981 *	5.940 *	5.973 *	5.992 *
AL	.032 6.000	.016 6.000	.044 6.000	.050 6.000	.019 6.000	.060 6.000	.027 6.000	.008 6.000
AL	3.967 *	3.970 *	3.970 *	3.978 *	3.984 *	3.927 *	4.003 *	3.990 *
TI	.016 *	.013 *	.010 *	.024 *	.024 *	.018 *	.014 *	.017 *
MG	.785 *	.636 *	.966 *	.589 *	.714 *	.784 *	.968 *	.760 *
CA	.681 *	.835 *	.972 *	.858 *	.760 *	.850 *	.564 *	.810 *
MN	1.166 *	1.366 *	.798 *	1.442 *	1.294 *	1.164 *	.832 *	1.136 *
FE	3.405 10.017	3.188 10.008	3.712 10.025	3.118 10.010	3.215 9.991	3.303 10.046	3.613 9.995	3.278 9.990
O	24.000 *	24.000 *	24.000 *	24.000 *	24.000 *	24.000 *	24.000 *	24.000 *
GROS	11.29	13.86	9.45	14.29	12.70	13.93	9.43	13.53
SPES	19.32	22.68	13.19	24.01	21.63	19.08	13.92	18.99
ALM	56.40	52.91	61.38	51.91	53.73	54.14	60.45	54.78
PYRP	13.00	10.55	15.97	9.80	11.94	12.84	16.20	12.69
F/M	5.822	7.166	4.670	7.746	6.311	5.701	4.592	5.811
F/FM	.853	.878	.824	.886	.863	.851	.821	.853

1 SAMPLE 78-66-417 CENTRAL
2 ANOTHER CENTRAL
3 AT EDGE
4 ANOTHER LARGER GRAIN CENTRAL
5 ANOTHER SPOT CENTRAL
6 INT SPOT
7 AT EDGE
8 ANOTHER GRAIN CENTRAL

SUPER RECAL — GARNET SAMPLES

	9	10	11	12
SIO2	37.23	37.30	37.60	37.01
A203	21.04	21.22	21.42	21.03
TIO2	.19	.15	.19	.11
FEO	23.60	24.91	26.42	23.41
MGO	2.56	3.17	3.73	2.62
MNO	10.58	8.72	10.37	7.07
CAO	4.71	4.37	5.00	3.74
SUM	99.91	99.84	104.71	94.97
SI	5.976 *	5.969 *	5.816 *	6.133 *
AL	.024 6.000	.031 6.000	.184 6.000	0.000 6.133
AL	3.956 *	3.971 *	3.721 *	4.107 *
TI	.023 *	.018 *	.022 *	.013 *
MG	.613 *	.757 *	.860 *	.647 *
CA	.810 *	.749 *	.828 *	.663 *
MN	1.439 *	1.182 *	1.358 *	.992 *
FE	3.168 10.009	3.334 10.010	3.418 10.207	3.244 9.666
O	24.000 *	24.000 *	24.000 *	24.000 *
GROS	13.44	12.43	12.81	11.96
SPES	23.86	19.62	21.01	17.89
ALM	52.55	55.37	52.87	58.49
PYRP	10.16	12.57	13.30	11.66
F/M	7.621	5.964	5.553	6.548
F/FM	.883	.856	.847	.868

9 ANOTHER GRAIN CENTRAL
10 AVERAGE
11 AVERAGE PLUS SIGMA
12 AVERAGE MINUS SIGMA

SUPER RECAL — GARNET SAMPLES

	1	2	3	4	5	6	7	8
SIO2	37.61	37.50	37.48	37.10	37.61	37.54	37.55	37.73
A203	21.37	21.57	21.48	21.16	21.55	21.24	21.75	21.33
TIO2	.04	.07	.11	.14	.11	.11	.05	.04
FEO	25.94	26.33	24.80	25.65	26.04	24.94	25.69	26.01
MGO	1.23	1.34	1.17	1.38	1.35	1.25	.88	1.19
MNO	7.13	6.88	6.79	7.51	7.33	7.45	7.05	6.54
CAO	7.66	7.23	8.26	6.77	7.14	7.03	7.07	7.74
SUM	100.98	100.92	100.09	99.71	101.13	99.56	100.04	100.58
SI	5.984 *	5.967 *	5.989 *	5.978 *	5.972 *	6.032 *	6.009 *	6.013 *
AL	.016 6.000	.033 6.000	.011 6.000	.022 6.000	.028 6.000	0.000 6.032	0.000 6.009	0.000 6.013
AL	3.991 *	4.011 *	4.034 *	3.996 *	4.005 *	4.022 *	4.101 *	4.006 *
TI	.005 *	.008 *	.013 *	.017 *	.013 *	.013 *	.006 *	.005 *
MG	.292 *	.318 *	.279 *	.331 *	.320 *	.299 *	.210 *	.283 *
CA	1.306 *	1.233 *	1.414 *	1.169 *	1.215 *	1.210 *	1.212 *	1.322 *
MN	.961 *	.927 *	.919 *	1.025 *	.986 *	1.014 *	.956 *	.883 *
FE	3.452 10.006	3.504 10.001	3.314 9.973	3.456 9.994	3.458 9.996	3.351 9.910	3.436 9.923	3.467 9.964
O	24.000 *	24.000 *	24.000 *	24.000 *	24.000 *	24.000 *	24.000 *	24.000 *
GROS	21.73	20.61	23.86	19.54	20.32	20.60	20.84	22.20
SPES	15.99	15.50	15.51	17.14	16.49	17.26	16.43	14.83
ALM	57.43	58.58	55.93	57.78	57.84	57.05	59.12	58.23
PYRP	4.85	5.31	4.70	5.54	5.34	5.10	3.61	4.75
F/M	15.127	13.942	15.191	13.521	13.908	14.581	20.932	15.387
F/FM	.938	.933	.938	.931	.933	.936	.954	.939

1 SAMPLE 78-67-397 CENTRAL
2 AT EDGE
3 ANOTHER SPOT
4 AT EDGE
5 ANOTHER POIK CENTRAL
6 AGAIN
7 AT EDGE
8 ANOTHER CENTRAL

SUPER RECAL — GARNET SAMPLES

	9	10	11	12
SIO2	37.41	37.50	37.67	37.34
A203	21.56	21.45	21.62	21.27
TIO2	.10	.09	.12	.05
FEO	26.05	25.72	26.21	25.22
MGO	1.14	1.21	1.36	1.07
MNO	6.81	7.05	7.37	6.74
CAO	6.78	7.30	7.76	6.83
SUM	99.85	100.32	102.10	98.53
SI	6.001 *	5.994 *	5.938 *	6.051 *
AL	0.000 6.001	.006 6.000	.062 6.000	0.000 6.051
AL	4.076 *	4.033 *	3.954 *	4.062 *
TI	.012 *	.010 *	.014 *	.006 *
MG	.273 *	.289 *	.319 *	.259 *
CA	1.165 *	1.250 *	1.311 *	1.186 *
MN	.928 *	.955 *	.983 *	.926 *
FE	3.495 9.946	3.437 9.974	3.455 10.037	3.419 9.858
O	24.000 *	24.000 *	24.000 *	24.000 *
GROS	19.89	21.07	21.61	20.49
SPES	15.80	16.10	16.21	15.99
ALM	59.66	57.95	56.93	59.05
PYRP	4.65	4.88	5.25	4.47
F/M	16.216	15.182	13.920	16.789
F/FM	.942	.938	.933	.944

9 AT EDGE
10 AVERAGE
11 AVERAGE PLUS SIGMA
12 AVERAGE MINUS SIGMA

SUPER RECAL GARNET SAMPLES

	1	2	3	4	5	6	7	8
SIO2	37.23	36.81	37.11	36.88	37.50	37.52	37.30	37.17
A2O3	21.09	20.55	20.71	21.16	20.91	20.94	21.23	20.82
TIO2	.25	.23	.30	.05	.13	.20	.19	.27
FEO	23.20	22.32	22.63	29.13	24.34	24.95	26.55	23.55
MGO	1.70	1.50	1.64	2.93	1.99	1.91	2.59	1.87
MNO	12.14	12.72	12.16	4.94	10.38	9.19	5.59	10.98
CAO	5.46	5.74	5.23	4.27	5.36	5.18	4.17	5.37
SUM	101.07	99.87	99.78	99.36	100.61	99.89	99.12	100.03

SI	5.949	*		5.964	*		5.995	*		5.951	*		5.999	*		6.027	*		6.010	*		5.983	*	
AL	.051	6.000		.036	6.000		.005	6.000		.049	6.000		.001	6.000		0.000	6.027		0.000	6.010		.017	6.000	
AL	3.920	*		3.888	*		3.937	*		3.974	*		3.941	*		3.964	*		4.031	*		3.933	*	
TI	.030	*		.028	*		.036	*		.006	*		.016	*		.024	*		.023	*		.033	*	
MG	.405	*		.362	*		.395	*		.705	*		.475	*		.457	*		.622	*		.449	*	
CA	.935	*		.996	*		.905	*		.738	*		.919	*		.891	*		.720	*		.926	*	
MN	1.643	*		1.746	*		1.664	*		.675	*		1.406	*		1.250	*		.763	*		1.497	*	
FE	3.100	10.033		3.024	10.044		3.057	9.995		3.931	10.029		3.256	10.012		3.352	9.938		3.780	9.939		3.170	10.007	
O	24.000	*		24.000	*		24.000	*		24.000	*		24.000	*		24.000	*		24.000	*		24.000	*	
GROS		15.37			16.26			15.03			12.20			15.17			14.98			12.23			15.33		
SPES		27.01			28.48			27.63			11.16			23.22			21.01			12.96			24.78		
ALM		50.97			49.35			50.77			64.98			53.77			56.32			64.23			52.47		
PYRP		6.66			5.91			6.56			11.65			7.84			7.68			10.57			7.43		
F/M		11.715			13.168			11.956			6.536			9.827			10.063			7.303			10.403		
F/FM		.921			.929			.923			.867			.908			.910			.880			.912		

1 SAMPLE 78-67-431.5
2 ANOTHER SPOT CENTRAL
3 INTERMEDIATE SPOT
4 AT EDGE OF GRAIN
5 ANOTHER GRAIN CENTRAL
6 INTERMEDIATE SPOT
7 EDGE
8 ANOTHER GRAIN CENTRAL

SUPER RECAL GARNET SAMPLES

	9	10	11	12
SIO2	36.88	37.16	37.40	36.91
A2O3	20.82	20.91	21.12	20.71
TIO2	.17	.20	.27	.13
FEO	26.00	24.91	27.17	22.65
MGO	2.38	2.06	2.51	1.61
MNO	7.64	9.53	12.26	6.80
CAO	4.71	5.05	5.57	4.54
SUM	98.60	99.81	106.29	93.34

SI	5.995	*		5.986	*		5.778	*		6.213	*	
AL	.005	6.000		.014	6.000		.222	6.000		0.000	6.213	
AL	3.963	*		3.956	*		3.623	*		4.107	*	
TI	.021	*		.024	*		.031	*		.016	*	
MG	.577	*		.494	*		.577	*		.403	*	
CA	.820	*		.872	*		.922	*		.819	*	
MN	1.052	*		1.300	*		1.604	*		.969	*	
FE	3.535	9.988		3.356	10.003		3.509	10.266		3.188	9.503	
O	24.000	*		24.000	*		24.000	*		24.000	*	
GROS		13.71			14.49			13.94			15.22	
SPES		17.58			21.59			24.25			18.02	
ALM		59.07			55.73			53.18			59.27	
PYRP		9.64			8.20			8.73			7.49	
F/M		7.954			9.427			8.858			10.315	
F/FM		.888			.904			.899			.912	

9 INT SPOT
10 AVERAGE
11 AVERAGE PLUS SIGMA
12 AVERAGE MINUS SIGMA

SUPER RECAL GARNET SAMPLES

	1	2	3	4	5	6	7	8
SIO2	37.53	37.56	37.70	37.28	37.24	37.28	37.05	37.54
A2O3	21.02	20.91	21.00	21.25	21.69	21.54	21.35	21.48
TIO2	.07	.16	.15	.09	.07	.07	.07	.08
FEO	27.71	28.36	28.43	27.05	27.73	27.57	29.85	28.27
MGO	2.89	2.92	3.19	3.30	3.66	3.56	3.61	3.79
MNO	6.22	5.91	5.44	5.90	5.92	5.54	3.39	5.55
CAO	3.97	4.38	4.26	4.84	3.89	4.31	3.93	4.05
SUM	99.41	100.20	100.17	99.71	100.20	99.72	100.29	100.76
SI	6.032 *	6.006 *	6.014 *	5.965 *	5.928 *	5.934 *	6.036 *	5.946 *
AL	0.000 6.032	0.000 6.006	0.000 6.014	.035 6.000	.072 6.000	.066 6.000	0.000 6.036	.054 6.000
AL	3.981 *	3.940 *	3.947 *	3.972 *	3.997 *	3.999 *	3.986 *	3.956 *
TI	.008 *	.019 *	.018 *	.011 *	.008 *	.005 *	.008 *	.010 *
MG	.692 *	.696 *	.758 *	.787 *	.866 *	.848 *	.853 *	.895 *
CA	.684 *	.750 *	.728 *	.830 *	.663 *	.738 *	.667 *	.687 *
MN	.847 *	.800 *	.735 *	.800 *	.798 *	.750 *	.755 *	.745 *
FE	3.724 9.936	3.792 9.998	3.792 9.979	3.620 10.019	3.692 10.027	3.686 10.026	3.956 9.925	3.745 10.037
O	24.000 *	24.000 *	24.000 *	24.000 *	24.000 *	24.000 *	24.000 *	24.000 *
GROS	11.50	12.43	12.11	13.75	11.02	12.26	11.25	11.32
SPES	14.24	13.25	12.22	13.25	13.26	12.46	7.67	12.26
ALM	62.63	62.80	63.06	59.97	61.31	61.20	66.70	61.68
PYRP	11.64	11.52	12.61	13.04	14.42	14.08	14.36	14.74
F/M	6.603	6.599	5.970	5.615	5.170	5.230	5.173	5.017
F/FM	.868	.868	.857	.849	.838	.839	.838	.834

1 SAMPLE 78-68-192 CENTRAL
2 ANOTHER SPOT CENTRAL
3 INT SPOT
4 AT EDGE
5 OPPOSITE EDGE
6 JUST INSIDE RIM
7 ANOTHER GRAIN CENTRAL
8 AT EDGE

SUPER RECAL GARNET SAMPLES

	9	10	11	12	13	14
SIO2	37.77	37.31	37.51	37.51	37.78	37.25
A2O3	20.95	20.82	21.74	21.25	21.57	20.94
TIO2	.18	.23	.07	.11	.17	.05
FEO	28.43	28.42	28.38	28.20	28.88	27.52
MGO	2.68	2.56	3.46	3.24	3.64	2.84
MNO	5.98	6.08	5.58	5.59	6.33	5.86
CAO	4.29	4.46	4.05	4.22	4.49	3.95
SUM	100.28	99.88	100.79	100.13	102.86	97.40
SI	6.032 *	5.998 *	5.941 *	5.985 *	5.899 *	6.074 *
AL	0.000 6.032	.002 6.000	.059 6.000	.015 6.000	.101 6.000	0.000 6.074
AL	3.942 *	3.942 *	3.999 *	3.980 *	3.868 *	4.023 *
TI	.022 *	.028 *	.008 *	.013 *	.020 *	.006 *
MG	.638 *	.613 *	.817 *	.770 *	.847 *	.689 *
CA	.734 *	.768 *	.687 *	.721 *	.751 *	.690 *
MN	.809 *	.829 *	.749 *	.756 *	.837 *	.671 *
FE	3.797 9.942	3.821 10.000	3.759 10.019	3.762 10.002	3.772 10.095	3.752 9.832
O	24.000 *	24.000 *	24.000 *	24.000 *	24.000 *	24.000 *
GROS	12.28	12.74	11.43	12.01	12.10	11.90
SPES	13.53	13.73	12.45	12.57	13.48	11.56
ALM	63.52	63.36	62.53	62.61	60.77	64.66
PYRP	10.67	10.17	13.59	12.81	13.65	11.88
F/M	7.220	7.578	5.519	5.667	5.440	6.416
F/FM	.878	.883	.847	.854	.845	.866

9 V LARGE GRAIN CENTRAL
10 INT SPOT
11 AT EDGE
12 AVERAGE
13 AVERAGE PLUS SIGMA
14 AVERAGE MINUS SIGMA

SUPER RECAL — GARNET SAMPLES

	1	2	3	4	5	6	7	8
SIO2	38.16	38.46	37.11	37.79	37.97	38.15	37.50	37.74
A2O3	21.88	21.75	21.98	22.01	22.04	21.50	21.53	21.75
TIO2	.08	.13	.05	.09	.08	.08	.05	.06
FEO	29.41	29.74	29.58	30.00	29.56	29.68	29.66	29.88
MGO	5.55	5.78	5.96	6.04	5.95	6.24	6.17	5.27
MNO	2.27	1.54	1.27	1.35	1.20	1.28	1.15	2.06
CAO	2.90	3.10	2.95	3.27	3.14	3.08	2.98	3.51
SUM	100.25	100.50	98.90	100.55	99.94	100.01	99.04	100.29

SI	5.985	*	6.006	*	5.898	*	5.913	*	5.956	*	5.987	*	5.948	*	5.943	*
AL	.015	6.000	0.000	6.006	.102	6.000	.087	6.000	.044	6.000	.013	6.000	.052	6.000	.057	6.000
AL	4.029	*	4.002	*	4.014	*	3.972	*	4.030	*	3.962	*	3.972	*	3.979	*
TI	.009	*	.015	*	.006	*	.011	*	.009	*	.009	*	.008	*	.009	*
MG	1.297	*	1.345	*	1.412	*	1.409	*	1.391	*	1.459	*	1.459	*	1.237	*
CA	.487	*	.519	*	.502	*	.548	*	.528	*	.518	*	.506	*	.592	*
MN	.302	*	.204	*	.171	*	.179	*	.159	*	.170	*	.154	*	.275	*
FE	3.857	9.982	3.884	9.969	3.931	10.036	3.926	10.044	3.878	9.995	3.895	10.014	3.934	10.032	3.935	10.027
O	24.000	*	24.000	*	24.000	*	24.000	*	24.000	*	24.000	*	24.000	*	24.000	*
GROS		8.29		8.71		8.35		9.04		8.86		8.57		8.37		9.81
SPES		5.07		3.42		2.84		2.95		2.68		2.82		2.55		4.55
ALM		64.90		65.26		65.34		64.76		65.11		64.46		64.99		65.16
PYRP		21.83		22.60		23.47		23.24		23.36		24.15		24.09		20.48
F/M		3.206		3.038		2.906		2.914		2.902		2.785		2.803		3.403
F/FM		.762		.752		.744		.744		.744		.736		.737		.773

1 SAMPLE 76-47-393-455 LARGE, CENTRAL
2 ANOTHER SPOT CENTRAL
3 AT EDGE
4 ANOTHER LARGE GRAIN CENTRAL
5 ANOTHER CENTRAL
6 INTERMEDIATE SPOT
7 AT EDGE OF THIS GRAIN
8 ANOTHER EXTREMELY LARGE GAR CENTRAL

SUPER RECAL — GARNET SAMPLES

	9	10	11	12	13	14
SIO2	37.94	37.77	38.31	37.90	38.26	37.54
A2O3	21.92	21.68	21.96	21.82	22.00	21.64
TIO2	.11	.12	.05	.08	.11	.06
FEO	29.72	29.52	29.99	29.76	29.88	29.52
MGO	5.34	5.16	5.99	5.77	6.13	5.41
MNO	1.85	2.15	1.23	1.58	1.98	1.17
CAO	3.27	3.37	2.83	3.13	3.33	2.93
SUM	100.15	99.77	100.36	99.98	101.70	98.26

SI	5.964	*	5.969	*	5.986	*	5.960	*	5.926	*	5.994	*				
AL	.036	6.000	.031	6.000	.014	6.000	.040	6.000	.074	6.000	.006	6.000				
AL	4.024	*	4.006	*	4.029	*	4.002	*	3.941	*	4.065	*				
TI	.013	*	.014	*	.006	*	.010	*	.013	*	.007	*				
MG	1.251	*	1.215	*	1.395	*	1.352	*	1.415	*	1.287	*				
CA	.551	*	.571	*	.474	*	.527	*	.552	*	.501	*				
MN	.246	*	.208	*	.163	*	.210	*	.260	*	.159	*				
FE	3.907	9.991	3.901	9.996	3.919	9.985	3.906	10.007	3.871	10.051	3.942	9.961				
O	24.000	*	24.000	*	24.000	*	24.000	*	24.000	*	24.000	*				
GROS		9.25		9.55		7.96		8.79		9.06		8.50				
SPES		4.14		4.82		2.74		3.50		4.26		2.69				
ALM		65.61		65.29		65.86		65.16		63.48		66.93				
PYRP		21.01		20.34		23.44		22.55		23.20		21.86				
F/M		3.320		3.447		2.926		3.045		2.926		3.186				
F/FM		.769		.775		.745		.753		.745		.761				

9 ANOTHER CENTRAL
10 INTERMEDIATE SPOT
11 AT EDGE
12 AVERAGE
13 AVERAGE PLUS SIGMA
14 AVERAGE MINUS SIGMA

SUPER RECAL

GARNET SAMPLES

	1	2	3	4	5	6	7	8
SIO2	37.39	37.13	37.53	37.28	38.11	37.50	37.58	37.50
A2O3	21.43	21.06	21.27	21.63	21.37	21.69	21.49	21.42
TIO2	.12	.12	.16	.16	.11	.13	.15	.14
FEO	26.36	28.10	27.07	7.23	26.82	26.93	27.14	24.24
MGO	4.68	5.23	4.57	4.87	5.00	4.98	4.89	4.87
MNO	6.45	4.44	6.48	.54	5.32	5.53	5.95	4.96
CAO	3.37	3.25	3.38	3.39	3.51	3.45	3.38	3.39
SUM	99.80	99.33	100.46	75.10	100.24	100.11	100.58	96.52

SI	5.945	*		5.932	*		5.947	*		6.859	*		6.005	*		5.932	*		5.932	*		6.063	*	
AL	.055	6.000		.068	6.000		.053	6.000		0.000	6.859		0.000	6.005		.068	6.000		.068	6.000		0.000	6.063	
AL	3.960	*		3.997	*		3.918	*		4.690	*		3.968	*		3.975	*		3.930	*		4.081	*	
TI	.014	*		.014	*		.019	*		.022	*		.013	*		.015	*		.018	*		.017	*	
MG	1.109	*		1.245	*		1.079	*		1.336	*		1.174	*		1.151	*		1.151	*		1.176	*	
CA	.574	*		.556	*		.574	*		.668	*		.593	*		.585	*		.572	*		.587	*	
MN	.869	*		.601	*		.870	*		.084	*		.710	*		.741	*		.796	*		.679	*	
FE	3.505	10.031		3.755	10.069		3.587	10.047		1.112	7.912		3.534	9.992		3.562	10.029		3.583	10.049		3.277	9.815	
O	24.000	*		24.000	*		24.000	*		24.000	*		24.000	*		24.000	*		24.000	*		24.000	*	
	GROS	9.49			9.04			9.39			20.88			9.86			9.68			9.37			10.27		
	SPES	14.34			9.76			14.23			2.63			11.81			12.27			13.04			11.88		
	ALM	57.87			60.98			58.71			34.76			58.79			58.99			58.73			57.31		
	PYRP	18.31			20.23			17.67			41.73			19.54			19.05			18.86			20.54		
	F/M	3.943			3.497			4.129			.896			3.614			3.740			3.805			3.368		
	F/FM	.798			.778			.805			.473			.783			.789			.792			.771		

1 SAMPLE-76-48-86-98 LARGE GRAIN CENTRAL
2 AT EDGE
3 RANDOM SPOT
4 APPARRENT CENTRE
5 ANOTHER GRAIN CENTRAL
6 ANOTHER
7 ANOTHER
8 AVERAGE

SUPER RECAL GARNET SAMPLES

	1	2	3	4	5	6	7	8
SIO2	37.15	37.62	36.91	37.24	37.78	37.25	36.23	37.93
A2O3	20.71	20.85	21.43	21.29	1.10	21.46	21.41	21.12
TIO2	.12	.13	.07	.06	.08	.04	.06	.14
FEO	28.48	28.57	28.79	28.91	28.70	28.29	28.56	28.56
MGO	4.85	4.85	5.31	4.78	4.99	5.16	5.00	4.81
MNO	4.38	4.27	3.13	3.91	3.91	3.83	4.28	4.04
CAO	2.98	3.05	3.21	3.11	2.98	2.98	2.88	3.06
SUM	98.67	99.34	98.85	99.00	79.54	98.91	100.41	99.66

SI	5.982	*	6.007	*	5.910	*	5.962	*	7.846	*	5.953	*	6.018	*	6.022	*
AL	.018	6.000	0.000	6.007	.090	6.000	.038	6.000	0.000	7.846	.047	6.000	0.000	6.018	0.000	6.022
AL	3.912	*	3.923	*	3.953	*	3.978	*	.259	*	3.994	*	3.972	*	3.951	*
TI	.015	*	.016	*	.008	*	.007	*	.012	*	.005	*	.007	*	.017	*
MG	1.164	*	1.154	*	1.267	*	1.141	*	1.545	*	1.229	*	1.173	*	1.138	*
CA	.514	*	.522	*	.551	*	.533	*	.663	*	.493	*	.486	*	.521	*
MN	.597	*	.577	*	.424	*	.530	*	.688	*	.518	*	.571	*	.543	*
FE	3.835	10.037	3.815	10.007	3.855	10.058	3.831	10.020	4.984	8.161	3.781	10.020	3.760	9.970	3.792	9.962
O	24.000	*	24.000	*	24.000	*	24.000	*	24.000	*	24.000	*	24.000	*	24.000	*
GPOS		8.41		8.60		9.03		8.84		8.41		8.19		8.11		8.68
SPES		9.78		9.52		6.96		8.79		8.73		8.61		9.53		9.06
ALM		62.76		62.87		63.22		63.47		63.25		62.79		62.77		63.26
PYRP		19.05		19.02		20.78		18.90		19.60		20.41		19.59		16.99
F/M		3.808		3.805		3.377		3.823		3.672		3.498		3.691		3.809
F/FM		.792		.792		.772		.793		.786		.778		.787		.792

1 SAMPLE 76-48-136.5-151 CENTRAL
2 ANOTHER SPOT CENTRAL
3 EDGE OF THIS GRAIN
4 ANOTHER GRAIN CENTRAL
5 ANOTHER SPOT CENTRAL
6 AT EDGE
7 LARGEST GRAIN IN SECTION CENTRAL
8 ANOTHER SPOT CENTRAL

SUPER RECAL GARNET SAMPLES

	9	10	11	12	13
SIO2	37.42	37.77	37.53	37.91	37.15
A2O3	21.71	21.77	19.29	25.36	13.21
TIO2	.11	.05	.09	.12	.05
FEO	29.00	28.37	28.59	28.79	28.40
MGO	5.09	5.30	5.01	5.20	4.83
MNO	3.68	2.94	3.84	4.29	3.38
CAO	3.08	3.41	3.06	3.21	2.91
SUM	100.09	99.61	97.41	104.88	89.94

SI	5.922	*	5.968	*	6.119	*	5.696	*	6.626	*		
AL	.078	6.000	.032	6.000	0.000	6.119	.304	6.000	0.000	6.620		
AL	3.971	*	4.022	*	3.709	*	4.185	*	2.775	*		
TI	.013	*	.006	*	.011	*	.014	*	.007	*		
MG	1.201	*	1.248	*	1.218	*	1.165	*	1.282	*		
CA	.522	*	.577	*	.535	*	.517	*	.556	*		
MN	.493	*	.394	*	.530	*	.546	*	.511	*		
FE	3.838	10.038	3.749	9.997	3.899	9.898	3.617	10.044	4.233	9.364		
O	24.000	*	24.000	*	24.000	*	24.000	*	24.000	*		
GPOS		8.63		9.67		8.66		8.85		8.45		
SPES		8.15		6.59		8.57		9.34		7.76		
ALM		63.39		62.82		63.06		61.88		64.31		
PYRP		19.83		20.92		19.71		19.92		19.48		
F/M		3.608		3.319		3.634		3.575		3.699		
F/FM		.783		.768		.784		.781		.787		

9 INTERMEDIATE SPOT
10 AT EDGE
11 AVERAGE
12 AVERAGE PLUS SIGMA
13 AVERAGE MINUS SIGMA

SUPER RECAL — GARNET SAMPLES

	1	2	3	4	5	6	7	8
SIO2	37.94	37.79	37.43	37.89	37.57	37.96	37.52	38.53
A203	21.61	21.25	21.54	21.63	21.40	21.30	21.70	21.61
TIO2	.06	.08	.11	.04	.16	.09	.10	.07
FEO	25.97	25.07	25.09	26.27	26.23	25.09	25.71	25.82
MGO	4.79	4.63	4.61	5.36	5.25	4.55	5.01	5.09
MNO	5.80	6.39	6.27	4.91	4.88	5.98	5.50	5.11
CAO	3.63	4.68	4.13	3.93	4.28	4.71	4.03	4.12
SUM	99.70	99.89	99.18	100.03	99.77	99.68	99.57	100.35

SI	5.989	*		5.984	*		5.961	*		5.966	*		5.944	*		6.010	*		5.944	*		6.032	*	
AL	.011	6.000		.016	6.000		.039	6.000		.034	6.000		.056	6.000		0.000	6.010		.056	6.000		0.000	6.032	
AL	4.019	*		3.949	*		4.003	*		3.980	*		3.933	*		3.974	*		3.994	*		3.987	*	
TI	.007	*		.010	*		.013	*		.005	*		.019	*		.011	*		.012	*		.008	*	
MG	1.130	*		1.093	*		1.094	*		1.258	*		1.238	*		1.074	*		1.183	*		1.168	*	
CA	.616	*		.794	*		.705	*		.663	*		.725	*		.799	*		.684	*		.691	*	
MN	.778	*		.857	*		.846	*		.655	*		.654	*		.802	*		.738	*		.678	*	
FE	3.437	9.987		3.320	10.022		3.342	10.003		3.459	10.020		3.470	10.040		3.322	9.981		3.406	10.017		3.361	9.932	
O	24.000	*		24.000	*		24.000	*		24.000	*		24.000	*		24.000	*		24.000	*		24.000	*	
GROS		10.33			13.09			11.77			10.99			11.92			13.32			11.38			11.54		
SPES		13.04			14.13			14.13			10.85			10.74			13.37			12.28			11.41		
ALM		57.67			54.75			55.82			57.32			57.01			55.40			56.66			56.94		
PYRP		18.96			18.02			18.28			20.84			20.34			17.91			19.68			20.01		
F/M		3.730			3.822			3.827			3.270			3.331			3.841			3.503			3.417		
F/FM		.789			.793			.793			.766			.769			.793			.778			.774		

1 SAMPLE 76-48-186-19E CENTRAL
2 ANOTHER CENTRAL
3 ANOTHER CENTRAL
4 ANOTHER GRAIN WITH BEDDING AT EDGE
5 TOWARD OPP EDGE ACROSS BEDDING
6 ANOTHER
7 SAME GENERAL AREA
8 CLOSER TO OTHER EDGE

SUPER RECAL — GARNET SAMPLES

	9	10	11	12	13
SIO2	38.08	37.29	37.79	38.13	37.45
A203	21.47	21.42	21.49	21.64	21.35
TIO2	.08	.08	.09	.12	.06
FEO	26.09	26.70	25.80	26.34	25.27
MGO	5.24	5.01	4.95	5.23	4.68
MNO	5.04	5.68	5.56	6.09	5.03
CAO	3.73	3.46	4.07	4.46	3.68
SUM	99.73	99.64	99.75	102.00	97.50

SI	6.007	*		5.931	*		5.977	*		5.925	*		6.031	*		
AL	0.000	6.007		.069	6.000		.023	6.000		.075	6.000		0.000	6.031		
AL	3.991	*		3.946	*		3.983	*		3.686	*		4.052	*		
TI	.009	*		.010	*		.010	*		.014	*		.007	*		
MG	1.232	*		1.188	*		1.168	*		1.212	*		1.122	*		
CA	.630	*		.590	*		.690	*		.743	*		.635	*		
MN	.673	*		.765	*		.744	*		.801	*		.686	*		
FE	3.442	9.978		3.552	10.050		3.413	10.008		3.423	10.078		3.403	9.904		
O	24.000	*		24.000	*		24.000	*		24.000	*		24.000	*		
GROS		10.55			9.68			11.47			12.02			10.86		
SPES		11.27			12.56			12.37			12.96			11.73		
ALM		57.58			58.28			56.74			55.40			59.21		
PYRP		20.61			19.49			19.42			19.61			19.20		
F/M		3.340			3.634			3.560			3.486			3.643		
F/FM		.770			.784			.781			.777			.785		

9 STILL CLOSER
10 OPPOSITE EDGE
11 AVERAGE
12 AVERAGE PLUS SIGMA
13 AVERAGE MINUS SIGMA

SUPER RECAL — GARNET SAMPLES

	1	2	3	4	5	6	7	8
SIO2	37.19	37.14	37.17	38.63	36.77	37.38	38.02	36.74
A2O3	21.05	21.11	20.68	21.05	21.07	20.99	21.15	20.83
TIO2	0.00	0.00	0.00	0.00	0.00	0.00	0.00	0.00
FEO	31.09	30.44	32.10	29.05	29.87	30.51	31.55	29.47
MGO	2.82	2.98	3.47	2.26	2.45	2.80	3.22	2.37
MNO	5.55	4.93	3.40	6.24	5.86	5.20	6.19	4.20
CAO	3.32	3.38	3.10	3.98	4.07	3.97	3.95	3.19
SUM	101.02	99.98	99.92	101.21	100.09	100.44	104.09	96.80
SI	5.948 *	5.970 *	5.982 *	6.112 *	5.933 *	5.989 *	5.922 *	6.061 *
AL	.052 6.000	.030 6.000	.018 6.000	0.000 6.112	.067 6.000	.011 6.000	.078 6.000	0.000 6.061
AL	3.915 *	3.969 *	3.904 *	3.924 *	3.938 *	3.953 *	3.803 *	-.051 *
TI	0.000 *	0.000 *	0.000 *	0.000 *	0.000 *	0.000 *	0.000 *	0.000 *
MG	.672 *	.714 *	.832 *	.533 *	.589 *	.668 *	.747 *	.583 *
CA	.569 *	.582 *	.535 *	.675 *	.704 *	.613 *	.660 *	.563 *
MN	.752 *	.671 *	.463 *	.836 *	.861 *	.705 *	.817 *	.587 *
FE	4.158 10.066	4.092 10.028	4.320 10.055	3.844 9.812	4.030 10.062	4.088 10.027	4.109 10.136	4.066 9.850
O	24.000 *	24.000 *	24.000 *	24.000 *	24.000 *	24.000 *	24.000 *	24.000 *
GROS	9.25	9.61	8.69	11.46	11.49	10.09	10.42	9.71
SPES	12.22	11.08	7.54	14.20	13.08	11.61	12.90	10.12
ALM	67.60	67.53	70.24	65.29	65.81	67.31	64.89	70.11
PYRP	10.93	11.78	13.53	9.05	9.62	10.99	11.80	10.06
F/M	7.304	6.671	5.747	8.781	8.200	7.173	6.592	7.975
F/FM	.880	.870	.852	.898	.891	.878	.868	.889

1 SAMPLE CA-2-B2 CENTRAL
2 INT
3 AT EDGE
4 ANOTHER GRAIN CENTRAL
5 AGAIN
6 AVERAGE
7 AVERAGE PLUS SIGMA
8 AVERAGE MINUS SIGMA

SUPER RECAL GARNET SAMPLES

	1	2	3	4	5	6	7	8
SIO2	36.92	37.55	36.86	37.11	37.79	36.74	36.54	37.25
A203	20.27	20.56	20.72	20.79	20.84	21.09	20.67	21.22
TIO2	0.00	0.00	0.00	0.00	0.00	0.00	0.00	0.00
FEO	30.49	30.96	30.25	32.46	27.43	26.88	28.36	31.91
MGO	2.63	2.79	2.80	3.13	1.74	1.86	2.41	3.22
MNO	4.77	4.82	4.35	3.40	7.80	7.99	5.22	2.88
CAO	3.73	3.64	3.69	2.90	4.84	5.16	5.50	3.20
SUM	98.81	100.32	98.87	99.73	100.44	99.42	98.70	99.68

SI	6.022	*	6.029	*	5.990	*	5.988	*	6.056	*	5.955	*	5.956	*	5.985	*
AL	0.000	6.022	0.000	6.029	.010	6.000	.012	6.000	0.000	6.056	.045	6.000	.044	6.000	.015	6.000
AL	3.896	*	3.890	*	3.958	*	3.942	*	3.936	*	3.983	*	3.925	*	.003	*
TI	0.000	*	0.000	*	0.000	*	0.000	*	0.000	*	0.000	*	0.000	*	.000	*
MG	.639	*	.668	*	.678	*	.753	*	.416	*	.449	*	.585	*	.771	*
CA	.652	*	.626	*	.677	*	.501	*	.831	*	.896	*	.960	*	.551	*
MN	.659	*	.655	*	.599	*	.465	*	1.059	*	1.097	*	.721	*	.392	*
FE	4.159	10.006	4.157	9.996	4.111	10.024	4.372	10.033	3.676	9.917	3.603	10.029	3.866	10.057	4.268	10.004
O	24.000	*	24.000	*	24.000	*	24.000	*	24.000	*	24.000	*	24.000	*	24.000	*
	GROS	10.67		10.25		11.17		8.23		13.89		14.82		15.66		9.18
	SPES	10.79		10.73		9.87		7.63		17.70		18.15		11.75		6.53
	ALM	68.08		68.08		67.78		71.78		61.46		59.60		63.04		71.44
	PYRP	10.47		10.93		11.18		12.36		6.95		7.43		9.55		12.85
	F/M	7.535		7.208		6.944		6.425		11.392		10.459		7.833		6.058
	F/FM	.883		.878		.874		.865		.919		.913		.887		.859

1 SAMPLE CA-284 GAR CENTRAL
2 ANOTHER
3 CENTRAL
4 EDGE
5 CENTRAL
6 ANOTHER CENTRAL
7 INT
8 EDGE

SUPER RECAL GARNET SAMPLES

	9	10	11
SIO2	37.10	37.49	36.70
A203	20.77	21.05	20.49
TIO2	0.00	0.00	0.00
FEO	29.80	31.78	27.82
MGO	2.57	3.08	2.07
MNO	5.15	6.89	3.41
CAO	4.11	4.99	3.22
SUM	99.50	105.28	93.72

SI	5.998	*	5.822	*	6.189	*
AL	.002	6.000	.178	6.000	0.000	6.189
AL	3.956	*	3.673	*	4.072	*
TI	0.000	*	0.000	*	0.000	*
MG	.520	*	.713	*	.519	*
CA	.712	*	.831	*	.582	*
MN	.706	*	.907	*	.488	*
FE	4.029	10.021	4.127	10.250	3.923	9.584
O	24.000	*	24.000	*	24.000	*
	GROS	11.73		12.63		10.56
	SPES	11.63		13.79		8.85
	ALM	66.42		62.74		71.17
	PYRP	10.22		10.84		9.42
	F/M	7.637		7.060		8.498
	F/FM	.884		.876		.895

9 AVERAGE
10 AVERAGE PLUS SIGMA
11 AVERAGE MINUS SIGMA

SUPER RECAL — GARNET SAMPLES

	1	2	3	4	5	6	7	8
SIO2	36.77	36.17	37.14	36.38	37.02	36.80	37.13	36.46
A2O3	20.73	20.83	21.35	21.23	20.86	21.00	21.24	20.76
TIO2	0.00	0.00	0.00	0.00	0.00	0.00	0.00	0.00
FEO	38.14	38.15	38.87	38.65	39.01	38.56	38.92	38.20
MGO	2.36	2.45	2.28	2.24	2.32	2.31	2.39	2.23
MNO	1.64	1.65	1.41	1.34	1.37	1.48	1.62	1.35
CAO	.71	.65	.58	.53	.71	.64	.71	.56
SUM	100.25	99.91	101.63	100.87	101.29	100.79	102.02	99.56

SI	5.979	*		5.912	*		5.952	*		5.954	*		5.966	*		5.953	*		5.938	*		5.967	*	
AL	.021	6.000		.088	6.000		.048	6.000		.046	6.000		.034	6.000		.047	6.000		.062	6.000		.033	6.000	
AL	3.950	*		3.924	*		3.984	*		3.993	*		3.927	*		3.956	*		3.942	*		3.970	*	
TI	0.000	*		0.000	*		0.000	*		0.000	*		0.000	*		0.000	*		0.000	*		0.000	*	
MG	.548	*		.599	*		.545	*		.539	*		.557	*		.557	*		.570	*		.545	*	
CA	.124	*		.114	*		.100	*		.092	*		.123	*		.110	*		.121	*		.099	*	
MN	.226	*		.228	*		.191	*		.183	*		.187	*		.203	*		.219	*		.187	*	
FE	5.186	10.034		5.215	10.080		5.210	10.030		5.218	10.025		5.257	10.051		5.217	10.044		5.206	10.058		5.229	10.029	
O	24.000	*		24.000	*		24.000	*		24.000	*		24.000	*		24.000	*		24.000	*		24.000	*	
	GROS	2.03			1.85			1.65			1.52			2.00			1.81			1.98			1.63		
	SPES	3.71			3.71			3.17			3.04			3.05			3.34			3.58			3.08		
	ALM	85.25			84.71			86.18			86.51			85.85			85.70			85.12			86.29		
	PYRP	9.00			9.73			9.01			8.94			9.10			9.16			9.32			8.99		
	F/M	9.881			9.082			9.917			10.021			9.770			9.723			9.520			9.940		
	F/FM	.908			.901			.908			.909			.907			.907			.905			.909		

1 SAMPLE CA 3A-1
2 ANOTHER
3 ANOTHER
4 AGAIN
5 AGAIN
6 AVERAGE
7 AVERAGE PLUS SIGMA
8 AVERAGE MINUS SIGMA

SUPER RECAL — GARNET SAMPLES

	1	2	3	4	5	6	7	8
SIO2	38.32	39.68	37.75	38.52	40.07	38.87	39.74	38.00
A2O3	21.04	20.29	20.90	21.06	19.80	20.62	21.11	20.12
TIO2	0.00	0.00	0.00	0.00	0.00	0.00	0.00	0.00
FEO	31.86	31.75	33.46	31.93	30.39	31.88	32.85	30.90
MGO	1.46	1.52	1.62	1.51	1.38	1.50	1.58	1.42
MNO	1.88	2.13	1.64	1.92	2.07	1.93	2.10	1.76
CAO	6.21	4.83	5.30	6.48	6.15	5.79	6.42	5.17
SUM	100.77	100.20	100.67	101.42	99.86	100.58	103.80	97.37
SI	6.094 *	6.305 *	6.043 *	6.090 *	6.370 *	6.181 *	6.142 *	6.222 *
AL	0.000 6.094	0.000 6.305	0.000 6.043	0.000 6.090	0.000 6.370	0.000 6.181	0.000 6.142	0.000 6.222
AL	3.943 *	3.799 *	3.943 *	3.924 *	3.709 *	3.863 *	3.845 *	3.883 *
TI	0.000 *	0.000 *	0.000 *	0.000 *	0.000 *	0.000 *	0.000 *	0.000 *
MG	.346 *	.360 *	.387 *	.356 *	.327 *	.355 *	.363 *	.346 *
CA	1.058 *	.822 *	.909 *	1.098 *	1.048 *	.987 *	1.063 *	.907 *
MN	.253 *	.287 *	.222 *	.257 *	.279 *	.260 *	.275 *	.244 *
FE	4.237 9.838	4.219 9.488	4.480 9.940	4.222 9.856	4.040 9.403	4.239 9.705	4.246 9.792	4.232 9.612
O	24.000 *	24.000 *	24.000 *	24.000 *	24.000 *	24.000 *	24.000 *	24.000 *
GROS	17.95	14.46	15.16	18.50	18.40	16.90	17.87	15.83
SPES	4.30	5.04	3.71	4.33	4.90	4.45	4.62	4.25
ALM	71.88	74.17	74.69	71.16	70.96	72.58	71.40	73.87
PYRP	5.87	6.33	6.45	6.00	5.74	6.08	6.11	6.05
F/M	12.975	12.516	12.164	12.587	13.208	12.671	12.448	12.920
F/FM	.928	.926	.924	.926	.930	.927	.926	.928

1 SAMPLE CA-483 COMP BANDED
2 ANOTHER
3 AGAIN
4 AGAIN
5 LAST ONE
6 AVERAGE
7 AVERAGE PLUS SIGMA
8 AVERAGE MINUS SIGMA

SUPER RECAL — GARNET SAMPLES

	1	2	3	4	5	6	7	8
SIO2	37.02	36.36	36.81	36.14	36.84	36.53	36.43	36.87
A2O3	21.12	20.71	21.10	20.45	20.92	21.29	20.93	20.78
TIO2	0.00	0.00	0.00	0.00	0.00	0.00	0.00	0.00
FEO	28.47	31.55	29.12	29.23	27.44	27.29	27.80	27.93
MGO	2.29	1.96	2.09	1.89	1.61	1.57	1.69	1.69
MNO	4.43	5.25	5.12	5.23	6.95	6.90	7.45	7.90
CAO	6.19	4.52	5.58	5.70	6.29	6.50	5.22	4.82
SUM	99.52	99.35	99.82	98.64	100.05	100.08	99.52	99.99
SI	5.963 *	5.932 *	5.941 *	5.931 *	5.948 *	5.897 *	5.926 *	5.978 *
AL	.037 6.000	.068 6.000	.059 6.000	.069 6.000	.052 6.000	.103 6.000	.074 6.000	.030 6.000
AL	3.972 *	3.914 *	3.953 *	3.886 *	3.928 *	3.947 *	3.938 *	3.935 *
TI	0.000 *	0.000 *	0.000 *	0.000 *	0.000 *	0.000 *	0.000 *	0.000 *
MG	.550 *	.477 *	.503 *	.462 *	.387 *	.378 *	.410 *	.408 *
CA	1.068 *	.790 *	.965 *	1.002 *	1.088 *	1.124 *	.910 *	.836 *
MN	.604 *	.726 *	.700 *	.727 *	.950 *	.943 *	1.026 *	1.084 *
FE	3.835 10.030	4.168 10.075	3.930 10.051	4.012 10.089	3.705 10.060	3.684 10.076	3.782 10.056	3.782 10.045
O	24.000 *	24.000 *	24.000 *	24.000 *	24.000 *	24.000 *	24.000 *	24.000 *
GROS	17.64	12.83	15.82	16.16	17.75	18.34	14.85	13.69
SPES	9.98	11.78	11.48	11.72	15.50	15.39	16.75	17.73
ALM	63.31	67.66	64.45	64.67	60.43	60.10	61.72	61.90
PYRP	9.08	7.74	8.24	7.45	6.32	6.16	6.69	6.68
F/M	8.675	10.267	9.210	10.250	12.016	12.251	11.735	11.929
F/FM	.890	.911	.902	.911	.923	.925	.921	.923

1 SAMPLE CA-6D
2 ANOTHER
3 ANOTHER
4 ANOTHER
5 NEW GRAIN
6 AGAIN
7 AGAIN
8 NEW

SUPER RECAL — GARNET SAMPLES

	9	10	11	12	13
SIO2	37.15	37.54	36.77	37.16	36.37
A2O3	21.14	21.30	20.97	21.23	20.72
TIO2	0.00	0.00	0.00	0.00	0.00
FEO	30.23	28.47	28.65	29.72	27.59
MGO	2.00	2.20	1.90	2.14	1.66
MNO	4.39	4.08	5.77	7.10	6.44
CAO	5.92	6.88	5.76	6.47	5.05
SUM	100.83	100.47	99.83	103.81	95.84
SI	5.944 *	5.980 *	5.943 *	5.835 *	6.058 *
AL	.056 6.000	.020 6.000	.057 6.000	.165 6.000	0.000 6.058
AL	3.930 *	3.979 *	3.938 *	3.764 *	4.066 *
TI	0.000 *	0.000 *	0.000 *	0.000 *	0.000 *
MG	.477 *	.522 *	.458 *	.500 *	.412 *
CA	1.015 *	1.174 *	.998 *	1.089 *	.901 *
MN	.595 *	.551 *	.790 *	.944 *	.627 *
FE	4.045 10.061	3.793 10.019	3.873 10.057	3.902 10.198	3.843 9.849
O	24.000 *	24.000 *	24.000 *	24.000 *	24.000 *
GROS	16.55	19.44	16.31	16.92	15.59
SPES	9.70	9.11	12.91	14.66	10.84
ALM	65.97	62.80	63.30	60.64	66.45
PYRP	7.78	8.65	7.48	7.78	7.12
F/M	9.728	8.315	10.192	9.682	10.850
F/FM	.907	.893	.911	.906	.918

9 AGAIN
10 ANOTHER
11 AVERAGE
12 AVERAGE PLUS SIGMA
13 AVERAGE MINUS SIGMA

SUPER RECAL — GARNET SAMPLES

	1	2	3	4	5
SIO2	37.40	37.55	37.48	37.55	37.40
A203	21.15	21.11	21.13	21.15	21.11
TIO2	0.00	0.00	0.00	0.00	0.00
FEO	30.91	28.73	29.82	30.91	28.73
MGO	1.97	2.20	2.09	2.20	1.97
MNO	4.64	5.93	5.29	5.93	4.64
CAO	5.42	5.61	5.52	5.61	5.42
SUM	101.49	101.13	101.31	103.35	99.27

SI	5.955	*	5.977	*	5.966	*	5.903	*	6.031	*
AL	.045	6.000	.023	6.000	.034	6.000	.097	6.000	0.000	6.031
AL	3.924	*	3.937	*	3.931	*	3.821	*	4.011	*
TI	0.000	*	0.000	*	0.000	*	0.000	*	0.000	*
MG	.468	*	.522	*	.495	*	.516	*	.474	*
CA	.925	*	.957	*	.941	*	.945	*	.936	*
MN	.626	*	.800	*	.713	*	.790	*	.634	*
FE	4.116	10.058	3.825	10.040	3.970	10.049	4.064	10.136	3.875	9.930
O	24.000	*	24.000	*	24.000	*	24.000	*	24.000	*
GROS		15.07		15.68		15.38		14.97		15.82
SPES		10.20		13.10		11.65		12.51		10.71
ALM		67.10		62.67		64.89		64.36		65.47
PYRP		7.62		8.55		8.09		8.16		8.00
F/M		10.142		8.859		9.465		9.415		9.521
F/FM		.910		.899		.904		.904		.905

1 SAMPLE CA-60 LARGE GAR
2 AGAIN
3 AVERAGE
4 AVERAGE PLUS SIGMA
5 AVERAGE MINUS SIGMA

SUPER RECAL — GARNET SAMPLES

	1	2	3	4	5	6	7	8
SIO2	38.59	38.66	38.16	38.61	37.93	38.39	38.68	38.10
A203	21.63	21.62	21.31	21.45	21.21	21.44	21.61	21.28
TIO2	.02	.05	.02	0.00	.10	.04	.07	.00
FEO	29.43	30.74	30.51	29.58	29.86	30.02	30.54	29.51
MGO	6.13	5.20	5.46	6.04	5.63	5.89	6.04	5.34
MNO	.73	.80	.80	.89	.80	.80	.85	.75
CAO	3.48	3.16	3.21	3.52	3.73	3.62	3.97	3.27
SUM	100.01	100.23	100.47	100.09	99.26	100.01	101.77	98.26

SI	6.032	*	6.059	*	5.991	*	6.040	*	6.007	*	6.026	*	5.982	*	6.071	*
AL	0.000	6.032	0.000	6.059	.009	6.000	0.000	6.040	0.000	6.007	0.000	6.026	.018	6.000	0.000	6.071
AL	3.984	*	3.993	*	3.933	*	3.954	*	3.958	*	3.966	*	3.919	*	3.995	*
TI	.002	*	.006	*	.002	*	0.000	*	.012	*	.004	*	.008	*	.000	*
MG	1.428	*	1.215	*	1.278	*	1.408	*	1.329	*	1.332	*	1.395	*	1.289	*
CA	.583	*	.531	*	.708	*	.590	*	.633	*	.609	*	.657	*	.559	*
MN	.097	*	.106	*	.106	*	.118	*	.107	*	.107	*	.112	*	.102	*
FE	3.847	9.940	4.029	9.879	4.008	10.033	3.870	9.940	3.955	9.994	3.941	9.959	3.949	10.039	3.933	9.858
O	24.000	*	24.000	*	24.000	*	24.000	*	24.000	*	24.000	*	24.000	*	24.000	*
GROS		9.79		9.02		11.61		9.86		10.51		10.17		10.75		9.53
SPES		1.62		1.81		1.74		1.97		1.78		1.79		1.83		1.73
ALM		64.61		68.51		65.69		64.65		65.65		65.81		64.63		67.09
PYRP		23.98		20.66		20.95		23.53		22.06		22.24		22.79		21.65
F/M		2.761		3.404		3.219		2.632		3.057		3.040		2.916		3.180
F/FM		.734		.773		.763		.739		.753		.752		.745		.761

1 SAMPLE A-188-5 AT EDGE
2 ANOTHER
3
4
5
6 AVERAGE
7 AVERAGE PLUS SIGMA
8 AVERAGE MINUS SIGMA

SUPER RECAL — GARNET SAMPLES

	1	2	3	4	5	6	7	8
SIO2	38.13	38.18	38.64	38.97	39.17	38.78	38.73	38.49
A2O3	20.77	21.32	21.52	21.90	21.44	21.57	21.68	21.24
TIO2	.02	.05	.04	.04	0.00	.04	.14	.19
FEO	28.32	30.86	30.83	31.85	31.63	31.33	31.19	24.99
MGO	2.12	2.99	3.42	4.54	3.89	3.98	3.99	3.73
MNO	5.88	3.37	2.17	1.67	2.89	3.17	2.14	3.05
CAO	4.72	3.61	3.97	2.17	1.81	1.78	2.70	3.46
SUM	99.96	100.38	100.59	101.14	100.83	100.65	100.57	100.15

SI	6.105	*		6.064	*		6.087	*		6.079	*		6.149	*		6.104	*		6.086	*		6.087	*	
AL	0.000	6.105	*	0.000	6.064	*	0.000	6.087	*	0.000	6.079	*	0.000	6.149	*	0.000	6.104	*	0.000	6.086	*	0.000	6.087	*
AL	3.919	*	*	3.990	*	*	3.994	*	*	4.025	*	*	3.966	*	*	4.001	*	*	4.014	*	*	3.958	*	*
TI	.002	*	*	.006	*	*	.005	*	*	.005	*	*	0.000	*	*	.005	*	*	.017	*	*	.023	*	*
MG	.506	*	*	.708	*	*	.803	*	*	1.056	*	*	.910	*	*	.934	*	*	.934	*	*	.879	*	*
CA	.810	*	*	.614	*	*	.670	*	*	.363	*	*	.304	*	*	.300	*	*	.955	*	*	.586	*	*
MN	.797	*	*	.453	*	*	.290	*	*	.221	*	*	.384	*	*	.423	*	*	.265	*	*	.409	*	*
FE	3.792	9.826	*	4.099	9.870	*	4.061	9.823	*	4.155	9.823	*	4.152	9.717	*	4.124	9.786	*	4.099	9.803	*	3.967	9.322	*
O	24.000	*		24.000	*		24.000	*		24.000	*		24.000	*		24.000	*		24.000	*		24.000	*	
GROS		13.71			10.46			11.50			6.26			5.29			5.19			7.87			10.04	
SPES		13.50			7.72			4.97			3.81			6.68			7.31			4.93			7.00	
ALM		64.22			69.78			69.74			71.71			72.20			71.34			71.00			67.91	
PYRP		8.57			12.05			13.79			18.22			15.83			16.15			16.19			15.05	
F/M		9.071			6.431			5.418			4.145			4.984			4.869			4.691			4.976	
F/FM		.901			.865			.844			.606			.833			.830			.824			.833	

1 SAMPLE A 189-1 LARGE GRAIN CENTRAL
2 TOWARD EDGE
3 CLOSER
4 CLOSER
5 OUTER EDGE
6 ANOTHER AT EDGE
7 BACK FROM EDGE
8 OTHER GRAIN AT EDGE

SUPER RECAL — GARNET SAMPLES

	9	10	11	12	13
SIO2	38.53	39.38	38.70	39.08	38.32
A2O3	21.52	21.59	21.46	21.74	21.17
TIO2	.02	.10	.06	.12	.01
FEO	27.86	27.52	30.14	31.69	28.59
MGO	2.20	2.38	3.32	4.13	2.51
MNO	5.96	5.59	3.59	5.13	2.05
CAO	4.84	4.60	3.37	4.50	2.24
SUM	100.93	101.16	100.64	106.39	94.88

SI	6.086	*		6.165	*		6.101	*		5.913	*		6.305	*		
AL	0.000	6.086	*	0.000	6.165	*	0.000	6.101	*	.087	6.000	*	0.000	6.305	*	
AL	4.005	*	*	3.983	*	*	3.986	*	*	3.790	*	*	4.104	*	*	
TI	.002	*	*	.012	*	*	.008	*	*	.014	*	*	.001	*	*	
MG	.518	*	*	.555	*	*	.781	*	*	.932	*	*	.617	*	*	
CA	.819	*	*	.772	*	*	.569	*	*	.729	*	*	.394	*	*	
MN	.797	*	*	.741	*	*	.479	*	*	.657	*	*	.286	*	*	
FE	3.680	9.822	*	3.603	9.665	*	3.973	9.795	*	4.010	10.132	*	3.933	9.335	*	
O	24.000	*		24.000	*		24.000	*		24.000	*		24.000	*		
GROS		14.09			13.61			9.80			11.52			7.54		
SPES		13.71			13.07			8.26			10.38			5.46		
ALM		63.29			63.53			68.48			63.36			75.21		
PYRP		8.91			9.79			13.46			14.73			11.79		
F/M		8.645			7.822			5.701			5.006			6.644		
F/FM		.896			.887			.851			.833			.873		

9 CENTRAL
10 AGAIN
11 AVERAGE
12 AVERAGE PLUS SIGMA
13 AVERAGE MINUS SIGMA

SUPER RECAL

GARNET SAMPLES

	1	2	3	4	5	6	7	8
SIO2	37.44	38.19	37.68	37.93	38.76	38.73	38.50	38.18
A2O3	21.54	21.50	21.67	21.58	21.21	21.14	22.02	21.52
TIO2	.09	.05	.07	.06	0.00	.05	.09	.06
FEO	24.57	24.59	25.55	25.07	25.22	24.54	24.36	24.84
MGO	3.36	3.45	3.01	3.23	2.52	2.54	3.31	3.06
MNO	8.49	8.52	8.82	8.67	9.47	9.00	8.73	8.81
CAO	4.12	4.13	3.41	3.76	3.37	5.07	4.37	4.03
SUM	99.61	100.43	100.21	100.30	100.55	101.07	101.38	100.51

SI	5.980	*	6.037	*	5.998	*	6.018	*	6.140	*	6.104	*	6.021	*	6.043	*
AL	.020	6.000	0.000	6.037	.002	6.000	0.000	6.018	0.000	6.140	0.000	6.104	0.000	6.021	0.000	6.043
AL	4.034	*	4.005	*	4.063	*	4.035	*	3.959	*	3.926	*	4.058	*	4.015	*
TI	.011	*	.006	*	.008	*	.007	*	0.000	*	.006	*	.011	*	.007	*
MG	.800	*	.813	*	.714	*	.764	*	.595	*	.597	*	.772	*	.722	*
CA	.705	*	.700	*	.582	*	.639	*	.572	*	.856	*	.732	*	.684	*
MN	1.149	*	1.141	*	1.169	*	1.165	*	1.271	*	1.201	*	1.156	*	1.182	*
FE	3.282	9.980	3.251	9.915	3.402	9.959	3.327	9.937	3.341	9.738	3.234	9.821	3.186	9.915	3.289	9.898
O	24.000	*	24.000	*	24.000	*	24.000	*	24.000	*	24.000	*	24.000	*	24.000	*
	GROS	11.98		11.85		9.88		10.84		9.90		14.54		12.52		11.64
	SPES	19.35		19.32		20.20		19.77		21.99		20.43		19.78		20.11
	ALM	55.29		55.06		57.78		56.43		57.82		54.93		54.50		55.96
	PYRP	13.48		13.77		12.13		12.96		10.30		10.13		13.20		12.29
	F/M	5.539		5.402		6.428		5.880		7.751		7.434		5.626		6.132
	F/FM	.847		.844		.865		.855		.886		.881		.849		.861

1 SAMPLE 190-3 CENTRAL
2 ANOTHER CENTRAL
3
4
5 LARGE POIK GRAIN CENTRAL
6
7 EDGE
8 AVERAGE

SUPER PECAL — GARNET SAMPLES

	1	2	3	4	5	6	7	8
SIO2	37.90	38.84	38.42	38.10	37.72	38.20	38.59	37.80
A2O3	20.86	21.18	20.97	20.89	20.64	20.91	21.08	20.73
TIO2	0.00	0.00	0.00	0.00	0.00	0.00	0.00	0.00
FEO	29.02	29.57	30.93	30.34	29.31	29.83	30.54	29.13
MGO	4.66	4.36	4.11	4.23	4.31	4.33	4.52	4.15
MNO	4.26	4.36	3.17	4.10	3.93	3.96	4.39	3.54
CAO	2.84	2.68	1.95	2.19	3.21	2.57	3.03	2.12
SUM	99.54	100.99	99.55	99.85	99.12	99.81	102.14	97.48
SI	6.042 *	6.096 *	6.119 *	6.070 *	6.050 *	6.075 *	6.027 *	6.126 *
AL	0.000 6.042	0.000 6.096	0.000 6.119	0.000 6.070	0.000 6.050	0.000 6.075	0.000 6.027	0.000 6.126
AL	3.919 *	3.917 *	3.936 *	3.922 *	3.901 *	3.919 *	3.879 *	3.960 *
TI	0.000 *	0.000 *	0.000 *	0.000 *	0.000 *	0.000 *	0.000 *	0.000 *
MG	1.107 *	1.020 *	.976 *	1.005 *	1.030 *	1.028 *	1.051 *	1.003 *
CA	.485 *	.451 *	.333 *	.374 *	.552 *	.439 *	.506 *	.368 *
MN	.575 *	.580 *	.428 *	.553 *	.534 *	.534 *	.580 *	.486 *
FE	3.869 9.955	3.861 9.848	4.120 9.792	4.043 9.896	3.931 9.948	3.969 9.888	3.968 10.005	3.949 9.766
O	24.000 *	24.000 *	24.000 *	24.000 *	24.000 *	24.000 *	24.000 *	24.000 *
GROS	8.04	7.60	5.68	6.26	9.12	7.35	8.27	6.35
SPES	9.53	9.77	7.30	9.26	8.83	8.95	9.47	8.37
ALM	64.09	65.43	70.35	67.67	65.01	66.49	65.10	68.01
PYRP	16.34	17.20	16.66	16.81	17.04	17.21	17.16	17.27
F/M	4.014	4.374	4.661	4.575	4.334	4.382	4.344	4.423
F/FM	.801	.814	.823	.821	.813	.814	.813	.816

1 SAMPLE A-190-4
2 CENTRE
3 EDGE
4 ANOTHER POIK CENTRAL
5
6 AVERAGE
7 AVERAGE PLUS SIGMA
8 AVERAGE MINUS SIGMA

SUPER RECAL — GARNET SAMPLES

	1	2	3	4	5	6	7	8
SIO2	37.79	37.59	36.54	37.37	38.21	37.91	37.68	39.06
A203	20.75	21.08	20.15	20.31	21.13	20.63	21.02	21.40
TIO2	0.00	0.00	0.00	0.00	0.00	0.00	0.00	0.00
FEO	24.71	25.05	25.24	25.68	24.99	24.27	24.10	23.79
MGO	3.17	3.36	2.98	3.68	3.59	3.21	3.10	3.04
MNO	9.50	9.17	10.06	7.70	8.40	9.73	10.12	10.59
CAO	4.09	3.71	3.40	3.67	3.73	4.08	4.57	3.67
SUM	100.01	99.96	98.37	98.41	100.05	99.83	100.59	101.55

SI	6.043	*		6.008	*		5.989	*		6.057	*		6.067	*		6.066	*		5.998	*		6.116	*	
AL	0.000	6.043		0.000	6.008		.011	6.000		0.000	6.057		0.000	6.067		0.000	6.066		.002	6.000		.000	6.116	
AL	3.910	*		3.970	*		3.881	*		3.879	*		3.954	*		3.890	*		3.941	*		3.948	*	
TI	0.000	*		0.000	*		0.000	*		0.000	*		0.000	*		0.000	*		0.000	*		0.000	*	
MG	.756	*		.800	*		.728	*		.889	*		.850	*		.766	*		.736	*		.709	*	
CA	.701	*		.635	*		.597	*		.637	*		.635	*		.699	*		.779	*		.616	*	
MN	1.287	*		1.241	*		1.397	*		1.057	*		1.130	*		1.319	*		1.364	*		1.404	*	
FE	3.364	9.957		3.348	9.996		3.460	10.063		3.481	9.944		3.319	9.886		3.248	9.921		3.208	10.028		3.115	9.793	
O	24.000	*		24.000	*		24.000	*		24.000	*		24.000	*		24.000	*		24.000	*		24.000	*	
GROS		11.59			10.54			9.66			10.51			10.70			11.60			12.80			10.53		
SPES		21.28			20.60			22.59			17.43			19.04			21.86			22.41			24.03		
ALM		54.64			55.57			55.97			57.40			55.94			53.85			52.70			53.30		
PYRP		12.49			13.28			11.78			14.66			14.32			12.69			12.08			12.14		
F/M		6.077			5.734			6.671			5.104			5.235			5.965			6.217			6.370		
F/FM		.859			.851			.870			.836			.840			.856			.861			.864		

1 SAMPLE A-191-8
2 CENTRAL
3 OTHER LARGER GRAIN CENTRAL
4 OUTER EDGE
5
6
7
8

SUPER RECAL — GARNET SAMPLES

	9	10	11	12	13
SIO2	38.78	37.68	37.86	38.53	37.19
A203	20.91	21.03	20.84	21.21	20.48
TIO2	0.00	0.00	0.00	0.00	0.00
FEO	25.70	23.92	24.75	25.41	24.08
MGO	3.31	2.99	3.24	3.47	3.01
MNO	8.27	10.34	9.39	10.31	8.46
CAO	4.01	3.68	3.86	4.17	3.55
SUM	100.98	99.64	99.94	103.11	96.76

SI	6.113	*		6.041	*		6.050	*		5.997	*		6.106	*		
AL	0.000	6.113		0.000	6.041		0.000	6.050		.003	6.000		0.000	6.106		
AL	3.884	*		3.973	*		3.924	*		3.887	*		3.961	*		
TI	0.000	*		0.000	*		0.000	*		0.000	*		0.000	*		
MG	.778	*		.714	*		.772	*		.806	*		.737	*		
CA	.677	*		.632	*		.661	*		.696	*		.624	*		
MN	1.104	*		1.404	*		1.271	*		1.360	*		1.177	*		
FE	3.388	9.831		3.207	9.930		3.307	9.935		3.307	10.056		3.306	9.806		
O	24.000	*		24.000	*		24.000	*		24.000	*		24.000	*		
GROS		11.39			10.61			11.00			11.28			10.68		
SPES		18.57			23.57			21.14			22.04			20.13		
ALM		56.97			53.83			55.01			53.61			56.57		
PYRP		13.08			11.99			12.85			13.06			12.61		
F/M		5.776			6.454			5.926			5.792			6.381		
F/FM		.852			.866			.856			.853			.859		

9 EDGE
10
11 AVERAGE
12 AVERAGE PLUS SIGMA
13 AVERAGE MINUS SIGMA

SUPER RECAL

GARNET SAMPLES

	1	2	3	4	5	6	7	8
SIO2	38.15	38.49	38.59	38.31	38.52	38.41	38.57	38.25
A2O3	21.58	21.53	21.32	21.02	21.41	21.37	21.57	21.17
TIO2	.03	.10	.08	.04	.04	.06	.09	.03
FEO	29.67	34.30	34.25	28.70	29.76	31.34	33.76	28.91
MGO	1.60	2.62	2.61	1.66	1.57	2.01	2.51	1.52
MNO	4.09	.80	.76	5.18	3.96	2.96	4.79	1.13
CAO	5.72	3.14	3.08	6.03	6.06	4.81	6.20	3.42
SUM	100.84	100.98	100.69	100.94	101.32	100.95	107.48	94.43
SI	6.052 *	6.084 *	6.114 *	6.082 *	6.081 *	6.083 *	5.856 *	6.329 *
AL	0.000 6.052	0.000 6.084	0.000 6.114	0.000 6.082	0.000 6.081	0.000 6.083	.144 6.000	0.000 6.329
AL	4.034 *	4.010 *	3.981 *	3.932 *	3.983 *	3.988 *	3.715 *	4.128 *
TI	.004 *	.012 *	.010 *	.005 *	.005 *	.007 *	.010 *	.004 *
MG	.378 *	.617 *	.616 *	.393 *	.369 *	.475 *	.567 *	.375 *
CA	.972 *	.532 *	.523 *	1.026 *	1.025 *	.815 *	1.008 *	.606 *
MN	.550 *	.107 *	.102 *	.697 *	.529 *	.397 *	.615 *	.158 *
FE	3.936 9.874	4.534 9.813	4.538 9.770	3.810 9.863	3.929 9.840	4.150 9.832	4.267 10.202	4.000 9.271
O	24.000 *	24.000 *	24.000 *	24.000 *	24.000 *	24.000 *	24.000 *	24.000 *
GROS	16.66	9.18	9.05	17.31	17.51	13.97	15.56	11.79
SPES	9.42	1.85	1.76	11.75	9.05	6.80	9.50	3.08
ALM	67.44	78.31	78.52	64.31	67.13	71.10	66.19	77.84
PYRP	6.48	10.66	10.66	6.63	6.31	8.14	8.75	7.29
F/M	11.857	7.519	7.528	11.474	12.069	9.574	8.648	11.102
F/FM	.922	.883	.883	.920	.923	.905	.896	.917

1 SAMPLE A-191-10 MASSIVE GARNET
2
3
4

5 MASSIVE GARNET
6 AVERAGE
7 AVERAGE PLUS SIGMA
8 AVERAGE MINUS SIGMA

SUPER RECAL AMPHIBOLE SAMPLES

SUB GROUP SI AL / AL TI MG FE MN NA CA K / O /	1	2	3	4	5	6	7	8
SIO2	51.72	52.25	51.18	51.47	50.75	51.09	51.42	51.41
TIO2	.13	.04	.09	0.00	0.00	0.00	0.00	.04
A203	.39	.35	.29	.50	.47	.43	.43	.41
FEO	34.76	35.60	36.17	34.88	34.88	36.19	36.13	35.52
MNO	0.00	0.00	0.00	.01	.02	.05	.04	.02
MGO	10.66	10.38	10.88	10.80	11.11	10.63	10.43	10.76
CAO	.03	.05	.01	.06	.06	.05	.06	.05
NA2O	0.00	0.00	0.00	.21	.15	.15	.13	.09
K2O	.03	0.00	.01	.01	0.00	0.00	0.00	.01
SUM	97.66	99.17	98.63	97.94	97.44	98.59	98.64	98.30

SI	7.971	*		7.947	*		7.874	*		7.925	*		7.872	*		7.871	*		7.906	*		7.909	*	
AL	.029	8.000		.053	8.000		.053	7.927		.075	8.000		.086	7.957		.078	7.949		.078	7.984		.074	7.984	
AL	.041	*		.010	*		0.000	*		.016	*		0.000	*		0.000	*		0.000	*		0.000	*	
TI	.015	*		.005	*		.010	*		0.000	*		0.000	*		0.000	*		0.000	*		.004	*	
MG	2.438	*		2.466	*		2.495	*		2.479	*		2.568	*		2.441	*		2.390	*		2.468	*	
FE	4.480	*		4.528	*		4.654	*		4.491	*		4.524	*		4.663	*		4.646	*		4.569	*	
MN	0.000	*		0.000	*		0.000	*		.001	*		.003	*		.007	*		.005	*		.002	*	
NA	0.000	*		0.000	*		0.000	*		.063	*		.045	*		.045	*		.039	*		.027	*	
CA	.005	*		.008	*		.002	*		.010	*		.010	*		.008	*		.010	*		.008	*	
K	.006	6.982		0.000	7.017		.002	7.163		.002	7.062		0.000	7.151		0.000	7.163		0.000	7.090		.001	7.080	
O	23.000	*		23.000	*		23.000	*		23.000	*		23.000	*		23.000	*		23.000	*		23.000	*	
F/M		1.840			1.836			1.865			1.813			1.763			1.913			1.946			1.853	
F/FM		.648			.647			.651			.644			.638			.657			.661			.649	

1 P14 GRUNERITE
2 ANOTHER GRAIN
3 ANOTHER
4
5
6
7
8 AVERAGE

SUPER RECAL AMPHIBOLE SAMPLES

	1	2	3	4	5	6	7	8
SIO2	54.63	54.55	54.27	55.26	55.01	55.20	54.86	54.45
TIO2	0.00	0.00	0.00	0.00	0.00	0.00	0.00	0.00
A2O3	1.63	1.47	.95	1.44	1.52	1.40	1.42	.71
FEO	23.32	22.82	24.29	22.82	23.28	22.65	23.47	23.97
MNO	.04	.06	.09	.03	.02	.09	.04	.05
MGO	18.71	19.20	18.44	19.20	19.20	18.48	19.31	18.94
CAO	.13	.18	.25	.15	.16	.13	.18	.23
NA2O	.07	.14	.05	.14	.09	.14	.03	.06
K2O	0.00	0.00	0.00	0.00	0.00	0.00	0.00	0.00
SUM	98.53	98.42	98.34	99.04	99.28	96.09	99.31	98.41

SI	7.864	*	7.852	*	7.880	*	7.890	*	7.855	*	7.949	*	7.842	*	7.887	*
AL	.136	8.000	.148	8.000	.120	8.000	.110	8.000	.145	8.000	.051	8.000	.158	8.000	.113	8.000
AL	.141	*	.102	*	.042	*	.132	*	.111	*	.187	*	.081	*	.009	*
TI	0.000	*	0.000	*	0.000	*	0.000	*	0.000	*	0.000	*	0.000	*	0.000	*
MG	4.015	*	4.119	*	3.991	*	4.086	*	4.086	*	3.967	*	4.114	*	3.989	*
FE	2.807	*	2.747	*	2.949	*	2.725	*	2.780	*	2.728	*	2.806	*	2.904	*
MN	.005	*	.007	*	.011	*	.004	*	.002	*	.011	*	.005	*	.006	*
NA	.020	*	.039	*	.014	*	.039	*	.025	*	.039	*	.006	*	.017	*
CA	.020	*	.028	*	.039	*	.023	*	.024	*	.020	*	.028	*	.036	*
K	0.000	7.007	0.000	7.042	0.000	7.046	0.000	7.008	0.000	7.029	0.000	6.951	0.000	7.042	0.000	7.060
O	23.000	*	23.000	*	23.000	*	23.000	*	23.000	*	23.000	*	23.000	*	23.000	*
F/M		.701		.669		.742		.668		.681		.690		.683		.712
F/FM		.412		.401		.426		.400		.405		.408		.406		.416

1 SAMPLE P58-4 GRUNERITE
2
3
4
5 AGAIN
6
7
8 SAMPLE P58-4

SUPER RECAL AMPHIBOLE SAMPLES

	9	10	11	12	13
SIO2	53.79	53.50	54.55	55.10	54.00
TIO2	0.00	0.00	0.00	0.00	0.00
A2O3	.91	.85	1.23	1.55	.91
FEO	24.44	24.46	23.55	24.21	22.89
MNO	.09	.16	.07	.11	.03
MGO	18.62	18.41	18.85	19.19	18.51
CAO	.28	.20	.19	.24	.14
NA2O	.12	.13	.10	.14	.06
K2O	0.00	0.00	0.00	0.00	0.00
SUM	98.25	97.71	98.54	100.53	96.54

SI	7.836	*	7.844	*	7.870	*	7.810	*	7.932	*						
AL	.156	7.993	.147	7.991	.130	8.000	.190	8.000	.068	8.000						
AL	0.000	*	0.000	*	.079	*	.068	*	.090	*						
TI	0.000	*	0.000	*	0.000	*	0.000	*	0.000	*						
MG	4.043	*	4.023	*	4.054	*	4.955	*	4.053	*						
FE	2.978	*	2.999	*	2.842	*	2.870	*	2.812	*						
MN	.011	*	.020	*	.006	*	.013	*	.003	*						
NA	.034	*	.037	*	.027	*	.038	*	.016	*						
CA	.044	*	.031	*	.029	*	.036	*	.022	*						
K	0.000	7.110	0.000	7.110	0.000	7.039	0.000	7.079	0.000	6.997						
O	23.000	*	23.000	*	23.000	*	23.000	*	23.000	*						
F/M		.739		.750		.703		.711		.695						
F/FM		.425		.429		.413		.416		.410						

9
10
11 AVERAGE
12 AVERAGE PLUS SIGMA
13 AVERAGE MINUS SIGMA

SUPER RECAL — AMPHIBOLE SAMPLES

	1	2	3	4	5	6	7	8
SIO2	52.51	51.15	52.23	52.37	50.78	51.39	51.10	51.21
TIO2	0.00	0.00	0.00	0.00	0.00	0.00	.03	.02
A2O3	.45	.49	.46	.56	.50	.50	.52	.54
FEO	34.06	33.38	34.39	34.61	35.13	34.74	34.50	34.95
MNO	.05	.04	.05	.08	.06	.01	.07	.06
MGO	11.87	11.47	11.80	11.32	11.54	11.34	11.45	11.29
CAO	.06	.09	.08	.04	.11	.09	.08	.11
NA2O	.11	.11	.08	.11	.15	.10	.10	.05
K2O	0.00	0.00	0.00	0.00	0.00	0.00	0.00	0.00
SUM	99.09	96.73	99.01	99.09	98.28	98.17	97.85	98.23

SI	7.936	*		7.927	*		7.916	*		7.937	*		7.820	*		7.889	*		7.871	*		7.869	*	
AL	.064	8.000		.073	8.000		.082	7.998		.063	8.000		.091	7.911		.090	7.980		.094	7.965		.098	7.967	
AL	.016	*		.016	*		0.000	*		.037	*		0.000	*		0.000	*		0.000	*		0.000	*	
TI	0.000	*		0.000	*		0.000	*		0.000	*		0.000	*		0.000	*		.003	*		.002	*	
MG	2.674	*		2.649	*		2.666	*		2.557	*		2.649	*		2.595	*		2.629	*		2.586	*	
FE	4.302	*		4.326	*		4.359	*		4.366	*		4.524	*		4.460	*		4.444	*		4.491	*	
MN	.006	*		.005	*		.006	*		.010	*		.008	*		.001	*		.009	*		.008	*	
NA	.032	*		.033	*		0.000	*		.032	*		.048	*		.030	*		.030	*		.015	*	
CA	.010	*		.015	*		.013	*		.006	*		.018	*		.015	*		.013	*		.018	*	
K	0.000	7.040		0.000	7.045		0.000	7.044		0.000	7.029		0.000	7.247		0.000	7.101		0.000	7.128		0.000	7.120	
O	23.000	*		23.000	*		23.000	*		23.000	*		23.000	*		23.000	*		23.000	*		23.000	*	
	F/M	1.611			1.635			1.638			1.719			1.711			1.719			1.694			1.740		
	F/FM	.617			.620			.621			.632			.631			.632			.629			.635		

1 SAMPLE CO-6 GRUNERITE
2 ANOTHER GRAIN
3 ANOTHER SPOT SAME GRAIN
4
5
6 ANOTHER GRAIN
7
8

SUPER RECAL — AMPHIBOLE SAMPLES

	9	10	11
SIO2	51.59	52.22	50.97
TIO2	.01	.02	-.00
A2O3	.50	.54	.47
FEO	34.47	34.98	33.95
MNO	.05	.07	.03
MGO	11.51	11.71	11.31
CAO	.08	.10	.06
NA2O	.09	.14	.05
K2O	0.00	0.00	0.00
SUM	98.31	99.79	96.83

SI	7.896	*		7.879	*		7.913	*	
AL	.091	7.986		.096	7.974		.086	7.999	
AL	0.000	*		0.000	*		0.000	*	
TI	.001	*		.002	*		-.001	*	
MG	2.628	*		2.634	*		2.616	*	
FE	4.411	*		4.414	*		4.408	*	
MN	.007	*		.009	*		.004	*	
NA	.027	*		.040	*		.014	*	
CA	.014	*		.017	*		.010	*	
K	0.000	7.085		0.000	7.117		0.000	7.053	
O	23.000	*		23.000	*		23.000	*	
	F/M	1.683			1.679			1.686	
	F/FM	.627			.627			.628	

9 AVERAGE
10 AVERAGE PLUS SIGMA
11 AVERAGE MINUS SIGMA

SUPER RECAL — AMPHIBOLE SAMPLES

	1	2	3	4	5	6
SIO2	52.30	52.54	52.21	52.35	52.49	52.21
TIO2	.06	0.00	.01	.02	.05	-.00
A2O3	.31	.27	.90	.49	.78	.21
FEO	31.73	31.16	31.16	31.35	31.62	31.08
MNO	0.00	0.00	0.00	0.00	0.00	0.00
MGO	12.59	12.14	12.00	12.24	12.50	11.99
CAO	.49	.49	.48	.49	.49	.48
NA2O	0.00	0.00	0.00	0.00	0.00	0.00
K2O	0.00	0.00	0.00	0.00	0.00	0.00
SUM	97.48	96.60	96.76	96.95	97.93	95.97

SI	7.963	*	8.043	*	7.980	*	7.995	*	7.941	*	8.051	*
AL	.037	8.000	0.000	8.043	.020	8.000	.005	8.000	.059	8.000	0.000	8.051
AL	.018	*	.049	*	.142	*	.084	*	.080	*	.037	*
TI	.007	*	0.000	*	.001	*	.003	*	.006	*	-.000	*
MG	2.857	*	2.770	*	2.734	*	2.787	*	2.818	*	2.756	*
FE	4.040	*	3.989	*	3.983	*	4.004	*	4.000	*	4.008	*
MN	0.000	*	0.000	*	0.000	*	0.000	*	0.000	*	0.000	*
NA	0.000	*	0.000	*	0.000	*	0.000	*	0.000	*	0.000	*
CA	.080	*	.080	*	.079	*	.080	*	.080	*	.080	*
K	0.000	7.002	0.000	6.889	0.000	6.938	0.000	6.958	0.000	6.984	0.000	6.881
O	23.000	*	23.000	*	23.000	*	23.000	*	23.000	*	23.000	*
F/M		1.414		1.440		1.457		1.437		1.420		1.454
F/FM		.586		.590		.593		.590		.587		.593

1 SAMPLE D-57-1 GRUNERITE
2
3

4 AVERAGE
5 AVERAGE PLUS SIGMA
6 AVERAGE MINUS SIGMA

SUPER RECAL — AMPHIBOLE SAMPLES

	1	2	3	4	5	6	7
SIO2	50.95	50.99	51.36	51.05	51.09	51.25	50.93
TIO2	.07	.02	.05	.10	.06	.09	.03
A2O3	.09	.25	.23	.21	.21	.28	.14
FEO	36.44	36.17	35.36	35.36	35.83	36.31	35.35
MNO	.26	.23	.14	.14	.19	.25	.14
MGO	9.41	9.55	10.06	9.83	9.71	9.96	9.46
CAO	.23	.34	.32	.25	.29	.33	.24
NA2O	.02	0.00	0.00	0.00	.01	.01	-.00
K2O	.02	0.00	0.00	0.00	.01	.01	-.00
SUM	97.49	97.55	97.55	96.96	97.39	98.50	96.28

SI	7.963	*	7.951	*	7.966	*	7.973	*	7.963	*	7.915	*
AL	.017	7.979	.046	7.997	.034	8.000	.027	8.000	.037	8.000	.050	7.955
AL	0.000	*	0.000	*	.014	*	.015	*	.002	*	0.000	*
TI	.008	*	.002	*	.006	*	.012	*	.007	*	.010	*
MG	2.192	*	2.220	*	2.326	*	2.288	*	2.257	*	2.294	*
FE	4.763	*	4.717	*	4.587	*	4.618	*	4.571	*	4.690	*
MN	.034	*	.030	*	.018	*	.019	*	.025	*	.032	*
NA	.006	*	0.000	*	0.000	*	0.000	*	.002	*	.004	*
CA	.079	*	.057	*	.053	*	.042	*	.048	*	.059	*
K	.004	7.046	0.000	7.026	0.000	7.004	0.000	6.994	.001	7.012	.003	7.088
O	23.000	*	23.000	*	23.000	*	23.000	*	23.000	*	23.000	*
F/M		2.188		2.139		1.980		2.026		2.081		2.059
F/FM		.686		.681		.664		.670		.675		.673

SI	8.013	*				
AL	0.000	8.013				
AL	.026	*				
TI	.000	*				
MG	2.219	*				
FE	4.652	*				
MN	.019	*				
NA	-.001	*				
CA	.040	*				
K	-.001	6.957				
O	23.000	*				
F/M		2.105				
F/FM		.678				

1 SAMPLE D 58-1 GRUNERITE
2
3 ANOTHER
4

5 AVERAGE
6 AVERAGE PLUS SIGMA
7 AVERAGE MINUS SIGMA

SUPER PECAL — AMPHIBOLE SAMPLES

	1	2	3	4	5	6
SIO2	51.02	51.53	50.82	51.12	51.42	50.82
TIO2	.10	.07	.05	.07	.09	.05
A2O3	.24	.27	.21	.24	.26	.22
FEO	39.12	38.75	39.34	39.07	39.31	38.83
MNO	.86	.73	.73	.77	.83	.71
MGO	7.11	6.89	6.93	6.98	7.07	6.88
CAO	.32	.27	.30	.30	.32	.28
NA2O	0.00	.08	.08	.05	.09	.02
K2O	.02	.01	0.00	.01	.02	.00
SUM	98.79	98.60	98.46	98.62	99.43	97.81

SI	7.982	*	8.046	*	7.988	*	8.005	*	7.990	*	8.020	*
AL	.018	8.000	0.000	8.046	.012	8.000	0.000	8.005	.010	8.000	0.000	8.020
AL	.026	*	.050	*	.027	*	.044	*	.039	*	.040	*
TI	.012	*	.008	*	.006	*	.009	*	.011	*	.006	*
MG	1.658	*	1.603	*	1.624	*	1.628	*	1.638	*	1.618	*
FE	5.118	*	5.060	*	5.171	*	5.116	*	5.109	*	5.124	*
MN	.114	*	.097	*	.097	*	.103	*	.110	*	.095	*
NA	0.000	*	.024	*	.024	*	.016	*	.027	*	.005	*
CA	.054	*	.045	*	.051	*	.050	*	.053	*	.047	*
K	.004	6.986	.002	6.889	0.000	6.999	.002	6.968	.004	6.990	.000	6.936
O	23.000	*	23.000	*	23.000	*	23.000	*	23.000	*	23.000	*
	F/M	3.156		3.216		3.245		3.205		3.186		3.225
	F/FM	.759		.763		.764		.762		.761		.763

1 SAMPLE D-58-2 GRUNERITE
2
3
4 AVERAGE
5 AVERAGE PLUS SIGMA
6 AVERAGE MINUS SIGMA

SUPER RECAL — AMPHIBOLE SAMPLES

	1	2	3	4	5	6
SIO2	50.71	51.57	52.18	51.49	52.09	50.88
TIO2	.04	.02	.07	.04	.06	.02
A203	.37	.20	.26	.28	.35	.21
FEO	35.41	35.76	35.18	35.45	35.69	35.21
MNO	.21	.22	.18	.20	.22	.19
MGO	9.95	9.87	10.08	9.94	9.99	9.89
CAO	.40	.31	.37	.36	.40	.32
NA20	0.00	0.00	.03	.01	.02	-.00
K20	0.00	0.00	0.00	0.00	0.00	0.00
SUM	97.09	97.95	98.27	97.77	98.82	96.72

SI	7.924	*	7.979	*	8.010	*	7.971	*	7.973	*	7.970	*
AL	.068	7.992	.021	8.000	0.000	8.010	.029	8.000	.027	8.000	.030	8.000
AL	0.000	*	.015	*	.047	*	.022	*	.036	*	.008	*
TI	.005	*	.002	*	.008	*	.005	*	.007	*	.003	*
MG	2.318	*	2.276	*	2.288	*	2.294	*	2.280	*	2.308	*
FE	4.628	*	4.627	*	4.516	*	4.590	*	4.568	*	4.612	*
MN	.028	*	.029	*	.023	*	.027	*	.029	*	.025	*
NA	0.000	*	0.000	*	.009	*	.003	*	.007	*	-.001	*
CA	.067	*	.051	*	.061	*	.060	*	.065	*	.054	*
K	0.000	7.045	0.000	7.001	0.000	6.953	0.000	7.000	0.000	6.992	0.000	7.008
O	23.000	*	23.000	*	23.000	*	23.000	*	23.000	*	23.000	*
	F/M	2.009		2.045		1.984		2.013		2.016		2.009
	F/FM	.668		.672		.665		.668		.668		.668

1 SAMPLE D-58-3 GRUNERITE
2
3

4 AVERAGE
5 AVERAGE PLUS SIGMA
6 AVERAGE MINUS SIGMA

SUPER RECAL AMPHIBOLE SAMPLES

	1	2	3	4	5	6	7	8
SIO2	52.75	52.75	53.33	53.39	53.42	53.41	51.91	53.39
TIO2	.03	.03	.01	.05	.04	.02	0.00	0.00
A203	.37	.50	.17	.54	.54	.66	1.05	.39
FEO	34.24	33.16	33.45	33.36	34.16	34.16	34.68	33.50
MNO	0.00	0.00	.01	0.00	0.00	0.00	.02	.03
MGO	10.51	10.89	10.50	9.97	10.13	9.98	9.75	10.44
CAO	.21	.19	.28	.15	.25	.19	.16	.27
NA2O	0.00	0.00	0.00	0.00	0.00	0.00	0.00	0.00
K2O	0.00	0.00	0.00	0.00	0.00	.04	.02	0.00
SUM	98.11	97.52	97.75	97.46	98.54	98.46	97.59	98.02

SI	8.049	*		8.056	*		8.128	*		8.147	*		8.095	*		8.098	*		7.991	*		8.113	*	
AL	0.000	8.049	*	0.000	8.056	*	0.000	8.128	*	0.000	8.147	*	0.000	8.095	*	0.000	8.098	*	.009	8.000	*	0.000	8.113	*
AL	.067		*	.098		*	.031		*	.097		*	.096		*	.118		*	.181		*	.076		*
TI	.003		*	.003		*	.001		*	.006		*	.005		*	.002		*	0.000		*	0.000		*
MG	2.390		*	2.479		*	2.385		*	2.268		*	2.288		*	2.255		*	2.237		*	2.365		*
FE	4.370		*	4.235		*	4.264		*	4.257		*	4.329		*	4.332		*	4.465		*	4.257		*
MN	0.000		*	0.000		*	.001		*	0.000		*	0.000		*	0.000		*	.003		*	.004		*
NA	0.000		*	0.000		*	0.000		*	0.000		*	0.000		*	0.000		*	0.000		*	0.000		*
CA	.034		*	.031		*	.046		*	.025		*	.041		*	.031		*	.026		*	.044		*
K	0.000	6.864	*	0.000	6.839	*	0.000	6.727	*	0.000	6.652	*	0.000	6.758	*	.008	6.746	*	.004	6.916	*	0.000	6.739	*
O	23.000		*	23.000		*	23.000		*	23.000		*	23.000		*	23.000		*	23.000		*	23.000		*
F/M		1.428			1.708			1.788			1.877			1.892			1.920			1.997			1.802	
F/FM		.646			.631			.641			.652			.654			.658			.666			.643	

1 SAMPLE A-22 GRUNERITE
2 GRUN SHEAF
3 AGAIN
4 AGAIN
5 ANOTHER GRAIN
6
7
8

SUPER RECAL AMPHIBOLE SAMPLES

	9	10	11	12	13
SIO2	51.42	50.94	52.67	53.55	51.79
TIO2	.05	.02	.03	.04	.01
A203	.50	.56	.53	.74	.31
FEO	35.50	35.42	34.16	34.95	33.37
MNO	.17	.14	.04	.10	-.02
MGO	10.02	10.65	10.28	10.63	9.94
CAO	.24	.31	.23	.28	.17
NA2O	0.00	0.00	0.00	0.00	0.00
K2O	0.00	0.00	.01	.02	-.01
SUM	97.90	98.04	97.94	100.31	95.57

SI	7.947	*		7.871	*		8.050	*		8.001	*		8.102	*		
AL	.053	8.000	*	.102	7.973	*	0.000	8.050	*	0.000	8.001	*	0.000	8.102	*	
AL	.038		*	0.000		*	.095		*	.131		*	.058		*	
TI	.006		*	.002		*	.003		*	.005		*	.001		*	
MG	2.308		*	2.453		*	2.343		*	2.367		*	2.317		*	
FE	4.588		*	4.577		*	4.367		*	4.367		*	4.366		*	
MN	.022		*	.018		*	.005		*	.012		*	-.003		*	
NA	0.000		*	0.000		*	0.000		*	0.000		*	0.000		*	
CA	.040		*	.051		*	.037		*	.044		*	.029		*	
K	0.000	7.002	*	0.000	7.102	*	.001	6.850	*	.000	6.930	*	-.001	6.766	*	
O	23.000		*	23.000		*	23.000		*	23.000		*	23.000		*	
F/M		1.997			1.874			1.866			1.850			1.883		
F/FM		.666			.652			.651			.649			.653		

9 SAMPLE A22 GRUNERITE
10
11 AVERAGE
12 AVERAGE PLUS SIGMA
13 AVERAGE MINUS SIGMA

SUPER FECAL AMPHIBOLE SAMPLES

	1		2		3		4		5		6		7		8	
SIO2	46.16		46.27		45.84		45.53		47.20		46.94		47.91		46.86	
TIO2	.38		.37		.45		.39		.45		.45		.38		.35	
A203	8.47		8.34		8.82		8.66		8.81		8.92		8.15		8.46	
FEO	16.82		16.83		16.64		17.12		17.23		17.54		16.64		16.25	
MNO	.34		.45		.36		.39		.46		.45		.41		.35	
MGO	12.50		12.26		12.44		12.06		12.05		11.60		12.76		12.12	
CAO	10.65		10.86		10.84		10.55		10.43		10.97		10.52		10.74	
NA20	2.00		1.67		2.15		1.96		1.72		1.64		1.74		1.82	
K20	.08		.06		.13		.11		.11		.08		.09		.09	
SUM	97.40		97.11		97.67		96.77		98.46		98.59		98.60		97.04	
SI	6.883	*	6.917	*	6.824	*	6.851	*	6.944	*	6.916	*	7.014	*	6.977	*
AL	1.117	8.000	1.083	8.000	1.176	8.000	1.149	8.000	1.056	8.000	1.082	8.000	.986	8.000	1.023	8.000
AL	.371	*	.386	*	.372	*	.386	*	.472	*	.467	*	.420	*	.461	*
TI	.043	*	.042	*	.050	*	.044	*	.050	*	.050	*	.042	*	.039	*
MG	2.778	*	2.732	*	2.760	*	2.705	*	2.643	*	2.548	*	2.784	*	2.699	*
FE	2.097	*	2.104	*	2.072	*	2.154	*	2.120	*	2.162	*	2.037	*	2.023	*
MN	.043	*	.057	*	.045	*	.050	*	.057	*	.056	*	.051	*	.044	*
NA	.578	*	.484	*	.621	*	.572	*	.491	*	.469	*	.494	*	.525	*
CA	1.701	*	1.739	*	1.729	*	1.701	*	1.644	*	1.732	*	1.650	*	1.713	*
K	.015	7.627	.011	7.554	.025	7.674	.021	7.633	.021	7.497	.015	7.499	.017	7.496	.017	7.513
O	23.000	*	23.000	*	23.000	*	23.000	*	23.000	*	23.000	*	23.000	*	23.000	*
F/M		.770		.791		.767		.815		.824		.870		.750		.769
F/FM		.435		.442		.434		.449		.452		.465		.429		.435

1 SAMPLE P53 HBLE HALF
2 ANOTHER HBLE HALF
3 HBLE HALF
4
5 P53 ANOTHER COMPOSITE GRAIN HBLE
6 ANOTHER HBLE
7 HBLE
8 SAMPLE P 53 HBLE

SUPER FECAL AMPHIBOLE SAMPLES

	9		10		11		12		13		14		15	
SIO2	47.51		47.01		47.16		45.28		46.64		47.42		45.86	
TIO2	.48		.38		.32		.43		.40		.45		.36	
A203	8.80		8.47		8.11		9.57		8.63		9.01		8.25	
FEO	16.96		17.18		17.46		18.13		17.07		17.54		16.59	
MNO	.41		.45		.43		.36		.41		.45		.36	
MGO	11.73		11.55		11.50		10.45		11.92		12.50		11.33	
CAO	10.09		10.44		10.64		10.43		10.60		10.83		10.37	
NA20	1.92		1.93		2.02		2.54		1.93		2.16		1.69	
K20	.06		.07		.09		.11		.09		.11		.07	
SUM	97.96		97.48		97.73		97.30		97.68		100.48		94.88	
SI	7.003	*	6.992	*	7.013	*	6.812	*	6.929	*	6.864	*	6.999	*
AL	.997	8.000	1.008	8.000	.987	8.000	1.188	8.000	1.071	8.000	1.136	8.000	1.001	6.000
AL	.532	*	.477	*	.434	*	.509	*	.441	*	.401	*	.383	*
TI	.053	*	.043	*	.036	*	.049	*	.045	*	.049	*	.041	*
MG	2.577	*	2.561	*	2.549	*	2.343	*	2.639	*	2.698	*	2.578	*
FE	2.091	*	2.137	*	2.171	*	2.281	*	2.121	*	2.123	*	2.118	*
MN	.051	*	.057	*	.054	*	.046	*	.051	*	.055	*	.047	*
NA	.549	*	.567	*	.582	*	.741	*	.585	*	.607	*	.550	*
CA	1.594	*	1.664	*	1.695	*	1.681	*	1.687	*	1.679	*	1.699	*
K	.011	7.458	.013	7.507	.017	7.539	.021	7.671	.017	7.555	.020	7.632	.015	7.474
O	23.000	*	23.000	*	23.000	*	23.000	*	23.000	*	23.000	*	23.000	*
F/M		.831		.857		.873		.993		.823		.807		.840
F/FM		.454		.461		.466		.498		.451		.447		.456

9 HBLE
10 P53 HBLE HALF
11 PALE HBLE IN C W GREEN
12 GREEN HBLE IN CONTACT
13 AVERAGE
14 AVERAGE PLUS SIGMA
15 AVERAGE MINUS SIGMA

SUPER RECAL AMPHIBOLE SAMPLES

	1	2	3	4	5	6	7	8
SIO2	53.06	53.09	53.45	53.45	53.11	52.32	54.84	55.15
TIO2	0.00	0.00	0.00	0.00	.04	0.00	.04	0.00
A2O3	.46	1.00	.67	.29	.61	.61	.63	.65
FEO	23.53	23.46	22.52	23.58	23.47	23.58	23.81	23.82
MNO	1.18	1.10	1.22	1.13	1.14	1.18	1.13	1.27
MGO	17.82	17.70	18.32	17.59	17.85	17.55	17.51	17.61
CAO	.87	1.62	1.08	.77	.97	.90	1.05	.91
NA2O	.04	.18	.08	.04	.06	.07	.22	.15
K2O	0.00	.01	0.00	0.00	0.00	0.00	.01	0.00
SUM	96.96	98.15	97.34	96.85	97.25	96.21	99.24	99.56

SI	7.866	*		7.788	*		7.856	*		7.923	*		7.848	*		7.833	*		7.925	*		7.937	*	
AL	.080	7.947		.173	7.960		.116	7.972		.051	7.973		.106	7.954		.108	7.941		.075	8.000		.063	8.000	
AL	0.000	*		0.000	*		0.000	*		0.000	*		0.000	*		0.000	*		.032	*		.047	*	
TI	0.000	*		0.000	*		0.000	*		0.000	*		.004	*		0.000	*		.004	*		0.000	*	
MG	3.938	*		3.870	*		4.013	*		3.886	*		3.931	*		3.916	*		3.771	*		3.778	*	
FE	2.917	*		2.878	*		2.768	*		2.923	*		2.900	*		2.952	*		2.877	*		2.867	*	
MN	.148	*		.137	*		.152	*		.142	*		.143	*		.150	*		.138	*		.155	*	
NA	.011	*		.051	*		.023	*		.011	*		.017	*		.020	*		.062	*		.042	*	
CA	.138	*		.255	*		.170	*		.122	*		.154	*		.144	*		.163	*		.140	*	
K	0.000	7.153		.002	7.192		0.000	7.126		0.000	7.085		0.000	7.149		0.000	7.183		.002	7.049		0.000	7.029	
O	23.000	*		23.000	*		23.000	*		23.000	*		23.000	*		23.000	*		23.000	*		23.000	*	
F/M		.778			.779			.728			.789			.774			.792				.800			.800	
F/FM		.438			.438			.421			.441			.436			.442				.444			.444	

1 SAMPLE P 53 CUMM
2 CUMM HALF
3 ANOTHER CUMM HALF
4 ANOTHER CUMM HALF
5
6 CUMM ALONE
7 CUMM SAME GRAIN
8 CUMM ALONE

SUPER RECAL AMPHIBOLE SAMPLES

	9	10	11	12	13	14
SIO2	54.91	54.73	54.58	53.88	54.81	52.95
TIO2	0.00	0.00	.02	.01	.02	-.01
A2O3	.33	.64	1.01	.63	.84	.41
FEO	23.70	23.99	23.32	23.53	23.89	23.16
MNO	1.24	1.15	1.13	1.17	1.22	1.12
MGO	17.97	17.81	17.61	17.75	17.97	17.53
CAO	.70	1.03	1.42	1.03	1.29	.77
NA2O	.10	.18	.14	.11	.17	.05
K2O	0.00	0.00	0.00	.00	.01	-.00
SUM	98.95	99.53	99.23	98.11	100.23	95.99

SI	7.955	*		7.894	*		7.878	*		7.882	*		7.854	*		7.911	*	
AL	.045	8.000		.106	8.000		.122	8.000		.108	7.990		.143	7.997		.072	7.984	
AL	.011	*		.003	*		.050	*		0.000	*		0.000	*		0.000	*	
TI	0.000	*		0.000	*		.002	*		.001	*		.003	*		-.001	*	
MG	3.859	*		3.829	*		3.789	*		3.870	*		3.838	*		3.904	*	
FE	2.871	*		2.894	*		2.815	*		2.878	*		2.863	*		2.894	*	
MN	.152	*		.141	*		.138	*		.145	*		.148	*		.142	*	
NA	.028	*		.050	*		.039	*		.032	*		.048	*		.016	*	
CA	.109	*		.159	*		.220	*		.161	*		.198	*		.123	*	
K	0.000	7.031		0.000	7.076		0.000	7.053		.000	7.088		.001	7.099		-.000	7.077	
O	23.000	*		23.000	*		23.000	*		23.000	*		23.000	*		23.000	*	
F/M		.794			.792			.779			.781			.785			.777	
F/FM		.439			.442			.438			.439			.440			.437	

9 CUMM IN CONTACT
10 CUMM AGAIN
11 AGAIN
12 AVERAGE
13 AVERAGE PLUS SIGMA
14 AVERAGE MINUS SIGMA

SUPER RECAL — AMPHIBOLE SAMPLES

	1	2	3	4	5	6
SIO2	53.50	52.91	51.67	52.69	53.46	51.93
TIO2	0.00	0.00	.10	.03	.08	-.01
A203	1.50	1.52	3.40	2.14	3.03	1.25
FEO	11.66	12.44	13.47	12.52	13.26	11.78
MNO	1.50	1.63	1.57	1.57	1.62	1.51
MGO	16.43	15.75	14.87	15.68	16.32	15.04
CAO	12.39	12.48	12.12	12.33	12.48	12.18
NA20	.06	.14	.43	.21	.37	.05
K20	.04	.04	.09	.06	.08	.03
SUM	97.08	96.91	97.72	97.24	100.71	93.77

SI	7.762	*	7.736	*	7.535	*	7.678	*	7.544	*	7.821	*
AL	.238	8.000	.262	7.998	.465	8.000	.322	8.000	.456	8.000	.179	8.000
AL	.019	*	0.000	*	.119	*	.045	*	.048	*	.042	*
TI	0.000	*	0.000	*	.011	*	.004	*	.009	*	-.002	*
MG	3.553	*	3.433	*	3.232	*	3.406	*	3.433	*	3.377	*
FE	1.415	*	1.521	*	1.643	*	1.526	*	1.566	*	1.484	*
MN	.184	*	.202	*	.194	*	.193	*	.194	*	.193	*
NA	.017	*	.040	*	.122	*	.059	*	.101	*	.019	*
CA	1.926	*	1.955	*	1.894	*	1.925	*	1.888	*	1.965	*
K	.007	7.121	.007	7.158	.017	7.231	.011	7.169	.014	7.253	.006	7.081
O	23.000	*	23.000	*	23.000	*	23.000	*	23.000	*	23.000	*
F/M		.450		.502		.568		.505		.512		.497
F/FM		.310		.334		.362		.335		.339		.332

1 SAMPLE P 51 HBLE
2 OTHER
3 OTHER

4 AVERAGE
5 AVERAGE PLUS SIGMA
6 AVERAGE MINUS SIGMA

SUPER RECAL AMPHIBOLE SAMPLES

	1	2	3	4	5	6	7	8
SIO2	42.29	43.92	43.28	43.48	43.53	43.30	43.85	42.75
TIO2	.47	.38	.43	.49	.40	.43	.48	.39
A2O3	13.08	11.77	11.94	12.55	11.59	12.19	12.74	11.63
FEO	20.55	19.54	19.12	19.93	19.23	19.67	20.19	19.15
MNO	.29	.27	.34	.29	.22	.28	.32	.24
MGO	8.46	9.46	9.20	8.37	9.12	8.92	9.35	8.49
CAO	10.56	10.67	10.73	10.71	10.63	10.66	10.72	10.60
NA2O	2.22	1.56	1.69	2.03	1.66	1.83	2.08	1.58
K2O	.34	.29	.29	.36	.26	.31	.34	.27
SUM	98.26	97.86	97.02	98.21	96.64	97.60	100.07	95.12

SI	6.393	*	6.601	*	6.565	*	6.538	*	6.622	*	6.544	*	6.475	*	6.617	*
AL	1.607	8.000	1.399	8.000	1.435	8.000	1.462	8.000	1.378	8.000	1.456	8.000	1.525	8.000	1.383	8.000
AL	.723	*	.686	*	.699	*	.762	*	.700	*	.714	*	.691	*	.738	*
TI	.053	*	.043	*	.049	*	.055	*	.046	*	.049	*	.053	*	.046	*
MG	1.906	*	2.119	*	2.080	*	1.876	*	2.066	*	2.010	*	2.098	*	1.959	*
FE	2.598	*	2.456	*	2.425	*	2.506	*	2.447	*	2.487	*	2.494	*	2.479	*
MN	.037	*	.034	*	.044	*	.037	*	.028	*	.036	*	.040	*	.032	*
NA	.651	*	.455	*	.497	*	.592	*	.490	*	.537	*	.596	*	.475	*
CA	1.710	*	1.718	*	1.744	*	1.726	*	1.733	*	1.726	*	1.696	*	1.758	*
K	.066	7.745	.056	7.567	.056	7.594	.069	7.624	.050	7.562	.059	7.618	.065	7.694	.054	7.540
O	23.000	*	23.000	*	23.000	*	23.000	*	23.000	*	23.000	*	23.000	*	23.000	*
	F/M	1.382		1.175		1.187		1.356		1.197		1.255		1.231		1.282
	F/FM	.580		.540		.543		.575		.545		.557		.552		.562

1 SAMPLE P 137 HBLE
2 ANOTHER
3
4
5
6 AVERAGE
7 AVERAGE PLUS SIGMA
8 AVERAGE MINUS SIGMA

SUPER RECAL — AMPHIBOLE SAMPLES

	1		2		3		4		5		6		7		8	
SIO2	53.85		51.91		53.54		52.07		54.19		54.52		53.35		54.35	
TIO2	.02		.09		.04		.10		.04		.02		.05		.08	
A2O3	2.18		3.57		2.11		4.41		1.96		2.04		2.71		3.65	
FEO	11.30		12.15		11.54		12.93		10.89		11.08		11.65		12.35	
MNO	.51		.58		.57		.64		.57		.52		.57		.61	
MGO	17.21		15.80		16.63		15.21		17.08		17.09		16.50		17.25	
CAO	12.64		12.48		12.70		12.34		12.70		13.08		12.66		12.89	
NA2O	.16		.20		.17		.34		.18		.13		.20		.26	
K2O	0.00		.01		0.00		.03		0.00		0.00		.01		.02	
SUM	97.87		96.79		97.30		96.07		97.61		96.48		97.69		101.46	
ST	7.702	*	7.555	*	7.717	*	7.500	*	7.754	*	7.741	*	7.662	*	7.535	*
AL	.298	8.000	.445	8.000	.283	8.000	.500	8.000	.246	8.000	.259	8.000	.338	8.000	.465	8.000
AL	.069	*	.167	*	.076	*	.248	*	.085	*	.082	*	.121	*	.131	*
TI	.002	*	.010	*	.004	*	.011	*	.004	*	.002	*	.006	*	.009	*
MG	3.669	*	3.427	*	3.573	*	3.265	*	3.643	*	3.617	*	3.533	*	3.565	*
FE	1.352	*	1.479	*	1.391	*	1.557	*	1.303	*	1.316	*	1.399	*	1.431	*
MN	.062	*	.071	*	.070	*	.078	*	.069	*	.063	*	.069	*	.071	*
NA	.044	*	.056	*	.048	*	.095	*	.050	*	.036	*	.055	*	.071	*
CA	1.937	*	1.946	*	1.961	*	1.904	*	1.947	*	1.990	*	1.948	*	1.914	*
K	0.000	7.134	.002	7.158	0.000	7.123	.006	7.165	0.000	7.101	0.000	7.104	.001	7.131	.003	7.195
O	23.000	*	23.000	*	23.000	*	23.000	*	23.000	*	23.000	*	23.000	*	23.000	*
F/M		.385		.452		.409		.501		.377		.381		.415		.422
F/FM		.278		.311		.290		.334		.274		.275		.294		.297

1 SAMPLE P 66 PALE GREEN HBLE
2
3
4 AMPH

5 PALE EDGE OF THIS GRAIN
6 ASSOC GRAIN
7 AVERAGE
8 AVERAGE PLUS SIGMA

SUPER RECAL AMPHIBOLE SAMPLES

	1	2	3	4	5	6	7	8
SIO2	43.98	44.06	44.00	43.25	42.16	41.38	41.84	41.25
TIO2	.44	.48	.43	.56	.61	.65	.45	.61
A2O3	13.52	13.39	13.59	14.68	14.04	14.91	15.53	14.63
FEO	16.83	16.95	16.59	16.68	16.66	16.73	17.16	16.60
MNO	.27	.29	.28	.31	.32	.32	.35	.33
MGO	10.97	10.68	10.82	10.18	10.13	9.70	9.51	9.49
CAO	10.63	10.82	10.59	10.48	10.77	10.99	10.80	10.69
NA2O	2.14	1.94	2.30	2.20	2.25	2.21	2.30	2.38
K2O	.19	.17	.17	.17	.16	.15	.22	.17
SUM	98.97	98.78	98.77	98.51	97.10	97.04	98.16	96.15

SI	6.453	*		6.478	*		6.462	*		6.370	*		6.330	*		6.227	*		6.225	*		6.264	*	
AL	1.547	8.000		1.522	8.000		1.538	8.000		1.630	8.000		1.670	8.000		1.773	8.000		1.775	8.000		1.736	8.000	
AL	.790	*		.798	*		.814	*		.918	*		.814	*		.871	*		.948	*		.882	*	
TI	.049	*		.053	*		.047	*		.062	*		.069	*		.074	*		.050	*		.070	*	
MG	2.399	*		2.340	*		2.369	*		2.235	*		2.267	*		2.176	*		2.109	*		2.148	*	
FE	2.065	*		2.084	*		2.038	*		2.055	*		2.092	*		2.106	*		2.135	*		2.109	*	
MN	.034	*		.036	*		.035	*		.039	*		.041	*		.041	*		.044	*		.042	*	
NA	.609	*		.553	*		.655	*		.628	*		.655	*		.645	*		.663	*		.701	*	
CA	1.671	*		1.704	*		1.666	*		1.654	*		1.733	*		1.772	*		1.722	*		1.739	*	
K	.036	7.651		.032	7.600		.032	7.656		.032	7.622		.031	7.701		.029	7.713		.042	7.714		.033	7.723	
O	23.000	*		23.000	*		23.000	*		23.000	*		23.000	*		23.000	*		23.000	*		23.000	*	
F/M		.875			.906			.875			.937			.941			.986				1.033			1.001	
F/FM		.467			.475			.467			.484			.485			.497				.508			.500	

1 SAMPLE P 46 HBLE
2
3
4

5 P 46 HBLE
6
7
8

SUPER RECAL AMPHIBOLE SAMPLES

	9	10	11
SIO2	42.74	43.88	41.60
TIO2	.53	.61	.45
A2O3	14.29	15.01	13.57
FEO	16.78	16.96	16.59
MNO	.31	.33	.28
MGO	10.19	10.74	9.63
CAO	10.72	10.57	10.57
NA2O	2.22	2.34	2.09
K2O	.18	.20	.16
SUM	97.93	100.93	94.94

SI	6.352	*		6.319	*		6.388	*	
AL	1.648	8.000		1.681	8.000		1.612	8.000	
AL	.856	*		.865	*		.843	*	
TI	.059	*		.066	*		.051	*	
MG	2.256	*		2.305	*		2.205	*	
FE	2.085	*		2.042	*		2.130	*	
MN	.039	*		.041	*		.037	*	
NA	.638	*		.653	*		.622	*	
CA	1.707	*		1.677	*		1.739	*	
K	.033	7.672		.036	7.685		.030	7.658	
O	23.000	*		23.000	*		23.000	*	
F/M		.941			.904			.983	
F/FM		.485			.475			.496	

9 AVERAGE
10 AVERAGE PLUS SIGMA

11 AVERAGE MINUS SIGMA

SUPER RECAL — AMPHIBOLE SAMPLES

	1		2		3		4		5		6		7		8	
SIO2	40.26		39.96		40.21		40.51		40.86		40.12		40.32		40.61	
TIO2	.23		.25		.26		.23		.35		.28		.27		.31	
A2O3	17.41		17.39		17.87		17.39		16.34		17.04		17.24		17.71	
FEO	17.56		18.21		17.43		17.87		18.21		18.31		17.93		18.27	
MNO	.64		.50		.52		.41		.39		.42		.48		.57	
MGO	7.94		7.77		7.82		7.79		8.14		7.62		7.85		8.01	
CAO	11.09		11.42		11.07		11.66		11.13		11.38		11.29		11.51	
NA2O	1.79		1.96		1.29		1.64		1.88		1.72		1.71		1.93	
K2O	.39		.40		.39		.40		.36		.39		.39		.40	
SUM	97.31		97.86		96.86		97.90		97.66		97.28		97.48		99.31	
SI	6.069	*	6.020	*	6.067	*	6.076	*	6.150	*	6.074	*	6.076	*	6.021	*
AL	1.931	8.000	1.980	8.000	1.933	8.000	1.924	8.000	1.850	8.000	1.926	8.000	1.924	8.000	1.979	8.000
AL	1.161	*	1.107	*	1.244	*	1.149	*	1.048	*	1.114	*	1.137	*	1.114	*
TI	.026	*	.028	*	.029	*	.026	*	.040	*	.032	*	.030	*	.034	*
MG	1.784	*	1.745	*	1.759	*	1.741	*	1.826	*	1.719	*	1.762	*	1.769	*
FE	2.214	*	2.294	*	2.199	*	2.241	*	2.292	*	2.318	*	2.260	*	2.265	*
MN	.082	*	.064	*	.066	*	.052	*	.050	*	.054	*	.061	*	.071	*
NA	.523	*	.572	*	.377	*	.477	*	.349	*	.505	*	.501	*	.554	*
CA	1.791	*	1.843	*	1.790	*	1.874	*	1.795	*	1.846	*	1.823	*	1.828	*
K	.075	7.656	.077	7.731	.075	7.540	.077	7.637	.069	7.669	.075	7.663	.075	7.6-9	.076	7.712
O	23.000	*	23.000	*	23.000	*	23.000	*	23.000	*	23.000	*	23.000	*	23.000	*
F/M		1.287		1.352		1.288		1.317		1.282		1.380		1.317		1.320
F/FM		.563		.575		.563		.568		.562		.580		.568		.569

1 SAMPLE P27A AMPH AT CENTRE
2 EDGE
3 ANOTHER CENTRAL
4 EDGE
5 BASAL SECTION CENTRAL
6 EDGE
7 AVERAGE
8 AVERAGE PLUS SIGMA

SUPER PECAL

AMPHIBOLE SAMPLES

	1	2	3	4	5	6	7	8
SIO2	40.77	40.65	40.94	41.91	41.18	41.03	40.82	41.04
TIO2	.26	.37	.06	.55	.09	.30	.15	.25
A2O3	16.32	16.86	16.24	14.27	17.16	16.80	16.68	16.33
FEO	17.61	18.06	18.31	18.61	18.19	17.65	18.04	18.07
MNO	.52	.75	.41	.74	.67	.51	.55	.59
MGO	7.96	8.14	7.73	8.85	7.92	8.27	7.89	8.11
CAO	10.95	10.58	11.12	11.10	10.86	10.98	11.18	10.97
NA2O	1.69	1.66	1.47	.95	2.10	1.90	1.88	1.66
K2O	.36	.32	.42	.34	.32	.33	.33	.35
SUM	96.44	97.39	96.70	97.32	98.49	97.77	97.52	97.36

SI	6.193	*	6.123	*	6.216	*	6.330	*	6.138	*	6.146	*	6.149	*	6.185	*
AL	1.807	8.000	1.877	8.000	1.784	8.000	1.670	8.000	1.862	8.000	1.854	8.000	1.851	8.000	1.815	8.000
AL	1.114	*	1.116	*	1.122	*	.869	*	1.153	*	1.111	*	1.110	*	1.069	*
TI	.030	*	.042	*	.007	*	.062	*	.010	*	.034	*	.017	*	.029	*
MG	1.802	*	1.928	*	1.749	*	1.992	*	1.760	*	1.846	*	1.772	*	1.821	*
FE	2.237	*	2.275	*	2.325	*	2.350	*	2.268	*	2.211	*	2.273	*	2.277	*
MN	.067	*	.096	*	.053	*	.095	*	.085	*	.065	*	.070	*	.076	*
NA	.498	*	.485	*	.433	*	.278	*	.607	*	.552	*	.549	*	.486	*
CA	1.782	*	1.708	*	1.809	*	1.796	*	1.734	*	1.762	*	1.804	*	1.771	*
K	.070	7.599	.061	7.610	.081	7.579	.065	7.509	.061	7.677	.063	7.644	.063	7.656	.066	7.611
O	23.000	*	23.000	*	23.000	*	23.000	*	23.000	*	23.000	*	23.000	*	23.000	*
F/M		1.278		1.297		1.359		1.227		1.337		1.233		1.322		1.292
F/FM		.561		.565		.576		.551		.572		.552		.569		.564

1 SAMPLE P278 GREEN HBLE
2 ANOTHER GRAIN CENTRAL
3 SAME GRAIN AT END
4 ANOTHER LARGE GRAIN CENTRAL
5 AT EDGE
6 ANOTHER GRAIN CENTRAL
7 AT EDGE
8 AVERAGE

SUPER RECAL — AMPHIBOLE SAMPLES

	1	2	3	4	5
SIO2	54.95	53.99	54.47	54.95	53.99
TIO2	0.00	0.00	0.00	0.00	0.00
A2O3	.59	.85	.72	.85	.59
FEO	22.65	22.33	22.49	22.65	22.33
MNO	1.29	1.28	1.29	1.29	1.28
MGO	18.57	18.44	18.51	18.57	18.44
CAO	.51	.55	.53	.55	.51
NA2O	0.00	0.00	0.00	0.00	0.00
K2O	0.00	.02	.01	.02	.00
SUM	98.56	97.46	98.01	98.88	97.14

SI	7.939	*		7.893	*		7.916	*		7.913	*		7.919	*	
AL	.061	8.000		.107	8.000		.084	8.000		.087	8.000		.081	8.000	
AL	.039	*		.039	*		.039	*		.057	*		.021	*	
TI	0.000	*		0.000	*		0.000	*		0.000	*		0.000	*	
MG	3.999	*		4.018	*		4.008	*		3.986	*		4.031	*	
FE	2.737	*		2.730	*		2.733	*		2.728	*		2.739	*	
MN	.158	*		.158	*		.158	*		.157	*		.159	*	
NA	0.000	*		0.000	*		0.000	*		0.000	*		0.000	*	
CA	.079	*		.086	*		.083	*		.085	*		.080	*	
K	0.000	7.011		.004	7.036		.002	7.023		.004	7.017		.000	7.030	
O	23.000	*		23.000	*		23.000	*		23.000	*		23.000	*	
	F/M	.724			.719			.721			.724			.719	
	F/FM	.420			.418			.419			.420			.418	

1 SAMPLE A-191-8 CUMM
2 OTHER CLEAR
3 AVERAGE
4 AVERAGE PLUS SIGMA
5 AVERAGE MINUS SIGMA

SUPER RECAL — AMPHIBOLE SAMPLES

	1	2	3	4	5	6	7
SIO2	44.46	43.86	44.41	43.07	43.95	44.51	43.39
TIO2	.33	.28	.32	.34	.32	.34	.29
A203	12.77	14.44	13.20	14.54	13.74	14.51	12.97
FEO	16.95	16.68	16.68	17.30	16.90	17.16	16.85
MNO	.32	.38	.33	.37	.35	.38	.32
MGO	10.70	10.34	10.63	9.83	10.38	10.72	10.03
CAO	11.00	10.62	10.91	10.74	10.82	10.96	10.87
NA20	1.80	1.90	1.96	1.91	1.89	1.95	1.83
K20	.14	.18	.09	.17	.15	.18	.11
SUM	98.47	98.68	98.53	98.27	98.49	100.70	96.27

SI	6.555	*	6.438	*	6.533	*	6.380	*	6.476	*	6.415	*	6.540	*
AL	1.445	8.000	1.562	8.000	1.467	8.000	1.620	8.000	1.524	8.000	1.585	8.000	1.460	8.000
AL	.773	*	.936	*	.821	*	.918	*	.862	*	.879	*	.844	*
TI	.037	*	.031	*	.035	*	.038	*	.035	*	.037	*	.033	*
MG	2.351	*	2.262	*	2.331	*	2.170	*	2.279	*	2.302	*	2.254	*
FE	2.090	*	2.048	*	2.052	*	2.143	*	2.083	*	2.068	*	2.099	*
MN	.040	*	.047	*	.041	*	.046	*	.044	*	.046	*	.041	*
NA	.514	*	.541	*	.559	*	.549	*	.541	*	.545	*	.536	*
CA	1.738	*	1.670	*	1.719	*	1.705	*	1.708	*	1.693	*	1.723	*
K	.026	7.569	.034	7.568	.017	7.575	.032	7.602	.027	7.578	.033	7.604	.021	7.552
O	23.000	*	23.000	*	23.000	*	23.000	*	23.000	*	23.000	*	23.000	*
	F/M	.906		.926		.898		1.009		.933		.918		.949
	F/FM	.475		.481		.473		.502		.483		.479		.487

1 SAMPLE A-191-8 COEXIST HBLE
2 COEXIST HBLE
3 ANOTHER AGAIN
4 ANOTHER HBLE

5 AVERAGE
6 AVERAGE PLUS SIGMA
7 AVERAGE MINUS SIGMA

SUPER RECAL AMPHIBOLE SAMPLES

	1	2	3	4	5	6	7
SIO2	43.70	44.28	43.74	43.62	43.84	44.10	43.57
TIO2	.28	.32	.31	.29	.30	.32	.28
A2O3	14.36	13.40	14.08	13.41	13.81	14.23	13.39
FEO	15.95	16.38	15.67	16.60	16.15	16.51	15.79
MNO	.12	.12	.12	.12	.12	.12	.12
MGO	10.85	11.39	10.72	10.98	10.99	11.24	10.73
CAO	11.17	10.36	11.04	9.88	10.61	11.14	10.09
NA2O	1.80	1.66	1.44	1.87	1.69	1.86	1.53
K2O	.16	.14	.16	.21	.17	.19	.14
SUM	98.39	98.05	97.28	96.98	97.67	99.70	95.65

SI	6.417	*	6.516	*	6.476	*	6.503	*	6.478	*	6.405	*	6.553	*
AL	1.583	8.000	1.484	8.000	1.524	8.000	1.497	8.000	1.522	8.000	1.595	8.000	1.447	8.000
AL	.901	*	.839	*	.932	*	.859	*	.883	*	.841	*	.926	*
TI	.031	*	.035	*	.035	*	.033	*	.033	*	.034	*	.032	*
MG	2.375	*	2.498	*	2.366	*	2.440	*	2.420	*	2.433	*	2.406	*
FE	1.959	*	2.016	*	1.940	*	2.078	*	1.996	*	2.006	*	1.989	*
MN	.015	*	.015	*	.015	*	.015	*	.015	*	.015	*	.015	*
NA	.512	*	.474	*	.413	*	.541	*	.485	*	.523	*	.446	*
CA	1.757	*	1.633	*	1.751	*	1.578	*	1.680	*	1.733	*	1.528	*
K	.030	7.580	.026	7.536	.030	7.482	.040	7.575	.032	7.543	.036	7.621	.027	7.463
O	23.000	*	23.000	*	23.000	*	23.000	*	23.000	*	23.000	*	23.000	*
	F/M	.831		.813		.827		.854		.831		.831		.832
	F/FM	.454		.448		.453		.461		.454		.454		.454

1 SAMPLE 188-5 HBLE AMD CUMM
2 ANOTHER HBLE
3 ANOTHER HBLE
4 RIMMED GRAIN

5 AVERAGE
6 AVERAGE PLUS SIGMA
7 AVERAGE MINUS SIGMA

SUPER RECAL — AMPHIBOLE SAMPLES

	1		2		3		4		5		6		7	
SIO2	54.29		52.14		50.74		49.95		51.78		53.43		50.13	
TIO2	0.00		.03		0.00		.04		.02		.04		.00	
A203	1.16		4.89		4.94		5.71		4.18		2.95		2.44	
FEO	22.04		21.76		22.14		21.64		21.95		22.10		21.79	
MNO	.23		.25		.21		.26		.24		.26		.22	
MGO	18.20		17.69		17.59		17.26		17.69		18.02		17.35	
CAO	.60		.48		.48		.46		.51		.56		.45	
NA20	.10		.45		.41		.64		.40		.59		.21	
K20	0.00		0.00		0.00		0.00		0.00		0.00		0.00	
SUM	96.62		97.69		96.51		96.16		96.74		100.94		92.99	
SI	7.947	*	7.557	*	7.479	*	7.394	*	7.595	*	7.486	*	7.719	*
AL	.053	8.000	.443	8.000	.521	8.000	.606	8.000	.405	8.000	.514	8.000	.285	8.000
AL	.147	*	.392	*	.337	*	.390	*	.316	*	.467	*	.150	*
TI	0.000	*	.003	*	0.000	*	.004	*	.002	*	.004	*	.000	*
MG	3.971	*	3.821	*	3.865	*	3.808	*	3.866	*	3.764	*	3.976	*
FE	2.698	*	2.637	*	2.729	*	2.704	*	2.592	*	2.589	*	2.805	*
MN	.029	*	.031	*	.028	*	.033	*	.030	*	.030	*	.028	*
NA	.028	*	.126	*	.117	*	.184	*	.114	*	.161	*	.062	*
CA	.094	*	.076	*	.076	*	.073	*	.079	*	.084	*	.074	*
K	0.000	6.967	0.000	7.085	0.000	7.150	0.000	7.195	0.000	7.099	0.000	7.100	0.000	7.098
O	23.000	*	23.000	*	23.000	*	23.000	*	23.000	*	23.000	*	23.000	*
F/M		.687		.698		.713		.719		.704		.696		.712
F/FM		.407		.411		.416		.418		.413		.410		.416

1 CUMM RIM
2 ANOTHER
3 ANOTHER
4 CUMM AGAIN

5 AVERAGE
6 AVERAGE PLUS SIGMA
7 AVERAGE MINUS SIGMA

SUPER RECAL — AMPHIBOLE SAMPLES

	1	2	3	4	5	6	7	8
SIO2	50.46	50.71	53.66	54.46	54.17	52.69	54.43	50.95
TIO2	.04	.02	.04	0.00	0.00	.02	.04	.00
A2O3	4.74	4.64	.96	.64	1.02	2.40	4.27	.53
FEO	24.74	25.08	25.33	25.21	25.28	25.13	25.34	24.92
MNO	.30	.27	.24	.25	.22	.26	.28	.23
MGO	16.21	15.69	17.50	17.77	17.79	16.99	17.86	16.12
CAO	.33	.22	.34	.28	.20	.27	.33	.22
NA2O	.27	.57	0.00	0.00	0.00	.17	.39	-.06
K2O	0.00	.01	0.00	.01	.04	.01	.03	-.00
SUM	97.09	97.21	98.07	98.62	98.72	97.94	102.98	92.90

SI	7.484	*	7.523	*	7.865	*	7.921	*	7.874	*	7.735	*	7.574	*	7.915	*
AL	.516	8.000	.477	8.000	.135	8.000	.079	8.000	.126	8.000	.265	8.000	.426	8.000	.085	8.000
AL	.312	*	.334	*	.031	*	.030	*	.049	*	.150	*	.275	*	.011	*
TI	.004	*	.002	*	.004	*	0.000	*	0.000	*	.002	*	.004	*	.000	*
MG	3.583	*	3.469	*	3.823	*	3.852	*	3.854	*	3.718	*	3.705	*	3.732	*
FE	3.068	*	3.112	*	3.105	*	3.066	*	3.073	*	3.085	*	2.949	*	3.237	*
MN	.038	*	.034	*	.030	*	.031	*	.027	*	.032	*	.033	*	-.030	*
NA	.078	*	.164	*	0.000	*	0.000	*	0.000	*	.048	*	.106	*	-.018	*
CA	.052	*	.035	*	.053	*	.044	*	.031	*	.043	*	.049	*	-.036	*
K	0.000	7.136	.002	7.152	0.000	7.047	.002	7.025	.007	7.042	.002	7.080	.005	7.127	-.001	7.028
O	23.000	*	23.000	*	23.000	*	23.000	*	23.000	*	23.000	*	23.000	*	23.000	*
	F/M	.867		.907		.820		.804		.804		.838		.809		.875
	F/FM	.464		.476		.451		.446		.446		.456		.446		.467

1 SAMPLE A 190-4 CUMM AND GED
2
3 IMMED ADJ TO CHL LATH
4 RIM ON GEDFITE
5 MAIN GRAIN
6 AVERAGE
7 AVERAGE PLUS SIGMA
8 AVERAGE MINUS SIGMA

SUPER RECAL AMPHIBOLE SAMPLES

	1	2	3	4
SIO2	42.32	42.32	42.32	42.32
TIO2	.13	.13	.13	.13
A203	15.07	15.07	15.07	15.07
FEO	24.96	24.96	24.96	24.96
MNO	.42	.42	.42	.42
MGO	11.89	11.89	11.89	11.89
CAO	.33	.33	.33	.33
NA20	1.86	1.86	1.86	1.86
K20	0.00	0.00	0.00	0.00
SUM	96.98	96.98	96.98	96.98

SI	6.379	*	6.379	*	6.379	*	6.379	*
AL	1.621	8.000	1.621	8.000	1.621	8.000	1.621	8.000
AL	1.056	*	1.056	*	1.056	*	1.056	*
TI	.015	*	.015	*	.015	*	.015	*
MG	2.671	*	2.671	*	2.671	*	2.671	*
FE	3.146	*	3.146	*	3.146	*	3.146	*
MN	.054	*	.054	*	.054	*	.054	*
NA	.544	*	.544	*	.544	*	.544	*
CA	.053	*	.053	*	.053	*	.053	*
K	0.000	7.538	0.000	7.538	0.000	7.538	0.000	7.538
O	23.000	*	23.000	*	23.000	*	23.000	*
F/M		1.198		1.198		1.198		1.198
F/FM		.545		.545		.545		.545

1 SAMPLE A-190-4 GEDRITE
2 AVERAGE
3 AVERAGE PLUS SIGMA
4 AVERAGE MINUS SIGMA

SUPER RECAL — AMPHIBOLE SAMPLES

	1	2	3	4	5	6	7
SIO2	44.56	43.88	44.43	45.19	44.52	44.98	44.05
TIO2	.34	.40	.38	.37	.37	.39	.35
A2O3	11.99	12.58	13.08	11.91	12.39	12.87	11.91
FEO	17.35	17.86	17.55	17.31	17.52	17.74	17.30
MNO	.39	.49	.50	.50	.47	.52	.42
MGO	10.48	10.02	9.98	10.48	10.24	10.48	10.00
CAO	10.55	9.83	10.09	10.62	10.27	10.60	9.95
NA2O	1.96	2.02	1.87	1.69	1.89	2.01	1.76
K2O	.14	.12	.13	.15	.14	.15	.12
SUM	97.76	97.20	98.01	98.22	97.80	99.73	98.87

SI	6.630	*	6.577	*	6.583	*	6.679	*	6.617	*	6.565	*	6.671	*
AL	1.370	8.000	1.423	8.000	1.417	8.000	1.321	8.000	1.383	8.000	1.435	8.000	1.329	8.000
AL	.732	*	.798	*	.866	*	.753	*	.787	*	.777	*	.798	*
TI	.038	*	.045	*	.042	*	.041	*	.042	*	.043	*	.040	*
MG	2.324	*	2.238	*	2.204	*	2.309	*	2.269	*	2.280	*	2.257	*
FE	2.159	*	2.239	*	2.174	*	2.139	*	2.178	*	2.165	*	2.191	*
MN	.049	*	.062	*	.063	*	.063	*	.059	*	.064	*	.054	*
NA	.565	*	.587	*	.537	*	.484	*	.543	*	.569	*	.517	*
CA	1.682	*	1.579	*	1.602	*	1.662	*	1.636	*	1.657	*	1.614	*
K	.027	7.576	.023	7.571	.025	7.513	.028	7.498	.026	7.539	.027	7.582	.024	7.495
O	23.000	*	23.000	*	23.000	*	23.000	*	23.000	*	23.000	*	23.000	*
F/M		.950		1.028		1.015		.954		.986		.977		.995
F/FM		.487		.507		.504		.488		.496		.494		.499

1 SAMPLE A-190-3 HBLE
2 OTHER ORIENT OF HBLE
3 ASSOC HBLE
4 ASSOC HBLE

5 AVERAGE
6 AVERAGE PLUS SIGMA
7 AVERAGE MINUS SIGMA

SUPER RECAL AMPHIBOLE SAMPLES

	1	2	3	4	5	6
SIO2	54.82	53.00	54.29	54.04	54.80	53.27
TIO2	.06	.05	.11	.07	.10	.05
A203	.71	2.82	.90	1.48	2.43	.52
FEO	23.35	21.90	23.52	22.92	23.65	22.20
MNO	1.75	1.42	1.77	1.65	1.81	1.49
MGO	17.20	15.82	17.57	16.86	17.62	16.11
CAO	.68	1.63	.63	.98	1.44	.52
NA20	.03	.20	.07	.10	.17	.03
K20	0.00	.01	.03	.01	.03	.00
SUM	98.60	96.85	98.89	98.11	102.04	94.18

SI	7.960	*	7.809	*	7.880	*	7.884	*	7.717	*	8.063	*
AL	.040	8.000	.191	8.000	.120	8.000	.116	8.000	.283	8.000	0.000	8.063
AL	.082	*	.298	*	.034	*	.137	*	.120	*	.093	*
TI	.007	*	.006	*	.012	*	.008	*	.011	*	.005	*
MG	3.723	*	3.474	*	3.801	*	3.667	*	3.697	*	3.634	*
FE	2.836	*	2.698	*	2.855	*	2.797	*	2.785	*	2.810	*
MN	.215	*	.177	*	.218	*	.203	*	.216	*	.191	*
NA	.008	*	.057	*	.020	*	.028	*	.047	*	.006	*
CA	.106	*	.257	*	.098	*	.153	*	.217	*	.084	*
K	0.000	6.976	.002	6.970	.006	7.043	.002	6.997	.005	7.097	.000	6.826
O	23.000	*	23.000	*	23.000	*	23.000	*	23.000	*	23.000	*
F/M		.820		.828		.808		.818		.812		.823
F/FM		.450		.453		.447		.450		.448		.452

1 SAMPLE A 190-3 CUMM IN C WITH HBLE
2 ANOTH AMPH PAIR,CUMM
3 CUMM ALONE

4 AVERAGE
5 AVERAGE PLUS SIGMA
6 AVERAGE MINUS SIGMA

SUPER PECAL — AMPHIBOLE SAMPLES

	1	2	3	4	5	6	7
SIO2	52.99	53.84	54.15	52.63	53.40	54.02	52.79
TIO2	0.00	.01	.01	0.00	.01	.01	.00
A2O3	.95	.64	.48	.71	.70	.86	.53
FEO	26.00	26.03	25.40	25.47	25.73	26.02	25.43
MNO	.70	.72	.74	.82	.75	.79	.70
MGO	16.54	16.88	16.75	16.79	16.74	16.86	16.62
CAO	.44	.45	.49	.45	.46	.48	.44
NA2O	.23	.15	.18	.23	.20	.23	.16
K2O	.01	.01	.01	.02	.01	.02	.01
SUM	97.86	98.73	98.21	97.12	97.98	99.29	96.67
SI	7.845 *	7.887 *	7.948 *	7.847 *	7.882 *	7.869 *	7.896 *
AL	.155 8.000	.110 7.998	.052 8.000	.125 7.972	.118 8.000	.131 8.000	.093 7.989
AL	.011 *	0.000 *	.031 *	0.000 *	.003 *	.017 *	0.000 *
TI	0.000 *	.001 *	.001 *	0.000 *	.001 *	.001 *	.000 *
MG	3.650 *	3.686 *	3.664 *	3.731 *	3.683 *	3.662 *	3.744 *
FE	3.219 *	3.189 *	3.118 *	3.176 *	3.175 *	3.169 *	3.182 *
MN	.088 *	.089 *	.092 *	.104 *	.093 *	.098 *	.089 *
NA	.066 *	.043 *	.051 *	.066 *	.057 *	.065 *	.047 *
CA	.070 *	.071 *	.077 *	.072 *	.072 *	.074 *	.070 *
K	.002 7.106	.002 7.080	.002 7.036	.002 7.153	.002 7.086	.003 7.090	.002 7.094
O	23.000 *	23.000 *	23.000 *	23.000 *	23.000 *	23.000 *	23.000 *
F/M	.906	.889	.876	.879	.888	.892	.883
F/FM	.475	.471	.467	.468	.470	.472	.469

1 SAMPLE A-190-8 AMPH
2 CUMM AGAIN
3 AGAIN
4 CUMM AGAIN
5 AVERAGE
6 AVERAGE PLUS SIGMA
7 AVERAGE MINUS SIGMA

SUPER RECAL

AMPHIBOLE SAMPLES

	1		2		3		4		5		6		7		8	
SIO2	50.08		51.63		45.96		51.57		51.26		50.10		52.24		47.97	
TIO2	.24		.18		.31		.16		.13		.20		.27		.14	
A203	8.88		7.54		13.59		8.02		7.62		9.13		11.41		6.85	
FEO	10.57		9.12		11.48		10.35		9.06		10.12		11.04		9.20	
MNO	.11		.13		.14		.15		.11		.13		.14		.11	
MGO	14.91		16.75		12.77		16.34		16.55		15.46		16.96		13.97	
CAO	11.78		11.86		11.88		11.44		12.19		11.83		12.07		11.59	
NA20	.57		.40		1.07		.47		.56		.61		.85		.38	
K20	0.00		0.08		.10		0.00		0.00		.02		.06		-.02	
SUM	97.14		97.61		97.32		98.50		97.48		97.61		105.04		90.18	
SI	7.174	*	7.300	*	6.650	*	7.258	*	7.272	*	7.133	*	6.926	*	7.373	*
AL	.826	8.000	.700	8.000	1.350	8.000	.742	8.000	.728	8.000	.867	8.000	1.074	8.000	.627	6.000
AL	.673	*	.557	*	.966	*	.589	*	.546	*	.665	*	.709	*	.614	*
TI	.026	*	.019	*	.034	*	.017	*	.014	*	.022	*	.027	*	.016	*
MG	3.184	*	3.530	*	2.753	*	3.428	*	3.499	*	3.281	*	3.351	*	3.200	*
FE	1.266	*	1.078	*	1.386	*	1.218	*	1.075	*	1.204	*	1.224	*	1.182	*
MN	.013	*	.016	*	.017	*	.018	*	.013	*	.015	*	.016	*	.016	*
NA	.158	*	.110	*	.300	*	.128	*	.154	*	.169	*	.219	*	.113	*
CA	1.808	*	1.797	*	1.841	*	1.725	*	1.553	*	1.804	*	1.714	*	1.909	*
K	0.000	7.129	0.000	7.106	.018	7.317	0.000	7.123	0.000	7.154	.004	7.165	.015	7.269	-.004	7.044
O	23.000	*	23.000	*	23.000	*	23.000	*	23.000	*	23.000	*	23.000	*	23.000	*
	F/M	.402		.310		.511		.361		.311		.372		.376		.374
	F/FM	.287		.237		.338		.265		.237		.271		.270		.272

1 A-190-2 HBLE
2 ANOTHER
3 ANOTHER
4
5 IN C WITH ANTH
6 AVERAGE
7 AVERAGE PLUS SIGMA
8 AVERAGE MINUS SIGMA

SUPER RECAL AMPHIBOLE SAMPLES

	1		2		3		4		5		6		7	
SIO2	54.62		54.02		55.19		55.24		54.77		55.26		54.27	
TIO2	0.00		0.00		0.00		0.00		0.00		0.00		0.00	
A2O3	2.12		2.77		1.84		2.13		2.22		2.56		1.87	
FEO	18.27		17.77		19.90		19.45		18.85		19.71		17.99	
MNO	.41		.46		.52		.51		.48		.52		.43	
MGO	20.11		19.63		20.66		20.41		20.20		20.59		19.82	
CAO	1.69		2.69		.42		.48		1.32		2.26		.38	
NA2O	.18		.14		.05		.07		.11		.16		.06	
K2O	0.00		0.00		0.00		0.00		0.00		0.00		0.00	
SUM	97.40		97.48		98.58		98.29		97.94		101.05		94.82	
SI	7.824	*	7.743	*	7.835	*	7.845	*	7.812	*	7.693	*	7.937	*
AL	.176	8.000	.257	8.000	.165	8.000	.155	8.000	.188	8.000	.307	8.000	.063	8.000
AL	.181	*	.211	*	.143	*	.202	*	.184	*	.112	*	.260	*
TI	0.000	*	0.000	*	0.000	*	0.000	*	0.000	*	0.000	*	0.000	*
MG	4.293	*	4.194	*	4.372	*	4.320	*	4.295	*	4.271	*	4.320	*
FE	2.189	*	2.130	*	2.363	*	2.310	*	2.258	*	2.294	*	2.200	*
MN	.050	*	.056	*	.063	*	.061	*	.057	*	.061	*	.053	*
NA	.050	*	.039	*	.014	*	.019	*	.030	*	.044	*	.016	*
CA	.259	*	.413	*	.064	*	.073	*	.202	*	.337	*	.060	*
K	0.000	7.022	0.000	7.042	0.000	7.018	0.000	6.986	0.000	7.017	0.000	7.119	0.000	6.909
O	23.000	*	23.000	*	23.000	*	23.000	*	23.000	*	23.000	*	23.000	*
F/M		.521		.521		.555		.549		.537		.551		.522
F/FM		.343		.343		.357		.354		.349		.355		.343

1 SAMPLE A-190-2 ANTH
2 ANOTHER SPOT SAME GRAIN
3 ANOTHER GRAIN
4 ANOTHER SPOT

5 AVERAGE
6 AVERAGE PLUS SIGMA
7 AVERAGE MINUS SIGMA

SUPER RECAL AMPHIBCLE SAMPLES

	1		2		3		4		5		6		7		8	
SIO2	52.95		47.82		47.58		47.94		48.39		50.03		51.30		49.14	
TIO2	.06		.20		.27		.16		.17		.16		.09		.21	
A203	4.93		10.17		11.59		11.37		11.07		8.81		6.84		9.71	
FEO	8.70		10.93		10.77		10.57		8.45		11.32		8.62		10.64	
MNO	.14		.22		.19		.18		.11		.25		.11		.17	
MGO	17.39		14.45		13.83		13.94		15.20		15.14		16.81		14.57	
CAO	12.71		11.66		12.18		12.08		12.13		10.66		12.84		12.07	
NA20	.34		.56		.68		.75		.67		.58		.29		.66	
K20	0.00		.07		.02		.04		.02		.02		0.00		.03	
SUM	97.22		96.08		97.11		97.03		96.21		96.97		96.90		97.20	
SI	7.519	*	6.967	*	6.858	*	6.905	*	6.952	*	7.186	*	7.318	*	7.059	*
AL	.481	8.000	1.033	8.000	1.142	8.000	1.095	8.000	1.048	8.000	.814	8.000	.682	8.000	.941	8.000
AL	.344	*	.713	*	.827	*	.834	*	.827	*	.678	*	.468	*	.702	*
TI	.006	*	.022	*	.029	*	.017	*	.018	*	.017	*	.010	*	.023	*
MG	3.681	*	3.138	*	2.971	*	2.993	*	3.255	*	3.241	*	3.574	*	3.120	*
FE	1.033	*	1.332	*	1.298	*	1.273	*	1.015	*	1.360	*	1.028	*	1.278	*
MN	.017	*	.027	*	.023	*	.022	*	.013	*	.030	*	.013	*	.021	*
NA	.094	*	.158	*	.190	*	.209	*	.187	*	.162	*	.080	*	.184	*
CA	1.934	*	1.820	*	1.881	*	1.864	*	1.867	*	1.641	*	1.963	*	1.858	*
K	.000	7.108	.013	7.223	.004	7.224	.007	7.220	.004	7.186	.004	7.132	0.000	7.137	.005	7.190
O	23.000	*	23.000	*	23.000	*	23.000	*	23.000	*	23.000	*	23.000	*	23.000	*
F/M		.285		.433		.445		.433		.316		.429		.291		.416
F/FM		.222		.302		.308		.302		.240		.300		.226		.294

1 SAMPLE A-190-9 ACTINOLITE
2
3
4 ANOTHER
5
6
7
8

SUPER RECAL AMPHIBOLE SAMPLES

	9		10		11		12		13	
SIO2	50.77		47.46		49.34		51.11		47.57	
TIO2	.17		.23		.17		.23		.11	
A203	8.12		11.78		9.44		11.59		7.29	
FEO	8.51		11.14		9.96		11.12		8.81	
MNO	.18		.19		.17		.22		.13	
MGO	16.42		13.36		15.11		16.48		13.82	
CAO	12.23		12.09		12.07		12.53		11.50	
NA20	.48		.67		.57		.71		.72	
K20	0.00		.07		.03		.05		.00	
SUM	96.88		96.99		96.86		104.06		89.65	
SI	7.232	*	6.860	*	7.087	*	6.864	*	7.343	*
AL	.768	8.000	1.140	8.000	.913	8.000	1.136	8.000	.657	8.000
AL	.595	*	.866	*	.685	*	.699	*	.569	*
TI	.018	*	.025	*	.019	*	.023	*	.013	*
MG	3.486	*	2.878	*	3.235	*	3.293	*	3.180	*
FE	1.014	*	1.347	*	1.197	*	1.250	*	1.137	*
MN	.022	*	.023	*	.021	*	.025	*	.017	*
NA	.133	*	.188	*	.158	*	.186	*	.126	*
CA	1.867	*	1.872	*	1.857	*	1.818	*	1.302	*
K	0.000	7.134	.013	7.212	.005	7.176	.009	7.292	.000	7.044
O	23.000	*	23.000	*	23.000	*	23.000	*	23.000	*
F/M		.297		.476		.377		.388		.363
F/FM		.229		.322		.274		.280		.266

9
10
11 AVERAGE

12 AVERAGE PLUS SIGMA
13 AVERAGE MINUS SIGMA

SUPER RECAL — AMPHIBOLE SAMPLES

	1	2	3	4	5	6	7	8
SIO2	53.96	51.81	52.78	52.60	53.27	51.66	52.70	52.68
TIO2	.02	.09	.08	.14	.11	.07	.12	.09
A2O3	1.27	2.71	2.93	2.58	2.40	2.23	2.33	2.35
FEO	25.74	24.95	25.18	24.43	24.98	24.75	24.68	24.96
MNO	.32	.44	.53	.59	.77	.78	.57	.53
MGO	17.30	17.23	16.91	18.27	17.42	17.10	17.29	17.36
CAO	.38	.23	.18	.17	.11	.19	.18	.21
NA2O	0.00	.30	.32	.11	.21	.26	.08	.18
K2O	0.00	0.00	.01	0.00	0.00	0.00	0.00	.00
SUM	98.99	97.76	98.92	98.89	99.27	96.74	97.95	98.36

SI	7.846	*	7.638	*	7.679	*	7.637	*	7.717	*	7.695	*	7.727	*	7.706	*
AL	.154	8.000	.362	8.000	.321	8.000	.363	8.000	.283	8.000	.305	8.000	.273	8.000	.294	8.000
AL	.063	*	.109	*	.182	*	.078	*	.126	*	.086	*	.130	*	.111	*
TI	.002	*	.010	*	.009	*	.015	*	.012	*	.008	*	.013	*	.010	*
MG	3.749	*	3.786	*	3.667	*	3.954	*	3.761	*	3.796	*	3.779	*	3.785	*
FE	3.130	*	3.076	*	3.064	*	2.966	*	3.026	*	3.083	*	3.026	*	3.053	*
MN	.039	*	.055	*	.066	*	.073	*	.094	*	.061	*	.071	*	.065	*
NA	0.000	*	.086	*	.090	*	.081	*	.059	*	.075	*	.023	*	.052	*
CA	.059	*	.036	*	.028	*	.026	*	.017	*	.030	*	.022	*	.032	*
K	0.000	7.043	0.000	7.159	.002	7.107	0.000	7.143	0.000	7.096	0.000	7.139	0.000	7.070	.000	7.108
O	23.000	*	23.000	*	23.000	*	23.000	*	23.000	*	23.000	*	23.000	*	23.000	*
F/M		.845		.827		.853		.769		.830		.828		.820		.824
F/FM		.458		.453		.460		.435		.453		.453		.450		.452

1 SAMPLE 189-1 CUMM
2
3 OTHER GRAIN
4

5
6
7
8 AVERAGE

SUPER RECAL — AMPHIBOLE SAMPLES

	1		2		3		4		5		6		7	
SIO2	40.01		41.13		40.57		43.67		41.35		42.74		39.95	
TIO2	.32		.38		.35		.22		.32		.38		.26	
A2O3	16.16		14.89		15.53		12.10		14.67		16.22		13.12	
FEO	18.66		18.46		18.55		18.75		18.61		18.71		18.50	
MNO	.45		.40		.42		.31		.40		.45		.34	
MGO	8.43		8.59		8.50		9.46		8.75		9.16		8.33	
CAO	10.20		10.43		10.32		10.59		10.39		10.53		10.24	
NA2O	2.63		2.41		2.52		2.23		2.45		2.60		2.50	
K2O	.26		.15		.20		.18		.20		.24		.16	
SUM	97.12		96.84		96.96		97.51		97.11		101.03		93.19	
SI	6.083	*	6.250	*	6.168	*	6.576	*	6.270	*	6.208	*	6.336	*
AL	1.917	8.000	1.750	8.000	1.832	8.000	1.424	8.000	1.730	8.000	1.792	8.000	1.662	8.000
AL	.979	*	.917	*	.950	*	.723	*	.892	*	.984	*	.791	*
TI	.037	*	.043	*	.040	*	.025	*	.036	*	.041	*	.031	*
MG	1.910	*	1.946	*	1.926	*	2.123	*	1.977	*	1.983	*	1.970	*
FE	2.373	*	2.346	*	2.358	*	2.361	*	2.360	*	2.273	*	2.454	*
MN	.058	*	.051	*	.054	*	.040	*	.051	*	.055	*	.048	*
NA	.775	*	.710	*	.743	*	.651	*	.729	*	.731	*	.708	*
CA	1.662	*	1.698	*	1.681	*	1.709	*	1.687	*	1.638	*	1.741	*
K	.050	7.844	.029	7.741	.039	7.791	.035	7.667	.038	7.760	.044	7.749	.032	7.773
O	23.000	*	23.000	*	23.000	*	23.000	*	23.000	*	23.000	*	23.000	*
	F/M	1.272		1.232		1.253		1.131		1.219		1.174		1.269
	F/FM	.560		.552		.556		.531		.549		.540		.559

1 A-189-4 HBLE
2
3
4 GREEN HBLE

5 AVERAGE
6 AVERAGE PLUS SIGMA
7 AVERAGE MINUS SIGMA

SUPER RECAL — AMPHIBOLE SAMPLES

	1	2	3	4	5
SIO2	52.25	53.79	53.02	53.79	52.25
TIO2	.01	.03	.02	.03	.01
A203	1.02	.92	.97	1.02	.92
FEO	25.00	24.39	24.70	25.00	24.39
MNO	1.16	1.05	1.11	1.16	1.05
MGO	16.63	16.90	16.77	16.90	16.63
CAO	.44	.73	.59	.73	.44
NA20	.14	.26	.20	.26	.14
K20	.05	.01	.03	.05	.01
SUM	96.70	98.38	97.39	98.94	95.84

SI	7.822	*	7.892	*	7.857	*	7.851	*	7.863	*
AL	.178	8.000	.108	8.000	.143	8.000	.149	8.000	.137	8.000
AL	.002	*	.051	*	.027	*	.027	*	.027	*
TI	.001	*	.003	*	.002	*	.003	*	.001	*
MG	3.711	*	3.696	*	3.703	*	3.677	*	3.730	*
FE	3.130	*	2.993	*	3.061	*	3.052	*	3.070	*
MN	.147	*	.130	*	.139	*	.143	*	.134	*
NA	.041	*	.074	*	.057	*	.074	*	.041	*
CA	.071	*	.118	*	.093	*	.114	*	.071	*
K	.010	7.112	.002	7.063	.006	7.087	.009	7.099	.002	7.075
O	23.000	*	23.000	*	23.000	*	23.000	*	23.000	*
F/M		.883		.845		.864		.869		.859
F/FM		.469		.458		.463		.465		.462

1 SAMPLE A-189-4 CUMM AT EDGE
2 CUMM AT EDGE
3 AVERAGE
4 AVERAGE PLUS SIGMA
5 AVERAGE MINUS SIGMA

SUPER RECAL — AMPHIBOLE SAMPLES

	1	2	3	4	5	6	7	8
SIO2	41.76	54.59	54.53	42.26	54.34	43.38	43.59	47.78
TIO2	.40	.02	.04	.32	.07	.19	.28	.19
A2O3	14.87	.97	.95	15.11	.89	14.04	14.21	8.72
FEO	18.98	25.80	26.26	18.82	26.32	18.88	19.08	22.02
MNO	.14	.50	.52	.26	.55	.18	.18	.33
MGO	7.52	16.07	15.39	7.52	15.77	8.25	8.16	11.31
CAO	10.28	.77	.64	10.05	.55	10.82	10.20	6.19
NA2O	2.29	.09	.02	2.22	0.00	1.80	2.26	1.24
K2O	.37	.02	.03	.28	.02	.27	.27	.18
SUM	96.61	98.83	98.88	96.84	98.51	97.81	98.23	97.96

SI	6.357	*		7.957	*		7.958	*		6.395	*		7.964	*		6.495	*		6.498	*		7.101	*	
AL	1.643	8.000		.043	8.000		.042	8.000		1.605	8.000		.036	8.000		1.505	8.000		1.502	8.000		.899	8.000	
AL	1.025	*		.123	*		.121	*		1.090	*		.117	*		.972	*		.994	*		.625	*	
TI	.046	*		.002	*		.004	*		.036	*		.008	*		.021	*		.031	*		.021	*	
MG	1.706	*		3.491	*		3.456	*		1.696	*		3.445	*		1.841	*		1.813	*		2.506	*	
FE	2.416	*		3.145	*		3.205	*		2.382	*		3.226	*		2.364	*		2.379	*		2.737	*	
MN	.018	*		.062	*		.064	*		.033	*		.068	*		.023	*		.023	*		.042	*	
NA	.676	*		.025	*		.006	*		.651	*		0.000	*		.523	*		.653	*		.357	*	
CA	1.677	*		.120	*		.100	*		1.629	*		.086	*		1.736	*		1.629	*		.985	*	
K	.072	7.636		.004	6.972		.006	6.962		.054	7.572		.004	6.954		.052	7.531		.051	7.574		.034	7.310	
O	23.000	*		23.000	*		23.000	*		23.000	*		23.000	*		23.000	*		23.000	*		23.000	*	
F/M		1.427			.918			.946			1.424			.956			1.296			1.324			1.109	
F/FM		.588			.479			.486			.587			.489			.565			.570			.526	

1 SAMPLE CA-28-6 LONG HBLE LATH
2 SAME COLOURLESS RIM
3 COLOURLESS RIM ON DEEP GREEN BASAL SECT
4 HBLE IN CONTACT
5 CUMM AGAIN
6 SAMPLE CA-286 HBLE
7 CUMM HALF
8 AVERAGE

SUPER RECAL — AMPHIBOLE SAMPLES

	1	2	3	4	5	6	7	8
SIO2	42.41	43.15	54.27	54.09	54.23	43.56	48.62	54.21
TIO2	.30	.39	.08	0.00	.07	.51	.23	.41
A2O3	15.19	15.41	1.25	.78	.94	14.66	8.04	15.09
FEO	18.85	18.87	25.32	25.52	26.40	19.14	22.35	25.76
MNO	.21	.17	.57	.46	.60	.25	.38	.55
MGO	7.31	7.87	16.10	15.88	15.90	7.91	11.83	15.97
CAO	10.48	10.31	.71	.82	.57	10.30	5.53	10.36
NA2O	2.21	2.40	.03	.10	.03	2.26	1.17	2.29
K2O	.31	.22	.02	.03	.01	.20	.13	.25
SUM	97.27	98.79	98.35	97.68	98.75	98.79	98.27	124.89

SI	6.395	*	6.390	*	7.934	*	7.977	*	7.936	*	6.457	*	7.188	*	6.393	*
AL	1.605	8.000	1.610	8.000	.066	8.000	.023	8.000	.064	8.000	1.543	8.000	.812	8.000	1.607	8.000
AL	1.094	*	1.080	*	.149	*	.113	*	.099	*	1.017	*	.586	*	.491	*
TI	.034	*	.043	*	.009	*	0.000	*	.008	*	.057	*	.025	*	.037	*
MG	1.643	*	1.737	*	3.508	*	3.491	*	3.468	*	1.746	*	2.606	*	2.807	*
FE	2.377	*	2.337	*	3.096	*	3.148	*	3.231	*	2.373	*	2.763	*	2.541	*
MN	.027	*	.021	*	.071	*	.057	*	.074	*	.031	*	.047	*	.055	*
NA	.646	*	.689	*	.009	*	.029	*	.009	*	.649	*	.336	*	.524	*
CA	1.693	*	1.636	*	.111	*	.130	*	.069	*	1.636	*	.876	*	1.310	*
K	.060	7.573	.042	7.585	.004	6.956	.006	6.972	.002	6.980	.038	7.549	.025	7.267	.037	7.801
O	23.000	*	23.000	*	23.000	*	23.000	*	23.000	*	23.000	*	23.000	*	23.000	*
F/M		1.463		1.358		.903		.918		.953		1.376		1.078		.925
F/FM		.594		.576		.474		.479		.488		.579		.519		.481

1 SAMPLE CA-284 CENTRAL HBLE ZONE
2 OUTER HBLE ZONE
3 CENTRAL CUMM ZONE AGAIN
4 ADJACENT FIBROUS CUMM
5 ANOTHER PAIR X CUMM HALF
6 HBLE HALF
7 AVERAGE
8 AVERAGE PLUS SIGMA

SUPER FECAL — AMPHIBOLE SAMPLES

	1	2	3	4	5	6	7
SIO2	54.03	43.38	53.51	43.83	48.69	53.78	43.60
TIO2	0.00	.30	.02	.24	.14	.27	.01
A2O3	1.02	14.69	.78	13.39	7.47	14.06	.88
FEO	26.34	19.16	26.13	19.57	22.80	26.24	19.36
MNO	.80	.16	.82	.23	.50	.81	.19
MGO	15.95	8.29	15.98	8.61	12.21	15.97	8.47
CAO	.60	10.34	.44	10.66	5.51	10.50	.52
NA2O	.04	2.14	0.00	2.04	1.06	2.09	.02
K2O	.03	.35	.03	.26	.17	.31	.03
SUM	98.81	98.81	97.71	98.83	98.54	124.02	73.06
SI	7.913 *	6.434 *	7.926 *	6.518 *	7.201 *	6.418 *	8.476 *
AL	.087 8.000	1.566 8.000	.074 8.000	1.482 8.000	.799 8.000	1.582 8.000	0.000 8.476
AL	.089 *	1.001 *	.062 *	.865 *	.502 *	.395 *	.202 *
TI	0.000 *	.033 *	.002 *	.027 *	.016 *	.024 *	.001 *
MG	3.482 *	1.933 *	3.526 *	1.909 *	2.691 *	2.840 *	2.446 *
FE	3.226 *	2.376 *	3.237 *	2.434 *	2.820 *	2.619 *	3.148 *
MN	.099 *	.020 *	.103 *	.029 *	.063 *	.082 *	.032 *
NA	.011 *	.615 *	0.000 *	.588 *	.303 *	.486 *	.007 *
CA	.094 *	1.643 *	.070 *	1.699 *	.873 *	1.343 *	.108 *
K	.006 7.007	.066 7.588	.006 7.007	.049 7.599	.032 7.299	.047 7.834	.007 5.953
O	23.000 *	23.000 *	23.000 *	23.000 *	23.000 *	23.000 *	23.000 *
F/M	.955	1.308	.947	1.290	1.071	.951	1.299
F/FM	.489	.567	.486	.563	.517	.487	.565

1 SAMPLE CA-283 CUMM RIM
2 HOLE HALF
3 ANOTHER PAIR CUMM
4 HOLE
5 AVERAGE
6 AVERAGE PLUS SIGMA
7 AVERAGE MINUS SIGMA

SUPER RECAL — AMPHIBOLE SAMPLES

	1	2	3	4	5	6	7	8
SIO2	54.27	44.04	53.69	44.25	54.66	43.04	48.99	54.23
TIO2	0.00	.35	.03	.39	.02	.32	.19	.35
A2O3	.48	12.86	.66	13.46	.59	13.53	6.93	13.29
FEO	27.27	20.61	26.56	20.31	27.13	19.68	23.59	27.00
MNO	.97	.29	.83	.37	.96	.29	.62	.92
MGO	15.42	8.18	14.53	7.86	14.98	7.80	11.46	14.99
CAO	.50	10.37	.51	10.23	.48	10.15	5.37	10.25
NA2O	0.00	1.89	.01	1.84	0.00	1.77	.92	1.83
K2O	.04	.23	0.00	.34	.02	.23	.14	.27
SUM	98.95	98.82	96.81	99.05	98.84	96.81	98.21	123.14

SI	7.973	*		6.573	*		8.034	*		6.572	*		8.020	*		6.532	*		7.269	*		6.526	*	
AL	.027	8.000		1.427	8.000		0.000	8.034		1.428	8.000		0.000	8.020		1.468	8.000		.711	8.000		1.474	8.000	
AL	.056	*		.874	*		.115	*		.928	*		.102	*		.951	*		.504	*		.410	*	
TI	0.000	*		.039	*		.003	*		.044	*		.002	*		.037	*		.021	*		.032	*	
MG	3.376	*		1.820	*		3.241	*		1.748	*		3.276	*		1.764	*		2.542	*		2.688	*	
FE	3.350	*		2.572	*		3.324	*		2.523	*		3.329	*		2.498	*		2.936	*		2.718	*	
MN	.121	*		.037	*		.105	*		.047	*		.119	*		.037	*		.078	*		.094	*	
NA	0.000	*		.547	*		.003	*		.530	*		0.300	*		.521	*		.265	*		.228	*	
CA	.079	*		1.658	*		.082	*		1.628	*		.075	*		1.656	*		.357	*		1.322	*	
K	.007	6.989		.044	7.551		0.000	6.872		.064	7.502		.004	6.908		.045	7.503		.027	7.228		.042	7.734	
O	23.000	*		23.000	*		23.000	*		23.000	*		23.000	*		23.000	*		23.000	*		23.000	*	
F/M		1.028			1.434			1.058			1.477			1.053			1.437			1.186			1.046		
F/FM		.507			.589			.514			.596			.513			.590			.542			.511		

1 SAMPLE CA-1F CUMM HALF
2 HBLE HALF
3 CUMM LATH
4 ADJ HBLE
5 CUMM
6 HBLE
7 AVERAGE
8 AVERAGE PLUS SIGMA

SUPER RECAL AMPHIBOLE SAMPLES

	1	2	3	4	5	6	7	8
SIO2	53.30	43.18	54.21	43.24	54.02	41.06	54.29	42.09
TIO2	.05	.37	.03	.29	.04	.33	.04	.37
A2O3	.68	14.22	1.00	13.61	.73	14.70	.88	14.77
FEO	26.00	19.56	26.15	20.11	26.57	20.38	27.05	20.41
MNO	.59	.20	.61	.27	.70	.26	.78	.27
MGO	14.00	7.81	15.39	7.72	15.29	6.89	15.15	7.29
CAO	.73	10.07	.64	10.17	.69	10.17	.48	10.30
NA2O	.04	2.16	.07	1.83	0.00	2.15	.06	2.03
K2O	.03	.22	.01	.31	.03	.24	0.00	.23
SUM	95.42	97.79	98.31	97.55	98.07	96.18	98.73	97.76

SI	8.074	*		6.480	*		7.961	*		6.526	*		7.977	*		6.326	*		7.972	*		6.362	*	
AL	0.000	8.074	*	1.520	8.000	*	.039	8.000	*	1.474	8.000	*	.023	8.000	*	1.674	8.000	*	.028	8.000	*	1.638	8.000	*
AL	.121	*	*	.995	*	*	.134	*	*	.946	*	*	.104	*	*	.995	*	*	.124	*	*	.993	*	*
TI	.006	*	*	.042	*	*	.003	*	*	.033	*	*	.004	*	*	.038	*	*	.004	*	*	.042	*	*
MG	3.161	*	*	1.747	*	*	3.413	*	*	1.737	*	*	3.365	*	*	1.562	*	*	3.316	*	*	1.642	*	*
FE	3.294	*	*	2.455	*	*	3.212	*	*	2.538	*	*	3.281	*	*	2.626	*	*	3.322	*	*	2.580	*	*
MN	.076	*	*	.025	*	*	.076	*	*	.035	*	*	.088	*	*	.034	*	*	.097	*	*	.039	*	*
NA	.012	*	*	.629	*	*	.020	*	*	.535	*	*	0.000	*	*	.642	*	*	.017	*	*	.595	*	*
CA	.118	*	*	1.619	*	*	.101	*	*	1.644	*	*	.109	*	*	1.679	*	*	.076	*	*	1.668	*	*
K	.006	6.794	*	.042	7.554	*	.002	6.960	*	.060	7.528	*	.006	6.958	*	.047	7.644	*	0.000	6.956	*	.044	7.599	*
O	23.000	*		23.000	*		23.000	*		23.000	*		23.000	*		23.000	*		23.000	*		23.000	*	
F/M		1.066			1.420			.963			1.481			1.001			1.681			1.031			1.592		
F/FM		.516			.587			.491			.597			.500			.627			.508			.614		

1 SAMPLE CA-682 CUMM HALF
2 HBLE HALF
3 CUMM
4 CUMM
5 CUMM
6 HBLE
7 CUMM
8 HBLE

SUPER RECAL AMPHIBOLE SAMPLES

	9	10	11
SIO2	48.17	54.00	42.35
TIO2	.19	.34	.04
A2O3	7.57	14.33	.81
FEO	23.28	26.46	20.09
MNO	.46	.68	.24
MGO	11.22	15.04	7.39
CAO	5.41	10.18	.63
NA2O	1.04	2.05	.04
K2O	.13	.25	.01
SUM	97.48	123.33	71.62

SI	7.219	*		6.467	*		8.474	*	
AL	.781	8.000	*	1.533	8.000	*	0.000	8.474	*
AL	.556	*	*	.490	*	*	.192	*	*
TI	.021	*	*	.031	*	*	.006	*	*
MG	2.505	*	*	2.685	*	*	2.205	*	*
FE	2.917	*	*	2.551	*	*	3.362	*	*
MN	.058	*	*	.059	*	*	.041	*	*
NA	.303	*	*	.475	*	*	.015	*	*
CA	.868	*	*	1.306	*	*	.136	*	*
K	.026	7.255	*	.039	7.746	*	.004	5.960	*
O	23.000	*		23.000	*		23.000	*	
F/M		1.188			1.613			1.543	
F/FM		.543			.603			.607	

9 AVERAGE
10 AVERAGE PLUS SIGMA
11 AVERAGE MINUS SIGMA

SUPER RECAL — AMPHIBOLE SAMPLES

	1	2	3	4	5	6	7	8
SIO2	55.04	55.35	53.34	57.51	53.02	52.96	56.16	55.23
TIO2	0.00	.03	.07	0.00	.10	.08	.04	.02
A203	2.69	2.84	4.50	.56	5.88	5.51	2.31	2.46
FEO	7.65	8.14	8.24	6.96	9.55	9.29	7.57	7.84
MNO	.22	.30	.20	.35	.27	.37	.20	.25
MGO	19.20	18.47	17.67	19.51	17.03	17.06	19.02	19.46
CAO	12.89	12.27	12.75	12.76	12.32	12.25	12.76	12.13
NA20	.11	.25	.34	.08	.62	.51	.10	.09
K20	.02	.06	.05	0.00	.07	.08	.03	0.00
SUM	97.82	97.71	97.16	97.73	98.86	98.31	98.19	97.48

SI	7.721	*	7.773	*	7.565	*	8.019	*	7.434	*	7.462	*	7.624	*	7.760	*
AL	.279	8.000	.227	8.000	.435	8.000	0.000	8.019	.566	8.000	.538	8.000	.176	8.000	.240	8.000
AL	.165	*	.243	*	.317	*	.092	*	.406	*	.393	*	.203	*	.167	*
TI	0.000	*	.003	*	.007	*	0.000	*	.011	*	.008	*	.004	*	.002	*
MG	4.014	*	3.866	*	3.736	*	4.055	*	3.559	*	3.583	*	3.949	*	4.075	*
FE	.897	*	.956	*	.977	*	.812	*	1.120	*	1.095	*	.882	*	.921	*
MN	.026	*	.036	*	.024	*	.041	*	.032	*	.044	*	.024	*	.033	*
NA	.030	*	.068	*	.093	*	.022	*	.169	*	.167	*	.027	*	.025	*
CA	1.937	*	1.846	*	1.938	*	1.906	*	1.851	*	1.849	*	1.905	*	1.826	*
K	.004	7.074	.011	7.028	.009	7.102	0.000	6.927	.013	7.159	.014	7.154	.005	6.999	0.000	7.046
O	23.000	*	23.000	*	23.000	*	23.000	*	23.000	*	23.000	*	23.000	*	23.000	*
F/M		.230		.257		.268		.210		.324		.318		.229		.233
F/FM		.187		.204		.211		.174		.245		.241		.187		.189

1 SAMPLE CA-1E MATRIX AMPH
2 ANOTHER
3 ANOTHER
4 DEEPER GREEN BLADED
5 GREEN RIM
6 AGAIN
7 NARROW CUMM AT MARGIN
8 COLOURLESS FIBROUS INST AREA

SUPER RECAL — AMPHIBOLE SAMPLES

	9	10	11
SIO2	54.83	56.34	53.31
TIO2	.04	.08	.01
A203	3.36	5.06	1.65
FEO	8.16	8.97	7.34
MNO	.27	.33	.21
MGO	18.43	19.40	17.45
CAO	12.52	12.80	12.24
NA20	.28	.49	.06
K20	.04	.07	.01
SUM	97.91	103.54	92.27

SI	7.695	*	7.505	*	7.908	*
AL	.305	8.000	.495	8.000	.092	8.000
AL	.250	*	.299	*	.197	*
TI	.004	*	.008	*	.001	*
MG	3.855	*	3.852	*	3.859	*
FE	.957	*	1.000	*	.910	*
MN	.032	*	.037	*	.026	*
NA	.075	*	.126	*	.018	*
CA	1.882	*	1.826	*	1.945	*
K	.007	7.063	.011	7.159	.002	6.957
O	23.000	*	23.000	*	23.000	*
F/M		.257		.269		.243
F/FM		.204		.212		.195

9 AVERAGE
10 AVERAGE PLUS SIGMA
11 AVERAGE MINUS SIGMA

NOTICE

PAGE(S) Plates 1+2 ~~IS~~/ARE ~~EST~~/SONT Large colored maps

WHICH WILL NOT REPRODUCE ON MICROFICHE.
AVEC LE RESULTAT QU'ELLE(S) NE PEUT (VENT) PAS
ETRE REPRODUITE(S) SUR MICROFICHE.

PLEASE WRITE TO THE AUTHOR FOR INFORMATION, OR CONSULT THE ARCHIVAL COPY HELD IN THE DEPARTMENT OF ARCHIVES AND SPECIAL COLLECTIONS, ELIZABETH DAFOE LIBRARY, UNIVERSITY OF MANITOBA, WINNIPEG, MANITOBA, CANADA R3T 2N2

VEUILLEZ ECRIRE A L'AUTEUR POUR LES RENSEIGNEMENTS OU VEUILLEZ CONSULTER L'EXEMPLAIRE DONT POSSEDE LE DEPARTEMENT DES ARCHIVES ET DES COLLECTIONS SPECIALES, BIBLIOTHEQUE ELIZABETH DAFOE, UNIVERSITE DU MANITOBA, WINNIPEG, MANITOBA, CANADA, R3T 2N2

Ellisville GD
Rt
Gr
Rt + RFt
RFt
Festn
Sh
RDt
Fe stn
Gr
Gr
Sh
Fe stn
Gr Gn
fQ
Ky Q
fGn
Si Fe fm
A
A'
MgS
Rt
GD
Tron
RD-Dt + At, Fl

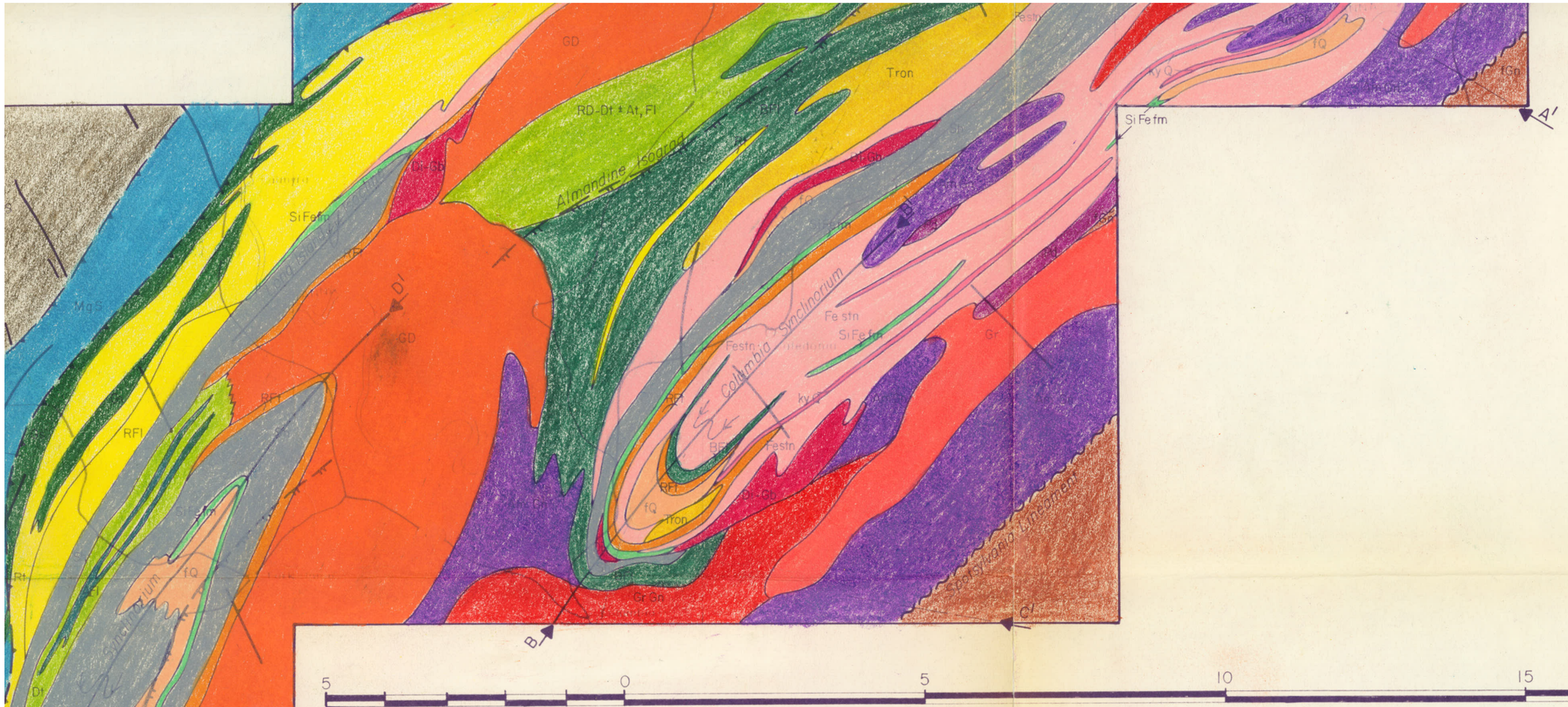

ROCK TYPES

Stratified Rocks

fanglomerate	
arenite	Ar
siltstone	St
shale	Sh
silicate facies iron formation	Si Fe fm
kyanite quartzite	ky Q
feldspathic quartzite	fQ
metakomatiite flow	KFl

Intrusive Rocks

diabase dykes	
granite	Gr
granodiorite	GD
trondhjemite	Tron
diorite	Di
gabbro	Gb
peridotite	Pd
granite gneiss	Gr Gn

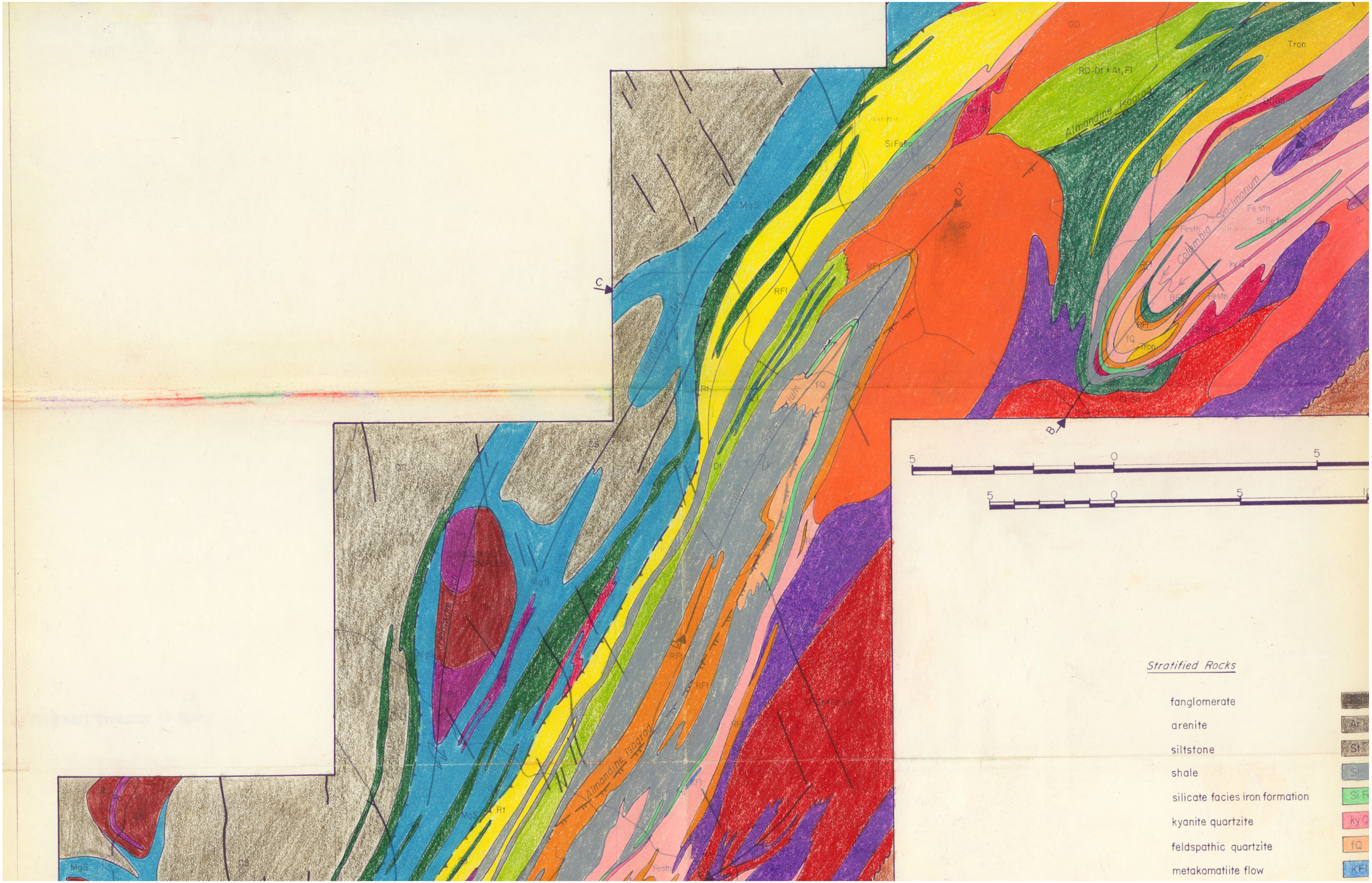

Stratified Rocks
fanglomerate
arenite
siltstone
shale
silicate facies iron formation
kyanite quartzite
feldspathic quartzite
metakomatiite flow
Almandine Isograd
Columbia Synclinorium
Tron
GD
RD-Dt ± At, Fl
SiFefm
Fe stn
Festn
MgS
RFl
fQ
Rt
Dt
C
B
5
0
5

kyanite quartzite	kyQ
feldspathic quartzite	fQ
metakomatiite flow	KFl
metarhyolite flow tuff	RFt
ironstone w/ iron formation bands	Festn
tuffaceous siltstone	tSt
metarhyolite tuff, flow	Rt, RFl
metarhyodacite tuff	RDt
metadacite tuff	Dt
meta-andesite tuff, flow	AN, ATl
metabasalt flow	BFl
greenstone flow	Gs
Candler schists	CS
amphibolite gneiss	Am Gn
feldspathic gneiss	fGn

gabbro	Gb
peridotite	Pd
granite gneiss	Gr Gn
diorite gneiss	Dr Gn
Hardware magnesian schist	MgS

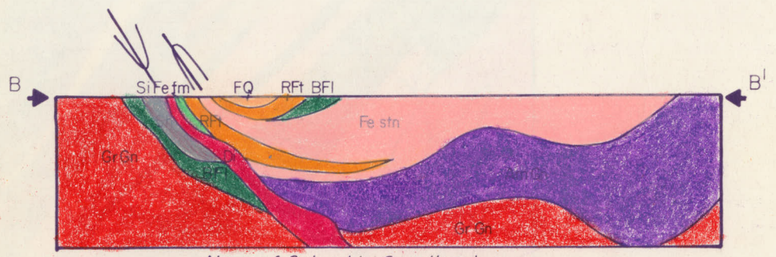

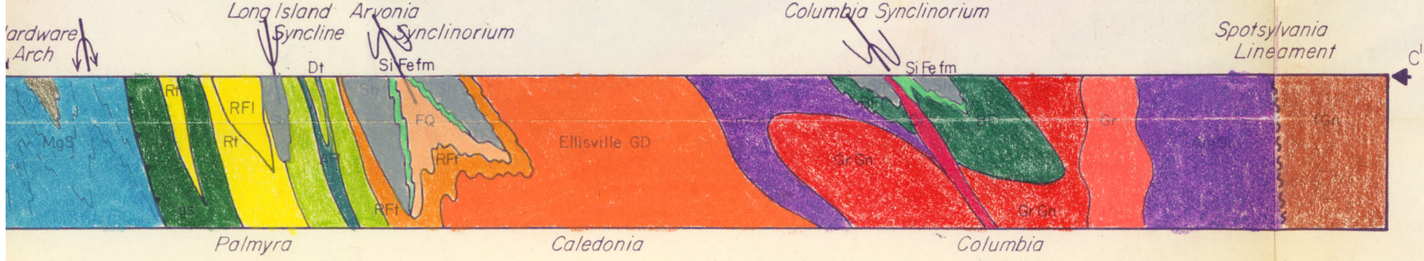

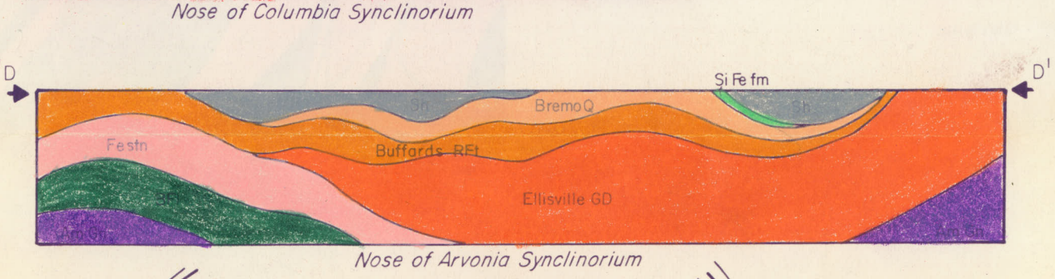

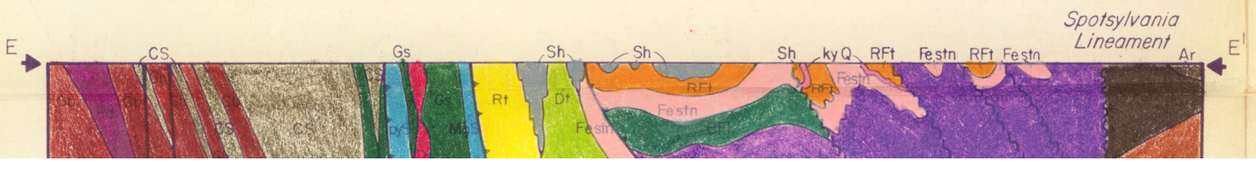

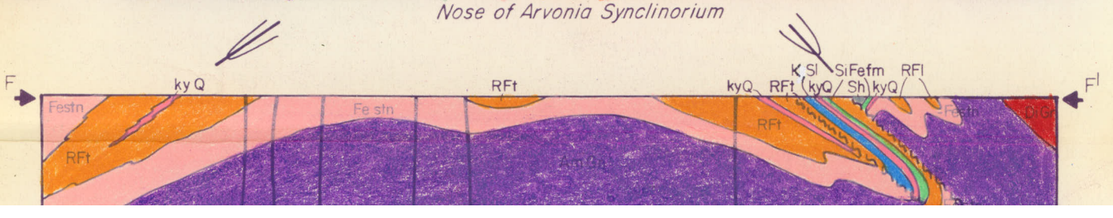

silicate facies iron formation — Si Fe
kyanite quartzite — kyQ
feldspathic quartzite — fQ
metakomatiite flow — KFt
metarhyolite flow tuff — RFt
ironstone w/ iron formation bands — Fest
tuffaceous siltstone — tSt
metarhyolite tuff, flow — Rt, R
metarhyodacite tuff — RDt
metadacite tuff — Dt
meta-andesite tuff, flow — At
metabasalt flow — BFt
greenstone flow — Gs
Candler schists — CS
amphibolite gneiss — Am
feldspathic gneiss — fGn

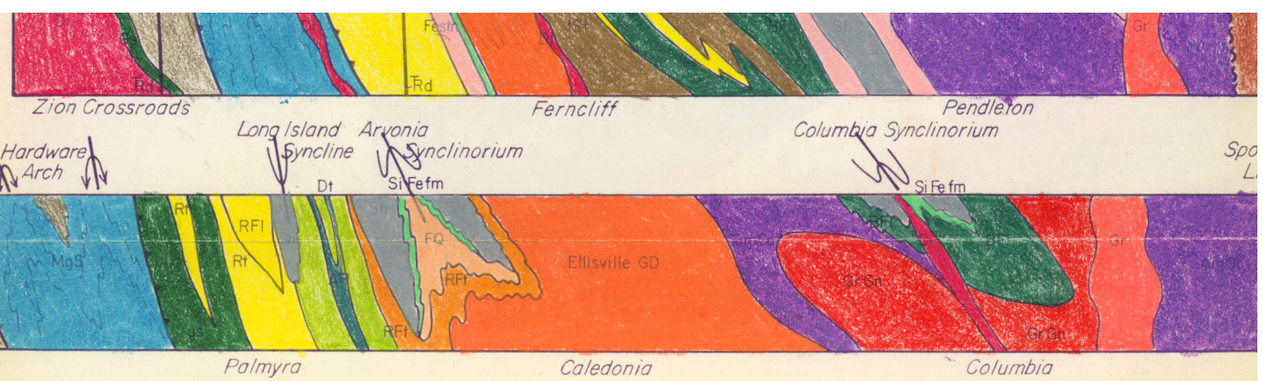

PLATE I: LITHOLOGICAL MAP OF THE LAKE ANNA TO APPOMATTOX

THE CHOPAWAMSIC METAVOLCANIC BELT

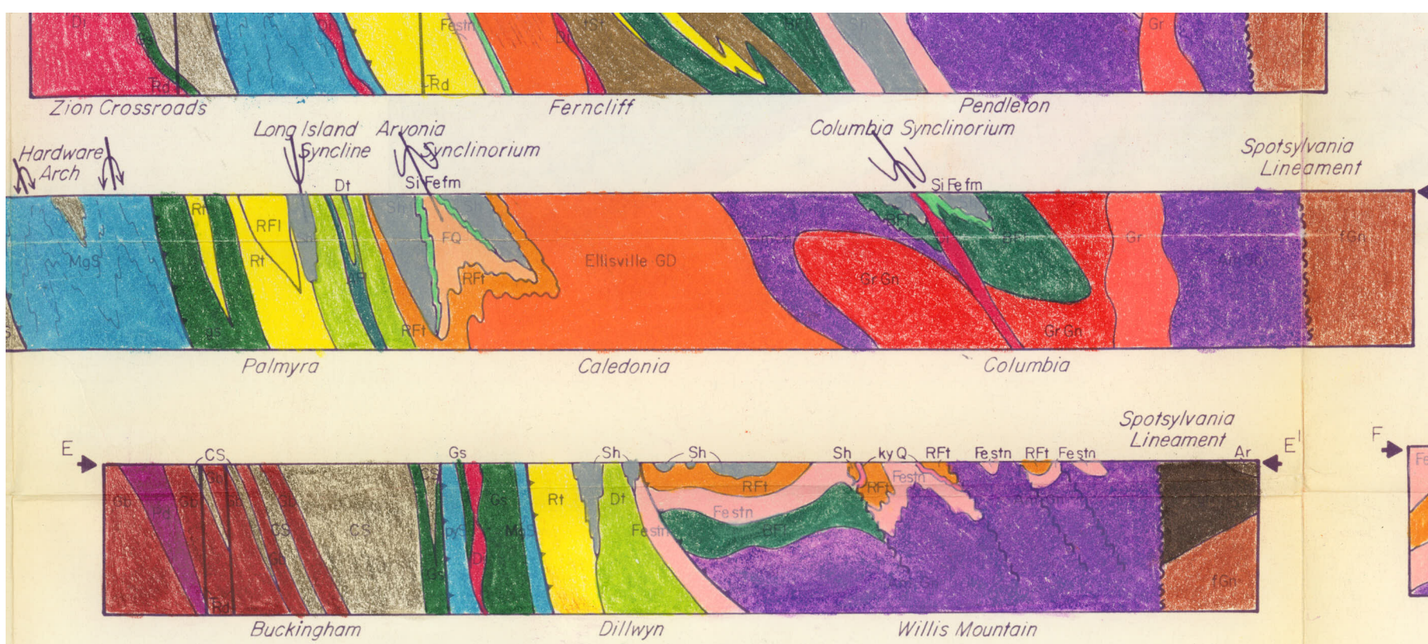

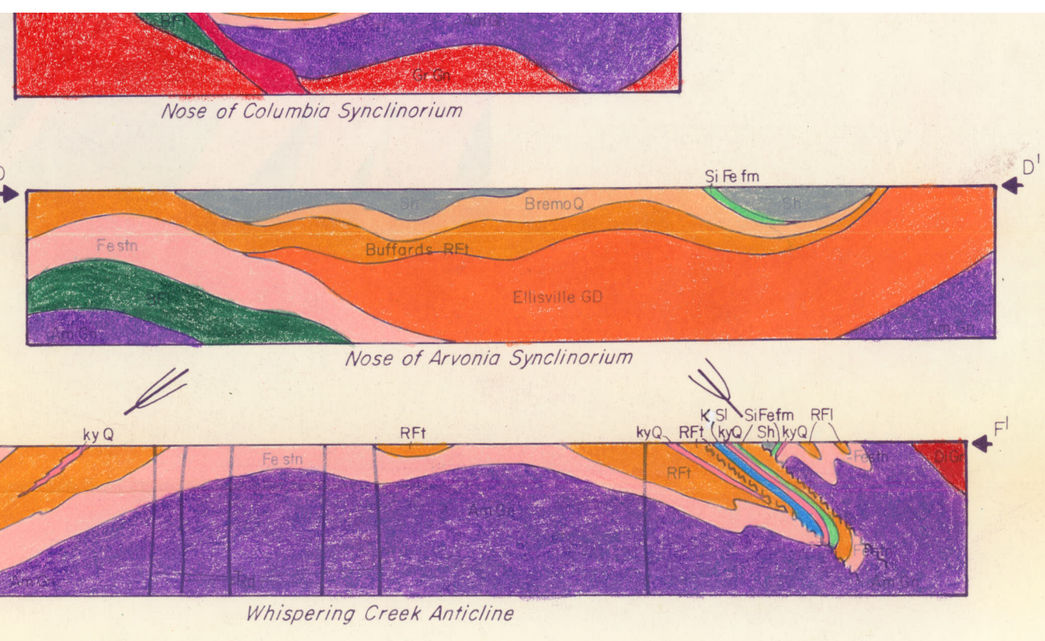

MAP OF THE LAKE ANNA TO APPOMATTOX RIVER SEGMENT OF THE CHOPAWAMSIC METAVOLCANIC BELT

LITHOLOGICAL CORRELATION CHART

age	stratified rocks		intrusive rocks
Triassic	ŦRm		ŦRd
Carboniferous			Ci
Ordovician	Osh/IO Fe fm		
Cambrio-Ordovician	Є-Ovs	Є-Ok	Є-Oi, Є-Oei
Cambrian	Єpv { Єmv	PЄ-Єv	Єi, Єgsi, Єcgi, Єhi
Precambrian-Cambrian	PЄ-Єs { PЄ-Єgs PЄ-Єav	PЄ-Єv	PЄ-Єbi, dmi
late Precambrian			PЄhs
Precambrian	PЄs		

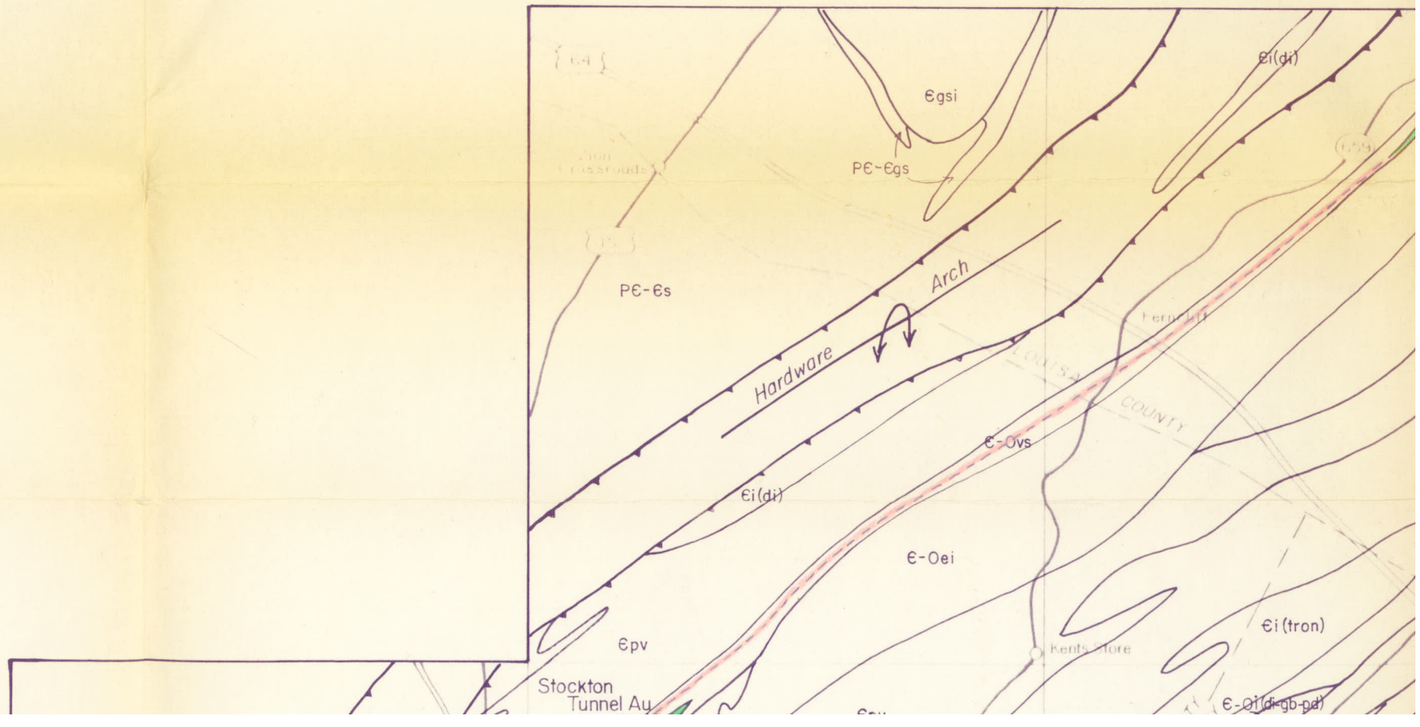

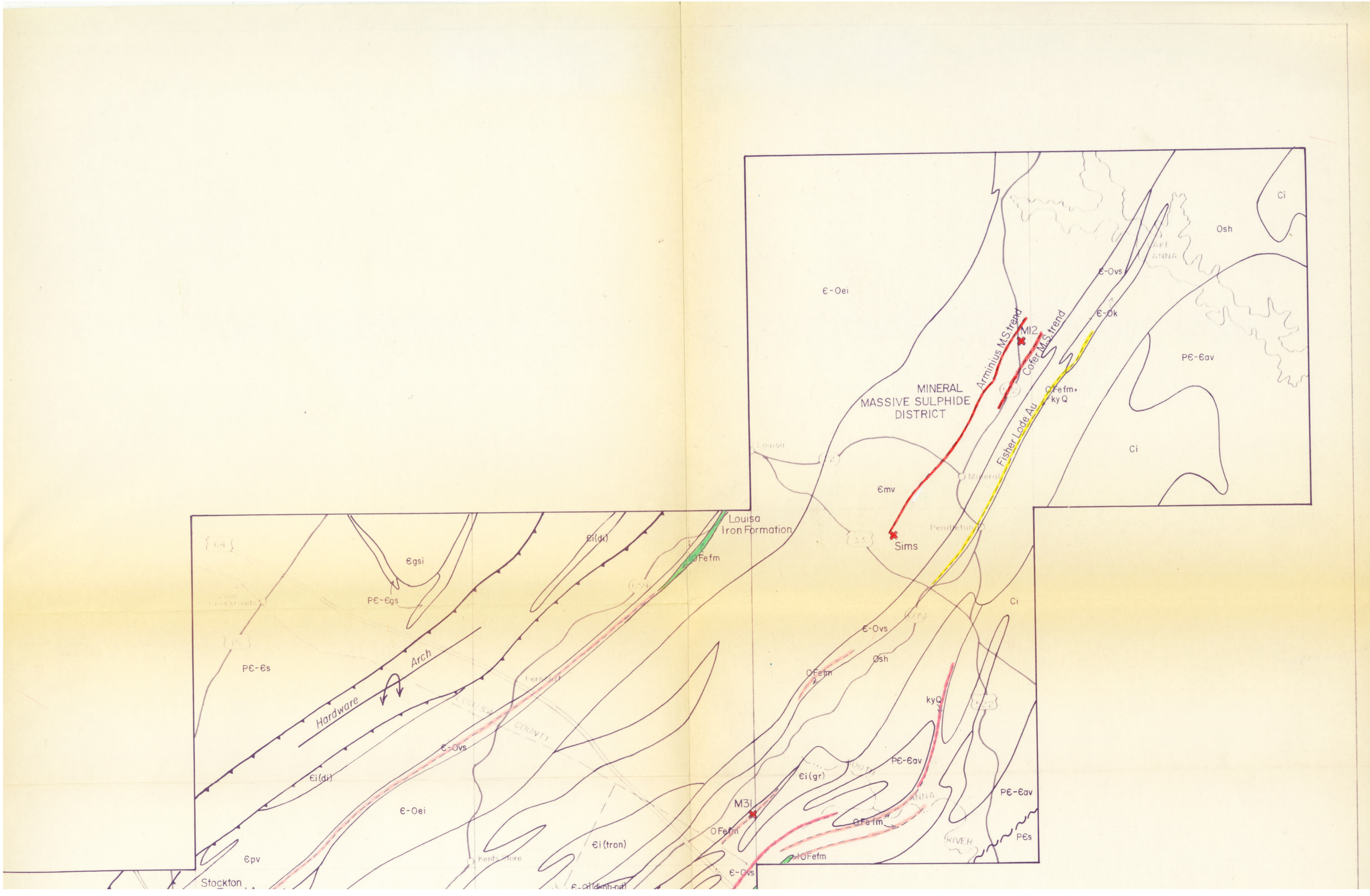

MINERAL
MASSIVE SULPHIDE
DISTRICT
Arminius M.S. trend
Cofer M.S. trend
Fisher Lode Au
M12
M31
Sims
Louisa
Iron Formation
Hardware
Arch
Louisa
County
Stockton
Ci
Osh
Є-Ovs
Є-Ok
PЄ-Єav
Є-Oei
Єmv
Єgsi
PЄ-Єgs
PЄ-Єs
Єi(di)
Єi(gr)
Єi(tron)
Єpv
kyQ
PЄs
OFefm

DESCRIPTION OF LITHOLOGIES

Stratified Rocks

Trm — MOLASSE OF THE FARMVILLE BASIN - coarse fanglomerate a western borders transitions through central arkosic s to lacustrian mudstones along the eastern border.

Osh — LONG ISLAND, ARVONIA, AND COLUMBIA METASHALE FORM includes an upper metashale facies, which occurs as grey slate at low metamorphic grades and as a micaceous garnet phyllite at medium grades, plus silicate iron formation facies (IOFefm), which occurs as green oolitic chloritite at low metamorphic grades an coarsely porphyroblastic garnet-grunerite amphibol medium grades.

Є-Ovs — UNDIFFERENTIATED UPPER CHOPAWAMSIC VOLCANICS AND SEDI includes regional two-amphibole ironstone, fer quartzite, and oxide iron formation, plus more re kyanite quartzite, tourmalinite, staurolite-gahnite qu feldspathic quartzite (Bremo Fm), and quartz-mica schi

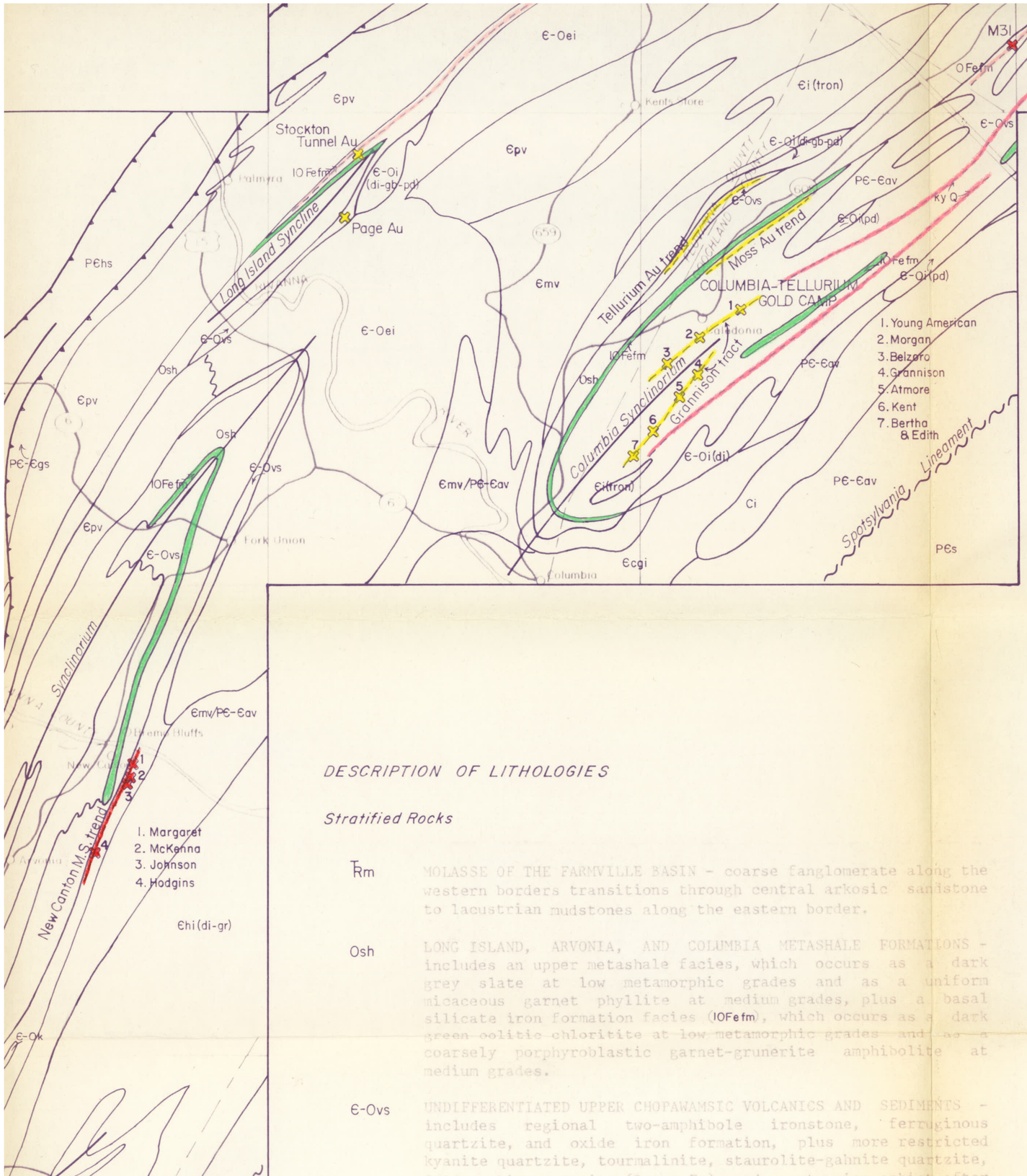

DESCRIPTION OF LITHOLOGIES

Stratified Rocks

Trm MOLASSE OF THE FARMVILLE BASIN - coarse fanglomerate along the western borders transitions through central arkosic sandstone to lacustrian mudstones along the eastern border.

Osh LONG ISLAND, ARVONIA, AND COLUMBIA METASHALE FORMATIONS - includes an upper metashale facies, which occurs as a dark grey slate at low metamorphic grades and as a uniform micaceous garnet phyllite at medium grades, plus a basal silicate iron formation facies (10Fefm), which occurs as a dark green oolitic chloritite at low metamorphic grades and as a coarsely porphyroblastic garnet-grunerite amphibolite at medium grades.

Є-Ovs UNDIFFERENTIATED UPPER CHOPAWAMSIC VOLCANICS AND SEDIMENTS - includes regional two-amphibole ironstone, ferruginous quartzite, and oxide iron formation, plus more restricted kyanite quartzite, tourmalinite, staurolite-gahnite quartzite, feldspathic quartzite (Bremo Fm), and quartz-mica schist after

Intrusive Rocks

Ci UNNAMED INTRUSIVE SUITE - Dykes and sills (not shown on map) and small plutons of fine to medium-grained granitoid rocks; probably correlative to the Falmouth Intrusive Suite of Pavlides (1980).

Є-Oi UNNAMED MAFIC INTRUSIVE BODIES - small composite diorite - gabbro - peridotite bodies occurring along the limbs of the major metashale synclines.

Є-Oei ELLISVILLE INTRUSION - comprises a northerly porphyritic quartz monzonite stock and a southerly gneissic-textured granodiorite sill (note: Є-Oi(gd), the unnamed porphyritic granodiorite stock in the Appomattox River area, was probably intruded coeval with the Ellisville body).

Єi UNNAMED FELSIC INTRUSIVE BODIES - includes (a) Єi(tron), small granophyric-textured trondhjemite bodies in the Mineral metavolcanic suite, and (b) Єi(di-gr), dioritic to granitic

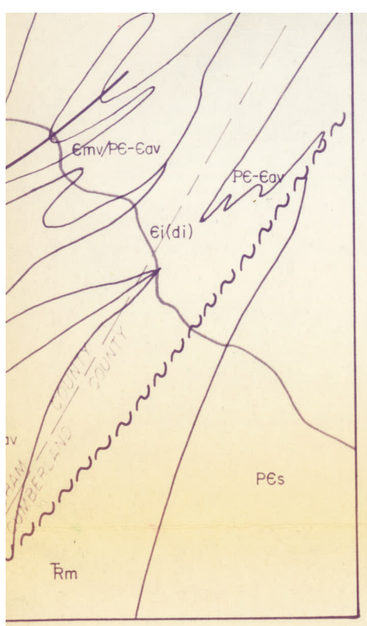

Є-Ovs UNDIFFERENTIATED UPPER CHOPAWAMSIC VOLCANICS AND SEDIMENTS - includes regional two-amphibole ironstone, ferruginous quartzite, and oxide iron formation, plus more restricted kyanite quartzite, tourmalinite, staurolite-gahnite quartzite, feldspathic quartzite (Bremo Fm), and quartz-mica schist after rhyolite ash flow tuff (Buffards Fm); ultramafic orthoamphibolites (Є-Ok) interlayered with iron formation are tentatively identified as metakomatiite flows.

PЄ-Єv UNDIFFERENTIATED CHOPAWAMSIC METAVOLCANICS - includes: Єpv, the Palmyra metavolcanic suite comprising (a) metarhyolite tuff and lesser flows west of the Long Island syncline, and (b) metadacite crystal tuff and meta-andesite lapilli tuff and lesser flows east of the Long Island syncline; Єmv, the Mineral metavolcanic suite comprising fine-grained epiclastic metasediment interlayered with bimodal metavolcanics and multifacies ironstone; PЄ-Єgs, the greenstone horizons basal to the Palmyra metavolcanic suite; and PЄ-Єav, the easterly unnamed amphibolitic gneisses which are probably correlative to the Ta River Metamorphic Suite of Pavlides (1980).

PЄ-Єs UNDIFFERENTIATED CANDLER METASEDIMENTS - composed mainly of chloritic and sericitic paper schists with minor impure quartzite and rare metagreywacke; greenstone flows (PЄ-Єgs) are locally interbedded with the metasediments.

PЄs UNDIFFERENTIATED FELDSPATHIC PARAGNEISS - unnamed paragneiss occurring east of the Chopawamsic metavolcanics; this lithology is at least in part correlative to the Po River Metamorphic Suite of Pavlides (1980).

Єi UNNAMED FELSIC INTRUSIVE BODIES - includes (a) Єi(tron), small granophyric-textured trondhjemite bodies in the Mineral metavolcanic suite, and (b) Єi(di-gr), dioritic to granitic orthogneisses lying along the eastern side of the Chopawamsic metavolcanics and incorporating Єhi, the gneisses of the Hatcher complex, and Єcgi, the Columbia granite gneiss.

Єgsi GREEN SPRINGS INTRUSION - a medium-grained dioritic stock with central tonalitic and peripheral granodioritic facies.

PЄ-Є bi,dmi BUCKINGHAM AND DIANA MILLS MAFIC INTRUSIVE COMPLEXES - multiple sill injection complexes in Hardware schist and/or Candler metasediment, including: (a) larger sills characterized by basal ultramafic cumulate, layered gabbro main zones, and minor quartz diorite segregations in their upper parts, and (b) peripheral sills constituted primarily of quartz diorite.

PЄhs HARDWARE SCHIST - severely tectonized Mg chlorite - talc - magnetite schist likely derived through extreme cataclasis and retrogression of ultramafic igneous material.

Mineralization

- prospects
- iron formation horizons
- massive sulphide trend
- trends of lode gold prospects
- kyanite quartzite horizons

5 0 5 10 15 20 miles

5 0 5 10 15 20 25 30 kilometers

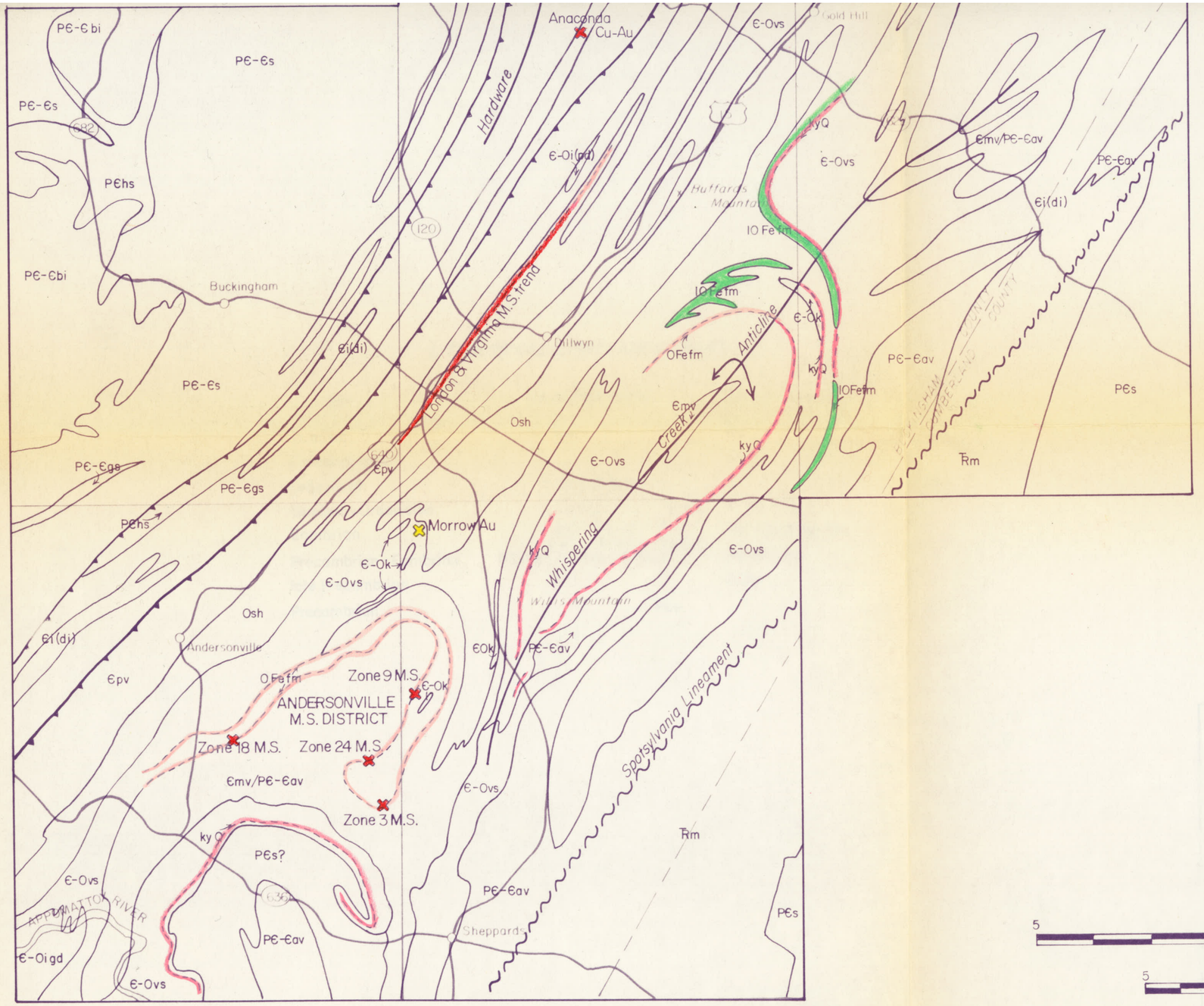
Anaconda Cu-Au
Gold Hill
Pε-Єbi
Pε-Єs
Pε-Єs
Pεhs
Pε-Єbi
Buckingham
Dillwyn
Hardware
Huffards Mountain
Huffards Mountain
London & Virginia M.S. trend
Anticline
Creek
Whispering
Whispering
Mountain
Spotsylvania Lineament
Єi(di)
Pε-Єs
Pε-Єgs
Pε-Єgs
Pεhs
Morrow Au
Osh
Osh
Andersonville
Єpv
Єi(di)
Zone 9 M.S.
Zone 18 M.S.
Zone 24 M.S.
Zone 3 M.S.
ANDERSONVILLE
M.S. DISTRICT
Єmv/Pε-Єav
Єmv/Pε-Єav
Pε-Єav
Pε-Єav

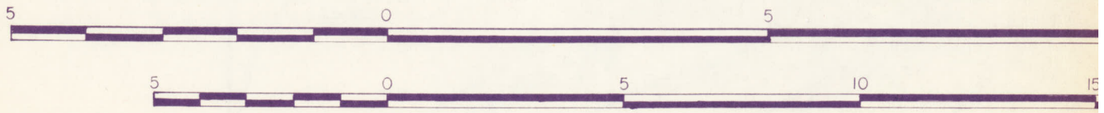

PLATE 2: REGIONAL GEOLOGICAL MAP OF THE LAKE ANNA TO APPOM

THE CHOPAWAMSIC METAVOLCANIC BELT

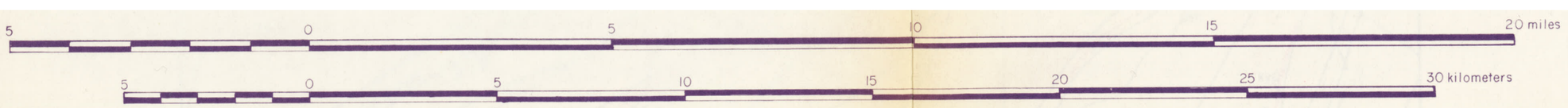

LOGICAL MAP OF THE LAKE ANNA TO APPOMATTOX RIVER SEGMENT OF

THE CHOPAWAMSIC METAVOLCANIC BELT